



Aromatic Ynamines: A New Bio-orthogonal Reactive Group for Step-efficient, Sequential Bioconjugation

Marine Hatit

Thesis submitted to the University of Strathclyde in fulfilment of the
requirements for the degree of Doctor of Philosophy

November 2018

Academic Supervisor: Prof Glenn A. Burley

Declaration of Copyright

This thesis is a result of the author's original research. It has been composed by the author and has not been previously submitted for examination which has led to the award of a degree. The copyright of this thesis belongs to the author under the terms of the United Kingdom Copyright Acts as qualified by University of Strathclyde Regulation 3.50. Due acknowledgement must always be made of the use of any material contained in, or derived from, this thesis.

Signed:

Date: November 2018

Table of Content

PUBLICATIONS LIST	7
ACKNOWLEDGEMENTS	8
ABSTRACT	9
ABBREVIATIONS.....	10
1 CHAPTER 1.....	12
1.1 INTRODUCTION TO BIOCONJUGATION.....	13
1.2 SITE-SPECIFIC BIOCONJUGATION BASED ON NATIVE FUNCTIONALITIES.....	14
1.2.1 Peptides and Proteins	14
1.2.2 Carbohydrates.....	18
1.2.3 Nucleic Acids	19
1.2.4 The Need for the Development of New Bio-orthogonal Reactions	20
1.3 BIO-ORTHOGONAL REACTIONS BASED ON EXTRINSIC FUNCTIONALITIES.....	20
1.3.1 Condensation of Ketones and Aldehydes	22
1.3.2 Staudinger Ligation.....	23
1.3.3 CpO/CpS Phosphine Ligation.....	26
1.3.4 Azide/Alkyne Cycloadditions.....	27
1.3.5 Strain-Promoted Alkyne/Nitrone Cycloaddition.....	39
1.3.6 Inverse Electron-Demand Diels-Alder with Tetrazine and Strained Alkene/Alkyne.....	39
1.3.7 Tandem [3 + 2] Cycloaddition-Retro-Diels-Alder.....	41
1.4 HYPOTHESIS	43
1.5 AIMS OF THIS PROJECT.....	44
2 CHAPTER 2.....	46
2.1 CHEMOSELECTIVITY OF ALKYNE AND AZIDE SUBSTRATES IN CuAAC REACTIONS	47
2.1.1 Sequential Chemoselective CuAAC Reactions Using Alkyne Protecting Groups.....	48
2.1.2 Sequential Chemoselective CuAAC Reactions Using Iodo/Bromo-Alkynes.....	50
2.1.3 Sequential Chemoselective CuAAC Reactions Using Chelate-Directed Azides.....	51
2.1.4 Sequential Chemoselective CuAAC Reactions using Transient Copper Complexation....	53
2.2 AROMATIC YNAMINES AS SYNTHONS FOR CuAAC REACTIONS	54
2.2.1 Ynamine Reactivity.....	54
2.2.2 Synthesis of Aromatic Ynamines	55

2.3	HYPOTHESIS TO BE TESTED.....	56
2.4	AIMS OF THIS CHAPTER	57
2.5	RESULTS AND DISCUSSION.....	58
2.5.1	<i>Optimisation of Aromatic Ynamine Synthesis</i>	58
2.5.2	<i>Aromatic Ynamine as a Synthron for CuAAC Reactions – Optimisation of the Reaction.</i>	60
2.5.3	<i>Aromatic Ynamine as a Synthron for CuAAC Reactions – Substrate Scope</i>	63
2.5.4	<i>Aromatic Ynamine as a Synthron for CuAAC Reactions – Chemoselective Profile.....</i>	64
2.5.5	<i>Aromatic Ynamine as a Synthron for CuAAC Reactions – Orthogonality Profile</i>	67
2.5.6	<i>Exploring Ynamine Reactivity vs Representative Terminal Alkynes in CuAAC Reactions</i>	71
2.5.7	<i>Ynamine Chemoselectivity vs Azide Chelate-Directed Strategy</i>	72
2.6	SUMMARY	73
2.7	EXPERIMENTAL	74
2.7.1	<i>Reagents and Solvents</i>	74
2.7.2	<i>Analysis of Products</i>	74
2.7.3	<i>General Procedures.....</i>	75
2.7.4	<i>Synthetic procedures.....</i>	77
3	CHAPTER 3.....	116
3.1	THE NEED FOR SEQUENTIAL BIOCONJUGATION	117
3.2	THE CURRENT <i>STATE-OF-ART</i> OF ORTHOGONAL BIOCONJUGATION	118
3.3	DUAL MODIFICATION OF BIOMOLECULES USING BIO-ORTHOGONAL CHEMISTRY	121
3.3.1	<i>Dual Labelling Using Sequential CuAAC Reactions.....</i>	121
3.3.2	<i>Dual Labelling Strategies which Combine CuAAC with Another Reaction.....</i>	123
3.3.3	<i>The Need for New Strategies for Sequential Bioconjugation</i>	131
3.4	HYPOTHESIS TO BE TESTED	132
3.5	AIMS OF THIS CHAPTER	133
3.6	RESULTS AND DISCUSSION.....	134
3.6.1	<i>Phosphoramidite Synthesis</i>	134
3.6.2	<i>Synthesis of Aromatic Ynamine- and Alkyne-Modified Oligodeoxyribonucleotides (ODNs)</i> <i>137</i>	
3.6.3	<i>Calculation of ODN Extinction Coefficients</i>	138
3.6.4	<i>Optimisation of CuAAC ligations using an Aromatic Ynamine-Modified ODN.....</i>	143
3.6.5	<i>Optimisation of CuAAC ligations using Phenylacetylene-Modified ODN</i>	147
3.6.6	<i>Substrate Scope.....</i>	148
3.6.7	<i>Site-Dependent Modulation of Ynamine Reactivity</i>	149
3.6.8	<i>Chemoselective, Sequential CuAAC Ligations of ODNs</i>	151

3.6.9	<i>Impact of Aromatic Ynamine Moiety into DNA Structure</i>	155
3.7	SUMMARY	156
3.8	EXPERIMENTAL	157
3.8.1	<i>Reagents and Solvents</i>	157
3.8.2	<i>Analysis of Products</i>	157
3.8.3	<i>Synthetic procedures</i>	158
3.8.4	<i>Solid Phase Synthesis of Oligodeoxyribonucleotides (ODNs)</i>	166
3.8.5	<i>Synthesis of triazole-ODNs via CuAAC ligations</i>	168
4	CHAPTER 4	173
4.1	BENEFITS OF FLOW CHEMISTRY	174
4.1.1	<i>Benefits of Flow Chemistry - Faster Reactions</i>	175
4.1.2	<i>Benefits of Flow Chemistry - Safer Reactions</i>	176
4.1.3	<i>Benefits of Flow Chemistry - Integrated Synthesis, Work-up and Analysis</i>	178
4.1.4	<i>Benefits of Flow Chemistry – High Throughput</i>	181
4.2	COPPER-CATALYSED REACTIONS IN CONTINUOUS FLOW PROCESSES.....	182
4.2.1	<i>C–C Bond Formation Using Cu-Catalysed Continuous Flow Processes</i>	182
4.2.2	<i>C–N Bond Formation Using Cu-Catalysed Continuous Flow Processes</i>	185
4.3	HYPOTHESIS TO BE TESTED.....	190
4.4	AIMS OF THIS CHAPTER	191
4.5	RESULTS AND DISCUSSION.....	192
4.5.1	<i>Cu-Loading for CuAAC Reactions with Aromatic Ynamines</i>	192
4.5.2	<i>Developing a Flow Platform for Mild CuAAC Ligation of Small Molecules</i>	193
4.5.3	<i>Developing a Flow Platform for Mild, Efficient Synthesis of Biomedical Imaging Markers</i> 202	
4.5.4	<i>Developing a Flow Platform for Mild, Efficient, Degradation-Free Bioconjugation of Peptides and Oligodeoxyribonucleotides</i>	204
4.6	SUMMARY	211
4.7	EXPERIMENTAL	211
4.7.1	<i>Reagents and Solvents</i>	211
4.7.2	<i>Analysis of Products</i>	211
4.7.3	<i>General Procedures</i>	214
4.7.4	<i>Synthetic procedures</i>	217
4.7.5	<i>Characterisation of ODNs</i>	241
4.7.6	<i>Characterisation of Peptides</i>	242
4.7.7	<i>Peptide-PMO Conjugate Synthesis and Characterisation Data</i>	244

5	CHAPTER 5	245
	REFERENCES	249
	APPENDIX	273
5.1	RP-HPLC AND LC-MS METHOD PARAMETERS.....	274
5.1.1	RP-HPLC.....	274
5.1.2	LC-MS.....	276
5.2	RP-HPLC TRACES	276
5.2.1	RP-HPLC Traces from Scheme 3.18	276
5.2.2	HPLC Chromatograms from Figure 3.14	279
5.2.3	RP-HPLC Chromatograms from Scheme 3.19.....	280
5.2.4	RP-HPLC Chromatograms from Figure 3.15.....	286
5.2.5	RP-HPLC Chromatograms from Figure 3.16.....	286
5.2.6	RP-HPLC Chromatograms from Scheme 3.20.....	287
5.3	NMR AND MS SPECTRUMS	288
5.4	MALDI SPECTRA	302

Publications List

- [4] **Hatit, M. Z. C.**, Reichenbach, L. F., Tobin, J. M., Vilela, F., Burley, G. B., Watson, A. J. B. “A flow platform for degradation-free CuAAC bioconjugation” *Nat. Comm.* **2018**, *9*, 4021–4028.
- [3] Buchanan, H. S., Pauff, S. M., Kosmidis, T. D., Taladriz-Sender, A., Rutherford, O. I., **Hatit, M. Z. C.**, Fenner, S., Watson, A. J. B., Burley, G. B. “Modular, step-efficient palladium-catalyzed cross-coupling strategy to access C6-heteroaryl-2-aminopurine ribonucleosides” *Org. Lett.* **2017**, *19*, 3759–3762.
- [2] **Hatit, M. Z. C.**, Seath, C. P., Watson, A. J. B., Burley, G. A. “A strategy for conditional orthogonal CuAAC reactions using protected aromatic ynamines” *J. Org. Chem.* **2017**, *82*, 5461–5468.
- [1] **Hatit, M. Z. C.**, Sadler, J. C., McLean, L. A., Whitehurst, B. C., Seath, C. P., Humphreys, L. D., Young, R. J., Watson, A. J. B., Burley, G. A. “Chemoselective sequential click ligations directed by enhanced reactivity of an aromatic ynamine” *Org. Lett.* **2016**, *18*, 1694–1697.

Acknowledgements

First, I would like to thank Prof Glenn Burley, Dr Allan Watson and the University of Strathclyde for giving me the opportunity to work on this project. I have learned so much and I am really grateful for it!

I would also like to thank all the people who have contributed to this project: Liam McLean, Dr Ciaran Seath, Dr Linus Reichenbach, Dr Joanna Sadler and Dr Benjamin Withehurst. Your help has been invaluable.

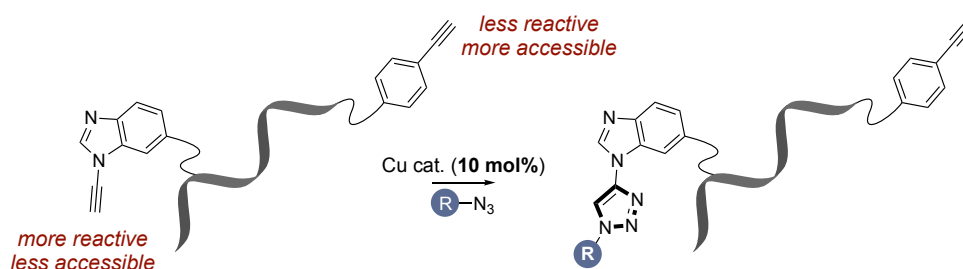
I would like to thank Dr Filipe Vilela and Dr John Tobin for introducing me to flow chemistry and for all the very interesting discussions about chemistry.

I would also like to acknowledge present and past members of the Burley and Watson groups. I extend a massive thanks to Dr Steven Pauff for his friendship, help and support, particularly during this difficult last year. Thank you for the constant reminder of who I am! And since I have to, I would also like to thank you for your beautiful hair, we will never stop being jealous of it! I offer a big thanks to Dr Olivia Rutherford, Helena Buchanan, Dr Kirsty Wilson and Dr Jamie Withers for your support, your friendship and all the good laughs. My PhD would not have been as great without you five! I would also like to thank Dr Steven Pauff, Dr Jamie Withers, Dr Andrea Taladriz-Sender and Dr Amanda Hughes for your advices and proof-reading this document.

On a personal note, I would like to thank my friends and my parents, particularly my mom Joelle Ducos, for her unconditional love and support! Finally, I would also like to thank all the wonderful people that I have met in Glasgow, in particular Kevin Hart for all of his love, his support and all the amazing moments we shared together.

Abstract

The Cu-catalysed alkyne-azide cycloaddition (CuAAC) or “click” reaction is a powerful and robust bio-orthogonal reaction that exclusively produces 1,4-substituted triazoles. Despite its extensive utility in chemical biology, the ability to differentiate alkyne subtypes has received little attention as a tool for the construction of discrete bioconjugates. This work highlights the utility of aromatic ynamines as a new click reagent for sequential bioconjugation. Aromatic ynamines are superior click reagents with enhanced chemical reactivity relative to conventional alkynes. This unique and orthogonal reactivity profile circumvents the need for conventional protecting group strategies. This project will also highlight the biocompatibility of these reagents as a new tool for protecting-group free sequential CuAAC bioconjugation of oligonucleotides in the presence of more accessible competing alkyne substrate (Scheme 1). This strategy allows the formation of a new platform for specific labelling using fluorescent and PET probes as much as specific targeting and drug delivery. Importantly, higher reactivity of aromatic ynamines allows lower copper loading, thereby decreases toxicity and side reactions on biomolecules.



enhanced reactivity of ynamine allows chemoselective CuAAC ligations of oligonucleotides at low copper loading (10 mol%)

Scheme 1. Chemoslective, sequential CuAAC bioconjugation using enhanced reactivity of aromatic ynamines.

Abbreviations

Ad	Adamantane
AMTC	1-(<i>Trans</i> -2-hydroxycyclohexyl)-4-(<i>N,N</i> -dimethylaminomethyl)-1,2,3-triazole)
ApoE	Apolipoprotein E
BTAA	2-(4-((Bis((1-(<i>tert</i> -butyl)-1 <i>H</i> -1,2,3-triazol-4-yl)methyl)amino)methyl)-1 <i>H</i> -1,2,3-triazol-1-yl)acetic acid
BTES	2-(4-((Bis((1-(<i>tert</i> -butyl)-1 <i>H</i> -1,2,3-triazol-4-yl)methyl)amino)methyl)-1 <i>H</i> -1,2,3-triazol-1-yl)ethylhydrogensulfate
BTTP	3-(4-((Bis((1-(<i>tert</i> -butyl)-1 <i>H</i> -1,2,3-triazol-4-yl)methyl)amino)methyl)-1 <i>H</i> -1,2,3-triazol-1-yl)propan-1-ol
CuAAC	Cu-Catalysed Azide-Alkyne Cycloaddition
Cu(OAc) ₂	Copper(II) acetate
DCC	<i>N,N'</i> -dicyclohexylcarbodiimide
DCM	Dichloromethane
DFT	Density functional theory
DIPEA	Diisopropylethylamine
DMF	Dimethylformamide
DMSO	Dimethyl sulfoxide
DNA	Deoxyribonucleic acid
EDTA	Ethylenediaminetetraacetic acid
equiv.	Equivalent
Et ₂ O	Diethylether
EtOAc	Ethyl acetate
EtOH	Ethanol
Fc	Ferrocene
HATU	<i>N</i> -[(dimethylamino)-1 <i>H</i> -1,2,3-triazolo-[4,5- <i>b</i>]pyridin-1-ylmethylene]- <i>N</i> -methylmethanaminiumhexafluorophosphate <i>N</i> -oxide
Hex	Hexane
HPA	3-Hydroxypicolinic acid

HRMS	High-resolution mass spectra
ICP-MS	Inductively coupled plasma mass spectrometry
<i>i</i> PrOH	<i>Iso</i> -propanol
LC-MS	Liquid chromatography-mass spectrometry
MALDI-TOF	Matrix-assisted laser desorption/ionisation-time of flight spectrometer
MeCN	Acetonitrile
MeOH	Methanol
NaAsc	Sodium ascorbate
NMR	Nuclear magnetic resonance spectroscopy
Oct	Octane
ODN	Oligodeoxyribonucleotide
PE	Petroleum ether
PEG-400	Polyethylene glycol 400
PFA	Perfluoroalkoxy alkane
RP-HPLC	Reverse phase - High performance liquid chromatography
rt	Room temperature
R _T	Retention time
SM	Starting material
SPAAC	Strain-promoted azide-alkyne cycloaddition
TBAF	Tetrabutylammonium fluoride
TBTA	Tris((1-benzyl-1 <i>H</i> -1,2,3-triazol-4-yl)methyl)amine
<i>t</i> BuOH	<i>Tert</i> -butanol
TEAA	Triethylammonium acetate
THF	Tetrahydrofuran
THPTA	Tris((1-hydroxypropyl-1 <i>H</i> -1,2,3-triazole-4-yl)methyl)amine
TIPS	Triisopropylsilane
TLC	Thin layer chromatography
TMS	Trimethylsilyl
t _R	Residence time
Ts	Tosyl

Chapter 1

Bioconjugation: A Powerful Tool For Studying Living Systems

1.1 Introduction to Bioconjugation

Understanding the roles of biomolecules in their native environments is challenging due to the complexity of living systems. The discovery of whole genome sequencing in 1995 has provided us with the opportunity to view the “blueprints” of living organisms.¹ Advancements in crystallography and spectroscopy methods have provided detailed snapshots of biomolecular structure and dynamics.² Unfortunately, complex biological function cannot truly be understood through genetics and structural studies. These functions are an interconnected highway, dependent on interactions with countless other molecules, all occurring within the compact environment of the cell. The discovery and development of the green fluorescent protein (GFP) revolutionised our understanding of certain protein functions by allowing, for the first time, their imaging and tracking in living cells.³ Nonetheless, its use is limited to the study of proteins and cannot be expanded to other biomolecules. Furthermore, owing to the large size of the fluorescent protein domain, GFP-tagging could perturb the target protein’s structure and function. To overcome these limitations, scientists have focused on developing new methods for the selective, covalent modification of biological entities within living systems, termed bioconjugation.

Antibody-drug conjugates (ADCs) illustrate perfectly the power of bioconjugation. Indeed, the ability to conjugate an antibody to cytotoxics has provided an effective technique for potent and selective chemotherapy. As compared to traditional chemotherapeutics, ADCs display superior specificity, longer half-lives and increased stability in blood circulation.⁴ ADCs are rapidly becoming lead therapeutic agents, with two ADC drugs currently approved by the FDA and another 50 at different stages of clinical development.⁴

Over the last decade, a variety of chemical strategies have been described for the ligation of biomolecules to numerous molecules including antibodies,⁵ peptides,⁶ lipids,⁷ drugs⁸ and fluorophores.⁹ Along with providing researchers with invaluable biological discoveries, this work detailed the requirements for effective bioconjugation. Optimal bioconjugation reactions should be rapid, selective towards the desired functional groups and generate only the desired, stable, non-toxic product. The ligation reaction kinetics are particularly important as bioconjugation reactions generally follow second-order kinetics, where reaction rates are dependent on the concentrations of both reagents, necessitating a large excess of one reagent (micromolar to millimolar) when performing the ligation *in vivo*. In turn, the excessive concentration of reagents required leads to reduced solubility and increased toxicity.¹⁰ Researchers have therefore been investigating the use of non-natural, highly reactive chemical

functional groups to increase the efficiency of bioconjugation. Despite the current focus on non-natural functional groups, ligation *via* native functional groups remains widely employed and understanding the benefits and limitations of these techniques provides the foundation for advances in chemical biology.

1.2 Site-Specific Bioconjugation Based on Native Functionalities

1.2.1 Peptides and Proteins

Proteins are responsible for many functions in living systems from catalysing metabolic reactions¹¹ to transporting molecules through membranes.¹² Recently, a variety of synthetic approaches have been developed to selectively modify proteins, providing the opportunity to understand the structure/function relationships of these essential biomolecules.¹³ Modification strategies must be site-selective, proceed under mild conditions and must not alter overall protein structure. For *in vivo* applications, the position of the modification in the primary sequence highly influences both the pharmacokinetics and biodistribution.^{14,15}

The strategy for chemoselective ligation to any of the 20 naturally-occurring amino acids (AAs) is dependent on its reactivity (Figure 1.1). The polyamide backbone of proteins and peptides is unreactive toward bioconjugation strategies, with the exception of the *N*-terminal amine and the *C*-terminal carboxylic acid. Consequently, ligation methodologies predominantly focus on targeting the AA side chains.¹³ The carboxylic acid side chains of aspartate (Asp) and glutamate (Glu) can function, upon activation, as electrophiles in reactions with amines. The thiol and thioether groups of cysteine (Cys) and methionine (Met), the amine groups of arginine (Arg), histidine (His), lysine (Lys) and tryptophan (Trp), and the hydroxyl and phenol groups of serine (Ser), threonine (Thr) and tyrosine (Tyr) have the potential to function as nucleophiles for bioconjugation. However, the ability to perform efficient conjugation with these AAs will highly depend on reaction conditions, including the pH of the reaction and the reactivity of the corresponding electrophile (Figure 1.1). Moreover, their reactivity varies significantly with their location within the protein and their interactions with neighbouring amino acid residues.¹⁶ The remaining AAs are generally unreactive toward traditional bioconjugate chemistries (Figure 1.1). The following sections will describe the most commonly used of the extensive list of available strategies for the selective ligation of amino acids.

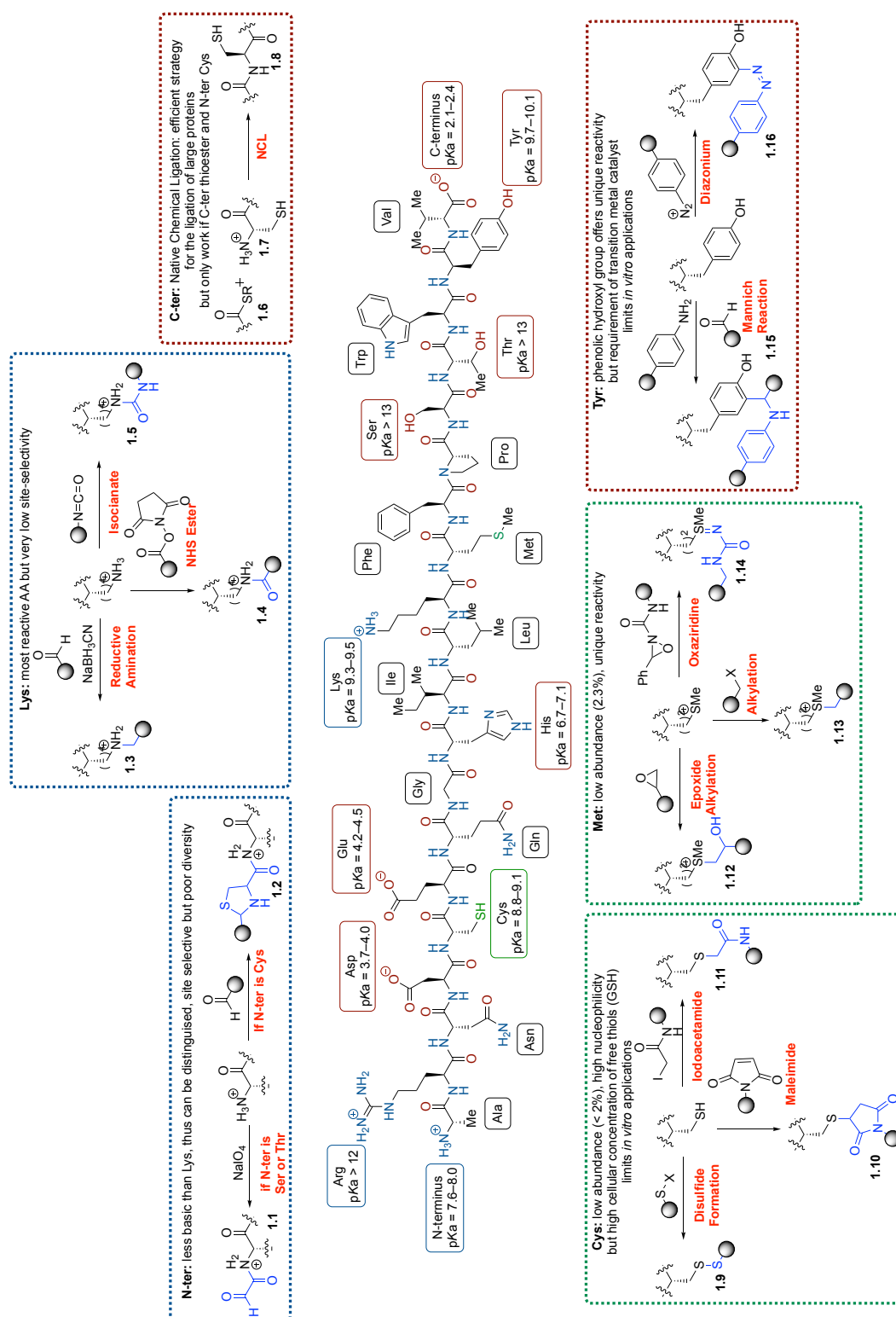


Figure 1.1. Structures of the 20 naturally occurring amino acids (AA), their pKa values in aqueous media at pH = 7 and the most commonly used strategies for their bioconjugation.¹⁷

1.2.1.1 Commonly Used Strategies for Lysine Bioconjugation

Lysine residues are a common choice for bioconjugation due to the numerous chemical reactions available for modifying nucleophilic primary amines (Figure 1.1).¹³ Most of these reactions use slightly alkaline pH, in which lysine can react with activated esters, anhydrides, carbonates, isocyanates, and a range of other acylating and alkylating agents (Figure 1.1).¹⁸ However, their high abundance in living systems means that multiple lysines could be targeted in a non-specific manner. Additionally, some of the strategies employed for lysine conjugation can have off-target effects with other nucleophilic side chains. For example, *N*-hydroxysuccinimide (NHS) esters, the most popular group used for lysine conjugation and labelling, can cross-react with the hydroxyl group of tyrosine, histidine, serine and threonine side-chains, forming an ester bond. Moreover, the pH required for lysine conjugation using isothiocyanate (~ 9) would be unsuitable for modifying alkaline-sensitive proteins.

1.2.1.2 Commonly Used Strategies for Cysteine Bioconjugation

The modification of cysteine residues has been highly exploited due to its superior nucleophilic properties as compared to other amino acids.¹³ Cysteine residues' low abundance (< 2%) in the proteome favours site-selective modification.¹⁹ However, they are rarely found on solvent-accessible surfaces of a protein.²⁰ Therefore, most conjugation methods require pre-treatment with a reducing agent, such as dithiothreitol (DTT), to cleave accessible disulfides. Under basic conditions, cysteine residues will be deprotonated to give a thiolate nucleophile which can then react with soft electrophiles, such as maleimide or iodoacetamide (Figure 1.1). Unfortunately, the high concentration of free thiols present in cells, *e.g.* glutathione, limits these approaches to *in vitro* applications. Moreover, Kiick *et al.* have reported that the thiol-maleimide conjugate can be labile under physiologically relevant conditions.²¹

1.2.1.3 Commonly Used Strategies for Methionine Bioconjugation

The low abundance (2.3%)²² and unique reactivity of methionine make this residue more attractive than cysteine for chemoselective, site-specific protein bioconjugation. Deming *et al.* reported the chemoselective alkylation of methionine residues, affording relatively stable sulfonium derivatives, such as compound **1.13** (Figure 1.1).²³ No undesired side-products were obtained, even in the presence of lysine residues. Using epoxides as alkylating agents, the same group was able to achieve the chemoselective introduction of a variety of functionalisations into proteins.²⁴ The advantage of the epoxide strategy, as compared to the

previously reported alkylation method, is that the reaction can be conducted in physiological conditions and the sulfonium derivatives, such as **1.12** (Figure 1.1), display increased stability. More recently, the Chang group developed a new platform for chemoselective methionine bioconjugation using oxaziridine-based reagents (ReACT, Figure 1.1).²⁵ Taking advantage of the redox potential of methionine, they were able to achieve rapid (≤ 10 min) and selective ligations in the context of various substrates.

1.2.1.4 Commonly Used Strategies for Tyrosine Bioconjugation

Another amino acid often pursued for chemical ligation is tyrosine due to the reactivity of its phenolic hydroxyl group.²⁶ Tyrosine conjugation with a diazonium has been of special interest ever since its discovery in 1959 (Figure 1.1).²⁷ However, the poor selectivity of the ligation, the relative instability of the diazonium salts and the strongly acidic conditions required for their *in-situ* preparation, which are incompatible with pH-sensitive proteins, prevented the widespread application of this methodology. An alternative approach was reported by Francis *et al.* using a three-component Mannich-type strategy involving the *in-situ* reaction of a Tyr residue, an amine and formaldehyde (Figure 1.1).²⁸ Using α -chymotrypsinogen A protein as a model, they demonstrated selective modification of tyrosine residues. This procedure allowed the use of mild conditions (pH = 6.5, 25–37 °C) and low protein concentrations (20–200 μ M), which are conducive to *in vivo* applications; however, the long reaction times (18 h) required to reach a reasonable level of tagging diminished the efficacy of this approach.

1.2.1.5 Commonly Used Strategies for N-terminal Bioconjugation

While the primary amine of lysine's side chain represents the most nucleophilic group available in the majority of proteins, they are protonated at physiological pH, resulting in a dramatic decrease in reactivity.¹⁸ The difference between the pKa of the α -amine of an N-terminal AA and the ϵ -amine of Lys (8 and 10, respectively; Figure 1.1) results in an increased selectivity for bioconjugation at the N-terminus at physiological pH. Additionally, the type of reaction that can be performed is influenced by the identity of the N-terminal AA.¹⁸ For example, an N-terminal cysteine can react with an aldehyde in a condensation reaction to form the thiazolidine product **1.2** (Figure 1.1).

1.2.1.6 Commonly Used Strategies for C-Terminus Bioconjugation

The most commonly used strategy for protein ligation at the C-terminus is the Native Chemical Ligation (NCL) of a C-terminal thioether and a N-terminal cysteine (Figure 1.1).²⁹ Relying on the ability of thioesters to undergo S-N acyl rearrangement, this strategy allows the chemoselective formation of an amide bond in the presence of unprotected nucleophilic AAs. Furthermore, this methodology can be performed in physiological buffer, typically PBS (pH 7.0–8.5), at 37 °C and affords high yields in short reaction times (~ 1 h), increasing its utility in bioconjugation. However, it is important to prevent the oxidation of the N-terminal cysteine's thiolate to a disulfide-linked dimer which is unreactive in the ligation.

1.2.2 Carbohydrates

Carbohydrates are a class of molecules including monosaccharides, such as glucose, mannose and galactose (Figure 1.2), polysaccharides and oligosaccharides. Similar to proteins, carbohydrates play important roles in living systems where they are involved in energy production, cell wall construction and protein recognition, to cite a few.³⁰

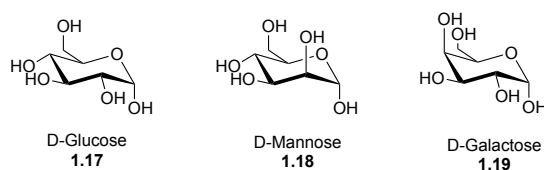
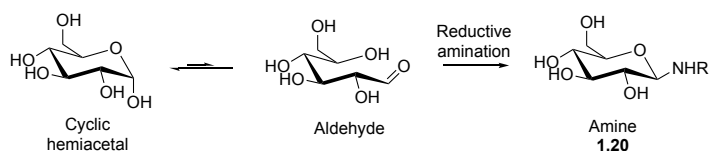


Figure 1.2. Structures of naturally-occurring carbohydrates.

The most abundant functional groups in carbohydrates are the hydroxyl groups, which are poor nucleophiles in aqueous media. Consequently, very few strategies have been developed for bioconjugation using native functionalities of carbohydrates. The most commonly used approaches take advantage of carbohydrates' propensity to isomerise between their cyclic hemiacetal form and open aldehyde/keto form (Scheme 1.1). In the latter structure, the carbonyl group can undergo reductive amination or react with phenyl hydrazide (Scheme 1.1), introducing functionalities which can then be used for bioconjugation.³¹



Scheme 1.1. Functionalising carbohydrates for bioconjugation.³¹

1.2.3 Nucleic Acids

Nucleic acids, DNA (deoxyribonucleic acid) and RNA (ribonucleic acid), are the biopolymers responsible for carrying genetic information. Information encoded by DNA is converted into RNA, and research has found that gene expression is affected by the structural organisation of DNA.³² RNA plays a variety of roles within the cell including co- and post-transcriptional regulation³³ as well as in protein translation. Therefore, the ability to monitor the structural organisation, localisation and abundance of nucleic acids within cells provides essential insights into cellular processes.

DNA and RNA are composed of nucleotides which consist of a purine or pyrimidine base attached to a deoxyribose (DNA) or ribose (RNA) sugar, linked by phosphate groups (Figure 1.3). The purine bases, adenine (A) and guanine (G), form Watson–Crick base pairs with their respective pyrimidine bases, cytosine (C) and thymine (T), in the DNA double helix. In RNA, thymine is replaced by uracil (U). The sugar-phosphate backbone of DNA is formed such that a phosphate group marks the 5' end and the 3' end terminates with a hydroxyl group. In RNA, the ribose sugar has a 2' hydroxyl group, making it more susceptible towards hydrolysis and enzymatic degradation than DNA.³⁰

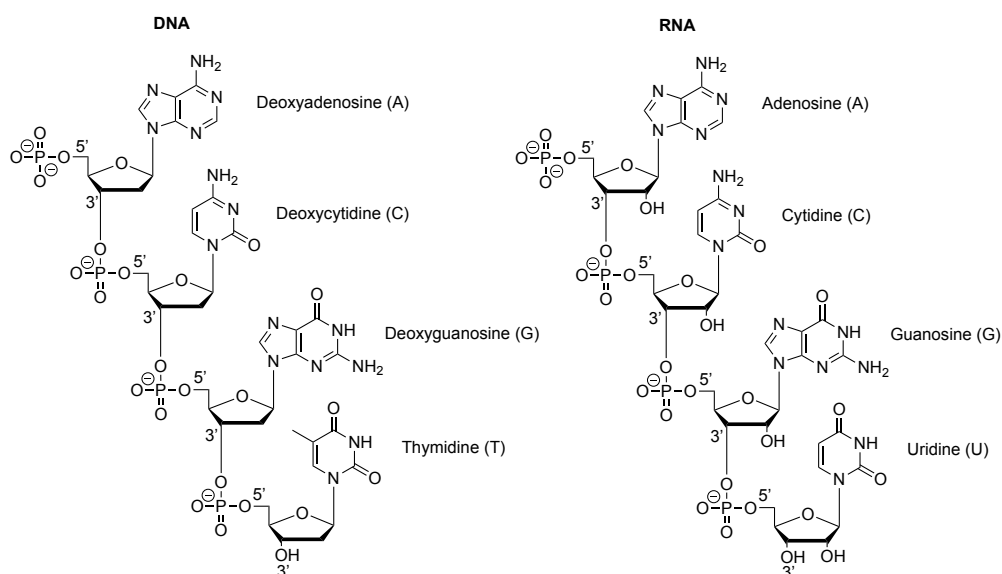
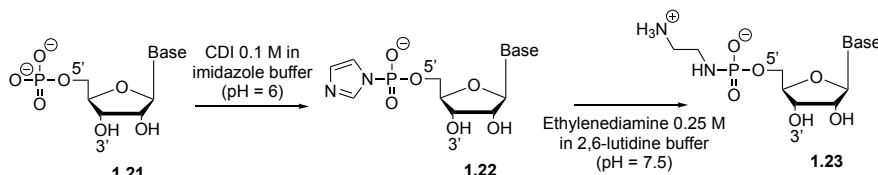


Figure 1.3. Chemical structures of nucleic acids.

There are fewer functional groups available for modifying native nucleic acids than found in proteins. Modifications at the terminal positions are possible *via* activation of the 5'-phosphate group with carbodiimides, followed by reaction with an amine (Scheme 1.2),³⁴ or the oxidation

of the RNA vicinal diol with sodium periodate.³⁵ Nucleobase modifications would be possible, but are often restricted by base pairing interactions.³⁰ In addition, site-specific modifications of native DNA or RNA nucleobases are generally not possible due to their repetitive characteristics. Since synthetic oligonucleotides are prepared *via* solid-phase synthesis,³⁶ modifications of the nucleobases, phosphates or the 3'- and 5'-terminus using phosphoramidite chemistry are more easily achieved than for naturally-occurring nucleic acids.³⁷



Scheme 1.2. Functionalising nucleic acids for bioconjugation.³⁴

1.2.4 The Need for the Development of New Bio-orthogonal Reactions

While bioconjugation using native functionalities has been employed for a variety of biological applications, all suffer from inherent limitations. As many of these reactions are sensitive towards hydrolysis, high reagent concentrations are required to obtain the desired product at any reasonable yield. The reagents employed for functionalisation are often poorly soluble in water and require the addition of toxic co-solvents (*e.g.* DMF, DMSO, MeCN). These features prevent the application of these techniques within living systems. Complicating the issue further is the inability to accurately and consistently target a precise site or a particular molecule, as most biomolecules are polymers consisting of repeated sequences of a limited number of monomers (*e.g.* amino acids in proteins, saccharides in carbohydrates and nucleotides in nucleic acids). To overcome these limitations and expand bioconjugate chemistry into the realm of complex living organisms, research has focused on the development of bio-orthogonal strategies for bioconjugation.

1.3 Bio-orthogonal Reactions Based on Extrinsic Functionalities

A primary goal of bioconjugation research over the past 15 years has been to increase its efficiency by employing highly reactive, non-natural functional groups rather than the native functionalities present within cells (Figure 1.4).^{10,20,38,39} Research has focused on developing strategies using chemical functionalities which are unable to react with biological moieties and react specifically with one another under physiological conditions (ambient temperature and pressure, aqueous media, neutral pH). Moreover, as the target of bioconjugation is application

within living systems, these bio-orthogonal reagents should be non-toxic and metabolically stable.

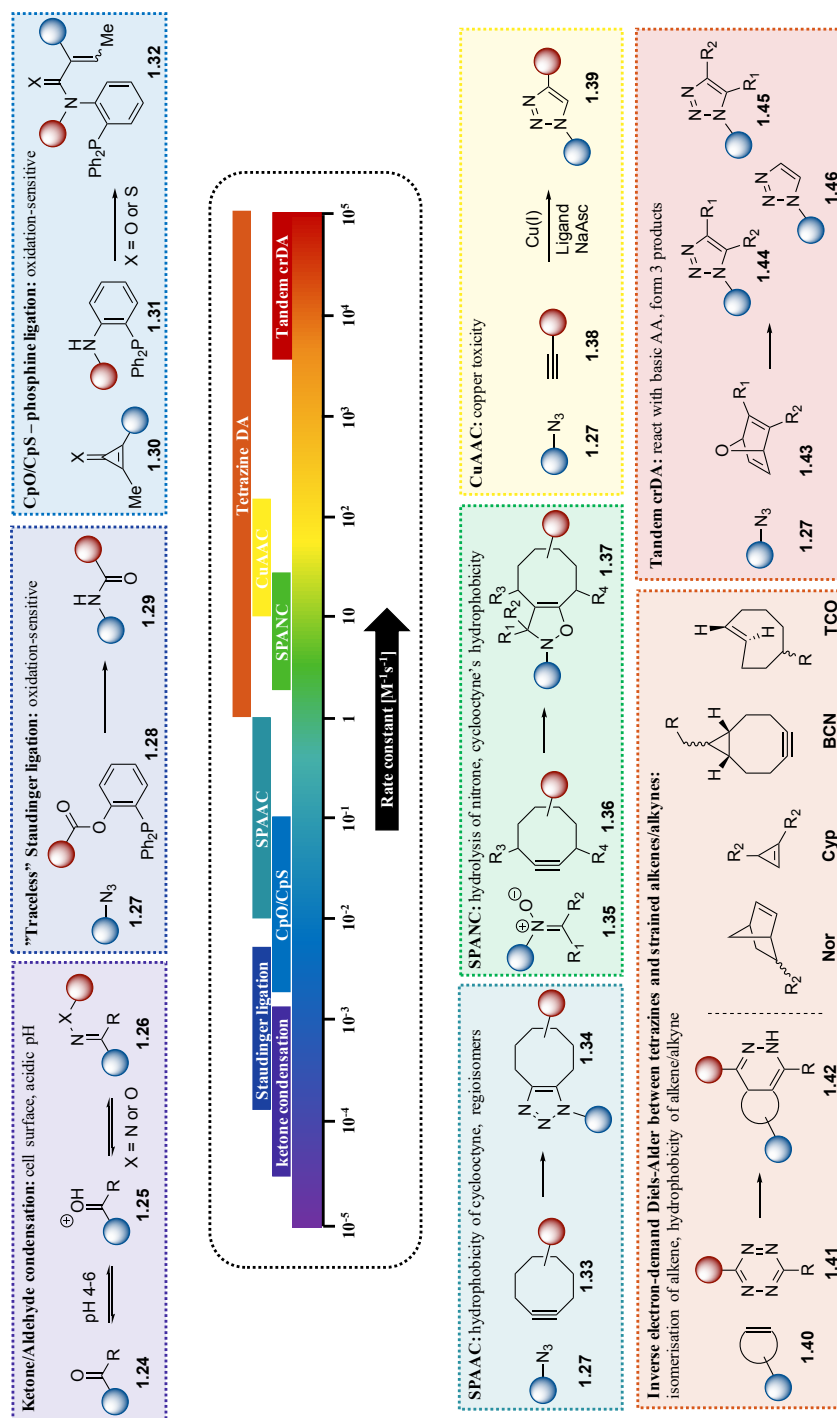
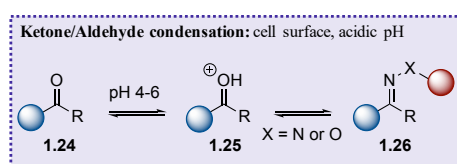


Figure 1.4. Bio-orthogonal reactions based on extrinsic functionalities.³⁹

As with the strategies described for ligations using native functionalities, the concentration of reagents needed to successfully perform the bio-orthogonal ligation is directly correlated with its kinetics. Consequently, rapid ligation kinetics will minimise reagent concentrations, further limiting the potential for toxic side-effects. While the development of these novel methodologies has met with many challenges, remarkable progress has been reported for bio-orthogonal ligations of biomolecules. This section will outline the most commonly used strategies for bioconjugation, detailing both their mode of action and limitations.

1.3.1 Condensation of Ketones and Aldehydes



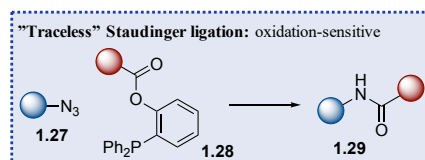
One of the first strategies reported for the bio-orthogonal ligation of biomolecules was the acidic (pH = 4 – 6) condensation of ketones and aldehydes with an amine to afford Schiff base intermediates (Figure 1.4).⁴⁰ While these functionalities are not completely absent from biomolecules, their small size and synthetic accessibility rendered them attractive for the development of bioconjugation methodologies. Additionally, they are easily integrated into living systems, further increasing their applicability.

Displaying the utility of this methodology, Bertozzi *et al.* reported the integration of a ketone as a chemical handle for the modification of cell surface glycoproteins known to be overexpressed in a variety of cancers.⁴¹ Using a non-natural sialic acid, they were able to introduce a reactive ketone functionality onto cell surface sialic acid residues. These modified surface markers were then reacted with an aminoxy-derivatised probe containing an MRI enhancer (lanthanide ion chelate), providing a novel and general platform for cancer diagnostics. Tirrell *et al.* used a ketone-modified phenylalanine to site-specifically incorporate reactive aryl ketones into recombinant proteins, further demonstrating the application of this strategy.⁴²

While useful, the slow kinetics of ketone/aldehyde condensations ($k \sim 10^{-4}$ to $10^{-3} \text{ M}^{-1}\text{s}^{-1}$) necessitates high concentrations of the reagents to ensure efficient labelling, resulting in increased toxicity of this strategy.⁴³ Moreover, the requirement of acidic pH for successfully

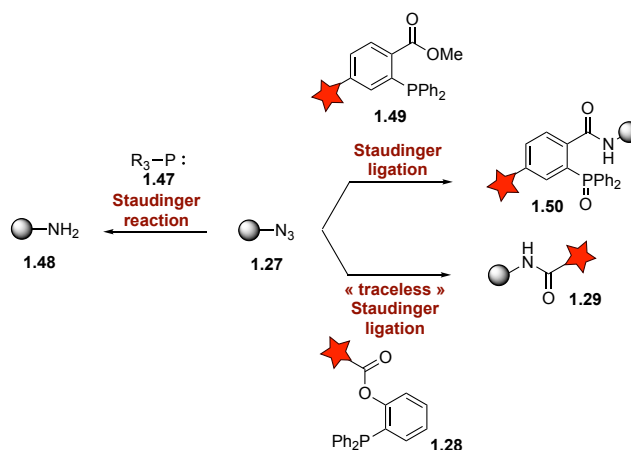
performing the reaction limits this strategy to *in vitro* and cell-surface labelling, as optimal conditions are difficult to obtain intracellularly.³⁹ Finally, intracellular applications of this methodology are limited due to off-target effects with carbonyl-bearing metabolites.

1.3.2 Staudinger Ligation



While the reaction between a phosphine and an azide was initially described in 1919 by Staudinger *et al.*,⁴⁴ the rediscovery of this strategy by Bertozzi *et al.* in 2000 paved the way for numerous applications in chemical biology (Figure 1.4).⁴⁵⁻⁴⁷

Although the original methodology afforded the formation of a primary amine, such as **1.48** (Scheme 1.3),⁴⁴ the revisited Staudinger ligation enables the formation of an amide bond (**1.50**), eliminating production of the hydrolysis-sensitive aza-ylide intermediate.⁴⁵



Scheme 1.3. The different variations of Staudinger reactions.⁴⁴⁻⁴⁶

In this context, the Staudinger ligation employs a phosphine that also functions as an acyl donor. The phosphorus first attacks the azide to form an iminophosphorane, which is then acylated to release nitrogen gas. This results in the formation of an amidophosphonium salt which, upon hydrolysis, yields the desired amide **1.50**.⁴⁵ Another version of this reaction, the

“traceless” Staudinger ligation, employs a cleavable linker (typically an ester or a thioester) that yields an acyclic amidophosphonium salt, resulting in the amide product **1.29** lacking the phosphine oxide moiety.⁴⁶

One of the many benefits of the Staudinger ligation is its use of an azide. Azides are essentially absent from living systems and is wholly inert towards biological functionalities. Their small size, intermediate polarity and inability to participate in any significant hydrogen bonding make them unlikely to perturb biomolecular structure or function. Furthermore, the reaction between an azide and a phosphine is highly selective and proceeds efficiently under mild and physiological conditions, fulfilling most of the criteria necessary for selective bio-orthogonal ligation.

While both azide and phosphine moieties are easily incorporated into biomolecules, azides are usually preferred due to their small size and higher stability under physiological conditions. The incorporation of an azide into proteins, glycans or oligonucleotides can be achieved *via* chemical modifications or biosynthetic pathways (Figure 1.5).^{47–52} To date, numerous azide-modified biomolecules are available (Figure 1.5) and the choice of a specific one will depend on the target to be investigated.

Bertozi *et al.* successfully reported the use of an azide as a bio-orthogonal reporter for glycan imaging *via* incorporation of *N*-azidoacetylmannosamine **1.53** (Ac₄ManNAz).⁴⁵ Incubation of Jurkat cells with saccharide **1.53** resulted in its incorporation into glycans through the sialic acid biosynthetic pathway. ManNAz units were subsequently visualised by performing a Staudinger ligation with a phosphine–modified biotin probe which, upon treatment with fluorescein-labelled avidin, afforded an increase in the fluorescence of the biotin–avidin complex.

The development of azide-containing thymidine analogues, such as **1.54** and **1.55**, has also permitted the successful functionalisation of DNA. For example, Marx *et al.* reported the incorporation of azide-modified nucleoside triphosphate building blocks into a growing DNA strand *via* DNA polymerase.⁵³ Functionalisation of the DNA was then successfully achieved *via* Staudinger ligations with phosphines bearing several functional groups, such as biotin.

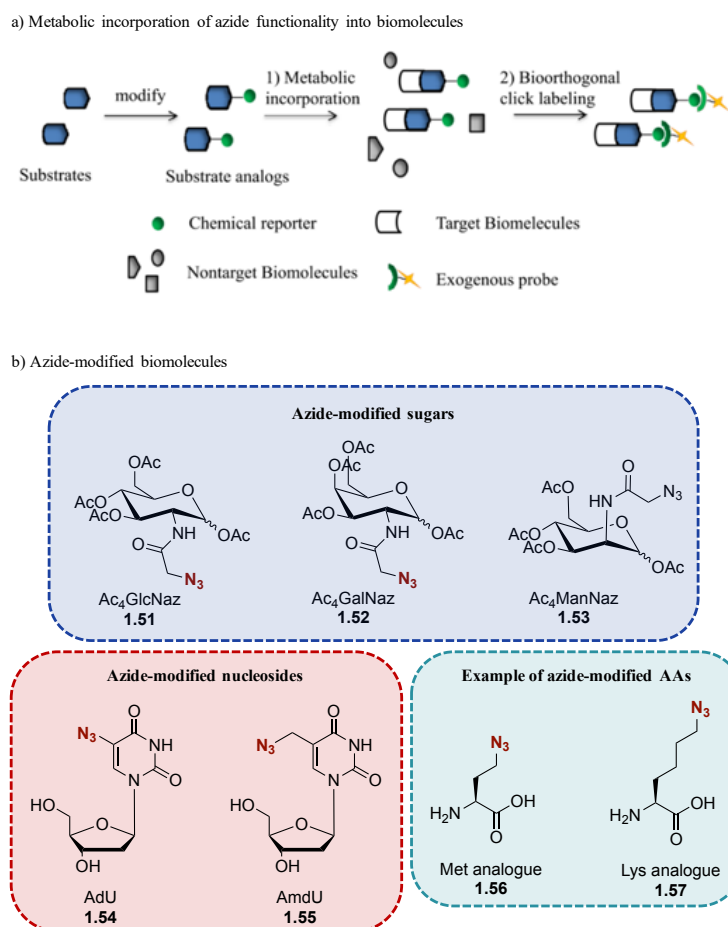
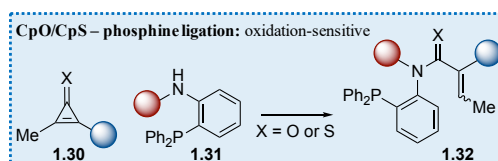


Figure 1.5. Incorporation of azide functionality into biomolecules. *a*) Metabolic incorporation of azide functionality into biomolecules. *b*) Examples of azide-modified biomolecules.⁵²

Site-specific incorporation of modified-AAAs has been reported by Schultz *et al.* using a unique codon–tRNA pair with a corresponding aminoacyl-tRNA synthetase.⁵⁴ This strategy relies on the generation of an orthogonal tRNA that is not recognised by any natural aminoacyl synthetases. As a result, only its azide-modified AA is inserted in response to the amber stop codon. Next, a synthetase is fashioned to specifically recognise this unique tRNA. Therefore, its substrate specificity is evolved to recognise only the desired non-natural AA, and no endogenous AA. This strategy can be used to efficiently incorporate a large variety of non-natural AA into proteins in *Escherichia coli*, yeast, and mammalian cells.⁵⁴ By applying this strategy, Yokoyama *et al.* successfully introduced azido-modified phenylalanine into *E. coli* transcripts which, following Staudinger ligations, resulted in site-specific protein modifications.⁵⁵

Although numerous examples of bioconjugation *via* the Staudinger ligation have been described,⁴⁷ the oxidation-sensitive properties of phosphine towards air or metabolic enzymes dramatically decreases the applicability of the reaction *in vivo*. Moreover, kinetic studies have shown that the use of stabilised phosphines, such as **1.28** and **1.49** (Scheme 1.3), decreases the rate of reaction up to ten-fold, thus imposing the use of high concentrations of reagents.⁵⁶

1.3.3 CpO/CpS Phosphine Ligation



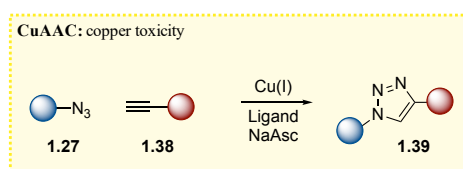
An alternative to the Staudinger ligation is the cyclopropenone (CpO)/phosphine ligation, where a CpO is reacted with a soft nucleophile, such as triarylphosphine (Figure 1.4).⁵⁷ The latter initiates a Michael-type addition to CpO **1.30** which, upon ring opening, forms a ketene ylide intermediate. While sensitive to nucleophilic attack, these ketene ylides have shown enough stability to be isolated under ambient, moisture-free conditions. However, these moieties are susceptible to rapid reaction with strong nucleophiles (*e.g.*, amines). Therefore, the amine-containing phosphine **1.31** has been designed to increase the selectivity of this ligation. This hemiaminal can then undergo elimination/proton transfer to provide the final ligated product **1.32** and the regenerated phosphine.

Similar to azides, CpOs are small and, depending on their substitutions, inert towards other biological functions.⁵⁸ Furthermore, CpOs are found in natural products and synthetic drugs, suggesting that they are metabolically stable. Preschner *et al.* have shown that these functionalities could readily be incorporated into proteins *via* NHS ester chemistry.⁵⁷ They prepared a non-canonical AA containing a CpO and incorporated it into GFP *via* amber codon suppression. The main advantage of this approach is that while CpOs are non-reactive toward other bio-orthogonal ligation strategies (*e.g.*, cycloaddition), the ligated product, such as **1.32** (Figure 1.4), has been shown to react with azides, suggesting compatibility with tandem labelling experiments.

Despite the advantages of this methodology, the slow kinetics ($\sim 10^{-2} \text{ M}^{-1}\text{s}^{-1}$) and sensitivity towards oxidation limits application for *in vivo* experiments. Recently, Preschner *et al.* have

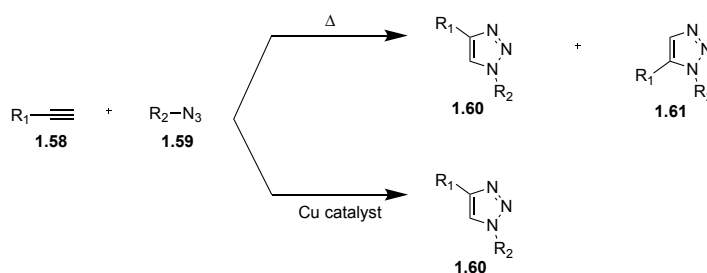
reported up to 300-fold faster ligations when replacing CpOs with cyclopropenethiones (CpS, Figure 1.4).⁵⁹ CpS differs from CpO by only a single atom and therefore maintains minimal perturbation effect on target biomolecules. In addition, the products derived from the ligation of CpS with phosphine, thiocarbonyls, are widely used in fluorescence quenching and other biophysical experiments with proteins, demonstrating their stability and biocompatibility.^{60,61} However, while this strategy has been shown to be efficient for labelling biomolecules *in vitro* and in cell lysate, the oxidation-sensitive property of phosphine still limits its applicability for *in vivo* studies.⁵⁹

1.3.4 Azide/Alkyne Cycloadditions



The exploration of 1,3-dipolar cycloadditions began in the late nineteenth century when Curtius⁶² and, later, Buchner⁶³ reported the first 1,3-dipolar cycloaddition of the diazoacetic ester with α,β -unsaturated esters. In the subsequent years, various 1,3-dipolar cycloadditions have been discovered, including the well-known Diels-Alder reaction.⁶⁴

In 1963, Huisgen reported the thermal cycloaddition between an azide and an alkyne to form both 1,4 and 1,5-substituted triazoles (**1.60** and **1.61**, Scheme 1.4). The formation of the two regioisomers was rationalised by the following phenomena. Firstly, organic azides contain three linear nitrogens and a C-N angle of 114° , which must bend during the activation process to make contact with the π -bond of the alkyne. This results in rotation around the C-N bond axis prior to ring closure.⁶⁵ Secondly, organic azides react with angularly strained triple bonds with enthalpy values between 8 to 15 kcal/mol and entropy values between -30 to -50 cal/deg.⁶⁶ The moderate enthalpy lends credence to a concerted process while the high, negative entropy suggests that effective collisions with the correct orientation (*cis*) occur rarely, thus resulting in the formation of the two regioisomers. Finally, triazole formation results in the creation of two σ -bonds ensuring a gain of free energy that compensates for the loss of π -bond energy of the reactants.



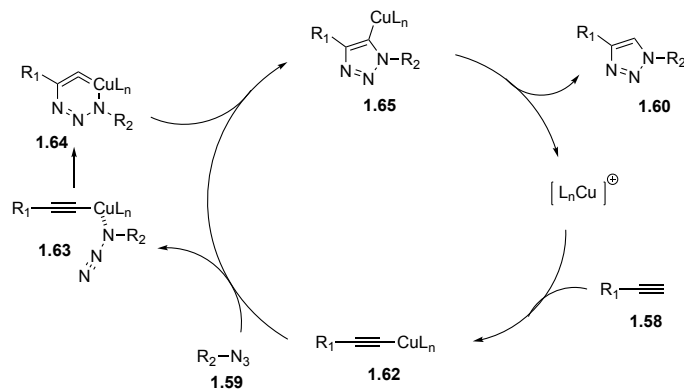
Scheme 1.4. Difference in regioselectivity of 1,3-dipolar cycloadditions under thermal⁶⁶ and catalytic conditions.⁶⁷

In 2002, the groups of Fokin and Sharpless⁶⁷ and Meldal⁶⁸ independently reported that the rate of [3+2] cycloaddition of a terminal alkyne and an azide was enhanced 10⁷-fold using copper(I) catalysis.⁶⁹ This method also resulted in the exclusive formation of 1,4-substituted triazoles (Scheme 1.4). CuAAC is now the most commonly used 1,3-dipolar cycloaddition in organic chemistry.⁷⁰ This reaction has been investigated extensively, with over 3420 publications reported by SciFinder as of 2018. The advantages of the CuAAC reaction include: (i) short reaction times, (ii) regioselectivity, producing exclusively the 1,4-triazole, (iii) bio-orthogonality, *i.e.*, the reaction is specific for the azide and alkyne functional groups, and (iv) the reaction can be carried out under mild conditions (room temperature in water without the need for inert conditions). As a result of these interesting attributes, CuAAC reactions have been employed in a variety of fields, including polymer and material sciences,^{71,72} drug discovery,⁷³ combinatorial chemistry,⁷⁴ and bioconjugation.^{20,75}

1.3.4.1 Mechanistic Considerations in the Copper-Catalysed Azide/Alkyne Cycloaddition

Copper chemistry is particularly rich because Cu(0), Cu(I), Cu(II) and Cu(III) oxidation states are easily accessible, enabling both one-electron and two-electron processes.⁷⁶ Furthermore, the different oxidation states of copper allow for reactions with a wide range of functional groups *via* Lewis acid interactions or π -coordination. In 2002, Sharpless *et al.* reported that Cu(I) was required for the CuAAC reaction to proceed and proposed a stepwise mechanism for Cu(I) catalysis (Scheme 1.5).⁶⁷ The stepwise mechanics of this reaction were explained using DFT calculations which predicted that the concerted [2+3] cycloaddition would be strongly disfavoured ($\Delta G = 15$ kcal/mol). The authors suggested that the CuAAC mechanism involves the formation of copper-acetylide **1.62**, a feature supported by the observation that cycloadditions failed to occur when using internal alkynes.⁶⁷ The formation of **1.62** is followed by the chelation of the α -N of the azide **1.59**. This chelation sets up the alkyne and azide for a cycloaddition to afford the six-membered, strained metallocycle **1.64** which, after

protodemetalation of intermediate **1.65**, forms the desired triazole **1.60** and regenerates the copper catalyst.



Scheme 1.5. Earlier mechanistic considerations reported by Sharpless *et al.*⁶⁷

While this mechanism offered valuable insights into the reaction, it failed to detailed the effects of either the nature of the counterion or the geometry of the copper.⁷⁰ Structural data obtained from the Cambridge Crystal Database revealed around 35 different copper acetylide structures, which typically show the alkyne coordinating to 3 atoms of copper (structure C, Figure 1.6).⁷⁰

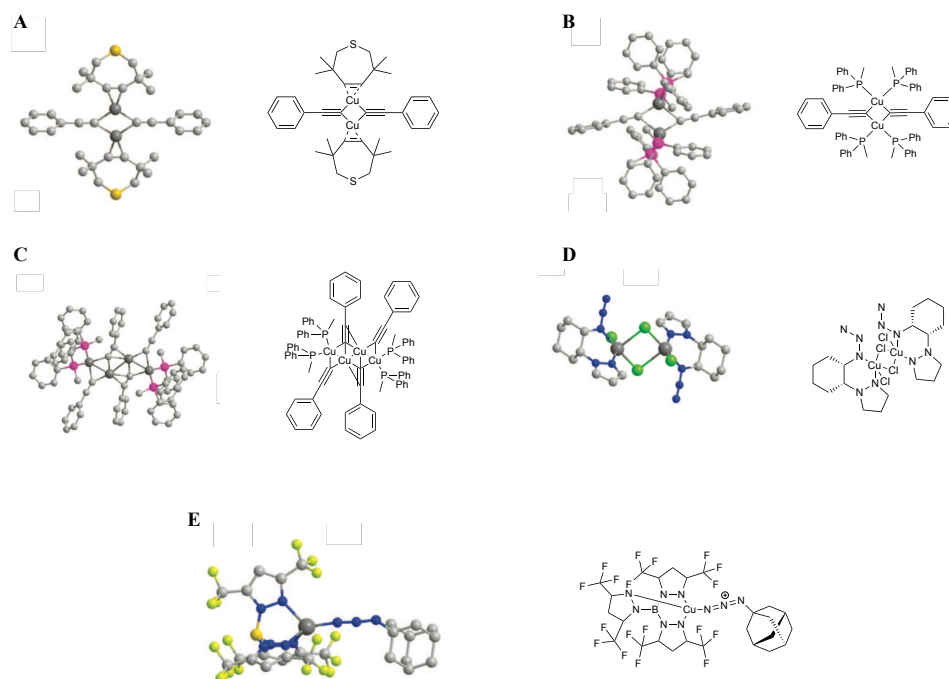


Figure 1.6. Examples of copper-acetylide crystal structures.⁷⁰

The coordination number and angle of the three bonds in C-C-Cu (structure C) indicates that the π -electron density of the alkyne is strongly involved in the coordination, suggesting that the second carbon possesses a large partial positive charge (Figure 1.7).⁷⁷ A dinuclear complex is also possible, with a C-C-Cu angle of approximately 130-140° (Figure 1.6, *e.g.*, A, B, D).⁷⁰ Few mononuclear complexes have been found; the most well-known example is copper (I) chloride which has a C-C-Cu angle of 180°. These findings indicate that the copper source strongly influences the kinetics of copper acetylide formation and therefore the formation of the triazole.

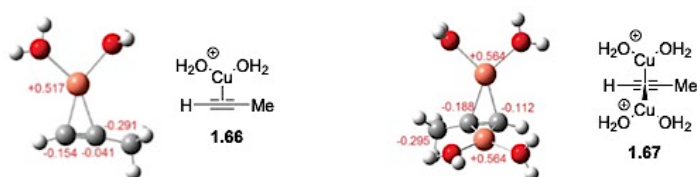


Figure 1.7. Partial charges of copper-acetylide mononuclear **1.66** and dinuclear **1.67** complexes.⁷⁷

Initially, copper(I) salts, such as CuI, were used to catalyzed CuAAC,^{67,68} generally requiring one equivalent of a nitrogenous base (*e.g.*, 2,6-lutidine, triethylamine, pyridine). However, the formation of by-products (diacetylenes, bis-triazole and 5-hydroxytriazoles) was often observed.^{67,68} Additionally, the use of Cu(I) salts required an inert atmosphere and/or anhydrous solvent to prevent aggregation and/or oxidation of the catalyst. To bypass these drawbacks, alternative routes to access the catalytically competent Cu(I) were investigated. The *in-situ* oxidation of Cu(0) is possible, although the time to reach completion of the reaction can be long (48 h).⁷⁰ Disproportionation of Cu(0) and Cu(II) is another route to produce the unstable Cu(I) oxidation state *in situ*.^{78,79} However, the most extensively applied strategy to produce Cu(I) is *via* the reduction of copper (II) sulfate with sodium ascorbate (NaAsc). Indeed, this system is effective for a range of different alkynes (aliphatic, aromatic) at room temperature with low catalyst loading (typically 5 - 10 mol %), producing the 1,4-triazole product in 82 - 94% yield.⁷³

Despite the benefits associated with this strategy, a key limiting factor when using NaAsc has been the variable reaction times observed for unactivated azides and alkynes. This effect is exacerbated for bioconjugation, where the toxicity of copper (classified as a Class 2 metal by the European Medicines Agency, maximum oral exposure of 250 ppm per day) and its reduction by NaAsc, leading to the formation of deleterious reactive oxygen species (ROS), prevent its widespread use *in vivo*.⁸⁰ ROS can cleave the phosphodiester backbone of nucleic

acids non-specifically, resulting in disintegration *via* radical-induced reactions.⁸¹ As a consequence, a key unmet challenge in the development of bio-orthogonal reactions is to minimise the inherent toxicity of Cu(I) in cells (*i.e.* reducing ROS formation). To this end, research has been focused on the synthesis of copper-ligands to mitigate the formation of ROS in CuAAC reactions.⁷⁰

Early mechanistic studies of CuAAC reactions revealed that certain bases/ligands, such as 2,6-lutidine, exhibited unusually high reaction rates, suggesting that these reactions could be autocatalytic.⁶⁷ Building from this, Sharpless *et al.* showed that the triazole ligand TBTA (Figure 1.8) accelerated the CuAAC reaction between phenylacetylene and benzyl azide, resulting in formation of the 1,4-triazole product with 84% yield after 24 h compared to 1% in the uncatalysed version.⁸²

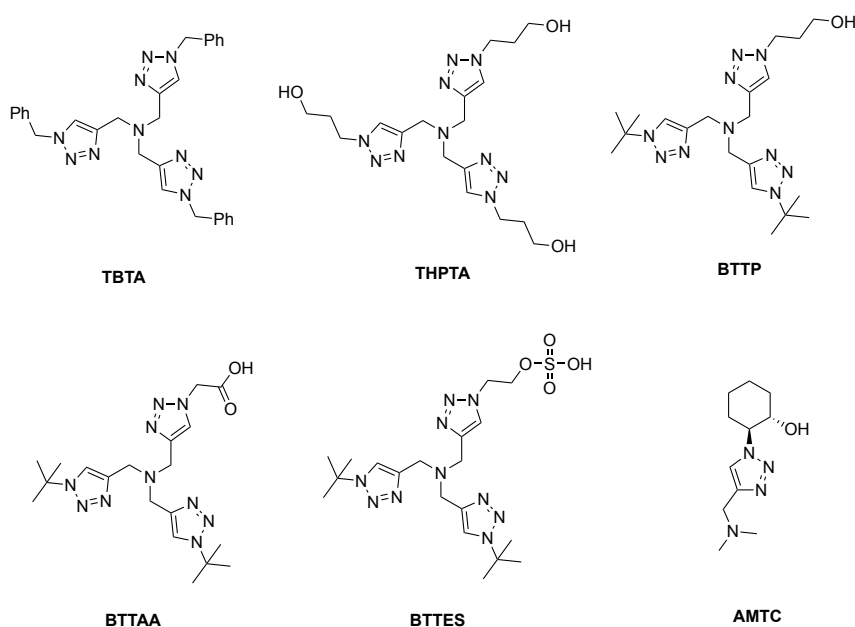
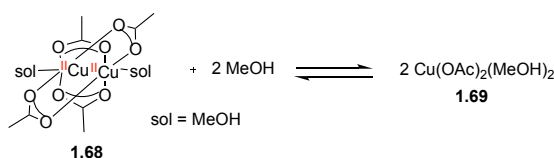


Figure 1.8. Examples of Cu(I) ligands for CuAAC reactions.

Sharpless *et al.* suggested that the observed rate acceleration arose from the tetradentate chelation of TBTA to the Cu(I) centre, producing a mononuclear complex. The tertiary amine of TBTA would accelerate the reaction rate by increasing the electron density on the copper centre, while the more labile triazole groups temporarily disassociate from the metal centre to allow the formation of the copper(I)-acetylide/ligand complex. Since the discovery of TBTA, a variety of CuAAC ligands have been developed to prevent the biological damage caused by copper ions and overcome the solubility limitations of TBTA in aqueous media. Some of the

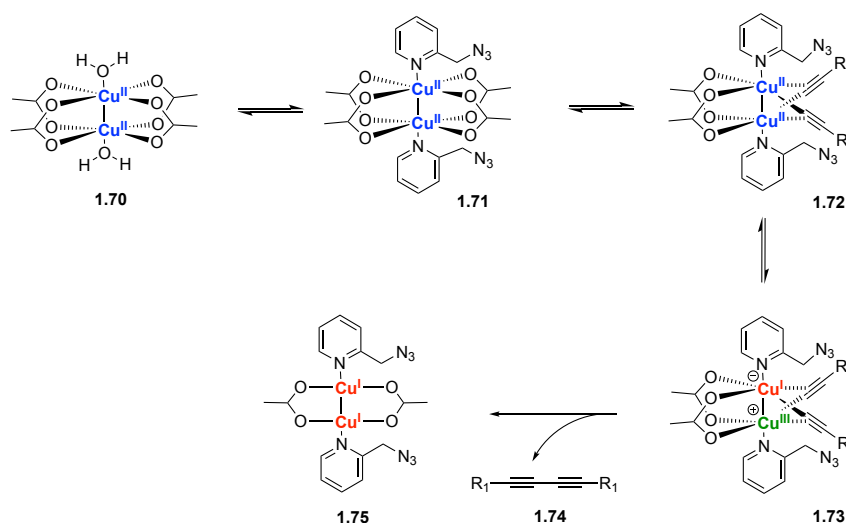
most notable examples are THPTA⁸³, BTTP⁸⁴, BTAA⁸⁵ and BTES⁸⁶ (Figure 1.8). Recently, Cegla *et al.* reported a new water soluble ligand, AMTC (Figure 1.8), which is readily synthesised, and more importantly, requires even lower copper loading than TBTA/THPTA (1 mol % compared to 10 mol %).⁸⁷

One of the defining characteristics of CuAAC is the wide range of solvents in which the reaction can be performed, including non-coordinating (toluene, chloroform, DCM), weakly coordinating (THF, pyridine, dioxane), polar (acetone, MeCN, DMF, DMSO, alcohols), and aqueous solvents and mixtures of the same.⁶⁸ Protic and aprotic solvents lead to Cu(I) formation *via* two different pathways. In aprotic solvent, the generation of Cu(I) is produced *via* formation of the Glaser product.^{88,89} When protic solvents are used, the formation of Cu(I) occurs *via* a redox-equilibrium between the solvent and copper species; this method is typically observed with alcohols.⁸⁸ In their mechanistic study of the copper(II)-mediated oxidative coupling of arylboronic acids and heteroatom nucleophiles, Stahl *et al.* showed that using methanol as the solvent with copper (II) acetate breaks the dinuclear copper complex **1.68** to form the mononuclear complex **1.69** (Scheme 1.6).⁹⁰ It should be noted that protonation of the triazole, the final step of the mechanism, would be kinetically less favourable in an aprotic solvent, which may explain the difference in reactivity between protic and aprotic solvents.⁸⁸



Scheme 1.6. Mononuclear complex formation with MeOH.⁹⁰

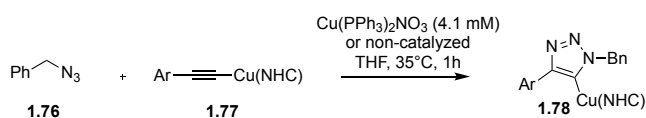
Zhu *et al.* published a mechanistic study on a chelate-assisted copper(II) acetate-accelerated azide-alkyne cycloaddition.⁸⁸ Fluorescence and NMR assays showed that Cu(OAc)₂ reacted as a dinuclear complex, which led to the conclusion that the acetate group was facilitating reduction to the catalytically-active copper(I) species when in a non-oxidisable solvent, such as MeCN. Kinetic and NMR studies showed that in MeCN, chelating azides have a zero-order reaction rate, indicating that they are the first to react with copper (Scheme 1.7). The use of chelating azides enhances the strength of the interaction with copper, which in turn facilitates the formation of the corresponding copper(I) acetylide **1.72**, presumed to be the rate-determining step of the reaction. Reduction of copper complex **1.73** is then made through the formation of the Glaser product **1.74**.⁹¹



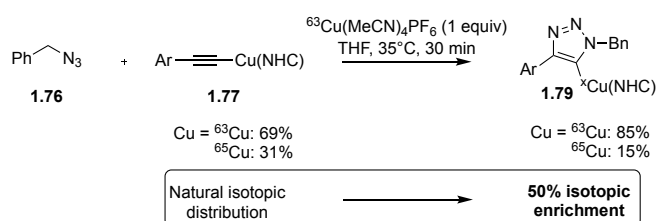
Scheme 1.7. Reduction of copper (II) acetate by Glaser reaction.⁸⁸

Considering the second-order kinetics⁹² of copper observed by Finn *et al.*⁹³ and Zhu *et al.*,⁸⁸ it is unlikely that only a single atom of copper is engaged in CuAAC catalysis. However, it had not been determined if the azide and alkyne were chelating the same copper atom. Fokin *et al.* confirmed the need for two atoms of copper by carrying out CuAAC reactions directly with copper-acetylide **1.77** in catalysed and non-catalysed conditions (Scheme 1.8).⁹⁴

a) Direct evidence for the requirement of a second copper atom:



b) ⁶³Cu-labelling studies:



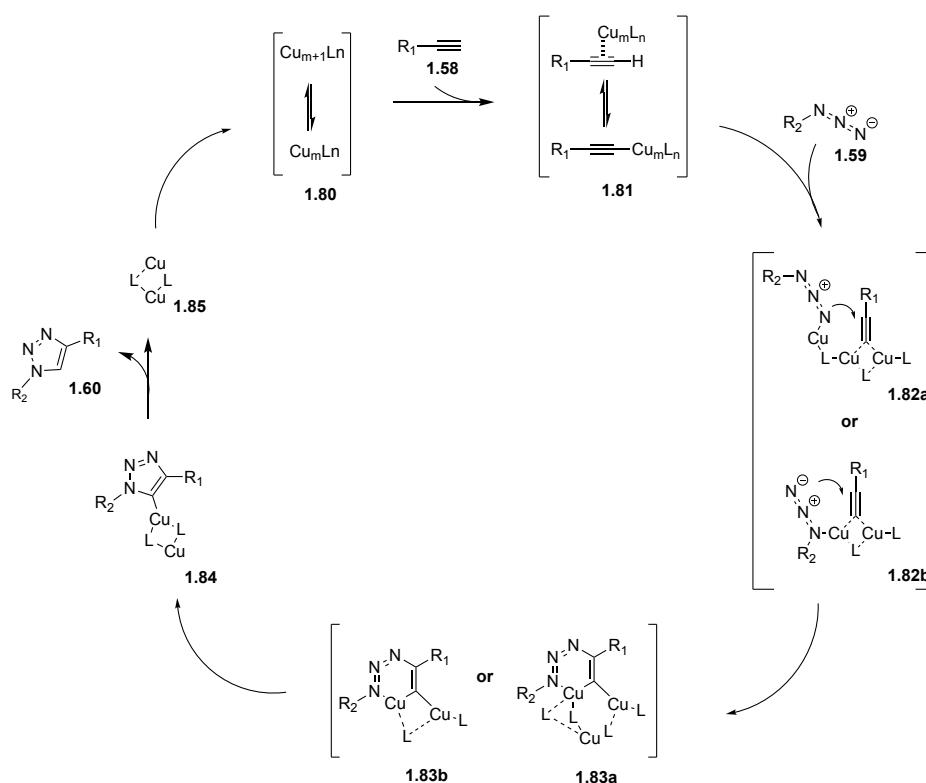
Scheme 1.8. Fokin's mechanistic studies supporting the necessity for a second copper atom for CuAAC reactions.

a) Direct evidence for the requirement of a second copper atom. b) ⁶³Cu-labelling studies.⁹⁴

Kinetic studies have shown that only catalytic conditions allowed the formation of the expected triazole **1.79**. Experiments with labelled ⁶³Cu were used in an attempt to determine the respective roles of each copper atom (Scheme 1.8).⁹⁴ An isotopically pure copper(II)

complex ($^{63}\text{Cu}(\text{MeCN})_4\text{PF}_6$) was used to catalyse the CuAAC reaction. Isotopic studies on the intermediate **1.78** unexpectedly showed 50% isotopic enrichment, disproving independent roles for the two copper atoms (Scheme 1.8). Reactions between ^{63}Cu and **1.79** have shown no isotopic enrichment, proving that the enrichment must occur during the cycloaddition steps, and therefore that the two atoms of copper must chelate the alkyne.

Based on these results, a plausible mechanism of the reaction is presented in Scheme 1.9.⁹⁴



Scheme 1.9. Plausible mechanism of CuAAC.⁹⁴

In 2015, mono- and bis(copper) intermediates were isolated by Bertrand *et al.*, further improving our understanding of the CuAAC mechanism (Figure 1.9).⁹⁵ Crystal structures of these intermediates allowed confirmation of alkyne chelation by two atoms of copper (structures A and C, Figure 1.9) but also showed, for the first time, the presence of a bis(copper)triazole intermediate (structure B, Figure 1.9). Kinetic studies have shown a dramatic rate acceleration of benzyl azide-copper chelation when the bimetallic complex is used ($1.76 \times 10^{-2} \text{ s}^{-1}$) over the monometallic ($1.86 \times 10^{-4} \text{ s}^{-1}$). Furthermore, kinetic studies of the catalytic reaction between phenylacetylene and benzyl azide confirmed the superior

catalytic activity of dinuclear complexes (quantitative yield after 600 min) over their mononuclear counterparts (20% yield after 2100 min).⁹⁵

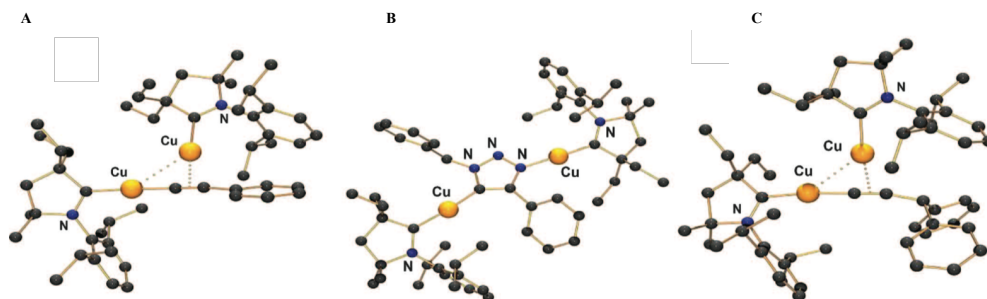


Figure 1.9. Crystal structures of copper-complex intermediates in the reaction between phenylacetylene and benzyl azide in the presence of (CAAC)CuOAc. CAAC = cyclic (alkyl)(amino) carbene.⁹⁵

1.3.4.2 Applications and Limitations of CuAAC Ligation for Bioconjugation

The CuAAC reaction has been widely employed across many scientific disciplines. It has been used in the development of self-healing polymers⁹⁶ and solar cells.⁹⁷ It has been essential for the production of a variety of biomolecular sensors of carbohydrates,^{98,99} proteins¹⁰⁰ and antibodies.¹⁰¹ It is in bioconjugation, however, that the CuAAC reaction has had its greatest effect.

In 2003, Finn *et al.* reported the first successful biological application of CuAAC.¹⁰² The authors introduced azide or alkyne moieties on the surface of Cowpea Mosaic Virus (CPMV) through ligation to lysine¹⁰³ or engineered cysteine residues.¹⁰⁴ Cycloaddition efficiency was quantified by the use of an alkyne- or azide-modified fluorescein. Importantly, the authors established that addition of a ligand, such as TBTA, was critical for efficient conjugation. Subsequently, extensive studies using CuAAC reactions for selectively labelling biomolecules were reported, illustrating its application both *in vitro* and *in vivo* and throughout the spectrum of biomolecules.^{42,54,105}

CuAAC methodology has benefited the field of activity-based protein profiling (ABPP) by promoting its use *in vivo*. ABPP employs chemical probes that interact with and label the active site of target proteins on a whole proteome level.¹⁰⁶ Limited cellular uptake and poor distribution, in addition to the potential perturbation of natural enzyme structure and activity, have limited the application of traditional, biotin-based probes (Figure 1.10). The advantage of using CuAAC methodology derives from its use of a small azide or alkyne moiety, which

is less likely to interfere with the biological target (Figure 1.10).¹⁰⁷ The small moiety is then reacted with its CuAAC surrogate to allow for protein capture. This approach helps to ensure that enrichment and visualisation are only achieved on the target site due to the bio-orthogonality of the probe's functionalities.

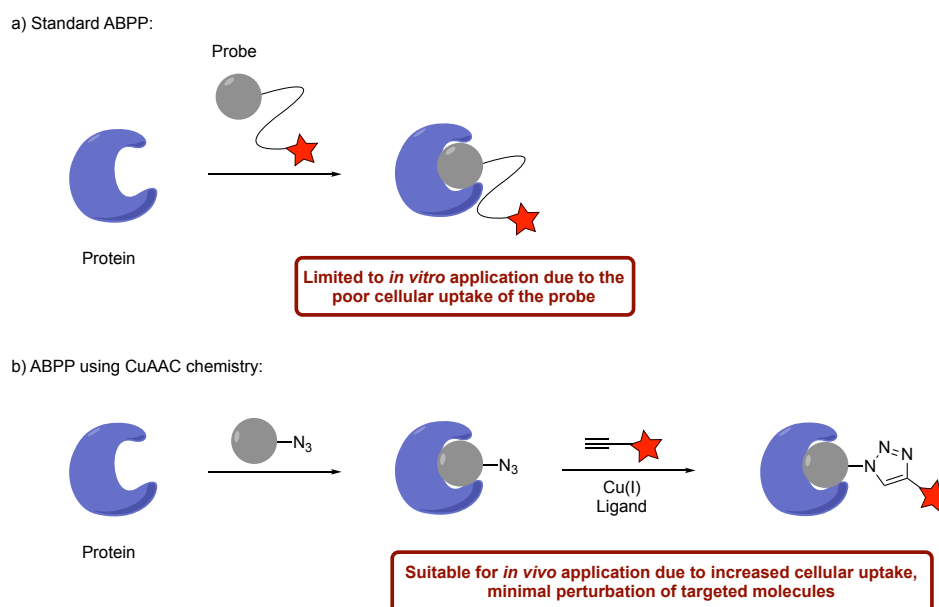


Figure 1.10. Activity-based protein profiling methodologies. *a*) Standard ABPP. *b*) ABPP using CuAAC chemistry.

While both the alkyne and azide moieties are easily incorporated into biomolecules, the higher stability of azides within biological systems render them more attractive. Indeed, undesired side reactions between alkynes and glutathione (GSH) have previously been reported.⁸³ Unfortunately, copper toxicity remains a serious limitation of this methodology. The copper-mediated formation of reactive oxygen species (ROS) leads to oxidative damage to biomolecules (Figure 1.11). Exacerbating this situation, (super)stoichiometric loading of copper is generally necessary due to inhibition of the catalyst when in the presence of abundant biomolecules possessing copper-chelation sites (Figure 1.11).^{81,108} The subsequently high copper concentration required to efficiently ligate biomolecules results in increased cellular toxicity.

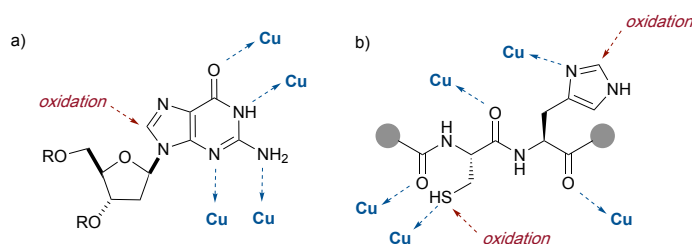
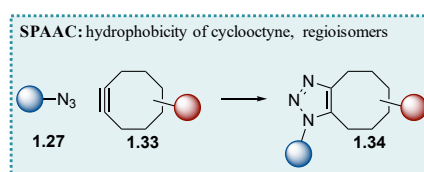


Figure 1.11. Examples of copper-mediated oxidative damage (red arrows) and potential copper-chelation sites (blue arrows) in nucleic acids *a*) and peptides *b*).

1.3.4.3 Strain-Promoted Azide/Alkyne Cycloaddition



To overcome the limitations observed in the CuAAC reaction, Bertozzi *et al.* have exploited the increased reactivity conferred by strained alkynes, such as cyclooctyne **1.33** (Figure 1.4), to develop a copper-free alternative for bioconjugation.¹⁰⁹ When reacted with an azide, ground state destabilisation owing to bond angle deformation of the acetylene to 163° skews the reaction equilibrium, favouring product formation without the need for catalyst or additive.^{110,111}

This strategy has been extensively used for bioconjugation, in particular for labelling carbohydrates, in a variety of *in vivo* contexts, including mammalian cells and animals.¹¹² Undeniably, carbohydrates' incompatibility with genetically encoded reporters has strongly limited their development as molecular imaging targets; therefore, bio-orthogonal strategies are particularly important for the study of these biomolecules. SPAAC methodology has successfully been employed for studying the dynamics of glycan trafficking in live cells, allowing identification of a population of sialoglycoconjugates with unexpectedly rapid internalisation kinetics.¹¹³ SPAAC bioconjugation has also been used for non-invasive imaging of carbohydrates in live, developing zebrafish.¹¹⁴

Significant efforts have been made to overcome SPAAC limitations by increasing the rate, biocompatibility and pharmacokinetic properties of cyclooctynes in order to obtain the optimal balance between reactivity and stability (Figure 1.12). Superior reaction rates were observed

by generating amplified strain energy through the addition of either electron withdrawing groups (MOFO, DIFO)^{113,115} or aryl rings (DIBO, DIBAC and BARAK) at the propargylic position.^{116–118} Addition of a ring fusion cyclopropyl (BCN) has also proven to dramatically increase cyclooctyne's reactivity.¹¹⁹ Unfortunately, higher reactivity is often accompanied by lower stability; BARAC, for example, has a 100-fold increase in kinetics, yet, intramolecular rearrangement under acidic conditions and hydrolysis in phosphate buffered saline has limited its application *in vivo*.¹²⁰ Moreover, side reactions between cyclooctynes and native biological functions have been observed. Reactions with cellular nucleophiles, such as glutathione and cysteine sulfenic acid, remain a serious limitation for SPAAC as they proceed up to 100-fold faster than the desired cycloaddition.^{51,121,122}

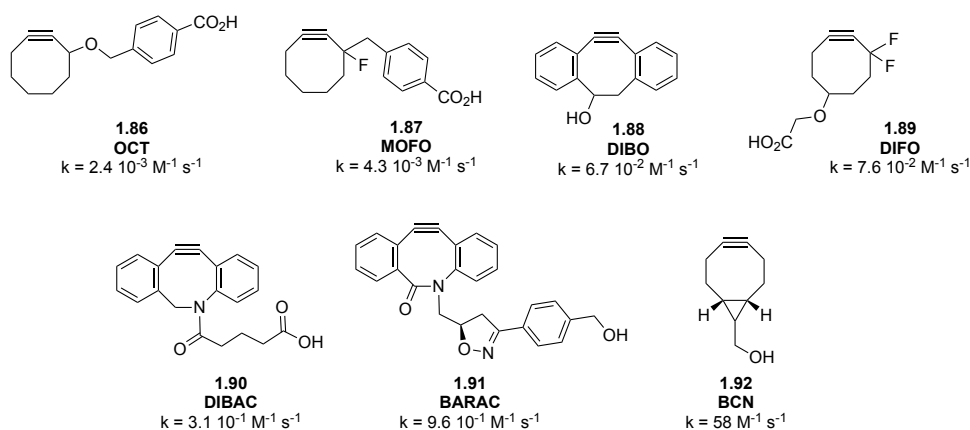
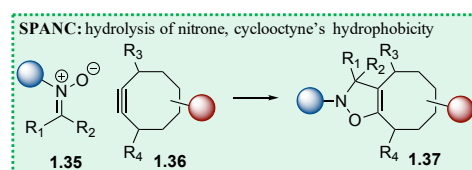


Figure 1.12. Cyclooctynes commonly employed in SPAAC reaction and their rate constants (k) when reacted with benzyl azide.²⁰

Further limitations of SPAAC derive from the large size and hydrophobic nature of cyclooctynes. These features result in decreased cell permeability, limited intracellular distribution, and an increased capacity to perturb the properties of the biological target. For example, Lemke *et al.* have reported that dibenzocyclooctynes, such as DIBO or DIBAC, could not be site-specifically incorporated into proteins *via* amber stop codons.¹²³ Finally, the formation of the 1,4- and 1,5-regioisomers obtained during SPAAC ligations remains a significant limitation of this strategy.¹⁰⁹

1.3.5 Strain-Promoted Alkyne/Nitrone Cycloaddition

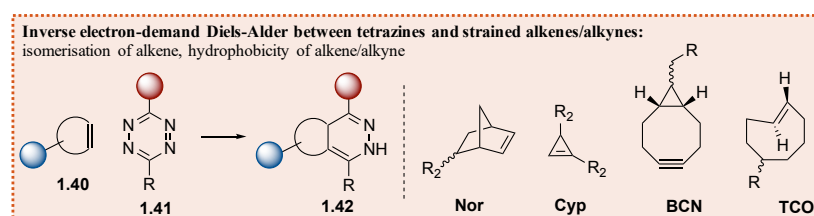


To improve the kinetics and biocompatibility of the SPAAC reaction, alternative 1,3-dipoles, such as nitrones^{124,125} or nitrile oxides^{126,127} have been employed. The strain-promoted alkyne/nitrone cycloaddition (SPANC) has allowed for a 1000-fold increase in reaction rate compared to Bertozzi's original SPAAC ligation.

SPANC methodology has been used to effectively label the *N*-terminus of chemokine interleukin-8 (IL-8), a potent promoter of angiogenesis.¹²⁵ Previous labelling strategies of IL-8 relied on random lysine-targeted methodologies, resulting in variable labelling at the many lysine sites. In this study, Delft *et al.* demonstrated a one-pot, three-step approach for the site-selective ligation of IL-8. First, nitrones were introduced *via* aldehyde condensation with the *N*-terminal serine, followed by reaction with *N*-methylhydroxylamine. A PEG-modified dibenzocyclooctyne was then introduced to the media affording full conversion to the expected *N*-alkylated isoxazoline after 20 hours.

The use of nitrile oxides has also been explored as an alternative to SPAAC, resulting in the formation of an isoxazole product. However, nitrile oxide must be generated *in-situ* due to its high reactivity. Nonetheless, this alternative strategy has successfully been employed for the selective ligation of peptides,¹²⁸ nucleotides¹²⁸ and carbohydrates.¹²⁶

1.3.6 Inverse Electron-Demand Diels-Alder with Tetrazine and Strained Alkene/Alkyne



The remarkable kinetics observed when 1,2,4,5-tetrazines are reacted with electron-rich dienophiles *via* an inverse electron-demand Diels-Alder, followed by a retro [4 + 2] cycloaddition,^{129,130} has established a new standard within bioconjugation chemistry.¹³¹ The choice of dienophiles is vast (Figure 1.4), ranging from trans-cyclooctene (TCO),^{132,133} cyclooctyne (BCN),¹³⁴ cyclopropene (Cyp),¹³⁵ norbornene (Nor),^{136–138} and cyclobutene¹³⁹ to azetidine¹⁴⁰ and isonitrile.¹⁴¹ Early kinetics studies revealed that the use of TCO dramatically increases reaction rates.¹³¹ In fact, owing to its strained angle, its reaction rate is 7-fold faster than cis-cyclooctene. However, isomerisation of the alkene and product instability toward hydrolysis have limited its potential application to bioconjugation.¹⁴²

Research has focused on improving tetrazine and product stability, reaction kinetics and cell permeability of this technique.¹⁴² Addition of an electron-withdrawing group at position 3 or 6 of tetrazines dramatically increases the kinetics of the reaction (from $10^{-2} \text{ M}^{-1} \text{ s}^{-1}$ to $10^{-5} \text{ M}^{-1} \text{ s}^{-1}$).¹⁴² The use of non-encumbered substituents has also been found to increase reaction rates. Unfortunately, increasing tetrazine's reactivity results in diminished stability towards hydrolysis (from days to only hours).³⁸ Exchanging the dienophile can improve product stability, however, this is at the cost of reaction rate.¹⁴²

The extremely fast kinetics observed during the reaction between TCO and tetrazine is particularly useful for tracking fast biological processes and labelling low-abundance proteins. In 2010, Weissleder *et al.* reported an elegant alternative to the gold-standard biotin/streptavidin pulldown assay by combining the use of antibodies, nanoparticles and TCO/tetrazine chemistry (Figure 1.13). This platform, called "BioOrthogonal Nanoparticle Detection" (BOND) provides higher nanoparticle binding compared to conventional strategies due to the high reactivity and small size of TCO as compared to avidin.

The use of TCO/tetrazine chemistry has also found application in the synthesis of biomedical imaging markers.¹⁴³ Half-lives of radioisotopes are generally short (*e.g.* 110 min for ^{18}F), therefore fast reaction rates are critical for connecting the probe to the target. However, while high chemical yields were obtained when using TCO/tetrazine chemistry for PET imaging, the introduction of a large hydrophobic group (TCO) dramatically decreased the probe's affinity.

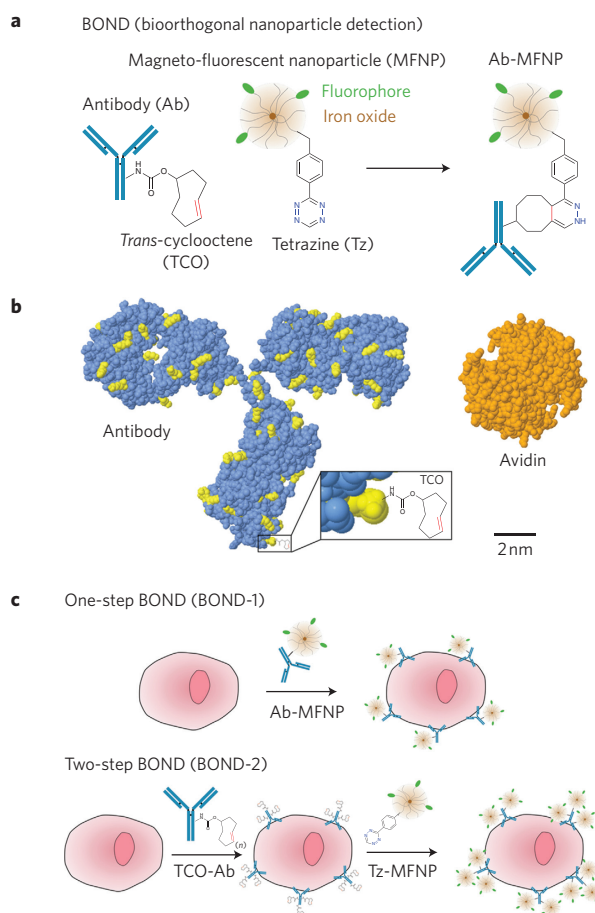
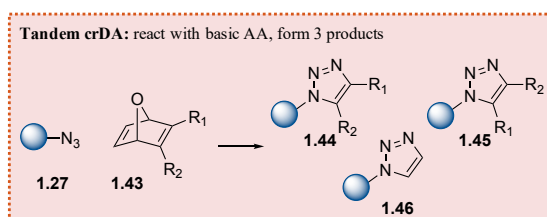


Figure 1.13. Bioorthogonal nanoparticle detection (BOND) platform. *a*) Strategy for the conjugation of an antibody to a nanoparticle. *b*) Comparison between TCO-modified mouse IgG2a antibody and avidin. *c*) Use of the BOND platform for direct (one-step) or indirect (two-step) cell targeting.

1.3.7 Tandem [3 + 2] Cycloaddition-Retro-Diels-Alder



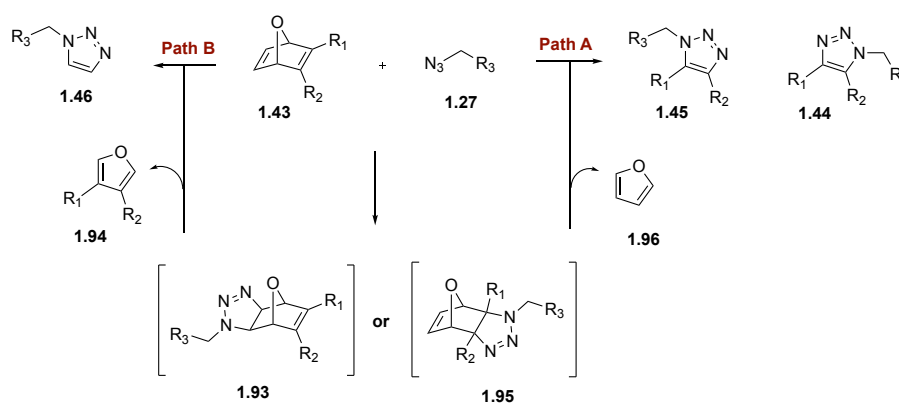
The spontaneous formation of 1,2,3-triazoles *via* a tandem [3 + 2] cycloaddition-retro-Diels-Alder reaction between azides and oxanorbornadienes, such as **1.43**, was recently reported by Rutjes *et al.* (Figure 1.4).¹⁴⁴ In this strategy, the authors take advantage of the ring strain and

electron deficiency of oxanorbornadienes to overcome the copper toxicity and cyclooctyne hydrophobicity usually encountered during triazole formation.

The spontaneous formation of 1,2,3-triazoles *via* a tandem [3 + 2] cycloaddition-retro-Diels-Alder reaction between azides and oxanorbornadienes, such as **1.43**, was recently reported by Rutjes *et al.* (Figure 1.4).¹⁴⁴ In this strategy, the authors take advantage of the ring strain and electron deficiency of oxanorbornadienes to overcome the copper toxicity and cyclooctyne hydrophobicity usually encountered during triazole formation.

An investigation into the kinetics of the reaction has shown a strong correlation with the substituents of oxanorbornadienes.¹⁴⁴ The authors reported a 20-fold decrease in the reaction rate when the oxanorbornadiene's R₂ substituent (Figure 1.4h) was changed from an ester to an amide (23.8 M⁻¹ s⁻¹ and 1.9 M⁻¹ s⁻¹, respectively). This observation may be due to the greater electron-withdrawing ability of the amide bond to alter the electron density of the adjacent carbon.

While this strategy has been used to successfully label biomolecules, such as the hen egg white lysozyme (HEWL), an enzyme responsible for antibacterial protection, the formation of multiple products during the ligation remains a critical limitation. Mechanistic investigations have shown that the cycloaddition between azide **1.27** and oxanorbornadiene **1.43** can occur at both alkene positions, potentially resulting in the production of three different triazoles (Scheme 1.10).¹⁴⁴ No selectivity of one triazole over another was observed, even when using the authors' optimal conditions, affording a ratio of 57/40/3 of triazoles **1.44/1.45/1.46**.



Scheme 1.10. Mechanism of the tandem [3 + 2] cycloaddition-retro-Diels-Alder ligation.¹⁴⁴

1.4 Hypothesis

Bio-orthogonal chemistry has been revealed as a critical tool for studying and understanding living systems. While extensive efforts have been made to enhance current strategies, crucial limitations remain. Many strategies are not inert towards native nucleophiles (*e.g.*, cysteine, lysine, glutathione), resulting in the formation of undesired side-products. Cellular uptake and probe affinity are negatively-impacted by scaffold size, thus limiting the available reagents. Despite the fact that research has focused on increasing the kinetics of the different bioconjugation strategies, very few display better kinetics than the native thiol/maleimide conjugation ($734 \text{ M}^{-1} \text{ s}^{-1}$).¹⁰⁸ Furthermore, cross-reactivity between the different strategies prevents their use in sequential ligations.

The CuAAC ligation remains the gold-standard for bioconjugation, despite the toxicity associated with the use of copper. It is one of the very few bio-orthogonal cycloadditions that combines the formation of a single product, fast kinetics and minimal perturbation of living systems. It has been widely demonstrated that increasing the reactivity of the bio-orthogonal reagents dramatically increases reaction kinetics, reducing the concentration of reagents and catalysts needed to efficiently perform bioconjugation. In fact, Ting *et al.* have demonstrated that using a metal-chelated strategy to activate the azide decreased the copper loading by 18-fold when targeting cell-surface proteins using CuAAC.⁸⁵ While this strategy is less damaging to the cells, it does not make the desired impact on reaction rate as copper acetylide formation has been reported by Fokin *et al.* to be the rate determining step of CuAAC reactions.⁹⁴

The hypothesis that was tested in this project is that modifying the reactivity of the alkyne surrogate would (*i*) increase the reaction rate, thus decreasing biomolecule/catalyst interaction times, (*ii*) reduce copper loading and (*iii*) modulate chemoselectivity to allow sequential bioconjugation (Figure 1.14). The work described herein focuses on the development of CuAAC bioconjugation using ynamines, alkynyl derivatives of enamines, where a nitrogen atom is directly conjugated to the alkyne, resulting in superior reactivity due to the electron-donating ability of the nitrogen strongly polarising the triple bond.¹⁴⁵

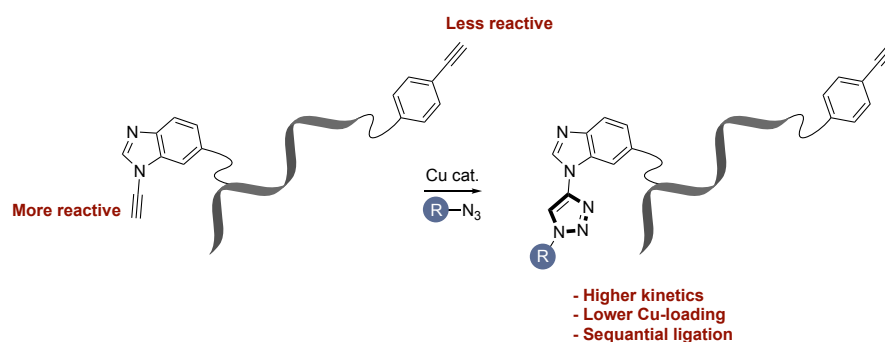


Figure 1.14. Proposed enhancement of CuAAC ligation reactivity through the use of ynamines.

1.5 Aims of This Project

The specific aims of this project are:

- (i) Optimise the synthesis of a focused series of aromatic ynamines (Figure 1.15 – Chapter 2).

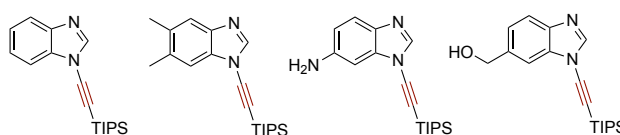


Figure 1.15. Examples of aromatic ynamines synthesised in this work.

- (ii) Determine the appropriate conditions for the chemoselective reaction of an aromatic ynamine in the presence of representative alkynes (Figure 1.16 – Chapter 2).

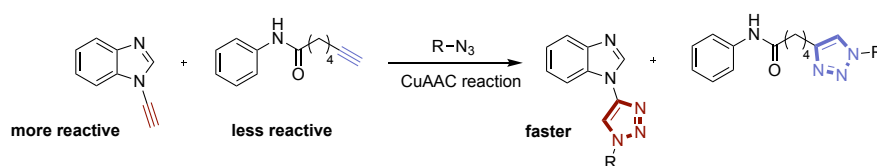


Figure 1.16. Determining optimal conditions for chemoselective CuAAC reaction.

- (iii) Establish chemoselective, sequential ligations of oligodeoxynucleotides (ODNs) using the enhanced reactivity of aromatic ynamines (Figure 1.17 – Chapter 3).

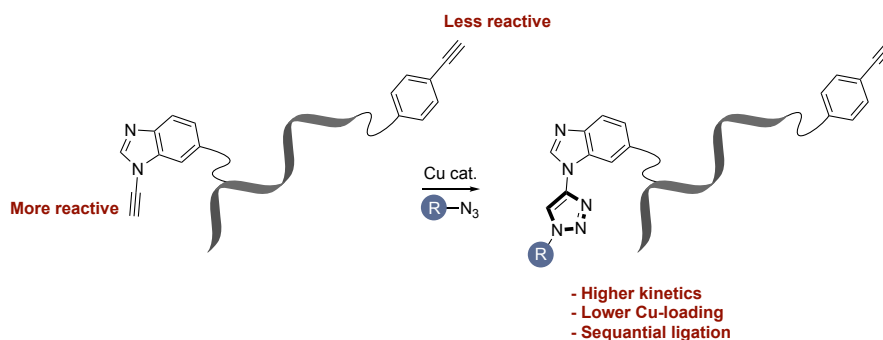


Figure 1.17. Determining optimal conditions for chemoselective, sequential CuAAC ligation of ODNs.

- (iv) Develop a flow-based platform for the fast, mild, degradation-free bioconjugation of peptide and oligonucleotide derivatives (Figure 1.18 – Chapter 4).

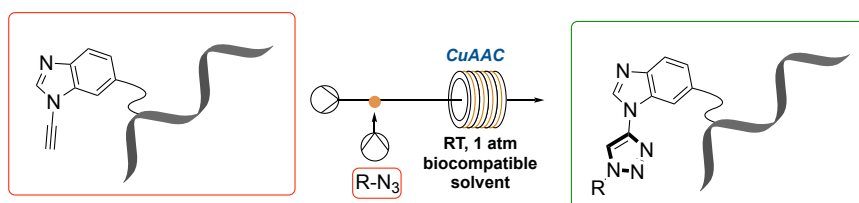


Figure 1.18. Flow-based platform for fast, mild, degradation-free bioconjugation.

Chapter 2

Interrogating the Chemoselective Profile of Aromatic Ynamines in Copper-Catalysed Azide-Alkyne Cycloadditions

The work in this chapter is based on the following publications:

- (i) M. Z. C. Hatit, J. C. Sadler, M. L. McLean, B. C. Whitehurst, C. P. Seath, L. D. Humphreys, R. J. Young, A. J. B. Watson, G. A. Burley, *Org. Lett.* **2016**, *18*, 1694–1697.
- (ii) M. Z. C. Hatit, C. P. Seath, A. J. B. Watson, G. A. Burley, *J. Org. Chem.* **2017**, *82*, 5461–5468.

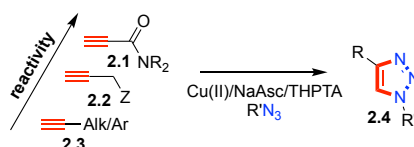
The work describe herein has been made in collaboration with Dr Joanna Sadler (substrate scope of ynamine CuAAC in MeCN), Liam McLean (azide syntheses), Dr Ben Whitehurst (bifunctional system synthesis) and Dr Ciaran Seath (kinetic data).

2.1 Chemoselectivity of Alkyne and Azide Substrates in CuAAC Reactions

As stated previously, copper-catalysed azide-alkyne cycloadditions are the gold-standard for biomolecule conjugation owing to their high efficiency and bio-orthogonality.^{67,68} Azide and alkyne functionalities are extremely rare in nature, making them ideal for chemistry within biological environments.^{146,147} Moreover, with but a single exception, these reactions consistently and specifically produce the desired 1,4-triazole targets.⁶⁸ Unfortunately, the high efficiency of CuAAC reactions results in limited chemoselectivity toward other alkyne/azide substrates, minimising the ability to employ distinct azide/alkyne moieties for targeted, sequential ligations.

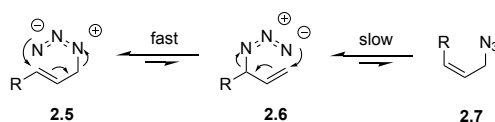
As the rate-determining step of CuAAC reactions is the formation of the copper-acetylide,⁹⁴ the chemoselectivity of alkyne/azide substrates in CuAAC reactions is influenced by the reactivity of the alkyne component. Finn *et al.* performed an in-depth study investigating the relative reactivity of various alkyne substrates in CuAAC reactions.¹⁴⁸ One of their hypotheses was that propiolate derivatives and ethynyl ketone/aldehyde groups would enhance the rate of cycloaddition in CuAAC reactions owing to the contributions of the electron-withdrawing ester groups towards [3 + 2] cycloadditions.⁶⁶ However, acetylenic ketones/aldehydes and alkylpropiolates are difficult to synthesise and, more importantly, result in cross-reactivity with biological macromolecules as they are excellent Michael acceptors.^{149,150} They therefore used propiolamides **2.1** as an alternative functionality because these are more synthetically accessible, have decreased Michael reactivity, and retain the potential for electronic activation as alkyne moieties in CuAAC reactions. Their work showed that secondary propiolamides, such as **2.1**, are the fastest alkyne substrates, followed by aromatic propargyl-ether derivatives

(Scheme 2.1a). Tertiary propiolamides, propargylamines and propargyl alcohols, such as **2.2**, showed similar reactivity, while aromatic and aliphatic alkynes substrates, such as **2.3**, were slower. However, differences in reactivity of these alkyne substrates were too little to ensure complete chemoselectivity when multiple alkynes were in competition.



Scheme 2.1. Reactivity difference of alkynes substrates in CuAAC reactions.¹⁴⁸

Alternatively, chemoselectivity in CuAAC reactions could be directed by the azide component. Organic azides are considerably more reactive than their inorganic counterparts, which permits one-pot strategies in which NaN_3 reacts first with an arylhalide followed by the triazole formation.¹⁵¹ Some organic azides, such as the allylic azide **2.5**, are so reactive that triazole formation is compromised by 1,3-sigmatropic rearrangements, which appear to be faster than the CuAAC reaction (Scheme 2.2).¹⁵² Differences in reactivity also exist between primary and secondary azides, indicating differential coordination of the azide with copper. However, these properties are not sufficient to ensure complete chemoselectivity of one azide over another.



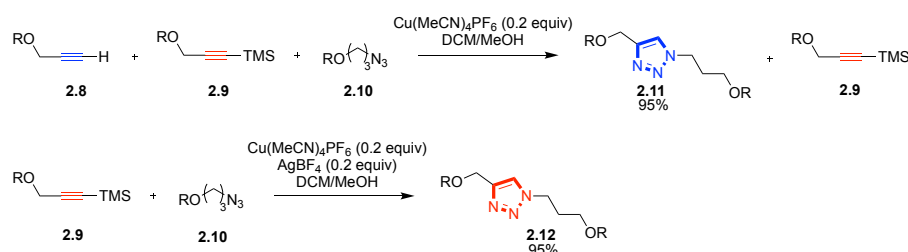
Scheme 2.2. 1,3-sigmatropic rearrangements of allylic azides.¹⁵²

2.1.1 Sequential Chemoselective CuAAC Reactions Using Alkyne Protecting Groups

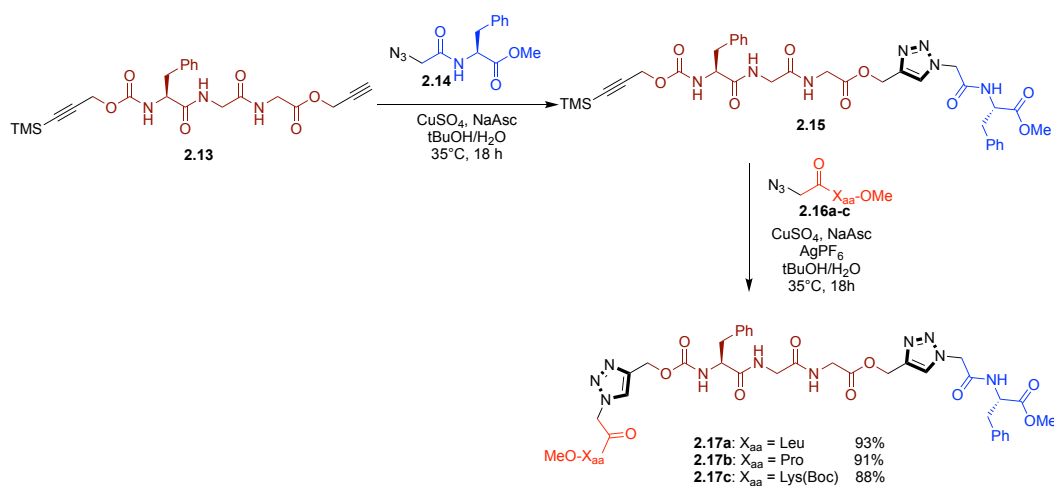
The high reactivity of CuAAC leads to limitations in chemoselectivity between different alkynes or azides. Few examples of chemoselective CuAAC reactions can be found in literature, and those that are reported generally rely on protection/deprotection strategies, disregarding any potential reactivity preferences that exist between alkyne subtypes. For example, Leigh *et al.* have employed a labile TMS-protecting group strategy for one-pot, consecutive, regioselective CuAAC (Scheme 2.3).¹⁵³

Using equimolar TMS-protected alkyne **2.9**, unprotected alkyne **2.8**, and azide **2.10** in the presence of catalytic $\text{Cu}(\text{MeCN})_4\text{PF}_6$ provided the expected 1,4-triazole **2.11** in 95% yield after 18 h (Scheme 2.3a). *In-situ* deprotection of **2.9** followed by CuAAC reaction with **2.10** allowed the subsequent formation of **2.12** in 95% yield, indicating that TMS-deprotection does not affect the azide or CuAAC reaction reactivity (Scheme 2.3a). This work was then applied to the bifunctional system **2.13** in which a TMS-protected alkyne and unprotected alkyne existed within the same molecule (Scheme 2.3b). These reactions required reoptimisation of solvent system, catalyst identity and load, as well as temperature due to partial deprotection of the TMS group, which obliterates the chemoselectivity profile of this strategy. Following optimisation, the desired bistriazole pseudononapeptides **2.17a-c** were obtained in 88-93% yields (Scheme 2.3b).

a) Intermolecular competition reaction between free and TMS-protected alkynes:



b) Intramolecular competition reaction between free and TMS-protected alkynes:

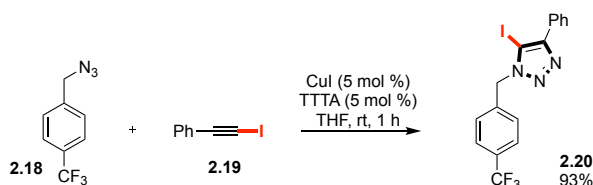


Scheme 2.3. Chemoselective control of triazole formation *via* protection/deprotection methodology. a) Intermolecular competition reaction between free and TMS-protected alkynes. b) Intramolecular competition reaction between free and TMS-protected alkynes.¹⁵³

While this strategy has been shown to efficiently allow sequential CuAAC ligations of bifunctional systems, such as **2.13**, addition of protecting/deprotecting steps and chemical reagents to perform the silyl deprotection limit its applicability in biological systems.

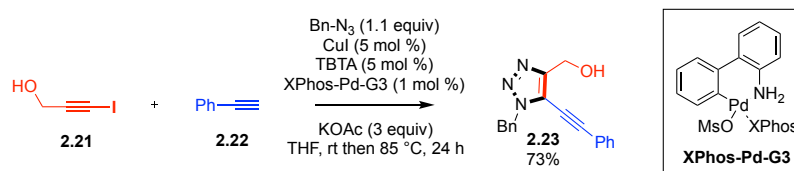
2.1.2 Sequential Chemoselective CuAAC Reactions Using Iodo/Bromo-Alkynes

Haloalkynes offer another potential route for modifying the chemoselectivity of CuAAC reactions. Fokin *et al.* reported copper-catalysed, rapid, regioselective formation of 5-iodo-1,4,5-trisubstituted-1,2,3-triazole **2.20** using 1-iodoalkyne **2.19** (Scheme 2.4).¹⁵⁴ While efficient, the use of supraequivalent triethylamine or catalytic tris((1-*tert*-butyl-1*H*-1,2,3-triazolyl)methyl)amine (TTTA) was necessary to avoid the formation of 5-proto and 5-alkynyl side products.



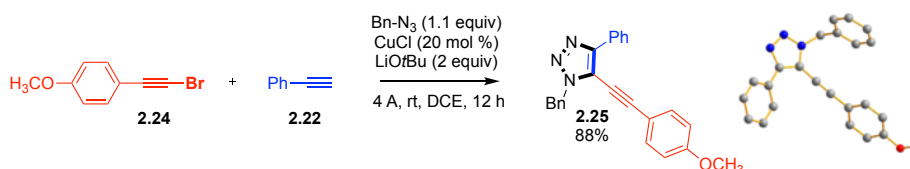
Scheme 2.4. Triazole formation using 1-iodoalkyne.¹⁵⁴

Taking advantage of the increased reaction rate offered by 1-iodoalkyne compared to terminal alkynes in CuAAC reactions, Lautens *et al.* described the one pot, chemoselective, tandem Cu- and Pd-catalysis to form the alkynyl-trisubstituted-triazole **2.23** (Scheme 2.5).¹⁵⁵ Using benzyl azide and catalytic CuI and TBTA in the presence of equimolar alkynes **2.21** and **2.22**, they were able to form predominantly the expected 5-iodotriazole, which was then reacted in a Sonogashira coupling to afford the final compound **2.23** in 73% yield. However, formation of numerous side products occurred using this method, rendering it unsuitable for bioconjugation.



Scheme 2.5. Chemoselective CuAAC reaction using 1-iodoalkyne.¹⁵⁵

Recently, Xu *et al.* reported reverse selectivity in CuAAC reactions by taking advantage of the less activated 1-bromoalkyne **2.24** in competition with terminal alkyne **2.22** (Scheme 2.6).¹⁵⁶ Using catalytic CuCl and LiOtBu as a base, they were able to synthesise chemoselectively the alkynyltriazole **2.25** in 88% yield. The crystal structure of **2.25** shows that the CuAAC reaction occurred with alkyne **2.22** (Scheme 2.6).



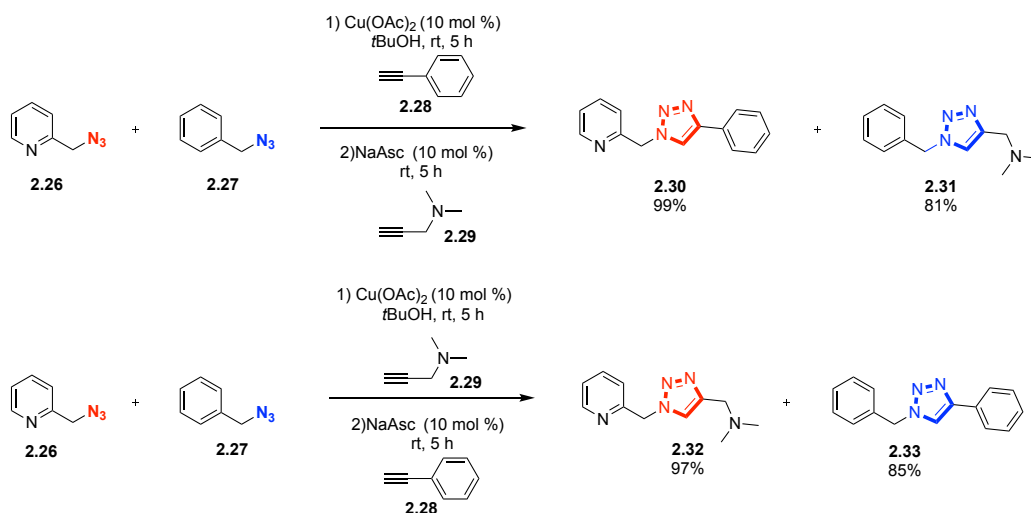
Scheme 2.6. Chemoselective CuAAC reaction using 1-bromoalkyne.¹⁵⁶

2.1.3 Sequential Chemoselective CuAAC Reactions Using Chelate-Directed Azides

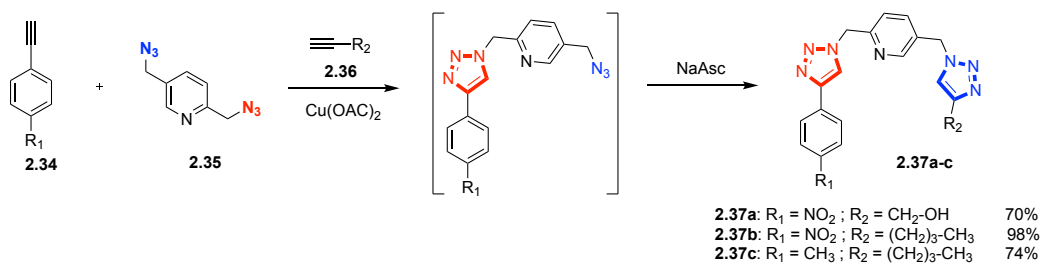
Zhu *et al.* has reported a chemoselective, three-component CuAAC reaction using a chelate-directed strategy which exploited the enhanced reactivity of azide groups in close proximity to a metal-chelating atom (Scheme 2.7).¹⁵⁷ This chelate-assisted approach enhances the reaction rate of picolyl azides and provides a reproducible platform for sequential ligation of two different alkynes. For example, both phenylacetylene **2.28** and chelating alkyne **2.29** react selectively with 2-picolylazide **2.26** over benzylazide **2.27**, showing that chelation by the azide directs the chemoselectivity of the reaction (Scheme 2.7a).

Unsymmetrical bisazides such as **2.35** containing both chelating and non-chelating azido groups were investigated for probing chemoselectivity in an intramolecular system. Crystal structures of unsymmetrical bisazides with Cu₂Cl₄ confirmed a selective azido-copper interaction with the chelating azido-group, leaving the nonchelating one unbound (Figure 2.1). Additionally, one-pot double click ligation experiments were performed using bisazide **2.35**, producing the expected bistriazole products **2.37a-c** in 70-98% yields (Scheme 2.7b).

a) intermolecular competition reaction between chelating and non-chelating azides:



b) intramolecular competition reaction between chelating and non-chelating azides:



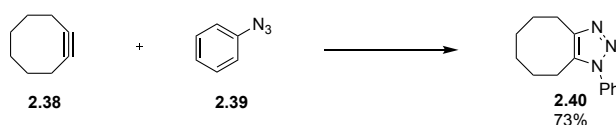
Scheme 2.7. Chemoselective CuAAC reaction *via* a chelate-directed azide strategy. *a*) Intermolecular competition reaction between chelating and non-chelating azides. *b*) Intramolecular competition reaction between chelating and non-chelating azides.¹⁵⁷



Figure 2.1. Crystal structure of unsymmetrical bisazides 2.35 with Cu₂Cl₄.¹⁵⁷

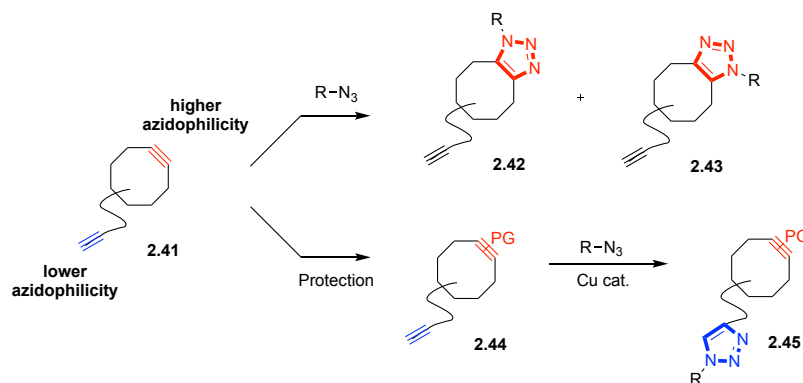
2.1.4 Sequential Chemoselective CuAAC Reactions using Transient Copper Complexation

In 1961, Wittig and Krebs reported that the neat reaction between cyclooctyne **2.38** and phenyl azide **2.39** “proceeded like an explosion to give a single triazole product” **2.40** (Scheme 2.8).¹¹⁰ The considerable bond angle deformation of the acetylene to 163° provides approximately 18 kcal/mol release of ring strain.^{110,111} This destabilisation of the ground state versus the transition state significantly enhances the reaction rate compared to unstrained alkynes.¹⁵⁸



Scheme 2.8. Reaction between cyclooctyne **2.38** and phenyl azide **2.39**.¹¹⁰

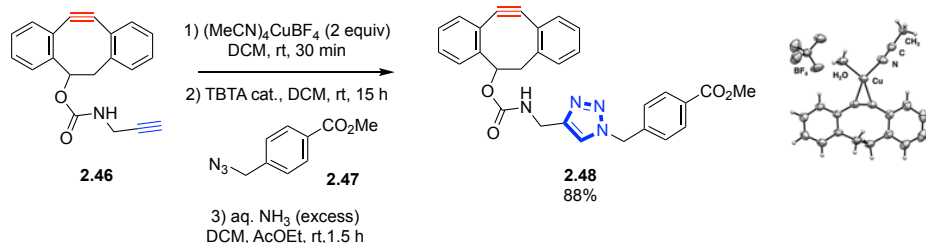
Bertozzi *et al.* exploited this property to develop the strain-promoted [3 + 2] cycloaddition of azides and cyclooctynes (SPAAC) reaction.¹⁰⁹ SPAAC offers a copper-free route to discriminate between alkyne subtypes (Scheme 2.9) which makes it attractive for use in biological systems; however, this reaction produces a regioisomeric mixture of triazole products which is generally undesirable.



Scheme 2.9. Discriminating alkyne reactivity by transient copper complexation of cyclooctyne.^{109,159}

Hosoya *et al.* developed a method to mask the “clickability” of a cyclooctyne by using the cationic copper(I) salt (MeCN)₄CuBF₄ (Scheme 2.9).¹⁵⁹ Treatment of the copper-cyclooctyne complex with excess aqueous ammonia regenerated the cyclooctyne. The utility of copper complexation to protect strained alkynes for chemoselective, sequential conjugation was then demonstrated in a one-pot, three-step procedure on the bifunctional system **2.46** (Scheme 2.10). Initial treatment of bifunctional system **2.46** with (MeCN)₄CuBF₄ results in the

protection of cyclooctyne only (Scheme 2.10, crystal structure). Azide **2.47** and catalytic TBTA were then added to the mixture to direct CuAAC exclusively at the terminal alkyne, followed by aqueous ammonia treatment to give the expected mono-triazole **2.48** with 88% yield.



Scheme 2.10. Click-modified cyclooctyne synthesis via transient strained alkyne protection.¹⁵⁹

Based on these observed differences in the reactivity of alkynes, a working hypothesis is that more strongly acidic terminal alkynes would react faster, potentially chemoselectively, with azides in CuAAC reactions.

2.2 Aromatic Ynamines as Synthons for CuAAC Reactions

2.2.1 Ynamine Reactivity

Ynamines are alkynyl derivatives of enamines (Figure 2.2), where a nitrogen atom is in direct conjugation with an alkyne. These were first reported and characterised by Zaugg *et al.* as a fortuitous accident in 1958.¹⁶⁰ In 1963, Viehe *et al.* reported the first general synthesis of ynamines.¹⁶¹ From that point, ynamines have been studied for their unique electronic properties. In particular, the electron-donating ability of the nitrogen strongly polarises the triple bond, giving it highly nucleophilic characteristics.¹⁴⁵

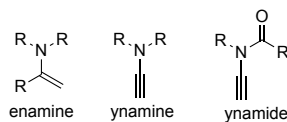
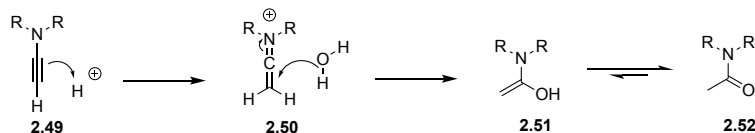


Figure 2.2. Structure of different *N*-alkynylheteroarenes.

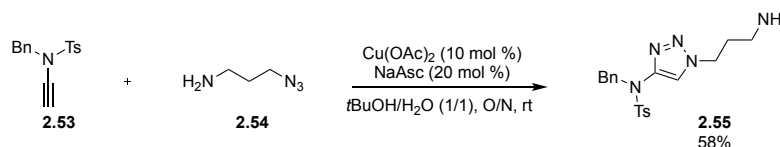
The reactivity and stability of ynamines are modulated by nitrogen substituents.¹⁶² Substitution with a strongly electron withdrawing group diminishes the electron-donating effect of the nitrogen lone pair on the triple bond; in the case of a trifluoromethyl group, no electron-donating effects are observed. Conversely, the most reactive ynamines are alkyl substituted,

such as ethyl or methyl groups. Unfortunately, the high reactivity of alkyl ynamines makes them highly susceptible to hydrolysis (Scheme 2.11).¹⁶³



Scheme 2.11. Hydrolysis of ynamines.¹⁶³

In order to reduce the electron-donating effects of the nitrogen, research has focused on the synthesis of ynamides (Figure 2.2). Ynamides employ the use of an additional electron withdrawing carbonyl substituent onto the nitrogen atom, which reduces the nitrogen's ability to donate electron density into the alkynyl group. Cintrat *et al.* used this strategy to prepare 1,4-disubstituted triazoles, such as **2.55**, in moderate yields using *N*-benzyl *N*-tosyl ynamide **2.53** and azide **2.54** (Scheme 2.12).¹⁶⁴

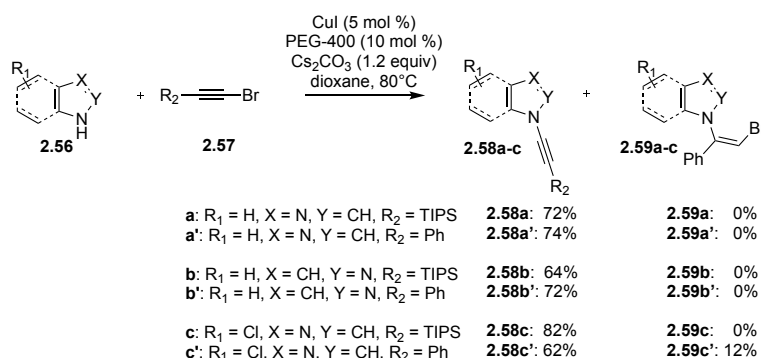


Scheme 2.12. The first example of CuAAC reaction with an ynamide.¹⁶⁴

2.2.2 Synthesis of Aromatic Ynamines

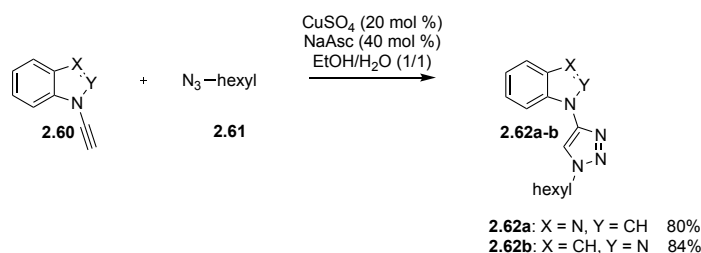
Comparable to ynamides, aromatic ynamines provide the ability to modulate the reactivity of ynamines. Ficini *et al.* have shown that aromatic substitution at the nitrogen diminishes ynamine reactivity.¹⁶² Aromatic ynamines, especially benzimidazole ynamine, have been shown to be stable towards hydrolysis. This stability likely results from the reduction of the nitrogen's ability to donate electron density into the triple bond due to delocalisation of its free electron pair into the aromatic system.

Burley *et al.* reported a step-efficient, Cu-catalysed synthesis of aromatic ynamines in which a key additive, PEG-400, was included and likely acts as both ligand and phase transfer agent (Scheme 2.13, **2.58a-c** and **2.58a'-c'**).^{165,166}



Scheme 2.13. Example of ynamines synthesised using conditions reported by Burley *et al.*¹⁶⁵

Preliminary studies, within the Burley group, have revealed that these aromatic ynamines are excellent substrates for CuAAC reactions. For example, reacting aromatic ynamines **2.60** with hexyl azide **2.61** in the presence of CuSO₄ and NaAsc provides the expected triazoles **2.62a** and **2.62b** in 80% and 84% yield, respectively, after only 5 min.¹⁶⁷ (Scheme 2.14).



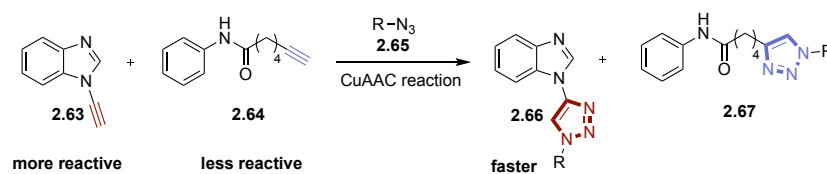
Scheme 2.14. The first example of CuAAC reaction with aromatic ynamine.¹⁶⁷

2.3 Hypothesis to Be Tested

There is extensive literature precedent showing that terminal ynamides are excellent substrates for a variety of Cu-catalysed C-C bond formations, such as Glaser couplings¹⁶⁸ or nucleophilic addition to mild electrophiles.¹⁶⁸ Terminal ynamide substrates such as **2.53** and aromatic ynamines **2.60** also display superior reactivity in CuAAC reactions (Scheme 2.12 and Scheme 2.14).^{164,167} The work described herein seeks to exploit the enhanced reactivity of aromatic ynamines as a new route for chemoselective, sequential CuAAC reactions by demonstrating that:

- (i) enhanced reactivity of aromatic ynamines will enable the preferential reaction of **2.63**, even in the presence of a competing alkyne such as **2.64** (Scheme 2.15).

- (ii) natural electronic bias present in aromatic ynamines would strike a balance with its enhanced reactivity in CuAAC reactions relative to an aliphatic alkyne.



Scheme 2.15. Hypothetical chemoselective CuAAC reaction based on the enhanced reactivity of ynamines.

2.4 Aims of this Chapter

The specific aims of this chapter are:

- (i) Optimize the synthesis of a focused series of aromatic ynamines (*e.g.*, **2.68-71**) and representative alkynes **2.64** and **2.72** (Figure 2.3).

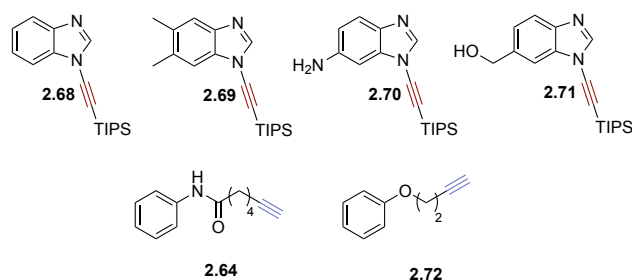
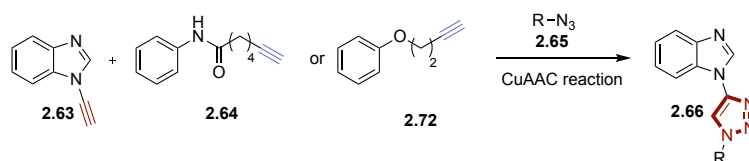


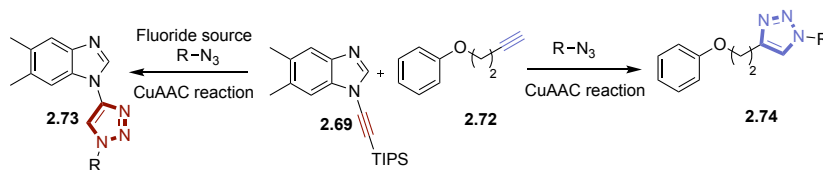
Figure 2.3. Example of ynamines and alkynes synthesised.

- (ii) Determine appropriate conditions for the chemoselective reaction of an aromatic ynamine (*e.g.*, **2.63**) in the presence of representative alkynes **2.64** and **2.72** (Scheme 2.16).



Scheme 2.16. Determining optimal conditions for chemoselective CuAAC reaction.

- (iii) Explore orthogonality of the reaction using silyl protecting groups (Scheme 2.17).



Scheme 2.17. Exploration of orthogonality of the CuAAC reaction.

2.5 Results and Discussion

2.5.1 Optimisation of Aromatic Ynamine Synthesis

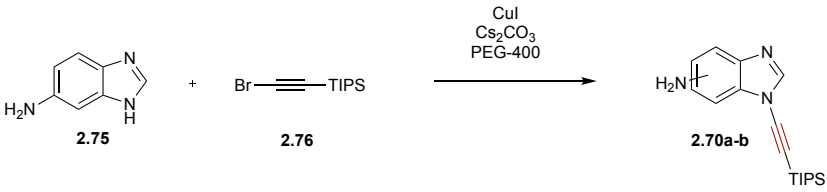
Initial work focused on the optimisation of conditions for the formation of aromatic ynamines **2.70a-b** (Table 2.1). DMSO and DMF were shown to solubilise starting material **2.75** but afforded numerous side products (Entry 2-3). Attempts to increase the reactivity of **2.76** by forming *in-situ* iodo-TIPS-acetylene resulted in the formation of only side products (Entry 4-6). Impurities were formed during ynamine synthesis from the dioxane-insoluble starting materials. The addition of 0.4% DMF to dioxane resulted in 81% conversion of the starting material **2.75**, producing the expected compounds **2.70a-b** after 48 h at 110 °C (Entry 7).

In order to decrease reaction times, we explored ynamine production *via* microwave-assisted synthesis (Entry 8-17). Repeating the reported conditions¹⁶⁵ resulted in only 34% conversion (by HPLC) after 20 min (Entry 8). Raising the temperature to 160 °C increased conversion from 34% to 80% after 20 min (Entry 9). Adding small amounts of DMF showed no improvement to the reaction (Entry 10-14). Interestingly, increasing the concentration of DMF above 50% resulted in the formation of an unknown compound as the major product (Entry 15-16). Zhao *et al.* recently published a study on the use of ynamides as coupling agents for the formation of amide bonds.¹⁶⁹ In the context of their findings, this observed impurity may be an amide derived from reaction with the free amine of **2.70a-b**.

The reaction scope confirmed that dioxane was required for the synthesis. Indeed, dioxane may function as a bidentate ligand for copper. To verify this hypothesis, the reaction was performed without PEG-400 which decreased the yield of expected products from 80% to only 7% (Entry 17). This result demonstrates that PEG-400 is required for an efficient reaction, which suggests that PEG-400 functions in the reaction as a copper chelator, which cannot be replaced by dioxane alone, or as a phase transfer reagent. To further explore the roles of

dioxane and PEG-400 within this reaction, a non-chelating phase transfer reagent, such as an ammonium salt, will be tested.

Table 2.1. Optimisation of the ynamine synthesis.¹⁷⁰

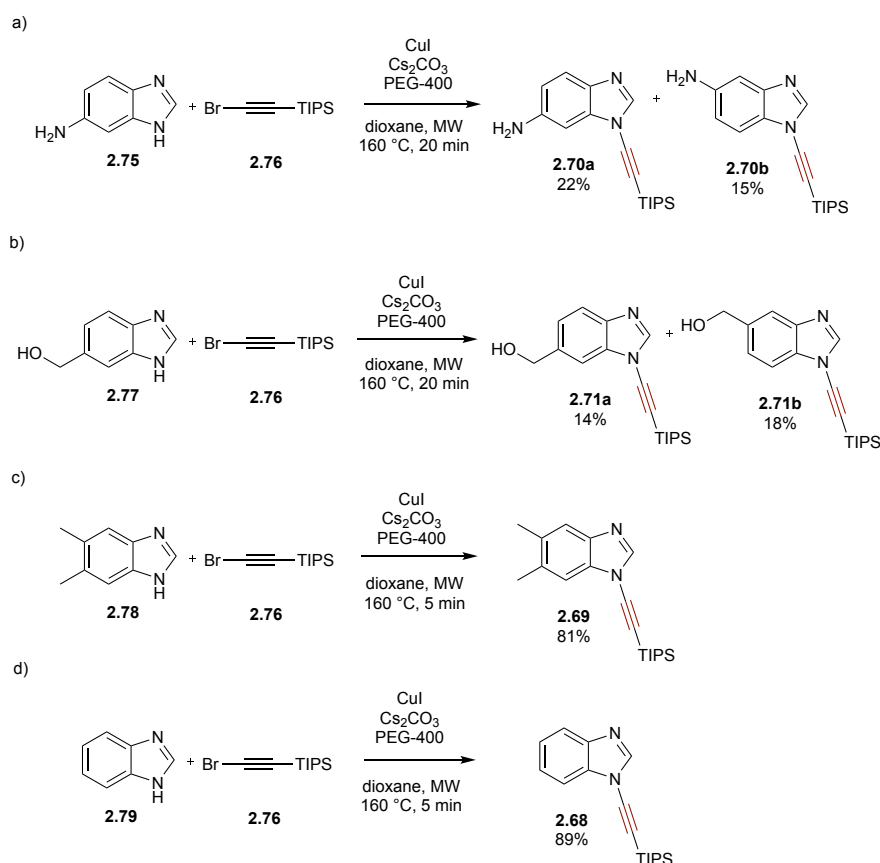


Entry	Conditions	(%)
1	dioxane, 90 °C, 48 h	0 ^[a]
2	DMSO, 90 °C, 48 h	20 ^[a]
3	DMF, 90 °C, 48 h	37 ^[a]
4	DMF, KI, without PEG-400, 160 °C, 48 h	0 ^[a]
5	DMF, KI, 160 °C, 48 h	0 ^[a]
6	DMF/dioxane (1/1), KI, 160 °C, 48 h	0 ^[a]
7	DMF/dioxane (0.4/9.6), 110 °C, 48 h	81 ^[a]
8	2.76 (2.2 equiv.), dioxane, 90 °C, MW, 20 min	34 ^[a]
9	2.76 (2.2 equiv.), dioxane, 160 °C, MW, 20 min	80 ^[b]
10	2.76 (2.2 equiv.), 0.1% DMF in dioxane, 160 °C, MW, 20 min	73 ^[b]
11	2.76 (2.2 equiv.), 1% DMF in dioxane, 160 °C, MW, 20 min	72 ^[b]
12	2.76 (2.2 equiv.), 2% DMF in dioxane, 160 °C, MW, 20 min	68 ^[b]
13	2.76 (2.2 equiv.), 4% DMF in dioxane, 160 °C, MW, 20 min	59 ^[b]
14	2.76 (2.2 equiv.), 10% DMF in dioxane, 160 °C, MW, 20 min	74 ^[b]
15	2.76 (2.2 equiv.), DMF/dioxane (1/1), 160 °C, MW, 20 min	23 ^[b]
16	2.76 (2.2 equiv.), DMF, 160 °C, MW, 20 min	11 ^[b]
17	2.76 (2.2 equiv.), dioxane, without PEG-400, 160 °C, MW, 20 min	7 ^[b]

^[a]Isolated yield. ^[b]Conversion calculated by RP-HPLC.

Having optimised the general reaction conditions, an additional screen was performed to increase atom efficiency by reducing the amount of bromo-TIPS-acetylene **2.76**. Unfortunately, using fewer than 2.2 equivalents of **2.76** was found to decrease the reaction rate dramatically. Extending the reaction time resulted in only a small increase in the conversion of **2.75**, suggesting that **2.76** is likely reacting with itself to form the Glaser compound.^{88,91}

To confirm that our optimised conditions were suitable for different substrates, a variety of benzimidazole ynamines were prepared (Scheme 2.18). Despite high conversions, low yields were obtained when using benzimidazoles **2.75** and **2.77** due to difficulties during extraction and purification. Nevertheless, ynamines **2.70a-b** and **2.71a-b** were obtained with yields between 14 and 22%. High yields were obtained after 5 min of reaction when less polar benzimidazoles were used, such as **2.78** or **2.79** (81 and 89%, respectively).¹⁷⁰



Scheme 2.18. Synthesis of different ynamines using optimised conditions. *Isolated Yields.*¹⁷⁰

2.5.2 Aromatic Ynamine as a Synthron for CuAAC Reactions – Optimisation of the Reaction

2.5.2.1 Reaction Optimization for Formation of Ynamine-1,4-Triazoles

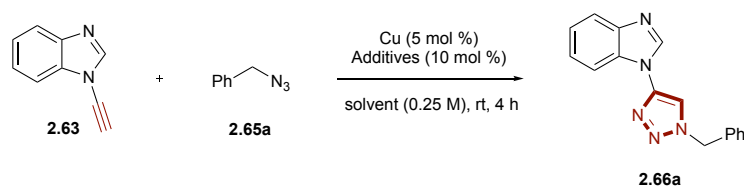
A screen was conducted to test the reactivity of aromatic ynamines as compared to aliphatic/aromatic alkynes in CuAAC reactions (Table 2.2).¹⁷¹ A variety of parameters including copper source, solvent, reductant, and ligand were explored. Initial evaluations for optimal CuAAC conditions were performed using benzimidazole ynamine **2.63**. 5 mol % of copper(II) acetate ($\text{Cu}(\text{OAc})_2$) was shown to be sufficient to catalyse the reaction. While other sources of copper(II) and copper(I) were able to catalyse the reaction, the rate of the reaction was dramatically decreased compared to $\text{Cu}(\text{OAc})_2$ (Entries 15-26).

Having established $\text{Cu}(\text{OAc})_2$ as the optimal catalyst for this reaction, the impact of the solvent was next explored (Entries 1-14). MeOH, MeOH/ H_2O , and DMSO/ H_2O were shown to be the

best solvent systems. In particular, MeOH significantly increased the rate of the reaction, producing triazole **2.66a** in quantitative yield within 2 h as compared to 4 h for MeCN. Visually, reactions using protic versus aprotic solvents differed; protic solvents (*e.g.*, MeOH) resulted in yellow to blue homogenous solutions, whereas aprotic solvents (*e.g.*, MeCN) produced heterogeneous mixtures ranging from blue to green. These observations suggest that the reduction of copper(II) to the active copper(I) in protic versus aprotic environments proceeds *via* different pathways.

The addition of a reductant, such as sodium ascorbate, to Cu(OAc)₂ and copper (II) sulfate (CuSO₄; Entries 27-32) significantly decreased the reaction rate and afforded a variety of side-products. The inclusion of TBTA as a ligand (Entry 34) ameliorated the formation of the undesired side products, affording **2.66a** in 81% yield. However, even with the benefits associated with TBTA, the presence of the reductant negatively impacts the efficiency of the Cu(OAc)₂-catalysed production of **2.66a** (80% compared to 95%, Entry 33-vs-Entry 4), suggesting that the acetate itself plays a role in the formation and stability of copper (I).

Table 2.2. Optimisation of ynamine CuAAC reaction.¹⁷¹



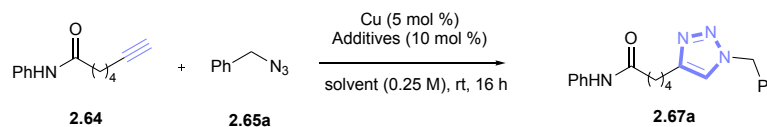
Entry	Catalyst	Solvent	Additive	Yield (%)
1	Cu(OAc) ₂	MeCN		92
2	Cu(OAc) ₂	MeCN/H ₂ O (1/1)		91
3	Cu(OAc) ₂	MeOH		Quant
4	Cu(OAc) ₂	MeOH/H ₂ O (1/1)		95
5	Cu(OAc) ₂	EtOH		83
6	Cu(OAc) ₂	EtOH/H ₂ O (1/1)		88
7	Cu(OAc) ₂	<i>i</i> PrOH		89
8	Cu(OAc) ₂	<i>i</i> PrOH/H ₂ O (1/1)		62
9	Cu(OAc) ₂	DMSO		84
10	Cu(OAc) ₂	DMSO/H ₂ O (1/1)		98
11	Cu(OAc) ₂	DMF		86
12	Cu(OAc) ₂	DMF/H ₂ O (1/1)		90
13	Cu(OAc) ₂	dioxane		73
14	Cu(OAc) ₂	dioxane/H ₂ O (1/1)		85
15	CuSO ₄	MeCN		50
16	CuSO ₄	MeCN/H ₂ O (1/1)		58
17	CuSO ₄	MeOH		70
18	CuSO ₄	MeOH/H ₂ O (1/1)		66
19	CuSO ₄	DMSO		54

20	CuSO ₄	DMSO/H ₂ O (1/1)		63
21	CuI	MeOH		90
22	CuI	MeOH/H ₂ O (1/1)		Quant
23	CuBr	MeOH		62
24	CuBr	MeOH/H ₂ O (1/1)		47
25	CuCl	MeOH		55
26	CuCl	MeOH/H ₂ O (1/1)		69
27	Cu(OAc) ₂	MeCN/H ₂ O (1/1)	NaAsc	47
28	Cu(OAc) ₂	MeOH/H ₂ O (1/1)	NaAsc	50
29	Cu(OAc) ₂	DMSO/H ₂ O (1/1)	NaAsc	21
30	CuSO ₄	MeCN/H ₂ O (1/1)	NaAsc	19
31	CuSO ₄	MeOH/H ₂ O (1/1)	NaAsc	24
32	CuSO ₄	DMSO/H ₂ O (1/1)	NaAsc	14
33	Cu(OAc) ₂	MeOH/H ₂ O (1/1)	NaAsc/TBTA	80
34	CuSO ₄	MeOH/H ₂ O (1/1)	NaAsc/TBTA	81

Compound **2.63** (1.0 equiv., 0.5 mmol, 0.25 M), **2.65a** (1 equiv., 0.5 mmol, 0.25 M), Air, rt. Cu catalyst 5 mol %, additives 10 mol %. Isolated yields.

2.5.2.2 Reaction Optimization for the Formation of Alkyne-1,4-Triazoles

To compare the reactivity of aromatic ynamines to an aliphatic alkyne, our CuAAC optimisation screen was repeated using *N*-phenyl-6-heptynamide **2.64** (1 equiv.) and benzyl azide **2.65a** (1 equiv.) (Table 2.3).¹⁷¹ The expected product was not observed after 4 h; in fact, at least 16 h was required for formation of **2.67a**. Using Cu(OAc)₂ as the catalyst, solvent screening showed the expected triazole **2.67a** was only produced in MeOH (76%, entry 3), DMSO (79%, entry 9), dioxane (73%, entry 13) and aqueous mixtures of these solvents (entry 4, 10 and 14). All other solvent systems contained only starting materials, even after 16 h. As expected, the use of standard CuAAC conditions (CuSO₄ 5 mol %, NaAsc 10 mol %, TBTA 10 mol %) produced **2.67a** in quantitative yield (entry 17); however, these conditions are sub-optimal for ynamine **2.63**. As TBTA was not as beneficial ligand for the ynamine reaction, alternative ligands were explored, such as AMTC which has shown to be extremely effective, even in the context of alkyne substrates (93%, entry 19). Moreover, as it is water-soluble, purification of the reaction is simplified. Interestingly, the ynamine click product **2.66a** functions as well as TBTA in this reaction (quantitative yield, entry 20), suggesting that **2.66a** contributes to its own production and therefore explains why aromatic ynamines, such as **2.63**, do not require the addition of a ligand for efficient CuAAC ligations.

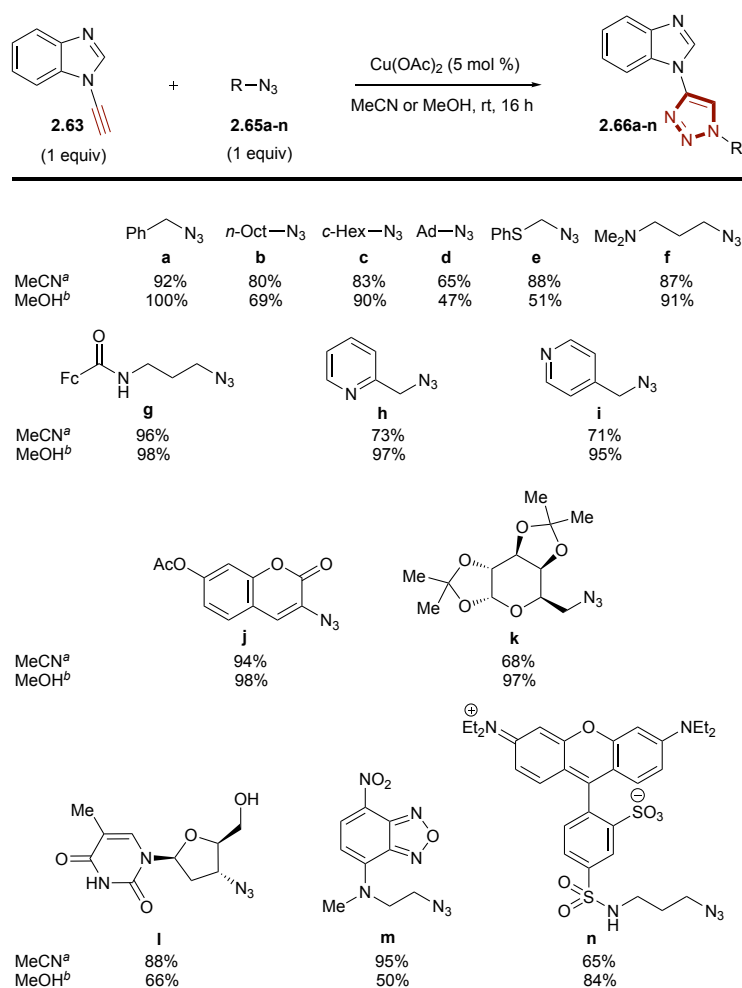
Table 2.3. Optimisation of alkyne CuAAC reaction.¹⁷¹

Entry	Catalyst	Solvent	Additive	Yield (%)
1	Cu(OAc) ₂	MeCN		0
2	Cu(OAc) ₂	MeCN/H ₂ O (1/1)		0
3	Cu(OAc) ₂	MeOH		76
4	Cu(OAc) ₂	MeOH/H ₂ O (1/1)		88
5	Cu(OAc) ₂	<i>i</i> PrOH		0
6	Cu(OAc) ₂	<i>i</i> PrOH/H ₂ O (1/1)		0
7	Cu(OAc) ₂	EtOH		0
8	Cu(OAc) ₂	EtOH/H ₂ O (1/1)		0
9	Cu(OAc) ₂	DMSO		79
10	Cu(OAc) ₂	DMSO/H ₂ O (1/1)		84
11	Cu(OAc) ₂	DMF		0
12	Cu(OAc) ₂	DMF/H ₂ O (1/1)		0
13	Cu(OAc) ₂	dioxane		73
14	Cu(OAc) ₂	dioxane/H ₂ O (1/1)		97
15	Cu(OAc) ₂	MeOH/H ₂ O (1/1)	NaAsc	64
16	CuSO ₄	MeOH/H ₂ O (1/1)	NaAsc	77
17	CuSO ₄	MeOH/H ₂ O (1/1)	NaAsc/TBTA	Quant
18	CuSO ₄	MeOH/H ₂ O (1/1)	NaAsc/THPTA	75
19	CuSO ₄	MeOH/H ₂ O (1/1)	NaAsc/AMTC	93
20	CuSO ₄	MeOH/H ₂ O (1/1)	NaAsc/ 2.66a	Quant

Compound **2.64** (1.0 equiv., 0.5 mmol, 0.25 M), **2.65a** (1 equiv., 0.5 mmol, 0.25 M), Air, rt. Cu catalyst 5 mol %, additive (10 mol %). Isolated yields.

2.5.3 Aromatic Ynamine as a Synthon for CuAAC Reactions – Substrate Scope

The substrate scope of ynamine **2.63** was investigated using our optimised CuAAC conditions of 5 mol % copper(II) acetate in MeOH or MeCN (Scheme 2.19).¹⁷¹ The reaction tolerated a wide range of azides containing varied steric constraints (*e.g.*, **b**, **c**, **d**), oxidisable functionalities (**e**, **l**), potential Cu-chelating substrates (**e**, **f**, **h**, **i**, **l**, **m**, **n**) and fluorophores (**m**, **n**).



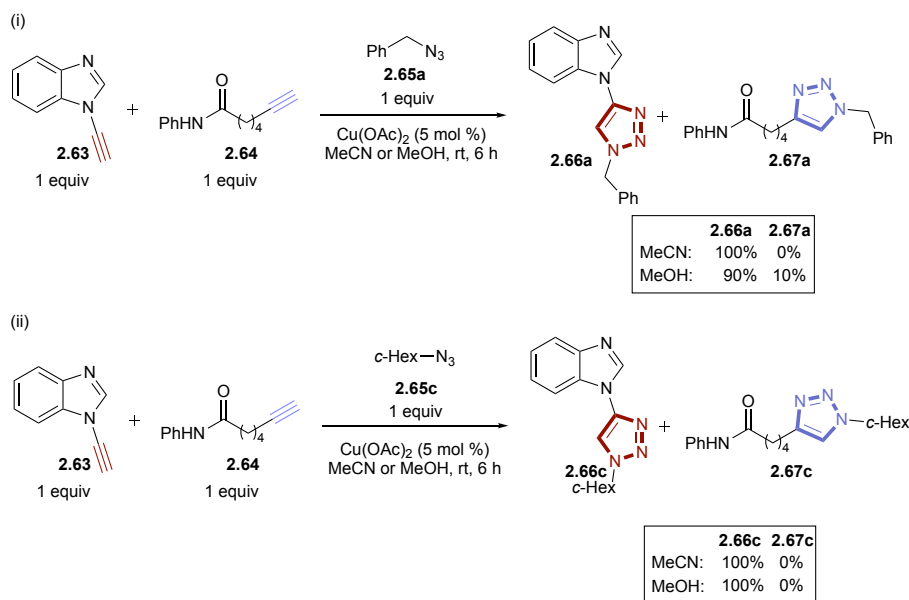
Scheme 2.19. Substrate scope of ynamine CuAAC reaction. ^a Isolated yields. ^b NMR yields. Fc = Ferrocene.¹⁷¹

2.5.4 Aromatic Ynamine as a Synthron for CuAAC Reactions – Chemoselective Profile

2.5.4.1 Intermolecular Chemoselective CuAAC Ligations

To explore the ability of an aromatic ynamine to react preferentially with an azide, intermolecular competition reactions between ynamine **2.63** and alkyne **2.64** were investigated.¹⁷¹ Products were resolved and identified by gradient HPLC. In MeCN, benzyl azide **2.65a** was fully converted to triazole **2.66a** rather than triazole **2.67a** (Scheme 2.20i). On the other hand, a small loss of chemoselectivity was observed in MeOH, where 10% of the product composition was attributable to triazole **2.67a**. Complete selectivity for the ynamine click product **2.66c** was observed in both MeCN and MeOH when cyclohexyl azide **2.65c** was

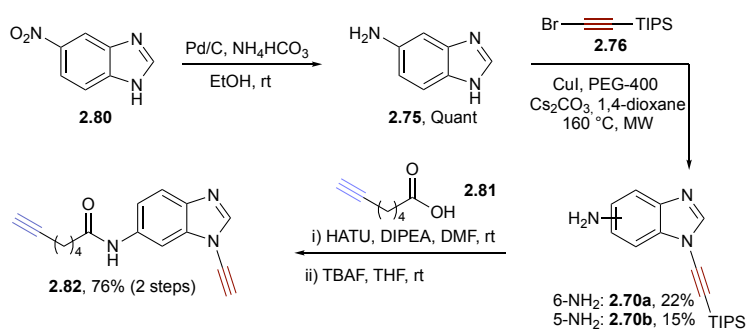
used as the corresponding azide (Scheme 2.20ii), which could be attributed either to the lower reactivity of aliphatic azides or to its increased steric component.



Scheme 2.20. Intermolecular competition reaction between **2.63** and **2.64** with two different azides (**2.65a** and **2.65c**). HPLC ratios.¹⁷¹

2.5.4.2 Intramolecular Chemoselective CuAAC Ligations

To further define the ynamine chemoselectivity profile, a CuAAC reaction using bifunctional scaffold **2.82** containing both an aromatic ynamine and a corresponding aliphatic alkyne was explored (Scheme 2.21).¹⁷¹

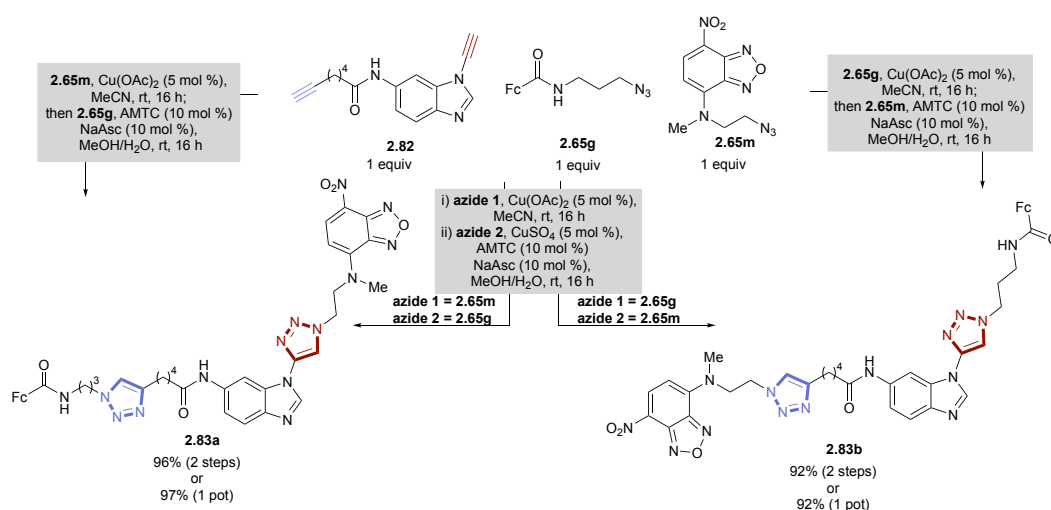


Scheme 2.21. Synthesis of the bifunctional system **2.82**. Isolated yields.¹⁷¹

Synthesis of **2.75** was achieved *via* hydrogenation of 5-nitrobenzimidazole **2.80**, affording 5-aminobenzimidazole **2.75** in quantitative yield. Copper-catalysed cross-coupling of **2.75** with

bromo-TIPS-acetylene **2.76** produced **2.70a** and **2.70b** (22% and 15%, respectively). Notably, no coupling of **2.76** at the anilinic site was observed. The major product **2.70a** was then used to form **2.82** via coupling with the corresponding acid **2.81**, followed by TIPS deprotection to produce **2.82** in 76% over two steps.

Two biologically-relevant azides **2.65g**-**2.65m** were chosen to test the chemoselectivity of the bifunctional system **2.82**. Ferrocene azide **2.65g** has been used extensively as an electrochemical reporter,¹⁷² while the green dye of NBD azide **2.65m** is widely used as a fluorescent probe for lipid membranes.¹⁷³ Consistent with the intermolecular competition reactions (Scheme 2.20), the reaction of **2.82** with **2.65m**, followed by **2.65g**, resulted in the exclusive formation of **2.83a** in a final yield of 96% (Scheme 2.22). Following the first click reaction, a workup procedure was conducted to confirm that it had occurred exclusively at the ynamine functionality. Reversing the sequence of addition (*i.e.*, **2.65g** followed by **2.65m**) produced the reverse click product **2.83b** in 92% yield, exemplifying the flexibility of the sequential ligation approach. Finally, the formation of **2.83a** and **2.83b** was achieved in a one-pot process controlled simply by the sequence of addition of the corresponding azide. Exclusive formation of the first CuAAC reaction at the ynamine position was observed in the presence of one equivalent of azide and Cu(OAc)₂. Addition of the second azide with ligand AMTC (10 mol %) and NaAsc (10 mol %), resulted in a second CuAAC reaction at the aliphatic alkyne position. This modular one-pot process resulted in the formation of **2.83a** and **2.83b** (97% and 92%, respectively).¹⁷¹



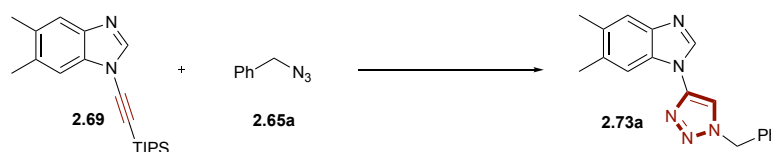
Scheme 2.22. Chemoselective sequential and one-pot CuAAC reactions with bifunctional system **2.82**. Isolated yields. Fc = Ferrocene.¹⁷¹

2.5.5 Aromatic Ynamine as a Synthon for CuAAC Reactions – Orthogonality Profile

2.5.5.1 Establishing Reaction Conditions for In-Situ TIPS-Deprotection/CuAAC Reactions with Aromatic Ynamines

It has been demonstrated that ynamines can be efficiently used in CuAAC reactions in a variety of standard conditions and with a wide range of azides. The reactivity differences between ynamines and aliphatic alkynes have also been established, allowing discrimination between the two alkynes in intermolecular and intramolecular contexts, even without protecting groups. In order to explore the orthogonality of the reaction, sequential CuAAC ligations using aromatic ynamine protecting groups is investigated below. The unique reactivity of aromatic ynamines may eliminate the need for conventional protecting group strategies through the use of a rapid *in-situ* deprotection of the silyl-protecting group, allowing improved modularity in the reaction. To test this hypothesis, a screen of *in-situ* TIPS-deprotection strategies followed by CuAAC reaction was investigated using **2.69** and benzyl azide **2.65a**.¹⁷⁴ Copper source, deprotecting agent, solvent, reductant, and ligand were surveyed (Table 2.4).

TIPS-deprotection was monitored by TLC and products were isolated upon reaction completion. TBAF resulted in extremely fast deprotection (< 2 min), whereas 3 h were required when using fluoride on polymer. DMSO was chosen as the solvent as protic solvents dramatically decrease the rate of deprotection when TBAF is used (1 h in MeOH, 2 h in DMSO/H₂O).^{175,176} Following deprotection, benzyl azide **2.65a** and Cu(OAc)₂ were added, affording the expected triazole **2.73a** after 30 min (66% with TBAF, 83% with fluoride on polymer, Entry 1-2). KHF₂ was also investigated as a deprotecting agent, giving a similar deprotection rate as TBAF, however, no subsequent CuAAC reaction was observed (Entry 3). Altering the solvent or adding reductant/ligand in the context of KHF₂ was not able to recover CuAAC reactivity and produced only the deprotected ynamine even after 16 h of reaction (Entry 4-5). The use of copper(II) fluoride (1 equiv.) in the presence of sodium ascorbate (NaAsc) and AMTC afforded the expected triazole **2.73a** after 16 h (90%, Entry 6). Attempts to decrease the amount of CuF₂ resulted in incomplete deprotection of the starting material **2.69**.

Table 2.4. Optimisation of in-situ TIPS-deprotection/CuAAC reaction.¹⁷⁴

Entry	Catalyst	Solvent	Additive	Deprotecting agent	Yield (%)
1	Cu(OAc) ₂	DMSO		TBAF	66
2	Cu(OAc) ₂	DMSO		Fluoride on polymer	83
3	Cu(OAc) ₂	DMSO		KHF ₂	0
4	Cu(OAc) ₂	DMSO/H ₂ O	NaAsc/AMTC	KHF ₂	0
5	Cu(OAc) ₂	MeOH		KHF ₂	0
6	CuF ₂	MeOH/H ₂ O	NaAsc/AMTC		90

2.69 (1.0 equiv., 0.15 mmol, 0.15 M), **2.65a** (1 equiv., 0.15 mmol, 0.15 M), Air, rt. Cu(OAc)₂ 5 mol %, CuF₂ (1 equiv.), (CH₃CN)₄Cu⁺PF₆⁻ (1 equiv.), additives (1.1 equiv.), deprotecting agents (1.1 equiv.). Isolated yields.

2.5.5.2 Controlling CuAAC Ligations using Aromatic Ynamine Protecting Groups

The chemoselectivity profile of TIPS-protected aromatic ynamine **2.69** and terminal alkyne **2.72** in the presence of benzyl azide **2.65a** was then investigated (Figure 2.4).¹⁷⁴

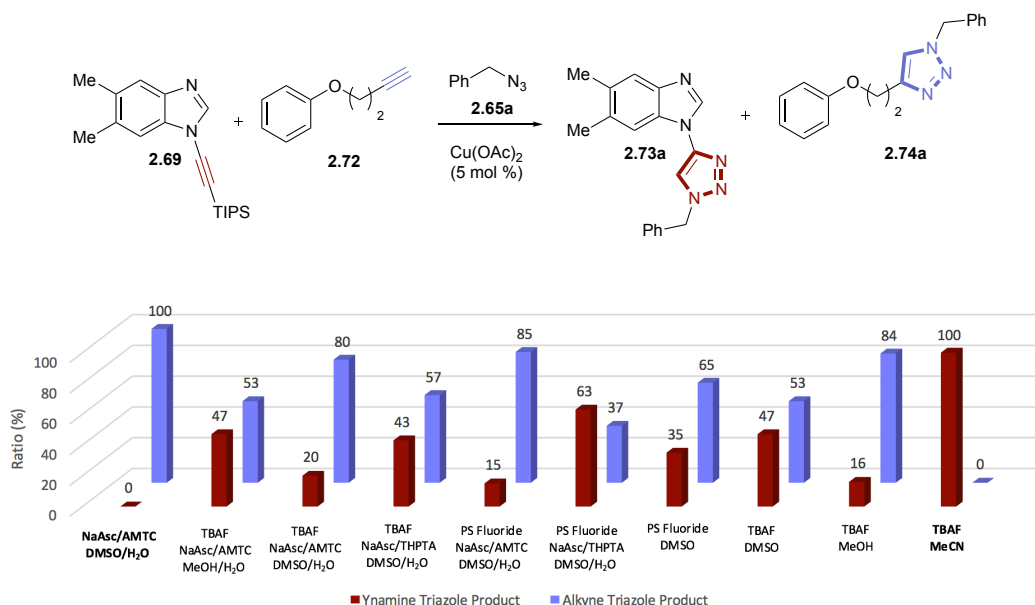


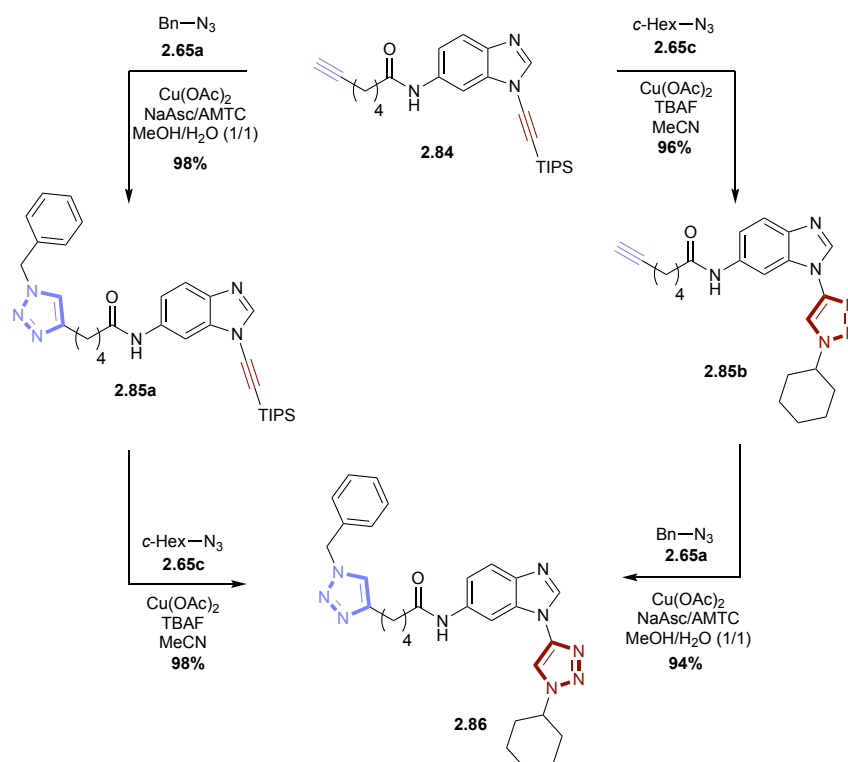
Figure 2.4. Optimisation of competition reaction between **2.69** and **2.72**. **2.69** (1.0 equiv., 0.031 mmol, 0.031 M), **2.72** (1.0 equiv., 0.031 mmol, 0.031 M), **2.65a** (1 equiv., 0.031 mmol, 0.031 M), Air, rt. Cu(OAc)₂ 5 mol %, additives (10 mol %), deprotecting agents (1.1 equiv.). NMR ratios.¹⁷⁴

Standard CuAAC conditions⁷⁰ - without adding deprotecting agent - afforded triazole **2.74a** without any degradation of the protected ynamine **2.69**. Adding TBAF or fluoride on polymer,

with or without reductant/ligand, afforded a mixture of both triazoles **2.73a** and **2.74a**. Negligible selectivity was observed in protic solvents, affording products **2.73a** and **2.74a** in a 16/84 mixture. A decrease in the rate of the CuAAC reaction was observed when MeCN was used as a solvent.¹⁷¹ An aprotic solvent presumably slows down the reduction of copper(II) (through the formation of the Glaser product)^{88,91} but also slows down the protonation of the copper-triazole complex.⁸⁸ Complete selectivity, in favour of **2.73a**, was obtained when Cu(OAc)₂ and TBAF were used in MeCN.

2.5.5.3 Substrate Scope of *In-Situ* TIPS-Deprotection/CuAAC Reactions

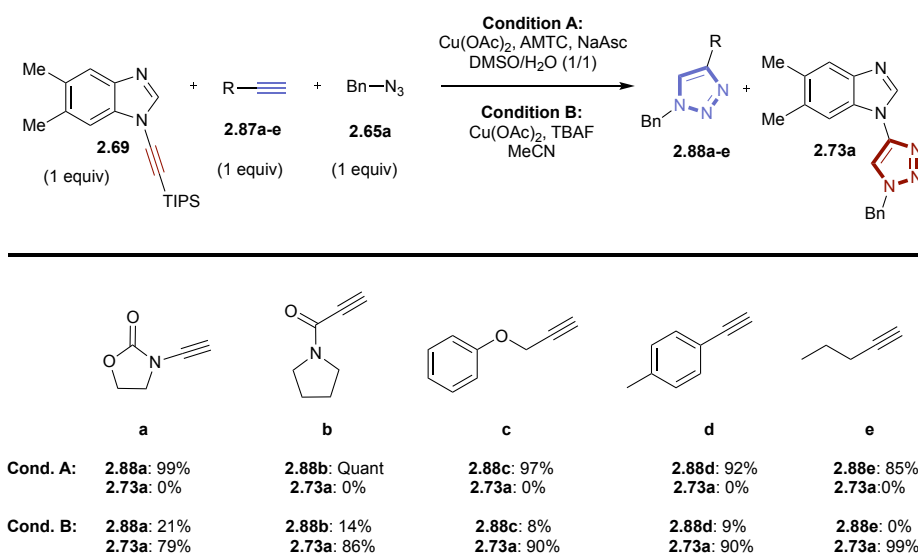
With the conditions for orthogonal, chemoselective CuAAC reactions established, the substrate scope was explored using the two optimised conditions (Scheme 2.23).¹⁷⁴ To promote the synthesis of ynamine triazoles **2.73a-s**, 5 mol % Cu(OAc)₂ and 1.1 equivalents of TBAF in MeCN were used. To promote the synthesis of alkyne triazoles **2.74a-s**, 5 mol % Cu(OAc)₂, 10 mol % NaAsc, and 10 mol % AMTC in DMSO/H₂O (1/1) were used. The reaction conditions tolerated a wide range of azides with varying steric bulk (*e.g.*, **d**, **o**), oxidisable functionalities (**i**) or potential Cu-chelating substrates (**h**, **m**, **p**, **q**, **r**, **s**). Reaction conditions also tolerated fluorophore azides (**m**, **q**, **r**), affording the expected triazoles in high yields. No loss of chemoselectivity was observed using either condition A or B. A notable exception was the CuAAC reactions of both **2.69** and **2.72** with azide **2.65r** which, due to the limited solubility of the FITC group, were conducted in MeOH and MeOH/H₂O, respectively. As seen previously during reaction optimisation (Figure 2.4), the use of MeOH results in a reduction of chemoselectivity. *In situ* TIPS-deprotection/CuAAC reaction between **2.69** and **2.65i** in these conditions still allowed the formation of the expected triazole **2.73r** with 85% yield after 16 h.



Scheme 2.24. Orthogonal CuAAC reactions using bifunctional system **2.84**, azides **2.65a** and **2.65c**. **2.84** (1.0 equiv., 0.2 M), **2.65a/2.65c** (1 equiv.), Cu(OAc)₂ (5 mol %), NaAsc (10 mol %), AMTC (10 mol %), TBAF (1.1 equiv.). Isolated yields.¹⁷⁴

2.5.6 Exploring Ynamine Reactivity vs Representative Terminal Alkynes in CuAAC Reactions

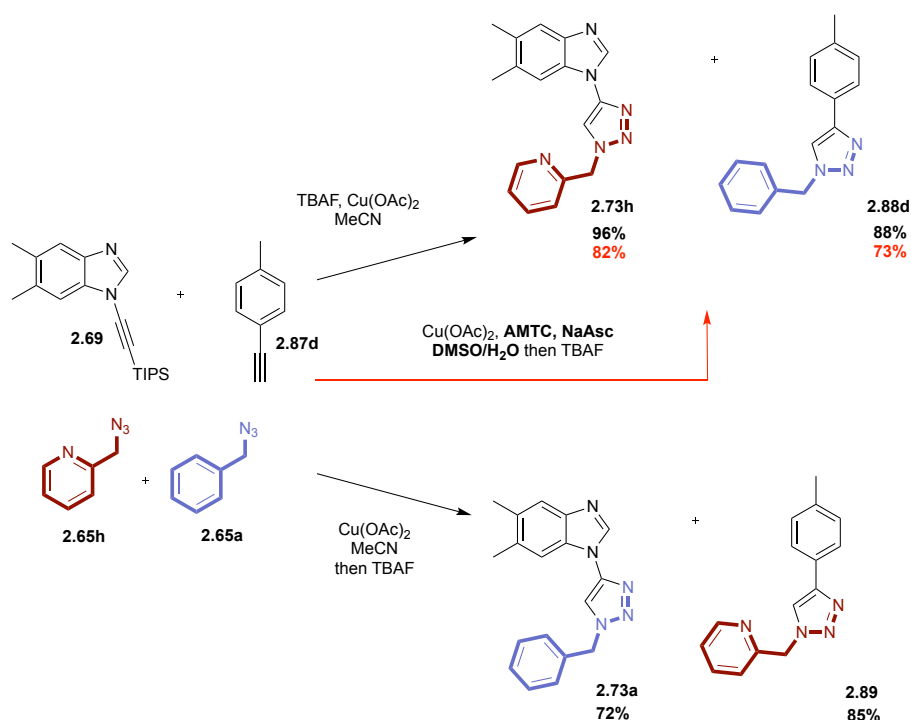
In order to compare the reactivity of aromatic ynamines with the different classes of alkynes present in the literature, competition reactions between aromatic ynamine **2.69** and alkynes **2.87a-e** were performed (Scheme 2.25).¹⁷⁴ Ynamide **2.87a**, developed by Hsung *et al.*,¹⁷⁷ propiolamide **2.87b**, developed by Finn *et al.*,¹⁴⁸ propargyl **2.87c**, aromatic **2.87d** and aliphatic **2.87e** alkynes were used as model substrates. When no deprotecting agent was used (Scheme 2.25, Condition A), full conversion to the expected alkyne triazoles **2.88a-e** was observed, with yields ranging between 85% to quantitative. Competition reactions between **2.69** and **2.87a-e** (Scheme 2.25, Condition B) showed high selectivity for the formation of the ynamine triazole **2.73a**. Only 21% of ynamide triazole **2.88a** and 14% of the propiolamide triazole **2.88b** was observed. Propargyl **2.87c** and aromatic **2.87d** alkynes showed similar reactivities (8% and 9%, respectively). Finally, when aliphatic alkyne **2.87e** was used, full selectivity for the formation of the ynamine triazole **2.73a** was observed.



Scheme 2.25. Competition reactions between **2.69** with a variety of representative alkynes. **2.69/2.87a-e** (1.0 equiv., 0.41 mmol, 0.2 M), **2.65a** (1 equiv., 0.41 mmol), $\text{Cu}(\text{OAc})_2$ (5 mol %), *NaAsc* (10 mol %), *AMTC* (10 mol %), *TBAF* (1.1 equiv.). Isolated yields.¹⁷⁴

2.5.7 Ynamine Chemoselectivity vs Azide Chelate-Directed Strategy

With the orthogonal chemoselectivity of the CuAAC reaction demonstrated in both intermolecular and intramolecular contexts, 2 + 2 competition reactions were explored using aromatic ynamine **2.69**, aromatic alkyne **2.87d**, chelating azide **2.65h**, and benzyl azide **2.65a** (Scheme 2.26).¹⁷⁴ Employing our optimised conditions and Zhu's chelate-directed strategy¹⁵⁷ provided triazoles **2.73h** and **2.88d** in 96% and 88% yield, respectively. Conversely, adding *TBAF* after the first CuAAC reaction allowed the formation of **2.73a** and **2.89** in 72% and 85% yield, respectively. Interestingly, the addition of reductant and ligand (*AMTC*) to the reaction resulted in the formation of **2.73h** (82%) and **2.88d** (73%). These results show that, by using the enhanced reactivity of aromatic ynamines in conjunction with a chelate-directed strategy at the ynamine and azide moieties, our optimised conditions allow chemoselective and orthogonal CuAAC ligations.



Scheme 2.26. 2 + 2 competition reaction using aromatic ynamine **2.69**, aromatic alkyne **2.87d**, azides **2.65a** and **2.65h**. **2.69/2.87d** (1.0 equiv., 0.2 M), **2.65a/2.65h** (1 equiv.), Cu(OAc)_2 (5 mol %), NaAsc (10 mol %), AMTC (10 mol %), TBAF (1.1 equiv.). Isolated yields.¹⁷⁴

2.6 Summary

This work describes the optimisation of orthogonal, chemoselective CuAAC reactions using the enhanced reactivity of aromatic ynamines. The rapid preparation of aromatic ynamines was facilitated by microwave-assisted synthesis (5 min versus 48 h for benzimidazole ynamine). Ynamines were shown to be reactive substrates in CuAAC reactions in a variety of conditions and with a wide range of azides. The reactivity differences between ynamines and aliphatic alkynes was established, allowing discrimination between the two alkynes in both intermolecular and intramolecular contexts without the need for protecting groups. Additionally, silyl protection of aromatic ynamines enabled CuAAC reactions to take place with less reactive alkyne substrates first. The higher reactivity of aromatic ynamines was further demonstrated in competition reactions with representative terminal alkynes, even in the presence of the most competitive alkynes previously described in the literature. Finally, the utility of an azide chelate-directed strategy was shown to be limited when a reductant and ligand were included in the reaction, whereas similar yields were obtained with or without the

use of reductant/ligand when aromatic ynamines are used. These findings represent a novel strategy for the chemoselective ligation of biomolecules.

2.7 Experimental

2.7.1 Reagents and Solvents

All reagents were used as supplied from commercial sources (Fisher, Fluorochem, Sigma-Aldrich) and used without further purification unless otherwise stated. PEG-400 was supplied from ABCR. Solvents were all HPLC grade and were used without further purification, unless otherwise stated.

2.7.2 Analysis of Products

2.7.2.1 NMR Spectroscopy

NMR spectroscopy was carried out using either a Bruker AV3 400 MHz UltraShield™ B-ACS 60 spectrometer or AV Bruker DRX 500 MHz. All chemical shifts (δ) were referenced to the deuterium lock and are reported in parts per million (ppm). Coupling constants are quoted in hertz (Hz). Abbreviations for splitting patterns are s (singlet), br. s (broad singlet), d (doublet), t (triplet), q (quartet), app. quint (apparent quintuplet) and m (multiplet). All NMR data was processed using TopSpin 3.2 software. Proton and carbon chemical shifts were assigned using proton (^1H), carbon (^{13}C), Heteronuclear Single Quantum Coherence (HSQC), Heteronuclear Multiple-Bond Correlation Spectroscopy (HMBC) and Correlation Spectroscopy (COSY).

2.7.2.2 Liquid Chromatography-Mass Spectrometry (LC-MS) and High-Performance Liquid Chromatography (HPLC)

LC-MS was carried out on an Agilent HPLC instrument in conjunction with an Agilent Quadrupole mass detector. Electrospray ionization (ESI) was used in all cases. HPLC was carried out on a Dionex Ultimate 3000 series instrument (see Appendix for method and column parameters).

2.7.2.3 *Infra-Red (IR) Spectroscopy*

IR data was collected on an Agilent spectrometer and the data processed using Spectrum One software. Only major absorbances are reported (> 50 %).

2.7.3 *General Procedures*

General Procedure A: General conditions for the synthesis of aromatic ynamines (Scheme 2.18)

To a degassed solution of amine (1 equiv.), PEG-400 (0.1 equiv.), CuI (0.05 equiv.) and Cs₂CO₃ (1.2 equiv.) in 1,4-dioxane (0.2 M) under argon was added bromo-TIPS-acetylene **2.76** (2.2 equiv.). The mixture was heated to 160 °C in a microwave (Biotage Initiator+ Sixty) and stirred for 1 h, after which Et₂O (50 mL) was added. The mixture was washed with aq. EDTA (10 mg/mL, 10 mL), and brine (2 x 10 mL), dried over Na₂SO₄ and then concentrated under reduced pressure. The resulting residue was purified by flash chromatography (silica gel) to provide the desired compound.

General Procedure B: Optimisation of the synthesis of **2.66a** (Table 2.2)

To a solution of 1-ethynyl-1*H*-benzo[d]imidazole **2.63** (71 mg, 0.5 mmol, 1 equiv.) and benzyl azide **2.65a** (63 µL, 0.5 mmol, 1 equiv.) in 2 mL of solvent was added 5 mol % catalyst. The reaction was stirred at rt for 4 h, after which EtOAc was added. The mixture was washed with aq. EDTA (10 mg/mL, 10 mL) and brine (2 x 10 mL), dried over Na₂SO₄ and then concentrated under reduced pressure. The resulting residue was purified by flash chromatography (silica gel, hexane/EtOAc 3/7) to provide the desired compound.

General Procedure C: Optimisation of the synthesis of **2.67a** (Table 2.3)

To a solution of *N*-phenyl-6-heptynamide **2.64** (11 mg, 0.05 mmol, 1 equiv.) and benzyl azide **2.65a** (6 µL, 0.05 mmol, 1 equiv.) in 1 mL of solvent was added 5 mol % catalyst. The reaction was stirred at rt for 16 h, after which EtOAc was added. The mixture was washed with aq. EDTA (10 mg/mL, 10 mL) and brine (2 x 10 mL), dried over Na₂SO₄ and then concentrated under reduced pressure. The resulting residue was purified by flash chromatography (silica gel, hexane/EtOAc 3/7) to provide the desired compound.

General Procedure D: Synthesis of compounds **2.66a-n** (Scheme 2.19)

To a solution of 1-ethynyl-1*H*-benzo[d]imidazole **2.63** (71 mg, 0.5 mmol, 1 equiv.) and azide **2.65a-n** (0.5 mmol, 1 equiv.) in 2 mL of solvent was added Cu(OAc)₂ (4.5 mg, 0.03 mmol,

0.05 equiv.). The reaction was stirred at rt for 16 h, before being filtered through celite and concentrated under reduced pressure. The resulting residue was purified by flash chromatography (silica gel) to provide the desired compounds.

General Procedure E: Optimisation of the synthesis of **2.73a** (Table 2.4)

To a solution of 5,6-dimethyl-1-((triisopropylsilyl)ethynyl)-1*H*-benzo[*d*]imidazole **2.69** (50 mg, 0.15 mmol, 1 equiv.) and benzyl azide **2.65a** (19 μ L, 0.15 mmol, 1 equiv.) in 1 mL of solvent was added deprotecting agent (1.1 equiv.) followed by copper catalyst (0.05 equiv.). The reaction was stirred at rt and monitored by TLC (hexane/EtOAc 1/1) until completion, after which EtOAc was added. The mixture was washed with aq. EDTA (10 mg/mL, 10 mL) and brine (2 x 10 mL), dried over Na₂SO₄ and then concentrated under reduced pressure. The resulting residue was purified by flash chromatography (silica gel, hexane/EtOAc 3/7) to provide the desired compound.

General Procedure F: Optimisation of the synthesis of **2.73a/2.74a** (Figure 2.3)

To a solution of 5,6-dimethyl-1-((triisopropylsilyl)ethynyl)-1*H*-benzo[*d*]imidazole **2.69** (10 mg, 0.031 mmol, 1 equiv.), (but-3-yn-1-yloxy)benzene **2.72** (5 mg, 0.031 mmol, 1 equiv.) and benzyl azide **2.65a** (4 μ L, 0.031 mmol, 1 equiv.) in 1 mL of solvent was added deprotecting agent (0.034 mmol, 1.1 equiv.) followed by copper catalyst (0.05 equiv.). The reaction was stirred at rt for 16 h, after which EtOAc was added. The mixture was washed with aq. EDTA (10 mg/mL, 5 mL) and brine (2 x 5 mL), dried over Na₂SO₄ and then concentrated under reduced pressure. NMR of crude material was used to determine compound identity and composition.

General Procedure G: Synthesis of compounds **2.73a-s** (Scheme 2.23)

To a solution of 5,6-dimethyl-1-((triisopropylsilyl)ethynyl)-1*H*-benzo[*d*]imidazole **2.69** (45 mg, 0.14 mmol, 1 equiv.), (but-3-yn-1-yloxy)benzene **2.72** (20 mg, 0.14 mmol, 1 equiv.) and azide **2.65a-s** (0.14 mmol, 1 equiv.) in MeCN (1 mL) was added TBAF (49 μ L, 0.15 mmol, 1.1 equiv.) followed by Cu(OAc)₂ (1 mg, 0.007 mmol, 0.05 equiv.). The reaction was stirred at rt for 16 h, after which EtOAc was added. The mixture was washed with aq. EDTA (10 mg/mL, 10 mL) and brine (2 x 10 mL), dried over Na₂SO₄ and then concentrated under reduced pressure. The resulting residue was purified by flash chromatography (silica gel) to provide the desired compounds.

General Procedure H: Synthesis of compounds **2.74a-s** (Scheme 2.23)

To a solution of 5,6-dimethyl-1-((triisopropylsilyl)ethynyl)-1*H*-benzo[*d*]imidazole **2.69** (45 mg, 0.14 mmol, 1 equiv.), (but-3-yn-1-yloxy)benzene **2.72** (20 mg, 0.14 mmol, 1 equiv.) and azide **2.65a-s** (0.14 mmol, 1 equiv.) in DMSO/H₂O (1/1, 1 mL) was added AMTC (3 mg, 0.014 mmol, 0.1 equiv.) followed by Cu(OAc)₂ (1 mg, 0.007 mmol, 0.05 equiv.) and NaAsc (3 mg, 0.014 mmol, 0.1 equiv.). The reaction was stirred at rt for 16 h, after which EtOAc was added. The mixture was washed with aq. EDTA (10 mg/mL, 10 mL) and brine (2 x 10 mL), dried over Na₂SO₄ and then concentrated under reduced pressure. The resulting residue was purified by flash chromatography (silica gel) to provide the desired compounds.

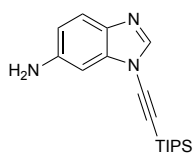
General Procedure I: Synthesis of compound **2.73a** (Scheme 2.25).

To a solution of 5,6-dimethyl-1-((triisopropylsilyl)ethynyl)-1*H*-benzo[*d*]imidazole **2.69** (132 mg, 0.41 mmol, 1 equiv.), alkyne **2.87a-e** (0.41 mmol, 1 equiv.) and benzyl azide **2.65a** (53 μL, 0.41 mmol, 1 equiv.) in MeCN (2 mL) was added TBAF (147 μL, 0.45 mmol, 1.1 equiv.) followed by Cu(OAc)₂ (3 mg, 0.02 mmol, 0.05 equiv.). The reaction was stirred at rt for 16 h, after which EtOAc was added. The mixture was washed with aq. EDTA (10 mg/mL, 10 mL) and brine (2 x 10 mL), dried over Na₂SO₄ and then concentrated under reduced pressure. The resulting residue was purified by flash chromatography (silica gel) to provide the desired compound.

General Procedure J: Synthesis of compounds **2.88a-e** (Scheme 2.25).

To a solution of 5,6-dimethyl-1-((triisopropylsilyl)ethynyl)-1*H*-benzo[*d*]imidazole **2.69** (132 mg, 0.41 mmol, 1 equiv.), alkyne **2.87a-e** (0.41 mmol, 1 equiv.) and benzyl azide **2.65a** (53 μL, 0.41 mmol, 1 equiv.) in DMSO/H₂O (1/1, 1 mL) was added AMTC (9 mg, 0.041 mmol, 0.1 equiv.) followed by Cu(OAc)₂ (3 mg, 0.02 mmol, 0.05 equiv.) and NaAsc (9 mg, 0.041 mmol, 0.1 equiv.). The reaction was stirred at rt for 16 h, after which EtOAc was added. The mixture was washed with aq. EDTA (10 mg/mL, 10 mL) and brine (2 x 10 mL), dried over Na₂SO₄ and then concentrated under reduced pressure. The resulting residue was purified by flash chromatography (silica gel) to provide the desired compounds.

2.7.4 Synthetic procedures**2.7.4.1 Product from Scheme 2.18****2.70a:** 1-((Triisopropylsilyl)ethynyl)-1*H*-benzo[*d*]imidazol-6-amine



Prepared according to General Procedure A using 1*H*-benzo[*d*]imidazol-5-amine **2.75** (1 g, 7.5 mmol, 1 equiv.), cesium carbonate (3 g, 9 mmol, 1.2 equiv.), copper iodide (72 mg, 0.38 mmol, 0.05 equiv.), PEG-400 (1.3 g) and (bromoethynyl)triisopropylsilane **2.76** (4.3 g, 16.5 mmol, 2.2 equiv.) in dioxane (10 mL). The resulting residue was purified by flash chromatography (silica gel, 0-30% EtOAc/hexane) to provide the desired product as a white solid (0.5 g, 22%).

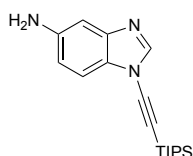
¹H-NMR (CDCl₃, 400 MHz): δ 7.86 (s, 1H, Ar-H), 7.53 (d, *J* = 8.4 Hz, 1H, Ar-H), 6.77 (d, *J* = 1.5 Hz, 1H, Ar-H), 6.70 (dd, *J* = 8.5, 1.5 Hz, 1H, Ar-H), 3.86 (br. s, 2H, NH₂), 1.15 (br. s, 21H, TIPS).

¹³C-NMR (CDCl₃, 100 MHz): δ 144.2, 141.2, 135.4, 134.5, 120.7, 112.9, 95.4, 90.0, 71.9, 18.1, 10.7.

IR ν_{\max} (neat): 3361, 3209, 2941, 2863, 2185, 1619, 1498, 1459, 1209, 1072, 884, 821, 746 cm⁻¹.

HRMS (ESI): C₁₈H₂₈N₃Si [M+H]⁺ calculated 314.2052, found 314.2047.

2.70b: 1-((Triisopropylsilyl)ethynyl)-1*H*-benzo[*d*]imidazol-5-amine



Prepared according to General Procedure A using 1*H*-benzo[*d*]imidazol-5-amine **2.75** (1 g, 7.5 mmol, 1 equiv.), cesium carbonate (3 g, 9 mmol, 1.2 equiv.), copper iodide (72 mg, 0.38 mmol, 0.05 equiv.), PEG-400 (1.3 g) and (bromoethynyl)triisopropylsilane **2.76** (4.3 g, 16.5 mmol, 2.2 equiv.) in dioxane (10 mL). The resulting residue was purified by flash chromatography (silica gel, 50-100% EtOAc/hexane) to provide the desired product as a white solid (0.3 g, 15%).

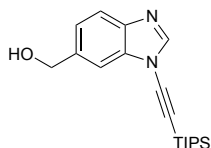
¹H-NMR (CDCl₃, 400 MHz): δ 7.97 (s, 1H, Ar-H), 7.29 (d, *J* = 8.4 Hz, 1H, Ar-H), 7.06 (s, 1H, Ar-H), 6.79 (d, *J* = 8.2 Hz, 1H, Ar-H), 3.75 (br. s, 2H, NH₂), 1.15 (br. s, 21H, TIPS).

¹³C-NMR (CDCl₃, 100 MHz): δ 144.0, 143.8, 143.1, 128.2, 114.4, 111.3, 105.6, 90.6, 72.4, 18.7, 11.3.

IR ν_{\max} (neat): 3330, 3208, 2943, 3864, 2181, 1621, 1594, 1486, 1450, 1238, 1141, 994, 854 cm⁻¹.

HRMS (ESI): C₁₈H₂₈N₃Si [M+H⁺] calculated 314.2052, found 314.2045.

2.71a: (1-((Triisopropylsilyl)ethynyl)-1*H*-benzo[*d*]imidazol-6-yl)methanol



Prepared according to General Procedure A using (1*H*-benzo[*d*]imidazol-6-yl)methanol **2.77** (1 g, 6.8 mmol, 1 equiv.), cesium carbonate (2.6 g, 8.1 mmol, 1.2 equiv.), copper iodide (64 mg, 0.34 mmol, 0.05 equiv.), PEG-400 (1.1 g) and (bromoethynyl)triisopropylsilane **2.76** (3.9 g, 14.9 mmol, 2.2 equiv.) in dioxane (11 mL). The resulting residue was purified by flash chromatography (silica gel, 50-70% EtOAc/hexane) to provide the desired product as a yellow oil (304 mg, 14%).

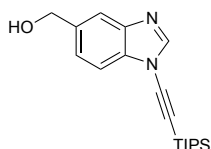
¹H-NMR (CDCl₃, 400 MHz): δ 8.02 (s, 1H, Ar-H), 7.68 (d, *J* = 8.3 Hz, 1H, Ar-H), 7.56 (s, 1H, Ar-H), 7.30 (dd, *J* = 8.3, 1.5 Hz, 1H, Ar-H), 4.83 (s, 2H, CH₂), 3.23 (br. s, 1H, OH), 1.14 (br. s, 21H, TIPS).

¹³C-NMR (CDCl₃, 100 MHz): δ 144.3, 138.3, 123.4, 121.0, 109.6, 65.6, 18.8, 11.4.

IR ν_{max} (neat): 3290, 2937, 2885, 2859, 2181, 1621, 1500, 1444, 1281, 1219, 1074, 883, 818 cm⁻¹.

HRMS (ESI): C₁₉H₂₈N₂OSi [M+H⁺] calculated 329.2044, found 329.2045.

2.71b: (1-((Triisopropylsilyl)ethynyl)-1*H*-benzo[*d*]imidazol-5-yl)methanol



Prepared according to General Procedure A using (1*H*-benzo[*d*]imidazol-6-yl)methanol **2.77** (1 g, 6.8 mmol, 1 equiv.), cesium carbonate (2.6 g, 8.1 mmol, 1.2 equiv.), copper iodide (64 mg, 0.34 mmol, 0.05 equiv.), PEG-400 (1.1 g) and (bromoethynyl)triisopropylsilane **2.76** (3.9 g, 14.9 mmol, 2.2 equiv.) in dioxane (11 mL). The resulting residue was purified by flash chromatography (silica gel, 50-70% EtOAc/hexane) to provide the desired product as a white solid (0.4 mg, 18%).

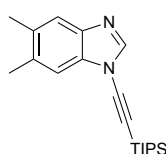
¹H-NMR (CDCl₃, 400 MHz): δ 8.08 (s, 1H, Ar-H), 7.80–7.79 (m, 1H, Ar-H), 7.53 (d, *J* = 8.3 Hz, 1H, Ar-H), 7.43 (dd, *J* = 8.3, 1.4 Hz, 1H, Ar-H), 4.82 (d, *J* = 5.6 Hz, 2H, CH₂), 1.93 (t, *J* = 5.9 Hz, 1H, OH), 1.17 (br. s, 21H, TIPS).

¹³C-NMR (CDCl₃, 100 MHz): δ 137.4, 124.4, 119.4, 111.2, 73.3, 65.6, 60.5, 21.2, 18.8, 11.4.

IR ν_{max} (neat): 3296, 2937, 2885, 2859, 2188, 1498, 1463, 1439, 1277, 1203, 1095, 883, 786 cm⁻¹.

HRMS (ESI): C₁₉H₂₈N₂OSi [M+H]⁺ calculated 329.2044, found 329.2045.

2.69: 5,6-Dimethyl-1-((triisopropylsilyl)ethynyl)-1*H*-benzo[*d*]imidazole¹⁶⁵

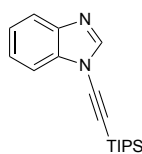


Prepared according to General Procedure A using 5,6-dimethyl-1*H*-benzo[*d*]imidazole **2.78** (1 g, 6.8 mmol, 1 equiv.), cesium carbonate (2.7 g, 8.2 mmol, 1.2 equiv.), copper iodide (65 mg, 0.34 mmol, 0.05 equiv.), PEG-400 (1.1 g) and (bromoethynyl)triisopropylsilane **2.76** (2 g, 7.5 mmol, 1.1 equiv.) in dioxane (11 mL). The resulting residue was purified by flash chromatography (silica gel, hexane/EtOAc 9/1) to provide the desired product as an orange oil (1.8 g, 81%).

¹H-NMR (CDCl₃, 500 MHz): δ 7.96 (s, 1H, Ar-H), 7.55 (s, 1H, Ar-H), 7.29 (s, 1H, Ar-H), 2.41 (s, 3H, CH₃), 2.38 (s, 3H, CH₃), 1.72–1.64 (m, 21H, TIPS).

¹³C-NMR (CDCl₃, 100 MHz): δ 143.1, 140.4, 134.3, 133.1, 133.0, 120.9, 111.2, 90.7, 72.5, 20.7, 20.3, 18.8, 11.4.

2.68: 1-((Triisopropylsilyl)ethynyl)-1*H*-benzo[*d*]imidazole¹⁶⁵



Prepared according to General Procedure A using 5,6-dimethyl-1*H*-benzo[*d*]imidazole **2.79** (2 g, 16.9 mmol, 1 equiv.), cesium carbonate (6.6 g, 20.3 mmol, 1.2 equiv.), copper iodide (160 mg, 0.85 mmol, 0.05 equiv.), PEG-400 (2.2 g) and (bromoethynyl)triisopropylsilane **2.76** (4.9 g, 18.6 mmol, 1.1 equiv.) in dioxane (10 mL). The resulting residue was purified by flash

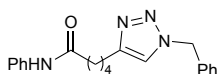
chromatography (silica gel, hexane/EtOAc 9/1) to provide the desired product as an orange oil (4.5 g, 89%).

¹H-NMR (CDCl₃, 500 MHz): δ 8.08 (s, 1H, Ar-H), 7.81 (d, *J* = 8.3 Hz, 1H, Ar-H), 7.56 (d, *J* = 8.1 Hz, 1H, Ar-H), 7.43–7.40 (m, 1H, Ar-H), 7.36 (td, *J* = 7.9, 1.1 Hz, 1H, Ar-H), 1.17 (br. s, 21H, TIPS).

¹³C-NMR (CDCl₃, 100 MHz): δ 143.7, 141.8, 134.6, 124.8, 124.0, 120.8, 111.0, 90.1, 73.0, 18.6, 17.7.

2.7.4.2 Product from Table 2.3

2.67a: 5-(1-Benzyl-1*H*-1,2,3-triazol-4-yl)-*N*-phenylpentanamide



Prepared according to General Procedure C using *N*-phenyl-6-heptynamide **2.64** (11 mg, 0.05 mmol, 1 equiv.), benzyl azide **2.65a** (6 μL, 0.05 mmol, 1 equiv.), AMTC (1 mg, 0.005 mmol, 0.1 equiv.), CuSO₄ (0.4 mg, 0.0025 mmol, 0.05 equiv.) and NaAsc (1 mg, 0.005 mmol, 0.1 equiv.) in MeOH/H₂O (1/1, 1 mL). The resulting residue was purified by flash chromatography (silica gel, hexane/EtOAc 3/7) to provide the desired product as a white solid (108 mg, 93%).

¹H-NMR (CDCl₃, 400 MHz): δ 8.11 (s, 1H, triazole-H), 7.59–7.56 (m, 2H, Ar-H), 7.35–7.34 (m, 5H, Ar-H), 7.29–7.22 (m, 2H, Ar-H), 7.07–7.04 (m, 1H, Ar-H), 5.46 (s, 2H, benzylic CH₂), 2.73 (t, *J* = 7.0 Hz, 2H, triazole-CH₂), 2.39 (t, *J* = 6.7 Hz, 2H, CO-CH₂), 1.75 (br. s, 4H, CH₂).

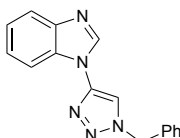
¹³C-NMR (CDCl₃, 125 MHz): δ 171.6, 138.4, 134.8, 129.2, 129.0, 128.8, 128.1, 124.0, 119.9, 54.3, 37.1, 29.8, 28.6, 25.3, 25.0.

IR ν_{\max} (neat): 3294, 3110, 3062, 3036, 2932, 2855, 1653, 1602, 1545, 1532, 1444, 1316, 1178, 1132, 1056, 1030, 710, 693 cm⁻¹.

HRMS (ESI): C₂₀H₂₂N₄NaO [M+Na]⁺ calculated 357.1672, found 357.1672.

2.7.4.3 Products from Scheme 2.19

2.66a: 1-(1-Benzyl-1*H*-1,2,3-triazol-4-yl)-1*H*-benzo[*d*]imidazole



Prepared according to General Procedure D using 1-ethynyl-1*H*-benzo[d]imidazole **2.63** (71 mg, 0.5 mmol, 1 equiv.), benzyl azide **2.65a** (63 μ L, 0.5 mmol, 1 equiv.) and Cu(OAc)₂ (5 mg, 0.025 mmol, 0.05 equiv.). The resulting residue was purified by flash chromatography (silica gel, hexane/EtOAc 3/7) to provide the desired product as a white solid (126 mg, 92% in MeCN).

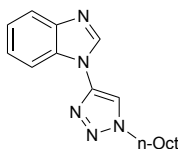
¹H-NMR (CDCl₃, 400 MHz): δ 8.32 (s, 1H, Ar-H), 7.84–7.82 (m, 1H, Ar-H), 7.70 (s, 1H, triazole-H), 7.64–7.62 (m, 1H, Ar-H), 7.42–7.31 (m, 7H, 7 x Ar-H), 5.61 (s, 2H, benzylic CH₂).

¹³C-NMR (CDCl₃, 125 MHz): δ 143.9, 142.8, 141.4, 133.9, 129.5, 129.3, 128.3, 124.3, 123.3, 120.8, 113.8, 111.1, 55.2.

IR ν_{\max} (neat): 2924, 2855, 1615, 1584, 1496, 1495, 1455, 1302, 1264, 1214, 1212, 1200, 950, 764, 745, 713 cm⁻¹.

HRMS (ESI): C₁₆H₁₄N₅ [M+H]⁺ calculated 276.1249, found 276.1244.

2.66b: 1-(1-Octyl-1*H*-1,2,3-triazol-4-yl)-1*H*-benzo[d]imidazole



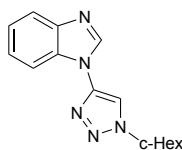
Prepared according to General Procedure D using 1-ethynyl-1*H*-benzo[d]imidazole **2.63** (71 mg, 0.5 mmol, 1 equiv.), 1-azidooctane **2.65b** (78 mg, 0.5 mmol, 1 equiv.) and Cu(OAc)₂ (5 mg, 0.025 mmol, 0.05 equiv.). The resulting residue was purified by flash chromatography (silica gel, 20-90% EtOAc/petroleum ether) to provide the desired product as a colourless oil (118 mg, 80%).

¹H-NMR (CDCl₃, 500 MHz): δ 8.38 (s, 1H, Ar-H), 7.87 (d, J = 7.4 Hz, 1H, Ar-H), 7.79 (s, 1H, triazole-H), 7.67 (d, J = 7.5 Hz, 1H, Ar-H), 7.38 (app. quint, J = 6.8 Hz, 2H, Ar-H), 4.47 (t, J = 7.3 Hz, 2H, triazole-CH₂), 2.01 (app. quint, J = 7.1 Hz, 2H, CH₂), 1.43–1.26 (m, 10H, CH₂), 0.88 (t, J = 6.7 Hz, 3H, CH₃).

¹³C-NMR (CDCl₃, 126 MHz): δ 144.0, 142.5, 141.4, 132.8, 124.4, 123.4, 120.9, 113.8, 111.1, 51.5, 31.8, 30.4, 29.2, 29.1, 26.6, 22.7, 14.2.

IR ν_{\max} (neat): 3120, 2925, 2855, 1614, 1584, 1493, 1454, 1301, 1204, 1136, 1055, 948, 740 cm⁻¹.

HRMS (ESI): C₁₇H₂₄N₅ [M+H]⁺ calculated 298.2032, found 298.2032.

2.66c: 1-(1-Cyclohexyl-1*H*-1,2,3-triazol-4-yl)-1*H*-benzo[d]imidazole

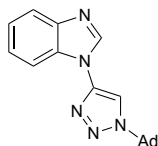
Prepared according to General Procedure D using 1-ethynyl-1*H*-benzo[d]imidazole **2.63** (71 mg, 0.5 mmol, 1 equiv.), azidocyclohexane **2.65c** (63 mg, 0.5 mmol, 1 equiv.) and Cu(OAc)₂ (5 mg, 0.025 mmol, 0.05 equiv.). The resulting residue was purified by flash chromatography (silica gel, hexane/EtOAc 3/7) to provide the desired product as a white solid (112 mg, 83%).

¹H-NMR (CDCl₃, 500 MHz): δ 8.37 (s, 1H, Ar-H), 7.87 (dd, *J* = 7.2, 2.3 Hz, 1H, Ar-H), 7.80 (s, 1H, triazole-H), 7.69 (dd, *J* = 6.7, 1.8 Hz, 1H, Ar-H), 7.40–7.34 (m, 2H, Ar-H), 4.56 (tt, *J* = 12.0, 4.6 Hz, 1H, CH), 2.33 (dd, *J* = 13.4, 2.4 Hz, 2H, CH₂), 2.00 (dt, *J* = 13.5, 3.0 Hz, 2H, CH₂), 1.87–1.81 (m, 3H, CH₂ and 1 x H from diastereotopic CH₂), 1.55–1.51 (m, 2H, CH₂), 1.35 (tt, *J* = 13.3, 3.5 Hz, 1H, 1 x H from diastereotopic CH₂).

¹³C-NMR (CDCl₃, 126 MHz): δ 143.9, 142.1, 141.5, 124.3, 123.4, 120.8, 112.0, 111.1, 61.3, 33.6, 25.2.

IR *v*_{max} (neat): 2927, 2854, 1610, 1579, 1448, 1293, 1125, 1055, 1203, 948, 756, 773 cm⁻¹.

HRMS (ESI): C₁₅H₁₈N₅ [M+H]⁺ calculated 268.1557, found 268.1548.

2.66d: 1-(1-(Adamantan-1-yl)-1*H*-1,2,3-triazol-4-yl)-1*H*-benzo[d]imidazole

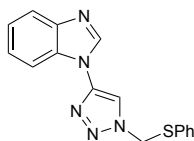
Prepared according to General Procedure D using 1-ethynyl-1*H*-benzo[d]imidazole **2.63** (71 mg, 0.5 mmol, 1 equiv.), 1-azidoadamantane **2.65d** (89 mg, 0.5 mmol, 1 equiv.) and Cu(OAc)₂ (5 mg, 0.025 mmol, 0.05 equiv.). The resulting residue was purified by flash chromatography (silica gel, hexane/EtOAc 3/7) to provide the desired product as a white solid (103 mg, 65%).

¹H-NMR (CDCl₃, 500 MHz): δ 8.40 (s, 1H, Ar-H), 7.89 (d, *J* = 5.0 Hz, 1H, Ar-H), 7.84 (s, 1H, triazole-H), 7.73 (br. s, 1H, Ar-H), 7.38–7.37 (m, 2H, Ar-H), 2.35 (app. s, 10H, 2 x CH and 4 x CH₂), 1.85 (s, 5H, 1 x CH and 2 x CH₂).

¹³C-NMR (CDCl₃, 126 MHz): δ 124.3, 123.3, 120.8, 111.3, 111.0, 61.1, 43.1, 35.9, 31.0, 29.6.

IR *v*_{max} (neat): 3131, 2913, 2850, 1614, 1580, 1453, 1296, 1212, 1134, 1013, 815, 739 cm⁻¹.

HRMS (ESI): C₁₉H₂₂N₅ [M+H]⁺ calculated 320.1870, found 320.1862.

2.66e: 1-(1-((Phenylthio)methyl)-1*H*-1,2,3-triazol-4-yl)-1*H*-benzo[d]imidazole

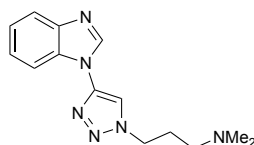
Prepared according to General Procedure D using 1-ethynyl-1*H*-benzo[d]imidazole **2.63** (71 mg, 0.5 mmol, 1 equiv.), azidomethylphenylsulfane **2.65e** (83 mg, 0.5 mmol, 1 equiv.) and Cu(OAc)₂ (5 mg, 0.025 mmol, 0.05 equiv.). The resulting residue was purified by flash chromatography (silica gel, hexane/EtOAc 3/7) to provide the desired product as a white solid (133 mg, 89%).

¹H-NMR (CDCl₃, 500 MHz): δ 8.39 (s, 1H, Ar-H), 7.88 (s, 1H, triazole-H), 7.68 (s, 2H, Ar-H), 7.46–7.35 (m, 7H, Ar-H), 5.65 (s, 2H, benzylic CH₂).

¹³C-NMR (CDCl₃, 126 MHz): δ 133.8, 129.6, 129.4, 128.4, 124.4, 123.3, 120.9, 113.8, 111.4, 55.3.

IR ν_{max} (neat): 2922, 1613, 1584, 1455, 1297, 1208, 1031, 945, 869, 813, 747 cm⁻¹.

HRMS (ESI): C₁₆H₁₄N₅S [M+H]⁺ calculated 308.0964, found 308.0956.

2.66f: 3-(4-(1*H*-Benzo[d]imidazol-1-yl)-1*H*-1,2,3-triazol-1-yl)-*N,N*-dimethylpropan-1-amine

Prepared according to General Procedure D using 1-ethynyl-1*H*-benzo[d]imidazole **2.63** (71 mg, 0.5 mmol, 1 equiv.), 3-azido-*N,N*-dimethylpropan-1-amine **2.65f** (64 mg, 0.5 mmol, 1 equiv.) and Cu(OAc)₂ (5 mg, 0.025 mmol, 0.05 equiv.). The resulting residue was purified by flash chromatography (silica gel, MeOH/DCM 1/9) to provide the desired product as a colourless solid (117 mg, 87%).

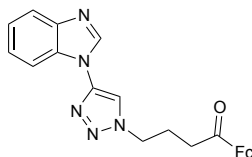
¹H-NMR (CDCl₃, 500 MHz): δ 8.39 (s, 1H, Ar-H), 7.89–7.87 (m, 2H, Ar-H and triazole-H), 7.69 (dd, *J* = 6.8, 1.5 Hz, 1H, Ar-H), 7.40–7.35 (m, 2H, Ar-H), 4.56 (t, *J* = 6.9 Hz, 2H, α-CH₂), 2.35 (t, *J* = 6.6 Hz, 2H, γ-CH₂), 2.26 (s, 6H, CH₃), 2.17 (app. quint, *J* = 6.7 Hz, 2H, β-CH₂).

¹³C-NMR (CDCl₃, 126 MHz): δ 143.9, 142.2, 141.4, 132.7, 124.4, 123.4, 120.9, 114.6, 111.0, 55.6, 49.0, 45.4, 28.0.

IR ν_{max} (neat): 3098, 2937, 2765, 1584, 1454, 1301, 1204, 1041, 950, 743 cm⁻¹.

HRMS (ESI): C₁₄H₁₉N₆ [M+H]⁺ calculated 271.1666, found 271.1660.

2.66g: *N*-(3-(4-(1*H*-Benzo[d]imidazol-1-yl)-1*H*-1,2,3-triazol-1-yl)propyl)ferrecenyl carboxamide



Prepared according to General Procedure D using 1-ethynyl-1*H*-benzo[d]imidazole **2.63** (71 mg, 0.5 mmol, 1 equiv.), *N*-(3-azidopropyl)ferrecenylcarboxamide **2.65g** (156 mg, 0.5 mmol, 1 equiv.) and Cu(OAc)₂ (5 mg, 0.025 mmol, 0.05 equiv.). The resulting residue was purified by flash chromatography (silica gel, MeOH/DCM 1/9) to provide the desired product as a yellow solid (224 mg, 96%).

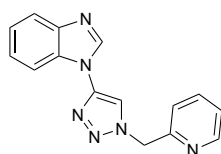
¹H-NMR (MeOD, 400 MHz): δ 8.57 (s, 1H, Ar-H), 8.55 (br. s, 1H, triazole-H), 7.84 (d, *J* = 8.0 Hz, 1H, Ar-H), 7.78 (d, *J* = 7.8 Hz, 1H, Ar-H), 7.45–7.37 (m, 2H, Ar-H), 4.78 (t, *J* = 1.9 Hz, 2H, 2 x CH), 4.63 (t, *J* = 6.9 Hz, 2H, α-CH₂), 4.39 (t, *J* = 1.9 Hz, 2H, 2 x CH), 4.21 (br. s, 5H, 5 x CH), 3.44 (t, *J* = 6.7 Hz, 2H, CONH-CH₂), 2.32 (app. quint, *J* = 6.8 Hz, 2H, CH₂).

¹³C-NMR (CDCl₃, 126 MHz): δ 171.3, 142.6, 124.4, 123.4, 120.8, 115.1, 111.3, 75.6, 70.9, 69.9, 68.2, 48.9, 36.6, 30.7, 29.8.

IR ν_{max} (neat): 3751, 1621, 1600, 1535, 1297, 825, 740 cm⁻¹.

HRMS (ESI): C₂₅H₂₀FeN₆O [M+H]⁺ calculated 454.1204, found 454.1191.

2.66h: 1-(1-(Pyridin-2-ylmethyl)-1*H*-1,2,3-triazol-4-yl)-1*H*-benzo[d]imidazole



Prepared according to General Procedure D using 1-ethynyl-1*H*-benzo[d]imidazole **2.63** (71 mg, 0.5 mmol, 1 equiv.), 2-(azidomethyl)pyridine **2.65h** (67 mg, 0.5 mmol, 1 equiv.) and Cu(OAc)₂ (5 mg, 0.025 mmol, 0.05 equiv.). The resulting residue was purified by flash chromatography (silica gel, MeOH/DCM 1/9) to provide the desired product as a pale brown solid (101 mg, 73%).

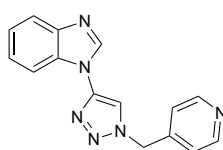
¹H-NMR (CDCl₃, 500 MHz): δ 8.64 (d, *J* = 4.8 Hz, 1H, Ar-H), 8.39 (br. s, 1H, triazole-H), 8.06 (s, 1H, Ar-H), 7.86 (d, *J* = 7.3 Hz, 1H, Ar-H), 7.75 (td, *J* = 7.8, 1.8 Hz, 1H, Ar-H), 7.69 (d, *J* = 7.5 Hz, 1H, Ar-H), 7.38–7.30 (m, 4H, Ar-H), 5.75 (s, 2H, CH₂).

¹³C-NMR (CDCl₃, 126 MHz): δ 153.6, 150.2, 144.0, 142.8, 141.4, 124.4, 124.0, 123.4, 123.0, 120.9, 114.6, 111.2, 56.6.

IR ν_{\max} (neat): 3069, 1597, 1459, 1418, 1054, 892, 766, 743 cm⁻¹.

HRMS (ESI): C₁₅H₁₂N₆Na [M+Na]⁺ calculated 299.1016, found 299.1006.

2.66i: 1-(1-(Pyridin-2-ylmethyl)-1*H*-1,2,3-triazol-4-yl)-1*H*-benzo[d]imidazole



Prepared according to General Procedure D using 1-ethynyl-1*H*-benzo[d]imidazole **2.63** (71 mg, 0.5 mmol, 1 equiv.), 4-(azidomethyl)pyridine **2.65i** (67 mg, 0.5 mmol, 1 equiv.) and Cu(OAc)₂ (5 mg, 0.025 mmol, 0.05 equiv.). The resulting residue was purified by flash chromatography (silica gel, MeOH/DCM 1/9) to provide the desired product as an orange oil (98 mg, 71%).

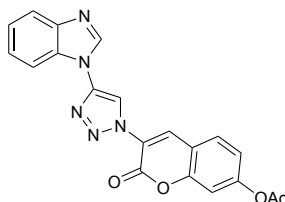
¹H-NMR (CDCl₃, 500 MHz): δ 8.69 (dd, *J* = 4.6, 1.6 Hz, 2H, Ar-H), 8.39 (s, 1H, Ar-H), 7.88–7.87 (m, 1H, Ar-H), 7.79 (s, 1H, triazole-H), 7.67–7.65 (m, 1H, Ar-H), 7.40–35 (m, 2H, Ar-H), 7.22 (d, *J* = 5.7 Hz, 2H, Ar-H), 5.68 (s, 2H, CH₂).

¹³C-NMR (CDCl₃, 126 MHz): δ 151.0, 143.9, 143.3, 142.8, 141.2, 132.5, 124.5, 123.6, 122.3, 121.0, 113.9, 111.0, 53.8.

IR ν_{\max} (neat): 3067, 2934, 1597, 1457, 1418, 1288, 1139, 743 cm⁻¹.

HRMS (ESI): C₁₅H₁₂N₆Na [M+Na]⁺ calculated 299.1016, found 299.1009.

2.66j: 3-(4-(1*H*-Benzo[d]imidazol-1-yl)-1*H*-1,2,3-triazol-1-yl)-2-oxo-2*H*-chromen-7-yl acetate



Prepared according to General Procedure D using 1-ethynyl-1*H*-benzo[*d*]imidazole **2.63** (71 mg, 0.5 mmol, 1 equiv.), 3-azido-2-oxo-2*H*-chromen-7-yl acetate **2.65j** (123 mg, 0.5 mmol, 1 equiv.) and Cu(OAc)₂ (5 mg, 0.025 mmol, 0.05 equiv.). The reaction mixture was dissolved in hot EtOAc (50 mL) and filtered over Celite. The filtrate was concentrated under vacuum to provide the desired product as a yellow solid (90 mg, 95%).

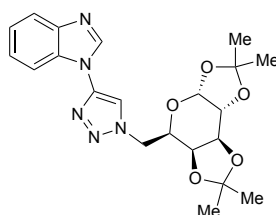
¹H-NMR-(DMSO-*d*₆, 500 MHz): δ 9.26 (s, 1H, Ar-H), 8.90 (s, 1H, Ar-H), 8.83 (br. s, 1H, triazole-H), 8.04 (d, *J* = 8.5 Hz, 1H, Ar-H), 7.95 (d, *J* = 8.1 Hz, 1H, Ar-H), 7.82 (d, *J* = 8.0 Hz, 1H, Ar-H), 7.50 (d, *J* = 1.7 Hz, 1H, Ar-H), 7.44 (t, *J* = 7.3 Hz, 1H, Ar-H), 7.38 (t, *J* = 7.6 Hz, 1H, Ar-H), 7.33 (dd, *J* = 8.4, 2.0 Hz, 1H, Ar-H), 2.35 (s, 3H, CH₃).

¹³C-NMR (DMSO-*d*₆, 126 MHz): δ 169.2, 156.1, 154.4, 153.7, 143.9, 143.2, 142.5, 136.1, 133.0, 131.1, 124.6, 123.6, 123.0, 120.5, 120.2, 117.7, 116.4, 112.3, 110.8, 21.4.

IR ν_{\max} (neat): 3133, 3077, 1770, 1729, 1615, 1584, 1497, 1453, 1367, 1306, 1225, 1185, 1145, 1053, 990, 909, 814, 739 cm⁻¹.

HRMS (ESI): C₂₀H₁₄N₅O₄ [M+H]⁺ calculated 388.1040, found 388.1105.

2.66k: 1-(1-(((3*aR*,5*R*,5*aS*,8*aS*,8*bR*)-2,2,7,7-Tetramethyltetrahydro-5*H*-bis([1,3]dioxolo)[4,5-*b*:4',5'-*d*]pyran-5-yl)methyl)-1*H*-1,2,3-triazol-4-yl)-1*H*-benzo[*d*]imidazole



Prepared according to General Procedure D using 1-ethynyl-1*H*-benzo[*d*]imidazole **2.63** (71 mg, 0.5 mmol, 1 equiv.), (3*aR*,5*R*,5*aS*,8*aS*,8*bR*)-5-(azidomethyl)-2,2,7,7-tetramethyltetrahydro-3*aH*-bis([1,3]dioxolo)[4,5-*b*:4',5'-*d*]pyran **2.65k** (143 mg, 0.5 mmol, 1 equiv.) and Cu(OAc)₂ (5 mg, 0.025 mmol, 0.05 equiv.). The resulting residue was purified by flash chromatography (silica gel, hexane/EtOAc 3/7) to provide the desired product as a colourless oil (145 mg, 68%).

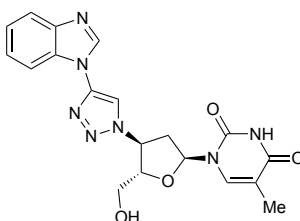
¹H-NMR (CDCl₃, 500 MHz): δ 8.41 (s, 1H, Ar-H), 8.07 (s, 1H, triazole-H), 7.88 (dd, *J* = 6.7, 1.7 Hz, 1H, Ar-H), 7.69 (dd, *J* = 6.4, 1.1 Hz, 1H, Ar-H), 7.40–7.34 (m, 2H, Ar-H), 5.58 (d, *J* = 5.0 Hz, 1H, O-CH), 4.77 (dd, *J* = 14.5, 3.3 Hz, 1H, CH), 4.69 (dd, *J* = 7.8, 2.5 Hz, 1H, 1 x H of diastereotopic CH₂), 4.58 (dd, *J* = 14.5, 9.0 Hz, 1H, 1 x H of diastereotopic CH₂), 4.38 (dd, *J* = 5.0, 2.6 Hz, 1H, O-CH), 4.30 (dd, *J* = 7.8, 1.8 Hz, 1H, CH), 4.26–4.23 (m, 1H, CH), 1.52 (s, 3H, CH₃), 1.41 (s, 3H, CH₃), 1.39 (s, 3H, CH₃), 1.31 (s, 3H, CH₃).

$^{13}\text{C-NMR}$ (CDCl_3 , 126 MHz): δ 142.2, 141.5, 124.3, 123.3, 120.9, 115.4, 111.1, 110.2, 109.4, 96.4, 71.4, 70.9, 70.4, 67.4, 51.7, 26.2, 26.1, 25.0, 24.5.

IR ν_{max} (neat): 2923, 1615, 1589, 1455, 1371, 1202, 1075, 1005, 888, 745 cm^{-1} .

HRMS (ESI): $\text{C}_{21}\text{H}_{26}\text{N}_5\text{O}_5$ $[\text{M}+\text{H}]^+$ calculated 428.1928, found 428.1913.

2.661: 1-((2*R*,4*S*,5*S*)-4-(4-(1*H*-Benzo[d]imidazol-1-yl)-1*H*-1,2,3-triazol-1-yl)-5-(hydroxymethyl)-tetrahydrofuran-2-yl)-5-methylpyrimidine-2,4(1*H*,3*H*)-dione



Prepared according to General Procedure D using 1-ethynyl-1*H*-benzo[d]imidazole **2.63** (71 mg, 0.5 mmol, 1 equiv.), 1-((2*S*,4*S*,5*S*)-4-azido-5-(hydroxymethyl)tetrahydrofuran-2-yl)-5-methylpyrimidine-2,4(1*H*,3*H*)-dione **2.651** (134 mg, 0.5 mmol, 1 equiv.) and $\text{Cu}(\text{OAc})_2$ (5 mg, 0.025 mmol, 0.05 equiv.). The reaction mixture was dissolved in MeOH, filtered and concentrated under vacuum. The resulting residue was purified by flash chromatography (silica gel, hexane/EtOAc 1/1 then MeOH/DCM 2/8) to provide the desired product as a white solid (178 mg, 88%).

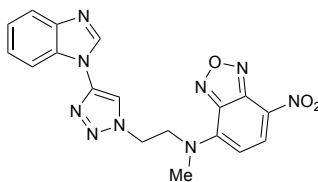
$^1\text{H-NMR}$ (DMSO-d_6 , 500 MHz): δ 11.40 (s, 1H, NH), 8.97 (s, 1H, Ar-H), 8.70 (s, 1H, triazole-H), 7.91 (d, $J = 8.0$ Hz, 1H, Ar-H), 7.86 (d, $J = 0.9$ Hz, 1H, N-CH), 7.80 (d, $J = 8.0$ Hz, 1H, Ar-H), 7.41 (t, $J = 7.8$ Hz, 1H, Ar-H), 7.37–7.34 (m, 1H, Ar-H), 6.48 (t, $J = 6.6$ Hz, 1H, CH), 5.50 (dt, $J = 8.8, 5.2$ Hz, 1H, CH), 5.34 (t, $J = 5.3$ Hz, 1H, CH), 4.38–4.35 (m, 1H, OH), 3.79–3.69 (m, 2H, CH_2), 2.92–2.86 (m, 1H, 1 x H diastereotopic CH_2), 2.78–2.72 (m, 1H, 1 x H diastereotopic CH_2), 1.83 (d, $J = 0.7$ Hz, 3H, CH_3).

$^{13}\text{C-NMR}$ (DMSO-d_6 , 126 MHz): δ 163.8, 150.5, 141.8, 136.3, 124.0, 123.0, 120.0, 115.8, 111.7, 109.7, 84.3, 83.9, 60.8, 60.3, 37.0, 12.3.

IR ν_{max} (neat): 3441, 3099, 2838, 1707, 1656, 1600, 1407, 1277, 1264, 1143, 1111, 1037, 881 cm^{-1} .

HRMS (ESI): $\text{C}_{19}\text{H}_{20}\text{N}_7\text{O}_4$ $[\text{M}+\text{H}]^+$ calculated 410.1571, found 410.1555.

2.66m: *N*-(2-(4-(1*H*-Benzo[d]imidazol-1-yl)-1*H*-1,2,3-triazol-1-yl)ethyl)-*N*-methylbenzo[*c*][1,2,5]oxadiazol-4-amine



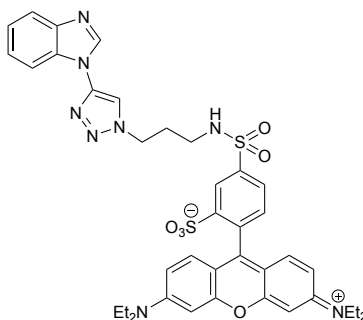
Prepared according to General Procedure D using 1-ethynyl-1*H*-benzo[*d*]imidazole **2.63** (71 mg, 0.5 mmol, 1 equiv.), *N*-(2-azidoethyl)-*N*-methyl-7-nitrobenzo[*c*][1,2,5]oxadiazol-4-amine **2.65m** (132 mg, 0.5 mmol, 1 equiv.) and Cu(OAc)₂ (5 mg, 0.025 mmol, 0.05 equiv.). The reaction mixture was filtered, and the solid residue was washed with an excess of MeCN to provide the desired product as an orange solid (192 mg, 95%).

¹H-NMR (CDCl₃, 500 MHz): δ 8.74 (s, 1H, Ar-H), 8.55 (s, 1H, triazole-H), 8.49 (d, *J* = 9.1 Hz, 1H, Ar-H), 7.77–7.76 (m, 1H, CH), 7.55–7.53 (m, 1H, Ar-H), 7.33–7.32 (m, 2H, Ar-H), 6.43 (d, *J* = 9.2 Hz, 1H, CH), 4.94 (t, *J* = 5.3 Hz, 2H, CH₂), 4.71 (s, 2H, CH₂), 3.37 (s, 3H, CH₃).

IR ν_{max} (neat): 3119, 1613, 1558, 1534, 1271, 1217, 1002, 768, 756, 742 cm⁻¹.

HRMS (ESI): C₁₈H₁₅N₉NaO [M+Na]⁺ calculated 428.1190, found 428.1176.

2.66n: 5-(*N*-(3-(4-(1*H*-Benzo[*d*]imidazol-1-yl)-1*H*-1,2,3-triazol-1-yl)propyl)sulfamoyl)-2-(6-(diethylamino)-3-(diethyliminio)-3*H*-xanthen-9-yl)benzenesulfonate



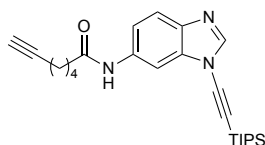
Prepared according to General Procedure D using 1-ethynyl-1*H*-benzo[*d*]imidazole **2.63** (10 mg, 0.07 mmol, 1 equiv.), 5-(*N*-(3-azidopropyl)sulfamoyl)-2-(6-(diethylamino)-3-(diethyliminio)-3*H*-xanthen-9-yl)benzenesulfonate **2.65n** (45 mg, 0.07 mmol, 1 equiv.) and Cu(OAc)₂ (0.7 mg, 0.035 mmol, 0.05 equiv.). The resulting residue was purified by flash chromatography (silica gel, DCM/MeOH 15/1) to provide the desired product as a dark purple solid (36 mg, 65%).

IR ν_{max} (neat): 3876, 1595, 1418, 1320, 1173, 1074, 1026, 724, 686 cm⁻¹.

HRMS (ESI): $C_{39}H_{43}N_8O_6S_2$ $[M+H]^+$ calculated 783.2741, found 783.2710. $C_{39}H_{42}N_8NaO_6S_2$ $[M+Na]^+$ calculated 805.2561, found 805.2530.

2.7.4.4 Products from Scheme 2.21

2.84: *N*-(1-((Triisopropylsilyl)ethynyl)-1*H*-benzo[*d*]imidazol-6-yl)hept-6-ynamide



To a solution of hept-6-ynoic acid **2.81** (61 μ L, 0.5 mmol, 1 equiv.) in DMF (3 mL) was added DIPEA (0.3 mL, 1.9 mmol, 4 equiv.) and HATU (0.18 g, 0.5 mmol, 1 equiv.). The resulting mixture was stirred at rt for 30 minutes, after which 1-((triisopropylsilyl)ethynyl)-1*H*-benzo[*d*]imidazol-6-amine **2.70a** (0.15 g, 0.5 mmol, 1 equiv.) was added. The reaction was then stirred at rt for 20 h, after which EtOAc (100 mL) was added. The mixture was washed with sat. aq. $NaHCO_3$ (1 x 50 mL) and brine (1 x 50 mL), dried over Na_2SO_4 and concentrated under reduced pressure. The resulting residue was purified by flash chromatography (silica gel, hexane/EtOAc 7/3) to provide the desired product as an orange oil (0.2 g, 97%).

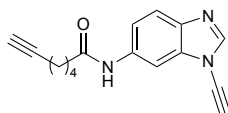
1H -NMR ($CDCl_3$, 400 MHz): δ 8.12 (s, 1H, Ar-H), 8.09 (br. s, 1H, NH), 8.02 (s, 1H, Ar-H), 7.64 (d, $J = 8.6$ Hz, 1H, Ar-H), 7.24 (dd, $J = 8.6, 1.9$ Hz, 1H, Ar-H), 2.41 (t, $J = 7.6$ Hz, 2H, α - CH_2), 2.20 (td, $J = 7.0, 2.6$ Hz, 2H, δ - CH_2), 1.94 (t, $J = 2.6$ Hz, 1H, alk-H), 1.85 (app. quint, $J = 7.6$ Hz, 1H, β - CH_2), 1.59 (app. quint, $J = 7.0$ Hz, 1H, χ - CH_2), 1.14–1.13 (m, 21H, TIPS).

^{13}C -NMR ($CDCl_3$, 100 MHz): δ 171.3, 143.9, 138.3, 135.8, 135.1, 120.8, 116.9, 102.7, 89.9, 84.1, 68.8, 37.2, 28.0, 24.9, 18.7, 11.3.

IR ν_{max} (neat): 3306, 3080, 2943, 2865, 2186, 1664, 1604, 1550, 1485, 1442, 1217, 882, 677 cm^{-1} .

HRMS (ESI): $C_{25}H_{36}N_3OSi$ $[M+H]^+$ calculated 422.2628, found 422.2628.

2.82: *N*-(1-Ethynyl-1*H*-benzo[*d*]imidazol-6-yl)hept-6-ynamide



To a solution of *N*-(1-((triisopropylsilyl)ethynyl)-1*H*-benzo[*d*]imidazol-6-yl)hept-6-ynamide **2.84** (2.2 g, 5.2 mmol, 1 equiv.) in THF (285 mL) was added TBAF (1 M in THF, 5.5 mL, 5.5 mmol, 1.05 equiv.). The reaction was then stirred at rt for 30 minutes, after which the solution

was concentrated under reduced pressure in the dark. The resulting residue was purified by flash chromatography (silica gel, hexane/EtOAc 4/6) to provide the desired product as a white solid that was stored at 0 °C (1.3 g, 91%).

¹H-NMR (400 MHz, MeOD): δ 8.38 (s, 1H, Ar-H), 8.26 (d, $J = 2.0$ Hz, 1H, Ar-H), 7.65 (d, $J = 8.6$ Hz, 1H, Ar-H), 7.33 (dd, $J = 8.6, 2.0$ Hz, 1H, Ar-H), 4.07 (s, 1H, ynamine-H), 2.44 (t, $J = 7.6$ Hz, 2H, α -CH₂), 2.27–2.22 (m, 3H, Alk-H and δ -CH₂), 1.88–1.80 (m, 2H, β -CH₂), 1.63–1.57 (m, 2H, χ -CH₂).

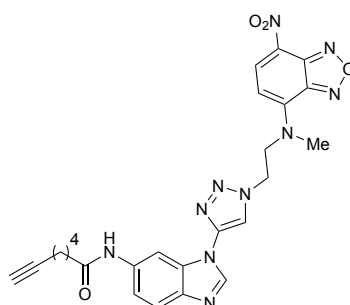
¹³C-NMR (100 MHz, MeOD): δ 174.4, 145.9, 138.6, 136.0, 135.9, 121.0, 118.3, 103.3, 84.6, 70.5, 69.8, 64.2, 37.4, 29.2, 25.9, 18.8.

IR ν_{\max} (neat): 3278, 3193, 2938, 2156, 1655, 1620, 1596, 1529, 1500, 1488, 1446, 1414, 1309, 1281, 1252, 1212, 1177, 969, 848, 817, 657 cm⁻¹.

HRMS (ESI): C₁₆H₁₆N₃O [M+H]⁺ calculated 266.1293, found 266.1320.

2.7.4.5 Products from Scheme 2.22

S1: *N*-(1-(1-(2-(Methyl(7-nitrobenzo[*c*][1,2,5]oxadiazol-4-yl)amino)ethyl)-1*H*-1,2,3-triazol-4-yl)-1*H*-benzo[*d*]imidazol-6-yl)hept-6-ynamide



To a solution of *N*-(1-ethynyl-1*H*-benzo[*d*]imidazol-6-yl)hept-6-ynamide **2.82** (50 mg, 0.19 mmol, 1 equiv.) and *N*-(2-azidoethyl)-*N*-methyl-7-nitrobenzo[*c*][1,2,5]oxadiazol-4-amine **2.65m** (50 mg, 0.19 mmol, 1 equiv.) in MeCN (2 mL) was added Cu(OAc)₂ (1.7 mg, 0.0094 mmol, 0.05 equiv.). The reaction was stirred at rt for 16 h, after which EtOAc (20 mL) was added. The mixture was washed with aq. EDTA (10 mg/mL, 20 mL) and brine (2 x 20 mL), dried over Na₂SO₄ and concentrated under reduced pressure to provide the desired product as an orange solid (92 mg, 93%).

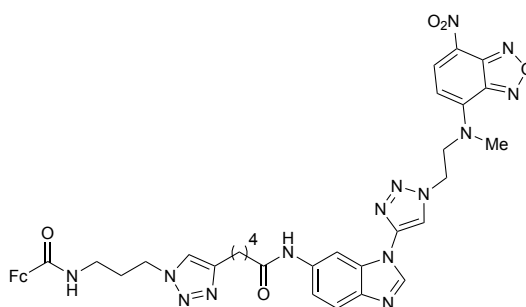
¹H-NMR (DMSO-*d*₆, 400 MHz): δ 10.04 (s, 1H, NH), 8.66 (s, 1H, Ar-H), 8.49 (d, $J = 8.3$ Hz, 1H, Ar-H), 8.42 (s, 1H, triazole-H), 8.27 (s, 1H, Ar-H), 7.66 (d, $J = 8.0$ Hz, 1H, Ar-H), 7.34 (d, $J = 7.6$ Hz, 1H, Ar-H), 6.43 (d, $J = 9.3$ Hz, 1H, Ar-H), 4.95 (t, $J = 5.6$ Hz, 2H, triazole-CH₂-CH₂), 4.68 (br. s, 2H, triazole-CH₂-CH₂), 3.36 (s, 3H, CH₃), 2.75 (t, $J = 2.6$ Hz, 1H, Alk-

H), 2.34 (t, $J = 7.3$ Hz, 2H, α -CH₂), 2.20 (dt, $J = 6.9, 2.2$ Hz, 2H, δ -CH₂), 1.69 (app. quint, $J = 7.7$ Hz, 2H, β -CH₂), 1.50 (app. quint, $J = 7.3$ Hz, 2H, γ -CH₂).

IR ν_{\max} (neat): 3300, 3263, 3237, 3125, 2847, 1679, 1613, 1582, 1554, 1539, 1496, 1483, 1435, 1275, 1219, 1095, 1043, 1006, 829, 816, 805, 740, 669 cm⁻¹.

HRMS (ESI): C₂₅H₂₄N₁₀NaO₄ [M+Na]⁺ calculated 551.1874, found 551.1861.

2.83a: 5-(1-((3-Propyl)ferrecenylcarboxamide)-1*H*-1,2,3-triazol-4-yl)-*N*-(1-(1-(2-(methyl(7-nitrobenzo[*c*][1,2,5]oxadiazol-4-yl)amino)ethyl)-1*H*-1,2,3-triazol-4-yl)-1*H*-benzo[*d*]imidazol-6-yl)pentanamide



Procedure A: To a solution of *N*-(1-(1-(2-(methyl(7-nitrobenzo[*c*][1,2,5]oxadiazol-4-yl)amino)ethyl)-1*H*-1,2,3-triazol-4-yl)-1*H*-benzo[*d*]imidazol-6-yl)hept-6-ynamide **S1** (30 mg, 0.06 mmol, 1 equiv.), *N*-(3-azidopropyl)ferrecenylcarboxamide **2.65g** (18 mg, 0.06 mmol, 1 equiv.) and AMTC (1.3 mg, 0.006 mmol, 0.1 equiv.) in MeOH/H₂O (1/1, 2 mL) were added CuSO₄ (0.5 mg, 0.003 mmol, 0.05 equiv.) and NaAsc (1.1 mg, 0.006 mmol, 0.1 equiv.). The reaction was stirred at rt for 16 h, after which EtOAc was added (20 mL). The mixture was washed with aq. EDTA (10 mg/mL, 20 mL) and brine (2 x 20 mL), dried over Na₂SO₄ and concentrated under reduced pressure to provide the desired product as a brown solid (48 mg, 98%).

Procedure B: To a solution of *N*-(1-ethynyl-1*H*-benzo[*d*]imidazol-6-yl)hept-6-ynamide **2.82** (20 mg, 0.08 mmol, 1 equiv.) and *N*-(2-azidoethyl)-*N*-methyl-7-nitrobenzo[*c*][1,2,5]oxadiazol-4-amine **2.65m** (20 mg, 0.08 mmol, 1 equiv.) in MeCN (2 mL) was added Cu(OAc)₂ (0.7 mg, 0.004 mmol, 0.05 equiv.). The reaction was stirred at rt for 16 h, after which MeOH/H₂O (1/1, 2 mL) was added followed by *N*-(3-azidopropyl)ferrecenylcarboxamide **2.65g** (23 mg, 0.008 mmol, 1 equiv.), AMTC (2 mg, 0.008 mmol, 0.1 equiv.) and NaAsc (1.5 mg, 0.008 mmol, 0.1 equiv.). The reaction was then stirred at rt for an additional 16 h, after which EtOAc (20 mL) was added. The mixture was washed with aq. EDTA (10 mg/mL, 20 mL) and brine (2 x 20 mL), dried over Na₂SO₄, and

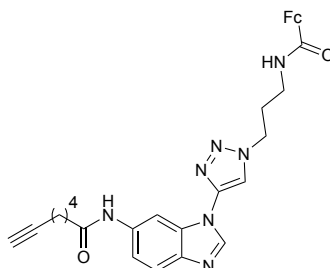
concentrated under reduced pressure to provide the desired product as a brown solid (61 mg, 97%).

¹H-NMR (DMSO-*d*₆, 400 MHz): δ 10.24 (s, 1H, NH), 8.82 (s, 1H, NH), 8.53 (s, 1H, Ar-H), 8.44 (d, $J = 9.2$ Hz, 1H, Ar-H), 8.39 (s, 1H, Ar-H), 8.12 (s, 1H, triazole-H), 7.88 (br. s, 1H, triazole-H), 7.66 (d, $J = 8.2$ Hz, 1H, Ar-H), 7.49 (d, $J = 8.7$ Hz, 1H, Ar-H), 6.35 (d, $J = 8.8$ Hz, 1H, Ar-H), 4.84 (s, 2H, 2 x CH), 4.74 (br. s, 2H, ynamine-triazole-CH₂-CH₂), 4.58–4.57 (m, 4H, Alk-triazole-CH₂-CH₂-CH₂ and ynamine-triazole-CH₂-CH₂), 4.34 (s, 2H, 2 x CH), 4.19–4.18 (m, 5H, 5 x CH), 3.29 (br. s, 5H, Alk-triazole-CH₂-CH₂-CH₂ and CH₃), 2.39–2.31 (m, 4H, α -CH₂ and δ -CH₂), 2.19–2.14 (m, 2H, Alk-triazole-CH₂-CH₂-CH₂), 1.51–1.49 (m, 4H, β -CH₂ and γ -CH₂).

IR ν_{\max} (neat): 3417, 3396, 3385, 3289, 3110, 2948, 2058, 1615, 1554, 1539, 1472, 1442, 1370, 1290, 1217, 1119, 1091, 1004, 820, 781, 742, 697, 684, 675, 662 cm⁻¹.

HRMS (ESI): C₃₉H₄₀FeN₁₄NaO₅ [M+Na]⁺ calculated 863.2548, found 863.2521.

S2: *N*-(1-(1-((3-Propyl)ferrecenylcarboxamide)-1*H*-1,2,3-triazol-4-yl)-1*H*-benzo[*d*]imidazol-6-yl)hept-6-ynamide



To a solution of *N*-(1-ethynyl-1*H*-benzo[*d*]imidazol-6-yl)hept-6-ynamide **2.82** (50 mg, 0.19 mmol, 1 equiv.) and *N*-(3-azidopropyl)ferrecenylcarboxamide **2.65g** (60 mg, 0.19 mmol, 1 equiv.) in MeCN (2 mL) was added Cu(OAc)₂ (1.7 mg, 0.0094 mmol, 0.5 equiv.). The reaction was stirred at rt for 16 h, after which EtOAc (20 mL) was added. The mixture was washed with aq. EDTA (10 mg/mL, 20 mL) and brine (2 x 20 mL), dried over Na₂SO₄ and concentrated under reduced pressure to provide the desired product as a brown solid (101 mg, 93%).

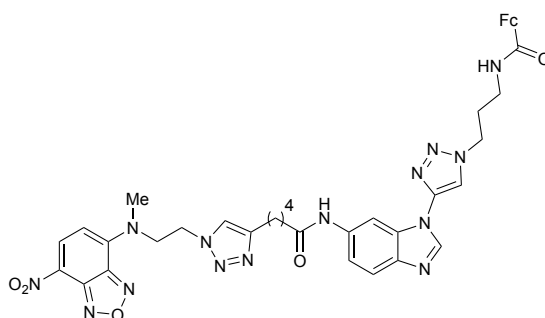
¹H-NMR (DMSO-*d*₆, 400 MHz): δ 10.06 (s, 1H, NH), 8.73 (s, 1H, NH), 8.52 (s, 1H, Ar-H), 8.36 (s, 1H, Ar-H), 7.94 (br. s, 1H, triazole-H), 7.68 (d, $J = 8.6$ Hz, 1H, Ar-H), 7.43 (d, $J = 8.6$ Hz, 1H, Ar-H), 4.80 (s, 2H, 2 x CH), 4.58 (t, $J = 6.7$ Hz, 2H, triazole-CH₂-CH₂-CH₂), 4.36 (s, 2H, 2 x CH), 4.19 (s, 5H, 5 x CH), 3.42–3.37 (m, 2H, triazole-CH₂-CH₂-CH₂), 2.77 (s, 1H,

Alk-H), 2.35 (t, $J = 6.8$ Hz, 2H, α -CH₂), 2.20–2.18 (m, 4H, triazole-CH₂-CH₂-CH₂ and δ -CH₂), 1.69 (app. quint, $J = 8.1$ Hz, 2H, γ -CH₂), 1.50 (app. quint, $J = 7.6$ Hz, 2H, β -CH₂).

IR ν_{\max} (neat): 3287, 3090, 2930, 2861, 2115, 1623, 1587, 1539, 1496, 1487, 1437, 1353, 1299, 1225, 1191, 1108, 1004, 946, 818, 734, 702 cm⁻¹.

HRMS (ESI): C₃₀H₃₂FeN₇O₂ [M+H]⁺ calculated 577.1889, found 577.1910.

2.83b: *N*-(1-(1-((3-Propyl)ferrecenylcarboxamide)1*H*-1,2,3-triazol-4-yl)-1*H*-benzo[*d*]imidazol-6-yl)-5-(1-(2-(methyl(7-nitrobenzo[*c*][1,2,5]oxadiazol-4-yl)amino)ethyl)-1*H*-1,2,3-triazol-4-yl)pentanamide



Procedure A: To a solution of *N*-(1-(1-((3-propyl)ferrecenylcarboxamide)-1*H*-1,2,3-triazol-4-yl)-1*H*-benzo[*d*]imidazole-6-yl)hept-6-ynamide **S2** (23 mg, 0.09 mmol, 1 equiv.), *N*-(2-azidoethyl)-*N*-methyl-7-nitrobenzo[*c*][1,2,5]oxadiazol-4-amine **2.65m** (11 mg, 0.09 mmol, 1 equiv.) and AMTC (4 mg, 0.009 mmol, 0.1 equiv.) in MeOH/H₂O (1/1, 2 mL) were added CuSO₄ (0.8 mg, 0.004 mmol, 0.05 equiv.) and NaAsc (2 mg, 0.009 mmol, 0.1 equiv.). The reaction was stirred at rt for 16 h, after which EtOAc (20 mL) was added. The mixture was washed with aq. EDTA (10 mg/mL, 20 mL) and brine (2 x 20 mL), dried over Na₂SO₄ and concentrated under reduced pressure to provide the desired product as a brown solid (66 mg, 90%).

Procedure B: To a solution of *N*-(1-ethynyl-1*H*-benzo[*d*]imidazol-6-yl)hept-6-ynamide **2.82** (20 mg, 0.08 mmol, 1 equiv.) and *N*-(3-azidopropyl)ferrecenylcarboxamide **2.65g** (23 mg, 0.008 mmol, 1 equiv.) in MeCN (2 mL) was added Cu(OAc)₂ (0.7 mg, 0.004 mmol, 0.05 equiv.). The reaction was stirred at rt for 16 h, after which MeOH/H₂O (1/1, 2 mL) were added followed by *N*-(2-azidoethyl)-*N*-methyl-7-nitrobenzo[*c*][1,2,5]oxadiazol-4-amine **2.65m** (20 mg, 0.08 mmol, 1 equiv.), AMTC (2 mg, 0.008 mmol, 0.1 equiv.) and NaAsc (2 mg, 0.008 mmol, 0.1 equiv.). The reaction was stirred at rt for an additional 16 h, after which EtOAc (20 mL) was added. The mixture was washed with aq. EDTA (10 mg/mL, 20 mL) and brine (2 x

20 mL), dried over Na₂SO₄ and concentrated under reduced pressure to provide the desired product as a brown solid (58 mg, 92%).

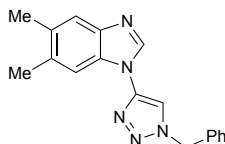
¹H-NMR (DMSO-d₆, 400 MHz): δ 10.23 (s, 1H, NH), 8.81 (s, 1H, NH), 8.52 (s, 1H, Ar-H), 8.43 (d, *J* = 9.4 Hz, 1H, Ar-H), 8.37 (s, 1H, Ar-H), 8.11 (s, 1H, triazole-H), 7.87 (br. s, 1H, triazole-H), 7.65 (d, *J* = 8.7 Hz, 1H, Ar-H), 7.48 (d, *J* = 8.7 Hz, 1H, Ar-H), 6.34 (d, *J* = 8.7 Hz, 1H, Ar-H), 4.83 (s, 2H, 2 x CH), 4.72 (t, *J* = 5.5 Hz, 2H, triazole-CH₂-CH₂-N-CH₃), 4.57 (t, *J* = 5.9 Hz, 4H, triazole-CH₂-CH₂-CH₂-NHCO and triazole-CH₂-CH₂-N-CH₃), 4.33 (s, 2H, 3 x CH), 4.17 (s, 5H, 5 x CH), 3.25 (br. s, 5H, triazole-CH₂-CH₂-CH₂-NHCO and CH₃), 2.33 (br. s, 4H, α-CH₂ and δ-CH₂), 2.18–2.13 (m, 2H, triazole-CH₂-CH₂-CH₂-NHCO), 1.64–1.50 (m, 4H, β-CH₂ and γ-CH₂).

IR ν_{max} (neat): 3417, 3396, 3385, 3289, 3110, 2948, 2058, 1615, 1554, 1539, 1472, 1442, 1370, 1290, 1217, 1119, 1091, 1004, 820, 781, 742, 697, 684, 675, 662 cm⁻¹.

HRMS (ESI): C₃₉H₄₀FeN₁₄NaO₅ [M+Na]⁺ calculated 863.2548, found 863.2521.

2.7.4.6 Products from Scheme 2.23

2.73a: 1-(1-Benzyl-1*H*-1,2,3-triazol-4-yl)-5,6-dimethyl-1*H*-benzo[*d*]imidazole



Prepared according to General Procedure G using 5,6-dimethyl-1-((triisopropylsilyl)ethynyl)-1*H*-benzo[*d*]imidazole **2.69** (50 mg, 0.15 mmol, 1 equiv.), (but-3-yn-1-yloxy)benzene **2.72** (22 mg, 0.15 mmol, 1 equiv.), benzyl azide **2.65a** (19 μL, 0.15 mmol, 1 equiv.), TBAF (56 μL, 0.17 mmol, 1.1 equiv.) and Cu(OAc)₂ (1.5 mg, 0.0077 mmol, 0.05 equiv.). The resulting residue was purified by flash chromatography (silica gel, hexane/EtOAc 3/7) to provide the desired product as a white solid (31 mg, 66%).

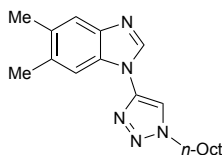
¹H-NMR (CDCl₃, 400 MHz): δ 8.20 (br. s, 1H, triazole-H), 7.67 (s, 1H, Ar-H), 7.58 (br. s, 1H, Ar-H), 7.39–7.45 (m, 4H, Ar-H), 7.37–7.34 (m, 2H, Ar-H), 5.62 (s, 2H, CH₂), 2.37 (s, 6H, CH₃).

¹³C-NMR (CDCl₃, 100 MHz): δ 143.2, 142.4, 140.4, 134.0, 133.6, 132.2, 131.1, 129.5, 129.3, 128.3, 120.7, 113.5, 111.3, 55.2, 20.7, 20.3.

IR ν_{max} (neat): 3086, 2922, 2854, 1724, 1584, 1495, 1459, 1407, 1284, 1213, 1053, 867, 718 cm⁻¹.

HRMS (ESI): $C_{18}H_{17}N_5$ $[M+H]^+$ calculated 304.1557, found 304.1551.

2.73b: 5,6-Dimethyl-1-(1-octyl-1*H*-1,2,3-triazol-4-yl)-1*H*-benzo[*d*]imidazole



Prepared according to General Procedure G using 5,6-dimethyl-1-((triisopropylsilyl)ethynyl)-1*H*-benzo[*d*]imidazole **2.69** (45 mg, 0.14 mmol, 1 equiv.), (but-3-yn-1-yloxy)benzene **2.72** (20 mg, 0.14 mmol, 1 equiv.), 1-azidooctane **2.65b** (21 mg, 0.14 mmol, 1 equiv.), TBAF (49 μ L, 0.15 mmol, 1.1 equiv.) and $Cu(OAc)_2$ (1.2 mg, 0.007 mmol, 0.05 equiv.). The resulting residue was purified by flash chromatography (silica gel, hexane/EtOAc 3/7) to provide the desired product as a white solid (88 mg, 98%).

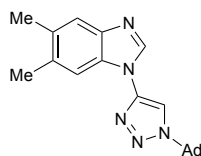
1H -NMR ($CDCl_3$, 500 MHz): δ 8.62 (br. s, 1H, triazole-H), 7.77–7.68 (m, 3H, Ar-H), 4.45 (t, $J = 7.1$ Hz, 2H, Ar-H), 2.40 (s, 3H, CH_3), 2.38 (s, 3H, CH_3), 2.00 (app. quint, $J = 6.6$ Hz, 2H, CH_2), 1.40–1.26 (m, 10H, CH_2), 0.87 (t, $J = 7.2$ Hz, 3H, CH_3).

^{13}C -NMR ($CDCl_3$, 100 MHz): δ 133.9, 132.0, 113.8, 51.5, 31.8, 30.4, 29.8, 29.2, 29.1, 26.6, 22.7, 20.7, 20.4, 14.2.

IR ν_{max} (neat): 3135, 2924, 2857, 1740, 1597, 1500, 1470, 1383, 1292, 1206, 1156, 1091, 1053, 1033, 949, 869, 785 cm^{-1} .

HRMS (ESI): $C_{19}H_{27}N_5$ $[M+H]^+$ calculated 326.2339, found 326.2323.

2.73d: 1-(1-((3*S*,5*S*,7*S*)-Adamantan-1-yl)-1*H*-1,2,3-triazol-4-yl)-5,6-dimethyl-1*H*-benzo[*d*]imidazole



Prepared according to General Procedure G using 5,6-dimethyl-1-((triisopropylsilyl)ethynyl)-1*H*-benzo[*d*]imidazole **2.69** (45 mg, 0.14 mmol, 1 equiv.), (but-3-yn-1-yloxy)benzene **2.72** (20 mg, 0.14 mmol, 1 equiv.), 1-azidoadamantane **2.65d** (24 mg, 0.14 mmol, 1 equiv.), TBAF (49 μ L, 0.15 mmol, 1.1 equiv.) and $Cu(OAc)_2$ (1.2 mg, 0.007 mmol, 0.05 equiv.). The resulting residue was purified by flash chromatography (silica gel, hexane/EtOAc 3/7) to provide the desired product as a white solid (95 mg, 99%).

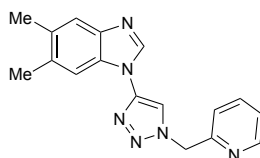
¹H-NMR (CDCl₃, 400 MHz): δ 8.22 (br. s, 1H, triazole-H), 7.82 (s, 1H, Ar-H), 7.60 (s, 1H, Ar-H), 7.47 (s, 1H, Ar-H), 2.39 (s, 3H, CH₃), 2.38 (s, 3H, CH₃), 2.33 (br. s, 9H, CH), 1.83 (br. s, 6H, CH).

¹³C-NMR (CDCl₃, 100 MHz): δ 142.4, 142.1, 140.7, 133.5, 132.1, 131.4, 120.7, 111.4, 110.6, 61.0, 43.1, 35.9, 29.8, 29.6, 20.7, 20.4.

IR ν_{\max} (neat): 3080, 2917, 2852, 1725, 1586, 1495, 1467, 1448, 1281, 1216, 1149, 1019, 948, 861, 844 cm⁻¹.

HRMS (ESI): C₂₁H₂₆N₅ [M+H]⁺ calculated 348.2183, found 348.2179.

2.73h: 5,6-Dimethyl-1-(1-(pyridin-2-ylmethyl)-1H-1,2,3-triazol-4-yl)-1H-benzo[d]imidazole



Prepared according to General Procedure G using 5,6-dimethyl-1-((triisopropylsilyl)ethynyl)-1H-benzo[d]imidazole **2.69** (45 mg, 0.14 mmol, 1 equiv.), (but-3-yn-1-yloxy)benzene **2.72** (20 mg, 0.14 mmol, 1 equiv.), 2-(azidomethyl)pyridine **2.65h** (18 mg, 0.14 mmol, 1 equiv.), TBAF (49 μ L, 0.15 mmol, 1.1 equiv.) and Cu(OAc)₂ (1.2 mg, 0.007 mmol, 0.05 equiv.). The resulting residue was purified by flash chromatography (silica gel, hexane/EtOAc 3/7) to provide the desired product as a yellow oil (83 mg, 99%).

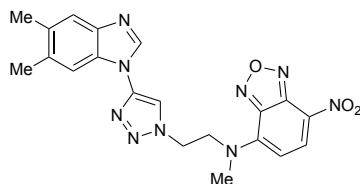
¹H-NMR (CDCl₃, 500 MHz): δ 8.61 (d, J = 4.5 Hz, 1H, Ar-H), 8.24 (s, 1H, triazole-H), 8.03 (s, 1H, Ar-H), 7.72 (dt, J = 7.7, 1.7 Hz, 1H, Ar-H), 7.57 (s, 1H, Ar-H), 7.45 (s, 1H, Ar-H), 7.33 (d, J = 7.7 Hz, 1H, Ar-H), 7.30–7.27 (m, 1H), 5.72 (s, 2H, benzylic CH₂), 2.36 (app. s, 6H, 2 x CH₃).

¹³C-NMR (CDCl₃, 100 MHz): δ 153.6, 150.1, 143.0, 142.3, 140.4, 137.6, 132.2, 132.1, 123.8, 122.8, 120.6, 114.3, 111.3, 56.4, 20.6, 20.3.

IR ν_{\max} (neat): 3105, 2960, 2917, 2852, 1586, 1502, 1465, 1435. cm⁻¹.

HRMS (ESI): C₁₇H₁₆N₆ [M+H]⁺ calculated 305.1509, found 305.1508.

2.73m: *N*-(2-(4-(5,6-dimethyl-1*H*-benzo[*d*]imidazol-1-yl)-1*H*-1,2,3-triazol-1-yl)ethyl)-*N*-methyl-7-nitrobenzo[*c*][1,2,5]oxadiazol-4-amine



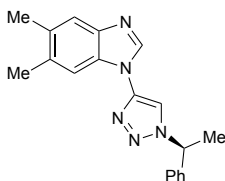
Prepared according to General Procedure G using 5,6-dimethyl-1-((trisopropylsilyl)ethynyl)-1*H*-benzo[*d*]imidazole **2.69** (50 mg, 0.29 mmol, 1 equiv.), (but-3-yn-1-yloxy)benzene **2.72** (41 mg, 0.29 mmol, 1 equiv.), *N*-(2-azidoethyl)-*N*-methyl-7-nitrobenzo[*c*][1,2,5]oxadiazol-4-amine **2.65m** (77 mg, 0.29 mmol, 1 equiv.), TBAF (104 μ L, 0.31 mmol, 1.1 equiv.) and Cu(OAc)₂ (2.5 mg, 0.015 mmol, 0.05 equiv.). The resulting residue was purified by flash chromatography (silica gel, hexane/EtOAc 1/9) to provide the desired product as a red solid (119 mg, 95%).

¹H-NMR (CDCl₃, 400 MHz): δ 8.49–8.48 (m, 2H, Ar-H), 7.63 (s, 1H, Ar-H), 7.49 (br. s, 1H, Ar-H), 6.38 (d, $J = 9.3$ Hz, 1H, Ar-H), 4.98 (t, $J = 4.5$ Hz, 2H, triazole-CH₂-CH₂), 3.45–3.42 (m, 2H, triazole-CH₂-CH₂), 2.40–2.39 (m, 6H, 2 x CH₃), 2.03 (s, 3H, CH₃).

IR ν_{\max} (neat): 3599, 3108, 3082, 2917, 2852, 1613, 1597, 1550, 1424, 1288, 1216, 1149, 1087, 1002, 918, 732 cm⁻¹.

HRMS (ESI): C₂₀H₂₀N₉O₃ [M+H]⁺ calculated 434.1684, found 434.1613.

2.73o: (*S*)-5,6-Dimethyl-1-(1-(1-phenylethyl)-1*H*-1,2,3-triazol-4-yl)-1*H*-benzo[*d*]imidazole



Prepared according to General Procedure G using 5,6-dimethyl-1-((trisopropylsilyl)ethynyl)-1*H*-benzo[*d*]imidazole **2.69** (50 mg, 0.15 mmol, 1 equiv.), (but-3-yn-1-yloxy)benzene **2.72** (22 mg, 0.15 mmol, 1 equiv.), (*S*)-(1-azidoethyl)benzene **2.65o** (23 mg, 0.15 mmol, 1 equiv.), TBAF (56 μ L, 0.17 mmol, 1.1 equiv.) and Cu(OAc)₂ (1.7 mg, 0.008 mmol, 0.05 equiv.). The resulting residue was purified by flash chromatography (silica gel, hexane/EtOAc 3/7) to provide the desired product as a white solid (46 mg, 95%).

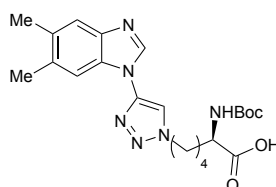
¹H-NMR (CDCl₃, 400 MHz): δ 8.20 (br. s, 1H, triazole-H), 7.63 (s, 1H, Ar-H), 7.59 (br. s, 1H, Ar-H), 7.45–7.35 (m, 6H, Ar-H), 5.88 (q, *J* = 7.0 Hz, 1H, CH), 2.37 (s, 6H, CH₃), 2.09 (d, *J* = 7.1 Hz, 3H, CH₃).

¹³C-NMR (CDCl₃, 100 MHz): δ 139.3, 133.6, 132.3, 129.4, 126.7, 120.7, 112.6, 111.5, 61.5, 29.8, 21.3, 20.7, 20.4.

IR ν_{\max} (neat): 3110, 2926, 2857, 1724, 1590, 1498, 1459, 1383, 1286, 1212, 1143, 910, 731 cm⁻¹.

HRMS (ESI): C₁₉H₁₉N₅ [M+H]⁺ calculated 318.1713, found 318.1704.

2.73p: (*S*)-2-((*Tert*-butoxycarbonyl)amino)-6-(4-(5,6-dimethyl-1*H*-benzo[*d*]imidazol-1-yl)-1*H*-1,2,3-triazol-1-yl)hexanoic acid



Prepared according to General Procedure G using 5,6-dimethyl-1-((triisopropylsilyl)ethynyl)-1*H*-benzo[*d*]imidazole **2.69** (44 mg, 0.14 mmol, 1 equiv.), (but-3-yn-1-yloxy)benzene **2.72** (20 mg, 0.14 mmol, 1 equiv.), Boc-Lys(N₃)-OH **2.65p** (50 mg, 0.14 mmol, 1 equiv.), TBAF (42 μL, 0.16 mmol, 1.1 equiv.) and Cu(OAc)₂ (1.2 mg, 0.006 mmol, 0.05 equiv.). The resulting residue was purified by flash chromatography (silica gel, DCM/MeOH 9/1 + 0.01% AcOH) to provide the desired product as a yellow solid (56 mg, 94%).

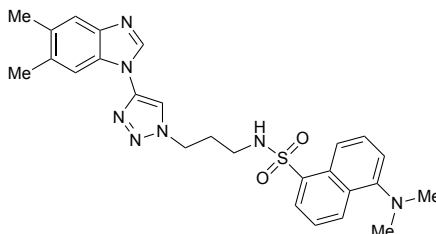
¹H-NMR (CDCl₃, 400 MHz): δ 9.80 (br. s, 1H, triazole-H), 8.79 (s, 1H, Ar-H), 7.91 (s, 1H, Ar-H), 7.71 (s, 1H, Ar-H), 4.60 (br. s, 2H, triazole-CH₂-CH₂-CH₂-CH₂-CH), 4.08 (br. s, 1H, triazole-CH₂-CH₂-CH₂-CH₂-CH), 2.48 (s, 6H, 2 x CH₃), 2.08 (br. s, 2H, triazole-CH₂-CH₂-CH₂-CH₂-CH), 1.89 (br. s, 1H, triazole-CH₂-CH₂-CH₂-CH₂-CH), 1.74 (br. s, 1H, triazole-CH₂-CH₂-CH₂-CH₂-CH), 1.51 (br. s, 2H, triazole-CH₂-CH₂-CH₂-CH₂-CH), 1.41 (s, 9H, Boc).

¹³C-NMR (CDCl₃, 100 MHz): δ 175.9, 158.1, 141.0, 139.2, 138.9, 119.9, 116.0, 114.8, 80.4, 54.6, 52.4, 32.2, 30.6, 28.7, 23.9, 20.7, 20.5.

IR ν_{\max} (neat): 3382, 3127, 2974, 2867, 2485, 2233, 2071, 1686, 1591, 1422, 1392, 1368, 1247, 1165, 1119, 1052, 974 cm⁻¹.

HRMS (ESI): C₂₂H₃₁N₆O₄ [M+H]⁺ calculated 443.2401, found 443.2389.

2.73q: *N*-(3-(4-(5,6-Dimethyl-1*H*-benzo[*d*]imidazol-1-yl)-1*H*-1,2,3-triazol-1-yl)propyl)-5-(dimethylamino)naphthalene-1-sulfonamide



Prepared according to General Procedure G using 5,6-dimethyl-1-((triisopropylsilyl)ethynyl)-1*H*-benzo[*d*]imidazole **2.69** (30 mg, 0.09 mmol, 1 equiv.), (but-3-yn-1-yloxy)benzene **2.72** (13 mg, 0.09 mmol, 1 equiv.), *N*-(3-azidopropyl)-5-(dimethylamino)naphthalene-1-sulfonamide **2.65q** (31 mg, 0.09 mmol, 1 equiv.), TBAF (30 μ L, 0.1 mmol, 1.1 equiv.) and Cu(OAc)₂ (0.8 mg, 0.004 mmol, 0.05 equiv.). The resulting residue was purified by flash chromatography (silica gel, DCM/MeOH 9/1) to provide the desired product as a yellow solid (43 mg, 92%).

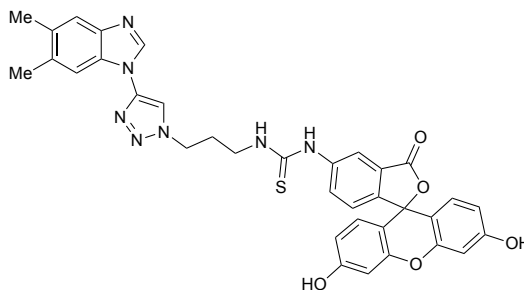
¹H-NMR (CDCl₃, 500 MHz): δ 8.52 (d, J = 8.6 Hz, 1H, Ar-H), 8.27 (d, J = 8.6 Hz, 1H, Ar-H), 8.24 (s, 1H, triazole-H), 8.21 (d, J = 8.6 Hz, 1H, Ar-H), 7.80 (s, 1H, Ar-H), 7.61 (s, 1H, Ar-H), 7.55 (t, J = 7.6 Hz, 1H, Ar-H), 7.50–7.46 (m, 2H, Ar-H), 7.16 (d, J = 7.6 Hz, 1H, Ar-H), 5.38 (t, J = 6.5 Hz, 1H, Ar-H), 4.54 (t, J = 5.5 Hz, 2H, α -CH₂), 2.94 (q, J = 6.2 Hz, 2H, β -CH₂), 2.86 (s, 6H, CH₃), 2.39 (s, 6H, CH₃), 2.16–2.14 (m, 2H, γ -CH₂).

¹³C-NMR (CDCl₃, 100 MHz): δ 152.4, 142.6, 142.4, 140.5, 134.2, 133.8, 132.4, 131.0, 130.1, 129.9, 129.6, 128.9, 123.4, 120.7, 118.3, 115.5, 114.7, 111.4.

IR ν_{\max} (neat): 3127, 2924, 2857, 2794, 1750, 1597, 1457, 1396, 1325, 1312, 1234, 1146, 1092, 1042, 951, 789 cm⁻¹.

HRMS (ESI): C₂₆H₃₀N₇O₂S [M+H]⁺ calculated 504.2176, found 504.2153.

2.73r: 1-(3',6'-Dihydroxy-3-oxo-3*H*-spiro[isobenzofuran-1,9'-xanthen]-5-yl)-3-(3-(4-(5,6-dimethyl-1*H*-benzo[*d*]imidazol-1-yl)-1*H*-1,2,3-triazol-1-yl)propyl)thiourea

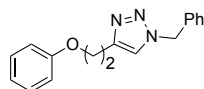


Prepared according to General Procedure G using 5,6-dimethyl-1-((triisopropylsilyl)ethynyl)-1*H*-benzo[*d*]imidazole **2.69** (39 mg, 0.12 mmol, 1 equiv.), (but-3-yn-1-yloxy)benzene **2.72** (17 mg, 0.12 mmol, 1 equiv.), 1-(3-azidopropyl)-3-(3',6'-dihydroxy-3-oxo-3*H*-spiro[isobenzofuran-1,9'-xanthen]-5-yl)thiourea **2.65r** (56 mg, 0.12 mmol, 1 equiv.), TBAF (38 μ L, 0.13 mmol, 1.1 equiv.) and Cu(OAc)₂ (1.1 mg, 0.006 mmol, 0.05 equiv.) in MeOH (2 mL). After 16 h, DCM (10 mL) was added, and the mixture was washed with HCl (1 M, 10 mL), aq. EDTA (10 mg/mL, 10 mL) and brine (10 mL). The resulting residue was purified by flash chromatography (silica gel, DCM/MeOH 9/1) to provide the desired product as a red solid (66 mg, 85%).

¹H-NMR (CDCl₃, 400 MHz): δ 9.32 (br. s, 1H, triazole-H), 9.00 (s, 1H, Ar-H), 8.45 (s, 1H, Ar-H), 7.86 (d, J = 8.0 Hz, 1H, Ar-H), 7.82 (s, 1H, Ar-H), 7.65–7.62 (m, 2H, Ar-H), 7.16 (d, J = 8.3 Hz, 1H, Ar-H), 6.72–6.68 (m, 2H, Ar-H), 6.60–6.56 (m, 3H, Ar-H), 4.66 (t, J = 6.9 Hz, 2H, triazole-CH₂-CH₂-CH₂-NH), 3.51 (s, 2H, triazole-CH₂-CH₂-CH₂-NH), 3.16 (s, 2H, triazole-CH₂-CH₂-CH₂-NH), 2.40 (s, 3H, CH₃), 2.38 (s, 3H, CH₃).

IR ν_{\max} (neat): 2924, 2113, 1716, 1593, 1541, 1457, 1381, 1303, 1245, 1210, 854 cm⁻¹.

HRMS (ESI): C₃₅H₂₉N₇O₅S [M+H]⁺ calculated 658.1878, found 642.1632 [M-OH]⁺.

2.74a: 1-Benzyl-4-(2-phenoxyethyl)-1*H*-1,2,3-triazole

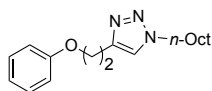
Prepared according to General Procedure H using 5,6-dimethyl-1-((triisopropylsilyl)ethynyl)-1*H*-benzo[*d*]imidazole **2.69** (45 mg, 0.14 mmol, 1 equiv.), (but-3-yn-1-yloxy)benzene **2.72** (20 mg, 0.14 mmol, 1 equiv.), benzylazide **2.65a** (18 μ L, 0.14 mmol, 1 equiv.), AMTC (3 mg, 0.014 mmol, 0.1 equiv.), Cu(OAc)₂ (1 mg, 0.007 mmol, 0.05 equiv.) and NaAsc (3 mg, 0.014 mmol, 0.1 equiv.). The resulting residue was purified by flash chromatography (silica gel, hexane/EtOAc 3/7) to provide the desired product as a white solid (81 mg, Quant.).

¹H-NMR (CDCl₃, 400 MHz): δ 7.40–7.34 (m, 4H, 3 x Ar-H and 1 x triazole-H), 7.29–7.26 (m, 2H, Ar-H), 7.25–7.24 (m, 2H, Ar-H), 6.94 (tt, $J = 7.4, 1.1$ Hz, 1H, Ar-H), 6.89–6.85 (m, 2H, Ar-H), 5.50 (s, 2H, CH₂), 4.23 (t, $J = 6.5$ Hz, 2H, α -CH₂), 3.19 (t, $J = 6.5$ Hz, 2H, β -CH₂).

¹³C-NMR (CDCl₃, 100 MHz): δ 158.8, 135.0, 129.6, 129.2, 128.8, 128.1, 122.0, 121.1, 114.7, 66.8, 54.2, 26.4.

IR ν_{\max} (neat): 3120, 3071, 3038, 2958, 2935, 1604, 1590, 1496, 1459, 1251, 1219, 1176, 1059, 1042, 890, 828, 789, 752, 720 cm⁻¹.

HRMS (ESI): C₁₇H₁₇N₃NaO [M+Na]⁺ calculated 302.1264, found 302.1256.

2.74b: 1-Octyl-4-(2-phenoxyethyl)-1*H*-1,2,3-triazole

Prepared according to General Procedure H using 5,6-dimethyl-1-((triisopropylsilyl)ethynyl)-1*H*-benzo[*d*]imidazole **2.69** (45 mg, 0.14 mmol, 1 equiv.), (but-3-yn-1-yloxy)benzene **2.72** (20 mg, 0.14 mmol, 1 equiv.), 1-azido-octane **2.65b** (21 mg, 0.14 mmol, 1 equiv.), AMTC (3 mg, 0.014 mmol, 0.1 equiv.), Cu(OAc)₂ (1 mg, 0.007 mmol, 0.05 equiv.) and NaAsc (3 mg, 0.014 mmol, 0.1 equiv.). The resulting residue was purified by flash chromatography (silica gel, hexane/EtOAc 3/7) to provide the desired product as a white solid (78 mg, 94%).

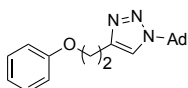
¹H-NMR (CDCl₃, 400 MHz): δ 7.41 (s, 1H, triazole-H), 7.29–7.25 (m, 2H, Ar-H), 6.96–6.89 (m, 3H, Ar-H), 4.30 (t, $J = 7.2$ Hz, 2H, α -CH₂), 4.24 (t, $J = 6.5$ Hz, 2H, CH₂), 3.21 (t, $J = 6.5$ Hz, 2H, β -CH₂), 1.87 (app. quint, $J = 7.1$ Hz, 2H, CH₂), 1.30–1.25 (m, 10H, 5 x CH₂), 0.87 (t, $J = 6.6$ Hz, 3H, CH₃).

¹³C-NMR (CDCl₃, 100 MHz): δ 158.7, 144.6, 129.6, 121.7, 121.0, 114.6, 66.8, 50.3, 31.8, 30.4, 29.1, 29.0, 26.6, 26.3, 22.7, 14.1.

IR ν_{\max} (neat): 3142, 2956, 2922, 2852, 1604, 1591, 1500, 1487, 1388, 1247, 1217, 1176, 1057, 1035, 886, 817, 756, 694 cm^{-1} .

HRMS (ESI): $\text{C}_{18}\text{H}_{27}\text{N}_3\text{NaO}$ $[\text{M}+\text{Na}]^+$ calculated 324.2046, found 324.2035.

2.74d: 1-((3*s*,5*s*,7*s*)-Adamantan-1-yl)-4-(2-phenoxyethyl)-1*H*-1,2,3-triazole



Prepared according to General Procedure H using 5,6-dimethyl-1-((triisopropylsilyl)ethynyl)-1*H*-benzo[*d*]imidazole **2.69** (45 mg, 0.14 mmol, 1 equiv.), (but-3-yn-1-yloxy)benzene **2.72** (20 mg, 0.14 mmol, 1 equiv.), 1-azidoadamantane **2.65d** (24 mg, 0.14 mmol, 1 equiv.), AMTC (3 mg, 0.014 mmol, 0.1 equiv.), $\text{Cu}(\text{OAc})_2$ (1 mg, 0.007 mmol, 0.05 equiv.) and NaAsc (3 mg, 0.014 mmol, 0.1 equiv.). The resulting residue was purified by flash chromatography (silica gel, hexane/EtOAc 3/7) to provide the desired product as a white solid (81 mg, Quant.).

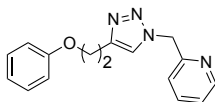
$^1\text{H-NMR}$ (CDCl_3 , 400 MHz): δ 7.49 (s, 1H, triazole-H), 7.30–7.28 (m, 2H, Ar-H), 7.00–6.90 (m, 3H, Ar-H), 4.25 (t, $J = 6.6$ Hz, 2H, $\alpha\text{-CH}_2$), 3.22 (t, $J = 6.6$ Hz, 2H, $\beta\text{-CH}_2$), 2.25–2.23 (m, 9H, CH), 1.82–1.75 (m, 6H).

$^{13}\text{C-NMR}$ (CDCl_3 , 100 MHz): δ 158.9, 143.7, 129.6, 121.0, 118.2, 114.7, 67.1, 59.4, 43.1, 36.1, 29.6, 26.5.

IR ν_{\max} (neat): 2909, 2857, 1599, 1590, 1556, 1500, 1476, 1457, 1420, 1348, 1292, 1243, 1035, 1016, 780, 759, 694 cm^{-1} .

HRMS (ESI): $\text{C}_{20}\text{H}_{25}\text{N}_3\text{NaO}$ $[\text{M}+\text{Na}]^+$ calculated 346.1890, found 346.1881.

2.74h: 2-((4-(2-Phenoxyethyl)-1*H*-1,2,3-triazol-1-yl)methyl)pyridine



Prepared according to General Procedure H using 5,6-dimethyl-1-((triisopropylsilyl)ethynyl)-1*H*-benzo[*d*]imidazole **2.69** (45 mg, 0.14 mmol, 1 equiv.), (but-3-yn-1-yloxy)benzene **2.72** (20 mg, 0.14 mmol, 1 equiv.), 2-(azidomethyl)pyridine **2.65h** (18 mg, 0.14 mmol, 1 equiv.), AMTC (3.1 mg, 0.014 mmol, 0.1 equiv.), $\text{Cu}(\text{OAc})_2$ (1.2 mg, 0.007 mmol, 0.05 equiv.) and NaAsc (2.7 mg, 0.014 mmol, 0.1 equiv.). The resulting residue was purified by flash chromatography (silica gel, hexane/EtOAc 3/7) to provide the desired product as a white solid (60 mg, 79%).

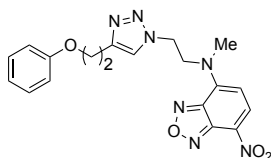
¹H-NMR (CDCl₃, 400 MHz): δ 8.60 (s, 1H, triazole-H), 7.67 (tt, *J* = 7.8, 1.8 Hz, 1H, Ar-H), 7.60 (s, 1H, Ar-H), 7.29–7.24 (m, 4H, Ar-H), 7.15 (d, *J* = 7.7 Hz, 1H, Ar-H), 6.93 (tt, *J* = 7.3, 1.2 Hz, 1H, Ar-H), 6.92–6.87 (m, 1H, Ar-H), 5.63 (s, 2H, benzylic CH₂), 4.25 (t, *J* = 6.5 Hz, 2H, α-CH₂), 3.22 (t, *J* = 6.5 Hz, 2H, β-CH₂).

¹³C-NMR (CDCl₃, 100 MHz): δ 158.8, 137.5, 129.6, 123.5, 121.1, 114.7, 66.8, 55.7, 26.4.

IR ν_{max} (neat): 3142, 2932, 1601, 1590, 1496, 1474, 1441, 1295, 1241, 1052, 1022, 1035, 998, 752, 692 cm⁻¹.

HRMS (ESI): C₁₆H₁₆N₄NaO [M+Na]⁺ calculated 303.1216, found 303.1214.

2.74m: *N*-methyl-7-nitro-*N*-(2-(4-(2-phenoxyethyl)-1*H*-1,2,3-triazol-1-yl)ethyl)benzo[*c*][1,2,5]oxadiazol-4-amine

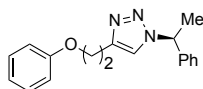


Prepared according to General Procedure H using 5,6-dimethyl-1-((triisopropylsilyl)ethynyl)-1*H*-benzo[*d*]imidazole **2.69** (59 mg, 0.34 mmol, 1 equiv.), (but-3-yn-1-yloxy)benzene **2.72** (50 mg, 0.34 mmol, 1 equiv.), *N*-(2-azidoethyl)-*N*-methyl-7-nitrobenzo[*c*][1,2,5]oxadiazol-4-amine **2.65m** (90 mg, 0.34 mmol, 1 equiv.), AMTC (7.5 mg, 0.034 mmol, 0.1 equiv.), Cu(OAc)₂ (2.8 mg, 0.017 mmol, 0.05 equiv.) and NaAsc (6.6 mg, 0.034 mmol, 0.1 equiv.). The resulting residue was purified by flash chromatography (silica gel, hexane/EtOAc 1/9) to provide the desired product as a yellow solid (118 mg, 85%).

¹H-NMR (CDCl₃, 500 MHz): δ 8.37 (d, *J* = 9.0 Hz, 1H, Ar-H), 7.86 (br. s, 1H, triazole-H), 7.24 (t, *J* = 7.7 Hz, 2H, Ar-H), 6.92 (t, *J* = 7.3 Hz, 1H, Ar-H), 6.84 (d, *J* = 8.0 Hz, 2H, Ar-H), 6.20 (d, *J* = 8.9 Hz, 1H, Ar-H), 4.68 (br. s, 2H, triazole-CH₂-CH₂), 4.01 (t, *J* = 6.0 Hz, 2H, O-CH₂-CH₂), 3.03 (t, *J* = 6.0 Hz, 2H, O-CH₂-CH₂), 1.34–1.29 (m, 5H, triazole-CH₂-CH₂ and CH₃).

IR ν_{max} (neat): 3142, 1617, 1556, 1483, 1429, 1303, 1281, 1095, 1035, 1000, 801, 756, 682 cm⁻¹.

HRMS (ESI): C₁₉H₁₉N₇NaO₄ [M+Na]⁺ calculated 432.1391, found 432.1376.

2.74o: (*S*)-4-(2-Phenoxyethyl)-1-(1-phenylethyl)-1*H*-1,2,3-triazole

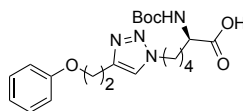
Prepared according to General Procedure H using 5,6-dimethyl-1-((triisopropylsilyl)ethynyl)-1*H*-benzo[*d*]imidazole **2.69** (89 mg, 0.3 mmol, 1 equiv.), (but-3-yn-1-yloxy)benzene **2.72** (40 mg, 0.3 mmol, 1 equiv.), (*S*)-(1-azidoethyl)benzene **2.65o** (40 mg, 0.3 mmol, 1 equiv.), AMTC (6 mg, 0.003 mmol, 0.1 equiv.), Cu(OAc)₂ (2 mg, 0.01 mmol, 0.05 equiv.) and NaAsc (5 mg, 0.03 mmol, 0.1 equiv.). The resulting residue was purified by flash chromatography (silica gel, hexane/EtOAc 3/7) to provide the desired product as a white solid (67 mg, 84%).

¹H-NMR (CDCl₃, 400 MHz): δ 7.38–7.32 (m, 8H, Ar-H), 6.94 (tt, *J* = 7.4, 1.1 Hz, 1H, Ar-H), 6.88–6.85 (m, 2H, Ar-H), 5.78 (q, *J* = 7.2 Hz, 1H, CH), 4.23 (t, *J* = 6.5 Hz, 2H, α-CH₂), 3.19 (t, *J* = 6.5 Hz, 2H, β-CH₂), 1.97 (d, *J* = 7.1 Hz, 3H, CH₃).

¹³C-NMR (CDCl₃, 100 MHz): δ 158.7, 144.6, 140.2, 129.6, 129.1, 128.5, 126.6, 121.0, 120.8, 114.7, 66.8, 60.2, 25.4, 21.4.

IR ν_{max} (neat): 3170, 3066, 3030, 3045, 2941, 2924, 2870, 1604, 1588, 1498, 1463, 1387, 1366, 1305, 1251, 1038, 811, 756, 733, 705, 694 cm⁻¹.

HRMS (ESI): C₁₈H₁₉N₃NaO [M+Na]⁺ calculated 316.1420, found 316.1410.

2.74p: (*R*)-2-((*Tert*-butoxycarbonyl)amino)-6-(4-(2-phenoxyethyl)-1*H*-1,2,3-triazol-1-yl)hexanoic acid

Prepared according to General Procedure H using 5,6-dimethyl-1-((triisopropylsilyl)ethynyl)-1*H*-benzo[*d*]imidazole **2.69** (44 mg, 0.14 mmol, 1 equiv.), (but-3-yn-1-yloxy)benzene **2.72** (20 mg, 0.14 mmol, 1 equiv.), Boc-Lys(N₃)-OH **2.65p** (50 mg, 0.14 mmol, 1 equiv.), AMTC (3 mg, 0.014 mmol, 0.1 equiv.), Cu(OAc)₂ (1.2 mg, 0.007 mmol, 0.05 equiv.) and NaAsc (2.6 mg, 0.014 mmol, 0.1 equiv.). The resulting residue was purified by flash chromatography (silica gel, DCM/MeOH 9/1, 0.1% AcOH) to provide the desired product as a white solid (46 mg, 82%).

¹H-NMR (MeOD, 500 MHz): δ 7.83 (br. s, 1H, triazole-H), 7.24 (t, *J* = 7.8 Hz, 2H, Ar-H), 6.92–6.89 (m, 3H, Ar-H), 4.37 (t, *J* = 7.1 Hz, 2H, triazole-CH₂-CH₂-CH₂-CH₂-CH), 4.22 (t, *J* = 6.5 Hz, 2H, O-CH₂-CH₂), 4.08–4.05 (m, 1H, triazole-CH₂-CH₂-CH₂-CH₂-CH), 3.15 (t, *J* =

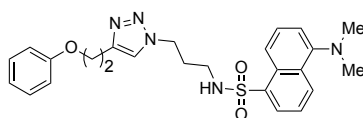
6.4 Hz, 2H, O-CH₂-CH₂), 1.94–1.89 (m, 2H, triazole-CH₂-CH₂-CH₂-CH), 1.87–1.80 (m, 2H, triazole-CH₂-CH₂-CH₂-CH), 1.70–1.55 (m, 2H, triazole-CH₂-CH₂-CH₂-CH), 1.42 (s, 9H, Boc).

¹³C-NMR (MeOD, 100 MHz): δ 176.0, 160.1, 158.1, 130.5, 121.9, 115.6, 80.5, 67.7, 54.6, 52.2, 51.1, 32.3, 32.2, 30.7, 29.4, 28.7, 26.9, 24.1, 23.9.

IR ν_{max} (neat): 3398, 2952, 2922, 2868, 2482, 2242, 2071, 1688, 1600, 1368, 1167, 1119, 974 cm⁻¹.

HRMS (ESI): C₂₁H₃₀N₄NaO₅ [M+Na]⁺ calculated 441.2108, found 441.2102.

2.74q: 5-(Dimethylamino)-N-(3-(4-(2-phenoxyethyl)-1H-1,2,3-triazol-1-yl)propyl)naphthalene-1-sulfonamide



Prepared according to General Procedure H using 5,6-dimethyl-1-((triisopropylsilyl)ethynyl)-1H-benzo[d]imidazole **2.69** (30 mg, 0.09 mmol, 1 equiv.), (but-3-yn-1-yloxy)benzene **2.72** (13 mg, 0.09 mmol, 1 equiv.), (S)-(1-azidoethyl)benzene **2.65q** (31 mg, 0.09 mmol, 1 equiv.), AMTC (2 mg, 0.009 mmol, 0.1 equiv.), Cu(OAc)₂ (1 mg, 0.004 mmol, 0.05 equiv.) and NaAsc (2 mg, 0.009 mmol, 0.1 equiv.). The resulting residue was purified by flash chromatography (silica gel, DCM/MeOH 9/1) to provide the desired product as a yellow solid (38 mg, 87%).

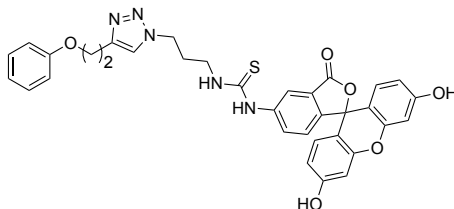
¹H-NMR (CDCl₃, 400 MHz): δ 8.53 (dt, *J* = 8.5, 0.9 Hz, 1H, Ar-H), 8.27 (dt, *J* = 8.5, 0.9 Hz, 1H, Ar-H), 8.18 (dd, *J* = 7.3, 1.2 Hz, 1H, Ar-H), 7.55 (dd, *J* = 8.6, 7.6 Hz, 1H, Ar-H), 7.47 (dd, *J* = 8.5, 7.2 Hz, 1H, Ar-H), 7.33 (s, 1H, triazole-H), 7.28–7.24 (m, 2H, Ar-H), 7.16 (d, *J* = 7.6 Hz, 1H, Ar-H), 6.95–6.88 (m, 3H, Ar-H), 5.41 (t, *J* = 6.5 Hz, 1H, CH₂), 4.32 (t, *J* = 6.6 Hz, 2H, CH₂), 4.20 (t, *J* = 6.3 Hz, 2H, α-CH₂), 3.15 (t, *J* = 6.3 Hz, 2H, β-CH₂), 2.87 (s, 6H, CH₃), 2.04–1.98 (m, 4H, CH₂).

¹³C-NMR (CDCl₃, 100 MHz): δ 158.7, 152.2, 134.5, 130.8, 130.0, 129.8, 129.6, 128.7, 123.3, 121.0, 118.6, 115.4, 114.7, 66.7, 46.9, 45.5, 40.1, 32.0, 30.4, 29.8, 26.2, 14.3, 14.2.

IR ν_{max} (neat): 3293, 3142, 2935, 2870, 2790, 1603, 1590, 1577, 1500, 1457, 1409, 1396, 1314, 1236, 1145, 1038, 947, 910, 791, 757, 731, 694 cm⁻¹.

HRMS (ESI): C₂₅H₂₉N₅NaO₃S [M+Na]⁺ calculated 502.1883, found 502.1862.

2.74r: 1-(3',6'-Dihydroxy-3-oxo-3*H*-spiro[isobenzofuran-1,9'-xanthen]-5-yl)-3-(3-(4-(2-phenoxyethyl)-1*H*-1,2,3-triazol-1-yl)propyl)thiourea



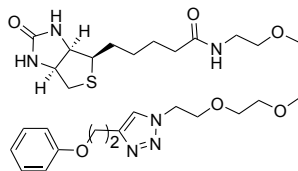
Prepared according to General Procedure H using 5,6-dimethyl-1-((triisopropylsilyl)ethynyl)-1*H*-benzo[*d*]imidazole **2.69** (39 mg, 0.12 mmol, 1 equiv.), (but-3-yn-1-yloxy)benzene **2.72** (17 mg, 0.12 mmol, 1 equiv.), 1-(3-azidopropyl)-3-(3',6'-dihydroxy-3-oxo-3*H*-spiro[isobenzofuran-1,9'-xanthen]-5-yl)thiourea **2.65r** (56 mg, 0.12 mmol, 1 equiv.), AMTC (2.7 mg, 0.012 mmol, 0.1 equiv.), Cu(OAc)₂ (1.1 mg, 0.006 mmol, 0.05 equiv.) and NaAsc (2.3 mg, 0.012 mmol, 0.1 equiv.) in MeOH/H₂O (1/1, 2 mL). After 16 h, DCM (10 mL) was added, and the mixture was washed with HCl (1 M, 10 mL), aq. EDTA (10 mg/mL, 10 mL) and brine (10 mL). The crude material was purified by flash chromatography (silica gel, DCM/MeOH 9/1) to provide the desired product as a red solid (68 mg, 91%).

¹H-NMR (CDCl₃, 500 MHz): δ 8.72 (br. s, 1H, triazole-H), 8.38 (s, 1H, Ar-H), 8.06 (s, 1H, Ar-H), 7.83 (d, *J* = 7.7 Hz, 1H, Ar-H), 7.27 (t, *J* = 7.1 Hz, 2H, Ar-H), 7.17 (d, *J* = 7.1 Hz, 1H, Ar-H), 6.96–6.90 (m, 2H, Ar-H), 6.71 (s, 3H, Ar-H), 6.58 (q, *J* = 8.2 Hz, 3H, Ar-H), 4.45 (t, *J* = 6.4 Hz, 2H, O-CH₂-CH₂), 4.22 (t, *J* = 6.6 Hz, 4H, triazole-CH₂-CH₂-CH₂), 3.51 (br. s, 2H, triazole-CH₂-CH₂-CH₂), 3.09 (t, *J* = 6.4 Hz, 2H, O-CH₂-CH₂).

IR ν_{max} (neat): 2928, 1638, 1591, 1541, 1457, 1381, 1295, 1238, 1210, 1176, 1120, 852 cm⁻¹.

HRMS (ESI): C₃₄H₂₉N₅O₆S [M+H]⁺ calculated 634.1766, found 618.2001 [M-OH]⁺.

2.74s: 5-((3*aR*,4*R*,6*aS*)-2-oxohexahydro-1*H*-thieno[3,4-*d*]imidazol-4-yl)-*N*-(2-(2-(2-(2-(4-(2-phenoxyethyl)-1*H*-1,2,3-triazol-1-yl)ethoxy)ethoxy)ethoxy)ethyl)pentanamide



Prepared according to General Procedure H using 5,6-dimethyl-1-((triisopropylsilyl)ethynyl)-1*H*-benzo[*d*]imidazole **2.69** (20 mg, 0.06 mmol, 1 equiv.), (but-3-yn-1-yloxy)benzene **2.72** (9 mg, 0.06 mmol, 1 equiv.), biotin-PEG3-azide **2.65s** (27 mg, 0.06 mmol, 1 equiv.), AMTC (1.4 mg, 0.006 mmol, 0.1 equiv.), Cu(OAc)₂ (0.5 mg, 0.003 mmol, 0.05 equiv.) and NaAsc (1.2

mg, 0.006 mmol, 0.1 equiv.). The resulting residue was purified by flash chromatography (silica gel, DCM/MeOH 9/1) to provide the desired product as a white solid (32 mg, 88%).

¹H-NMR (CDCl₃, 400 MHz): δ 7.96 (br. s, 1H, triazole-H), 7.25 (t, *J* = 7.7 Hz, 2H, Ar-H), 6.92 (d, *J* = 7.2 Hz, 3H, Ar-H), 4.56 (t, *J* = 4.6 Hz, 2H, Ar-H), 4.47 (dd, *J* = 7.6, 5.6 Hz, 1H, CH), 4.28 (dd, *J* = 7.9, 4.3 Hz, 1H, CH), 4.24 (t, *J* = 5.1 Hz, 2H, α-CH₂), 3.88 (t, *J* = 4.7 Hz, 2H, β-CH₂), 3.63–3.54 (m, 8H, 4 x CH₂), 3.50 (t, *J* = 5.1 Hz, 2H, CH₂), 3.37–3.33 (m, 2H, CH₂), 3.20–3.17 (m, 3H, CH and CH₂), 2.90 (dd, *J* = 12.5, 4.8 Hz, 1H, CH), 2.70 (d, *J* = 12.7 Hz, 1H, CH), 2.19 (t, *J* = 7.4 Hz, 2H, CH₂), 1.75–1.54 (m, 4H, 2 x CH₂), 1.41 (app. quint, *J* = 7.5 Hz, 2H, CH₂).

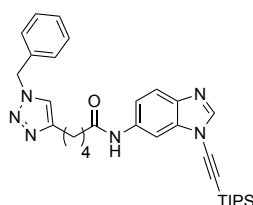
¹³C-NMR (CDCl₃, 100 MHz): δ 176.1, 166.1, 160.2, 130.5, 121.9, 115.7, 71.6, 71.5, 71.4, 71.2, 10.6, 70.4, 67.8, 63.4, 61.6, 57.0, 51.5, 41.1, 40.3, 36.7, 29.7, 29.5, 27.0, 26.8.

IR ν_{max} (neat): 3274, 3071, 2917, 2861, 1695, 1679, 1643, 1545, 1474, 1238, 1104, 1035, 756 cm⁻¹.

HRMS (ESI): C₂₈H₄₃N₆O₆S [M+H]⁺ calculated 591.2959, found 591.2811.

2.7.4.7 Products from Scheme 2.24

2.85a: 5-(1-benzyl-1*H*-1,2,3-triazol-4-yl)-*N*-(1-((triisopropylsilyl)ethynyl)-1*H*-benzo[*d*]imidazol-6-yl)pentanamide



To a solution of *N*-(1-((triisopropylsilyl)ethynyl)-1*H*-benzo[*d*]imidazol-6-yl)hept-6-ynamide **2.84** (50 mg, 0.119 mmol, 1 equiv.) in MeOH/H₂O (1/1, 2 mL) was added benzyl azide **2.65a** (15 μL, 0.119 mmol, 1 equiv.), AMTC (3 mg, 0.012 mmol, 0.1 equiv.), Cu(OAc)₂ (1 mg, 0.006 mmol, 0.05 equiv.) and NaAsc (3 mg, 0.012 mmol, 0.1 equiv.). The reaction was stirred at rt for 16 h, after which DCM (10 mL) was added. The mixture was washed with aq. EDTA (10 mg/mL, 10 mL) and brine (2 x 10 mL), dried over Na₂SO₄ and concentrated under reduced pressure. The resulting residue was purified by flash chromatography (silica gel, hexane/EtOAc 3/7) to provide the desired product as a white solid (62 mg, 98%).

¹H-NMR (CDCl₃, 400 MHz): δ 8.75 (s, 1H, Ar-H), 8.24 (s, 1H, Ar-H), 8.05 (br. s, 1H, triazole-H), 7.64 (br. s, 1H, NH), 7.35–7.30 (m, 4H, Ar-H), 7.23–7.21 (m, 3H, Ar-H), 5.45 (s, 2H,

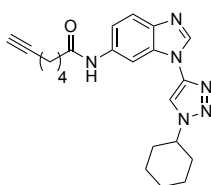
benzylic CH₂), 2.71 (t, $J = 6.9$ Hz, 2H, α -CH₂), 2.43 (t, $J = 6.9$ Hz, 2H, δ -CH₂), 1.79–1.70 (m, 4H, β -CH₂ and γ -CH₂), 1.14 (s, 21H, TIPS).

¹³C-NMR (CDCl₃, 100 MHz): δ 171.8, 136.3, 134.8, 129.2, 128.8, 128.1, 120.6, 117.0, 102.6, 73.5, 54.2, 37.1, 29.8, 28.6, 25.1, 25.0, 18.7, 11.3.

IR ν_{\max} (neat): 3251, 2937, 2859, 2184, 1664, 1602, 1548, 1498, 1441, 1216, 909, 883, 730 cm⁻¹.

HRMS (ESI): C₃₂H₄₂N₆NaOSi [M+Na]⁺ calculated 577.3082, found 577.3122.

2.85b: *N*-(1-(1-cyclohexyl-1*H*-1,2,3-triazol-4-yl)-1*H*-benzo[*d*]imidazol-6-yl)hept-6-ynamide



To a solution of *N*-(1-((triisopropylsilyl)ethynyl)-1*H*-benzo[*d*]imidazol-6-yl)hept-6-ynamide **2.84** (50 mg, 0.12 mmol, 1 equiv.) in MeCN (1 mL) was added cyclohexylazide **2.65c** (15 mg, 0.12 mmol, 1 equiv.), TBAF (43 μ L, 0.13 mmol, 1.1 equiv.) and Cu(OAc)₂ (1 mg, 0.006 mmol, 0.05 equiv.). The reaction was stirred at rt for 16 h, after which DCM (10 mL) was added. The mixture was washed with aq. EDTA (10 mg/mL, 10 mL) and brine (2 x 10 mL), dried over Na₂SO₄ and concentrated under reduced pressure. The resulting residue was purified by flash chromatography (silica gel, 7/3 EtOAc/hexane) to provide the desired product as a white solid (45 mg, 96%).

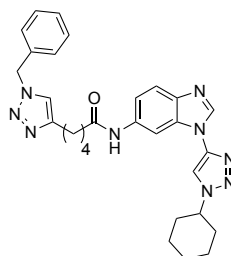
¹H-NMR (CDCl₃, 400 MHz): δ 8.40 (br. s, 1H, triazole-H), 8.34 (s, 1H, Ar-H), 8.08 (br. s, 1H, NH), 7.85 (s, 1H, Ar-H), 7.68 (br. s, 1H, Ar-H), 7.07 (d, $J = 5.9$ Hz, 1H, Ar-H), 4.48 (tt, $J = 11.8, 3.6$ Hz, 1H, *hex*-CH), 2.41 (t, $J = 7.4$ Hz, 2H, α -CH₂), 2.27 (d, $J = 12.4$ Hz, 2H, δ -CH₂), 2.21 (dt, $J = 7.2, 2.1$ Hz, 2H, *hex*-CH₂), 1.96 (m, 3H, Alk-H and *hex*-CH₂), 1.89–1.82 (m, 4H, β -CH₂ and γ -CH₂), 1.59 (app. quint, $J = 7.8$ Hz, 2H, *hex*-CH₂), 1.52–1.41 (m, 2H, *hex*-CH₂), 1.32 (dt, $J = 12.8, 2.7$ Hz, 2H, *hex*-CH₂).

¹³C-NMR (CDCl₃, 100 MHz): δ 171.5, 141.7, 135.1, 120.7, 116.1, 112.4, 102.7, 84.1, 68.9, 61.4, 37.2, 33.5, 28.0, 25.2, 25.1, 24.8, 18.3.

IR ν_{\max} (neat): 3289, 3259, 3123, 3080, 2930, 2855, 1673, 1604, 1587, 1550, 1487, 1442, 1299, 1240, 911, 803, 730 cm⁻¹.

HRMS (ESI): C₂₂H₂₆N₆NaO [M+Na]⁺ calculated 413.2060, found 413.2049.

2.86: 5-(1-benzyl-1*H*-1,2,3-triazol-4-yl)-*N*-(1-(1-cyclohexyl-1*H*-1,2,3-triazol-4-yl)-1*H*-benzo[*d*]imidazol-6-yl)pentanamide



Procedure A: To a solution of 5-(1-benzyl-1*H*-1,2,3-triazol-4-yl)-*N*-(1-((triisopropylsilyl)ethynyl)-1*H*-benzo[*d*]imidazol-6-yl)pentanamide **2.85a** (64 mg, 0.12 mmol, 1 equiv.) in MeCN (1 mL) was added cyclohexylazide **2.65c** (15 mg, 0.12 mmol, 1 equiv.), TBAF (43 μ L, 0.13 mmol, 1.1 equiv.) and Cu(OAc)₂ (1 mg, 0.006 mmol, 0.05 equiv.). The reaction was stirred at rt for 16 h, after which DCM (10 mL) was added. The mixture was washed with aq. EDTA (10 mg/mL, 10 mL) and brine (2 x 10 mL), dried over Na₂SO₄ and concentrated under reduced pressure. The resulting residue was purified by flash chromatography (silica gel, 9/1 EtOAc/hexane) to provide the desired product as a white solid (61 mg, 98%).

Procedure B: To a solution of 5-(1-benzyl-1*H*-1,2,3-triazol-4-yl)-*N*-(1-((triisopropylsilyl)ethynyl)-1*H*-benzo[*d*]imidazol-6-yl)pentanamide **2.85b** (20 mg, 0.051 mmol, 1 equiv.) in MeOH/H₂O (1/1, 2 mL) was added benzyl azide **2.65a** (7 μ L, 0.051 mmol, 1 equiv.), AMTC (1 mg, 0.0051 mmol, 0.1 equiv.), Cu(OAc)₂ (0.5 mg, 0.0026 mmol, 0.05 equiv.) and NaAsc (1 mg, 0.0026 mmol, 0.1 equiv.). The reaction was stirred at rt for 16 h, after which DCM (10 mL) was added. The mixture was washed with aq. EDTA (10 mg/mL, 10 mL) and brine (2 x 10 mL), dried over Na₂SO₄ and concentrated under reduced pressure. The resulting residue was purified by flash chromatography (silica gel, 9/1 EtOAc/hexane) to provide the desired product as a white solid (25 mg, 94%).

¹H-NMR (CDCl₃, 400 MHz): δ 8.23 (s, 1H, Ar-H), 8.40 (br. s, 1H, triazole-H), 8.38 (s, 1H, Ar-H), 7.92 (s, 1H, NH), 7.68 (d, J = 7.5 Hz, 1H, Ar-H), 7.33–7.30 (m, 4H, Ar-H), 7.23–7.20 (m, 3H, Ar-H), 5.45 (s, 2H, benzylic CH₂), 4.47 (tt, J = 11.8, 3.8 Hz, 1H, *hex*-CH), 2.69 (t, J = 6.5 Hz, 2H, α -CH₂), 2.43 (t, J = 6.7 Hz, 2H, δ -CH₂), 2.25 (dd, J = 12.7, 2.4 Hz, 2H, *hex*-CH₂), 1.95–1.89 (m, 2H, β -CH₂), 1.84 (dd, J = 12.1, 3.6 Hz, 2H, *hex*-CH₂), 1.79–1.70 (m, 6H, γ -CH₂ and *hex*-CH₂), 1.47 (tt, J = 12.9, 3.5 Hz, 2H, *hex*-CH₂).

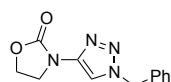
$^{13}\text{C-NMR}$ (CDCl_3 , 100 MHz): δ 172.0, 135.5, 134.9, 129.2, 128.8, 128.1, 121.1, 120.6, 116.3, 112.3, 102.4, 61.3, 54.1, 37.1, 33.4, 28.6, 25.3, 26.2, 25.1, 25.0.

IR ν_{max} (neat): 3257, 3125, 3062, 2922, 2852, 2093, 1671, 1584, 1547, 1496, 1485, 1446, 1299, 1216, 1050, 816, 799, 729 cm^{-1} .

HRMS (ESI): $\text{C}_{29}\text{H}_{33}\text{N}_9\text{NaO}$ $[\text{M}+\text{Na}]^+$ calculated 546.2700, found 546.2660.

2.7.4.8 Products from Scheme 2.25

2.88a: 3-(1-Benzyl-1*H*-1,2,3-triazol-4-yl)oxazolidin-2-one¹⁷⁸

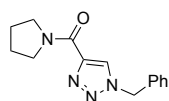


Prepared according to General Procedure J using 5,6-dimethyl-1-((triisopropylsilyl)ethynyl)-1*H*-benzo[*d*]imidazole **2.69** (132 mg, 0.41 mmol, 1 equiv.), 3-ethynyloxazolidin-2-one **2.87a** (46 mg, 0.14 mmol, 1 equiv.), benzyl azide **2.65a** (53 μL , 0.41 mmol, 1 equiv.), AMTC (9 mg, 0.041 mmol, 0.1 equiv.), $\text{Cu}(\text{OAc})_2$ (3 mg, 0.02 mmol, 0.05 equiv.) and NaAsc (9 mg, 0.041 mmol, 0.1 equiv.). The resulting residue was purified by flash chromatography (silica gel, hexane/EtOAc 7/3) to provide the desired product as a white solid (99 mg, 99%).

$^1\text{H-NMR}$ (CDCl_3 , 400 MHz): δ 7.82 (s, 1H, triazole-H), 7.36–7.33 (m, 3H, Ar-H), 7.28–7.26 (m, 2H, Ar-H), 5.48 (s, 2H, benzylic CH_2), 4.56–4.52 (m, 2H, N- CH_2), 4.25–4.21 (m, 2H, O- CH_2).

$^{13}\text{C-NMR}$ (CDCl_3 , 100 MHz): δ 154.9, 144.1, 134.4, 129.2, 129.0, 128.2, 111.9, 63.4, 54.9, 43.7.

2.88b: (1-benzyl-1*H*-1,2,3-triazol-4-yl)(pyrrolidin-1-yl)methanone



Prepared according to General Procedure J using 5,6-dimethyl-1-((triisopropylsilyl)ethynyl)-1*H*-benzo[*d*]imidazole **2.69** (132 mg, 0.41 mmol, 1 equiv.), 1-(pyrrolidin-1-yl)prop-2-yn-1-one **2.87b** (50 mg, 0.14 mmol, 1 equiv.), benzyl azide **2.65a** (53 μL , 0.41 mmol, 1 equiv.), AMTC (9 mg, 0.041 mmol, 0.1 equiv.), $\text{Cu}(\text{OAc})_2$ (3 mg, 0.02 mmol, 0.05 equiv.) and NaAsc (9 mg, 0.041 mmol, 0.1 equiv.). The resulting residue was purified by flash chromatography (silica gel, hexane/EtOAc 7/3) to provide the desired product as a white solid (105 mg, Quant.).

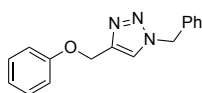
¹H-NMR (CDCl₃, 400 MHz): δ 8.02 (s, 1H, triazole-H), 7.36–7.34 (m, 3H, Ar-H), 7.28–7.26 (m, 2H, Ar-H), 5.52 (s, 2H, benzylic CH₂), 4.09 (t, *J* = 6.7 Hz, 2H, CH₂), 3.62 (t, *J* = 6.9 Hz, 2H, CH₂), 1.97 (app. quint, *J* = 7.1 Hz, 2H, CH₂), 1.88 (app. quint, *J* = 7.1 Hz, 2H, CH₂).

¹³C-NMR (CDCl₃, 100 MHz): δ 159.5, 145.5, 134.1, 129.3, 129.0, 128.3, 127.6, 54.3, 48.7, 47.0, 26.6, 23.8.

IR ν_{\max} (neat): 3298, 3099, 2939, 2861, 2190, 1600, 1543, 1498, 1424, 1342, 1279, 1229, 1048 cm⁻¹.

HRMS (ESI): C₁₄H₁₆N₄NaO [M+Na]⁺ calculated 279.1216, found 279.1206.

2.88c: 1-Benzyl-4-(phenoxyethyl)-1*H*-1,2,3-triazole¹⁷⁹

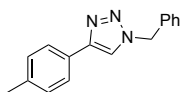


Prepared according to General Procedure J using 5,6-dimethyl-1-((triisopropylsilyl)ethynyl)-1*H*-benzo[*d*]imidazole **2.69** (132 mg, 0.41 mmol, 1 equiv.), (prop-2-yn-1-yloxy)benzene **2.87c** (54 mg, 0.14 mmol, 1 equiv.), benzyl azide **2.65a** (53 μL, 0.41 mmol, 1 equiv.), AMTC (9 mg, 0.041 mmol, 0.1 equiv.), Cu(OAc)₂ (3 mg, 0.02 mmol, 0.05 equiv.) and NaAsc (9 mg, 0.041 mmol, 0.1 equiv.). The resulting residue was purified by flash chromatography (silica gel, hexane/EtOAc 9/1) to provide the desired product as a white solid (106 mg, 97%).

¹H-NMR (CDCl₃, 400 MHz): δ 7.52 (s, 1H, triazole-H), 7.37–7.35 (m, 3H, Ar-H), 7.29–7.25 (m, 4H, Ar-H), 6.97–6.95 (m, 3H, Ar-H), 5.52 (s, 2H, O-CH₂), 5.18 (s, 2H, benzylic CH₂).

¹³C-NMR (CDCl₃, 100 MHz): δ 157.7, 144.2, 134.0, 129.0, 128.7, 128.3, 127.6, 122.1, 120.8, 114.3, 61.6, 53.7.

2.88d: 1-Benzyl-4-(*p*-tolyl)-1*H*-1,2,3-triazole¹⁸⁰

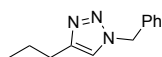


Prepared according to General Procedure J using 5,6-dimethyl-1-((triisopropylsilyl)ethynyl)-1*H*-benzo[*d*]imidazole **2.69** (132 mg, 0.41 mmol, 1 equiv.), 1-ethynyl-4-methylbenzene **2.87d** (48 mg, 0.14 mmol, 1 equiv.), benzyl azide **2.65a** (53 μL, 0.41 mmol, 1 equiv.), AMTC (9 mg, 0.041 mmol, 0.1 equiv.), Cu(OAc)₂ (3 mg, 0.02 mmol, 0.05 equiv.) and NaAsc (9 mg, 0.041 mmol, 0.1 equiv.). The resulting residue was purified by flash chromatography (silica gel, hexane/EtOAc 9/1) to provide the desired product as a white solid (94 mg, 92%).

¹H-NMR (CDCl₃, 400 MHz): δ 7.70 (s, 1H, triazole-H), 7.68 (s, 1H, Ar-H), 7.62 (s, 1H, Ar-H), 7.39–7.36 (m, 3H, Ar-H), 7.32–7.31 (m, 1H, Ar-H), 7.30–7.29 (m, 1H, Ar-H), 7.21 (s, 1H, Ar-H), 7.19 (s, 1H, Ar-H), 5.56 (s, 2H, benzylic CH₂), 2.36 (s, 3H, CH₃).

¹³C-NMR (CDCl₃, 100 MHz): δ 148.4, 138.1, 134.9, 129.6, 129.3, 128.9, 128.2, 127.9, 125.7, 119.3, 54.3, 21.4.

2.88e: 1-benzyl-4-propyl-1*H*-1,2,3-triazole¹⁸¹



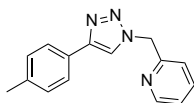
Prepared according to General Procedure J using 5,6-dimethyl-1-((triisopropylsilyl)ethynyl)-1*H*-benzo[*d*]imidazole **2.69** (132 mg, 0.41 mmol, 1 equiv.), pent-1-yne **2.87e** (28 mg, 0.14 mmol, 1 equiv.), benzyl azide **2.65a** (53 μL, 0.41 mmol, 1 equiv.), AMTC (9 mg, 0.041 mmol, 0.1 equiv.), Cu(OAc)₂ (3 mg, 0.02 mmol, 0.05 equiv.) and NaAsc (9 mg, 0.041 mmol, 0.1 equiv.). The resulting residue was purified by flash chromatography (silica gel, hexane) to provide the desired product as a white solid (70 mg, 85%).

¹H-NMR (CDCl₃, 400 MHz): δ 7.36–7.31 (m, 3H, Ar-H), 7.24–7.21 (m, 2H, Ar-H), 7.18 (s, 1H, triazole-H), 5.47 (s, 2H, benzylic CH₂), 2.64 (t, *J* = 7.4 Hz, 2H, α-CH₂), 1.64 (sext, *J* = 7.4 Hz, 2H, β-CH₂), 0.9 (t, *J* = 7.4 Hz, 3H, CH₃).

¹³C-NMR (CDCl₃, 100 MHz): δ 148.8, 135.1, 129.1, 128.6, 128.0, 120.7, 54.0, 27.8, 22.7, 13.8.

2.7.4.9 Product from Scheme 2.26

2.89: 2-((4-(*p*-tolyl)-1*H*-1,2,3-triazol-1-yl)methyl)pyridine¹⁸²



To a solution of 5,6-dimethyl-1-((triisopropylsilyl)ethynyl)-1*H*-benzo[*d*]imidazole **2.69** (49 mg, 0.15 mmol, 1 equiv.) and 1-ethynyl-4-methylbenzene **2.87d** (19 μL, 0.15 mmol, 1 equiv.) in MeCN (0.75 mL) was added 2-(azidomethyl)pyridine **2.65h** (20 mg, 0.15 mmol, 1 equiv.), (azidomethyl)benzene **2.65a** (19 μL, 0.15 mmol, 1 equiv.) and Cu(OAc)₂ (1.4 mg, 0.0075 mmol, 0.05 equiv.). The reaction was stirred at rt for 5 h before being filtered through celite and concentrated under reduced pressure. The crude mixture was dissolved in MeCN (0.75 mL) before adding Cu(OAc)₂ (1.4 mg, 0.0075 mmol, 0.05 equiv.) and TBAF (1 M in THF,

22.5 μ L, 0.225 mmol, 1.5 equiv.). The reaction was stirred at rt for an additional 16 h, after which EtOAc (10 mL) was added. The mixture was washed with aq. EDTA (10 mg/mL, 10 mL) and brine (2 x 10 mL), dried over Na₂SO₄ and concentrated under reduced pressure. The resulting residue was purified by flash chromatography (silica gel, Et₂O/MeOH/NEt₃ 20/1/1) to provide the desired product as a white solid (32 mg, 85%).

¹H-NMR (CDCl₃, 500 MHz): δ 8.61 (br. s, 1H, triazole-H), 7.89 (s, 1H, Ar-H), 7.72 (s, 1H, Ar-H), 7.71 (s, 1H, Ar-H), 7.68 (td, J = 7.6, 1.4 Hz, 1H, Ar-H), 7.26 (t, J = 5.4 Hz, 1H, Ar-H), 7.22 (t, J = 5.6 Hz, 3H, Ar-H), 5.69 (s, 2H, benzylic CH₂), 2.36 (s, 3H, CH₃).

¹³C-NMR (CDCl₃, 100 MHz): δ 154.7, 149.8, 148.5, 138.1, 137.5, 129.6, 127.8, 125.7, 123.6, 122.6, 120.0, 55.8, 21.4.

Chapter 3

Developing a New Bio-orthogonal Reactive Group for Step-Efficient, CuAAC Sequential Bioconjugation

Results presented in this chapter are unpublished. This work was performed in collaboration with Dr Linus Reichenbach (preparation of phosphoramidite building blocks and solid phase ODN synthesis).

3.1 The Need for Sequential Bioconjugation

The development of bio-orthogonal, site-selective chemical ligations has considerably improved our understanding of living systems.^{10,20,39,183} The ability to functionalise biomolecules with a probe (*e.g.*, fluorophore, biotin, NMR tag, for example), for example, has revealed their functions, interactions, localisations and structures.¹⁸⁴ While several strategies have been successfully developed for introducing a single chemical handle (see Chapter 1), site-selective and orthogonal sequential modifications of biomolecules remains challenging.

The ability to conjugate biomolecules sequentially and chemoselectively is essential for applications requiring at least two chemical handles, such as Förster resonance energy transfer (FRET).¹⁸⁵ FRET is a spectroscopy platform where a donor fluorophore, in an excited state, transfers energy to an acceptor fluorophore through dipole-dipole interaction.¹⁸⁶ Among a multitude of applications, FRET has been widely used for the detection of nucleic acids (Figure 3.1).¹⁸⁷ Unimolecular (Figure 3.1a) and bimolecular (Figure 3.1b) probes have been extensively developed for monitoring DNA hybridisations and mutations. Since the distance between the two chromophores is crucial for efficient FRET analysis, the advancement of site-selective, orthogonal dual modifications is essential.

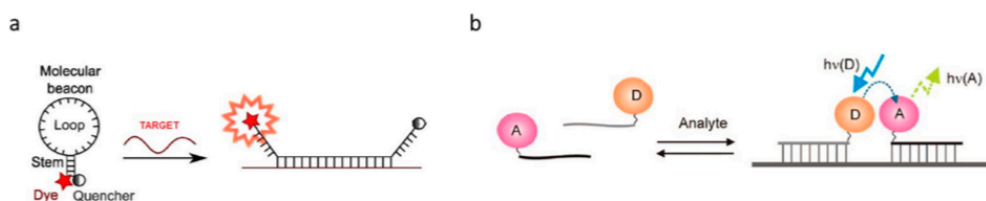
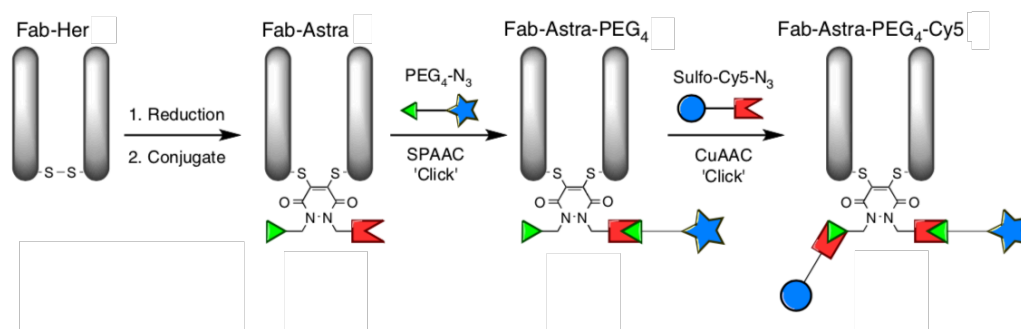


Figure 3.1. FRET probes design for nucleic acid detection. *a)* Example of a unimolecular probe also called a “molecular beacon”. *b)* Example of bimolecular probe.¹⁸⁷

Another example of the importance of biomolecule dual modification has recently been illustrated by Caddick *et al.* with the remarkable construction of a new antibody-drug conjugate (ADC) platform.¹⁸⁸ The authors started their investigations with the site-selective modification of a fragment antigen-binding (Fab) construct *via* the insertion of a dibromopyridazinedione, bearing two chemical handles, into disulfide bonds (Scheme 3.1).

The use of disulfide bonds has been shown to increase the (i) selectivity of the modification and (ii) stability of the construct toward hydrolysis compared to current strategy using lysine modification. Multi-functionalisation of the platform was then possible through sequential SPAAC and CuAAC ligations. Using this approach, the authors were able to incorporate several functionalities such as a fluorophore, a polyethylene glycol, and doxorubicin: a drug commonly used for the treatment of breast cancer.



Scheme 3.1. Sequential modification of native Fab-Her.¹⁸⁸

While SPAAC makes use of a strained alkyne to increase the reaction rate of triazole formation, the terminal alkynes used in CuAAC necessitate the use of a copper(I) catalyst, therefore, in the absence of a catalyst, terminal alkynes will remain inert and selective ligation can be performed at the strained alkyne site.¹⁸⁸ However, this strategy encounters several limitations due to a lack of orthogonality between the two chemical methodologies used (SPAAC ligation must be performed prior to CuAAC), reducing the flexibility of this process. More importantly, it has extensively been shown that the incorporation of the highly hydrophobic cyclooctyne moiety often results in lower probe affinity.^{123,189}

These examples represent only a few among many more uses of multifunctional scaffolds.¹⁹⁰ Improvement of orthogonal and bio-orthogonal ligations is therefore critical for expanding these applications and potentially developing next generation probes.

3.2 The Current *State-of-Art* of Orthogonal Bioconjugation

Bio-orthogonal strategies for biomolecule ligation necessitate non-native chemical functionalities to avoid cross-reactivity with cellular components. However, existing bio-orthogonal strategies (see Chapter 1) frequently employ the same type of reaction (*e.g.*, [3 + 2] cycloaddition) and use similar reactants for performing ligations (*e.g.*, azide, alkyne,

phosphine). This results in loss of orthogonality of one strategy toward another, making sequential conjugation challenging (see figure 3.2 depicting the current bio-orthogonal strategies for the ligation of biomolecules and their compatibility in a *one-pot* process).¹⁹¹ For example, the Staudinger ligation (Figure 3.2, reaction 2) reacts a phosphine with an azide, therefore all the methodologies requiring a phosphine (*e.g.*, CpO/CpS phosphine ligation, reaction 3) and an azide (*e.g.*, SPAAC, reaction 4; CuAAC, reaction 6 and tandem crDA, reaction 8) will not be compatible in a *one-pot* process. Similarly, the use of cyclooctyne is recurrent in the SPAAC, SPANC (Figure 3.2, reaction 5) and the inverse electron-demand Diels-Alder (reaction 7) resulting in a loss of orthogonality within these strategies.

From the available strategies developed for bioconjugation,^{10,20,39} the condensation of ketones and aldehydes (Figure 3.2, reaction 1) has fewest problems with cross-reactivity when used in combination with other strategies.¹⁹¹ However, potential side-reactions with carbonyl-bearing metabolites dramatically decreases its applicability for sequential ligations in living systems.²⁰

As the tandem [3 + 2] cycloaddition-retro-Diels-Alder reaction (tandem crDA, reaction 8) and the CpO/CpS phosphine ligation are relatively recent approaches,^{57,144} no data concerning their orthogonality toward other bio-orthogonal reactions have yet been reported. However, because the moieties needed to perform the ligations (cyclooctene and phosphine in the case of the CpO:CpS phosphine ligation; azide and norbornadiene in the case of the tandem crDA) are commonly used in other strategies, it is easy to predict that these ligations will not be compatible with the Staudinger ligation, the SPAAC, CuAAC, or the inverse electron-demand Diels-Alder reaction.

Among the current bio-orthogonal strategies, the CuAAC and the inverse electron-demand Diels-Alder (when using TCO) have been shown to be compatible due to their orthogonal reactive functional groups. This approach has successfully been used for the site-specific *one-pot* dual labelling of DNA (Scheme 3.2).¹⁹² A series of ODNs were synthesised, incorporating both TCO and terminal alkyne *via* phosphoramidite chemistry.³⁶

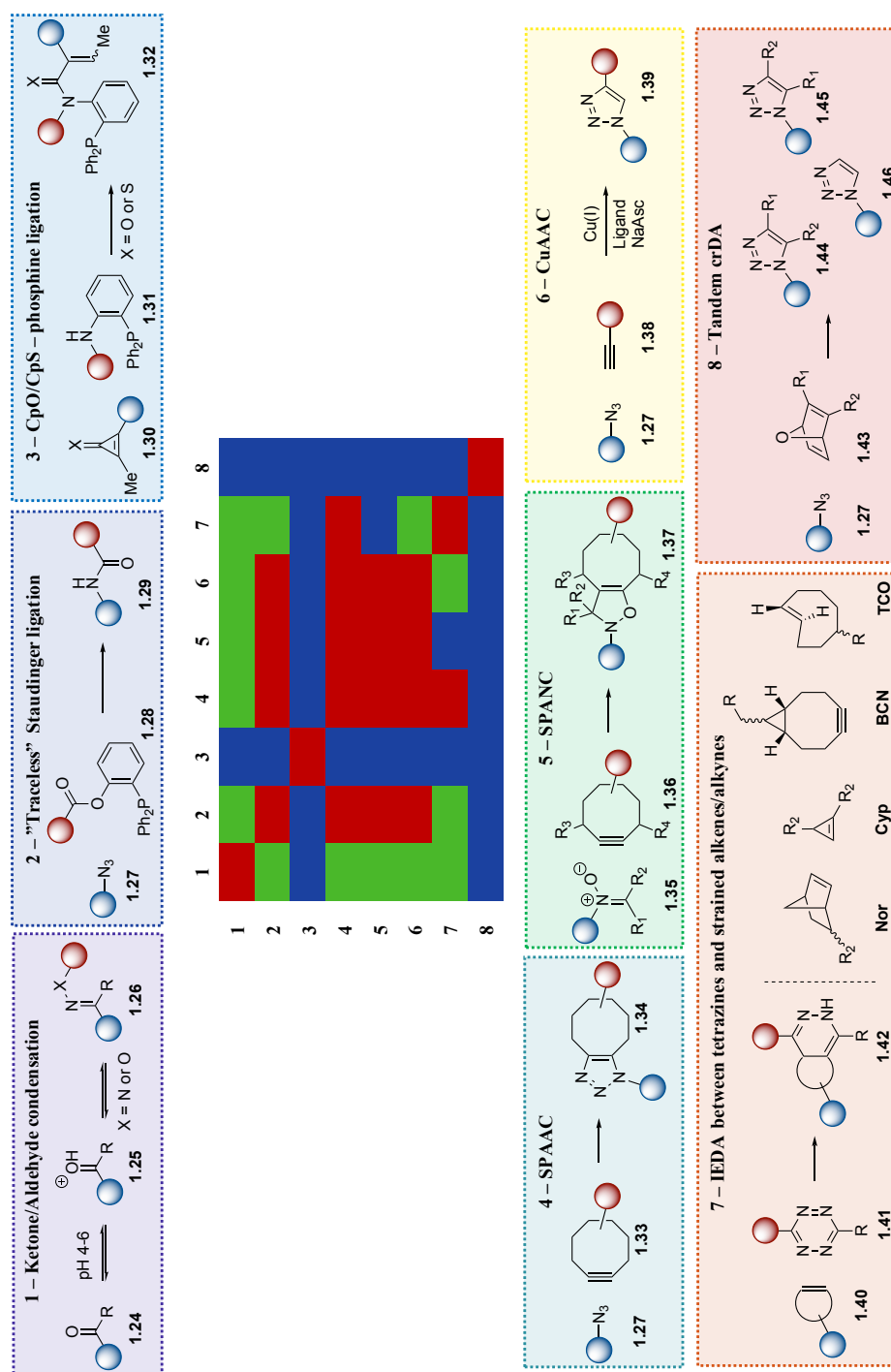
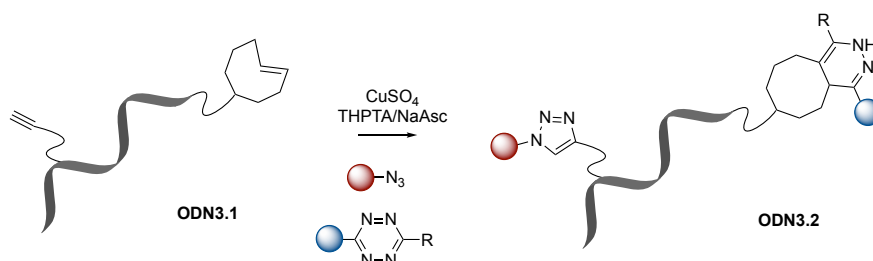


Figure 3.2. Orthogonality between the most commonly used bioconjugation strategies when achieved in a *one-pot* process. *green* = orthogonal, *red* = not orthogonal, *blue* = not reported.¹⁹¹

Control reactions with ODNs, containing either a terminal alkyne or a TCO moiety, were reacted with a tetrazine or an azide, respectively, affording no reaction in each case. These

data indicate a total orthogonality between the two strategies. The bifunctional **ODN3.1**, containing both TCO and terminal alkyne, was then reacted with Cy-5 azide and TAMRA-tetrazine in the presence of CuSO_4 , (100 equiv.) THPTA (500 equiv.) and NaAsc (200 equiv.) affording, after 3 h, the expected **ODN3.2** in 33% yield.



Scheme 3.2. Site-specific *one-pot* dual labelling of DNA.¹⁹²

While efficient, the requirement for supra-stoichiometric amounts (100 equiv.) of toxic copper species remains a serious limitation of this strategy for *in vivo* applications. As other current bio-orthogonal strategies are not compatible for *one-pot* procedures, research has been focused on alternative strategies to perform dual ligations of biomolecules.

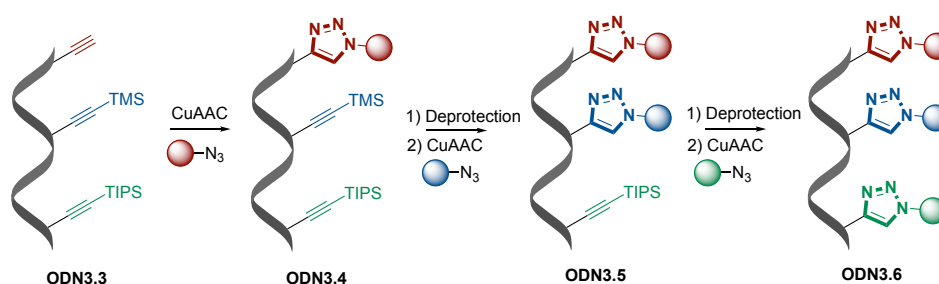
3.3 Dual Modification of Biomolecules using Bio-orthogonal Chemistry

The CuAAC reaction has been extensively explored for the ligation of biomolecules due to its various advantages (compatible with physiological conditions, relatively high reaction rates, accessibility of alkyne/azide surrogates, easy insertion of an alkyne/azide moiety into biomolecules). Importantly, it is one of the few current bio-orthogonal strategies which produces a single product, which is crucial when considering dual modifications of biomolecules. Therefore, to date, the few examples of biomolecules multi-functionalisation reported rely on CuAAC reactions only or combine this strategy to a compatible bio-orthogonal reaction.

3.3.1 Dual Labelling Using Sequential CuAAC Reactions

One of the earliest methods for incorporating two functionalities into biomolecules, described by Carell *et al.*, uses a protection/deprotection strategy providing DNA multi-functionalisation (Scheme 3.3).¹⁹³ Three modified nucleotides, containing either a free, a TMS- or a TIPS-protected alkyne, were incorporated into **ODN3.3** on solid phase, *via* phosphoramidite chemistry. As the CuAAC reaction involves the formation of a Cu-acetylide, silyl-protected

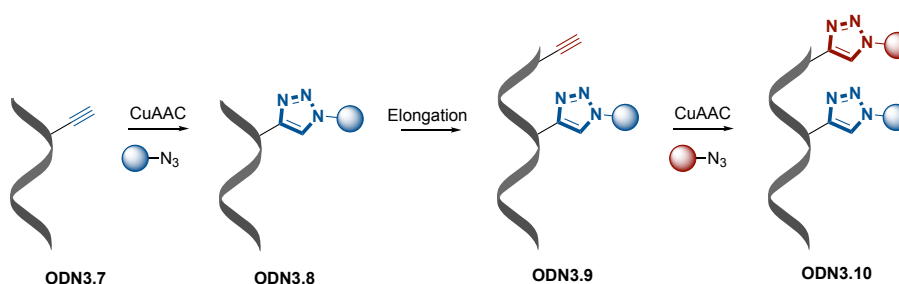
alkynes remain inert until deprotection, allowing the exclusive formation of **ODN3.4** when **ODN3.3** was reacted on the resin with benzyl azide, CuBr, TBTA and NaAsc. Conditions used for the cleavage of ODNs from the resin (32% aqueous ammonia solution) were sufficient for selective TMS-deprotection; no TIPS-deprotection was observed. After RP-HPLC purification, the intermediate was involved in a second CuAAC ligation in solution, affording the formation of **ODN3.5** which was then subsequently treated with TBAF, CuBr, TBTA and NaAsc, ensuring TIPS-deprotection and CuAAC reaction in a *one-pot* process. Crude **ODN3.6** was analysed by RP-HPLC which confirmed the high selectivity of this approach. After RP-HPLC purification, a series of **ODN3.6** were obtained in yields 45–52%.



Scheme 3.3. Chemoselective, sequential modification of ODNs *via* a protection/deprotection methodology.¹⁹³

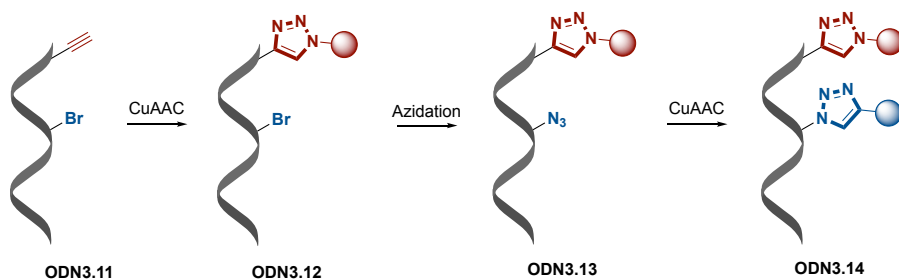
Although proven to be highly selective, this strategy is limited by the fact that the CuAAC ligation has to be performed on solid-support, as the TMS protecting group has shown to be labile in conditions used for cleavage of DNA from the support. This limits the scope of this strategy to the ligation of molecules which remain stable to the harsh cleavage conditions, which is not the case of most fluorophores, for example. Moreover, addition of multiple deprotection steps render this approach less straightforward.

To avoid additional protection/deprotection steps in the synthesis of multi-functionalised DNA, Wengel *et al.* carried out modification while synthesising ODNs *via* the interruption of DNA elongation (Scheme 3.4).¹⁹⁴ In this method, the authors stopped the synthesis of **ODN3.7** after 9 nucleotides, performed the first ligation on solid-support, affording the expected triazole **ODN3.8**. Elongation of the DNA was then continued for 4 nucleotides, incorporating a second alkyne-modified nucleotide. Subsequent CuAAC ligation was possible on solid-support or in solution affording **ODN3.10** in high yields. The main drawback of this method relies in the incompatibility between the aqueous conditions, necessary for CuAAC ligation, and oligonucleotide synthesis, which requires dry conditions. To overcome this issue, the authors had to include additional washing and drying steps to their synthesis.



Scheme 3.4. Dual labelling of DNA *via* elongation interruption.¹⁹⁴

The two strategies described previously rely on solid-support modifications. However, as stated previously, harsh conditions used to cleave DNA from the resin (ammonia, high temperature, 16 h) can result in degradation of sensitive molecules such as fluorophores. To overcome this issue, Morvan *et al.* described the dual modification of DNA using an alkyne- and a bromohexyl-modified nucleotides (Scheme 3.5).¹⁹⁵ The advantage of this approach comes from the ability to specifically achieve CuAAC reaction at the alkyne site, allowing the formation of ODN3.12, followed by the post-synthetic azidation (ODN3.13), giving access to a second chemical handle for modification. This approach also allows the incorporation of an azide moiety at an ODN internal position. Commonly used strategies are limited to the 3' position due to the incompatibility between azide and phosphoramidite chemistry (Staudinger ligation with P^{III}).¹⁹⁶



Scheme 3.5. Dual labelling of DNA *via* post-synthetic azidation.¹⁹⁵

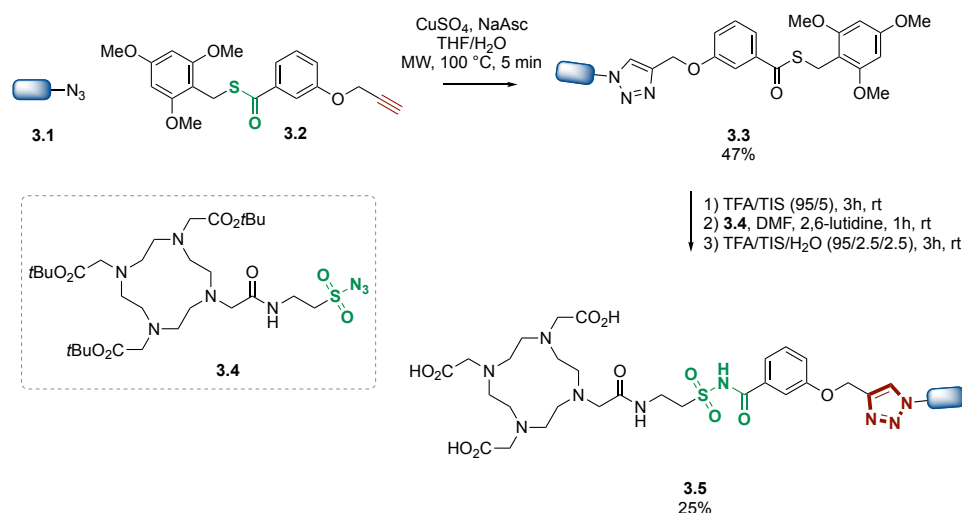
3.3.2 Dual Labelling Strategies which Combine CuAAC with Another Reaction

Several strategies have been successfully developed for DNA dual labelling using CuAAC methodologies. Methods relying on a protection/deprotection strategy or the interruption of DNA synthesis have shown to be efficient but are limited to *in vitro* investigations as modifications need to occur on solid-support. Incorporation of alkyl-bromide followed by *in situ* azidation does not necessitate solid-support modification, however the high temperature

(65 °C) necessary for azide formation is incompatible with biological systems and would most likely provoke protein denaturation and aggregation. Therefore, combination of the CuAAC reaction with other bio-orthogonal ligations had to be investigated for expanding applications of biomolecules sequential labelling.

3.3.2.1 Dual Labelling using Sequential CuAAC and "Sulfo-Click" Ligations

A pioneering strategy for the multi-functionalisation of peptides, combining CuAAC ligation with another bio-orthogonal reaction has been reported by Liskamp *et al.* in 2010.¹⁹⁷ In this study, the authors synthesised and evaluated a series of DOTA-conjugated monomeric, dimeric and tetrameric [Tyr³]octreotide-based analogues for radionuclide therapy and tumour imaging. The synthesis of the monomer is described in Scheme 3.6.

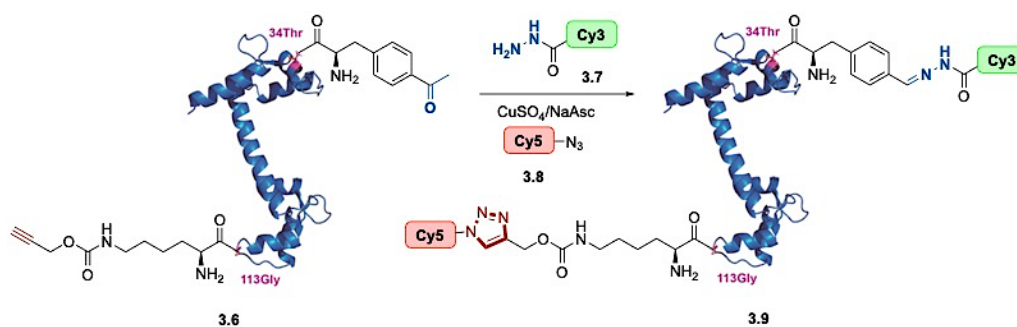


Scheme 3.6. Dual labelling using CuAAC/"sulfo click" strategy.¹⁹⁷

First, an azide-modified peptide **3.1** was reacted in a microwave with propargyl **3.2** in the presence of CuSO₄ and NaAsc affording triazole **3.3** in 47% yield. Ligation of azide-modified DOTA **3.4** was then achieved through a copper-free thio acid/sulfonyl azide amidation ("sulfo click", allowing the formation of compound **3.5** in 25% yield after RP-HPLC purification. The advantage of this methodology relies on the orthogonality of the two ligations with native peptide functionalities. Furthermore, performing the second ligation using the "sulfo click" strategy avoided copper contamination of the DOTA moiety, therefore ensuring efficient radiolabelling, using ¹¹¹In³⁺, of compound **3.5**. However, highly activated, thus extremely unstable, azides were necessary for performing the second ligation without catalyst which remain a limitation to this platform.

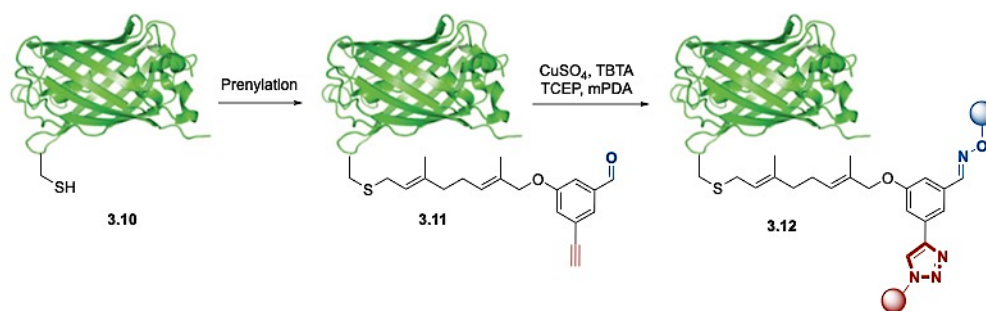
3.3.2.2 Dual Labelling using Sequential CuAAC Ligation and Ketone Condensation

As stated previously, ketone condensation has the advantage of being orthogonal toward other bio-orthogonal methodologies due to its singular reactivity. Therefore, the combination of both ketone condensation and CuAAC reaction has a great potential for *one-pot* site-selective multifunctionalisation of biomolecules. Dual labelling of calmodulin (CaM), a ubiquitous regulator protein involved in several calcium-mediated processes,¹⁹⁸ has successfully been accomplished using this strategy (Scheme 3.7).¹⁹⁹ Alkynyllysine and *p*-acetylphenylalanine were first genetically incorporated into CaM in position 113 and 34, respectively. Dual labelling using hydrazine **3.7** and azide **3.8**, in the presence of CuSO₄ and NaAsc, allowed the integration of the two fluorophores Cy3 and Cy5 to the system. FRET analysis was then performed in order to monitor CaM's conformational change upon calcium binding.



Scheme 3.7. Dual labelling of CaM *via* CuAAC and hydrazine reactions.¹⁹⁹

Alternatively, proteins have been modified using an aldehyde functional group, which could then be reacted to form an oxime (Scheme 3.8).²⁰⁰ In this study the authors multifunctionalised the green fluorescent protein (GFP) by combining CuAAC and oxime ligations. This allowed the introduction of several functionalities, such as TAMRA, fluorescein and dansyl dyes or a polyethylene glycol (PEG) group. However, this approach relies on the specific prenylation of proteins containing a C-terminal CaaX motif (C = cysteine, a = aliphatic amino acid and X = Met, Ser, Gln, Ala or Cys), considerably limiting its range of applications.

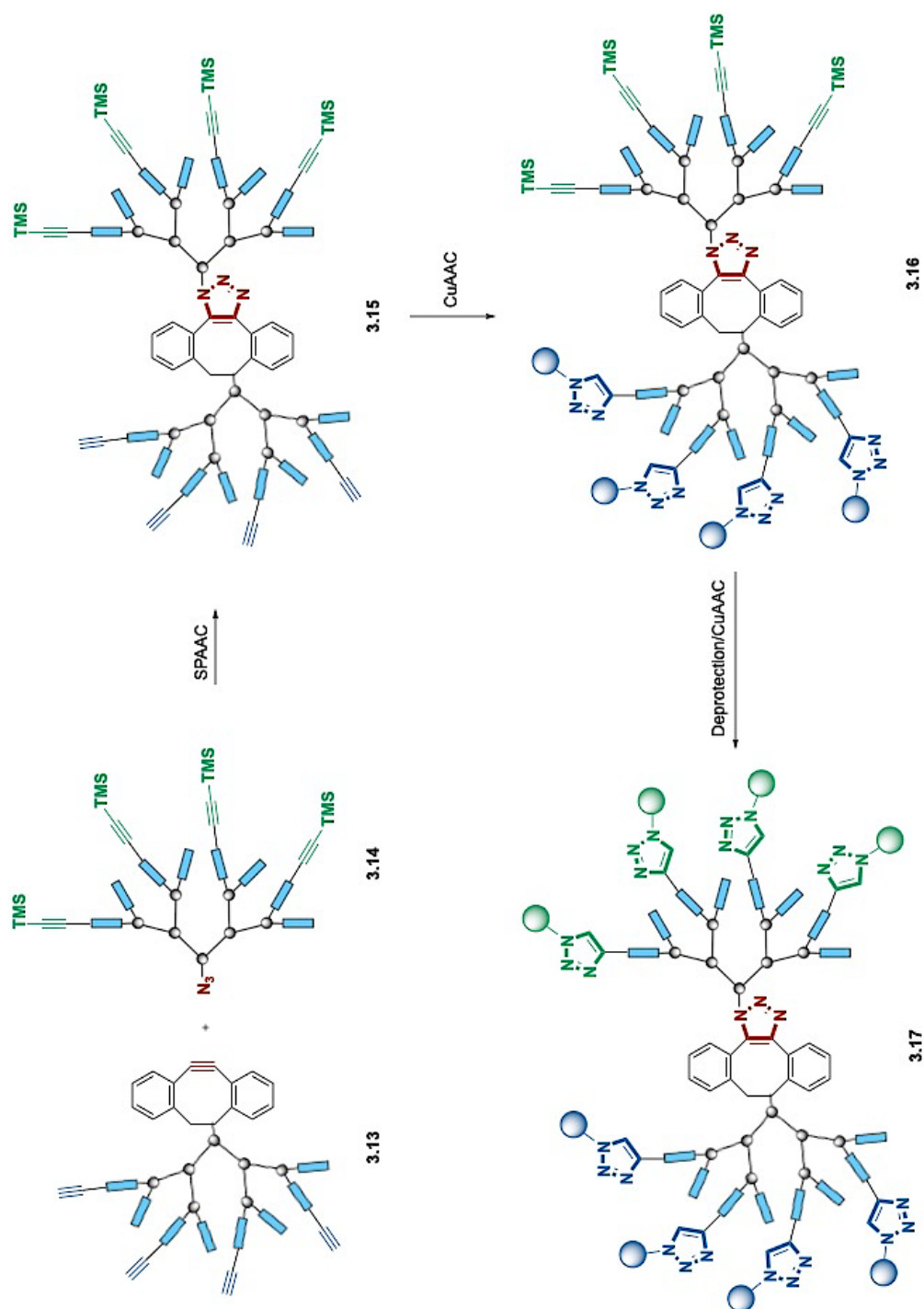


Scheme 3.8. Dual labelling of GFP via CuAAC and oxime ligations.²⁰⁰

This approach has recently been expanded to the dual modification of a lipase using an aldehyde-modified AA incorporated at the *N*-terminal position.²⁰¹ High selectivity was observed when using this strategy for dual modification of proteins. However, the poor selectivity previously observed with ketone condensation reactions limits its applicability to *in vitro* studies.²⁰²

3.3.2.3 Dual Labelling using Sequential CuAAC and SPAAC Ligations

Dual labelling of biomolecules combining CuAAC and SPAAC methodologies has first been described by Wolfbeis *et al.* in 2009.²⁰³ Taking advantage of the reactivity difference between terminal and strained alkynes, the authors were able to multi-functionalise silica-nanoparticles or proteins, such as bovine serum albumin (BSA), commonly used for several biochemical assays. RP-HPLC analyses for the ligations have shown high conversion (> 76%) and site-selectivity for the SPAAC ligations. However, 12 h was required for the reaction to reach completion. The slow reaction rate brings the disadvantage of requiring higher reagent concentration, therefore RP-HPLC purification is necessary between the two ligations to avoid cross-reactivity between the terminal alkyne and excess azide, once the copper-catalyst is added to the system. Nonetheless, this approach has been shown to be efficient for several applications. Combining SPAAC, CuAAC and a protection/deprotection strategy, Boons *et al.* were able to multi-functionalise dendrimers' surface.²⁰⁴ Dendrimers, containing multi-functionalities at their surface, have been studied for their promising characteristics for drug delivery as they can combine tissue targeting and imaging functionalities. In this study, the authors developed a methodology, relying on three sequential azide/alkyne cycloadditions for the assembly and multi-functionalisation of dendrimers (Scheme 3.9).

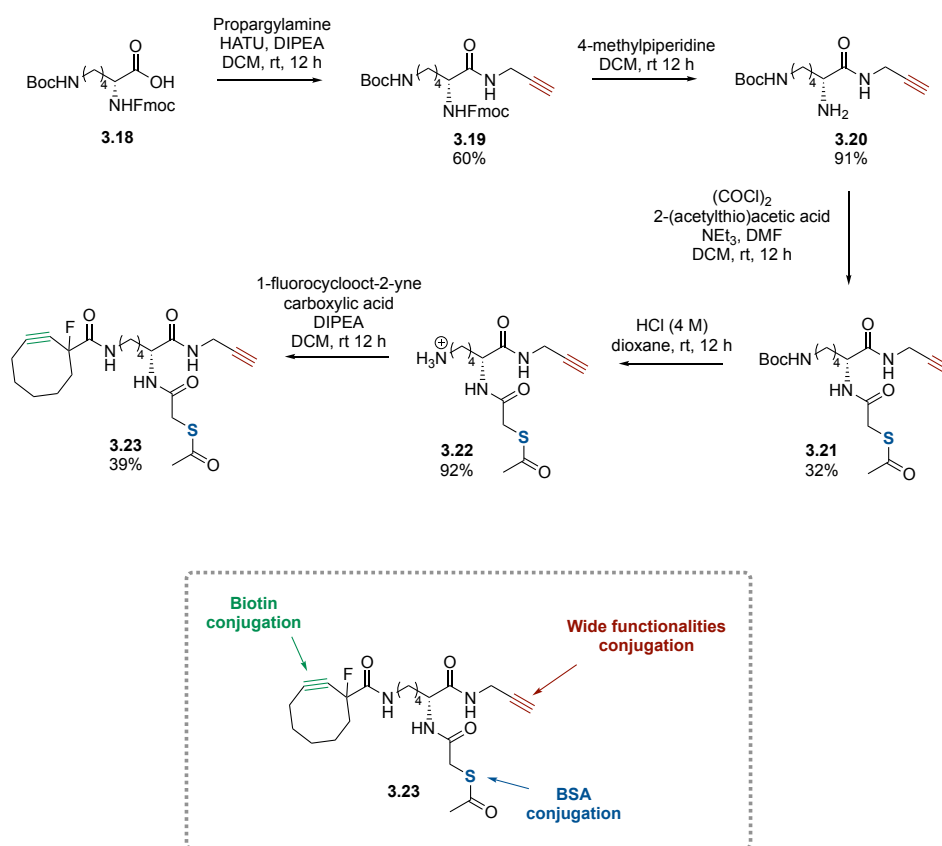


Scheme 3.9. Dual labelling of dendrimers *via* CuAAC/SPAAC ligations.²⁰⁴

First, a DIBO- and an azide-modified polyester dendron were assembled *via* SPAAC ligation. Despite the steric hindrance often observed at dendron focal points which often results in poor coupling conversions, SPAAC ligation afforded dendrimer **3.15** in 93% yield after 24 h.

The second ligation, with the unprotected terminal alkynes, was then performed in the presence of catalytic amount of CuI and DIPEA, resulting in the formation of **3.16** in 75% yield after 4 h. Finally, TMS-deprotection and third ligation was achieved in the presence of CuF₂ (8 equiv.), affording multi-functionalised dendrimer **3.17** after 40 h at 40 °C.

Dual labelling combining CuAAC/SPAAC sequential ligations, followed by the integration of this dual probe into BSA, *via* maleimide linkage, was also reported by Jones *et al.* in 2012.²⁰⁵ In this study, the authors synthesised the trifunctional scaffold **3.23** starting from the commercially available Fmoc-Lys(Boc)-OH **3.18** (Scheme 3.10).



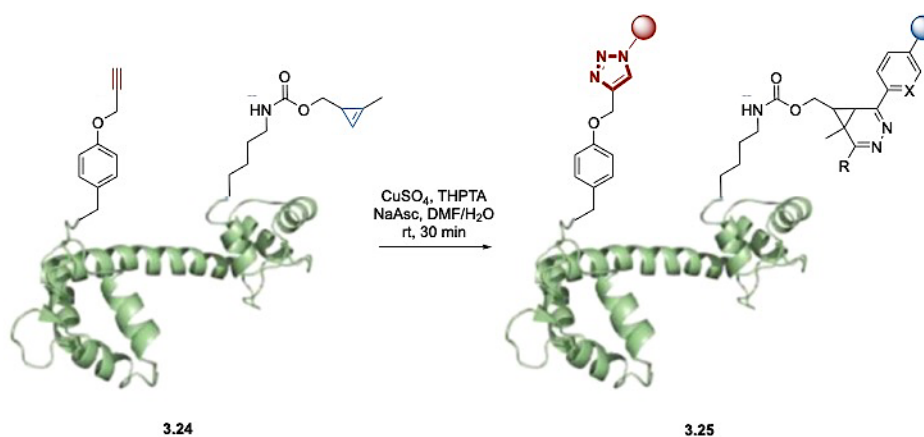
Scheme 3.10. Synthesis of a tri-functional probes and design for sequential multi-functionalisation of BSA.²⁰⁵

First, amide coupling of **3.18** and propargylamine in the presence of HATU and DIPEA afforded terminal alkyne **3.19** in 60% yield after 12 h. Fmoc deprotection, followed by amide coupling of **3.20** with *S*-acetylthioacetic acid, afforded compound **3.21** in 32% yield and resulted in the incorporation of the second functionality. Finally, cyclooctyne functionality was added to the system *via* Boc deprotection followed by amide coupling between **3.22** and

1-fluorocyclooct-2-yne carboxylic acid, allowing the formation of the final product **3.23** in 39%. Overall synthesis of the trifunctional scaffold **3.23** required 5 steps with an overall yield of 6%. It is important to note that cyclooctyne functionality must be incorporated last in this approach due to its instability toward strong acid.²⁰⁵ The applicability of this scaffold for multifunctionalisation was demonstrated with the conjugation of several functional groups, such as protein, peptide, sugar, lipid, fluoroalkane, biotin and fluorophores. The advantage of this approach relies on the fact that this small molecule scaffold was designed to avoid engineered biomolecules, therefore expanding its use. Indeed, the cyclooctyne and terminal alkyne moieties were used to introduce probes to the system while conjugation to biomolecules occurred *via* maleimide linkage, which can easily be incorporated into proteins. However, the instability of the thiol-maleimide linkage²¹ and hydrophobicity of the cyclooctyne moiety limit its applicability to *in vitro* investigations.

3.3.2.4 Dual Labelling using Sequential CuAAC and Inverse Electron-Demand Diels-Alder Ligations

While useful, the previous examples of sequential bioconjugation exhibited extremely slow reaction rates, sometimes requiring days for efficient ligations. Recently, Chin *et al.* have demonstrated that the combination of CuAAC and inverse electron-demand Diels-Alder methodologies allow for the efficient, fast (30 min) and site-selective multi-functionalisation of proteins, such as CaM (Scheme 3.11).²⁰⁶



Scheme 3.11. Dual labelling of CaM *via* CuAAC/inverse electron-demand DA strategies.²⁰⁶

In this objective, terminal alkyne- and cyclopropane-modified AAs were genetically encoded in proteins. Treatment of **3.24** with CuSO₄ (5 000 equiv.), THPTA (5 000 equiv.) and NaAsc

(5 000 equiv.) afforded quantitative dual labelling after 30 min. Importantly, ligations were achieved at physiological pH, temperature and pressure. However, a supra-stoichiometric amount of copper (5 000 equiv.) was needed to increase the rate of CuAAC ligation, limiting its applicability with biomolecules sensitive to copper-mediated oxidative damage.⁸⁰

An alternative approach for nucleic acid multi-functionalisation has recently been reported by Jäschke *et al.*, combining CuAAC, SPAAC and inverse electron-demand Diels-Alder methodologies (Figure 3.3).²⁰⁷ As explained previously, CuAAC and SPAAC reactions are not compatible in a *one-pot* process due to their use of same reactants (*e.g.*, azides). Therefore, to minimise side-reactions between the two ligations, it was necessary to perform and monitor the SPAAC ligation prior to CuAAC, ensuring its completion. Large excesses of azide were needed for the subsequent CuAAC reaction to ensure complete ligation with the ODN, even in the presence of excess competing cyclooctyne. Although cyclooctynes have previously been used for inverse electron-demand Diels-Alder reactions,¹¹⁹ ligation kinetics have been shown to be slower than for strained alkenes,³⁹ therefore no side reaction was observed between SPAAC and inverse electron-demand Diels-Alder reactions. A limitation that this strategy encounters comes from the incorporation of the azide moiety into ODNs, to ensure minimal side-reactions between CuAAC and SPAAC. As stated previously, azides are incompatible with phosphoramidite chemistry, resulting in Staudinger side-reactions. Therefore, they can only be incorporated at the 3' position during nucleic acid synthesis. Moreover, it has been reported that azide-modified AAs are prone to reduction, forming the corresponding amines when encoded into proteins.²⁰⁸ Potential side-reactions combined with the instability of the functional groups inserted into biomolecules thus limit the flexibility of this approach.

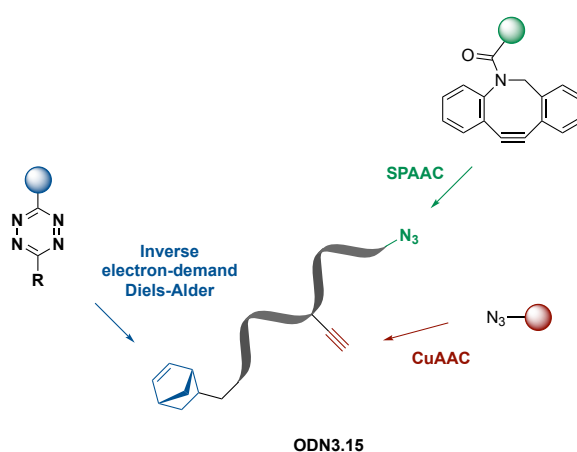


Figure 3.3. Design of triple “click” labelling of nucleic acids.²⁰⁷

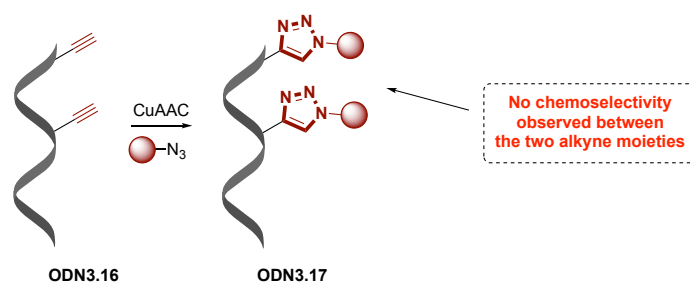
3.3.3 The Need for New Strategies for Sequential Bioconjugation

The different limitations observed with the previously described approaches for biomolecule multi-functionalisation highlight the need for more sophisticated methodology. An ideal platform for efficient sequential bioconjugation must (i) incorporate stable functionalities into biomolecules, (ii) use mild conditions for incorporating these functions and performing the ligations, (iii) achieve ligations with high reaction rate and yields and (iv) integrate small chemical moieties, that will therefore not disrupt biomolecules' structure and functionality.

Ketones have been shown to be easily encoded into biomolecules; however, potential side-reaction with carbonyl-bearing metabolites, slow kinetics and acidic pH, necessary for the ligations,⁴³ render this strategy ineffective for biomolecule dual labelling.

Both Staudinger and CpO/CpS phosphine ligations are not compatible for *in vivo* sequential labelling due to the oxidation-sensitive properties of phosphine moieties towards air or metabolic enzymes and their slow kinetics.⁴⁷ Strategies using large moieties, such as cyclooctynes in SPAAC and SPANC, or cyclooctene in inverse electron-demand Diels-Alder and tandem crDA, exhibit faster kinetics, which would then be favourable for sequential ligations. However, the large sizes and strong hydrophobicity of these functional groups result in (i) poor cell uptake for *in vivo* applications, and (ii) structure modifications of biomolecules.

Despite copper toxicity, the CuAAC methodology remains the favoured choice for bioconjugation due to its numerous advantages compared to the other bio-orthogonal strategies. Furthermore, incorporation of terminal alkyne moieties has extensively been reported. Nevertheless, current strategies using CuAAC methodology are often laborious. Indeed, the lack of chemoselectivity of alkyne and azides moieties, toward another alkyne/azide surrogate, results in the requirement of protecting groups or hidden reactive groups. The example of DNA dual labelling using CuAAC reactions without protected groups, reported by Astakhova *et al.* (Scheme 3.12),²⁰⁹ reflects the limitation of this strategy to discriminate one alkyne from another.



Scheme 3.12. Dual labelling of ODNs using CuAAC reactions without protecting groups.²⁰⁹

Recently, Chin *et al.* have reported the orthogonal, sequential dual labelling of proteins using inverse electron-demand Diels-Alder methodology only (Figure 3.4).²¹⁰ By exploiting the difference in reactivity between norbornene and strained cyclooctyne, as well as the difference between alkyl- and aryl-substituted tetrazines, the authors were able to achieve chemoselective protein multi-functionalisation in high yields.

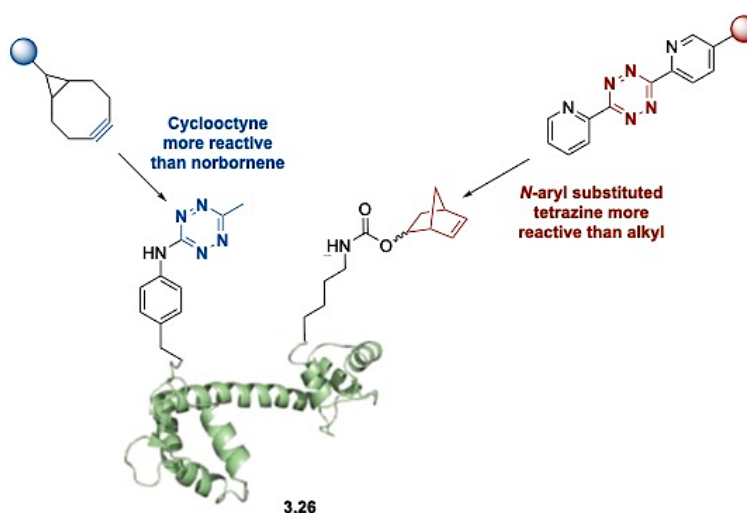


Figure 3.4. Chemoslective dual labelling of CaM *via* inverse electron-demand Diels-Alder.²¹⁰

3.4 Hypothesis to be Tested

The use of aromatic ynamines as a new reactive group for CuAAC reactions has been shown to dramatically increase reaction kinetics for small molecule ligation, even in the presence of low copper loading.^{170,171,174} Furthermore, the enhanced reactivity of aromatic ynamine has allowed chemoselective CuAAC ligations when in competition with regular alkynes. In fact, when an aromatic ynamine and an aliphatic alkyne were incorporated into a bifunctional

system, the superior reactivity of the aromatic ynamine afforded chemoselective, sequential CuAAC ligations in a *one-pot* process.

Analogous to the approach of Chin *et al.*, the work described herein seeks to exploit the enhanced reactivity of aromatic ynamines for developing a new methodology for sequential, chemoselective multi-functionalisation of ODNs. Such a platform would have the advantage of incorporating small chemical moieties, which should not have a strong impact on ODN structure. Furthermore, the enhanced reactivity of aromatic ynamines should allow considerably decreased copper loading, which would therefore minimise potential degradation of biomolecules.

3.5 Aims of this Chapter

The specific aims of this chapter are to:

- (i) Synthesise a focused series of aromatic ynamine phosphoramidites and incorporating them into ODNs (Collaboration with Dr Linus Reichenbach; Figure 3.5).

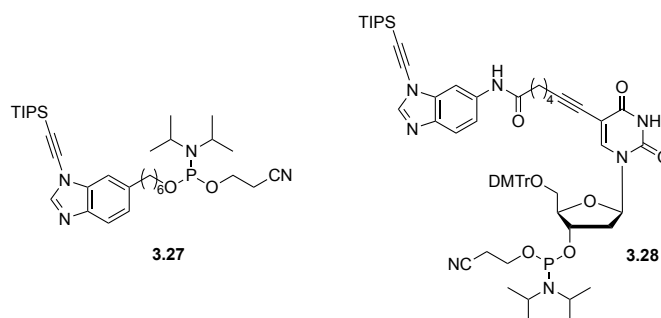
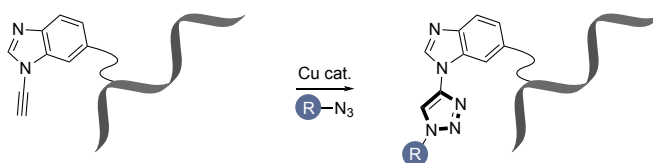


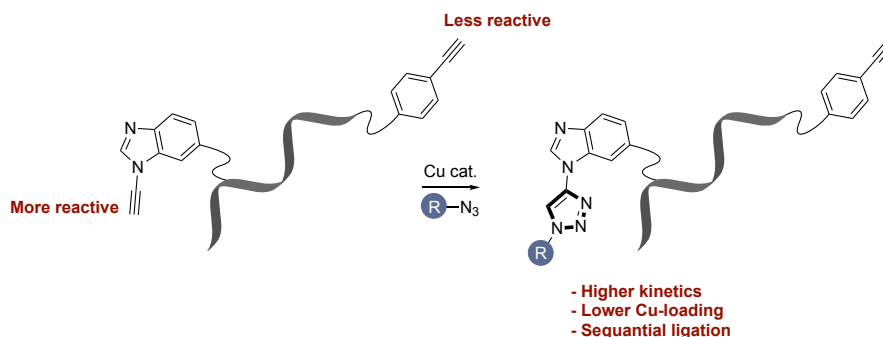
Figure 3.5. Example of ynamine phosphoramidite synthesised.

- (ii) Optimise reaction conditions for CuAAC ligation ynamine-modified ODNs (Scheme 3.13).



Scheme 3.13. Determine optimal conditions for ODNs CuAAC ligation using an aromatic ynamine.

- (iii) Establish reaction conditions for chemoselective, sequential ligations of ODNs using enhanced reactivity of aromatic ynamines (Scheme 3.14).



Scheme 3.14. Determining optimal conditions for chemoselective, sequential CuAAC ligation of ODNs.

3.6 Results and Discussion

3.6.1 Phosphoramidite Synthesis

Incorporation of aromatic ynamine and phenylacetylene moieties into ODNs was achieved either *via* phosphodiester linkage, when in a 5' terminal position, or directly conjugated to an internal thymidine. In this objective, aromatic ynamine- and phenylacetylene-modified phosphoramidite nucleotides were synthesised.

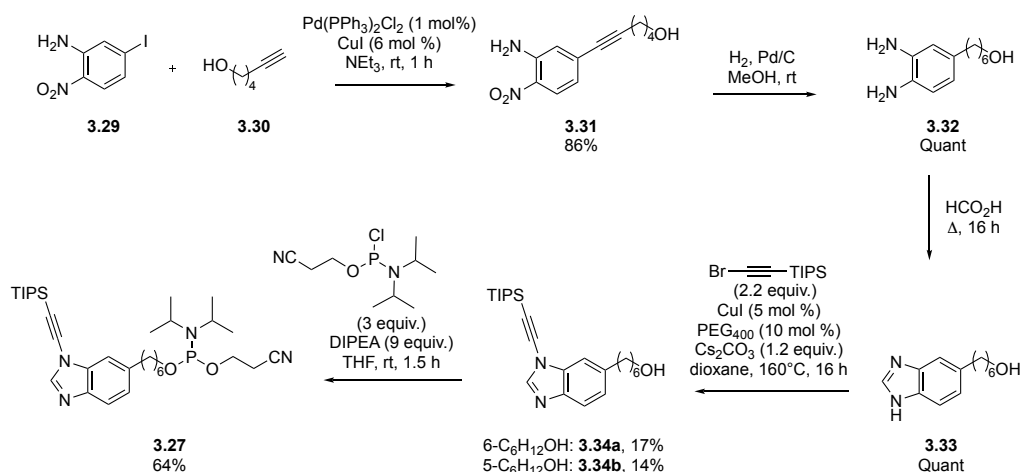
Since its discovery in 1981, the use of phosphoramidite nucleotides remain the gold standard for chemical DNA synthesis.²¹¹ They are easily activated by mild acid, such as tetrazole derivatives or 4,5-dicyanoimidazole, have shown high stability toward hydrolysis and oxidation and react with protected nucleotides in high yields (> 99%).²¹²

3.6.1.1 Synthesis of External Aromatic Ynamine Phosphoramidite*

When at the terminal 5' position, aromatic ynamine moiety was incorporated *via* a phosphodiester linkage. In this objective, phosphoramidite **3.27** was synthesised in 5 steps (Scheme 3.15), starting from a Sonogashira coupling between iodo-aryl **3.29** and terminal alkyne **3.30** in the presence of triethylamine and a catalytic amount of Pd(PPh₃)₂Cl₂ and CuI. After 1 h of reaction, internal alkyne **3.31** was obtained in 86% yield. Reduction of the nitro and alkyne groups was achieved *via* hydrogenation in the presence of Pd/C, affording

* Synthesis developed by Dr Linus Reichenbach (unpublished).

compound **3.32** in quantitative yield. Benzimidazole formation was completed through the reaction of **3.32** and formic acid, affording **3.33** in quantitative yield after 16 h. Cu-catalysed *N*-alkylation was then achieved in the presence of bromo-TIPS-acetylene, Cs₂CO₃ and catalytic amount of CuI and PEG-400, producing **3.34a** and **3.34b** in 17% and 14% yields, respectively. Finally, phosphoramidite **3.27** was obtained in 64% yield *via* the reaction of **3.34a** with chloro(diisopropylamino)- β -cyanoethoxyphosphine.

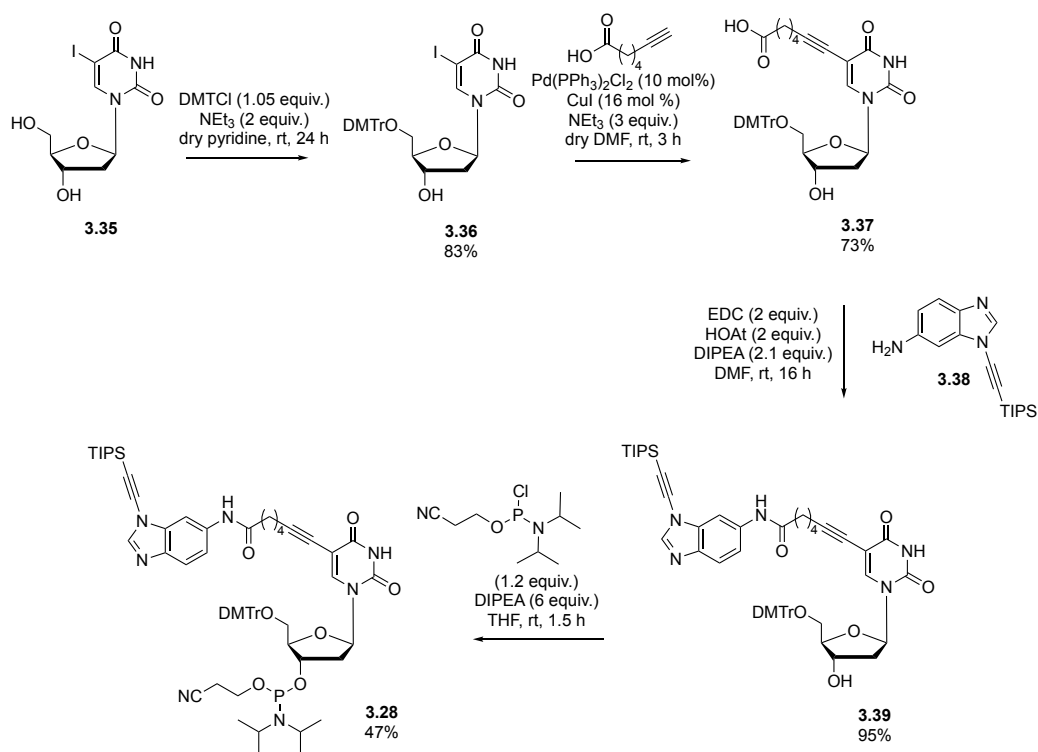


Scheme 3.15. Synthesis of external aromatic ynamine phosphoramidite **3.27**. *Isolated yields.*

3.6.1.2 Synthesis of Internal Aromatic Ynamine Phosphoramidite*

The aromatic ynamine functional group was conjugated to a thymidine *via* an amide linkage (Scheme 3.16). Synthesis of phosphoramidite **3.28** was first achieved by the DMT protection of 5-iodo-2'-deoxyuridine **3.35**, resulting in the formation of **3.36** in 83% yield. A Sonogashira cross-coupling was then performed in the presence of triethylamine and catalytic amount of Pd(PPh₃)₂Cl₂ and CuI, affording **3.37** in 73% yield after 3 h. Amide coupling between carboxylic acid **3.37** and amine **3.38**, in the presence of EDC, HOAt and DIPEA, ensured the incorporation of the aromatic ynamine moiety, affording compound **3.39** in 95% yield. Finally, phosphoramidite **3.28** was obtained in 47% yield *via* the reaction of **3.39** with chloro(diisopropylamino)- β -cyanoethoxyphosphine.

* Synthesis developed by Dr Linus Reichenbach (unpublished).

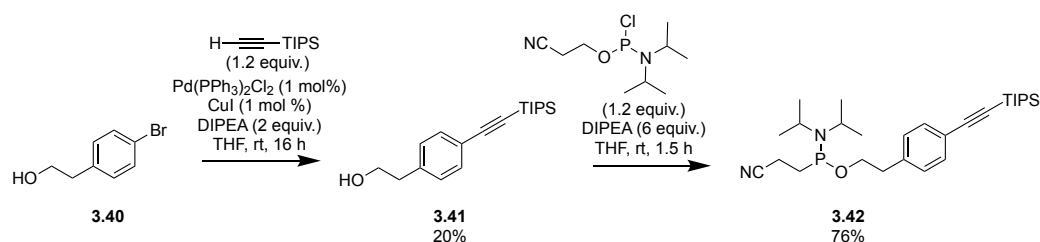


Scheme 3.16. Synthesis of internal aromatic ynamine phosphoramidite **3.28**. *Isolated yields.*

3.6.1.3 Synthesis of External Alkyne Phosphoramidite*

To compare the difference of reactivity between aromatic ynamine and more conventional alkynes in CuAAC bioconjugation, an external phenylacetylene phosphoramidite **3.42** was also synthesised (Scheme 3.17). In this objective, 2-(4-bromophenyl)ethan-1-ol **3.40** was first reacted in a Sonogashira coupling in the presence of DIPEA and catalytic amount of $\text{Pd(PPh}_3)_2\text{Cl}_2$ and CuI , affording **3.41** in 20% yield after 16 h. Phosphoramidite **3.42** was obtained in 76% yield *via* the reaction of **3.41** with chloro(diisopropylamino)- β -cyanoethoxyphosphine.

* Synthesis developed by Dr Linus Reichenbach (unpublished).

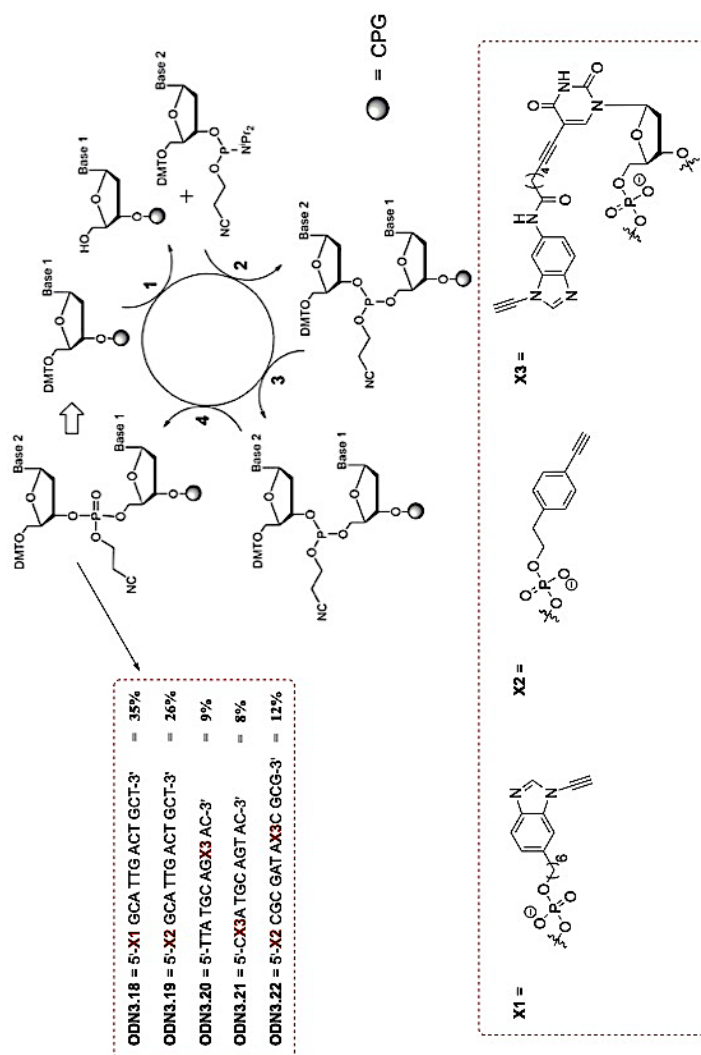


Scheme 3.17. Synthesis of external phenylacetylene phosphoramidite **3.42**. *Isolated yields.*

3.6.2 Synthesis of Aromatic Ynamine- and Alkyne-Modified Oligodeoxyribonucleotides (ODNs)*

ODNs were synthesised using standard solid-phase strategy on a controlled pore glass (CPG) support (Scheme 3.18). Synthesis of **ODN3.18-22** was performed from the 3'-position to the 5'-position, starting from DMT deprotection of the first nucleotide, usually attached to the CPG, in the presence of trifluoroacetic acid solution (3% in DCM), revealing the reactive 5'-hydroxyl group. Activation of the 3'- β -cyanodiisopropyl phosphoramidite group of a second nucleotide was then achieved using 5-benzylthio-1*H*-tetrazole, resulting in the formation of a linkage between the first nucleotide's 5'-hydroxyl group and the second nucleotide's 3'-phosphine group. Capping of potential unreacted 5'-hydroxyl group is performed with acetic anhydride, following by the oxidation of the phosphine, in the presence of I_2 in a pyridine/ H_2O mixture, to a more stable phosphate. This cycle is repeated as many times as needed to obtain expected ODNs. **ODN3.18-22** were obtained in yields 8–35% after cleavage of the CPG, performed using 32% aqueous ammonia solution at rt for 16 h and RP-HPLC purification.

* Synthesis developed by Dr. Linus Reichenbach (unpublished).



Scheme 3.18. Solid-phase ODNs synthesis. 1) DMT-deprotection. 2) Condensation. 3) Coupling. 4) Oxidation. Isolated yields.

3.6.3 Calculation of ODN Extinction Coefficients

Since a laboratory-scale synthesis of DNA is usually achieved on nano- to milli-molar scale, measuring a weight is not possible to obtain yields of reactions. However, the concentration of DNA samples can easily be quantified by UV/Vis spectroscopy at 260 nm, due to the conjugated double bonds of the base pairs. DNA concentration can then be calculated using the Beer Lambert law (Equation 3.1):

$$A_{260} = \epsilon_{260}Cl \quad \text{Equation 3.1}$$

Where A_{260} = absorbance at 260 nm, ϵ_{260} = oligonucleotide extinction coefficient at 260 nm ($\text{L}\cdot\text{mol}^{-1}\cdot\text{cm}^{-1}$), c = oligonucleotide concentration ($\text{mol}\cdot\text{L}^{-1}$) and l = pathlength (cm).

The extinction coefficient ϵ of ODNs depends on its sequence. The most commonly used method for calculating ϵ is based on the nearest neighbour method; ϵ is determined for pairs starting from the 5'- to the 3'-position.²¹³ The value for ϵ is then calculated following equation 3.2.

$$\epsilon = \left[\sum_1^{n-1} \epsilon_{\text{nearest neighbour}} \right] - \left[\sum_2^{n-1} \epsilon_{\text{individual}} \right] \quad \text{Equation 3.2}$$

It worth noting that this equation is an approximation of the real extinction coefficient value and the average error is believed to be around 4%.²¹⁴ In the case where ODNs were modified with chemical groups which would influence on the overall extinction coefficient, calculation of ϵ follows equation 3.3.

$$\epsilon = \left[\sum_1^{n-1} \epsilon_{\text{nearest neighbour}} \right] - \left[\sum_2^{n-1} \epsilon_{\text{individual}} \right] + \left[\sum_1^n \epsilon_{\text{modification}} \right] \quad \text{Equation 3.3}$$

To quantify the impact of aromatic ynamine (**3.43** and **3.44**) and phenylacetylene (**3.45**) moieties on the extinction coefficient of ODNs, absorbance measurements of the different modifications were measured at 260 nm (Figure 3.6). While both external and internal aromatic ynamine scaffolds (respectively **3.43** and **3.44**) have shown to absorb at 260 nm, phenylacetylene **3.45** has no significance absorbance at this wavelength, and consequently no influence on the extinction coefficient value.

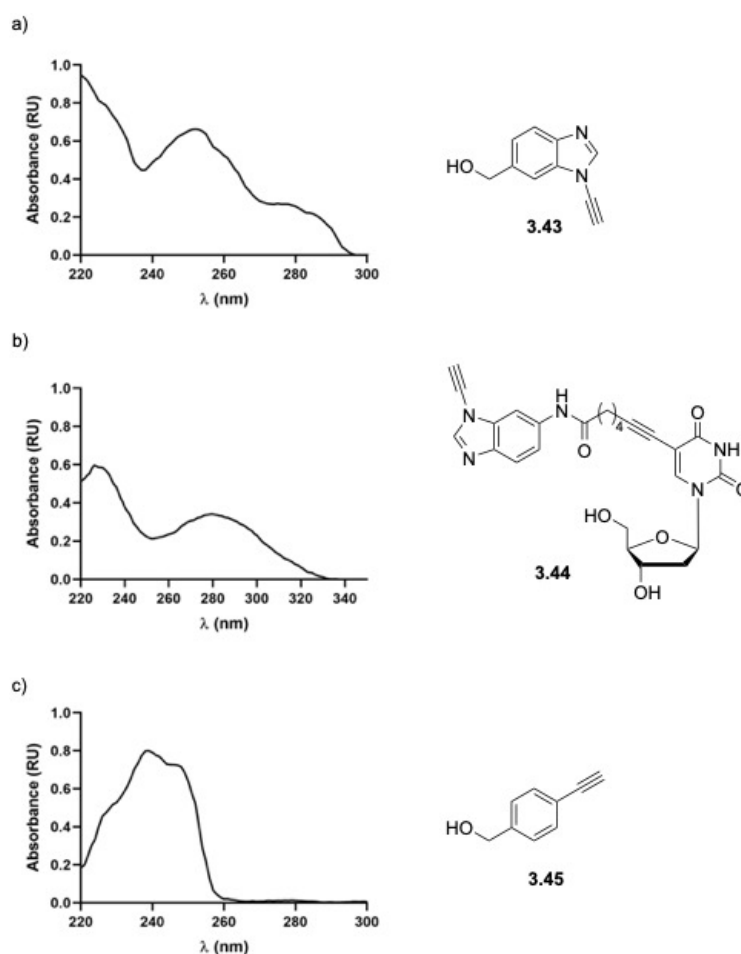


Figure 3.6. Absorbance measurements at 260 nm of aromatic ynamines **3.43** and **3.44** and phenylacetylene **3.45**.

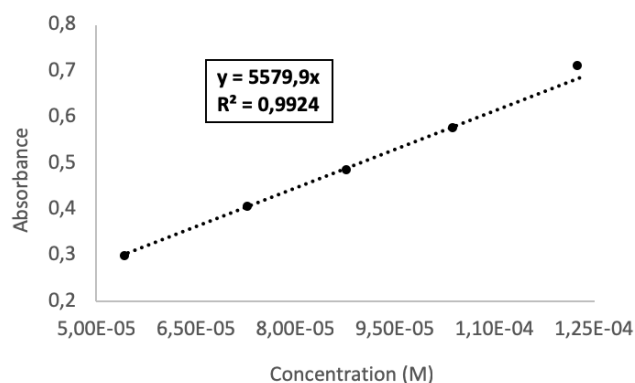
Since both compounds **3.43** and **3.44** have shown a significant absorbance at 260 nm, extinction coefficient was measured for both scaffolds. Measurements were performed in MeOH/H₂O (1/9) at different concentrations, starting from a stock solution containing 10 mg of compound **3.43** or **3.44**. Absorbance was measured in three duplicates for each concentration. Data obtained are presented in Tables 3.1 and 3.2 (for compound **3.43** and **3.44** respectively) and Figure 3.7 and 3.8 represent ϵ calculation (for compound **3.43** and **3.44** respectively). Following Beer Lambert law, extinction coefficient was calculated following equation 3.4.

$$\epsilon = \frac{A_{260}}{cl} \quad \text{Equation 3.4}$$

where $l = 1$ cm.

Table 3.1. Absorbance measurements for aromatic ynamine **3.43**.

Entry	Concentration (M)	A1	A2	A3	Absorbance (average)
1	$1.23 \cdot 10^{-4}$	0.707	0.714	0.704	0.708
2	$1.04 \cdot 10^{-4}$	0.585	0.563	0.568	0.572
3	$8.81 \cdot 10^{-5}$	0.483	0.491	0.476	0.483
4	$7.30 \cdot 10^{-5}$	0.392	0.407	0.403	0.401
5	$5.46 \cdot 10^{-5}$	0.295	0.291	0.295	0.294

**Figure 3.7.** Extinction coefficient calculation for compound **3.43**.

These data suggest that extinction of coefficient of compound **3.43** is $5\,580 \text{ L}\cdot\text{mol}^{-1}\cdot\text{cm}^{-1}$ and therefore that overall extinction coefficient of **ODN3.18** is $121\,847 \text{ L}\cdot\text{mol}^{-1}\cdot\text{cm}^{-1}$. The difference between the concentration using the modified and unmodified ($116\,200 \text{ L}\cdot\text{mol}^{-1}\cdot\text{cm}^{-1}$) extinction coefficients is approximately of 0.3 nmol .

Table 3.2. Absorbance measurements for aromatic ynamine **3.44**.

Entry	Concentration (M)	A1	A2	A3	Absorbance (average)
1	$1.95 \cdot 10^{-4}$	0.739	0.727	0.714	0.727
2	$1.61 \cdot 10^{-4}$	0.603	0.592	0.564	0.586
3	$1.34 \cdot 10^{-4}$	0.472	0.465	0.506	0.481
4	$1.07 \cdot 10^{-4}$	0.357	0.403	0.380	0.380
5	$8.05 \cdot 10^{-5}$	0.288	0.273	0.267	0.276

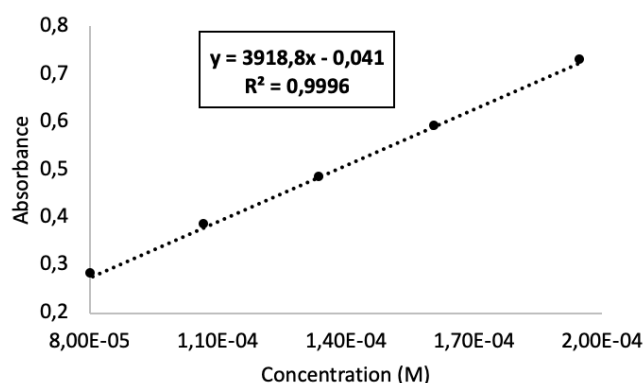


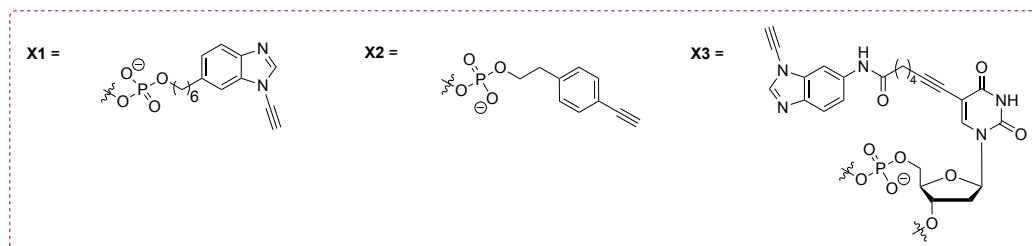
Figure 3.8. Extinction coefficient calculation for compound **3.44**.

These data suggest that extinction of coefficient of compound **3.44** is $3\,919\text{ L}\cdot\text{mol}^{-1}\cdot\text{cm}^{-1}$ and therefore that overall extinction coefficient of modified **ODN3.22** is $107\,919\text{ L}\cdot\text{mol}^{-1}\cdot\text{cm}^{-1}$. The difference between the concentration using the modified and unmodified ($112\,700\text{ L}\cdot\text{mol}^{-1}\cdot\text{cm}^{-1}$) extinction coefficients is approximately of 0.3 nmol.

The modified and unmodified extinction coefficient values for the ODNs synthesised in this project are summarised in Table 3.3.

Table 3.3. Modified and unmodified ODNs extinction coefficient values.

ODN	Sequence	$\epsilon_{\text{unmodified}}$ ($\text{L}\cdot\text{mol}^{-1}\cdot\text{cm}^{-1}$)	$\epsilon_{\text{modified}}$ ($\text{L}\cdot\text{mol}^{-1}\cdot\text{cm}^{-1}$)	[C] _{error} (nmol)
ODN3.18	5'- X1 GCA TTG ACT GCT-3'	116 200	121 847	0.28
ODN3.19	5'- X2 GCA TTG ACT GCT-3'	116 200	116 200	0
ODN3.20	5'-TTA TGC AG X3 AC-3'	119 000	114 119	0.26
ODN3.21	5'- CX3A TGC AGT AC-3'	116 300	111 419	0.27
ODN3.22	5'- X2 CGC GAT AX3C GCG-3'	112 700	107 919	0.29



Due to the error associated with the nearest neighbour calculation, it is often assumed that modifications made on ODNs do not change ϵ significantly and reaction yields are calculated from peak area using RP-HPLC, even when modifying ODNs with fluorophores.¹⁹³ Since

these data showed that aromatic ynamine scaffolds slightly influence ODN overall ϵ , reaction yields are calculated using both, modified and unmodified, extinction coefficient, subsequently providing average yields.

3.6.4 Optimisation of CuAAC ligations using an Aromatic Ynamine-Modified ODN

A screen was conducted to test the reactivity of aromatic ynamines as compared to aromatic alkynes when performing CuAAC ligations on ODNs. A variety of parameters including a screening of ligand and copper source and a screening of azide and copper loading were explored. Initial investigations were achieved to determine the need for additives (e.g., NaAsc, ligand) when performing CuAAC reaction on **ODN3.18** (Figure 3.9).

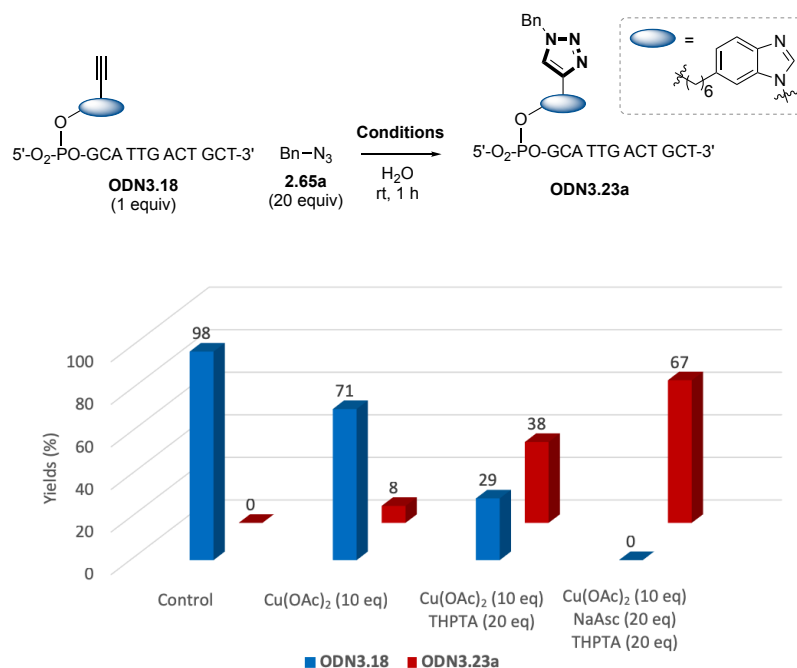


Figure 3.9. Optimization of CuAAC conditions to convert **ODN3.18** into triazole **ODN3.23a**

A control reaction between ynamine-modified **ODN3.18** and azide **2.65a**, without the use of copper catalyst, was performed, affording, as expected, no reaction. The addition of $\text{Cu}(\text{OAc})_2$ (10 equiv.) only provided **ODN3.23a** in $8 \pm 1\%$ yield. Reaction rate was dramatically increased when adding a ligand (e.g., THPTA) to the reaction mixture, consistent with observation made with regular alkynes,⁸² affording **ODN3.23a** in $38 \pm 1\%$ yield. Finally, the

addition of a Cu(II) reductant (*e.g.*, NaAsc) allowed the formation of **ODN3.23a** in $67 \pm 2\%$ yield after 1 h of reaction.

It has previously been reported that the use of triazole ligand, such as THPTA, dramatically accelerates CuAAC reaction rate. This is due to the tetradentate chelation of THPTA ligands with the Cu(I) centre (see Chapter 1 for more information on the impact of ligands on CuAAC kinetics). Commonly used ligands for CuAAC reactions are TBTA⁸² and THPTA.⁸³ Among the several ligands discovered, AMTC has shown to increase CuAAC reaction rate at lower copper loading and has the advantage of being water soluble and easily synthesised.⁸⁷ The reactivity difference of these ligands were then investigated for the formation of **ODN3.23a** (Figure 3.10).

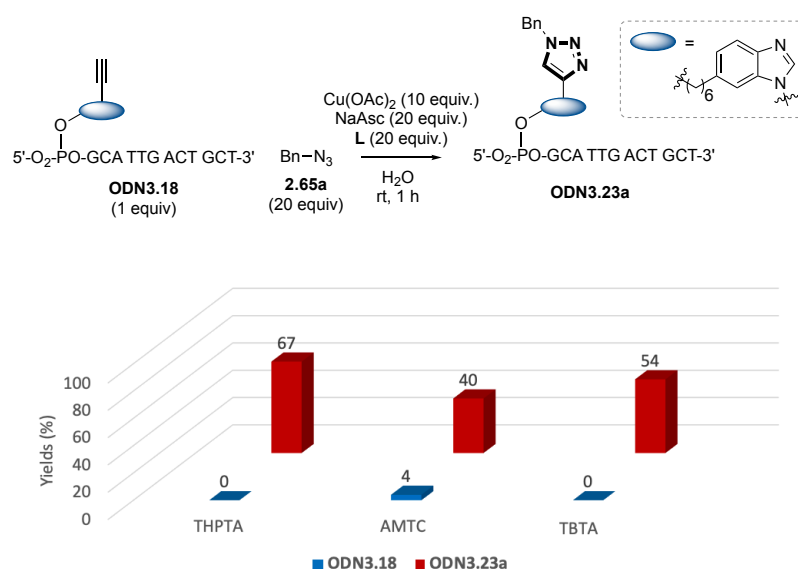


Figure 3.10. Ligand screening for the formation of **ODN3.23a**.

TBTA has shown to decrease the rate of **ODN3.23a** formation compared to THPTA (respectively $54 \pm 2\%$ and $67 \pm 2\%$), most likely due to its poor solubility in aqueous media. AMTC has been shown to decrease reaction rate furthermore ($40 \pm 1\%$ yield), most likely due to its small size.⁸⁷ Indeed, only $4 \pm 1\%$ of **ODN3.18** starting material was recovered, suggesting that most of ODN was degraded, *via* copper-induced oxidative damage, when using this ligand. Since THPTA has shown to generate higher reaction rates and improved ODN stability, it was used for the rest of this study.

A screening campaign was also carried out to investigate the effect of copper source on CuAAC reaction rate when using ynamine-modified **ODN3.18** and azide **2.65a** (Figure 3.11).

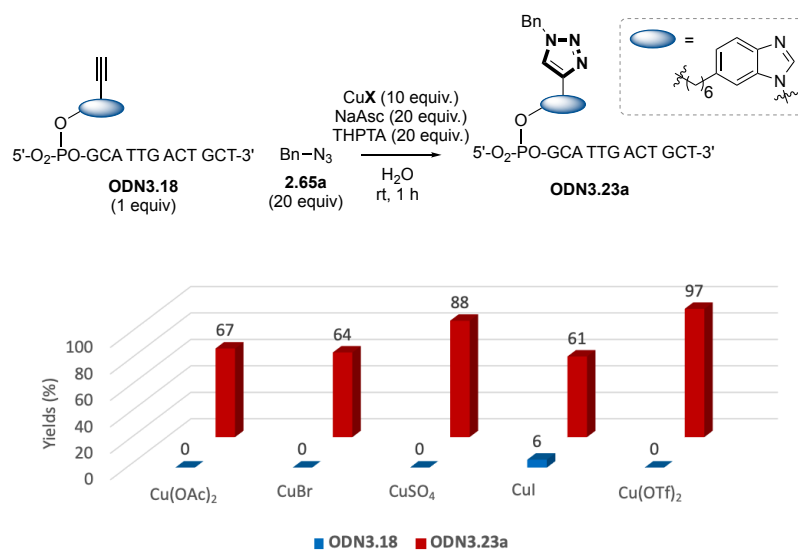


Figure 3.11. Copper source screening for the formation of **ODN3.23a**.

Consistent with observations previously made on small molecules,¹⁷¹ Cu(OAc)₂ has shown slower reaction rates than CuSO₄, when in the presence of a ligand such as THPTA (respectively 67 ± 2% and 88 ± 2%). This could be due to the fact that poly-triazole ligands, such as THPTA, accelerate reaction rate *via* the formation of a copper mononuclear complex.⁸² However, it has also been shown that Cu(OAc)₂ reacts faster as a dinuclear complex.⁸⁸ Therefore, addition of a hindered ligand, such as THPTA, could either slow down the reaction by forming a mononuclear complex, which would then be less favourable for Cu(OAc)₂ or the ligand could chelate the dinuclear complex, forming an extremely hindered, thus less accessible, copper complex. The use of Cu(I), such as CuBr and CuI, has also been shown to decrease the reaction yields (respectively 64 ± 3% and 61 ± 2%). The use of both CuSO₄ and Cu(OTf)₂ has allowed the formation of **ODN3.23a** in excellent yields 88 ± 2% and 97 ± 2%, respectively, after 1 h of reaction. Cu(OTf)₂ was chosen for the rest of this study.

As discussed previously, copper-induced oxidative damage on biomolecules remains a significant limitation of CuAAC methodology, limiting its applicability to bioconjugation. Enhanced reactivity of aromatic ynamine has allowed highly efficient triazole formation with small molecules, even at low copper loading.^{171,215} A study of the copper loading, when performing ligation on **ODN3.18**, was then explored (Figure 3.12).

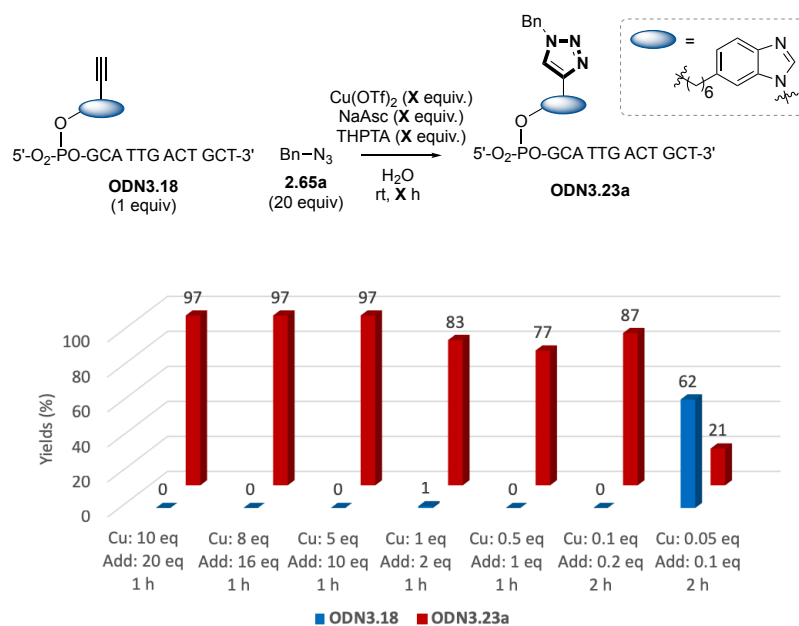


Figure 3.12. Screening of copper loading for the formation of **ODN3.23a**.

No difference in reactivity was observed when decreasing copper loading from 10 to 5 equiv., affording $97 \pm 2\%$ yield of product **ODN3.23a** after 1 h of reaction. Decreasing further to catalytic amount of $\text{Cu}(\text{OTf})_2$ (0.5 equiv.) resulted in only a small loss of reactivity, affording **ODN3.23a** in $77 \pm 2\%$ yield. When increasing the time of reaction to 2 h, triazole formation was efficiently achieved with 10 mol % of $\text{Cu}(\text{OTf})_2$, providing **ODN3.23a** in $87 \pm 2\%$ yield. Attempts to decrease copper loading furthermore afforded a majority of starting material and only $21 \pm 1\%$ yield of **ODN3.23a** after 2 h. It worth noting that, even though the rest of this study uses 10 mol % of $\text{Cu}(\text{OTf})_2$ to decrease reaction time, decreasing copper loading to 5 mol % will still catalyse the reaction and could allow completion of the reaction if reaction time was increased.

Finally, the stoichiometry of azide **2.65a** required to obtain formation of **ODN3.23a** was screened (Figure 3.13). Increasing the excess of azide resulted in a small loss of reactivity, affording **ODN3.23a** in $80 \pm 2\%$ yield, most likely due to the poor solubility of azide **2.65a** in aqueous media. However, decreasing the stoichiometry to 2 equiv. afforded **ODN3.23a** in $99 \pm 1\%$ yield after 2 h of reaction.

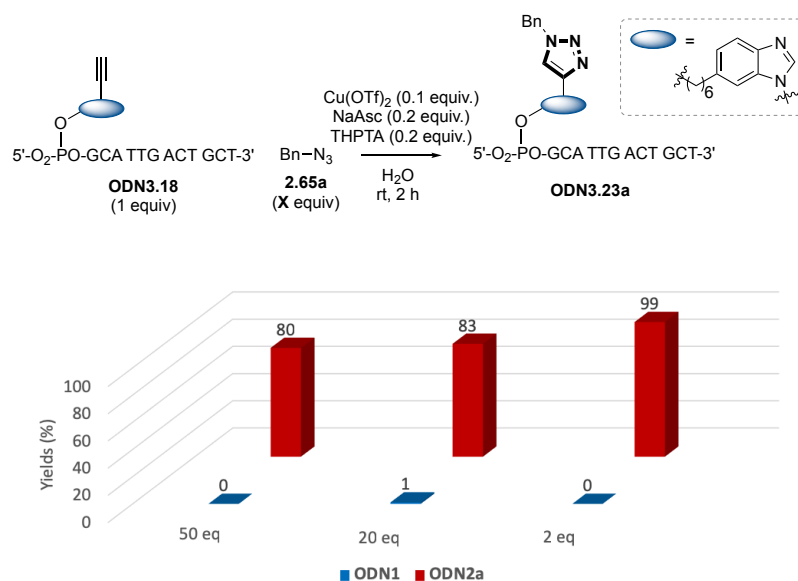


Figure 3.13. Screening of azide stoichiometry for the formation of **ODN3.23a**.

3.6.5 Optimisation of CuAAC ligations using Phenylacetylene-Modified ODN

To compare the reactivity of aromatic ynamine to conventional alkynes, CuAAC reactions using azide **2.65a** and **ODN3.19**, containing the same sequence but modified with a phenylacetylene moiety, were carried out (Figure 3.14). Enhanced reactivity of aromatic ynamines was first demonstrated by the fact that no reaction occurred between **2.65a** and **ODN3.19** after 2 h, even in the presence of 10 equiv. of Cu(OTf)_2 . Increasing reaction time to 16 h afforded the formation of **ODN3.24a** in quantitative yield. Decreasing copper loading to 5 equiv. provided the expected triazole in 88% yield. However, attempts to decrease copper loading further (1 equiv.) resulted in only 48% of **ODN3.24a** after 16 h. Attempts to perform the reaction using catalytic amount of copper resulted in the recovery of starting material only.

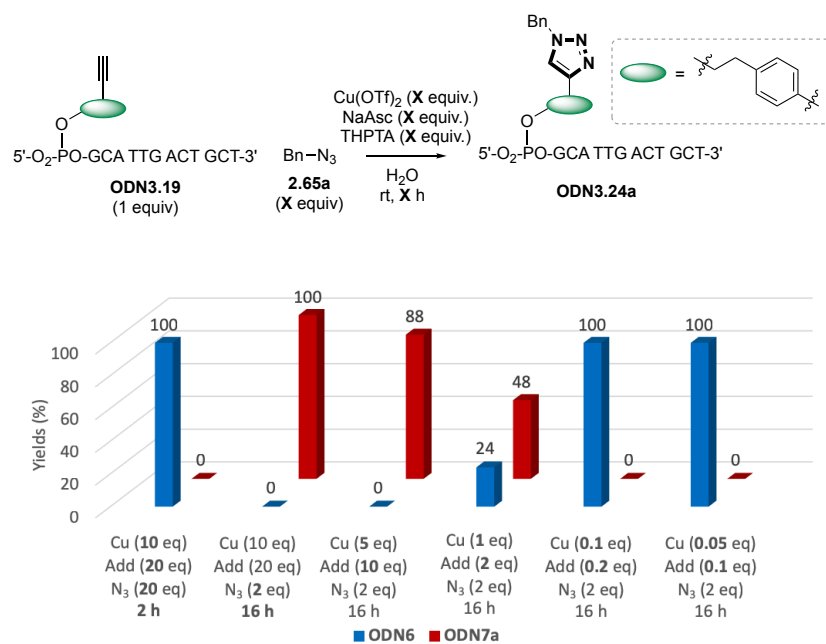


Figure 3.14. Optimisation of CuAAC conditions for the formation of **ODN3.24a**.

3.6.6 Substrate Scope

The substrate scope of aromatic ynamine-modified **ODN3.18** was investigated using $\text{Cu}(\text{OTf})_2$ (10 mol %), THPTA (20 mol %) and NaAsc (20 mol %) in H_2O (Scheme 3.19). The reaction tolerates a wide range of azides containing steric constraints (e.g., **2.65d**), copper-chelating groups (e.g., **2.65h**, **2.65q**, **2.65r**, **3.46a**, **3.46b**, **3.46c** and **3.46e**) and fluorophores (e.g., **2.65q**, **2.65r** and **3.46b**). Interestingly, this strategy allows for the efficient formation of bioconjugates which could be used in several applications. The synthesis of a mimic of a biomedical imaging marker¹⁸⁹ has been demonstrated with the ligation of **ODN3.18** with azide modified-PET probe mimic **3.46a**, affording **ODN3.23d** in $97 \pm 2\%$ yield. Ligation with **ODN3.18** with an azide-modified fluororous tail, commonly used in surface chemistry,²¹⁶ has also been shown, resulting in the formation of **ODN3.23i** in $68 \pm 2\%$ yield. This strategy could also be used for drug discovery with the ligation of azide-modified mannose²¹⁷ **3.46c**, azide-modified folate²¹⁸ **3.46e** and azide-modified cholesterol²¹⁹ **3.46f**, affording respectively **ODN3.23h** in $39 \pm 2\%$ yield, **ODN3.23k** in $65 \pm 1\%$ yield and **ODN3.23f** in $91 \pm 2\%$ yield. Finally, conjugation of **ODN3.18** with biotin azide **2.65s**, commonly used for pull-down assays,²²⁰ has also successfully been demonstrated, providing the formation of **ODN3.23j** in $87 \pm 2\%$ yield. It worth noting that for less reactive azides, such as **2.65d**, **3.46c**, **3.46d** and **3.46e**, higher copper loading was necessary for catalysing the reaction (0.5 to 1 equiv.).

$\text{Cu}(\text{OTf})_2$, 20 mol % of THPTA and NaAsc) afforded no reaction, only recovery of the starting material (Figure 3.15). This result suggests that the position of the modification has a significance influence on its reactivity. Increasing copper loading to 1 equiv. provided the expected triazole **ODN3.25a** in $92 \pm 2\%$ yield. More importantly, aromatic ynamine reactivity was also restored when increasing azide **2.65a** stoichiometry, allowing the formation of **ODN3.25a** in $82 \pm 2\%$ yield with only a catalytic amount of copper (0.1 equiv.).

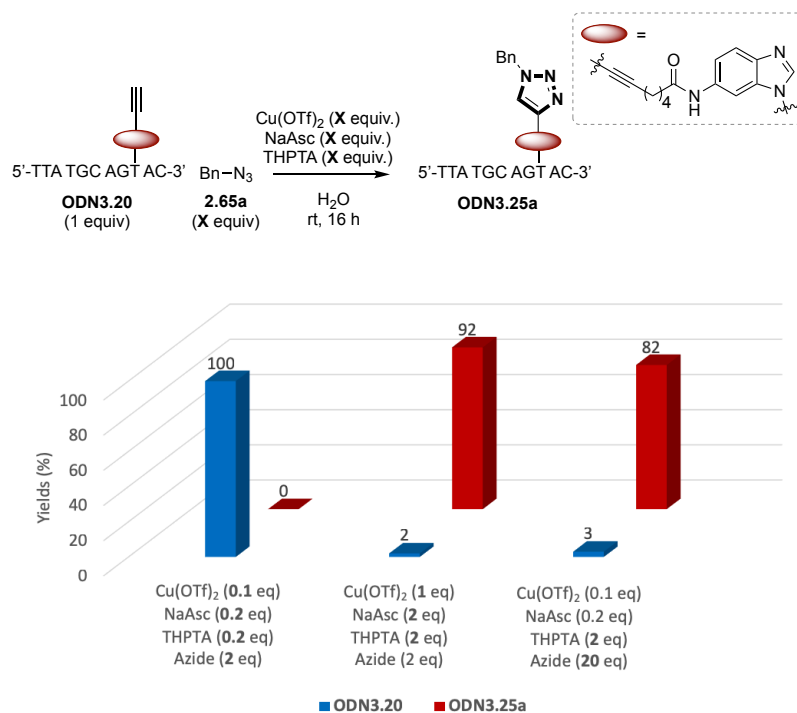


Figure 3.15. Optimisation of CuAAC conditions for the formation of **ODN3.25a**.

To further probe the influence of aromatic ynamine position on its reactivity, CuAAC reaction conditions using **ODN3.21** and azide **2.65a** were also investigated (Figure 3.16). Similar to the previous experiments, no reaction occurred when using the previously optimised conditions (10 mol % of $\text{Cu}(\text{OTf})_2$, 20 mol % of THPTA and NaAsc). Increasing copper loading to 1 equiv. afforded moderate reactivity with the formation of only $50 \pm 1\%$ of **ODN3.26a**. Comparable to **ODN3.20**, when using an excess of azide **2.65a**, CuAAC reaction was successfully performed, providing **ODN3.26a** in $78 \pm 2\%$ yield with only a catalytic amount of copper.

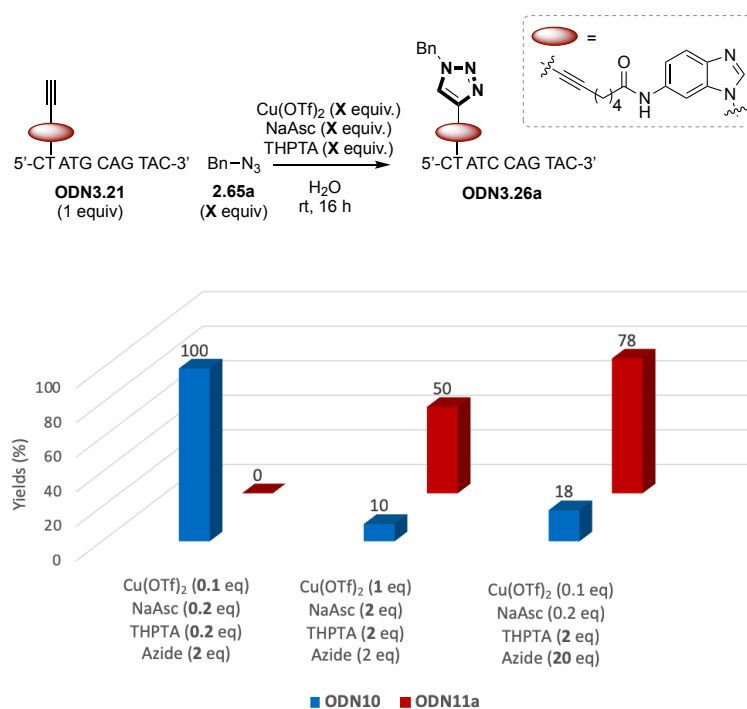
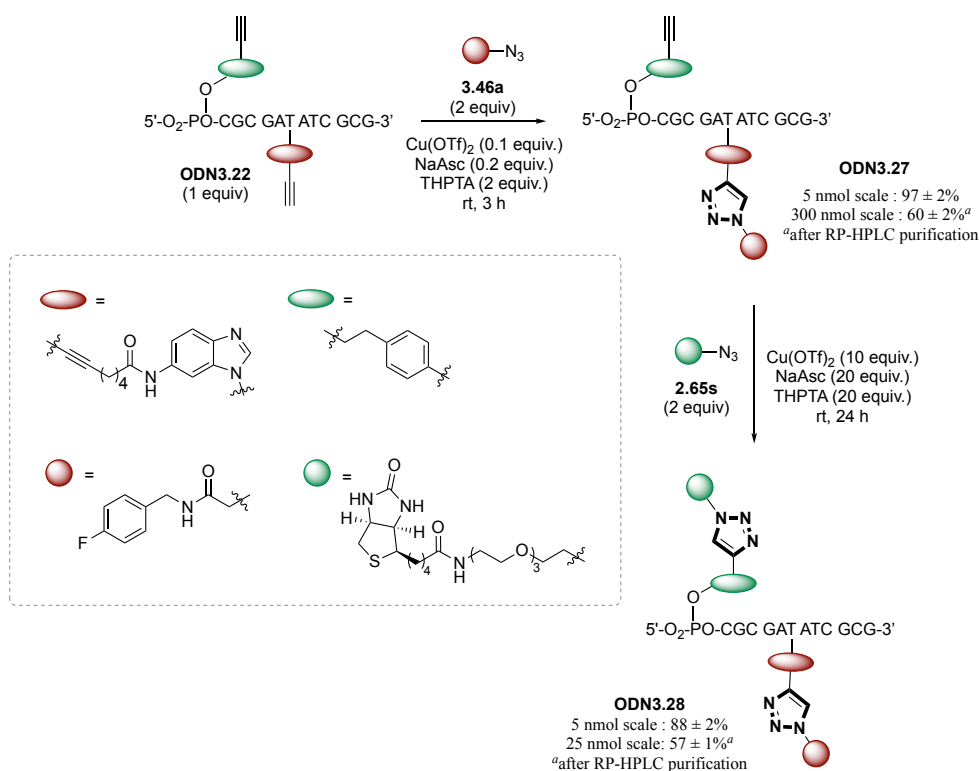


Figure 3.16. Optimisation of CuAAC conditions for the formation of **ODN3.26a**.

These data suggest that the position of the modification has a strong impact on its reactivity, consistent with the fact that, when incorporated in an internal position, aromatic ynamines are less accessible for reacting. However, the addition of an excess of azide restore aromatic ynamine reactivity and allow efficient ligation, even at low copper loading.

3.6.8 Chemoselective, Sequential CuAAC Ligations of ODNs

To demonstrate the potential of aromatic ynamine for performing chemoselective CuAAC bioconjugation, **ODN3.22** was designed to contain a phenylacetylene reactive group at the 3'-position, thus being potentially more accessible, and an aromatic ynamine functional group at an internal position. Furthermore, the sequence of **ODN3.22** has been carefully be chosen to be palindromic, potentially decreasing furthermore the accessibility of the aromatic ynamine moiety. **ODN3.22** was reacted with azide-modified PET-probe mimic **3.46a** in the presence of Cu(OTf)₂ (10 mol %), THPTA (20 mol %) and NaAsc (20 mol %) (Scheme 3.20). After 3 h of reaction, triazole **ODN3.27** was obtained in 97 ± 2% yield. RP-HPLC and MALDI-ToF analyses of the crude have indicated the formation of a single product (Figure 3.17). Scale-up of the reaction to 300 nmol provided compound **ODN3.27** in 60 ± 2% yield after RP-HPLC purification. A second ligation, at the alkyne site, was then performed with biotin azide **2.65s**



Scheme 3.20. Chemoselective, sequential CuAAC reactions on **ODN3.22**.

using Cu(OTf)_2 (10 equiv.), NaAsc (20 equiv.) and THPTA (20 equiv.). After 24 h of reaction, multi-functionalised **ODN3.28** was obtained in 88 \pm 2% yield. Scale-up of the reaction to 25 nmol scale afforded compound **ODN3.28** in 57 \pm 1% yield after RP-HPLC purification.

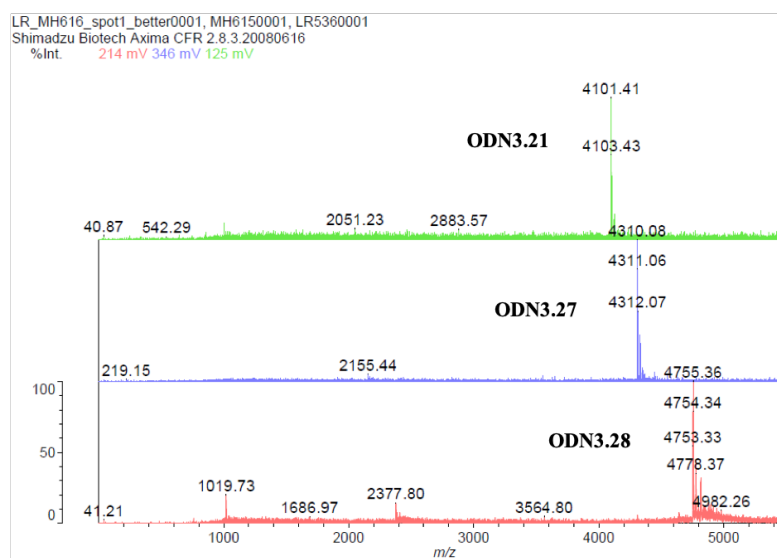


Figure 3.17. MALDI-TOF analysis of sequential CuAAC dual labelling of **ODN3.22**.

To demonstrate that the ligation occurred specifically at the aromatic ynamine position, an enzymatic digestion of **ODN3.27** was performed using ExoI and ExoIII exonucleases.

Exonuclease enzymes cleave nucleotides, one at a time, *via* hydrolysis of phosphodiester groups, either from the 3'- or the 5'-end of DNA.²²¹ ExoIII catalyses the digestion of double stranded DNA from the 3'- to the 5'-position and removes 3'-terminal phosphate groups, generating 3'- hydroxyls. ExoI also degrades DNA from the 3'- to the 5'-position but is only active on single stranded DNA. It releases 5'-monophosphate deoxyribonucleotides up to the last two nucleotides.

To ensure the formation of the DNA duplex, **ODN3.27** was first heated to 80 °C (denaturation) and slowly cooled down to rt (annealing). **ODN3.27** was subsequently incubated with ExoIII at 37 °C for 2 h. As ExoIII catalyses degradation of double stranded DNA, it will only digests **ODN3.27** up to half of the strand. ExoI was then added and the reaction mixture incubated at 37 °C for another 2 h, ensuring the complete degradation of **ODN3.27**. Inactivation of both enzymes, by heating the mixture to 80 °C for 20 min, followed by centrifugation, afforded digested **ODN3.27**, which was then analysed by LC-MS (Figure 3.18).

LC-MS analysis of the digest revealed the presence of unmodified 3'-hydroxyl 5'-phosphate nucleotides (peaks at 3.6 min (T), 5.2 min (C and G) and 7.5 min (A)). No non-digested **ODN3.27** was detected, indicating effective digestion. MS analysis of both peaks (34.2 and 41.9 min) showed mass corresponding to compounds **3.48** and **3.47**, respectively. The triazole product from phenylacetylene and azide **3.46a** was not observed. These data demonstrate that, in the absence of protecting group, aromatic ynamines perform chemoselective CuAAC ligation.

3.6.9 Impact of Aromatic Ynamine Moiety into DNA Structure

The development of bio-orthogonal strategies has allowed a better understanding of biomolecules' structures and functions. Therefore, to be fully effective for bioconjugation, it is important that the incorporated reactive groups, used for performing these bio-orthogonal strategies, does not alter biomolecule structure. Aromatic ynamines have been shown to be easily incorporated into ODNs. However, their impact onto DNA structure as yet not been established.

Although DNA can exist in several different conformations, the most commonly found structure within living systems is a right-handed helix, called B-DNA, which involves two antiparallel strands.²²² The stability of this duplex can be determined thermally by monitoring absorption changes at 260 nm, when submitting the DNA sample to a temperature ramp. Absorption changes usually follow a sigmoidal curve, where the point of inflection represents the temperature where DNA is in equilibrium with single and double strands. This temperature is called melting temperature T_M . A higher T_M values means that DNA duplex is more stable as it requires more energy to break.

To investigate the impact of an aromatic ynamine moiety onto DNA structure, a comparison of the melting temperature T_M between the unmodified DNA **ODN3.29** and modified **ODN3.22** was evaluated. The impact of the triazole (**ODN3.27**) was also assessed. For that, each ODN was successively subjected to temperature ramp (from 20 °C to 80 °C then back to 20 °C at 0.2 °C per minute) three times. ODN absorption was monitored every 0.2 °C.

The results obtained for the three different ODNs are summarised in Table 3.4. The average melting temperature of unmodified DNA, **ODN3.29**, has been shown to be 55.2 °C. After incorporation of aromatic ynamine moiety and phenylacetylene moieties, the average melting temperature has been shown to be 60.6 °C. This result suggests that these modifications stabilise the duplex. After CuAAC reaction, the melting temperature of the triazole product **ODN3.27** has shown a small destabilisation of the DNA duplex, compared to **ODN3.22**, however the melting temperature is comparable to the unmodified **ODN3.29**.

Table 3.4. Melting temperatures of unmodified **ODN3.29** and modified **ODN3.22** and **ODN3.27**.

ODN	T_{m1} (°C)	T_{m2} (°C)	T_{m3} (°C)	T_{mAv} (°C)
ODN3.29	54.2	55.5	55.9	55.2
ODN3.22	61.0	60.6	60.2	60.6
ODN3.27	56.7	54.8	55.2	55.6

The representative melting curves of **ODN3.22**, **ODN3.37** and **ODN3.29** are presented in Figure 3.19. These results suggest that incorporating an aromatic ynamine functional group into ODN for performing CuAAC ligation does not alter its structure and therefore could be used as a new reactive group for *in vitro* and *in vivo* bioconjugation applications.

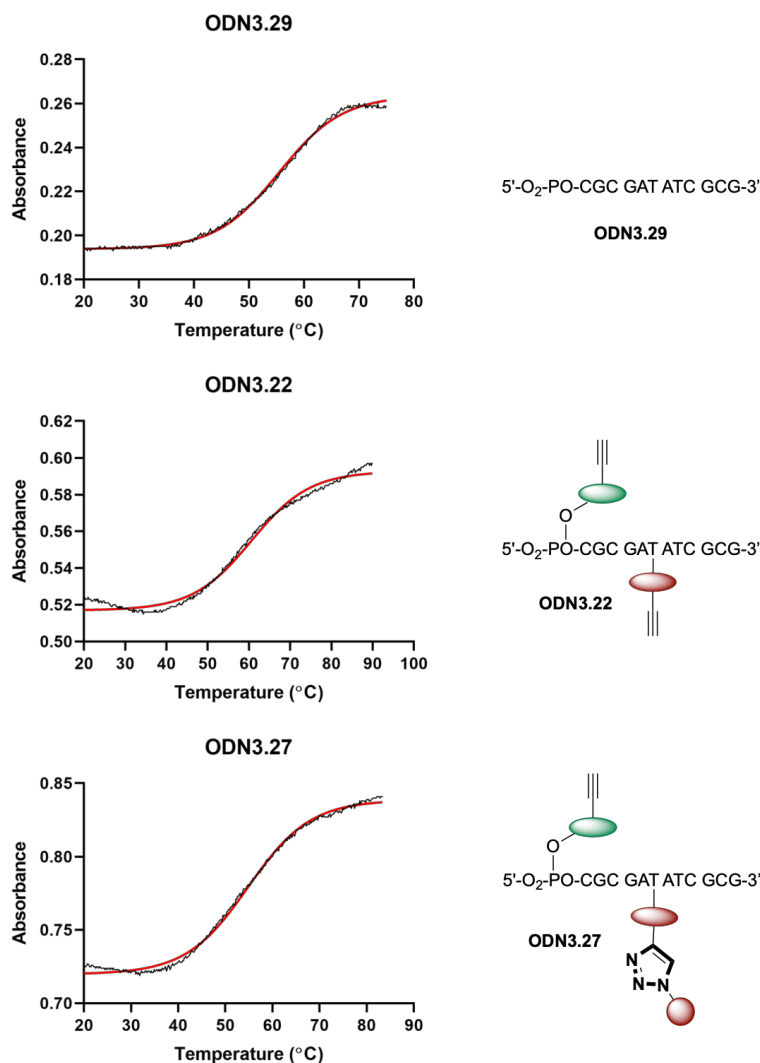


Figure 3.19. Representative melting curves of unmodified **ODN3.29** and modified **ODN3.22** and **ODN3.27**.

3.7 Summary

This work describes the optimisation of chemoselective, sequential CuAAC bioconjugation of oligodeoxyribonucleotides using the enhanced reactivity of aromatic ynamines. Aromatic ynamines have easily been incorporated into DNA, in both internal and external positions. No

degradation of the aromatic ynamine functional group was observed during their incorporation. Its enhanced reactivity has allowed for fast and efficient CuAAC ligations of ODNs with a wide range of azides. Importantly, the high reactivity of aromatic ynamines has allowed decreased copper loading to a catalytic amount (10 mol %) while supra-stoichiometric amounts of copper are usually required due to DNA's numerous Cu-chelation sites.^{81,108} The reactivity difference between aromatic ynamines and aromatic alkynes has also been shown, providing a new platform for chemoselective, sequential bioconjugation of ODNs. Finally, it has been shown that incorporating an aromatic ynamine moiety into DNA does not alter DNA structure. These findings represent a novel, efficient strategy for CuAAC chemoselective bioconjugation.

3.8 Experimental

3.8.1 Reagents and Solvents

All reagents were used as supplied from commercial sources (Fisher, Fluorochem, Sigma-Aldrich) and used without further purification unless otherwise stated. Solvents were all HPLC grade and were used without further purification, unless otherwise stated.

3.8.2 Analysis of Products

3.8.2.1 NMR Spectroscopy

NMR spectroscopy was carried out using either a Bruker AV3 400 MHz UltraShield™ B-ACS 60 spectrometer or Bruker DRX 500 MHz. All chemical shifts (δ) were referenced to the deuterium lock and are reported in parts per million (ppm). Coupling constants are quoted in hertz (Hz). Abbreviations for splitting patterns are s (singlet), br. s (broad singlet), d (doublet), t (triplet), q (quartet), app. quint (apparent quintuplet) and m (multiplet). All NMR data was processed using TopSpin 3.2 software. Proton and carbon chemical shifts were assigned using proton (^1H), carbon (^{13}C), Heteronuclear Single Quantum Coherence (HSQC), Heteronuclear Multiple-Bond Correlation Spectroscopy (HMBC) and Correlation Spectroscopy (COSY).

3.8.2.2 Liquid Chromatography-Mass Spectrometry (LC-MS) and High-Performance Liquid Chromatography (HPLC)

LC-MS was carried out on an Agilent HPLC instrument in conjunction with an Agilent Quadrupole mass detector. Electrospray ionization (ESI) was used in all cases. HPLC was

carried out on a Dionex Ultimate 3000 series instrument (see Appendix for method and column parameters).

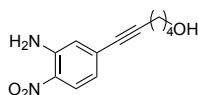
3.8.2.3 Infra-Red (IR) Spectroscopy

IR data was collected on an Agilent spectrometer and the data processed using Spectrum One software. Only major absorbances are reported (> 50 %).

3.8.3 Synthetic procedures

3.8.3.1 Product from Scheme 3.15

3.31: 6-(3-Amino-4-nitrophenyl)hex-5-yn-1-ol²²³

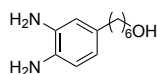


5-Iodo-2-nitroaniline **3.29** (2.7 g, 10 mmol, 1.00 equiv.) was dissolved in NEt₃ (51 mL). CuI (0.11 g, 0.6 mmol, 0.06 equiv.) and Pd(PPh₃)₂Cl₂ (0.08 g, 0.11 mmol, 0.01 equiv.) were added and the mixture was degassed by freeze-pump-thaw cycles. 5-hexyn-1-ol **3.30** (1.0 g, 11 mmol, 1.07 equiv.) was added and the mixture stirred at room temperature for 1.5h. Consumption of the starting material was monitored by TLC (PE/EtOAc, 1/1). The reaction mixture was diluted in Et₂O and filtered through a Celite pad. The organic phase was washed with 1M HCl (1 x 50 mL) and sat. solution of NaHCO₃ (1 x 50 mL), dried over Na₂SO₄, and concentrated under reduced pressure. The resulting residue was purified by flash chromatography (silica gel, PE/EtOAc, 1/1) to provide the desired product as an orange solid (2.1 g, 87%).

¹H-NMR (CDCl₃, 400 MHz): δ 8.17 (d, *J* = 1.9 Hz, 1H), 7.35 (dd, *J* = 8.6, 1.9 Hz, 1H), 6.72 (d, *J* = 8.7 Hz, 1H), 6.11 (br. s, 2H), 3.72 (t, *J* = 6.1 Hz, 2H), 2.44 (t, *J* = 6.7 Hz, 2H), 1.77–1.66 (m, 4H).

¹³C-NMR (CDCl₃, 100 MHz): δ 143.9, 138.5, 131.9, 129.3, 118.8, 113.0, 89.2, 79.2, 62.6, 32.0, 25.1, 19.3.

3.32: 6-(3,4-Diaminophenyl)hexan-1-ol



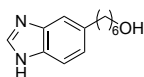
6-(3-Amino-4-nitrophenyl)hex-5-yn-1-ol **3.31** (2.1 g, 8.8 mmol, 1.0 equiv.) was dissolved in MeOH (50 mL). The mixture was degassed by freeze-pump-thaw cycles before adding palladium on carbon 10% (145 mg). Argon atmosphere was replaced by hydrogen atmosphere. The reaction was followed by disappearance of the yellow color of the solution. The reaction mixture was filtered through a Celite pad, washed with MeOH and concentrated under reduced pressure to provide the desired product as a red solid (1.8 g, quant).

¹H-NMR (MeOD, 500 MHz): δ 6.61 (d, $J = 7.8$ Hz, 1H), 6.56–6.55 (m, 1H), 6.43 (dd, $J = 7.8, 1.4$ Hz, 1H), 3.52 (t, $J = 6.6$ Hz, 2H), 2.43 (t, $J = 7.6$ Hz, 2H), 1.58–1.48 (m, 4H), 1.39–1.29 (m, 4H).

¹³C-NMR (MeOD, 125 MHz): δ 136.0, 135.6, 133.3, 120.6, 118.0, 117.9, 63.0, 36.3, 33.6, 32.9, 30.1, 26.8.

HRMS (ESI): C₁₂H₂₀N₂O [M+H]⁺ calculated 209.1648, found 209.1649.

3.33: 6-(1*H*-Benzo[*d*]imidazol-5-yl)hexan-1-ol



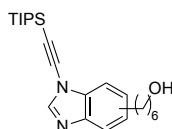
6-(3,4-Diaminophenyl)hexan-1-ol **3.32** (1.8 g, 8.8 mmol, 1.0 equiv.) was heated to reflux in formic acid (14 mL) for 16 h. Excess formic acid was removed under reduced pressure, providing the desired product as a brown solid (1.89 g, quant).

¹H-NMR (MeOD, 500 MHz): δ 8.33 (br. s, 1H), 8.07 (s, 1H), 7.56 (d, $J = 6.1$ Hz, 1H), 7.46 (s, 1H), 7.17 (d, $J = 8.2$ Hz, 1H), 4.14 (t, $J = 6.6$ Hz, 2H), 2.76 (t, $J = 7.6$ Hz, 2H), 1.72–1.63 (m, 4H), 1.44–1.38 (m, 4H).

¹³C-NMR (MeOD, 125 MHz): δ 163.0, 139.6, 125.5, 115.9, 115.0, 64.9, 36.9, 33.0, 29.8, 29.6, 26.8. Two signals not observed/coincident.

HRMS (ESI): C₁₃H₁₈N₂O [M+H]⁺ calculated 219.1492, found 219.1492.

3.34a and 3.34b: 6-(1-((Triisopropylsilyl)ethynyl)-1*H*-benzo[*d*]imidazol-5-yl)hexan-1-ol and 6-(1-((Triisopropylsilyl)ethynyl)-1*H*-benzo[*d*]imidazol-6-yl)hexan-1-ol



6-(1*H*-Benzo[*d*]imidazol-5-yl)hexan-1-ol **3.33** (0.7 g, 3.2 mmol, 1.0 equiv.), CuI (30 mg, 0.2 mmol, 0.05 equiv.), Cs₂CO₃ (1.2 g, 3.5 mmol, 1.2 equiv.), PEG400 (0.5 g, 0.3 mmol, 0.1

equiv.) in 1,4-dioxane (5.2 mL) were added in a sealed tube and degassed by freeze-pump-thaw. Bromo-TIPS-acetylene (1.8 g, 7.0 mmol, 2.2 equiv.) was added and the mixture stirred at 160 °C for 16 h. The reaction mixture was extracted with Et₂O (50 mL), washed with brine (2 x 50 mL), and aq. EDTA solution (10 mg/mL, 50 mL). The organic layer was dried over Na₂SO₄ and concentrated under reduced pressure. The resulting residue was purified by flash chromatography (silica gel, PE/EtOAc, 5/1 to 3/1) to provide the two regioisomers **3.34a** and **3.34b** in 17% and 14% yield, respectively. The absolute regiochemistry was determined by NOESY.

3.34a: 6-(1-((Triisopropylsilyl)ethynyl)-1*H*-benzo[*d*]imidazol-5-yl)hexan-1-ol

¹H-NMR (CDCl₃, 500 MHz): δ 8.04 (s, 1H), 7.59 (s, 1H), 7.45 (d, *J* = 8.3 Hz, 1H), 7.22 (d, *J* = 8.4, 1H), 3.63 (t, *J* = 6.5 Hz, 2H), 2.75 (t, *J* = 7.6 Hz, 2H), 1.68 (app. quint, *J* = 7.3 Hz, 2H), 1.56–1.55 (m, 2H), 1.39–1.38 (m, 4H), 1.18–1.16 (m, 21H).

¹³C-NMR (MeOD, 125 MHz): δ 145.8, 142.6, 141.0, 133.9, 127.3, 120.3, 111.4, 91.4, 73.7, 62.9, 36.8, 33.6, 33.1, 30.1, 26.8, 19.1, 12.4.

HRMS (ESI) : C₂₄H₃₈N₂OSi [M+H]⁺ calculated 399.2826, found 399.2823.

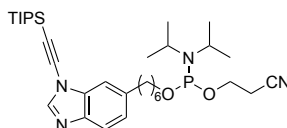
3.34b: 6-(1-((Triisopropylsilyl)ethynyl)-1*H*-benzo[*d*]imidazol-6-yl)hexan-1-ol

¹H-NMR (CDCl₃, 500 MHz): δ 8.01 (s, 1H), 7.69 (d, *J* = 8.2 Hz, 1H), 7.32 (s, 1H), 7.17 (dd, *J* = 8.3, 1.3 Hz, 1H), 3.64 (t, *J* = 6.3 Hz, 2H), 2.78 (t, *J* = 7.8 Hz, 2H), 1.73–1.67 (m, 2H), 1.41–1.40 (m, 4H), 1.27–1.24 (m, 2H), 1.18–1.17 (m, 21H).

¹³C-NMR (MeOD, 125 MHz): δ 143.4, 140.2, 140.1, 134.9, 125.0, 120.5, 110.3, 90.5, 72.9, 63.1, 36.2, 32.9, 31.8, 29.1, 25.8, 18.8, 11.4.

HRMS (ESI) : C₂₄H₃₈N₂OSi [M+H]⁺ calculated 399.2826, found 399.2823.

3.27: 2-Cyanoethyl(6-(1-((triisopropylsilyl)ethynyl)-1*H*-benzo[*d*]imidazol-6-yl)hexyl) diisopropylphosphoramidite



N,N-Diisopropylethylamine (0.8 mL, 2.7 mmol, 9 equiv.) and 2-cyanoethyl diisopropylchlorophosphoramidite (0.3 mL, 0.9 mmol, 3 equiv.) were added to a solution of 6-(1-((triisopropylsilyl)ethynyl)-1*H*-benzo[*d*]imidazol-6-yl)hexan-1-ol **2b** (0.2 g, 0.3 mmol, 1 equiv.) in THF (4 mL). The mixture was stirred at room temperature for 2 h, then was

partitioned between CHCl_3 (30 mL) and sat. NaHCO_3 (10 mL). The organic layer was washed with brine (2 x 30 mL), dried over Na_2SO_4 , and concentrated under reduced pressure. The resulting residue was purified by flash chromatography (silica gel, *n*-hexane/EtOAc, 8/1 + 1% NEt_3) to provide the desired product as a colorless oil (0.2 g, 64%).

$^1\text{H-NMR}$ (CDCl_3 , 500 MHz): δ 8.01 (s, 1H), 7.68 (d, $J = 8.3$ Hz, 1H), 7.32 (s, 1H), 7.17 (d, $J = 8.3$ Hz, 1H), 3.87–3.77 (m, 2H), 3.68–3.56 (m, 4H), 2.77 (t, $J = 7.7$ Hz, 2H), 2.63 (t, $J = 6.5$ Hz, 2H), 1.70–1.67 (m, 2H), 1.63–1.68 (m, 2H), 1.41–1.40 (m, 4H), 1.19–1.16 (m, 33H).

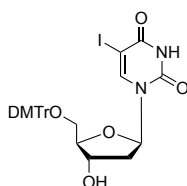
$^{13}\text{C-NMR}$ (CDCl_3 , 125 MHz): δ 143.4, 140.2, 140.1, 134.9, 125.0, 120.5, 117.6, 110.3, 90.5, 72.9, 63.9, 63.7, 58.5, 58.4, 43.2, 43.1, 36.3, 31.8, 31.3, 31.2, 29.1, 26.6, 24.9, 24.8, 24.7, 24.6, 20.5, 20.4, 18.9, 11.4.

$^{31}\text{P-NMR}$ (CDCl_3 , 202 MHz): 147.3.

HRMS (ESI): $\text{C}_{33}\text{H}_{55}\text{N}_4\text{O}_2\text{PSi}$ [$\text{M}+\text{H}$] $^+$ calculated 599.3905, found 599.3899.

3.8.3.2 Product from Scheme 3.16

3.36: 1-((2*R*,4*S*,5*R*)-5-((Bis(4-methoxyphenyl)(phenyl)methoxy)methyl)-4-hydroxytetrahydrofuran-2-yl)-5-iodopyrimidine-2,4(1*H*,3*H*)-dione²²⁴

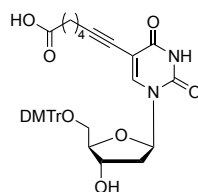


5'-Iodo-2'-deoxyuridine **3.35** (2.0 g, 5.6 mmol, 1 equiv.) was dissolved in anhydrous pyridine (56 mL). NEt_3 (1.6 mL, 11.3 mmol, 2 equiv.) and DMTrCl (2.0 g, 5.9 mmol, 1.1 equiv.) were added and the reaction mixture stirred for 24 h at room temperature. The mixture was quenched with water (20 mL) and the organic phase was extracted with CHCl_3 (3 x 100 mL). The combined organic phase was dried over Na_2SO_4 and concentrated under reduced pressure. The resulting residue was purified by flash chromatography (silica gel, DCM/MeOH, 1/0 to 96/4) to provide the desired product as a white solid (3.1 g, 83%).

$^1\text{H-NMR}$ (CDCl_3 , 500 MHz): δ 8.13 (s, 1H), 7.42–7.41 (m, 2H), 7.34–7.29 (m, 6H), 7.24–7.22 (m, 1H), 6.85 (d, $J = 8.8$ Hz, 4H), 6.31 (t, $J = 6.6$ Hz, 1H), 4.55–4.53 (m, 1H), 4.08 (br. s, 1H), 3.79 (s, 6H), 3.43–3.36 (m, 2H), 2.50–2.48 (m, 1H), 2.29 (app. quint, $J = 6.7$ Hz, 1H).

$^{13}\text{C-NMR}$ (CDCl_3 , 125 MHz): δ 158.9, 144.4, 135.6, 135.5, 130.3, 130.2, 128.3, 128.2, 127.3, 113.6, 87.3, 86.6, 85.8, 72.7, 63.6, 55.4, 41.6. Two signals not observed/coincident.

3.37: 7-(1-((2*R*,4*S*,5*R*)-5-((Bis(4-methoxyphenyl)(phenyl)methoxy)methyl)-4-hydroxytetrahydrofuran-2-yl)-2,4-dioxo-1,2,3,4-tetrahydropyrimidin-5-yl)hept-6-ynoic acid²²⁵

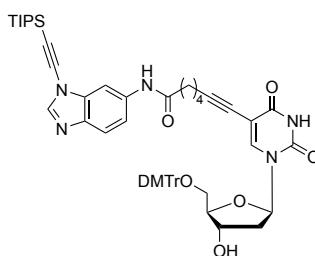


Pd(PPh₃)₂Cl₂ (0.1 g, 0.2 mmol, 0.09 equiv.), CuI (0.09 g, 0.3 mmol, 0.16 equiv.) and 1-((2*R*,4*S*,5*R*)-5-((bis(4-methoxyphenyl)(phenyl)methoxy)methyl)-4-hydroxytetrahydrofuran-2-yl)-5-iodopyrimidine-2,4(1*H*,3*H*)-dione **3.36** (1.3 g, 2.0 mmol, 1 equiv.) were placed in a dried flask filled with argon. Anhydrous DMF (22 mL) was added followed by heptynoic acid (2.6 g, 11.0 mmol, 5.1 equiv.). The mixture was degassed by freeze-pump-thaw cycles. NEt₃ (0.8 mL, 5.8 mmol, 2.9 equiv.) was added and the solution stirred at room temperature for 3 h. The reaction mixture was quenched with water (20 mL) and the organic phase was extracted with EtOAc (3 × 100 mL). The combined organic phase was washed with 10% aq. solution of LiCl (2 × 25 mL), aq. solution of EDTA (10 mg/mL, 25 mL) and brine (25 mL), dried over Na₂SO₄ and concentrated under reduced pressure. The resulting residue was purified by flash chromatography (silica gel, CHCl₃/MeOH, 98/2 to 94/6) to provide the desired product as a brown solid (1.0 g, 73%).

¹H-NMR (CDCl₃, 500 MHz): δ 8.00 (s, 1H), 7.42 (d, *J* = 7.6 Hz, 2H), 7.33 (dd, *J* = 8.7, 1.6 Hz, 4H), 7.29 (t, *J* = 7.4 Hz, 2H), 7.23–7.20 (m, 1H), 6.85–6.83 (m, 4H), 6.30 (t, *J* = 6.6 Hz, 1H), 4.52–4.49 (m, 1H), 4.06 (q, *J* = 3.2 Hz, 1H), 3.79 (s, 6H), 3.42 (dd, *J* = 10.8, 3.2 Hz, 1H), 3.32 (dd, *J* = 10.7, 3.7 Hz, 1H), 2.49–2.44 (m, 1H), 2.40–2.33 (m, 1H), 2.31–2.25 (m, 1H), 2.21 (t, *J* = 7.4 Hz, 2H), 2.11 (t, *J* = 7.1 Hz, 2H), 1.60–1.54 (m, 3H), 1.33–1.26 (m, 3H).

¹³C-NMR (CDCl₃, 125 MHz): δ 177.4, 162.4, 158.8, 149.3, 144.6, 141.9, 135.7, 130.1, 129.3, 128.2, 128.1, 127.1, 113.5, 101.0, 94.9, 87.2, 86.5, 85.6, 72.4, 71.3, 63.6, 55.4, 41.5, 33.3, 27.5, 24.1, 19.3, 8.7.

3.39: 7-(1-((2*R*,4*S*,5*R*)-5-((Bis(4-methoxyphenyl)(phenyl)methoxy)methyl)-4-hydroxytetrahydrofuran-2-yl)-2,4-dioxo-1,2,3,4-tetrahydropyrimidin-5-yl)-*N*-(1-((triisopropylsilyl)ethynyl)-1*H*-benzo[*d*]imidazol-6-yl)hept-6-ynamide



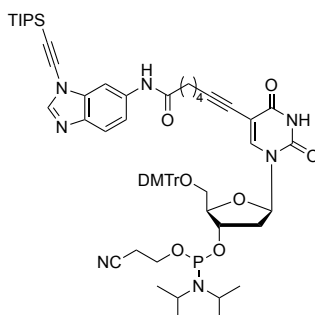
7-(1-((2*R*,4*S*,5*R*)-5-((Bis(4-methoxyphenyl)(phenyl)methoxy)methyl)-4-hydroxytetrahydrofuran-2-yl)-2,4-dioxo-1,2,3,4-tetrahydropyrimidin-5-yl)hept-6-ynoic acid **3.37** (0.5 g, 0.8 mmol, 1 equiv.) and 1-((triisopropylsilyl)ethynyl)-1*H*-benzo[*d*]imidazol-6-amine **3.38** (0.4 g, 1.1 mmol, 1.5 equiv.) were dissolved in dry DMF (6 mL). EDC (0.2 g, 1.5 mmol, 2 equiv.), HOAt (0.2 g, 1.5 mmol, 2 equiv.) and DIPEA (0.3 mL, 1.7 mmol, 2.1 equiv.) were added and stirred under argon atmosphere for 16 h at room temperature. The reaction mixture was diluted with EtOAc (100 mL), washed with 10% aq. solution of LiCl (2 × 15 mL) and brine (15 mL), dried over Na₂SO₄ and concentrated under reduced pressure. The resulting residue was purified by flash chromatography (silica gel, CHCl₃/MeOH, 98/2 to 94/6) to provide the desired product as a brown solid (0.7 g, 95%).

¹H-NMR (CDCl₃, 500 MHz): δ 8.55 (br. s, 1H), 8.33 (br. s, 1H), 8.08 (s, 1H), 8.01 (s, 1H), 7.71 (d, *J* = 8.6 Hz, 1H), 7.43 (d, *J* = 7.5 Hz, 2H), 7.36–7.34 (m, 5H), 7.29 (t, *J* = 7.6 Hz, 2H), 7.22 (t, *J* = 7.3 Hz, 1H), 6.85–6.83 (m, 4H), 6.39 (br. s, 1H), 4.61 (br. s, 1H), 4.12 (br. s, 1H), 3.79–3.78 (m, 6H), 3.41–3.36 (m, 2H), 2.70 (br. s, 1H), 2.53–2.50 (m, 1H), 2.46 (t, *J* = 7.9 Hz, 2H), 2.34–2.28 (m, 1H), 2.19–2.11 (m, 2H), 1.88–1.82 (m, 3H), 1.49–1.42 (m, 3H), 1.16–1.15 (m, 21H).

¹³C-NMR (CDCl₃, 125 MHz): δ 172.1, 162.5, 158.6, 150.0, 144.5, 143.5, 141.7, 137.4, 136.6, 135.7, 135.5, 134.8, 130.0, 129.9, 128.0, 127.9, 127.0, 120.2, 117.4, 113.3, 102.6, 101.1, 94.9, 89.9, 87.1, 86.7, 85.7, 77.2, 73.4, 72.4, 72.0, 63.7, 55.3, 41.8, 37.2, 26.1, 25.1, 18.7, 11.2.

HRMS (ESI): C₅₅H₆₃N₅O₈Si [M+Na]⁺ calculated 972.4338, found 972.4335.

3.28: (2*R*,3*S*,5*R*)-2-((Bis(4-methoxyphenyl)(phenyl)methoxy)methyl)-5-(2,4-dioxo-5-(7-oxo-7-((1-((triisopropylsilyl)ethynyl)-1*H*-benzo[*d*]imidazol-6-yl)amino)hept-1-yn-1-yl)-3,4-dihydropyrimidin-1(2*H*)-yl)tetrahydrofuran-3-yl (2-cyanoethyl) diisopropylphosphoramidite



N,N-Diisopropylethylamine (0.4 mL, 2.4 mmol, 6 equiv.) and 2-cyanoethyl diisopropylchlorophosphoramidite (0.1 mL, 0.5 mmol, 1.2 equiv.) were added to a solution of 7-(1-((2*R*,4*S*,5*R*)-5-((bis(4-methoxyphenyl)(phenyl)methoxy)methyl)-4-hydroxytetrahydrofuran-2-yl)-2,4-dioxo-1,2,3,4-tetrahydropyrimidin-5-yl)-*N*-(1-((triisopropylsilyl)ethynyl)-1*H*-benzo[*d*]imidazol-6-yl)hept-6-ynamide **3.39** (0.4 g, 0.4 mmol, 1 equiv.) in THF (2.7 mL). The reaction mixture was stirred at room temperature for 1.5 h, and then partitioned between CHCl₃ (50 mL) and aq. sat. solution of NaHCO₃ (10 mL). The organic layer was washed with brine (2 x 50 mL), dried over Na₂SO₄, and concentrated under reduced pressure. The resulting residue was purified by flash chromatography (silica gel, *n*-hexane/EtOAc, 1/1 to 0/1 +2% NEt₃) to provide the desired product as a white solid (0.2 g, 47%).

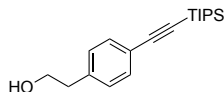
¹H-NMR (CDCl₃, 500 MHz): δ 8.32–8.30 (m, 1H), 8.22 (s, 1H), 8.12–8.07 (m, 1H), 8.01 (s, 1H), 7.67 (d, *J* = 7.8 Hz, 1H), 7.43 (d, *J* = 7.6 Hz, 2H), 7.35–7.33 (m, 4H), 7.30–7.27 (m, 3H), 7.24–7.20 (m, 1H), 6.86–6.83 (m, 4H), 6.32–6.27 (m, 1H), 4.64–4.62 (m, 1H), 4.21–4.16 (m, 1H), 3.85–3.83 (m, 1H), 3.79–3.78 (m, 6H), 3.75–3.73 (m, 1H), 3.60–3.54 (m, 2H), 3.47–3.39 (m, 1H), 3.32–3.30 (m, 1H), 2.62 (t, *J* = 6.2 Hz, 2H), 2.44 (t, *J* = 7.2 Hz, 2H), 2.33 (app. quint, *J* = 6.8 Hz, 1H), 2.11 (t, *J* = 6.8 Hz, 2H), 1.79 (t, *J* = 7.3 Hz, 2H), 1.26–1.24 (m, 2H), 1.18–1.16 (m, 28H), 1.78 (d, *J* = 6.8 Hz, 5H).

¹³C-NMR (CDCl₃, 125 MHz): δ 162.3, 158.7, 149.1, 144.5, 143.9, 142.0, 136.3, 135.8, 135.6, 135.1, 130.2, 130.1, 128.2, 128.1, 127.1, 120.7, 117.6, 117.0, 113.5, 102.7, 100.9, 95.3, 90.2, 87.2, 85.8, 73.8, 71.7, 63.3, 58.5, 58.4, 55.4, 43.5, 43.4, 40.9, 37.1, 32.1, 31.6, 30.5, 30.3, 29.8, 26.5, 25.3, 24.8, 24.7, 24.6, 22.8, 20.6, 20.5, 19.2, 18.8, 11.4.

³¹P-NMR (CDCl₃, 202 MHz): δ 149.1, 148.7.

HRMS (ESI): C₆₄H₈₀N₇O₉PSi [M+H]⁺ calculated 1150.5597, found 1150.5598.

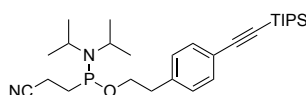
3.8.3.3 Product from Scheme 3.17

3.41: 2-(4-((Triisopropylsilyl)ethynyl)phenyl)ethan-1-ol²²⁶

To a degassed solution of 2-(4-bromophenyl)ethan-1-ol **3.40** (1.0 g, 5.0 mmol, 1.0 equiv.), (triisopropylsilyl)acetylene (1.1 g, 6.0 mmol, 1.2 equiv.), Pd(PPh₃)₂Cl₂ (0.04 g, 0.05 mmol, 0.01 equiv.) and CuI (0.01 g, 0.05 mmol, 0.01 equiv.) in THF (17 mL) was added diisopropylamine (1.3 g, 10 mmol, 2.0 equiv.). The reaction mixture was stirred at room temperature for 16h and then quenched with aq. sat. solution of NH₄Cl (50 mL). The reaction mixture was diluted with Et₂O (50 mL), washed with brine (2 x 50 mL), dried over Na₂SO₄ and concentrated under reduced pressure. The resulting residue was purified by flash chromatography (silica gel, PE/EtOAc, 19/1 to 5/1) to provide the desired product as a yellow oil (0.3 g, 20%).

¹H-NMR (CDCl₃, 500 MHz): δ 7.43 (d, *J* = 8.1 Hz, 2H), 7.17 (d, *J* = 8.1 Hz, 2H), 3.84 (q, *J* = 6.3 Hz, 2H), 2.86 (t, *J* = 6.5 Hz, 2H), 1.13 (s, 21H).

¹³C-NMR (CDCl₃, 125 MHz): δ 139.1, 132.4, 129.0, 121.9, 107.1, 90.4, 63.6, 39.3, 18.8, 11.5.

3.42: 2-Cyanoethyl (4-((triisopropylsilyl)ethynyl)phenethyl) diisopropylphosphoramidite

N,N-Diisopropylethylamine (1.6 mL, 9.4 mmol, 9.4 equiv.) and 2-cyanoethyl diisopropylchlorophosphoramidite (0.3 mL, 1.2 mmol, 1.2 equiv.) were added to a solution of 2-(4-((triisopropylsilyl)ethynyl)phenyl)ethan-1-ol **3.41** (0.3 g, 1.0 mmol, 1 equiv.) in dry THF (10 mL) under argon atmosphere. The reaction was stirred at room temperature for 1.5 h, and then partitioned between CHCl₃ (50 mL) and aq. sat. solution of NaHCO₃ (50 mL). The organic layer was washed with brine (3 x 20 mL), dried over Na₂SO₄, and concentrated under reduced pressure. The resulting residue was purified by flash chromatography (silica gel, *n*-hexane/EtOAc, 3/1) to provide the desired product as a colourless oil (0.4 g, 76%).

¹H-NMR (CDCl₃, 500 MHz): δ 7.39 (d, *J* = 7.7 Hz, 2H), 7.16 (d, *J* = 7.7 Hz, 2H), 3.87–3.73 (m, 4H), 3.61–3.55 (m, 2H), 2.91 (d, *J* = 7.2 Hz, 2H), 2.58 (d, *J* = 6.4 Hz, 2H), 1.20–1.17 (m, 12H), 1.15–1.12 (m, 21H).

^{13}C -NMR (CDCl_3 , 125 MHz): δ 139.3, 132.2, 129.1, 121.7, 117.8, 107.3, 90.2, 64.2, 58.5, 58.4, 43.3, 43.2, 37.9, 37.8, 24.8, 24.7, 24.6, 24.5, 18.8, 11.5.

^{31}P -NMR (CDCl_3 , 202 MHz): δ 147.5.

IR ν_{max} (neat): 2961, 2939, 2863, 2249, 2155, 1463, 1364, 1184, 1026 cm^{-1} .

HRMS (ESI): $\text{C}_{28}\text{H}_{47}\text{N}_2\text{O}_2\text{PSi}$ $[\text{M}+\text{H}]^+$ calculated. 503.3217, found 503.3209.

3.8.4 Solid Phase Synthesis of Oligodeoxyribonucleotides (ODNs)

ODNs were synthesized using phosphoramidite-based protocols (1 μmol scale) on an Applied Biosystems 392 nucleic acid synthesiser. Phosphoramidites and controlled pore glass (CPG) supports were purchased from LINK Technologies Ltd (Bellshill, UK). For the coupling of modified phosphoramidites (**3**, **7** and **S5**), longer coupling times of 3-9 minutes were used. TIPS deprotection was performed using a solution of 50 μL TBAF (1 M in THF) in 1.95 mL of MeCN. The mixture was repeatedly passed over the column containing the CPG support for 3 min. The CPG support was washed with MeCN (3×5 mL) and dried with air.

For ODNs (**ODN3**, **ODN8** and **ODN10**) incorporating phosphoramidite **7**, TIPS deprotection was conducted in solution. Crude ODNs (**ODN3**, **ODN8** and **ODN10**) were solubilized in DMSO (230 μL) before adding NEt_3 (120 μL). HF-Triethylamine (150 μL) was added and the reaction mixture was stirred at 65 $^\circ\text{C}$ for 2.5h. Ammonia (minimum 28%, 1.5 mL/mmol) was then added, and the suspension was shaken for 16 hours at room temperature. The supernatant was removed, and the CPG support was then washed with water (2×1.5 mL/mmol).

The combined aqueous phases were lyophilised and purified by RP-HPLC using a preparative column (Phenomenex Clarity 5 μM Oligo-RP, 250 \times 10 mm) at a flow rate of 3 mL/min, gradient 10–50% 0.1 M TEAA in MeCN in 32 min or 10–40% 0.1 M TEAA in MeCN in 22 min. Purity of resultant products was assessed with a Shimadzu Prominence HPLC using an analytical column (Phenomenex Clarity 5 μM Oligo-RP, 250 \times 4.6 mm) at a flow rate of 1 mL/min, gradient 10–50% 0.1 M TEAA in MeCN in 35 min.

Yields were calculated by measuring the absorbance of the ODNs with a NanoDrop 1000 spectrometer (Thermo Scientific) using extinction coefficient values of 121847 $\text{L}\cdot\text{mol}^{-1}\cdot\text{cm}^{-1}$ for **ODN3.18**, 116200 $\text{L}\cdot\text{mol}^{-1}\cdot\text{cm}^{-1}$ for **ODN3.19**, 111419 $\text{L}\cdot\text{mol}^{-1}\cdot\text{cm}^{-1}$ for **ODN3.20**, 114119 $\text{L}\cdot\text{mol}^{-1}\cdot\text{cm}^{-1}$ for **ODN3.21** and 107819 $\text{L}\cdot\text{mol}^{-1}\cdot\text{cm}^{-1}$ for **ODN3.22**. Extinction coefficient values were measured with a NanoDrop 1000 spectrometer (Thermo Scientific) or calculated using OligoAnalyzer 3.1 calculator on IDT DNA (<https://www.idtdna.com/calc/analyzer>).

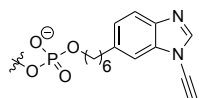
MALDI-TOF mass spectra were recorded using an HPA matrix with dibasic ammonium citrate as co-matrix on a Shimadzu Biotech Axima CFR spectrometer.

3.8.4.1 Spectroscopic Characterisation of ODNs

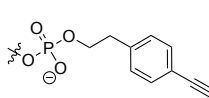
Table 3.5. ODN sequences.

Product	Sequence
ODN3.18	5'- X1 GCA TTG ACT GCT-3'
ODN3.19	5'- X2 GCA TTG ACT GCT-3'
ODN3.20	5'-TTA TGC AG X3 AC-3'
ODN3.21	5'- CX3A TGC AGT AC-3'
ODN3.22	5'- X2 CGC GAT AX3C GCG-3'

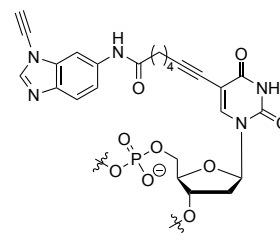
X1 =



X2 =



X3 =



ODN3.18: C₁₃₂H₁₆₆N₄₄O₇₅P₁₂ Yield: **35%**. MW 3940.70 g/mol.

MALDI-TOF (-ve mode; matrix 3-hydroxypicolinic acid) *m/z* [M-H]⁻ found 3941.80.

RP-HPLC R_T = 20.5 min.

ODN3.19: C₁₂₇H₁₅₈N₄₂O₇₅P₁₂ Yield: **26%**. MW 3844.57 g/mol.

MALDI-TOF (-ve mode; matrix 3-hydroxypicolinic acid) *m/z* [M-H]⁻ found 3844.72.

RP-HPLC R_T = 18.2 min.

ODN3.20: C₁₃₃H₁₆₀N₄₇O₇₂P₁₁ Yield: **9%**. MW 3909.71 g/mol.

MALDI-TOF (-ve mode; matrix 3-hydroxypicolinic acid) *m/z* [M-H]⁻ found 3909.16.

RP-HPLC R_T = 15.7 min.

ODN3.21: C₁₃₂H₁₅₉N₄₈O₇₁P₁₁ Yield: **8%**. MW 3894.70 g/mol.

MALDI-TOF (-ve mode; matrix 3-hydroxypicolinic acid) *m/z* [M-H]⁻ found 3893.33.

RP-HPLC R_T = 15.3 min.

ODN3.22: C₁₄₁H₁₆₇N₄₉O₇₄P₁₂ Yield: **12%**. MW 4103.84 g/mol.

MALDI-TOF (-ve mode; matrix 3-hydroxypicolinic acid) *m/z* [M-H]⁻ found 4103.50.

RP-HPLC R_T = 20.5; 21.1 min (two conformations: ssDNA and dsDNA).

3.8.5 Synthesis of triazole-ODNs via CuAAC ligations

3.8.5.1 General Procedure for CuAAC Ligations of alkyne-modified ODNs

To a solution of ODN (5 nmol, 1 equiv.) and azide **18a-1** (10 nmol, 2 equiv.) in H₂O (50 μL), was added THPTA (1 nmol, 0.2 equiv.) followed by Cu(OTf)₂ (0.5 nmol, 0.1 equiv.) and NaAsc (1 nmol, 0.2 equiv.). The reaction was shaken at room temperature for 3h. The reaction mixture was lyophilised and purified by RP-HPLC on a Dionex UltiMate 3000 HPLC using a semi-preparative column (Phenomenex Clarity 5 μM Oligo-RP, 250 × 10 mm) at a flow rate of 3 mL/min, gradient 10–50% 0.1 M triethylammonium acetate (TEAA) in MeCN in 32 min or 10–40% 0.1 M TEAA in MeCN in 22 min. The purity of resultant triazole ODN products was assessed with a Shimadzu Prominence HPLC using an analytical column (Phenomenex Clarity 5 μM Oligo-RP, 250 × 4.6 mm) at a flow rate of 1 mL/min, gradient 10–50% 0.1 M TEAA in MeCN in 35 min. Yields were calculated by measuring the absorbance of the ODNs with a Shimadzu Prominence HPLC using starting materials extinction coefficient values of 121847 L·mol⁻¹·cm⁻¹ for **ODN3.18**, 116200 L·mol⁻¹·cm⁻¹ for **ODN3.19**, 111419 L·mol⁻¹·cm⁻¹ for **ODN3.20**, 114119 L·mol⁻¹·cm⁻¹ for **ODN3.21** and 107819 L·mol⁻¹·cm⁻¹ for **ODN3.22**. Extinction coefficient values were measured with a NanoDrop 1000 spectrometer (Thermo Scientific) or calculated using OligoAnalyzer 3.1 calculator on IDT DNA (<https://www.idtdna.com/calc/analyzer>). The products were characterised by MALDI-TOF.

3.8.5.2 Spectroscopic Characterisation of ODNs from Scheme 3.19

ODN3.23a: Prepared according to General Procedure described in section 3.8.5.2 using **ODN3.18** (5 nmol, 1 equiv.), azide **2.65a** (10 nmol, 2 equiv.), THPTA (1 nmol, 0.2 equiv.), Cu(OTf)₂ (0.5 nmol, 0.1 equiv.) and NaAsc (1 nmol, 0.2 equiv.). No need for RP-HPLC purification. Yield: **99 ± 1%**.

C₁₃₉H₁₇₃N₄₇O₇₅P₁₂: MW 4073.85 g/mol.

MALDI-TOF (-ve mode; matrix 3-hydroxypicolinic acid) *m/z* [M-H]⁻ found 4074.87.

RP-HPLC R_T = 25.7 min.

ODN3.23b: Prepared according to General Procedure described in section 3.8.5.2 using **ODN3.18** (5 nmol, 1 equiv.), azide **2.65d** (10 nmol, 2 equiv.), THPTA (10 mmol, 2 equiv.), Cu(OTf)₂ (5 mmol, 1 equiv.), and NaAsc (10 mmol, 2 equiv.). Yield: **37 ± 1%**.

C₁₄₂H₁₈₁N₄₇O₇₅P₁₂: MW 4117.95 g/mol.

MALDI-TOF (+ve mode; matrix 3-hydroxypicolinic acid) *m/z* [M+H]⁺ found 4118.63.

RP-HPLC R_T = 28.0 min.

ODN3.23c: Prepared according to General Procedure described in section 3.8.5.2 using **ODN3.18** (5 nmol, 1 equiv.), azide **2.65h** (10 nmol, 2 equiv.), THPTA (1 nmol, 0.2 equiv.), Cu(OTf)₂ (0.5 nmol, 0.1 equiv.) and NaAsc (1 nmol, 0.2 equiv.). No need for RP-HPLC purification. Yield: **99 ± 1%**.

C₁₃₈H₁₇₂N₄₈O₇₅P₁₂: MW 4074.84 g/mol.

MALDI-TOF (-ve mode; matrix 3-hydroxypicolinic acid) *m/z* [M-H]⁻ found 4074.78.

RP-HPLC R_T = 21.6 min.

ODN3.23d: Prepared according to General Procedure described in section 3.8.5.2 using **ODN3.18** (5 nmol, 1 equiv.), azide **3.46a** (10 nmol, 2 equiv.), THPTA (1 nmol, 0.2 equiv.), Cu(OTf)₂ (0.5 nmol, 0.1 equiv.) and NaAsc (1 nmol, 0.2 equiv.). No need for RP-HPLC purification. Yield: **97 ± 2%**.

C₁₄₁H₁₇₅FN₄₈O₇₆P₁₂: MW 4148.89 g/mol.

MALDI-TOF (-ve mode; matrix 3-hydroxypicolinic acid) *m/z* [M-H]⁻ found 4148.70.

RP-HPLC R_T = 24.7 min.

ODN3.23e: Prepared according to General Procedure described in section 3.8.5.2 using **ODN3.18** (5 nmol, 1 equiv.), azide **3.46b** (10 nmol, 2 equiv.), THPTA (1 nmol, 0.2 equiv.), Cu(OTf)₂ (0.5 nmol, 0.1 equiv.) and NaAsc (1 nmol, 0.2 equiv.). Yield: **69 ± 2%**.

C₁₄₁H₁₇₁N₄₇O₇₈P₁₂: MW 4143.86 g/mol.

MALDI-TOF (+ve mode; matrix 3-hydroxypicolinic acid) *m/z* [M+H]⁺ found 4145.75.

RP-HPLC R_T = 22.8 min.

ODN3.23f: Prepared according to General Procedure described in section 3.8.5.2 using **ODN3.18** (5 nmol, 1 equiv.), azide **2.65q** (10 nmol, 2 equiv.), THPTA (1 nmol, 0.2 equiv.), Cu(OTf)₂ (0.5 nmol, 0.1 equiv.) and NaAsc (1 nmol, 0.2 equiv.). No need for RP-HPLC purification. Yield: **97 ± 2%**.

C₁₄₇H₁₈₅N₄₉O₇₇P₁₂S: MW 4274.11 g/mol.

MALDI-TOF (-ve mode; matrix 3-hydroxypicolinic acid) *m/z* [M-H]⁻ found 4272.16.

RP-HPLC R_T = 29.7 min.

ODN3.23g: Prepared according to General Procedure described in section 3.8.5.2 using **ODN3.18** (5 nmol, 1 equiv.), azide **2.65r** (10 nmol, 2 equiv.), THPTA (1 nmol, 0.2 equiv.), Cu(OTf)₂ (0.5 nmol, 0.1 equiv.) and NaAsc (1 nmol, 0.2 equiv.). Yield: **66 ± 2%**.

C₁₅₆H₁₈₅N₄₉O₈₀P₁₂S: MW 4430.20 g/mol.

MALDI-TOF (+ve mode; matrix 3-hydroxypicolinic acid) *m/z* [M+H]⁺ found 4433.52.

RP-HPLC R_T = 20.8 min.

ODN3.23h: Prepared according to General Procedure described in section 3.8.5.2 using **ODN3.18** (5 nmol, 1 equiv.), azide **3.46c** (10 nmol, 2 equiv.), THPTA (5 mmol, 1 equiv.), Cu(OTf)₂ (2.5 mmol, 0.5 equiv.) and NaAsc (5 mmol, 1 equiv.). Yield: **39 ± 2%**.

C₁₄₈H₁₈₉N₄₇O₈₅P₁₂: MW 4358.07 g/mol.

MALDI-TOF (+ve mode; matrix 3-hydroxypicolinic acid) *m/z* [M+H]⁺ found 4357.45.

RP-HPLC R_T = 23.4 min.

ODN3.23i: Prepared according to General Procedure described in section 3.8.5.2 using **ODN3.18** (5 nmol, 1 equiv.), azide **3.46d** (10 nmol, 2 equiv.), THPTA (10 mmol, 2 equiv.), Cu(OTf)₂ (5 mmol, 1 equiv.) and NaAsc (10 mmol, 2 equiv.). Yield: **68 ± 2%**.

C₁₄₂H₁₇₀F₁₇N₄₇O₇₅P₁₂: MW 4429.83 g/mol.

MALDI-TOF (+ve mode; matrix 3-hydroxypicolinic acid) *m/z* [M+H]⁺ found 4430.74.

RP-HPLC R_T = 39.5 min.

ODN3.23j: Prepared according to General Procedure described in section 3.8.5.2 using **ODN3.18** (5 nmol, 1 equiv.), azide **2.65s** (10 nmol, 2 equiv.), THPTA (1 nmol, 0.2 equiv.), Cu(OTf)₂ (0.5 nmol, 0.1 equiv.) and NaAsc (1 nmol, 0.2 equiv.). No need for RP-HPLC purification. Yield: **87 ± 2%**.

C₁₅₀H₁₉₈N₅₀O₈₀P₁₂S: MW 4385.25 g/mol.

MALDI-TOF (-ve mode; matrix 3-hydroxypicolinic acid) *m/z* [M-H]⁻ found 4384.37.

RP-HPLC $R_T = 20.7$ min.

ODN3.23k: Prepared according to General Procedure described in section 3.8.5.2 using **ODN3.18** (5 nmol, 1 equiv.), azide **3.46e** (10 nmol, 2 equiv.), THPTA (1 nmol, 0.2 equiv.), $\text{Cu}(\text{OTf})_2$ (0.5 nmol, 0.1 equiv.) and NaAsc (1 nmol, 0.2 equiv.). Yield: **65 ± 1%**.

$\text{C}_{158}\text{H}_{199}\text{N}_{55}\text{O}_{80}\text{P}_{12}$: MW 4520.32 g/mol.

MALDI-TOF (+ve mode; matrix 3-hydroxypicolinic acid) m/z $[\text{M}+\text{H}]^+$ found 4521.71.

RP-HPLC $R_T = 23.1$ min.

ODN3.23l: Prepared according to General Procedure described in section 3.8.5.2 using **ODN3.18** (5 nmol, 1 equiv.), azide **3.46f** (10 nmol, 2 equiv.), THPTA (1 nmol, 0.2 equiv.), $\text{Cu}(\text{OTf})_2$ (0.5 nmol, 0.1 equiv.) and NaAsc (1 nmol, 0.2 equiv.) in $\text{H}_2\text{O}/t\text{BuOH}$ (1/1). Yield: **91 ± 2%**.

$\text{C}_{163}\text{H}_{218}\text{N}_{48}\text{O}_{77}\text{P}_{12}$: MW 4453.48 g/mol.

MALDI-TOF (+ve mode; matrix 3-hydroxypicolinic acid) m/z $[\text{M}+\text{H}]^+$ found 4455.94.

RP-HPLC $R_T = 45.2$ min.

3.8.5.3 Spectroscopic Characterisation of ODNs from Scheme 3.20

ODN3.24a: Prepared according to General Procedure described in section 3.8.5.2 using **ODN3.19** (5 nmol, 1 equiv.), azide **2.65a** (10 nmol, 2 equiv.), THPTA (0.1 mmol, 20 equiv.), $\text{Cu}(\text{OTf})_2$ (50 nmol, 10 equiv.) and NaAsc (0.1 mmol, 20 equiv.). No need for RP-HPLC purification. Yield: **Quant.**

$\text{C}_{134}\text{H}_{165}\text{N}_{45}\text{O}_{75}\text{P}_{12}$: MW 3977.72 g/mol.

MALDI-TOF (-ve mode; matrix 3-hydroxypicolinic acid) m/z $[\text{M}-\text{H}]^-$ found 3976.69.

RP-HPLC $R_T = 20.9$ min.

3.8.5.4 Spectroscopic Characterisation of ODNs from Scheme 3.21

ODN3.25a: Prepared according to General Procedure described in section 3.8.5.2 using **ODN3.20** (5 nmol, 1 equiv.), azide **2.65a** (0.1 mmol, 20 equiv.), THPTA (10 nmol, 2 equiv.), $\text{Cu}(\text{OTf})_2$ (0.5 nmol, 0.1 equiv.) and NaAsc (1 nmol, 0.2 equiv.). No need for RP-HPLC purification. Yield: **82 ± 2%**.

$\text{C}_{140}\text{H}_{167}\text{N}_{50}\text{O}_{72}\text{P}_{11}$: MW 4042.87 g/mol.

MALDI-TOF (-ve mode; matrix 3-hydroxypicolinic acid) m/z $[\text{M}-\text{H}]^-$ found 4042.85.

RP-HPLC $R_T = 20.8$ min.

3.8.5.5 Spectroscopic Characterisation of ODNs from Scheme 3.22

ODN3.26a: Prepared according to General Procedure described in section 3.8.5.2 using **ODN3.21** (5 nmol, 1 equiv.), azide **2.65a** (0.1 mmol, 20 equiv.), THPTA (10 nmol, 2 equiv.), $\text{Cu}(\text{OTf})_2$ (0.5 nmol, 0.1 equiv.) and NaAsc (1 nmol, 0.2 equiv.). No need for RP-HPLC purification. Yield: **78 ± 2%**.

$\text{C}_{139}\text{H}_{166}\text{N}_{51}\text{O}_{71}\text{P}_{11}$: MW 4027.85 g/mol.

MALDI-TOF (-ve mode; matrix 3-hydroxypicolinic acid) m/z $[\text{M-H}]^-$ found 4027.37.

RP-HPLC $R_T = 20.8$ min.

3.8.5.6 Spectroscopic Characterisation of ODNs from Scheme 3.23

ODN3.27: Prepared according to General Procedure described in section 3.8.5.2 using **ODN3.22** (0.3 μmol , 1 equiv.), azide **3.46a** (0.6 μmol , 2 equiv.), THPTA (0.6 μmol , 2 equiv.), $\text{Cu}(\text{OTf})_2$ (30 nmol, 0.1 equiv.) and NaAsc (60 nmol, 0.2 equiv.). Yield: **60 ± 2%**.

$\text{C}_{150}\text{H}_{176}\text{FN}_{53}\text{O}_{75}\text{P}_{12}$: MW 4312.04 g/mol.

MALDI-TOF (-ve mode; matrix 3-hydroxypicolinic acid) m/z $[\text{M-H}]^-$ found 4310.08.

RP-HPLC $R_T = 25.0$ min.

ODN3.28: Prepared according to General Procedure described in section 3.8.5.2 using **ODN3.27** (25 nmol, 1 equiv.), azide **2.65s** (50 nmol, 2 equiv.), THPTA (0.5 μmol , 20 equiv.), $\text{Cu}(\text{OTf})_2$ (0.25 μmol , 10 equiv.) and NaAsc (0.5 μmol , 20 equiv.). Yield: **57 ± 1%**.

$\text{C}_{168}\text{H}_{208}\text{FN}_{59}\text{O}_{80}\text{P}_{12}\text{S}$: MW 4756.59 g/mol.

MALDI-TOF (-ve mode; matrix 3-hydroxypicolinic acid) m/z $[\text{M-H}]^-$ found 4755.36.

RP-HPLC $R_T = 24.3$ min.

Chapter 4

Developing a New Platform for Fast, Degradation-Free CuAAC Bioconjugation Using Flow Chemistry

The work in this chapter is based on the following publication: M. Z. C. Hatit, L. F. Reichenbach, J. M. Tobin, F. Vilela, G. A. Burley, A. J. B. Watson, *Nat. Comm.* **2018**, *9*, 4021–4029.

Aspects of the work described herein has been made in collaboration with Dr Linus Reichenbach (synthesis of phosphoramidite building blocks and solid phase ODN synthesis) and John Tobin (training of flow process).

4.1 Benefits of Flow Chemistry

Over the past two decades, synthetic organic chemistry has undergone a rapid evolution, transitioning from the standard chemical hood to modern automisation.^{227–229} A prime example is the introduction of microwave reactors into both academic and industrial research with the goal of optimising reaction efficiency. The microwave irradiation of the molecules results in fast and efficient heating of the reaction (microwave dielectric heating).²³⁰ The use of a sealed vessel allows the solvent to be heated above boiling temperatures (“super-heated” solvent). The combination of these features allows reactions to reach completion within minutes or even seconds.²³¹ Unfortunately, microwave-assisted synthesis is incompatible with large scale reactions due to the limited penetration depth of microwaves in reaction mixtures. This lack of scalability represents a serious limitation for industrial purposes; therefore, research has focused on translating microwave chemistry to continuous flow.²³²

Continuous flow processes are performed in microfluidic reactors in which the conditions of the reaction are rigorously controlled. Parameters such as temperature, pressure and flow rate can be easily established and monitored, providing a more reliable and reproducible process as compared to batch chemistry.²³³ Moreover, the superior heat and mass transfer obtained through flow systems permit dramatically increased reaction rates compared to batch reactions, rendering this process attractive for both academic and industrial applications.

There are currently four types of continuous flow reactors described in the literature, tolerating a wide range of reactions (Figure 4.1).²³³ Type I and II reactors are used when no catalyst is required (Figure 4.1a and 4.1b). However, all the reagents are flowed in the type I reactor, while a solid supported reactant is confined into the reactor type II. Type III and IV reactors are used when homogeneous (type III, Figure 4.1c) or supported-catalysis (type IV, Figure 4.1d) is necessary to obtain the expected product.

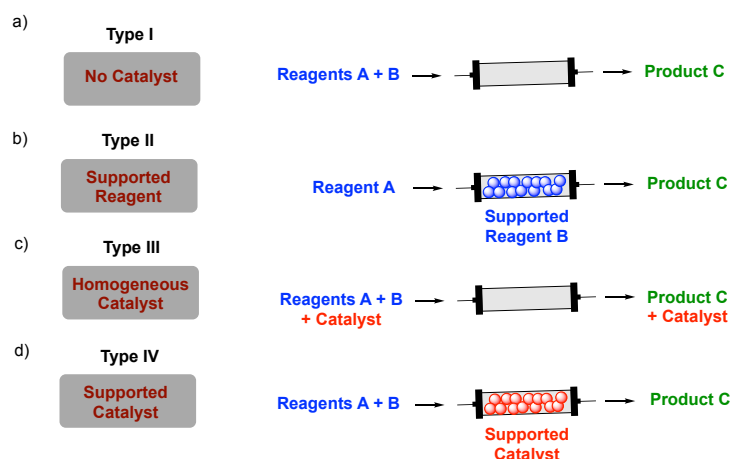


Figure 4.1. The four continuous flow systems currently available for organic synthesis.²³³

One of the main areas where flow chemistry has had a huge impact is drug discovery.^{233–235} Reduction of organic solvent required in the reaction, higher product purity and reduction of reaction time dramatically lower operating cost. Herein are presented a few key examples of Active Pharmaceutical Ingredients (APIs) synthesised *via* continuous flow chemistry which illustrate the main benefits of this technique. A schematic of the generalised components used in this chapter are diagrammed in Figure 4.2.

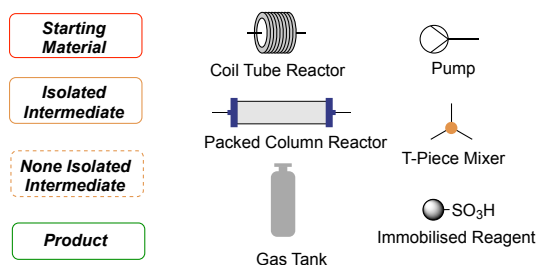
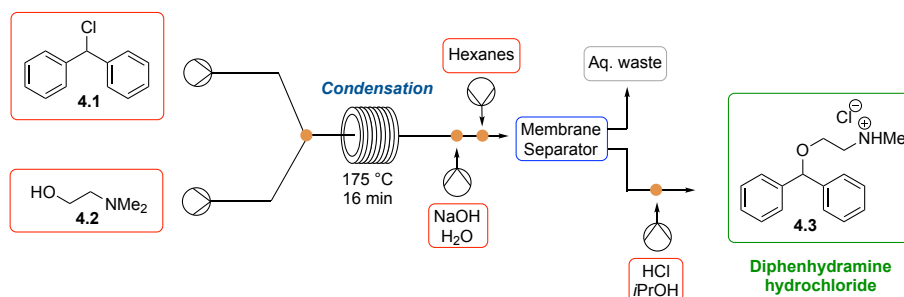


Figure 4.2. Schematic of components for continuous flow processes.

4.1.1 Benefits of Flow Chemistry - Faster Reactions

One of the main advantages of continuous flow processes, as compared to batch chemistry, is the ability to dramatically reduce reaction times. This arises from the superior heat and mass transfer provided by flow processes. Additionally, reactors are fitted with back-pressure regulators, allowing for a straightforward reproduction of the high temperatures/pressures obtained *via* the sealed vessels employed in microwave chemistry.^{232,236} These benefits were successfully illustrated by Jamison *et al.* in their study on the continuous flow synthesis of

diphenhydramine hydrochloride **4.3**, an antihistamine reportedly used at approximately 100 tons/year worldwide (Scheme 4.1).²³⁷



Scheme 4.1. Continuous flow synthesis of Diphenhydramine hydrochloride **4.3**.²³⁷

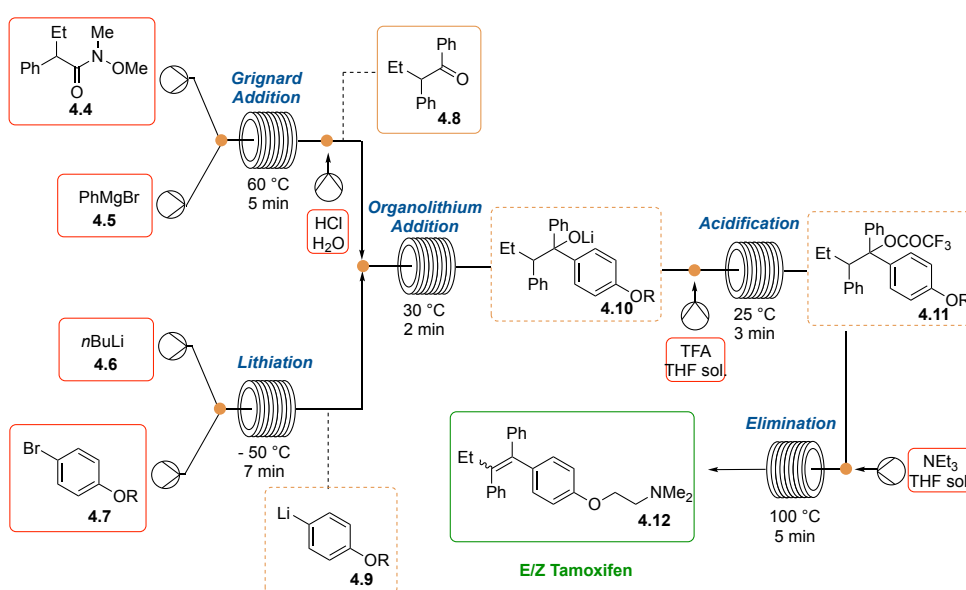
In this work, chlorodiphenylmethane **4.1** and dimethylethanolamine **4.2** were passed through a PFA reactor ($d = 0.5$ mm, $V = 720$ μ L) at 175 °C ($t_R = 16$ min). The resulting ammonium salt was neutralised with 3 M NaOH aq., before being extracted with hexanes. Treatment of the organic layer with 5 M HCl aq. afforded compound **4.3** in 89% yield. Along with decreasing the reaction time from 2 h to 16 min, this process has the advantage of being solvent-free and results in minimal side product formation. With a 720 μ L micro-reactor, the authors were able to synthesis 2.4 g of diphenhydramine hydrochloride **4.3** in 1 h, making this process optimal for its industrial production. A key challenge in applying the flow process to this synthesis arose during the quenching steps as the salts' insolubility resulted in line blockage. However, through their extensive efforts during optimisation, the authors were able to overcome any such issues.

4.1.2 Benefits of Flow Chemistry - Safer Reactions

Flow-based processes generally employ small volumes of reagents, affording safer handling of potential toxic and/or hazardous compounds. Additionally, owing to its modular set-up, flow technology offers the possibility to avoid handling unstable or hazardous intermediates by preparing them in a flow reactor *in-situ* prior to being passed through a second reactor.²³⁸ For example, Sach *et al.* successfully reported the *in-situ* generation of organic azides, followed by CuAAC reactions using a continuous flow platform.²³⁹ The use of organic azides on a preparative scale at industrial level is usually prohibited due to their explosive properties. Their synthesis, using NaN_3 , can generate the explosive and highly toxic hydrazoic acid. Consequently, the ability to generate organic azides *in-situ* and react them upon formation, thus avoiding their accumulation, considerably improves the safety of CuAAC reactions and

will allow industry to explore one of the most commonly used bioconjugation strategies employed in academia.

An additional safety feature of continuous flow processes is the ability to precisely control the reaction temperature and pressure. This can be most appreciated in the context of large-scale exothermic reactions, such as the formation of highly reactive organometallic intermediates. Ley *et al.* reported the continuous flow synthesis of Tamoxifen **4.12**, an oestrogen receptor antagonist used in the treatment of breast cancer, using highly reactive and air sensitive reagents, such as Grignard and organolithium compounds (Scheme 4.2).²⁴⁰



Scheme 4.2. Continuous flow synthesis of Tamoxifen **4.12**.²⁴⁰

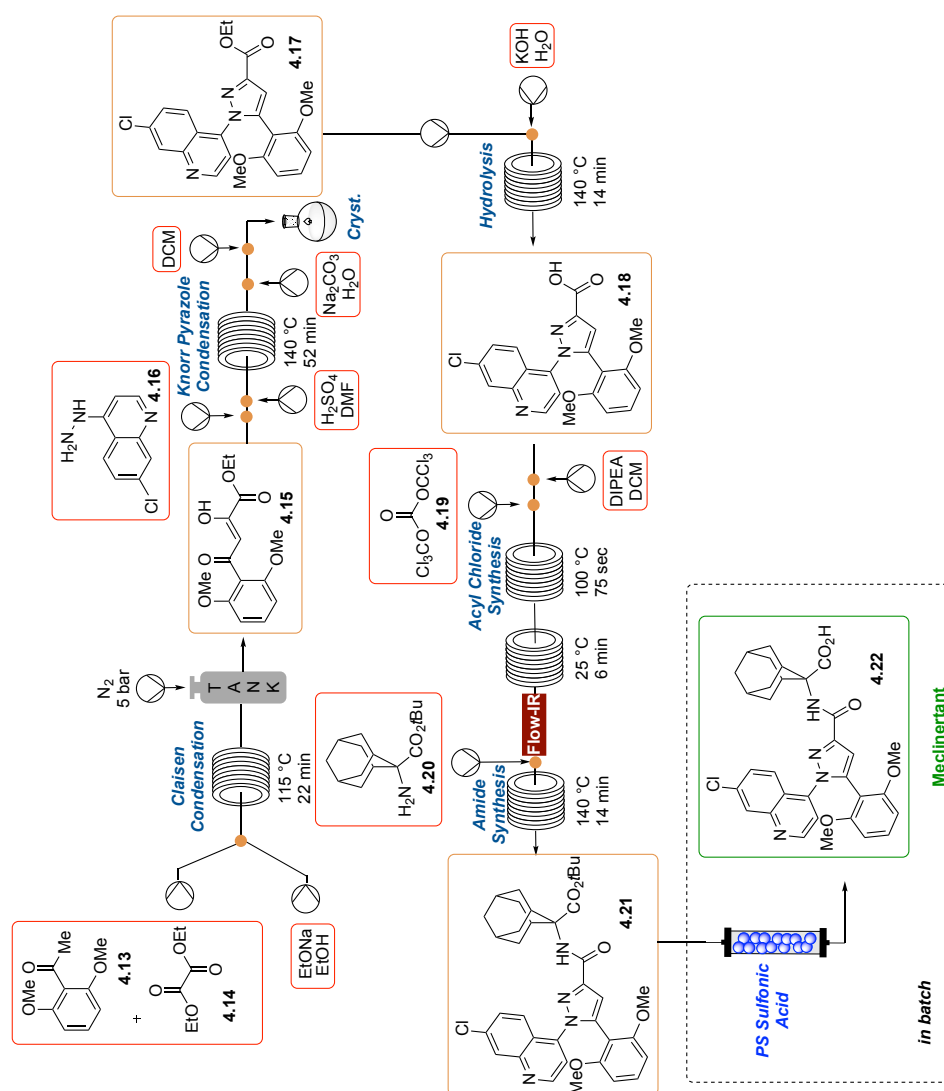
The first step of this synthesis was the Grignard addition of compound **4.5** to Weinreb amide **4.4** in a PFA reactor (d = 10 mm, V = 10 mL) at 60 °C for 5 min, affording ketone **4.8** upon quenching with HCl. Notably, while batch conditions generally necessitate the addition of a catalyst (*e.g.*, ZnCl₂) to ensure reasonable reaction rates (from 24 h to 2 h), no catalyst was required for the flow-based synthesis. Simultaneously to the Grignard addition, lithiation of **4.7** was performed in a separate PFA reactor (d = 10 mm, V = 10 mL) at –50 °C. After 7 min of reaction, aryl lithium **4.9** and ketone **4.8** were mixed and passed through another PFA reactor (d = 10 mm, V = 0.4 mL) at 30 °C, affording the lithium alkoxide **4.10** after only 2 min. TFA treatment of **4.10** (PFA reactor, d = 10 mm, V = 10 mL) at 25 °C followed by a final elimination step afforded Tamoxifen **4.12** in 84% yield and in a E/Z mixture of 25/75. This process provided, after only 80 min, 12.4 g of Tamoxifen, representing 900 days of treatment

for a single patient. More significant synthetically, both the Grignard addition and lithiation reactions require controlled temperatures for long periods of time, which is not always possible when reactions are performed in batch (e.g., for 24 h).

4.1.3 Benefits of Flow Chemistry - Integrated Synthesis, Work-up and Analysis

The previous examples have illustrated continuous flow technology's proficiency for successfully allowing automation of multiple chemical transformations. However, the modularity of this strategy also permits the integration of work-up, such as separation (Scheme 4.1) and crystallisation (Scheme 4.3), purification (Scheme 4.4) and analysis (Scheme 4.3) in a single, fully-automated, continuous process. An impressive example of this combined modular strategy was displayed by Ley *et al.* with the fully automated flow synthesis of the neurotensin receptor-1 antagonist Merclinerfant **4.21** (Scheme 4.3).²⁴¹

Claisen condensation between **4.13** and **4.14** was performed in a PFA reactor (d = 78 mm, V = 52 mL) at 115 °C. Reaction completion was obtained after 22 min, compared to the 3 h required for batch synthesis. To avoid potential blockage of the system arising from precipitation of the intermediate, a pressurised stainless-steel tank containing nitrogen (5 bar) was added to the system, allowing the formation of compound **4.15** in 74% yield. Knorr pyrazole condensation using **4.15** and hydrazine **4.16** (PFA reactor, d = 78 mm, V = 52 mL) at 140 °C for 52 min, followed by Na₂CO₃ aq. treatment, DCM extraction and crystallisation provided pyrazole ester **4.17** in 89% yield. Hydrolysis of ester **4.17** was performed at 140 °C for 14 min (PFA reactor, d = 78 mm, V = 14 mL) and delivered, after precipitation, carboxylic acid **4.18** in 90% yield. Amide formation was then achieved *via* activation of **4.18** to its corresponding acid chloride using triphosgene **4.19**, followed by coupling to amine **4.20**.

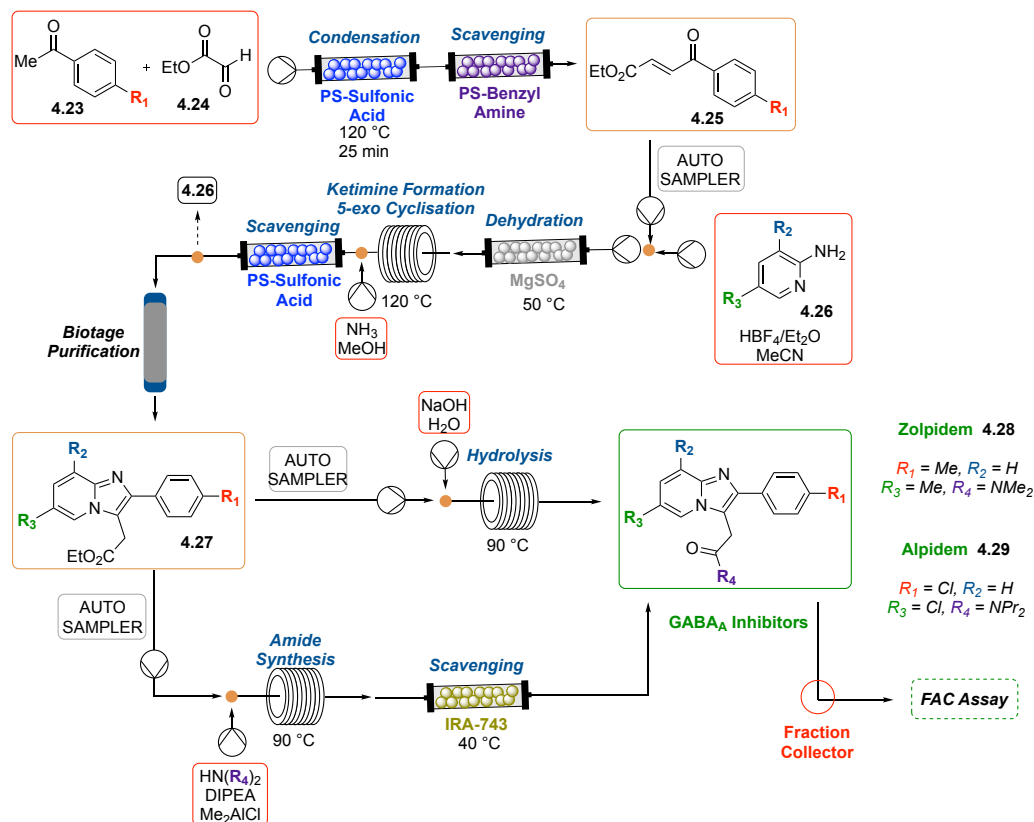


Scheme 4.3. Continuous flow synthesis of Meclintertant **4.22**.²⁴¹

To improve the safety of the process, formation of phosgene was monitored using an inline flow-FTIR spectrometer, thereby avoiding contact with the toxic gas.²⁴² After passing the reaction mixture through three PFA reactors, the Meclintertant ester **4.21** was obtained in 73% yield. This novel approach permitted the production of the final compound, seven reactions and their corresponding work-ups/analysis, in less than half a typical working day, a feat that is impossible to accomplish using general batch synthesis.

Another elegant example of a fully integrated continuous flow process was illustrated through the synthesis of two GABA_A inhibitor analogues, Zolpidem **4.28**, commonly used for treating insomnia, and Alpidem **4.29**, an anxiolytic drug (Scheme 4.4).²⁴³ The novelty of this platform

was the combination of a fully integrated organic synthesis process with frontal affinity chromatography (FAC) as an inline protein binding assay.



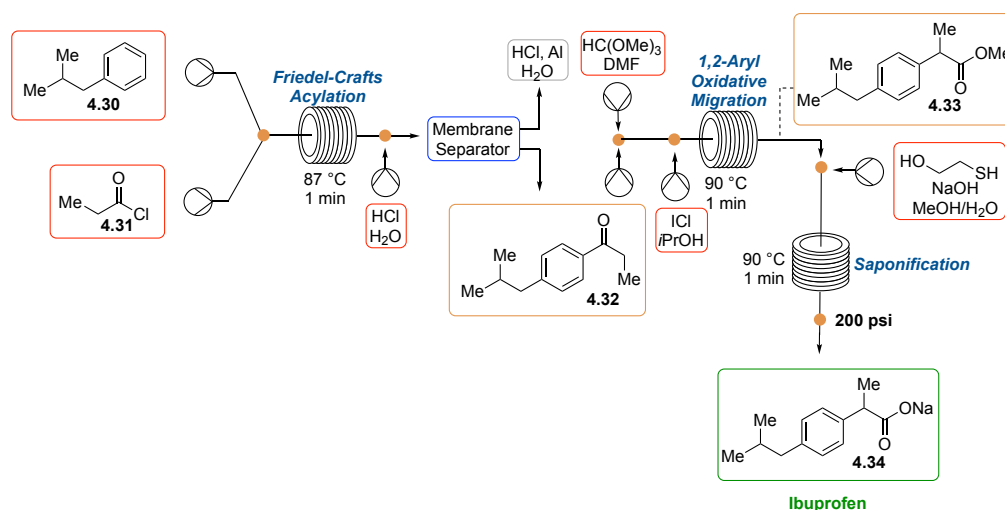
Scheme 4.4. Continuous flow synthesis of GABA_A inhibitors, Zolpidem 4.28 and Alpidem 4.29.²⁴³

First, the condensation of compounds 4.23 and 4.24 was performed using a polymer-supported sulphonic acid cartridge at 120 °C, affording, after 25 min, the unsaturated ketone 4.25 in yields between 76–85%. Excess glyoxalate 4.24 was scavenged using a benzyl amine polymer-supported cartridge to avoid the need for further purification. Ketone 4.25 and amine 4.26 were then pumped through a MgSO₄-packed cartridge, used as a dehydrating agent, followed by ketimine formation and 5-exo cyclisation in a PFA reactor (d = 10 mm, V = 14 mL). Excess amine 4.26 was removed using a polymer-supported sulfonic acid cartridge and the reaction mixture was directly injected into an inline chromatographic purification system, affording imidazopyridine 4.27. Saponification was achieved by heating 4.27 in the presence of NaOH at 90 °C. Reaction of 4.27 with a secondary amine in the presence of Me₂AlCl followed by removal of excess aluminium by passing through a polyol resin (IRA-743) allowed the formation of compounds 4.28 and 4.29 after 280 min. An aliquot of 22 analogues synthesised using this procedure was then directly subjected to FAC analysis, allowing the

direct investigation of their interactions with Human Serum Albumin (HSA). This example clearly shows the ability of flow technology to integrate organic synthesis and biological evaluation in a single process.

4.1.4 Benefits of Flow Chemistry – High Throughput

One of the main benefits of continuous flow technology, particularly for industrial purposes, is its capacity for high throughput applications. Jamison *et al.* “pushed the limits” of organic synthesis with their 3 min continuous flow synthesis of Ibuprofen **4.34** (Scheme 4.5), one of the most commonly used drugs worldwide.²⁴⁴



Scheme 4.5. Flow synthesis of Ibuprofen **4.34**.²⁴⁴

This three-step process begins with a Friedel-Crafts acylation using compounds **4.30** and **4.31** in a PFA reactor ($d = 0.8$ mm, $V = 250$ μ L) at 87 °C. After 1 min of reaction, the mixture was treated with HCl aq. then extracted through an inline membrane separator operating at 200 psi, thus avoiding the need of organic solvent. Intermediate **4.32** was then involved in a 1,2-aryl oxidative migration in the presence of trimethylorthoformate ($\text{HC}(\text{OMe})_3$) and ICl in a second PFA reactor ($d = 0.8$ mm, $V = 900$ μ L), affording aryl ester **4.33** after 1 min of reaction at 90 °C. The last step of this process combined quenching of the excess ICl and saponification of intermediate **4.33** in a PFA reactor ($d = 0.8$ mm, $V = 3.9$ mL). After 1 min of reaction at 90 °C, Ibuprofen **4.34** was obtained in an overall yield of 83%. This process uses inexpensive and readily available starting materials. Furthermore, using a system with a footprint of half the

size of standard laboratory fume hood, the authors were able to synthesis 8.1 g/h of Ibuprofen **4.34**.

While the previous examples have shown the power of continuous flow chemistry (increased kinetics, safer reactions, high throughput) and its potential towards the development of applied automation in drug discovery and organic methodology, another important factor offered by this process is the ability to perform immobilised catalysis. This would result in increased reaction safety as the operator would not contact the catalyst and decreased reaction cost as the catalyst can be used several times without loss of reactivity.

4.2 Copper-Catalysed Reactions in Continuous Flow Processes

The growing number of transition metal-catalysed cross-couplings have revolutionised chemical synthesis, allowing for milder reaction conditions, improved yields and the generation of higher-complexity molecules. However, the decreased abundance of transition-metals commonly used for catalysing reactions (*e.g.*, palladium) has led to rising prices of these vital catalysts. Research has therefore focused on expanding the library of immobilised-transition metal-catalysed cross-couplings. A key advantage of this technique is that the catalysts can be employed for multiple reactions, decreasing reaction costs. Flow processes are primed for performing transition metal-catalysed cross-couplings as catalysts can be easily immobilised in cartridges and reactors (Figure 4.1, Type IV reactor).

Copper catalysis has received much attention over the last decades due to copper's high abundance and the corresponding low cost of the catalysts. Additionally, the several oxidation states of copper are easily accessible, allowing for a wide range of reactions. Copper-catalysed chemistry has been highly developed on flow systems due to the ease of preparing copper reactors. The following sections describe the current copper-catalysed cross-couplings developed on flow systems.

4.2.1 C–C Bond Formation Using Cu-Catalysed Continuous Flow Processes

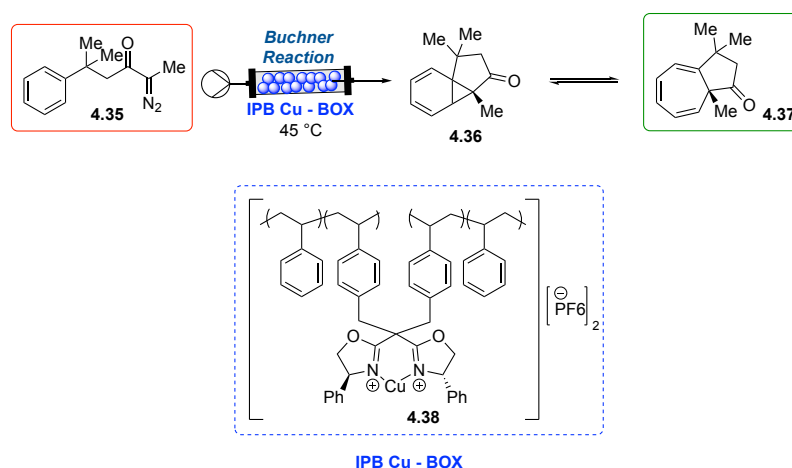
Carbon-carbon (C–C) bond formation is the foundation of organic chemistry. Whereas palladium catalysts are commonly employed for C–C bond formation, fewer methodologies have been developed using copper catalysis.

4.2.1.1 Buchner Ring Expansion

The Buchner ring expansion allows for the metal-catalysed 2-step formation of 7-membered rings.²⁴⁵ The first step of the reaction involves the formation of a carbene from diazoacetate compounds, such as **4.35** (Scheme 4.6), which then react to form a cyclopropane, such as **4.36**. Ring expansion then occurs to provide 7-membered ring products, such as **4.37**. Although rhodium was originally used to catalysing this reaction, the use of copper has been shown to increase the enantioselectivity of the reaction.²⁴⁶

Recently, Maguire *et al.* adapted this methodology to flow processes for the enantioselective, intramolecular Buchner reaction of α -diazoketone **4.35** using a copper-packed bed reactor (Scheme 4.6).²⁴⁷ Polymerisation of bis(oxazoline) ligand *via* Burguete's procedure,²⁴⁸ followed by copper-complexation, using $[\text{Cu}(\text{MeCN})_4]\text{PF}_6^-$ as a copper source, allowed the formation of IPB-Cu catalyst **4.38**. Prior reaction optimisation in batch synthesis revealed that the use of 4-phenyl bis(oxazoline) as a copper ligand improved enantioselectivity of the reaction.

Direct translation of these conditions to flow processes afforded the synthesis of azulenone **4.37** in 83 % *ee*. More importantly, atomic absorption spectroscopy indicated that **4.38** contained 0.24 mmol/g of catalyst. Therefore, this copper-packed bed reactor was able to catalyse the intramolecular Buchner reaction up to 7 times without any loss of activity, representing a significant advantage compared to current batch strategies.

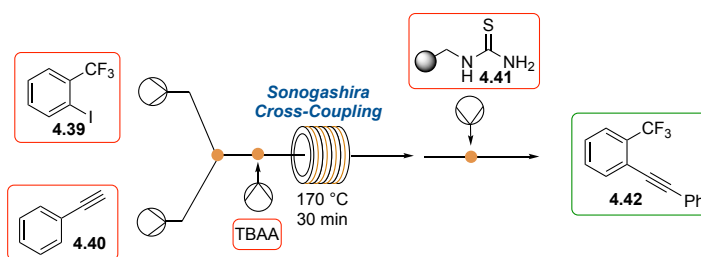


Scheme 4.6. Continuous flow synthesis of Azulenone **4.37**.²⁴⁷

4.2.1.2 Sonogashira Cross-coupling Reaction

Another important C–C bond formation reaction is the Sonogashira cross-coupling reaction, wherein a terminal alkyne is reacted with an aryl or vinyl halide in the presence of palladium and copper catalysts.²⁴⁹ Typical batch conditions require 1–10 mol % of palladium and copper catalysts and the addition of supra-stoichiometric amounts of an amine base. Reaction kinetics are generally slow, often requiring up to 24 h to reach completion.

Mainolfi *et al.* reported the continuous flow process of Sonogashira cross-coupling reactions using a copper tube flow reactor (Scheme 4.7).²⁵⁰ In this reactor, a copper coil is looped around a mesh support and inserted into a metal jacket, allowing the reactor to be heated up to 250 °C. The advantage of this type of reactor is that it directly promotes copper-catalysed reactions without the need for additional catalyst.



Scheme 4.7. Sonogashira cross-coupling via continuous flow using a copper reactor.²⁵⁰

Optimisation of the reaction found that the type of solvent used for the reaction was a critical parameter for the successful synthesis of arylalkynes, such as **4.42**. DMF was identified as the ideal solvent for the reaction, whereas THF, CH₃CN, EtOAc and EtOH afforded only small amounts of the expected product. Furthermore, increasing the temperature to 170 °C and addition of the ionic base tetra-*n*-butylammonium acetate (TBAA) allowed the formation of **4.42** in 90 % yield after 30 min without the need for the palladium catalyst. However, when less reactive substrates were used (*e.g.* bromobenzene or trimethylsilyl acetylene), a catalytic amount of Pd(PPh₃)₂Cl₂ (0.5 mol %) was required to obtain the desired products. In addition, no Glaser by-product^{89,91} was observed during these reactions.

While this method was able to rapidly and efficiently produce a variety of arylalkynes, a large amount of copper leaching from the reactor was observed in final products due to the extreme temperature used to perform the reaction. To alleviate this problem, an immobilised scavenger, Quadrapure Thiourea, was added to remove traces of copper and palladium.

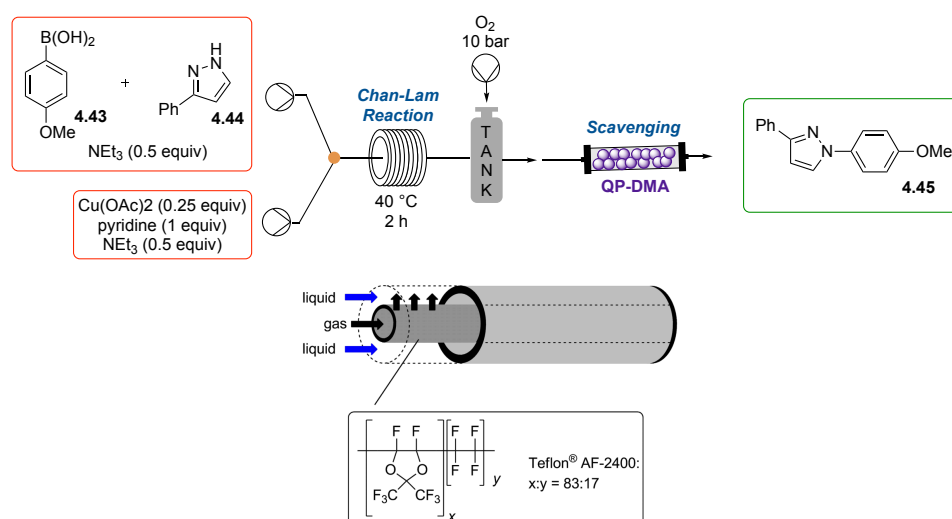
4.2.2 C–N Bond Formation Using Cu-Catalysed Continuous Flow Processes

The formation of carbon–nitrogen (C–N) bonds is extremely important as they are regularly found in natural products and bioactive molecules. Extensive efforts have been made to identify and improve methodologies for efficient C–N bond formations. Similar to C–C bond formation, the use of a catalyst, such as copper, has been shown to dramatically improve our ability to form C–N bonds.

4.2.2.1 Chan-Evans-Lam Reaction

The Chan-Evans-Lam reaction^{251–253} is particularly important as it allows the formation of aryl amine products which are of great interest to medicinal chemists.²⁵⁴ This process reacts a boronic acid with an amine in the presence of catalytic to stoichiometric amounts of a copper catalyst. The advantage of this strategy, with respect to other C–N bond formation methodologies, is that the reaction is performed under mild conditions and can support aerobic conditions. However, the kinetics of this reaction are relatively slow, requiring up to 24 h to reach completion, even when heated at 100 °C.

Baxendale *et al.* published a Chan-Evans-Lam study using catalytic amounts of $\text{Cu}(\text{OAc})_2$ and a ‘tube-in-tube’ flow reactor (Scheme 4.8),²⁵⁵ allowing for the safe delivery of oxygen to the reaction, even at high temperatures.

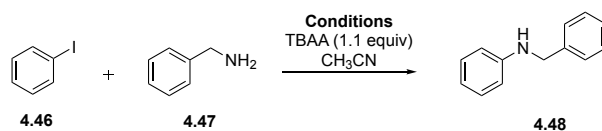


Scheme 4.8. Chan-Evans-Lam continuous flow process.²⁵⁵

Optimisation of the reaction between boronic acid **4.43** and amine **4.44** revealed that only a catalytic amount of $\text{Cu}(\text{OAc})_2$ was necessary to catalyse the reaction when oxygen was used to re-oxidise $\text{Cu}(\text{I})$ following C-N reductive elimination, whereas, without oxygen, stoichiometric amounts of copper were required. It is worth noting that this flow platform uses homogeneous catalysis and that the copper is solubilised prior to the reaction. The authors found that decreasing the equivalents of boronic acid **4.43** from 1.6 to 1.4 dramatically decreased the yield of **4.45** from 94% to 56%, respectively. To allow for the use of higher equivalents of boronic acid **4.43** and facilitate purification of the final product, a polymer-supported tertiary amine base, QP-DMA, was added to the system to trap excess **4.43**. Using their optimised continuous flow conditions, the authors were able to synthesis a small library of 1,3-disubstituted pyrazoles in 26-92% yields after only 2 h of reaction, a remarkable advancement when compared to modern batch techniques.

4.2.2.2 Ullmann Condensation

The Ullmann condensation refers to the reaction between an aryl halide and phenol or aniline in the presence of a catalytic amount of copper.²⁵⁶ As with the Chan-Evans-Lam reaction, this reaction usually requires high temperature (100 °C) and extended reaction time (24 h). Mainolfi *et al.* investigated the reactivity difference between flow, microwave and batch chemistry using the Ullmann condensation as a model (Table 4.1).²⁵⁰ Iodobenzene **4.46** (1 equiv) and benzylamine **4.47** (1.2 equiv) were reacted in the presence of TBAA (1.1 equiv) in MeCN. The use of a copper reactor at 150 °C for 30 min afforded 65% of expected product **4.48** (Entry 1). Decreasing the flow rate from 0.33 mL/min to 0.17 mL/min allowed the reaction to reach completion (Entry 2). Replacing the copper reactor with a PFA reactor, and without the addition of an external copper source, afforded only recovery of starting material (Entry 3), demonstrating that copper is necessary to catalyse the reaction. Microwave-assisted synthesis (400 W) using CuI (10 mol %) or Cu powder (10 mol %) afforded **4.48** in 50% and 31% yield, respectively, after 30 min (Entry 4-5). Finally, batch conditions using an oil bath at 90 °C afforded **4.48** in 40% yield after 16 h, demonstrating the enormous advantage of flow processes compared to microwave and batch chemistry.

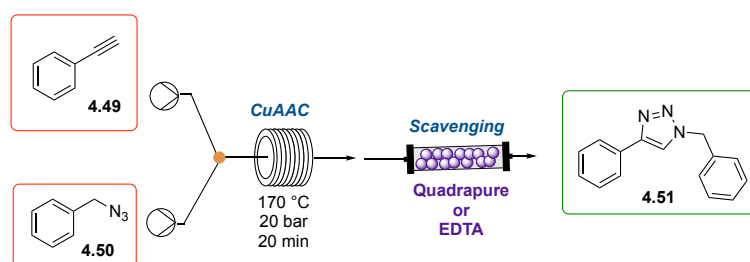
Table 4.1. Ullmann condensation using flow, microwave and batch conditions.²⁵⁰

Entry	Conditions	Temperature (°C)	Residence Time (min)	Flow Rate (mL/min)	Conversion (%)
1	Copper tube	150	30	0.33	65
2	Copper tube	150	120	0.17	100
3	PFA tube	150	30	0.33	0
4	Microwave	150	30		50
5	Microwave	150	30		31
6	Oil bath	90	960		40

4.2.2.3 Copper-Catalysed Azide-Alkyne Cycloaddition

The copper-catalysed azide/alkyne cycloaddition has also been employed for the synthesis and modification of polymers,²⁵⁷ surfaces²⁵⁸ and supramolecular assemblies.²⁵⁹ Despite the extensive efforts made to increase reaction rates, completion of the reaction can still take up to 16 h. Therefore, adaptation of this important methodology to flow chemistry has the potential to overcome the kinetics issue.

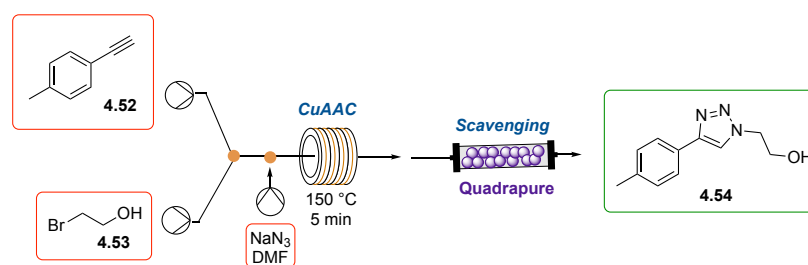
This was successfully accomplished by Kappe *et al.* in their investigation into the mechanism of the formation of 1,4-triazoles using a Cu/C packed column in continuous flow and phenylacetylene **4.49** and benzyl azide **4.50** as model substrates (Scheme 4.9).²⁶⁰ The authors hypothesised that Cu(0) could be used as a copper source to catalyse CuAAC reactions in flow as the copper metal would be continuously oxidised by the air, creating surface CuO and Cu₂O oxidative layers.²⁶¹ To test this hypothesis, the authors performed a series of CuAAC reactions using Cu turnings in a microwave at 160 °C, alternating between HCl treatment to remove the CuO/Cu₂O layers and H₂O₂ treatment to re-oxidise the copper surface.²⁶⁰ Upon treatment with HCl, conversion of **4.49** and **4.50** to triazole **4.51** was considerably decreased (3% to 11%). However, activation of the copper turnings with 35% H₂O₂ generated the active catalyst and afforded triazole **4.51** in 48% yield, confirming their hypothesis.



Scheme 4.9. CuAAC reactions using Cu/C packed column in flow.²⁶⁰

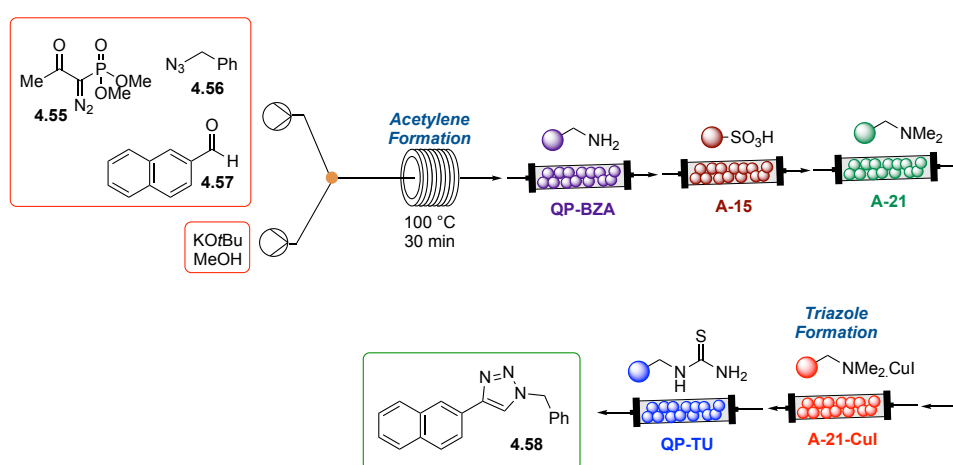
Flow experiments were then performed using a high-pressure flow reactor (X-Cube) and an immobilised, pre-packed Cu/C cartridge (60 × 4 mm) containing 250 mg of Cu/C (Scheme 4.9). Reaction between **4.49** and **4.50** in acetone at 170 °C (20 bars) afforded the expected triazole **4.51** in quantitative yield after 2 h. Decreasing the temperature of the reaction afforded incomplete conversion. Unfortunately, a high concentration of copper was detected by ICP-MS analysis in the final product (600 mg/kg), far above the acceptable concentrations for pharmaceuticals (15 mg/kg).²⁶² To decrease copper contamination, a scavenger was added to the continuous flow process. Following purification through Quadrapure TU (thiourea) resin packed in a stainless-steel cartridge (60 × 4 mm, 350 mg), the concentration of copper in the final product was decreased to 1 mg/kg. While efficient on a small scale (0.25 mmol), this scavenging method is problematic on large scales, as when scaled up to 250 mmol 60% of the pre-packed Cu/C had leached within 11 h. Multiple extractions with EDTA were then necessary, decreasing copper concentration to 2 mg/kg.

The same year, Sach *et al.* reported an *in-situ* azide synthesis, followed by 1,4-triazole formation using a copper flow reactor (Scheme 4.10).²³⁹ The use of a copper reactor eliminates the need for additional catalyst to perform the reaction. Optimisation of the reaction between alkyne **4.52** and azide **4.53** has shown that copper leaching is highly dependent on the solvent used for the reaction. For example, the amount of copper leaching present in the final product was only 78 ppm as determined by elemental analysis when ethanol was used at 150 °C, while 300 ppm were found with DMF. However, precipitation of phenylacetylene **4.52** occurred when ethanol was used. DMF was therefore chosen as a solvent for the reaction, and a Quadrapure TU cartridge was added to the process, reducing the copper concentration to 5 ppm. Using this strategy, the authors were able to synthesise a vast library of triazoles in 21-92% yields.



Scheme 4.10. CuAAC reactions using a copper flow reactor.²³⁹

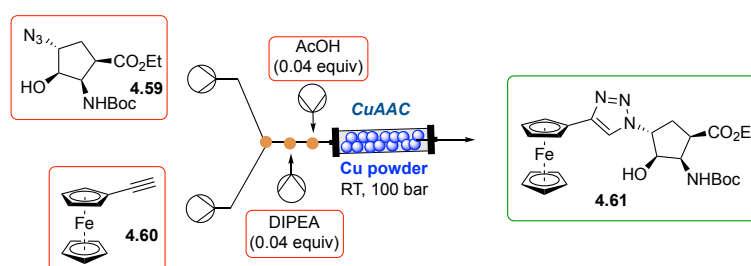
In-situ formation of the alkyne moiety followed by triazole formation was also demonstrated in a continuous flow process by Smith *et al.* (Scheme 4.11).²⁶³



Scheme 4.11. *In-situ* alkyne formation followed by a CuAAC reaction.²⁶³

Using a variety of in-line, immobilised reagents and scavengers, the authors were able to successfully synthesise triazole **4.58** without the need for further purification. Aldehyde **4.57** (1.3 equiv) and Bestmann-Ohira reagent **4.55** (1 equiv) were first reacted in a convection-flow coil (CFC, 10 mL) at 100 °C for 30 min in the presence of azide **4.56** and KO*t*Bu in MeOH. The reaction mixture was then flowed through a Quadrapure benzylamine cartridge (QP-BZA) at 70 °C to remove excess aldehyde **4.57**. The resulting mixture was pumped through an Amberlyst-15 sulfonic acid (A-15) support to remove the base and protonating phosphoric residues before being flowed through another Amberlyst-21 dimethyl amine resin (A-21), removing residual acid and affording pure acetylene product. Importantly, no degradation of azide **4.56** was observed. The CuAAC reaction was then performed by flowing the mixture through an immobilised copper-catalyst (A-21-CuI), affording triazole **4.58** in 69% yield after scavenging residual copper with a Quadrapure thiourea (QP-TU) flow tube.

While efficient and modular, these processes require elevated temperatures, which limits their use with biomolecules. However, Fülöp *et al.* published a study in which the use of additives allowed them to perform CuAAC reactions at room temperature (Scheme 4.12).²⁶⁴ Earlier studies had shown that adding an amine base dramatically increases the rate of CuAAC reactions by chelating and stabilising Cu(I) species.^{67,70} Other studies have found that adding catalytic amounts of acid could further increase the rate, accelerating the protonation of the Cu-triazole in the last step of the mechanism.²⁶⁵ By adding a combination of *N,N*-diisopropylethylamine (DIPEA, 0.04 equiv) and acetic acid (AcOH, 0.04 equiv) to their flow process, the authors were able to produce the desired triazoles in high yields, without the need for heating. This process allowed the ligation of cispentacin azide derivative **4.59**, a naturally occurring carbocyclic β -amino acid possessing antifungal properties, and ferrocene alkyne **4.60**, an electrochemical reporter, affording triazole **4.61** in 99% yield. More importantly, the use of milder conditions dramatically decreased copper leaching (7.1 mg/kg). However, high pressures (100 bar) were still necessary to activate the reaction and avoid any precipitation.



Scheme 4.12. CuAAC reaction using immobilised Cu powder and DIPEA/AcOH as additives.²⁶³

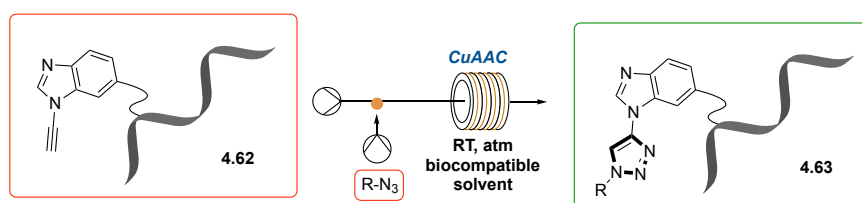
4.3 Hypothesis to Be Tested

The development of flow-based technologies has significantly advanced chemical synthesis, offering numerous advantages compared to batch and microwave chemistry. Furthermore, the higher reactivity observed in flow processes, due to enhanced mass transfer, has proven to be particularly beneficial for performing chemical reactions with large molecular weight biomolecules, in which structural conformations can significantly compromise functional groups' accessibility.^{266,267}

Despite these benefits, the development of a flow-based platform for CuAAC bioconjugation has not yet been possible due to the requirement for excess Cu catalyst and elevated

temperatures, conditions which cause biomolecule denaturation and degradation. In addition, the need for organic solvent has limited flow-based CuAAC applications to small molecules.

We have previously shown that aromatic ynamines are superior CuAAC reagents with enhanced chemical reactivity relative to conventional alkynes (Chapter 2).^{170,171,174} Additionally, incorporating a benzimidazole ynamine moiety into oligonucleotides allowed us to decrease Cu loading to 10 mol % while a large excess (10 equiv) is necessary when using conventional alkynes (Chapter 3). The hypothesis to be test in this work is that the enhanced reactivity of aromatic ynamines will allow for the development of a flow-based platform for the fast, mild, degradation-free bioconjugation of peptide and oligonucleotide derivatives (Scheme 4.13).

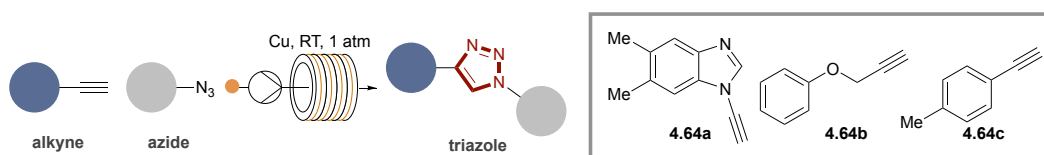


Scheme 4.13. Flow-based platform for CuAAC bioconjugation using the enhanced reactivity of aromatic ynamines.

4.4 Aims of this Chapter

The specific aims of this chapter are to:

- (i) Determine appropriate reaction conditions for fast and mild CuAAC reactions using a copper flow reactor with a range of alkynes **4.64a-c** (Scheme 4.14).



Scheme 4.14. Optimisation of flow CuAAC using copper tubing.

- (ii) Apply these conditions to the CuAAC bioconjugation of peptide and oligonucleotide derivatives using a copper flow reactor.

- (iii) Optimise reaction conditions for the ligation of a phosphorodiamidite morpholino oligomer (PMO) derivative and a cell-penetrating peptide (CPP) using a copper flow reactor (Figure 4.3).

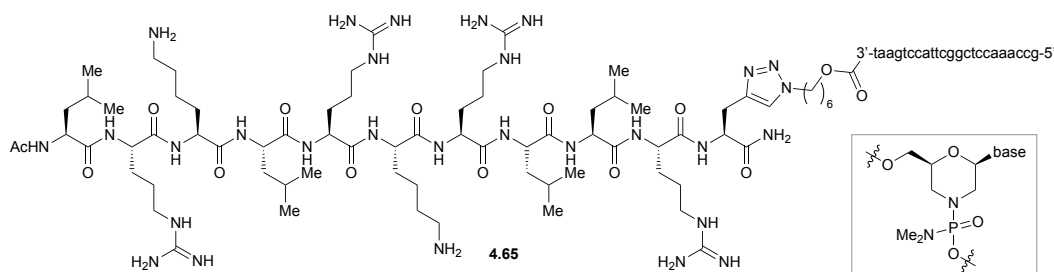


Figure 4.3. PMO-ApoE conjugate **4.65**.

4.5 Results and Discussion

4.5.1 Cu-Loading for CuAAC Reactions with Aromatic Ynamines

It is hypothesised that the Cu leaching from the tubing during continuous flow processes due to elevated temperatures and high pressures is sufficient to catalyse CuAAC reactions.²⁶⁰ The enhanced reactivity of aromatic ynamines has proven to dramatically decrease copper loading (10 mol % versus 10 equiv using phenylacetylene) when performing CuAAC ligations on oligonucleotides (see Chapter 3). This leads to the hypothesis that the higher reactivity of aromatic ynamines could allow for the development of a milder flow platform for CuAAC ligations, as less copper should be required to reach completion of the reaction.

To test this hypothesis, the amount of copper needed to perform CuAAC reactions between benzimidazole ynamine **4.64a** and benzyl azide **2.86a** was empirically determined in batch (Figure 4.4).

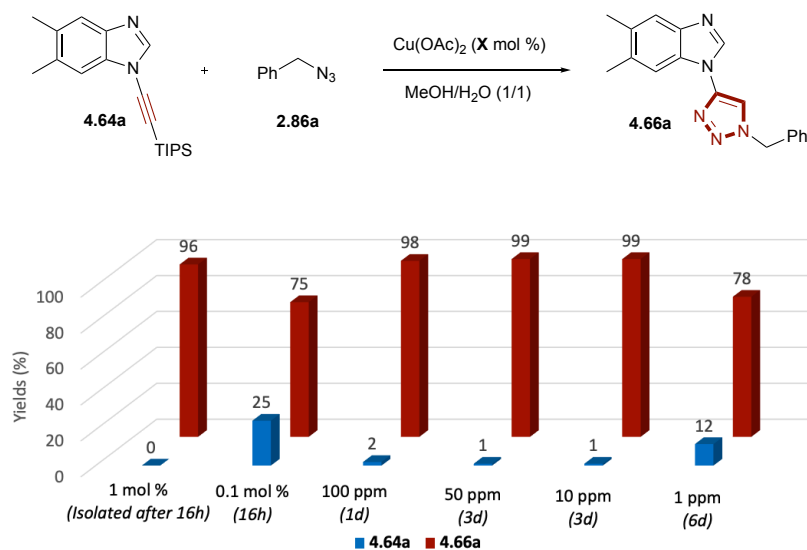


Figure 4.4. Investigating Cu loading required for the formation of **4.66a**. Isolated yields.

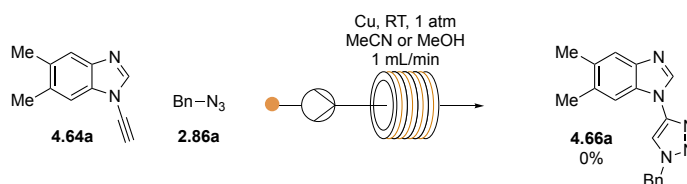
Decreasing Cu loading to 1 mol % had no impact on the reactivity of benzimidazole ynamine **4.64a** and afforded triazole **4.66a** in 96% yield after 16 h. A small drop in reactivity was observed when 0.1 mol % was used, still allowing the formation of **4.66a** in 75% yield. Serial dilutions of Cu(OAc)₂ were then used to explore the CuAAC reaction between **4.64a** and **2.86a** at even further reduced (ppm) amounts of copper. While slower, high yields of triazole **4.66a** were observed even when only 1 ppm Cu(OAc)₂ was used to catalyse the reaction. Remarkably, **4.66a** was obtained in 99% yield after 3 days when only 10 ppm Cu(OAc)₂ was used; notably, this is below the minimum copper concentration permitted in pharmaceuticals (15 ppm).²⁶² These results suggest that the amount of leaching from a copper flow reactor at ambient temperature could be sufficient for catalysing CuAAC reactions with aromatic ynamines, which could allow for the development of a flow platform for the ligation of more sensitive molecules, such as peptides or oligonucleotides.

4.5.2 Developing a Flow Platform for Mild CuAAC Ligation of Small Molecules

4.5.2.1 Effect of H₂O on Triazole Formation

The following CuAAC reactions were carried out in a commercial chemical flow reactor (easy-Scholar, Vapourtec) equipped with a copper reactor (Vapourtec, d = 1 mm, V = 10 mL). Alkyne and azide starting materials were solubilised in 10 mL of solvent before being pumped through the copper tubing at a flow rate of 1 mL/min (t_R = 10 min) at room temperature (25 °C), unless stated otherwise. Initial attempts to perform CuAAC reactions between ynamine

benzimidazole **4.64a** and benzyl azide **2.86a** using either MeOH or MeCN as solvent were unsuccessful; only starting materials were recovered after one pass through the reactor ($t_R = 10$ min, Scheme 4.15). Decreasing the flow rate to 0.25 mL/min ($t_R = 40$ min) also failed to yield product. Surprisingly, adding a small amount of water to MeOH (1/40 and 1/20) afforded **4.66a** in 11% and 24% yields, respectively. Changing the solvent to 40/1 MeCN/H₂O allowed for complete conversion of starting materials to **4.66a** after 10 min at room temperature.



Scheme 4.15. Initial attempts of flow CuAAC reaction with aromatic ynamine **4.64a** using copper tubing.²¹⁵

The effects of water on triazole formation were further investigated using three representative alkynes: benzimidazole ynamine **4.64a**, propargyl ether **4.64b** and aromatic alkyne **4.64c** (Figure 4.5).²¹⁵

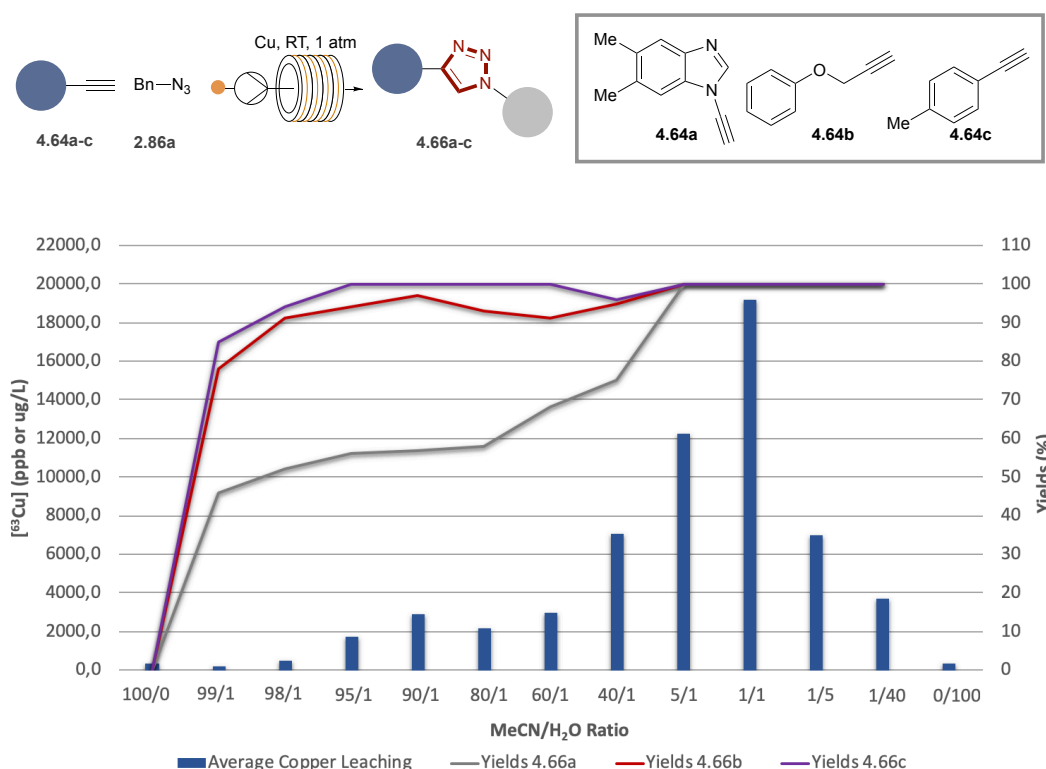


Figure 4.5. Effect of H₂O on triazole formation. Isolated yields.²¹⁵

Results from this study indicate that the addition of even a small amount of water to MeCN (1/99) has substantial impact on the extent of triazole formation, affording **4.66a**, **4.66b**, and **4.66c** in 46%, 78% and 85% yields, respectively. Increasing the proportion of water in the solvent system further improved yields, with the reaction reaching completion for alkynes **4.64a-c** when 5/1 MeCN/H₂O was used. It is worth noting that while ynamine **4.64a** exhibited superior reactivity in the batch system, owing to a pK_a modifying Cu-ligation,¹⁷⁰ this solvent system proved effective even with less reactive alkynes, such as **4.64b** and **4.64c**.

4.5.2.2 Effect of H₂O on Copper Leaching

As stated previously, it had been hypothesised that elevated temperatures were needed when performing CuAAC reactions in flow in order to solubilise enough copper to achieve the reaction.²⁶⁰ However, adding water to the eluent allowed the reaction to reach completion at room temperature and atmospheric pressure. In order to investigate if water is necessary to perform the reaction due to associated copper leaching, ICP-MS analysis was performed for each solvent system (Figure 4.5).²¹⁵ To achieve this, the eluents were pumped through the copper reactor at 1 mL/min at room temperature and analysed directly by ICP-MS. These data confirmed that increasing water content resulted in higher copper concentrations in the eluents, with a maximum occurring in 1/1 MeCN/H₂O. A direct comparison of copper leaching from a used (~300 reactions) and new (no reaction) reactor measured distinctly higher copper concentrations from the used one in equivalent solvent mixtures (Figure 4.6).

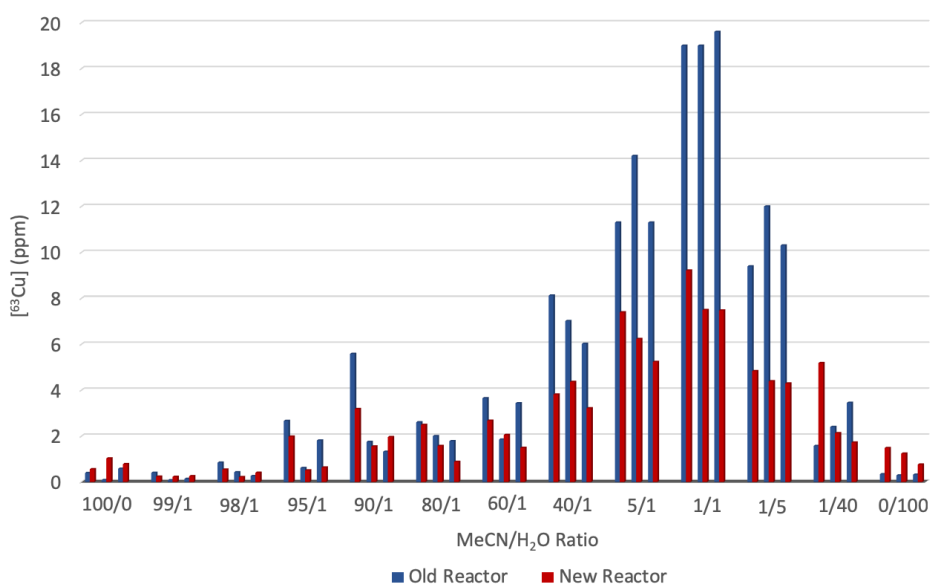
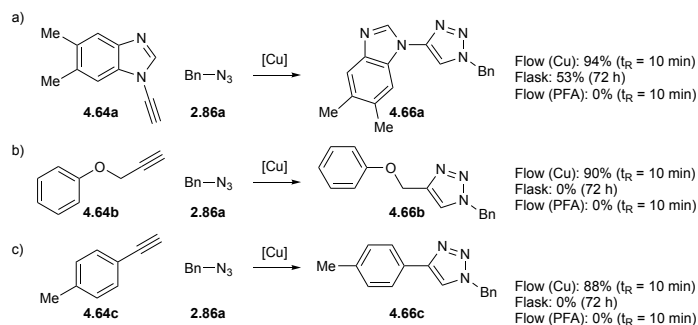


Figure 4.6. Copper leaching from new and used (~300 reactions) reactors.²¹⁵

These findings would be consistent with the higher solubility of CuO and Cu₂O, which form a coating on copper pipes, in water than in organic solvent. Therefore, these pipes are more prone to leaching after multiple exposures to water.²⁶¹ However, similar copper concentrations were observed when MeCN and 99/1 MeCN/H₂O were used as solvents (0.353 ppm and 0.206 ppm, respectively), even though the conversion of starting materials **4.64a-c** to products **4.66a-c** has been shown to be dramatically different. These data suggest that the role of water in the reaction mechanism is not simply to solubilise copper.

4.5.2.3 Investigating the Role of H₂O in the Reaction

Control experiments were performed in order to investigate whether copper solubilisation is necessary to catalyse CuAAC reactions between alkynes **4.64a-c** and benzyl azide **2.86a** (Scheme 4.16a-c).²¹⁵ Attempting CuAAC reactions in batch using a 5/1 MeCN/H₂O solvent mixture containing 12.3 ppm of copper, as determined by ICP-MS, proved unsuccessful for **4.64b** and **4.64c** and poor for **4.64a**, after 72 h. Repeating these experiments in flow using a PFA reactor (d = 1 mm, V = 10 mL) at 1 mL/min only recovers starting materials in the eluent for all three reactions. These results suggest that solution copper is not sufficient for the CuAAC reactions and that catalysis most likely occurs on the surface of the copper tubing.

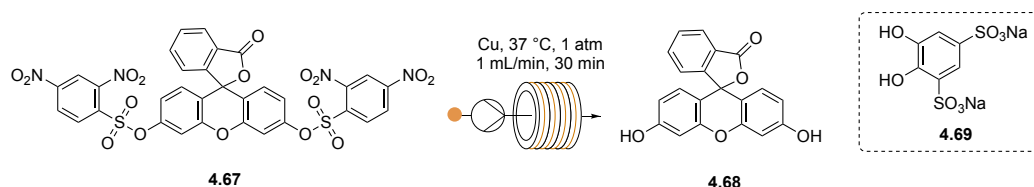


Scheme 4.16. Comparison of CuAAC efficiency in batch vs. flow containing 12.3 ppm Cu. *Isolated yields.*²¹⁵

Performing a CuAAC reaction between ynamine **4.64a** and benzyl azide **2.86a** in the copper flow reactor using a degassed solution of 5/1 MeCN/H₂O affords full conversion of the starting materials to the expected product **4.66a**. On the other hand, flowing O₂ (0.5 mL/min) into the reactor while performing the same reaction in MeCN alone also affords full conversion to **4.66a**. These experiments suggest that reactive oxygen species (ROS) may arise during the flow process, the presence of which could aid in the reaction progress *via* copper disproportionation. To verify their presence, continuous flow reactions were performed in the copper flow reactor using a variety of ROS probes. Benzenesulphonyl-protected fluorescein

4.67 is used to measure superoxide concentrations in biological systems, such as human Jurkat T cells.²⁶⁸ Deprotection of the sulphonyl groups occurs *via* a non-redox mechanism through nucleophilic substitution by superoxide. The main advantage of this probe is the fact that protected fluorescein **4.67** is not fluorescent, providing the opportunity to study living systems through fluorescence-based assays. To determine whether H₂O contributes to the formation of ROS in the copper flow reactor, protected fluorescein **4.67** was pumped through the system at 37 °C for 30 min using both MeCN and a 7/3 MeCN/H₂O mixture (Table 4.2). The reaction mixtures were then analysed directly by RP-HPLC. Only protected fluorescein **4.67** was observed when the reaction was performed in MeCN (Entry 1), while 64% of deprotected fluorescein **4.68** was obtained with the MeCN/H₂O mixture (Entry 2). Performing the reaction in the presence of one equivalent of sodium 4,5-dihydroxybenzene-1,3-disulfonate **4.69** (tiron),²⁶⁹ which scavenges free radicals such as superoxide, in 7/3 MeCN/H₂O afforded only the protected fluorescein **4.67** after 30 min.

Table 4.2. Deprotection of Fluorescein **4.67** using a copper flow reactor.

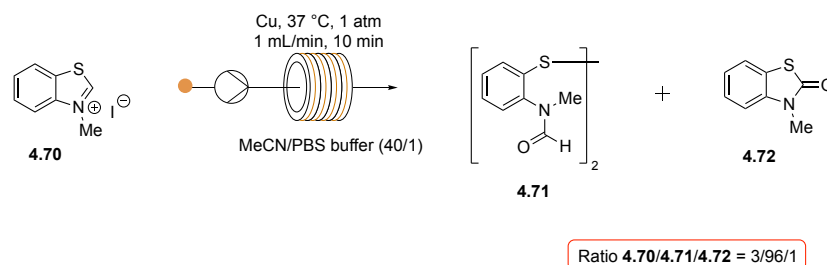


Entry	Solvent	ROS Inhibitor	Conversion (%) ^[a]
1	MeCN		0
2	MeCN/H ₂ O (7/3)		64
3	MeCN/H ₂ O (7/3)	4.69 (1 equiv)	0

^[a] Conversion calculated by peak area using RP-HPLC.

ROS in the flow system were also measurable using benzothiazolium iodide **4.70** (Scheme 4.17). Ohsawa *et al.* reported the selective oxidation of 3-methylthiazolium derivatives, such as **4.70**, with superoxide allowing the formation of both **4.71** and **4.72**.²⁷⁰ A solution of **4.70** in a 40/1 MeCN/PBS buffer (pH = 7.5) mixture was pumped through the copper flow reactor at 1 mL/min at 37 °C for 10 min. RP-HPLC analysis of the reaction mixture indicated 96% conversion of **4.70** to the oxidised product **4.71**, substantiating the presence of ROS in the flow system. Finally, histidine, known for its instability toward ROS, was dissolved in a 1/1 MeCN/H₂O mixture and flowed through the system at room temperature for 10 min. RP-HPLC analysis of the resulting mixture showed complete degradation of histidine. These data support the hypothesis that ROS are produced when H₂O is introduced into our flow platform. The requirement of water for performing CuAAC reactions using a copper flow reactor could

therefore be explained by ROS reactions with the Cu surface generating Cu(I) active species via *in-situ* Cu(I)/Cu(II) disproportionation.

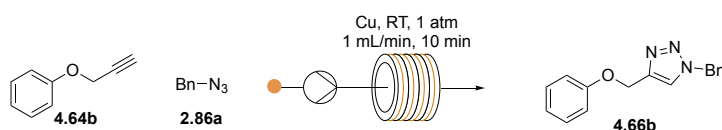


Scheme 4.17. Oxidation of 3-methylbenzothiazolium iodide **4.70** using a copper flow reactor. Conversion calculated by RP-HPLC.

4.5.2.4 Effect of Organic Solvent on Triazole Formation and Copper Leaching

To investigate the effect of organic solvent on the efficiency triazole formation, alkyne **4.64b** and azide **2.86a** were pumped through a copper flow reactor at 1 mL/min at room temperature and atmospheric pressure using different solvent systems (Table 4.3).²¹⁵

Table 4.3. Effect of organic solvent on Cu leaching and triazole **4.66b** formation.



Entry	Solvent	Yield (%) ^[a]	[Cu] (ppm)
1	MeCN	0	6.92
2	MeCN/H ₂ O (5/1)	90	40.9
3	MeOH	0	7.69
4	MeOH/H ₂ O (5/1)	13	1.84
5	DMF	0	8.17
6	DMF/H ₂ O (5/1)	30	9.24
7	DCM	7	1.2

^[a] Isolated yields.²¹⁵

Performing the reaction without H₂O at room temperature recovered only starting materials when MeCN, MeOH and DMF were used as solvents (Entry 1, Entry 3 and Entry 5, respectively) and was low yielding (7%) when DCM was used (Entry 7). The addition of H₂O to the solvent mixtures resulted in the formation of the expected product **4.66b**. However, low yields were obtained when 5/1 MeOH/H₂O or 5/1 DMF/H₂O were used (13% (Entry 4) and 30% (Entry 6), respectively). MeCN/H₂O was the best solvent system for the reaction, affording triazole **4.66b** in 90% yield. ICP-MS analyses of the reaction mixtures revealed

higher copper concentrations when MeCN/H₂O was used for the reaction. The superior reaction efficiency and higher copper concentration observed with this solvent system could be explained by a higher corrosion of the copper tubing, increasing the rate of Cu disproportionation.²⁶⁰

4.5.2.5 Effect of Flow Rate on Triazole Formation

As illustrated previously, the higher throughput offered by continuous flow technology represents one of the main benefits of this process, particularly for industrial purposes. To measure the maximum amount of triazole produced on our platform, a flow rate study was performed using alkynes **4.64a-c** and non-chelating azide **2.86a** (Figure 4.7) or chelating azide **2.86f** (Figure 4.8).²¹⁵

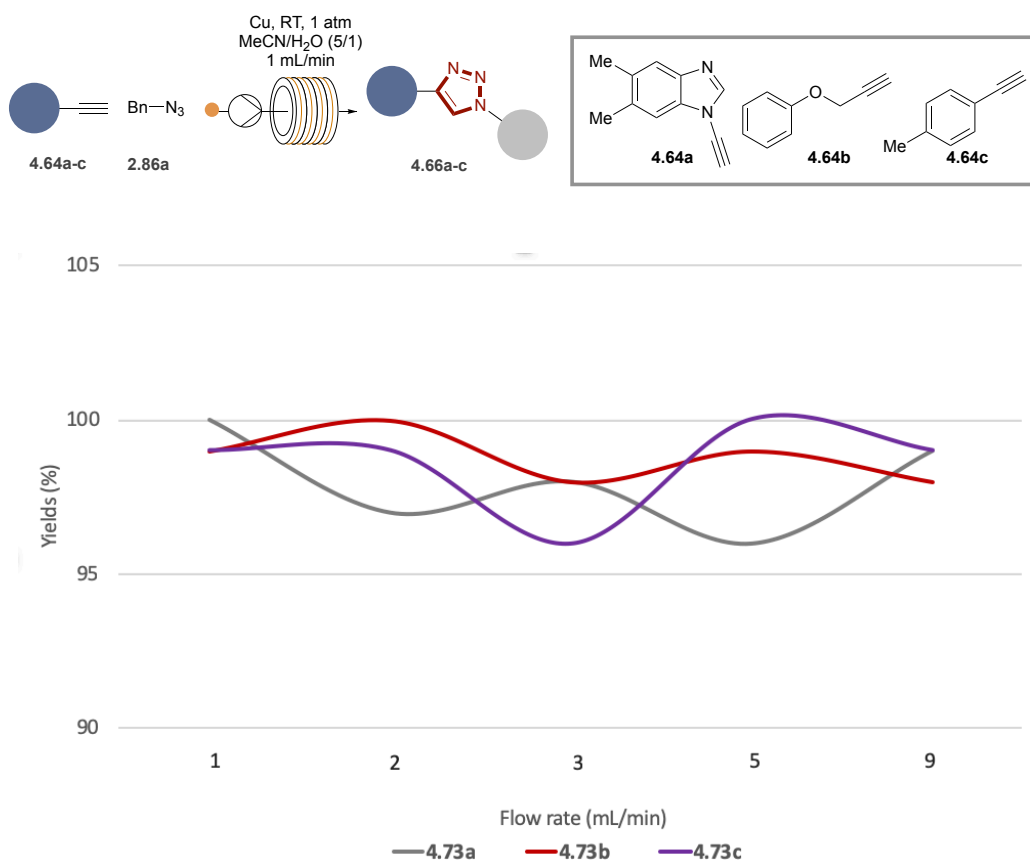


Figure 4.7. Flow rate vs efficiency of CuAAC reaction between alkynes **4.64a-c** and non-chelating azide **2.86a**. Isolated yields.²¹⁵

Reactions were performed on a 0.2 M scale using 5/1 MeCN/H₂O as the solvent. Increasing the flow rate from 1 mL/min to 3 mL/min did not decrease the efficiency of CuAAC reactions

when a non-chelating azide was used, such as benzyl azide **2.86a** (Figure 4.7). However, increasing the flow rate to 5 mL/min decreased the efficiency for both alkynes **4.64a** and **4.64c**. Performing the ligation at 3 mL/min would therefore allow the formation of approximately 1.1 kg of triazole **4.66a**, 0.98 kg of triazole **4.66b** and 0.99 kg of triazole **4.66c** after 1 h. Repeating these experiments using a chelating azide, such as **2.86f**, dramatically increased the efficiency of the reaction, affording high yields for alkynes **4.64a-c**, even when reactions were performed at 9 mL/min (Figure 4.8).²¹⁵ Performing the ligation at 9 mL/min would allow the formation of approximately 3.6 kg of triazole **4.73a**, 3.0 kg of triazole **4.73b** and 2.9 kg of triazole **4.73c** after 1 h. These results show that the increased reactivity of chelating azides observed in batch (see Chapter 2) is replicated in flow systems.

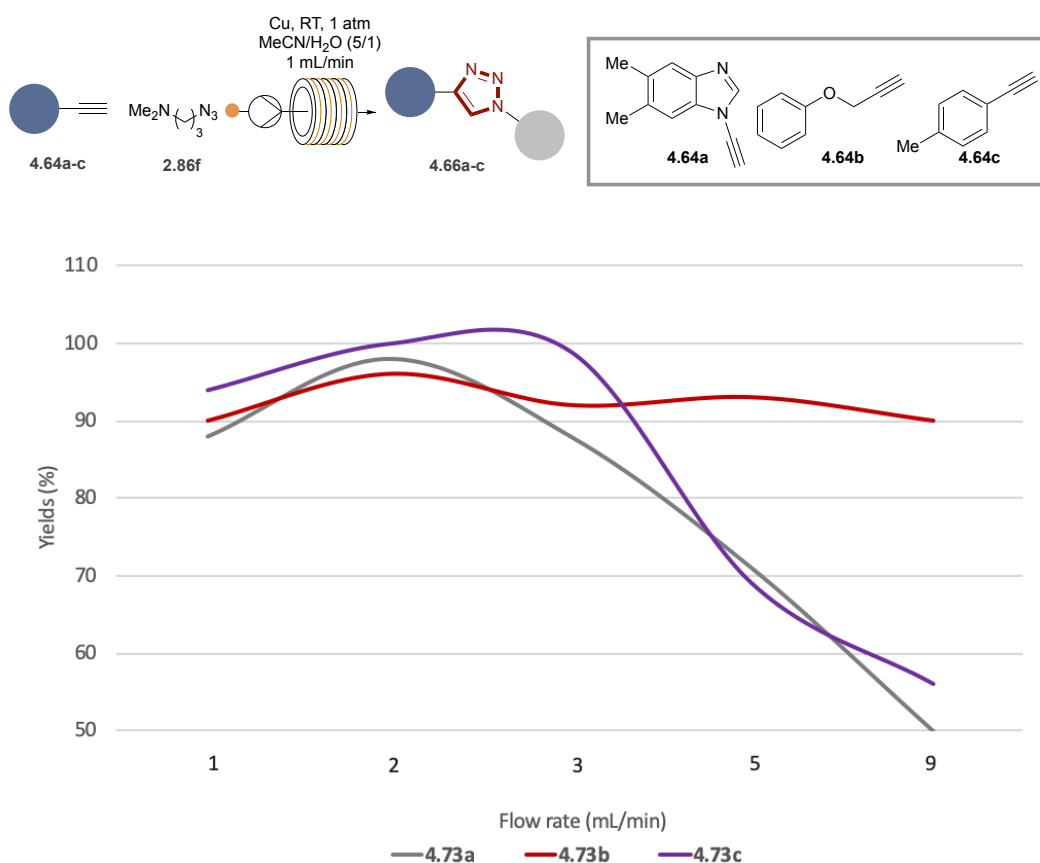
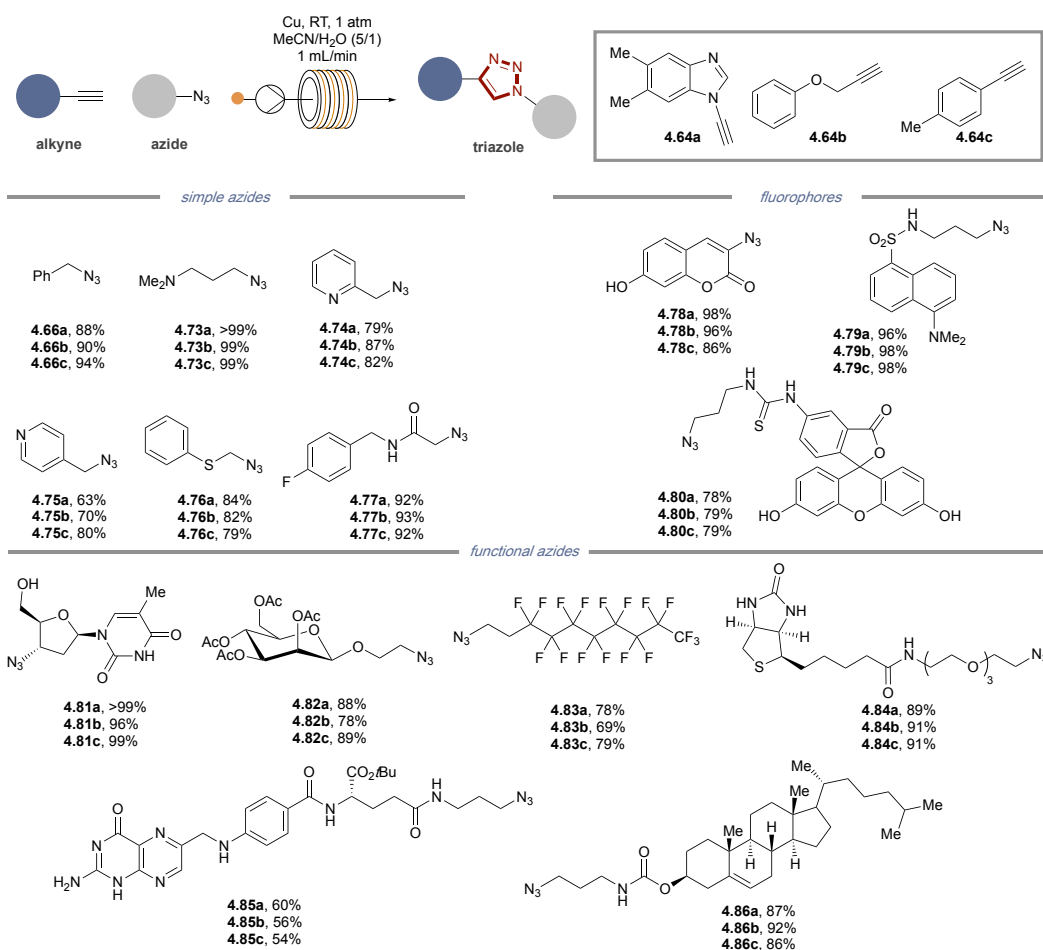


Figure 4.8. Flow rate vs efficiency of CuAAC reaction between alkynes **4.64a-c** and chelating azide **2.86f**. Isolated yields.²¹⁵

4.5.2.6 Substrate Scope of Triazole Formation using Optimized CuAAC Flow Conditions

The scope of our flow platform for CuAAC ligations was both broad and reproducible (Scheme 4.18).²¹⁵ Using three different alkynes **4.64a-c**, a variety of triazole products derived

from simple azides, azido fluorophores and azides possessing functionalities for downstream applications were all isolated in high yields after only a single pass through the Cu reactor.

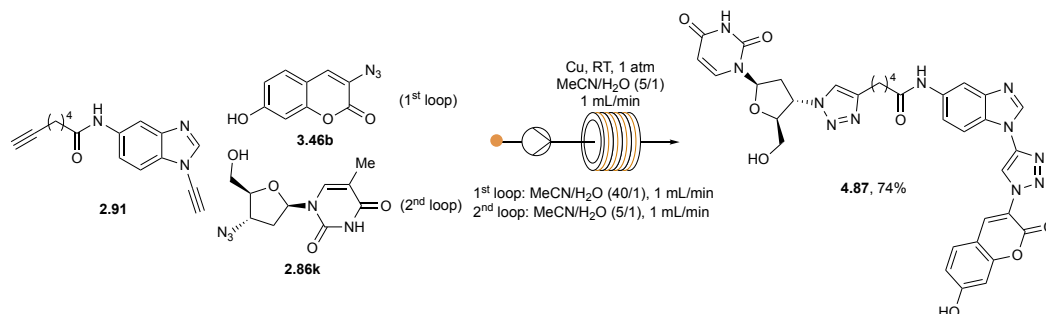


Scheme 4.18. Substrate scope of CuAAC flow process using alkynes **4.64a-c**. *Isolated yields.*²¹⁵

4.5.2.7 Chemoselective CuAAC Ligation in Flow

The compatibility of our flow platform with regards to established CuAAC chemoselectivity profiles¹⁷¹ was examined (Scheme 4.19).²¹⁵ Optimisation of the reaction using our flow platform has revealed that decreasing H₂O content in the eluent resulted in lower CuAAC efficiency. We surmised that we could achieve chemoselective CuAAC ligation by taking advantage of this feature. Diyne **2.91**, which contains a more reactive aromatic ynamine site and a less reactive aliphatic alkyne site, underwent chemoselective ligation with coumarin azide **3.46b** at its ynamine site using a 40/1 MeCN/H₂O mixture, followed by ligation of AZT azide **2.86k** at its alkyne site using a 5/1 MeCN/H₂O mixture. Complete chemoselectivity was

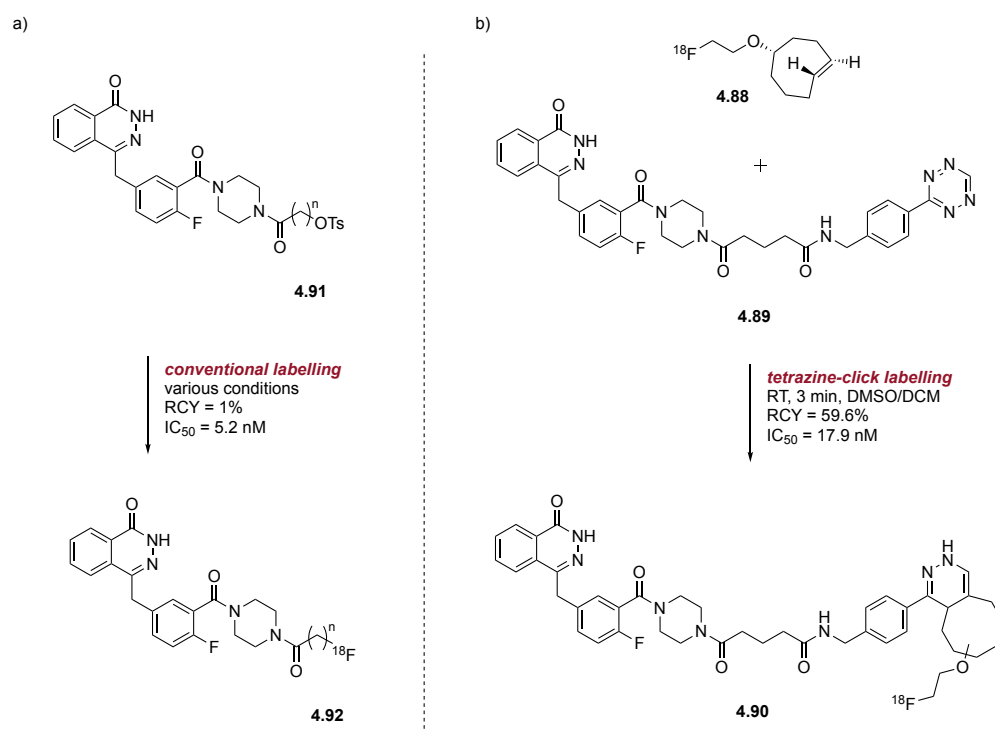
observed. This demonstrated that the established reactivity profiles are replicated in our flow platform with enhanced overall reaction kinetics even at very low [Cu].



Scheme 4.19. Chemoselective CuAAC ligation using a copper flow reactor. *Isolated yields.*²¹⁵

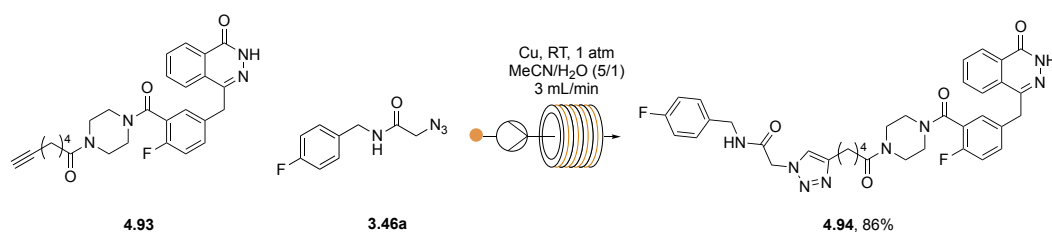
4.5.3 Developing a Flow Platform for Mild, Efficient Synthesis of Biomedical Imaging Markers

The development of new chemical strategies for radiolabelling biologically active molecules has been extensively pursued due to the increasing applications of positron emission tomography (PET) in nuclear medicine.¹⁸⁹ To be viable for PET imaging, the incorporation of radioisotopes, such as fluorine-18 (half-life 109.8 min), needs to be fast, regioselective, proceed under physiological conditions and in high yields. A comparison between conventional and tetrazine-click labelling strategies of Olaparib derivatives (Scheme 4.20), such as **4.89** and **4.91**,¹⁴³ was used as a paradigm for the development of this flow platform. Olaparib (AstraZeneca) is an FDA-approved, targeted therapy for breast, ovarian and prostate cancer which functions by inhibiting poly (ADP-ribose) polymerase (PARP), an enzyme involved in DNA repair.²⁷¹ In 2011, Weissleder *et al.* reported the 3 min synthesis of ¹⁸F-labelled Olaparib **4.90** *via* tetrazine-click labelling, providing high radiochemical yield (RCY, 60%) compared to the direct labelling of tosylate **4.91**, affording product **4.92** with an RCY of 1% after 6 h (Scheme 4.20).¹⁴³ However, tetrazine chemistry requires RP-HPLC purification of the final product to separate the two regioisomers formed during the reaction, decreasing the efficiency of this system. Moreover, the introduction of a large hydrophobic group to Olaparib, such as a cyclooctene, dramatically decreases the affinity of **4.90** for PARP1 as compared to **4.92** (IC₅₀ 17.9 nM and 5.2 nM, respectively).



Scheme 4.20. Comparison between a) conventional and b) tetrazine-click labelling strategies of a PARP1 inhibitor.¹⁴³

Building on this work, we demonstrated the utility of our flow platform for the synthesis of PET probes through the CuAAC ligation of Olaparib alkyne derivative **4.93** and a mimic of the commonly used ¹⁸F-azido probe²⁷² **3.46a** (scheme 4.21).²¹⁵ Solutions of **4.93** and **3.46a** in 5/1 MeCN/H₂O were pumped through the copper flow reactor at 3 mL/min at room temperature. After 3 min of reaction, triazole **4.94** was obtained in 86% yield without the need for purification. More importantly, ICP-MS analysis of the eluent measured only 6.21 ppm of copper, far below permissible copper concentrations (15 ppm), demonstrating the capacity of our flow platform to synthesise biomedical imaging markers.



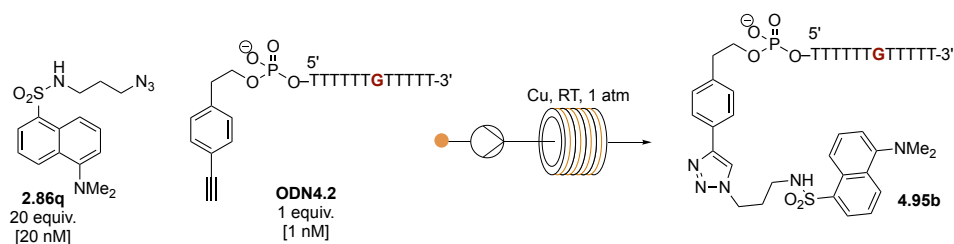
Scheme 4.21. Continuous flow CuAAC reaction between Olaparib derivative **4.93** and PET probe mimic **3.46a**. Isolated yields.²¹⁵

4.5.4 Developing a Flow Platform for Mild, Efficient, Degradation-Free Bioconjugation of Peptides and Oligodeoxyribonucleotides

4.5.4.1 Developing a Flow Platform for CuAAC Ligations of Oligodeoxyribonucleotides

While CuAAC has proven to be an efficient strategy for the ligation of biomolecules, such as oligodeoxyribonucleotides (ODNs), the requirement for (super)stoichiometric amounts of copper remains a severe limitation. The higher efficiency observed for flow processes, due to enhanced mass transfer, added to the use of a copper tubing should dramatically increase reaction kinetics and therefore decrease exposure of ODNs to copper, reducing potential degradation and damage. To test this hypothesis, **ODN4.2**, containing only one oxidation sensitive residue, and azido fluorophore **2.86q** were reacted using our flow platform (Table 4.4).²¹⁵ CuAAC reactions were performed in a commercial chemical flow reactor (easy-Scholar, Vapourtec) equipped with a copper reactor (Vapourtec, d = 1 mm, V = 2 mL). Alkyne and azide starting materials were dissolved in 100 μ L of solvent before being pumped through the copper reactor at room temperature (25 $^{\circ}$ C), unless stated otherwise.

Table 4.4. Optimisation of flow CuAAC reaction using **ODN4.2**.

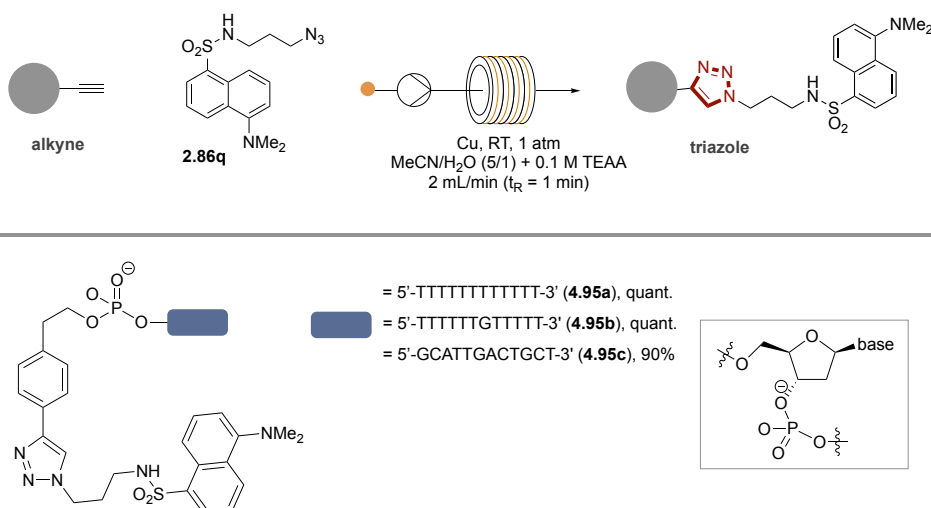


Entry	Solvent	Flow Rate (mL/min)	Yield (%)
1	H ₂ O	0.2 (t _R = 10 min)	0
2	H ₂ O	1 (t _R = 2 min)	7
3	MeOH/H ₂ O (5/1)	0.2 (t _R = 10 min)	4
4	MeOH/H ₂ O (5/1)	1 (t _R = 2 min)	21
5	MeOH/H ₂ O (5/1)	2 (t _R = 1 min)	59
6	MeOH/H ₂ O (5/1)	2 (3 cycles, t _R = 3 min)	36
7	MeOH/H ₂ O (5/1) + 0.1 M TEAA	2 (t _R = 1 min)	100

Yields determined by RP-HPLC peak integration relative to the ODN starting material.²¹⁵

Initial attempts to achieve the reaction in H₂O resulted in complete degradation of **ODN4.2** (Entries 1-2). Switching the solvent to 5/1 MeCN/H₂O generated the expected product **4.95b**; however, extensive oligonucleotide degradation was still observed. Increasing the flow rate, and therefore decreasing exposure of **ODN4.2** to the copper reactor, dramatically improved reaction yields (4% at 0.2 mL/min and 59% at 2 mL/min). Increasing the number of passes

through the reactor from one to three at 2 mL/min resulted in lower yield (36%, Entry 6). Triethylammonium acetate (TEAA) buffer is commonly used for RP-HPLC purification and analysis of ODNs, functioning as an ion pair to the negatively-charged ODN phosphate backbone to allow for increased resolution on hydrophobic C18 silica.²⁷³ TEAA also has the ability to function as a Cu chelator, competing with the purine and pyrimidine bases of ODNs, leading to decreased degradation of the ligated product. To investigate whether a reduction in ODN-Cu chelation would result in increased yield of the CuAAC product, 0.1 M TEAA was added to the solvent mixture, affording triazole **4.95b** in quantitative yield after 1 min of reaction (Entry 7). In comparison, performing this reaction in batch using Cu(OTf)₂ (10 equiv), THPTA (20 equiv) and NaAsc (20 equiv) required 24 h to reach completion. Using the optimised flow conditions, triazoles **4.95a-c** were obtained in high yields (90% to quantitative) after only 1 min of reaction and without the need for purification (Scheme 4.22).



Scheme 4.22. CuAAC ligations of representative ODNs using optimised conditions in a copper flow reactor. Yields determined by RP-HPLC peak integration relative to ODN starting material.²¹⁵

4.5.4.2 Developing a Flow Platform for CuAAC Ligations of Peptides

CuAAC methodology has been extensively used for peptide bioconjugation. Since the triazole linkage, formed during the ligation, is similar in size and polarity to the standard peptide linkage, there is minimal perturbation to the conjugate's biological function.²⁷⁴ However, as with ODN ligations, super-stoichiometric copper (10 to 100 equiv) and long reaction times (24 to 48 h) are required due to the numerous Cu-chelating sites present in peptides.²⁰ Moreover, Cu-mediated formation of ROS leads to the oxidative degradation of peptides, which is especially pronounced for cysteine, methionine, histidine and tyrosine containing

peptides.²⁷⁵ The remarkable results obtained for ODN ligation with our flow platform encouraged us to develop an assay for fast, degradation-free bioconjugation of peptides.²¹⁵ A peptide fragment of the ApoE protein was chosen as a model for this study (Figure 4.9). This peptide is arginine- and lysine-rich and therefore has strong Cu-chelating character. Its arginine residues make it a well-known cell penetrating peptide (CPP), commonly used as a delivery vehicle across the blood brain barrier (BBB).²⁷⁶ This peptide was modified at the C-terminus with a propargylglycine to allow for CuAAC ligations. Additionally, to investigate degradation during flow CuAAC reactions, the ApoE peptide core was modified at the N-terminus with oxidation-sensitive residues (Figure 4.9).

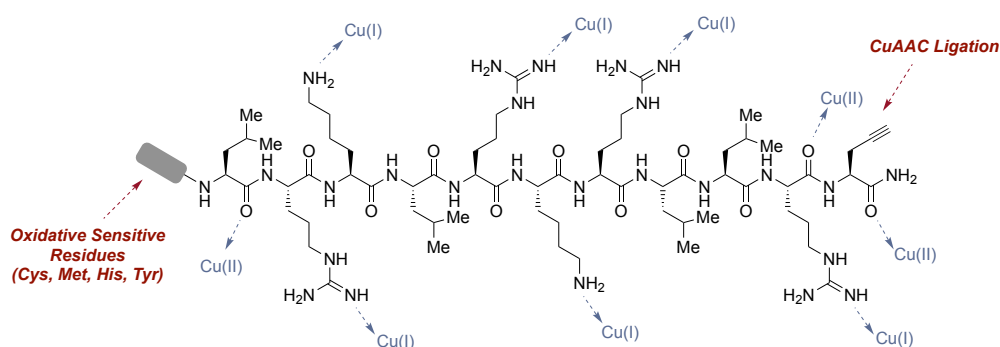
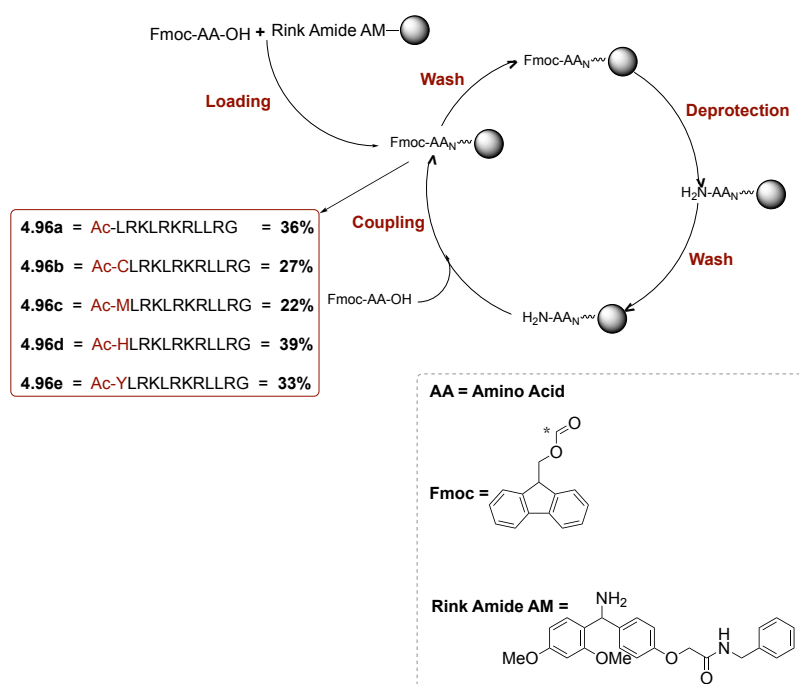


Figure 4.9. ApoE peptide used for the development of a flow CuAAC platform for peptide bioconjugation.²¹⁵

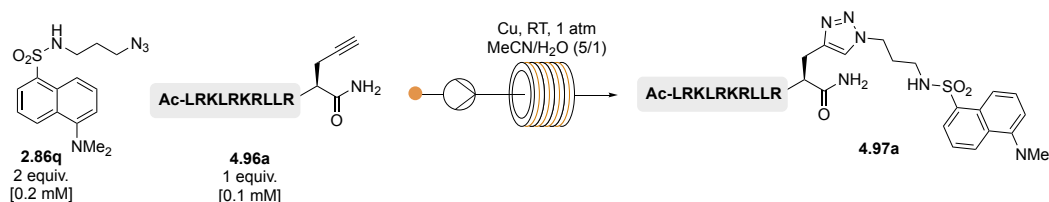
Peptides **4.96a-e** were prepared using standard Fmoc solid-phase peptide synthesis on a rink amide resin (Scheme 4.23). Peptides **4.96a-e** were obtained in 22-39% yields after RP-HPLC purification.



Scheme 4.23. Fmoc solid-phase peptide synthesis. *Isolated yields.*²¹⁵

CuAAC reactions were performed in a commercial chemical flow reactor (easy-Scholar, Vapourtec) equipped with a copper reactor (Vapourtec, $d = 1$ mm, $V = 2$ mL). Alkyne and azide starting materials were solubilised in 100 μ L of solvent before being pumped through the copper tube at room temperature (25 $^{\circ}$ C), unless stated otherwise. RP-HPLC analysis was used to determine the optimal flow rate for the ligation of peptide **4.96a** and dansyl azide **2.86q** in a copper flow reactor (Table 4.5).²¹⁵

Table 4.5. Optimisation of the flow rate for CuAAC reaction using peptide **4.96a**.



Entry	Flow Rate (mL/min)	Conversion (%)
1	0.2 ($t_R = 10$ min)	69
2	0.1 ($t_R = 20$ min)	79
3	1 ($t_R = 2$ min)	68
4	1 (2 cycles, $t_R = 4$ min)	96
5	1 (3 cycles, $t_R = 6$ min)	97
6	1 (4 cycles, $t_R = 8$ min)	100

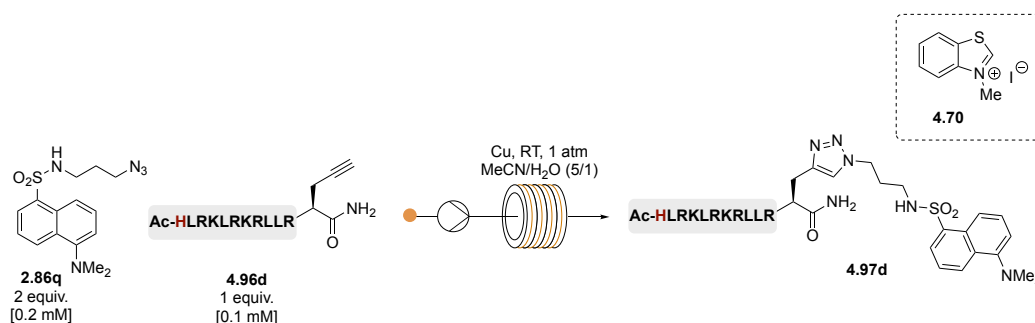
7	2 ($t_R = 1$ min)	47
8	2 (2 cycles, $t_R = 2$ min)	87
9	2 (3 cycles, $t_R = 3$ min)	84
10	2 (4 cycles, $t_R = 4$ min)	92

Conversion determined by RP-HPLC peak integration relative to peptide starting material.²¹⁵

A flow rate of 0.2 mL/min ($t_R = 10$ min) provided triazole **4.97a** in 69% yield; unfortunately, HPLC chromatography indicated the presence of multiple compounds, suggesting degradation of the starting materials and/or product (Entry 1). Decreasing the flow rate to 0.1 mL/min ($t_R = 20$ min) increased both yield and degradation (Entry 2). Increasing the flow rate to 1 mL/min ($t_R = 2$ min) afforded a similar yield (68%) but without the accompanying degradation (Entry 3). These results suggest that the CuAAC reaction occurs faster than peptide **4.96a** degradation and that reducing the time of contact between the peptide and the copper surface of the reactor would reduce potential chelation/degradation. To obtain complete conversion of peptide **4.96a**, the reaction mixture was pumped at 1 mL/min through the reactor several times and analysed by RP-HPLC after each pass (Entry 3-6). Full conversion of peptide **4.96a** to triazole **4.97a** was achieved after 4 passes, representing a total residence time in the reactor of 8 min (Entry 6). Repeating these experiments at 2 mL/min afforded 92% yield of triazole **4.97a** after 4 min in the reactor (Entry 10). In comparison, performing this reaction in batch using Cu(OTf)₂ (20 equiv), THPTA (40 equiv) and NaAsc (40 equiv) required 16 h to reach completion.

Degradation of oxidation-sensitive residues was then explored using the histidine-containing peptide **4.96d** (Table 4.6).

Table 4.6. Optimisation of the flow CuAAC reaction using peptide **4.96d**.

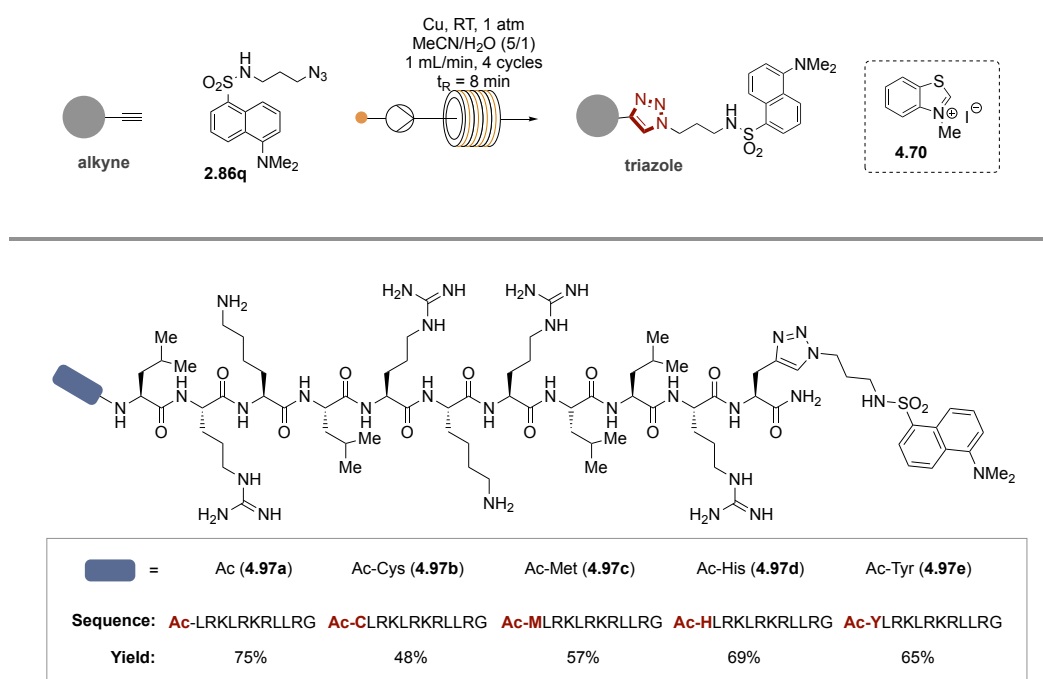


Entry	Additives	Flow Rate (mL/min)	Conversion (%)
1		0.2 ($t_R = 10$ min)	23
2		1 (4 cycles, $t_R = 8$ min)	77
3	4.70 (2 equiv)	1 (4 cycles, $t_R = 8$ min)	90

Conversion determined by RP-HPLC peak integration relative to peptide starting material.²¹⁵

Reaction between peptide **4.96d** and dansyl azide **2.86q** at 0.2 mL/min afforded only 23% conversion to triazole **4.97d** with several degradation products observed by RP-HPLC (Entry 1). Using the previously optimised conditions (1 mL/min, 4 cycles) increased the conversion of **4.96d** to triazole **4.97d** to 77%; however, degradation products were still detected by RP-HPLC (Entry 2). Several ROS scavengers, such as tiron **4.69** and DMSO, were employed to suppress the oxidative damage of peptide **4.96d**; unfortunately, this resulted in further degradation. However, addition of benzothiazolium iodide **4.70** (2 equiv), previously used as a superoxide probe (Scheme 4.17), resulted in 90% conversion of peptide **4.96d** to triazole **4.97d** after 8 min of reaction with no detectable degradation.

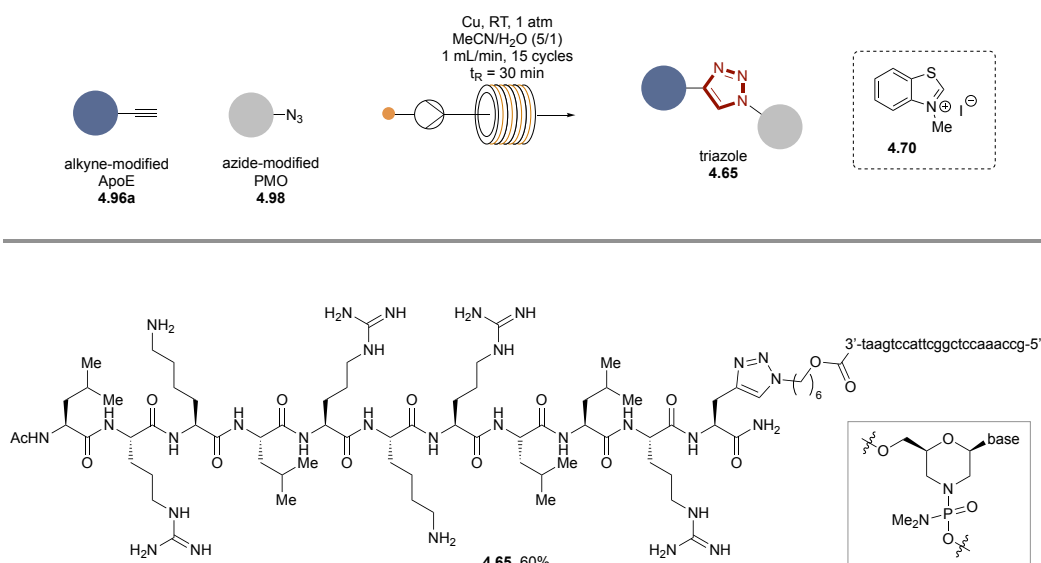
Applying these conditions to the ligation of peptides **4.96a-d** with azido fluorophore **2.86q** afforded triazoles **4.97a-d** in 48-75% yields after RP-HPLC purification (Scheme 4.24). No degradation was observed. Importantly, ICP-MS analysis of triazole **4.97d** measured only 7.13 ppm of copper in the final product. Triazole **4.97e** and the side-product resulting from the oxidation of **4.70** (Scheme 4.17) were unfortunately not separable by RP-HPLC. Omission of the ROS scavenger allowed isolation of triazole **4.97e** in 65% yield; interestingly, no degradation product was observed.



Scheme 4.24. CuAAC ligations of representative peptides using optimised conditions in a copper flow reactor. Isolated yields.²¹⁵

4.5.4.3 Developing a Flow Platform for the Fast, Mild, Degradation-Free Formation of a Peptide-Phosphoramidate Oligonucleotide Conjugate

The synthesis of the ApoE-PMO conjugate **4.65** was performed to illustrate the ability of our flow platform to achieve fast and efficient bioconjugation. Phosphorodiamidate morpholino oligomers (PMOs) are nucleic acid analogues, in which the sugar backbone is replaced by a morpholino ring and the phosphodiester linkage substituted with a phosphorodiamidate (Scheme 4.25). The improved stability of PMOs towards nuclease digestion due to these modifications has offered promise for antisense gene therapy.^{277,278} Owing to their neutral properties, PMOs have poor cellular uptake; however, this can be ameliorated by conjugation to a cell penetrating peptide (CPP). The bioconjugate triazole **4.65** was prepared from precursors derived from a PMO azide **4.98**, purchased at Gene Tools, with known *in vivo* efficacy as a splice-switching oligonucleotide for the treatment of Duchenne Muscular Dystrophy (DMD) and a peptide fragment **4.96a** of the ApoE protein (Scheme 4.25).^{279,280} Using our previously optimised flow conditions, the ApoE-PMO bioconjugate **4.65** was formed in 60% yield after 15 passes (1 mL/min; total $t_R = 30$ min). When performed under equivalent batch conditions, no reaction was observed after 24 h and only 26% yield of **4.65** was obtained after 48 h using 100 equiv Cu.



Scheme 4.25. Bioconjugation of ApoE peptide **4.96a** and PMO azide **4.98**. Isolated yields.²¹⁵

4.6 Summary

This chapter has described a rapid and mild continuous flow platform for CuAAC ligation. Reactions proceed under mild conditions (room temperature, ambient pressure) and without the need for additives. The efficiency of this platform was demonstrated for the ligation of small molecules (10 min) and the ligation of a PARP1 inhibitor to a PET probe mimic (3 min). Furthermore, we have shown that this platform could be used for the fast conjugation of biomolecules, such as oligonucleotides (1 min) and peptides (8 min), without degradation of even the most oxidation-sensitive substrates. Finally, the utility of this platform has been demonstrated for the mild, fast and degradation-free bioconjugation of an azide-modified PMO with an alkyne-modified CPP (30 min). This work therefore presents the opportunity to perform fast and efficient bioconjugation under conditions that are favourable to biomolecules.

4.7 Experimental

4.7.1 Reagents and Solvents

All reagents were obtained from commercial sources (Fisher, Fluorochem, Sigma-Aldrich) and used without further purification unless otherwise stated. All solvents were HPLC grade and were used without further purification, unless otherwise stated.

4.7.2 Analysis of Products

4.7.2.1 NMR Spectroscopy

NMR spectroscopy was carried out using either a Bruker 400 UltraShield™ B-ACS 60 spectrometer or Bruker DRX 500. All chemical shifts (δ) were referenced to the deuterium lock and are reported in parts per million (ppm). Coupling constants are quoted in hertz (Hz). Abbreviations for splitting patterns are s (singlet), br. s (broad singlet), d (doublet), t (triplet), q (quartet), app. quint (apparent quintuplet), app. sept (apparent septet) and m (multiplet). All NMR data was processed using TopSpin 3.2 software. Proton and carbon chemical shifts were assigned using proton (^1H), carbon (^{13}C), Heteronuclear Single Quantum Coherence (HSQC), Heteronuclear Multiple-Bond Correlation Spectroscopy (HMBC) and Correlation Spectroscopy (COSY).

4.7.2.2 *Liquid Chromatography-Mass Spectrometry (LC-MS) and High-Performance Liquid Chromatography (HPLC)*

LC-MS was carried out on an Agilent HPLC instrument in conjunction with an Agilent Quadrupole mass detector. Electrospray ionization (ESI) was used in all cases. RP-HPLC was carried out on a Dionex Ultimate 3000 series instrument or a Shimadzu Prominence HPLC (see Appendix for method and column parameters).

4.7.2.3 *Infra-Red (IR) Spectroscopy*

IR data was collected on an Agilent spectrometer and the data processed using Spectrum One software. Only major absorbances are reported (> 50 %).

4.7.2.4 *ICP-MS Results*

The instrument was operated in spectrum acquisition mode and three replicate runs per sample were obtained. The masses analysed for Cu were ^{63}Cu and ^{65}Cu . ^{103}Rh was used as an internal standard and added at a concentration of 20 $\mu\text{g/L}$. Each mass was analysed in full quantitation mode (three points per unit mass) and in standard 'no gas' mode. A series of standards from 1-1000 $\mu\text{g/L}$ Cu were prepared using single element 1000 mg/L Cu (Fischer Scientific) diluted with distilled water and MeCN to match the samples. An external reference standard CRM SLRS-4 (NRCC, Canada) was diluted 2-fold to check for accuracy of the standard graph.

The samples were collected directly after a single pass through the copper flow reactor (1 mL/min) and diluted to reduce the concentration of MeCN in the samples to 1% v/v. Samples without MeCN were spiked with MeCN to keep all samples/standards within the same matrix to minimise any changes in ionization, *etc.*

Parameters for No gas mode:

Ion Lenses:

Extract1: 0 V

Extract 2: -131 V

Omega Bias-ce: -20 V

Omega Lens-ce: 0 V

Cell Entrance: -30 V

QP focus: 3 V

Cell Exit: -34 V

Quadrupole Parameters:

OctP RF: 180 V

OctP Bias: -6 V

QP Bias: -3 V

Table 4.7. ICP-MS analysis of different solvent eluents from a used (~ 300 reactions) vs. a new (0 reactions) reactor.

Ratio MeCN/H ₂ O	[Cu] (ppm) of Used Reactor	[Cu] (ppm) of New Reactor
100/0	0.353	0.790
99/1	0.206	0.240
98/1	0.510	0.387
95/1	1.69	1.04
90/1	2.88	2.23
80/1	2.13	1.65
60/1	2.98	2.07
40/1	7.05	3.79
5/1	12.3	6.30
1/1	19.2	8.06
1/5	10.6	4.50
1/40	2.47	3.01
0/100	0.32	1.16

Table 4.8. ICP-MS analysis of biomolecules after CuAAC reactions in flow.

Product	[Cu] (ppm)
4.94	6.21
ODN6 (4.96c)	8.96
P9 (4.97d)	7.13
4.65	7.42

4.7.3 General Procedures

General Procedure A: Synthesis of triazoles under CuAAC flow conditions

Alkyne (0.2 mmol) and azide (0.2 mmol) were dissolved in 5/1 MeCN/H₂O (10 mL). The CuAAC reactions were carried out in a commercial chemical flow reactor equipped with a 10 mL copper reactor (easy-Scholar from Vapourtec). The reaction mixture was flowed through a copper tube (diameter = 1 mm, volume = 10 mL, surface area = 400 cm²) at a flow rate of 1 mL/min at rt (25 °C, t_R = 10 min). The reaction mixture was then collected and concentrated *in vacuo*.

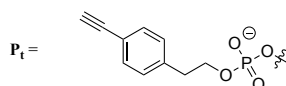
General Procedure B: Solid phase synthesis of ODNs

ODNs were synthesised using phosphoramidite-based solid phase synthesis protocols on an Applied Biosystems 392 DNA/RNA synthesizer. Phosphoramidites and controlled pore glass (CPG) supports were loaded with standard nucleotides purchased from LINK Technologies Ltd (Bellshill, UK). For the synthesis of ODNs containing the modified alkyne phosphoramidite **3.42** (see Chapter 3) installed on the 5' end, longer coupling times of 8 minutes were used. TIPS deprotection was performed using a solution of 1 M TBAF in THF (50 μ L) in MeCN (1.95 mL). The mixture was repeatedly passed over the column containing the CPG support for 3 min. The CPG support was washed with MeCN (3 \times 5 mL) and dried with air. Ammonia (DNA grade, 1.5 mL/mmol) was added and the suspension was shaken for 16 hours at room temperature. The supernatant was removed, and the CPG support was then washed with water (2 \times 1.5 mL/mmol). The combined aqueous phase was lyophilised and purified by RP-HPLC on a Dionex UltiMate 3000 HPLC using a preparative column (Phenomenex Clarity 5 μ M Oligo-RP, 250 \times 10 mm) at a flow rate of 3 mL/min, gradient 10–50% 0.1 M triethylammonium acetate (TEAA) in MeCN over 32 min or 10–40% 0.1 M TEAA in MeCN over 22 min. Purity of the resultant products was assessed with a Shimadzu Prominence HPLC using an analytical column (Phenomenex Clarity 5 μ M Oligo-RP, 250 \times 4.6 mm) at a flow rate of 1 mL/min, gradient 10–50% 0.1 M TEAA in MeCN over 35 min. Yields were calculated by measuring the absorbance of the products using extinction coefficient values of 97800 L/(mol \times cm) for **ODN4.1**, 100400 L/(mol \times cm) for **ODN4.2** and 108700 L/(mol \times cm) for **ODN4.3**.

Table 4.9. ODNs prepared in this study.

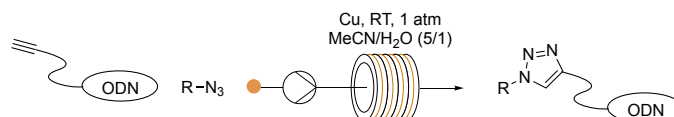
Product	Sequence	Yield (%) ^[a]
ODN4.1	5'-P _t TTT TTT TTT TTT-3'	16
ODN4.2	5'-P _t TTT TTT GTT TTT-3'	10
ODN4.3	5'-P _t GCA TTG ACT GCT-3'	26

^[a] Isolated yields after RP-HPLC purification.



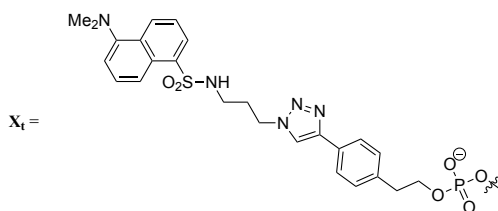
General Procedure C: CuAAC reactions using alkyne-modified ODNs

ODN4.1-3 (1 equiv) and azide (20 equiv) were dissolved in 0.1 M TEAA in 5/1 MeCN/H₂O (100 μL). The CuAAC reactions were carried out in a commercial chemical flow reactor equipped with a 2 mL copper reactor (easy-Scholar from Vapourtec). The reaction mixture was fed through the copper reactor (2 mL total volume) at a flow rate of 9 mL/min at rt (25 °C). The reaction mixture was collected following one cycle through the reactor and lyophilised. The purity of the triazole products **4.95a-c** was assessed using a Shimadzu Prominence HPLC on an analytical column (Phenomenex Clarity 5 μM Oligo-RP, 250 x 4.6 mm) at a flow rate of 1 mL/min, gradient 10–50% 0.1 M TEAA in MeCN over 35 min. Yields were calculated using the HPLC integrals ratio relative to the ODN starting materials.

Table 4.9. Experimental data for the synthesis of **4.95a-c**.

Product	Sequence	Yield (%) ^[a]
ODN4.4 (4.95a)	5'-X _t TTT TTT TTT TTT-3'	Quant
ODN4.5 (4.95b)	5'-X _t TTT TTT GTT TTT-3'	Quant
ODN4.6 (4.95c)	5'-X _t GCA TTG ACT GCT-3'	91

^[a] RP-HPLC yields.



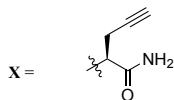
General Procedure D: Solid-phase peptide synthesis of **4.96a-e**

Solid-phase synthesis was performed on Rink amide resin (0.6–0.7 mmol/g, 100–200 mesh) (NovaBiochem) using a Protein Technologies Tribute automated synthesizer. Syntheses were performed from the C-terminus to the N-terminus using Fmoc-protected amino acids. Side chain functionalities were protected with a *t*-Bu group for Tyr, a Pbf group for Arg and a Boc group for Lys. The resin was swollen for 20 min in DCM. Fmoc deprotection was achieved using 20% piperidine in DMF (5 min). Each amino acid (5.0 equiv) was activated with HATU (4.5 equiv) and DIPEA (0.5 M in DMF) for 2 min (10 min for arginine and cysteine). The solution was then added to the resin, shaken for 20 min (2 h for arginine and cysteine), then washed with DMF. Double couplings were used for arginine and cysteine. Capping of **4.96a-e** was performed using a solution of 15% acetic anhydride in DMF. Deprotection, coupling, washing, and capping procedures were repeated until the final amino acid had been coupled to the peptide chain. The peptide was cleaved from the resin by shaking in a solution of TFA/phenol/H₂O/TIPS (90/5/2.5/2.5) for 2 h. The peptide was then collected by precipitating in cold Et₂O and centrifuged at 7000 rpm for 25 min (three times). Peptides **4.96a-e** were then purified by RP-HPLC on a Dionex UltiMate 3000 HPLC using a preparative column (Phenomenex C18, 150 × 21.2 mm) at a flow rate of 9 mL/min, gradient 5–100% MeCN/0.1% TFA over 95 min. Purity of the resultant products was assessed by analytical RP-HPLC (Phenomenex C18, 250 × 4.6 mm) at a flow rate of 1 mL/min, gradient 5–60% MeCN/0.1% TFA over 35 min.

Table 4.10. List of synthesised peptides **4.96a-e**, sequence and yields.

Product	Sequence	Yield (%) ^[a]
4.96a	Ac-LRKLKRLLRX	36
4.96b	Ac-CLRKLKRLLRX	27
4.96c	Ac-MLRKLKRLLRX	22
4.96d	Ac-HLRKLKRLLRX	39
4.96e	Ac-YLRKLKRLLRX	33

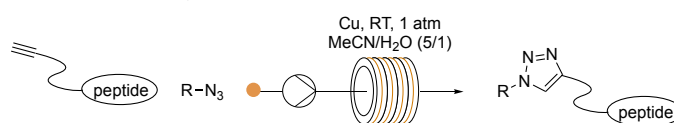
^[a] Isolated yields after RP-HPLC purification.

**General Procedure E:** CuAAC Reactions with Peptides

Alkyne **4.96a-e** (1 equiv), azide (2 equiv), and 3-methylbenzo[*d*]thiazol-3-ium **4.70** (2 equiv) were dissolved in 5/1 MeCN/H₂O (100 μL). The CuAAC reactions were carried out in a

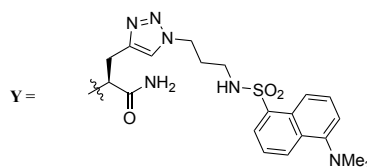
commercial chemical flow reactor equipped with a 2 mL copper reactor (easy-Scholar from Vapourtec). The reaction mixture was fed through the copper reactor (2 mL total volume) at a flow rate of 1 mL/min at rt (25 °C). The reaction mixture was collected after four cycles through the reactor, lyophilised, and purified by reverse phase HPLC on a Dionex UltiMate 3000 HPLC using a preparative column (Phenomenex C18, 150 × 21.2 mm) at a flow rate of 9 mL/min, gradient 5–100% MeCN/0.1% TFA over 95 min. Purity of the resultant products was assessed by analytical RP-HPLC (Phenomenex C18, 250 × 4.6 mm) at a flow rate of 1 mL/min, gradient 5–60% MeCN/0.1% TFA over 35 min.

Table 4.11. Experimental data for the synthesis of **4.97a-e**.



Product	Sequence	Isolated Yield (%) ^[a]
P6 (4.97a)	Ac-LRKLKRLRLRY	75
P7 (4.97b)	Ac-CLRKLKRLRLRY	48
P8 (4.97c)	Ac-MLRKLKRLRLRY	57
P9 (4.97d)	Ac-HLRKLKRLRLRY	69
P10 (4.97e)	Ac-YLRKLKRLRLRY	65

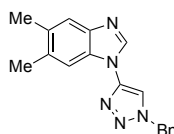
^[a] Isolated yields after RP-HPLC purification.



4.7.4 Synthetic procedures

4.7.4.1 Products from Scheme 4.18

4.66a: 1-(1-benzyl-1H-1,2,3-triazol-4-yl)-5,6-dimethyl-1H-benzo[d]imidazole¹⁷⁴

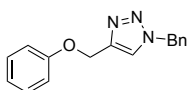


Prepared using General Procedure A. White amorphous solid (53 mg, 88%). Purification on silica gel using 7/3 PE/EtOAc.

¹H-NMR (CDCl₃, 400 MHz): δ 8.20 (s, 1H), 7.67 (s, 1H), 7.58 (s, 1H), 7.45–7.39 (m, 4H), 7.37–7.34 (m, 2H), 5.62 (s, 2H), 2.37 (s, 6H).

¹³C-NMR (CDCl₃, 100 MHz): δ 143.2, 142.4, 140.4, 134.0, 133.6, 132.3, 131.1, 129.5, 129.3, 128.3, 120.7, 113.5, 111.3, 55.2, 20.7, 20.3.

4.66b: 1-benzyl-4-(phenoxyethyl)-1*H*-1,2,3-triazole¹⁷⁹

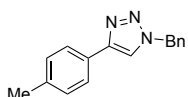


Prepared using General Procedure A. Colorless oil (48 mg, 90%). Purification on silica gel using 9/1 PE/EtOAc.

¹H-NMR (CDCl₃, 400 MHz): δ 7.52 (s, 1H), 7.38–7.35 (m, 3H), 7.28–7.26 (m, 4H), 6.98–6.94 (m, 3H), 5.53 (s, 2H), 5.19 (s, 2H).

¹³C-NMR (CDCl₃, 100 MHz): δ 158.3, 144.9, 134.6, 129.6, 129.3, 128.9, 128.3, 122.7, 121.4, 114.9, 62.2, 54.4.

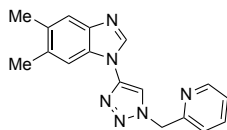
4.66c: 1-benzyl-4-(*p*-tolyl)-1*H*-1,2,3-triazole¹⁸⁰



Prepared using General Procedure A. Colorless oil (47 mg, 94%). Purification on silica gel using 9/1 PE/EtOAc.

¹H-NMR (CDCl₃, 400 MHz): δ 7.70–7.69 (m, 1H), 7.68–7.67 (s, 1H), 7.63 (s, 1H), 7.38–7.36 (m, 3H), 7.31–7.28 (m, 2H), 7.21–7.19 (m, 2H), 5.54 (s, 2H), 2.36 (s, 3H).

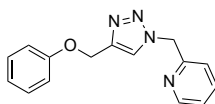
¹³C-NMR (CDCl₃, 100 MHz): δ 148.4, 138.1, 134.9, 129.6, 129.2, 128.8, 128.1, 127.8, 125.7, 119.3, 54.2, 21.3.

4.74a: 5,6-dimethyl-1-(1-(pyridin-2-ylmethyl)-1*H*-1,2,3-triazol-4-yl)-1*H*-benzo[*d*]imidazole¹⁷⁴

Prepared using General Procedure A. Pale yellow oil (48 mg, 79%). Purification on silica gel using 1/9 PE/EtOAc + 2% NEt₃.

¹H-NMR (CDCl₃, 400 MHz): δ 8.60 (d, *J* = 4.3 Hz, 1H), 8.26 (br. s, 1H), 8.03 (s, 1H), 7.71 (t, *J* = 7.6 Hz, 1H), 7.57 (s, 1H), 7.45 (s, 1H), 7.34–7.26 (m, 2H), 5.71 (s, 2H), 2.37–2.35 (m, 6H).

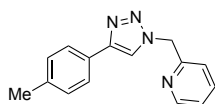
¹³C-NMR (CDCl₃, 100 MHz): δ 153.6, 150.1, 143.0, 142.3, 140.4, 137.6, 133.6, 132.2, 131.0, 123.8, 122.8, 120.6, 114.3, 111.3, 56.4, 20.6, 20.3.

4.74b: 2-((4-(phenoxy)methyl)-1*H*-1,2,3-triazol-1-yl)methylpyridine²⁸¹

Prepared using General Procedure A. Pale yellow oil (46 mg, 87%). Purification on silica gel using 4/6 PE/EtOAc.

¹H-NMR (CDCl₃, 400 MHz): δ 8.59 (br. s, 1H), 7.78 (s, 1H), 7.67 (dt, *J* = 1.7, 7.7 Hz, 1H), 7.30–7.24 (m, 3H), 7.18 (d, *J* = 7.7 Hz, 1H), 6.98–6.40 (m, 3H), 5.65 (s, 2H), 5.21 (s, 2H).

¹³C-NMR (CDCl₃, 100 MHz): δ 158.3, 154.4, 149.9, 144.8, 137.5, 129.6, 123.6, 123.4, 122.6, 121.4, 114.9, 62.1, 55.8.

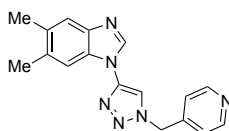
4.74c: 2-((4-(*p*-tolyl)-1*H*-1,2,3-triazol-1-yl)methyl)pyridine¹⁷⁹

Prepared using General Procedure A. Pale yellow oil (41 mg, 82%). Purification on silica gel using 9/1 PE/EtOAc.

¹H-NMR (CDCl₃, 400 MHz): δ 8.61 (br. s, 1H), 7.89 (s, 1H), 7.72–7.67 (m, 3H), 7.28–7.25 (m, 1H), 7.23–7.21 (m, 3H), 5.69 (s, 2H), 2.36 (s, 3H).

$^{13}\text{C-NMR}$ (CDCl_3 , 100 MHz): δ 154.7, 149.8, 148.4, 138.1, 137.5, 129.6, 127.8, 125.7, 123.6, 122.6, 120.0, 55.8, 21.4.

4.75a: 5,6-dimethyl-1-(1-(pyridin-4-ylmethyl)-1*H*-1,2,3-triazol-4-yl)-1*H*-benzo[*d*]imidazole



Prepared using General Procedure A. Yellow oil (38 mg, 63%). Purification on silica gel using 1/9 PE/EtOAc + 2% NEt_3 .

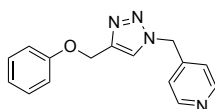
$^1\text{H-NMR}$ (CDCl_3 , 400 MHz): δ 8.63 (br. s, 2H), 8.26 (br. s, 1H), 7.88 (s, 1H), 7.55 (s, 1H), 7.45 (s, 1H), 7.18 (br. s, 2H), 5.62 (s, 2H), 2.34 (s, 6H).

$^{13}\text{C-NMR}$ (CDCl_3 , 100 MHz): δ 150.8, 143.5, 143.0, 142.2, 140.3, 133.9, 132.6, 130.9, 122.3, 120.7, 113.8, 111.4, 53.7, 20.7, 20.3.

IR ν_{max} (neat): 3129, 3073, 3030, 2967, 2935, 1656, 1595, 1498, 1465, 1416, 1288, 1203, 1056 cm^{-1} .

HRMS (ESI): $\text{C}_{17}\text{H}_{17}\text{N}_6$ $[\text{M}+\text{H}]^+$ calculated 305.1509, found 305.1510.

4.75b: 4-((4-(phenoxy)methyl)-1*H*-1,2,3-triazol-1-yl)methylpyridine



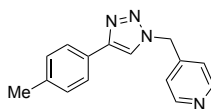
Prepared using General Procedure A. Yellow oil (37 mg, 70%). Purification on silica gel using 4/6 PE/EtOAc.

$^1\text{H-NMR}$ (CDCl_3 , 400 MHz): δ 8.62 (br. s, 2H), 7.30–7.26 (m, 3H), 7.10 (d, $J = 4.8$ Hz, 2H), 6.99–6.96 (m, 3H), 5.55 (s, 2H), 5.23 (s, 2H).

$^{13}\text{C-NMR}$ (CDCl_3 , 100 MHz): δ 158.2, 150.7, 145.4, 143.5, 129.7, 123.0, 122.3, 121.5, 114.9, 62.1, 52.9.

IR ν_{max} (neat): 3138, 3093, 3060, 3032, 2932, 2876, 1686, 1600, 1493, 1416, 1230, 1175, 1050, 1033 cm^{-1} .

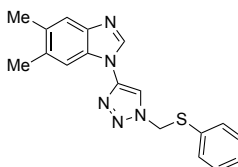
HRMS (ESI): $\text{C}_{15}\text{H}_{15}\text{N}_4\text{O}$ $[\text{M}+\text{H}]^+$ calculated 267.1240, found 267.1241.

4.75c: 4-((4-(*p*-tolyl)-1*H*-1,2,3-triazol-1-yl)methyl)pyridine²⁸²

Prepared using General Procedure A. Yellow oil (40 mg, 80%). Purification on silica gel using 9/1 PE/EtOAc.

¹H-NMR (CDCl₃, 400 MHz): δ 8.62 (br. s, 2H), 7.71–7.69 (m, 3H), 7.22 (d, *J* = 7.9 Hz, 2H), 7.14 (d, *J* = 5.1 Hz, 2H), 5.59 (s, 2H), 2.37 (s, 3H).

¹³C-NMR (CDCl₃, 100 MHz): δ 150.6, 148.9, 143.9, 138.5, 129.7, 127.5, 125.8, 122.2, 119.6, 52.9, 21.4.

4.76a: 5,6-dimethyl-1-(1-((phenylthio)methyl)-1*H*-1,2,3-triazol-4-yl)-1*H*-benzo[*d*]imidazole

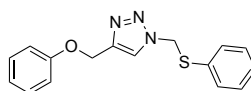
Prepared using General Procedure A. Yellow oil (56 mg, 84%). Purification on silica gel using 3/7 PE/EtOAc.

¹H-NMR (CDCl₃, 400 MHz): δ 8.24 (br. s, 1H), 7.73 (s, 1H), 7.58 (s, 1H), 7.39–7.38 (m, 2H), 7.34–7.31 (m, 4H), 5.69 (s, 2H), 2.36 (s, 6H).

¹³C-NMR (CDCl₃, 100 MHz): δ 133.8, 132.7, 132.3, 131.5, 129.9, 129.3, 121.0, 113.0, 111.5, 55.1, 20.7, 20.4. Four signals not observed/coincident.

IR ν_{\max} (neat): 3114, 2969, 2937, 2921, 1686, 1593, 1496, 1467, 1441, 1390, 1283, 1217, 1046, 1026 cm⁻¹.

HRMS (ESI): C₁₈H₁₈N₅S [M+H]⁺ calculated 336.1277, found 336.1277.

4.76b: 4-(phenoxy)methyl-1-((phenylthio)methyl)-1*H*-1,2,3-triazole

Prepared using General Procedure A. Pale yellow oil (49 mg, 82%). Purification on silica gel using 1/1 PE/EtOAc.

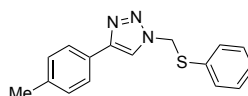
¹H-NMR (CDCl₃, 400 MHz): δ 7.60 (s, 1H), 7.31–7.26 (m, 7H), 6.99–6.95 (m, 3H), 5.61 (s, 2H), 5.19 (s, 2H).

¹³C-NMR (CDCl₃, 100 MHz): δ 158.2, 145.1, 132.5, 131.8, 129.6, 128.9, 122.3, 121.4, 114.9, 114.5, 62.1, 54.1.

IR ν_{\max} (neat): 3138, 3156, 2947, 2872, 1599, 1493, 1441, 1229, 1175, 1046 cm⁻¹.

HRMS (ESI): C₁₆H₁₆N₃OS [M+H]⁺ calculated 298.1009, found 298.1007.

4.76c: 1-((phenylthio)methyl)-4-(*p*-tolyl)-1*H*-1,2,3-triazole



Prepared using General Procedure A. Pale yellow oil (44 mg, 79%). Purification on silica gel using 8/2 PE/EtOAc.

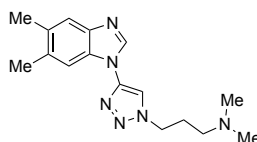
¹H-NMR (CDCl₃, 400 MHz): δ 7.73 (br. s, 1H), 7.69 (s, 1H), 7.67 (s, 1H), 7.36–7.34 (m, 2H), 7.29–7.28 (m, 3H), 7.22 (s, 1H), 7.20 (s, 1H), 5.62 (s, 2H), 2.37 (s, 3H).

¹³C-NMR (CDCl₃, 100 MHz): δ 138.1, 132.2, 132.0, 129.5, 129.4, 128.7, 127.6, 125.6, 118.8, 53.8, 21.3. One signal not observed/coincident.

IR ν_{\max} (neat): 3093, 3023, 2915, 2859, 1502, 1448, 1396, 1349, 1223, 1193 cm⁻¹.

HRMS (ESI): C₁₆H₁₆N₃S [M+H]⁺ calculated 282.1059, found 282.1056.

4.73a: 3-(4-(5,6-dimethyl-1*H*-benzo[*d*]imidazol-1-yl)-1*H*-1,2,3-triazol-1-yl)-*N,N*-dimethylpropan-1-amine



Prepared using General Procedure A. Pale yellow oil (60 mg, Quant). No purification needed.

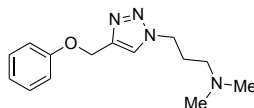
¹H-NMR (CDCl₃, 400 MHz): δ 8.21 (br. s, 1H), 7.84 (s, 1H), 7.61 (s, 1H), 7.46 (s, 1H), 4.53 (t, *J* = 6.8 Hz, 2H), 2.38 (d, *J* = 2.2 Hz, 6H), 2.32 (t, *J* = 6.6 Hz, 2H), 2.24 (s, 6H), 2.17–2.10 (m, 2H).

¹³C-NMR (CDCl₃, 100 MHz): δ 142.6, 133.6, 132.2, 120.8, 114.3, 111.3, 55.7, 49.0, 45.4, 28.0, 20.6, 20.3. Three signals not observed/coincident.

IR ν_{\max} (neat): 3103, 2941, 2816, 2766, 1625, 1587, 1495, 1461, 1377, 1331, 1286, 1219, 1089, 1041 cm⁻¹.

HRMS (ESI): $C_{16}H_{23}N_6$ $[M+H]^+$ calculated 299.1979, found 299.1977.

4.73b: *N,N*-dimethyl-3-(4-(phenoxy)methyl)-1*H*-1,2,3-triazol-1-yl)propan-1-amine



Prepared using General Procedure A. Pale yellow oil (51 mg, 99%). No purification needed.

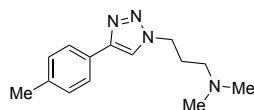
1H -NMR ($CDCl_3$, 400 MHz): δ 7.61 (s, 1H), 7.29–7.25 (m, 2H), 6.98–6.93 (m, 3H), 5.21 (s, 2H), 4.41 (t, $J = 6.9$ Hz, 2H), 2.22 (t, $J = 6.9$ Hz, 2H), 2.18 (s, 6H), 2.04 (app. quint, $J = 6.9$ Hz, 2H).

^{13}C -NMR ($CDCl_3$, 100 MHz): δ 158.3, 144.2, 129.6, 123.1, 121.3, 114.9, 62.2, 55.9, 48.2, 45.4, 28.2.

IR ν_{max} (neat): 3138, 2943, 2861, 2816, 2766, 1671, 1587, 1495, 1240, 1175, 1030 cm^{-1} .

HRMS (ESI): $C_{14}H_{21}N_4O$ $[M+H]^+$ calculated 261.1710, found 261.1709.

4.73c: *N,N*-dimethyl-3-(4-(*p*-tolyl)-1*H*-1,2,3-triazol-1-yl)propan-1-amine



Prepared using General Procedure A. Yellow oil (48 mg, 99%). No purification needed.

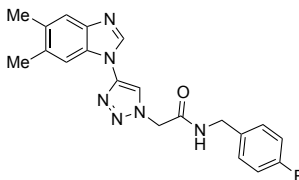
1H -NMR ($CDCl_3$, 400 MHz): δ 7.73 (s, 1H), 7.73–7.72 (m, 1H), 7.71–7.70 (m, 1H), 7.24 (s, 1H), 7.22 (s, 1H), 4.46 (t, $J = 6.9$ Hz, 2H), 2.37 (s, 3H), 2.28 (t, $J = 6.8$ Hz, 2H), 2.22 (s, 6H), 2.08 (app. quint, $J = 6.9$ Hz, 2H).

^{13}C -NMR ($CDCl_3$, 100 MHz): δ 147.8, 138.0, 129.6, 128.0, 125.7, 119.8, 55.9, 48.1, 45.3, 28.2, 21.4.

IR ν_{max} (neat): 3134, 3108, 2943, 2859, 2816, 2764, 1671, 1500, 1461, 1223, 1043 cm^{-1} .

HRMS (ESI): $C_{14}H_{21}N_4$ $[M+H]^+$ calculated 245.1761, found 245.1760.

4.77a: 2-(4-(5,6-dimethyl-1*H*-benzo[*d*]imidazol-1-yl)-1*H*-1,2,3-triazol-1-yl)-*N*-(4-fluorobenzyl)acetamide



Prepared using General Procedure A. Yellow oil (70 mg, 92%). Purification on silica gel using 9/1 DCM/MeOH + 2% NEt₃.

¹H-NMR (CDCl₃, 400 MHz): δ 8.26 (br. s, 1H), 8.02 (s, 1H), 7.57–7.54 (m, 1H), 7.43 (s, 1H), 7.27–7.21 (m, 2H), 7.02–6.97 (m, 2H), 6.83 (br. s, 1H), 5.18 (s, 2H), 4.45 (d, *J* = 5.3 Hz, 2H), 2.38 (s, 6H).

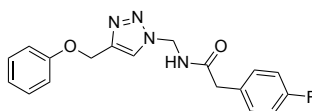
¹⁹F-NMR (DMSO-*d*₆, 376 MHz): δ 115.8.

¹³C-NMR (CDCl₃, 100 MHz): δ 165.1, 162.3, 160.3, 141.8, 134.9, 134.8, 132.7, 131.3, 129.5, 129.4, 120.0, 117.2, 115.2 (d, *J* = 20.9 Hz), 111.8, 52.4, 41.7, 20.1, 19.8.

IR ν_{max} (neat): 3426, 2251, 2127, 1666, 1511, 1054, 1026, 1007 cm⁻¹.

HRMS (ESI): C₂₀H₂₀FN₆O [M+H]⁺ calculated 379.1677, found 379.1677.

4.77b: 2-(4-fluorophenyl)-*N*-((4-(phenoxy)methyl)-1*H*-1,2,3-triazol-1-yl)methyl)acetamide



Prepared using General Procedure A. Yellow oil (63 mg, 93%). Purification on silica gel using 9/1 DCM/MeOH + 2% NEt₃.

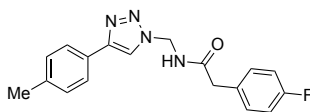
¹H-NMR (CDCl₃, 400 MHz): δ 7.79 (br. s, 1H), 7.33–7.28 (m, 2H), 7.19–7.16 (m, 2H), 7.01–6.97 (m, 5H), 5.22 (s, 2H), 5.08 (s, 2H), 4.69 (d, *J* = 2.4 Hz, 1H), 4.39 (d, *J* = 5.7 Hz, 2H).

¹⁹F-NMR (CDCl₃, 376 MHz): δ 114.3.

¹³C-NMR (CDCl₃, 100 MHz): δ 163.7, 161.3, 158.2, 133.1, 129.8, 129.6, 121.7, 121.6, 116.0 (d, *J* = 21.7 Hz), 115.0, 114.9, 55.9, 43.4, 29.8.

IR ν_{max} (neat): 3445, 2251, 2125, 1656, 1511, 1495, 1223, 1054, 1026, 1007 cm⁻¹.

HRMS (ESI): C₁₈H₁₈FN₄O₂ [M+H]⁺ calculated 341.1408, found 341.1412.

4.77c: 2-(4-fluorophenyl)-*N*-((4-(*p*-tolyl)-1*H*-1,2,3-triazol-1-yl)methyl)acetamide

Prepared using General Procedure A. Yellow oil (60 mg, 92%). Purification on silica gel using 1/9 PE/EtOAc + 2% NEt₃.

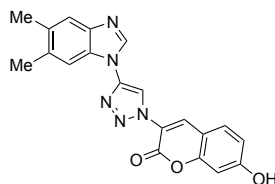
¹H-NMR (DMSO-*d*₆, 400 MHz): δ 8.84 (t, *J* = 5.9 Hz, 1H), 8.47 (s, 1H), 7.76–7.74 (m, 2H), 7.35–7.32 (m, 2H), 7.27–7.25 (m, 2H), 7.19–7.14 (m, 2H), 5.19 (s, 2H), 4.32 (d, *J* = 5.7 Hz, 2H), 2.33 (s, 3H).

¹⁹F-NMR (DMSO-*d*₆, 376 MHz): δ 115.9.

¹³C-NMR (CDCl₃, 100 MHz): δ 165.5, 162.5, 160.0, 146.2, 137.1, 135.0, 129.4, 128.0, 125.0, 122.5, 115.2 (d, *J* = 21.4 Hz), 51.7, 41.7, 20.8.

IR ν_{max} (neat): 3093, 3023, 2915, 2859, 1502, 1448, 1349, 1279, 1193, 1076, 1045 cm⁻¹.

HRMS (ESI): C₁₈H₁₈FN₄O [M+H]⁺ calculated 325.1459, found 325.1463.

4.78a: 3-(4-(5,6-dimethyl-1*H*-benzo[*d*]imidazol-1-yl)-1*H*-1,2,3-triazol-1-yl)-7-hydroxy-2*H*-chromen-2-one

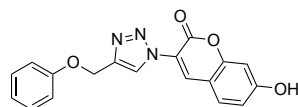
Prepared using General Procedure A. Yellow oil (73 mg, 98%). Purification on silica gel using 9/1 DCM/MeOH + 2% NEt₃.

¹H-NMR (DMSO-*d*₆, 400 MHz): δ 11.00 (s, 1H), 9.15 (s, 1H), 8.72 (s, 2H), 7.80–7.60 (m, 3H), 6.96–6.93 (m, 1H), 6.89 (d, *J* = 1.8 Hz, 1H), 2.38 (s, 3H), 2.34 (s, 3H).

¹³C-NMR (DMSO-*d*₆, 100 MHz): δ 162.8, 156.2, 154.9, 137.6, 132.9, 131.2, 119.1, 116.8, 114.4, 110.2, 102.3, 20.1, 19.8. Seven signals not observed/coincident.

IR ν_{max} (neat): 3126, 2921, 2949, 1722, 1703, 1607, 1590, 1465, 1417, 1380 cm⁻¹.

HRMS (ESI): C₂₀H₁₆N₅O₃ [M+H]⁺ calculated 374.1248, found 374.1249.

4.78b: 7-hydroxy-3-(4-(phenoxy)methyl)-1*H*-1,2,3-triazol-1-yl)-2*H*-chromen-2-one

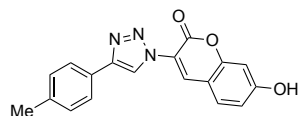
Prepared using General Procedure A. Yellow oil (64 mg, 96%). Purification on silica gel using 9/1 DCM/MeOH + 2% NEt₃.

¹H-NMR (DMSO-*d*₆, 500 MHz): δ 10.91 (br. s, 1H), 8.67 (s, 1H), 8.62 (s, 1H), 7.75 (d, *J* = 7.9 Hz, 1H), 7.32 (t, *J* = 7.6 Hz, 2H), 7.07 (d, *J* = 8.1 Hz, 2H), 6.96–6.95 (m, 1H), 6.94–6.85 (m, 2H), 5.25 (s, 2H).

¹³C-NMR (DMSO-*d*₆, 125 MHz): δ 158.0, 156.3, 142.9, 136.5, 131.0, 129.5, 125.5, 120.9, 114.7, 60.6. Six signals not observed/coincident.

IR ν_{max} (neat): 3014, 2994, 2981, 1687, 1625, 1614, 1597, 1421, 1389, 1229 cm⁻¹.

HRMS (ESI): C₁₈H₁₄N₃O₄ [M+H]⁺ calculated 336.0979, found 336.0984.

4.78c: 7-hydroxy-3-(4-(*p*-tolyl)-1*H*-1,2,3-triazol-1-yl)-2*H*-chromen-2-one

Prepared using General Procedure A. Yellow oil (55 mg, 86%). Purification on silica gel using 9/1 DCM/MeOH + 2% NEt₃.

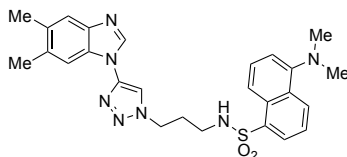
¹H-NMR (DMSO-*d*₆, 500 MHz): δ 10.95 (br. s, 1H), 8.93 (s, 1H), 8.64 (s, 1H), 7.84 (d, *J* = 7.7 Hz, 2H), 7.77 (d, *J* = 8.4 Hz, 1H), 7.30 (d, *J* = 7.7 Hz, 2H), 6.94–6.89 (m, 2H), 2.35 (s, 3H).

¹³C-NMR (DMSO-*d*₆, 125 MHz): δ 162.5, 156.3, 154.7, 146.5, 137.6, 136.7, 131.0, 129.5, 127.3, 125.3, 121.7, 119.2, 114.2, 110.3, 102.2, 20.8.

IR ν_{max} (neat): 3167, 3079, 3014, 1731, 1714, 1701, 1603, 1404, 1235 cm⁻¹.

HRMS (ESI): C₁₈H₁₄N₃O₃ [M+H]⁺ calculated 320.1030, found 320.1033.

4.79a: *N*-(3-(4-(5,6-Dimethyl-1*H*-benzo[*d*]imidazol-1-yl)-1*H*-1,2,3-triazol-1-yl)propyl)-5-(dimethylamino)naphthalene-1-sulfonamide¹⁷⁴

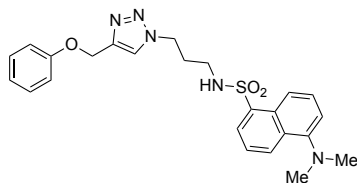


Prepared using General Procedure A (0.1 mmol scale). Yellow oil (52 mg, 96%). Purification on silica gel using 9/1 DCM/MeOH + 2% NEt₃.

¹H-NMR (CDCl₃, 500 MHz): δ 8.52 (d, *J* = 8.6 Hz, 1H), 8.27 (d, *J* = 8.9 Hz, 1H), 8.24 (s, 1H), 8.21 (d, *J* = 7.0 Hz, 1H), 7.80 (s, 1H), 7.61 (s, 1H), 7.55 (t, *J* = 7.8 Hz, 1H), 7.50–7.46 (m, 2H), 7.16 (d, *J* = 7.6 Hz, 1H), 5.38 (t, *J* = 6.0 Hz, 1H), 4.54 (t, *J* = 6.0 Hz, 2H), 2.95–2.92 (m, 2H), 2.86 (s, 6H), 2.39 (s, 6H), 2.18–2.13 (m, 2H).

¹³C-NMR (CDCl₃, 500 MHz): δ 152.4, 142.6, 142.4, 140.5, 134.2, 133.8, 132.4, 131.0, 130.1, 129.9, 129.6, 128.9, 123.4, 120.7, 118.3, 115.5, 114.7, 111.4, 47.7, 45.5, 39.9, 30.2, 20.7, 20.4. One signal not observed/coincident.

4.79b: 5-(dimethylamino)-*N*-(3-(4-(phenoxyethyl)-1*H*-1,2,3-triazol-1-yl)propyl)naphthalene-1-sulfonamide



Prepared using General Procedure A (0.1 mmol scale). Yellow oil (46 mg, 98%). Purification on silica gel using 9/1 DCM/MeOH + 2% NEt₃.

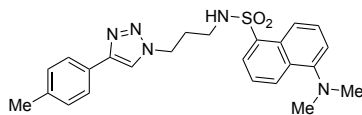
¹H-NMR (CDCl₃, 500 MHz): δ 8.54 (d, *J* = 8.4 Hz, 1H), 8.25 (d, *J* = 8.7 Hz, 1H), 8.19 (d, *J* = 7.1 Hz, 1H), 7.59 (t, *J* = 8.2 Hz, 1H), 7.51 (t, *J* = 7.9 Hz, 1H), 7.47 (s, 1H), 7.29 (t, *J* = 8.0 Hz, 2H), 7.19 (d, *J* = 7.6 Hz, 1H), 6.98 (d, *J* = 7.8 Hz, 3H), 5.17 (s, 2H), 4.96 (t, *J* = 6.2 Hz, 1H), 4.37 (t, *J* = 6.5 Hz, 2H), 2.88 (s, 6H), 2.87–2.85 (m, 2H), 2.04 (app. quint, *J* = 6.3 Hz, 2H).

¹³C-NMR (DMSO-*d*₆, 100 MHz): δ 158.3, 152.4, 134.4, 130.9, 130.1, 130.0, 129.7, 128.9, 123.4, 121.9, 121.5, 118.6, 115.5, 115.0, 114.9, 56.3, 45.5, 40.1, 30.2. Two signals not observed/coincident.

IR ν_{max} (neat): 3292, 3142, 3062, 2939, 2867, 2829, 2785, 1587, 1493, 1459, 1312, 1214, 1143 cm⁻¹.

HRMS (ESI): C₂₄H₂₈N₅O₃S [M+H]⁺ calculated 466.1907, found 466.1906.

4.79c: 5-(dimethylamino)-*N*-(3-(4-(*p*-tolyl)-1*H*-1,2,3-triazol-1-yl)propyl)naphthalene-1-sulfonamide



Prepared using General Procedure A (0.1 mmol scale). Yellow oil (44 mg, 98%). Purification on silica gel using 9/1 DCM/MeOH + 2% NEt₃.

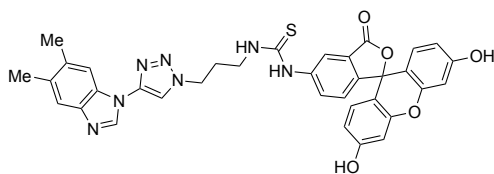
¹H-NMR (CDCl₃, 500 MHz): δ 8.53 (d, *J* = 8.6 Hz, 1H), 8.26 (d, *J* = 8.6 Hz, 1H), 8.21 (d, *J* = 7.5 Hz, 1H), 7.67 (d, *J* = 8.0 Hz, 2H), 7.60–7.56 (m, 2H), 7.49 (t, *J* = 8.0 Hz, 1H), 7.23 (d, *J* = 8.0 Hz, 2H), 7.19 (d, *J* = 7.8 Hz, 1H), 5.01 (t, *J* = 6.2 Hz, 1H), 4.42 (t, *J* = 6.4 Hz, 2H), 2.90 (t, *J* = 6.3 Hz, 2H), 2.88 (s, 6H), 2.38 (s, 3H), 2.07 (app. quint, *J* = 6.3 Hz, 2H).

¹³C-NMR (CDCl₃, 100 MHz): δ 138.3, 134.3, 130.9, 130.1, 130.0, 129.7, 128.9, 125.8, 123.4, 118.5, 115.5, 47.1, 45.5, 40.1, 30.4, 21.4. Five signals not observed/coincident.

IR ν_{max} (neat): 3285, 3132, 2928, 2865, 1688, 1574, 1455, 1316, 1143 cm⁻¹.

HRMS (ESI): C₂₄H₂₈N₅O₂S [M+H]⁺ calculated 450.1958, found 450.1966.

4.80a: 1-(3',6'-dihydroxy-3-oxo-3*H*-spiro[isobenzofuran-1,9'-xanthen]-5-yl)-3-(3-(4-(5,6-dimethyl-1*H*-benzo[*d*]imidazol-1-yl)-1*H*-1,2,3-triazol-1-yl)propyl)thiourea¹⁷⁴



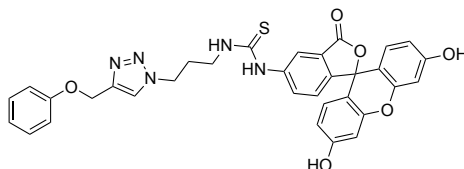
Prepared using General Procedure A (0.1 mmol scale). Orange gum (51 mg, 78%). Purification on silica gel using 9/1 DCM/MeOH + 2% NEt₃.

¹H-NMR (DMSO-*d*₆, 400 MHz): δ 9.32 (br. s, 1H), 9.00 (s, 1H), 8.45 (s, 1H), 7.86 (d, *J* = 8.0 Hz, 1H), 7.82 (s, 1H), 7.65–7.62 (m, 2H), 7.16 (d, *J* = 8.3 Hz, 1H), 6.72–6.68 (m, 2H), 6.60–6.56 (m, 3H), 4.66 (t, *J* = 6.9 Hz, 2H), 3.51 (s, 2H), 3.16 (s, 2H), 2.40 (s, 3H), 2.38 (s, 3H).

¹³C-NMR could not be obtained due to relaxation issues.

HRMS (ESI): C₃₅H₂₈N₇O₅S [M-OH]⁻ calculated 642.1923, found 642.1632. Error >5 ppm, due to fluorescein protonation state variation.²⁸³

4.80b: 1-(3',6'-dihydroxy-3-oxo-3*H*-spiro[isobenzofuran-1,9'-xanthen]-5-yl)-3-(3-(4-(phenoxy)methyl)-1*H*-1,2,3-triazol-1-yl)propyl)thiourea



Prepared using General Procedure A (0.1 mmol scale). Orange gum (52 mg, 79%). Purification on silica gel using 9/1 DCM/MeOH + 2% NEt₃.

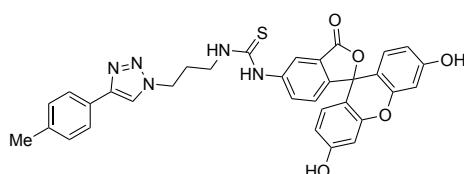
¹H-NMR (DMSO-*d*₆, 400 MHz): δ 8.39 (br. s, 1H), 8.31 (br. s, 1H), 7.91 (br. s, 1H), 7.19–6.92 (m, 14H), 5.08 (br. s, 2H), 4.45 (br. s, 2H), 3.54 (br. s, 2H), 2.17 (br. s, 2H).

¹³C-NMR could not be obtained due to relaxation issues.

IR ν_{\max} (neat): 3437, 2259, 2190, 2130, 1770, 1693, 1152, 1026 cm⁻¹.

HRMS (ESI) C₃₃H₂₈N₅O₆S [M+H-S]⁺ calculated 590.2034, found 590.2031; C₃₃H₂₈N₅O₆S [M+H-OH]⁺ calculated 605.1727, found 605.1678; C₃₃H₂₈N₅O₆S [M+H]⁺ calculated 606.1806, found 606.1979. Error >5 ppm due to fluorescein protonation state variation.²⁸³

4.80c: 1-(3',6'-dihydroxy-3-oxo-3*H*-spiro[isobenzofuran-1,9'-xanthen]-5-yl)-3-(3-(4-(*p*-tolyl)-1*H*-1,2,3-triazol-1-yl)propyl)thiourea



Prepared using General Procedure A (0.1 mmol scale). Orange gum (48 mg, 79%). Purification on silica gel using 9/1 DCM/MeOH + 2% NEt₃.

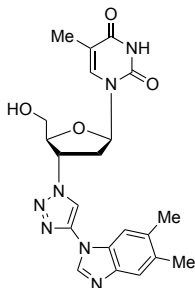
¹H-NMR (DMSO-*d*₆, 400 MHz): δ 8.43 (br. s, 2H), 7.96 (br. s, 1H), 7.65 (br. s, 2H), 7.18–6.97 (m, 11H), 4.48 (br. s, 2H), 3.58 (br. s, 2H), 2.22 (br. s, 5H). One drop of pyridine-*d*₅ was added to DMSO-*d*₆ for solubility, resulting in the loss of phenolic protons; basic form of fluorescein.²⁸⁴

¹³C-NMR could not be obtained due to relaxation issues.

IR ν_{\max} (neat): 3486, 2255, 1766, 1335, 1178, 1154, 1026, 1009 cm⁻¹.

HRMS (ESI): C₃₃H₂₈N₅O₅S [M+H]⁺ calculated 606.1806, found 606.1977; C₃₃H₂₇N₅O₅SNa [M+Na]⁺ calculated 628.1625, found 628.1800. Error >5 ppm due to fluorescein protonation state variation.²⁸³

4.81a: 1-((2*R*,4*S*,5*S*)-4-(4-(5,6-dimethyl-1*H*-benzo[*d*]imidazol-1-yl)-1*H*-1,2,3-triazol-1-yl)-5-(hydroxymethyl)tetrahydrofuran-2-yl)-5-methylpyrimidine-2,4(1*H*,3*H*)-dione



Prepared using General Procedure A (0.1 mmol scale). Yellow oil (44 mg, Quant). Purification on silica gel using 9/1 DCM/MeOH + 2% NEt₃.

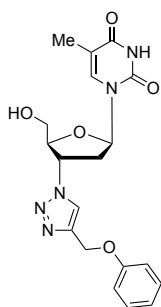
¹H-NMR (DMSO-*d*₆, 500 MHz): δ 11.38 (s, 1H), 8.90 (s, 2H), 7.85–7.61 (m, 3H), 6.49 (s, 1H), 5.50 (s, 1H), 5.38 (s, 1H), 4.38 (s, 1H), 3.78–3.74 (m, 2H), 2.89–2.76 (m, 2H), 2.36 (s, 3H), 2.32 (s, 3H), 1.83 (s, 3H).

¹³C-NMR (DMSO-*d*₆, 125 MHz): δ 165.3, 151.5, 137.5, 134.8, 117.0, 111.0, 85.3, 85.2, 61.7, 61.4, 37.8, 20.8, 20.6, 12.9. Seven signals not observed/coincident.

IR ν_{max} (neat): 3341, 2926, 2255, 2128, 1699, 1680, 1584, 1470, 1405, 1283 cm⁻¹.

HRMS (ESI): C₂₁H₂₄N₇O₄ [M+H]⁺ calculated 438.1884, found 438.1883.

4.81b: 1-((2*R*,4*S*,5*S*)-5-(hydroxymethyl)-4-(4-(phenoxyethyl)-1*H*-1,2,3-triazol-1-yl)tetrahydrofuran-2-yl)-5-methylpyrimidine-2,4(1*H*,3*H*)-dione²⁸⁵

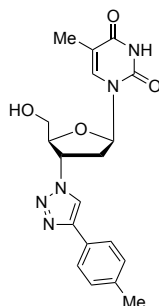


Prepared using General Procedure A (0.1 mmol scale). Yellow oil (38 mg, 96%). Purification on silica gel using 9/1 DCM/MeOH + 2% NEt₃.

¹H-NMR (DMSO-*d*₆, 500 MHz): δ 11.32 (br. s, 1H), 8.43 (s, 1H), 7.82 (s, 1H), 7.31 (t, *J* = 7.8 Hz, 2H), 7.04 (d, *J* = 8.0 Hz, 2H), 6.96 (t, *J* = 7.3 Hz, 1H), 6.43 (t, *J* = 6.4 Hz, 1H), 5.42–5.38 (m, 1H), 5.28 (t, *J* = 5.1 Hz, 1H), 5.15 (s, 2H), 4.25–4.22 (m, 1H), 3.73–3.69 (m, 1H), 3.65–3.58 (m, 1H), 2.78–2.72 (m, 1H), 2.41–2.24 (m, 1H), 1.81 (s, 3H).

$^{13}\text{C-NMR}$ (DMSO- d_6 , 125 MHz): δ 163.7, 158.0, 150.4, 136.2, 129.5, 124.2, 120.8, 114.6, 109.6, 84.4, 83.9, 61.0, 60.1, 59.3, 37.1, 36.1, 12.2.

4.81c: 1-((2*R*,4*S*,5*S*)-5-(hydroxymethyl)-4-(4-(*p*-tolyl)-1*H*-1,2,3-triazol-1-yl)tetrahydrofuran-2-yl)-5-methylpyrimidine-2,4(1*H*,3*H*)-dione



Prepared using General Procedure A (0.1 mmol scale). Yellow oil (39 mg, 99%). Purification on silica gel using 9/1 DCM/MeOH + 2% NEt_3 .

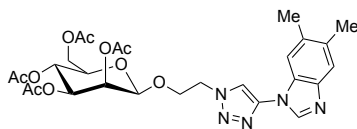
$^1\text{H-NMR}$ (DMSO- d_6 , 500 MHz): δ 11.35 (s, 1H), 8.72 (s, 1H), 7.83 (d, $J = 1.1$ Hz, 1H), 7.75 (s, 1H), 7.74 (s, 1H), 7.28 (s, 1H), 7.26 (s, 1H), 6.45 (t, $J = 6.5$ Hz, 1H), 5.41–5.37 (m, 1H), 4.29–4.27 (m, 1H), 3.74–3.65 (m, 2H), 3.30 (d, $J = 11.8$ Hz, 1H), 2.82–2.66 (m, 2H), 2.33 (s, 3H), 1.82 (s, 3H).

$^{13}\text{C-NMR}$ (DMSO- d_6 , 125 MHz): δ 163.7, 150.4, 146.6, 137.3, 136.2, 129.5, 127.8, 125.1, 120.5, 109.6, 84.4, 83.9, 60.8, 59.3, 37.1, 20.8, 12.2.

$\text{IR } \nu_{\text{max}}$ (neat): 3473, 2251, 2127, 1656, 1273, 1054, 1026, 1006 cm^{-1} .

HRMS (ESI): $\text{C}_{19}\text{H}_{22}\text{N}_5\text{O}_4$ $[\text{M}+\text{H}]^+$ calculated 384.1666, found 384.1669.

4.82a: (2*R*,3*R*,4*S*,5*S*,6*R*)-2-(acetoxymethyl)-6-(2-(4-(5,6-dimethyl-1*H*-benzo[*d*]imidazol-1-yl)-1*H*-1,2,3-triazol-1-yl)ethoxy)tetrahydro-2*H*-pyran-3,4,5-triyl triacetate



Prepared using General Procedure A (0.1 mmol scale). Yellow oil (52 mg, 88%). Purification on silica gel using 9/1 DCM/MeOH + 2% NEt_3 .

$^1\text{H-NMR}$ (DMSO- d_6 , 500 MHz): δ 8.79 (s, 1H), 8.50 (s, 1H), 7.61 (s, 1H), 7.54 (s, 1H), 5.10–5.09 (m, 1H), 5.04–5.02 (m, 2H), 4.96 (d, $J = 1.4$ Hz, 1H), 4.78 (t, $J = 5.8$ Hz, 2H), 4.12–4.08

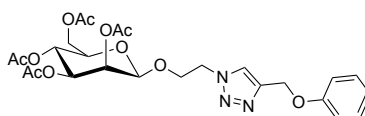
(m, 1H), 4.04–3.95 (m, 3H), 3.50–3.47 (m, 1H), 2.36 (s, 3H), 2.34 (s, 3H), 2.08 (s, 3H), 1.97 (s, 3H), 1.90 (s, 3H), 1.79 (s, 3H).

¹³C-NMR (MeOD, 100 MHz): 172.1, 171.5, 171.4, 171.2, 135.3, 133.9, 120.5, 118.1, 113.1, 98.3, 70.5, 70.3, 70.1, 66.9, 63.3, 53.7, 51.8, 47.8, 20.7, 20.6, 20.3, 20.2, 9.25. Four signals not observed/coincident.

IR ν_{\max} (neat): 2978, 2945, 2623, 2606, 2498, 2047, 1749, 1478, 1400, 1229, 1039 cm^{-1} .

HRMS (ESI): C₂₇H₃₄N₅O₁₀ [M+H]⁺ calculated 588.2300, found 588.2291.

4.82b: (2*R*,3*R*,4*S*,5*S*,6*R*)-2-(acetoxymethyl)-6-(2-(4-(phenoxy)methyl)-1*H*-1,2,3-triazol-1-yl)-ethoxy)tetrahydro-2*H*-pyran-3,4,5-triyl triacetate



Prepared using General Procedure A (0.1 mmol scale). Yellow oil (43 mg, 78%). Purification on silica gel using 9/1 DCM/MeOH + 2% NEt₃.

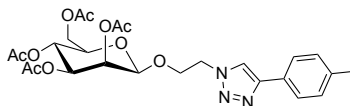
¹H-NMR (MeOD, 400 MHz): δ 8.13 (s, 1H), 7.30–7.26 (m, 2H), 7.03–7.01 (m, 2H), 6.95 (t, $J = 7.4$ Hz, 1H), 5.20–5.19 (m, 1H), 5.18 (s, 2H), 5.17–5.16 (m, 2H), 4.84–4.83 (m, 1H), 4.71–4.69 (m, 2H), 4.16–4.09 (m, 2H), 4.01–3.92 (m, 2H), 3.41–3.38 (m, 1H), 2.11 (s, 3H), 2.05 (s, 3H), 1.95 (s, 3H), 1.94 (s, 3H).

¹³C-NMR (MeOD, 100 MHz) 172.3, 171.5, 171.5, 171.4, 159.8, 145.3, 130.6, 126.3, 122.3, 115.9, 98.5, 70.6, 70.4, 70.1, 67.2, 66.9, 63.2, 62.4, 51.0, 20.6, 20.5. Two signals not observed/coincident.

IR ν_{\max} (neat): 3447, 3409, 2924, 1742, 1600, 1495, 1242, 1138, 1095, 1054, 1035 cm^{-1} .

HRMS (ESI): C₂₅H₃₂N₃O₁₁ [M+H]⁺ calculated 550.2031, found 550.2021.

4.82c: (2*R*,3*R*,4*S*,5*S*,6*R*)-2-(acetoxymethyl)-6-(2-(4-(*p*-tolyl)-1*H*-1,2,3-triazol-1-yl)ethoxy)tetrahydro-2*H*-pyran-3,4,5-triyl triacetate



Prepared using General Procedure A (0.1 mmol scale). Yellow oil (47 mg, 89%). Purification on silica gel using 9/1 DCM/MeOH + 2% NEt₃.

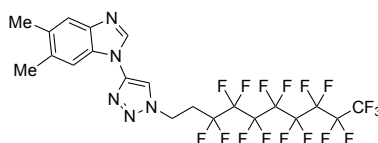
¹H-NMR (MeOD, 400 MHz): δ 8.32 (s, 1H), 7.74–7.72 (m, 2H), 7.26–7.24 (m, 2H), 5.23–5.22 (m, 1H), 5.17–5.08 (m, 2H), 4.86 (d, J = 1.6 Hz, 1H), 4.74–4.71 (m, 2H), 4.15–3.92 (m, 4H), 3.15–3.11 (m, 1H), 2.35 (s, 3H), 2.10 (s, 3H), 2.01 (s, 3H), 1.95 (s, 3H), 1.72 (s, 3H).

¹³C-NMR (MeOD, 100 MHz): δ 172.2, 171.6, 171.5, 171.4, 149.0, 139.5, 130.6, 128.8, 126.8, 123.1, 98.1, 70.6, 70.4, 69.9, 66.9, 66.8, 63.2, 51.1, 21.2, 20.6, 20.5, 20.2. One signal not observed/coincident.

IR ν_{\max} (neat): 3136, 3114, 2960, 2926, 1745, 1454, 1370, 1225, 1139, 1091, 1048 cm^{-1} .

HRMS (ESI): $\text{C}_{25}\text{H}_{32}\text{N}_3\text{O}_{10}$ $[\text{M}+\text{H}]^+$ calculated 534.2082, found 534.2071.

4.83a: 1-(1-(3,3,4,4,5,5,6,6,7,7,8,8,9,9,10,10,10-heptafluorodecyl)-1*H*-1,2,3-triazol-4-yl)-5,6-dimethyl-1*H*-benzo[*d*]imidazole



Prepared using General Procedure A (0.1 mmol scale). Yellow oil (51 mg, 78%). Purification on silica gel using 6/4 PE/EtOAc.

¹H-NMR (CDCl_3 , 400 MHz): δ 8.28 (br. s, 1H), 7.85 (s, 1H), 7.63 (s, 1H), 7.45 (s, 1H), 4.81 (t, J = 7.2 Hz, 2H), 3.01–2.87 (m, 2H), 2.41 (s, 3H), 2.40 (s, 3H).

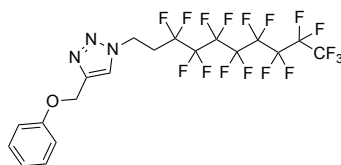
¹⁹F-NMR (CDCl_3 , 376 MHz): δ -80.7 (t, J = 9.9 Hz), -113.9 (app. quint, J = 15.3 Hz), -121.5, -121.8, -122.6, -123.3, -126.0.

¹³C-NMR could not be obtained due to relaxation issues.²⁸⁶

IR ν_{\max} (neat): 3447, 2251, 2125, 1656, 1054, 1026, 1007 cm^{-1} .

HRMS (ESI): $\text{C}_{21}\text{H}_{15}\text{F}_{17}\text{N}_5$ $[\text{M}+\text{H}]^+$ calculated 660.1051, found 660.1053.

4.83b: 1-(3,3,4,4,5,5,6,6,7,7,8,8,9,9,10,10,10-heptafluorodecyl)-4-(phenoxyethyl)-1*H*-1,2,3-triazole



Prepared using General Procedure A (0.1 mmol scale). Yellow oil (43 mg, 69%). Purification on silica gel using 6/4 PE/EtOAc.

¹H-NMR (CDCl₃, 400 MHz): δ 7.66 (s, 1H), 7.32–7.28 (m, 2H), 7.00–6.96 (m, 3H), 5.23 (s, 2H), 4.68 (t, *J* = 7.3 Hz, 2H), 2.84 (app. sept, *J* = 7.5 Hz, 2H).

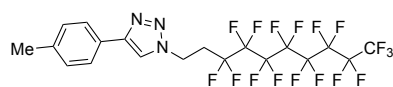
¹⁹F-NMR (CDCl₃, 376 MHz): δ -80.7 (t, *J* = 9.9 Hz), -114.0 (app. quint, *J* = 15.4 Hz), -121.5 (d, *J* = 10.2 Hz), -121.8, -122.6, -123.4, -126.0.

¹³C-NMR (MeOD, 100 MHz): δ 129.7, 123.2, 121.5, 114.9, 62.1, 29.8.

IR ν_{\max} (neat): 2919, 2850, 1602, 1498, 1459, 1199, 1147, 1082, 1045 cm⁻¹.

HRMS (ESI): C₁₉H₁₃F₁₇N₃O [M+H]⁺ calculated 622.0782, found 622.0777.

4.83c: 1-(3,3,4,4,5,5,6,6,7,7,8,8,9,9,10,10,10-heptafluorodecyl)-4-(*p*-tolyl)-1*H*-1,2,3-triazole



Prepared using General Procedure A (0.1 mmol scale). Yellow oil (48 mg, 79%). Purification on silica gel using 8/2 PE/EtOAc.

¹H-NMR (CDCl₃, 400 MHz): δ 7.78 (s, 1H), 7.72 (d, *J* = 8.1 Hz, 2H), 7.24 (s, 2H), 4.73 (t, *J* = 7.5 Hz, 2H), 2.87 (app. sept, *J* = 7.4 Hz, 2H), 2.39 (s, 3H).

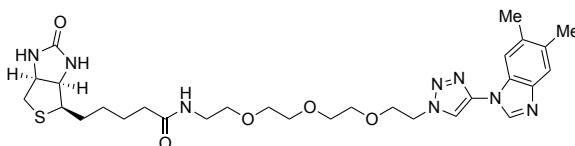
¹⁹F-NMR (CDCl₃, 376 MHz): δ -80.7 (t, *J* = 9.8 Hz), -114.0 (app. quint, *J* = 15.2 Hz), -121.5, -121.8, -122.6, -123.3, -126.0.

¹³C-NMR (MeOD, 100 MHz): δ 138.5, 129.8, 127.5, 125.9, 42.5, 32.1, 21.4.

IR ν_{\max} (neat): 3108, 2921, 1502, 1400, 1329, 1197, 1143, 1115, 1048 cm⁻¹.

HRMS (ESI): C₁₉H₁₃F₁₇N₃ [M+H]⁺ calculated 606.0833, found 606.0837.

4.84a: *N*-(2-(2-(2-(2-(4-(5,6-dimethyl-1*H*-benzo[*d*]imidazol-1-yl)-1*H*-1,2,3-triazol-1-yl)ethoxy)ethoxy)ethoxy)ethyl)-5-((3*aR*,4*R*,6*aS*)-2-oxohexahydro-1*H*-thieno[3,4-*d*]imidazol-4-yl)pentanamide¹⁷⁴



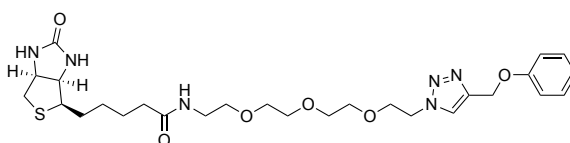
Prepared using General Procedure A (0.1 mmol scale). Yellow oil (55 mg, 89%). Purification on silica gel using 9/1 DCM/MeOH + 2% NEt₃.

¹H-NMR (MeOD, 400 MHz): δ 8.52 (s, 2H), 7.63 (br. s, 1H), 7.55 (br. s, 1H), 4.71 (t, *J* = 5.2 Hz, 2H), 4.45 (dd, *J* = 7.8, 4.9 Hz, 1H), 4.25 (dd, *J* = 7.9, 4.5 Hz, 1H), 3.99 (t, *J* = 4.9 Hz, 2H), 3.69–3.66 (m, 2H), 3.64–3.62 (m, 2H), 3.58–3.55 (m, 2H), 3.49–3.47 (m, 2H), 3.38 (t, *J* = 5.4

Hz, 2H), 3.24 (t, $J = 5.4$ Hz, 2H), 3.17–3.12 (m, 1H), 2.88 (dd, $J = 12.8, 5.0$ Hz, 1H), 2.68 (d, $J = 12.7$ Hz, 1H), 2.41 (s, 3H), 2.40 (s, 3H), 2.17–2.13 (m, 2H), 1.73–1.50 (m, 4H), 1.42–1.34 (m, 2H).

$^{13}\text{C-NMR}$ (MeOD, 100 MHz): δ 176.0, 166.1, 135.2, 133.9, 120.6, 118.2, 112.9, 71.5, 71.4, 71.1, 70.5, 63.3, 61.6, 57.0, 52.3, 41.0, 40.2, 36.7, 29.7, 29.4, 26.8, 20.7, 20.3. Six signals not observed/coincident.

4.84b: 5-((3*aR*,4*R*,6*aS*)-2-oxohexahydro-1*H*-thieno[3,4-*d*]imidazol-4-yl)-*N*-(2-(2-(2-(2-(4-(phoxymethyl)-1*H*-1,2,3-triazol-1-yl)ethoxy)ethoxy)ethoxy)ethyl)pentanamide



Prepared using General Procedure A (0.1 mmol scale). Yellow oil (52 mg, 91%). Purification on silica gel using 9/1 DCM/MeOH + 2% NEt₃.

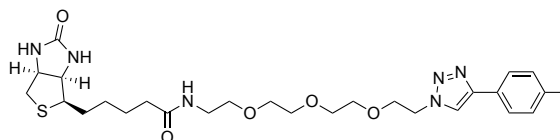
$^1\text{H-NMR}$ (MeOD, 500 MHz): δ 8.11 (s, 1H), 7.30–7.26 (m, 2H), 7.02–7.00 (m, 2H), 6.97–6.93 (m, 1H), 5.17 (s, 2H), 4.60 (t, $J = 5.0$ Hz, 2H), 4.49–4.46 (m, 1H), 4.28 (dd, $J = 7.9, 4.5$ Hz, 1H), 3.90 (t, $J = 5.0$ Hz, 2H), 3.61–3.58 (m, 4H), 3.56 (s, 4H), 3.49 (t, $J = 5.5$ Hz, 2H), 3.35–3.32 (m, 2H), 3.20–3.15 (m, 1H), 2.90 (dd, $J = 12.7, 5.0$ Hz, 1H), 2.69 (d, $J = 12.7$ Hz, 1H), 2.19 (t, $J = 7.4$ Hz, 2H), 1.76–1.54 (m, 4H), 1.46–1.40 (m, 2H).

$^{13}\text{C-NMR}$ (MeOD, 100 MHz): δ 176.1, 166.1, 159.8, 145.0, 130.6, 126.1, 122.3, 71.6, 71.5, 71.4, 71.2, 70.6, 70.3, 63.4, 62.3, 61.6, 57.0, 51.5, 41.0, 40.3, 36.7, 29.7, 29.5, 26.8. One signal not observed/coincident.

IR ν_{max} (neat): 3404, 2508, 2251, 2128, 2063, 1128, 1054, 1026, 1007 cm⁻¹.

HRMS (ESI): C₂₇H₄₁N₆O₆S [M+H]⁺ calculated 577.2803, found 577.2790.

4.84c: 5-((3*aR*,4*R*,6*aS*)-2-oxohexahydro-1*H*-thieno[3,4-*d*]imidazol-4-yl)-*N*-(2-(2-(2-(2-(4-(*p*-tolyl)-1*H*-1,2,3-triazol-1-yl)ethoxy)ethoxy)ethoxy)ethyl)pentanamide



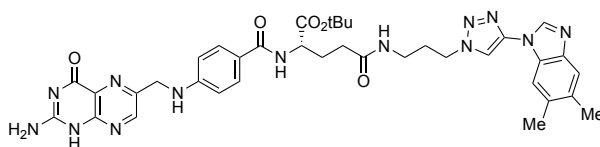
Prepared using General Procedure A (0.1 mmol scale). Yellow oil (51 mg, 91%). Purification on silica gel using 9/1 DCM/MeOH + 2% NEt₃.

¹H-NMR (CDCl₃, 400 MHz): δ 8.31–8.12 (m, 1H), 7.71–7.69 (m, 1H), 7.29–7.25 (m, 2H), 7.02–6.95 (m, 1H), 5.17–5.16 (m, 1H), 4.64–4.60 (m, 2H), 4.49–4.46 (m, 1H), 4.30–4.26 (m, 1H), 3.95–3.89 (m, 2H), 3.67–3.45 (m, 12H), 3.20–3.15 (m, 2H), 2.92–2.89 (m, 1H), 2.71–2.68 (m, 1H), 2.37–2.36 (m, 2H), 2.19–2.17 (m, 2H), 1.71–1.69 (m, 4H), 1.44–1.38 (m, 2H).
¹³C-NMR (MeOD, 100 MHz): δ 130.6, 126.7, 122.7, 122.3, 115.9, 71.6, 71.5, 71.2, 70.5, 70.3, 63.4, 62.3, 61.6, 57.0, 51.5, 41.0, 40.3, 36.7, 29.7, 29.5, 26.8, 21.3. Three signals not observed/coincident.

IR ν_{\max} (neat): 3404, 2474, 2244, 2214, 2138, 2071, 1125, 1093 cm⁻¹.

HRMS (ESI): C₂₇H₄₁N₆O₅S [M+H]⁺ calculated 561.2854, found 561.2841.

4.85a: *tert*-butyl-*N*₂-(4-(((2-amino-4-oxo-1,4-dihydropteridin-6-yl)methyl)amino)benzoyl)-*N*₅-(3-(4-(5,6-dimethyl-1*H*-benzo[*d*]imidazol-1-yl)-1*H*-1,2,3-triazol-1-yl)propyl)-*L*-glutamate



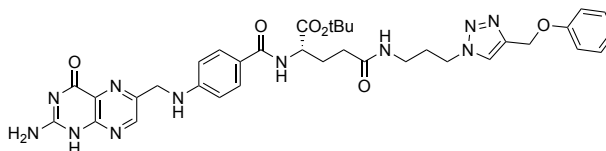
Prepared using General Procedure A (0.1 mmol scale). Yellow oil (45 mg, 60%). Purification on ISOLUTE Flash SCX-2 10g using NH₃ 7 M in MeOH. Purity of resultant product was assessed by analytical HPLC (Phenomenex C18, 250 × 4.6 mm) at a flow rate of 1 mL/min over 35 min.

RP-HPLC R_T = 21.2 min.

IR ν_{\max} (neat): 3493, 2251, 2125, 2062, 1126, 1056, 1026, 1007 cm⁻¹.

HRMS (ESI): C₃₇H₄₄N₁₃O₅ [M+H]⁺ calculated 750.3583, found 750.3573.

4.85b: *tert*-butyl *N*₂-(4-(((2-amino-4-oxo-1,4-dihydropteridin-6-yl)methyl)amino)benzoyl)-*N*₅-(3-(4-(phenoxy)methyl)-1*H*-1,2,3-triazol-1-yl)propyl)-*L*-glutamate



Prepared using General Procedure A (0.1 mmol scale). Yellow oil (40 mg, 56%). Purification on ISOLUTE Flash SCX-2 10g using NH₃ 7 M in MeOH. Purity of resultant product was

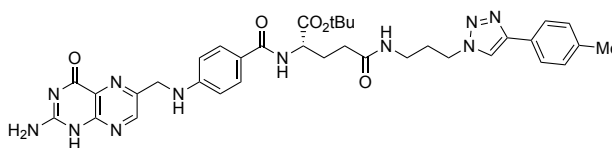
assessed by analytical HPLC (Phenomenex C18, 250 × 4.6 mm) at a flow rate of 1 mL/min, gradient 10–60% MeCN/0.1% TFA over 35 min.

RP-HPLC R_T = 23.0 min.

IR ν_{\max} (neat): 3415, 2519, 2253, 2125, 2063, 1126, 1054, 1026, 1007 cm^{-1} .

HRMS (ESI): $\text{C}_{35}\text{H}_{42}\text{N}_{11}\text{O}_6$ $[\text{M}+\text{H}]^+$ calculated 712.3314, found 712.1180.

4.85c: *tert*-butyl N_2 -(4-(((2-amino-4-oxo-1,4-dihydropteridin-6-yl)methyl)amino)benzoyl)- N_5 -(3-(4-(*p*-tolyl)-1*H*-1,2,3-triazol-1-yl)propyl)-*L*-glutamate



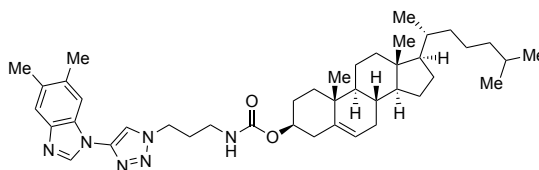
Prepared using General Procedure A (0.1 mmol scale). Yellow oil (38 mg, 54%). Purification on ISOLUTE Flash SCX-2 10g using NH_3 7 M in MeOH. Purity of resultant product was assessed by analytical HPLC (Phenomenex C18, 250 × 4.6 mm) at a flow rate of 1 mL/min, gradient 10–60% MeCN/0.1% TFA over 35 min.

RP-HPLC R_T = 25.5 min.

IR ν_{\max} (neat): 3437, 2498, 2257, 2132, 2069, 1461, 1217, 1125, 1050, 1026 cm^{-1} .

HRMS (ESI): $\text{C}_{35}\text{H}_{42}\text{N}_{11}\text{O}_5$ $[\text{M}+\text{H}]^+$ calculated 696.3365, found 696.3374.

4.86a: (1*R*,3*S*,8*R*,9*S*,13*R*,14*S*)-1,13-dimethyl-17-((*R*)-6-methylheptan-2-yl)-2,3,4,7,8,9,10,11,12,13,14,15,16,17-tetradecahydro-1*H*-cyclopenta[*a*]phenanthren-3-yl (3-(4-(5,6-dimethyl-1*H*-benzo[*d*]imidazol-1-yl)-1*H*-1,2,3-triazol-1-yl)propyl)carbamate



Prepared using General Procedure A (0.1 mmol scale in 3/3/1 MeCN/*t*BuOH/ H_2O). Yellow oil (59 mg, 87%). Purification on silica gel using 7/3 PE/EtOAc.

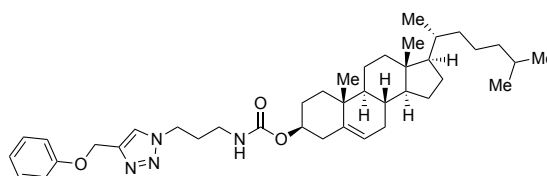
$^1\text{H-NMR}$ (CDCl_3 , 500 MHz): δ 8.08–7.65 (m, 4H), 5.32 (s, 1H), 5.10 (br. s, 1H), 4.53 (br. s, 2H), 4.47 (br. s, 1H), 3.27 (br. s, 2H), 2.38 (d, J = 16.7 Hz, 6H), 2.33–2.19 (m, 4H), 2.00–1.96 (m, 2H), 1.84–1.79 (m, 4H), 1.55–1.41 (m, 8H), 1.34–1.32 (m, 3H), 1.26–1.23 (m, 1H), 1.14–1.07 (m, 7H), 0.97 (s, 3H), 0.90 (d, J = 6.9 Hz, 3H), 0.85 (dd, J = 6.6, 2.2 Hz, 6H), 0.66 (s, 3H).

$^{13}\text{C-NMR}$ (CDCl_3 , 100 MHz) 156.7, 139.7, 133.8, 131.9, 12.7, 114.6, 74.9, 56.8, 56.2, 50.1, 48.5, 42.4, 39.8, 39.6, 38.6, 37.7, 37.0, 36.6, 36.3, 35.9, 32.0, 31.9, 30.8, 28.3, 28.2, 28.1, 24.4, 23.9, 22.9, 22.7, 21.1, 20.6, 20.4, 19.4, 18.8, 11.9. Six signals not observed/coincident.

IR ν_{max} (neat): 3400, 3127, 2935, 2867, 1690 1595, 1496, 1439, 1271, 1257, 1152, 1017 cm^{-1} .

HRMS (ESI): $\text{C}_{42}\text{H}_{63}\text{N}_6\text{O}_2$ $[\text{M}+\text{H}]^+$ calculated 683.5007, found 683.5000.

4.86b: (1*R*,3*S*,8*R*,9*S*,13*R*,14*S*)-1,13-dimethyl-17-((*R*)-6-methylheptan-2-yl)-2,3,4,7,8,9,10,11,12,13,14,15,16,17-tetradecahydro-1*H*-cyclopenta[*a*]phenanthren-3-yl (3-(4-(phenoxyethyl)-1*H*-1,2,3-triazol-1-yl)propyl)carbamate



Prepared using General Procedure A (0.1 mmol scale in 3/3/1 MeCN/*t*BuOH/ H_2O). Yellow oil (59 mg, 92%). Purification on silica gel using 8/2 PE/EtOAc.

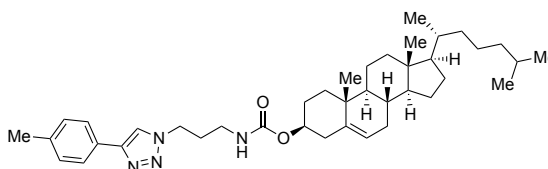
$^1\text{H-NMR}$ (CDCl_3 , 400 MHz): δ 7.73 (br. s, 1H), 7.28–7.26 (m, 2H), 6.98 (br. s, 2H), 5.37 (br. s, 1H), 5.22 (br. s, 1H), 4.92 (br. s, 1H), 4.45 (br. s, 2H), 3.20 (br. s, 2H), 2.34–2.27 (m, 2H), 2.13–1.83 (m, 8H), 1.56–1.43 (m, 7H), 1.33–1.25 (m, 5H), 1.15–1.10 (m, 7H), 1.00 (s, 6H), 0.91 (d, $J = 6.1$ Hz, 3H), 0.86 (d, $J = 6.2$ Hz, 6H), 0.67 (s, 3H).

$^{13}\text{C-NMR}$ (CDCl_3 , 100 MHz): δ 158.4, 156.5, 139.8, 129.7, 122.7, 121.4, 114.9, 74.7, 62.1, 56.9, 56.3, 50.1, 47.8, 42.4, 39.9, 39.6, 38.7, 37.8, 37.1, 36.7, 36.3, 35.9, 32.0, 31.9, 30.8, 28.3, 28.2, 28.1, 24.4, 24.0, 22.9, 22.7, 21.2, 19.4, 18.8, 12.0. One signal not observed/coincident.

IR ν_{max} (neat): 3369, 3341, 2930, 2863, 2091, 1692, 1599, 1439, 1223, 1046 cm^{-1} .

HRMS (ESI): $\text{C}_{40}\text{H}_{61}\text{N}_4\text{O}_3$ $[\text{M}+\text{H}]^+$ calculated 645.4738, found 645.4731.

4.86c: (1*R*,3*S*,8*R*,9*S*,13*R*,14*S*)-1,13-dimethyl-17-((*R*)-6-methylheptan-2-yl)-2,3,4,7,8,9,10,11,12,13,14,15,16,17-tetradecahydro-1*H*-cyclopenta[*a*]phenanthren-3-yl (3-(4-(*p*-tolyl)-1*H*-1,2,3-triazol-1-yl)propyl)carbamate



Prepared using General Procedure A (0.1 mmol scale in 3/3/1 MeCN/*t*BuOH/H₂O). Yellow oil (54 mg, 86%). Purification on silica gel using 9/1 PE/EtOAc.

¹H-NMR (CDCl₃, 400 MHz): δ 7.81 (br. s, 1H), 7.70 (d, *J* = 8.2 Hz, 2H), 7.21 (d, *J* = 8.2 Hz, 2H), 5.35–5.34 (m, 1H), 5.01 (t, *J* = 5.5 Hz, 1H), 4.45 (t, *J* = 6.7 Hz, 3H), 3.21 (q, *J* = 6.0 Hz, 2H), 2.37 (s, 3H), 2.33–2.21 (m, 2H), 2.13 (app. quint, *J* = 6.5 Hz, 2H), 2.02–1.92 (m, 2H), 1.86–1.80 (m, 3H), 1.58–1.44 (m, 7H), 1.42–1.40 (m, 1H), 1.38–1.33 (m, 3H), 1.33–1.24 (m, 2H), 1.16–1.05 (m, 9H), 0.98 (s, 3H), 0.91 (d, *J* = 6.5 Hz, 3H), 0.86 (dd, *J* = 6.6, 1.8 Hz, 6H), 0.67 (s, 3H).

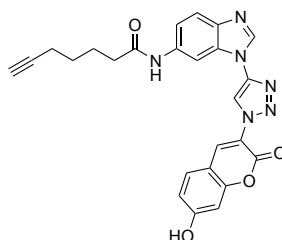
¹³C-NMR (CDCl₃, 100 MHz): δ 156.5, 148.1, 139.9, 138.1, 129.6, 127.9, 125.7, 122.6, 119.7, 74.7, 56.8, 56.3, 50.1, 47.8, 42.4, 39.8, 39.6, 38.6, 37.9, 37.1, 36.6, 36.3, 35.9, 32.0, 31.9, 30.8, 28.3, 28.2, 28.1, 24.4, 23.9, 22.9, 22.7, 21.4, 21.1, 19.4, 18.8, 12.0.

IR ν_{\max} (neat): 3350, 3331, 2935, 2867, 1693, 1532, 1465, 1437, 1366, 1253, 1033 cm⁻¹.

HRMS (ESI): C₄₀H₆₁N₄O₂ [M+H]⁺ calculated 629.4789, found 629.4789.

4.7.4.2 Products from Scheme 4.19

4.S1: *N*-(1-(1-(7-hydroxy-2-oxo-2*H*-chromen-3-yl)-1*H*-1,2,3-triazol-4-yl)-1*H*-benzo[*d*]imidazol-6-yl)hept-6-ynamide



Prepared using General Procedure A (0.2 mmol scale). Yellow oil (91 mg, 75%). Purification on silica gel using 9/1 DCM/MeOH + 2% NEt₃.

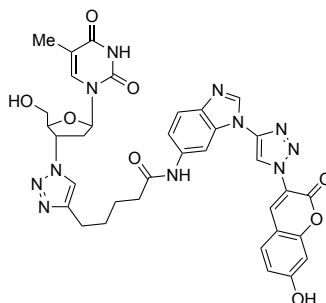
¹H-NMR (DMSO-*d*₆, 500 MHz): δ 10.08 (br. s, 1H), 9.10 (br. s, 1H), 8.72 (br. s, 1H), 8.46 (br. s, 1H), 7.78 (br. s, 2H), 7.45 (br. s, 1H), 6.88 (br. s, 2H), 2.35 (br. s, 1H), 2.19 (br. s, 2H), 2.07 (br. s, 1H), 1.69 (br. s, 2H), 1.50 (br. s, 2H), 1.31 (br. s, 2H). One proton under D₂O peak, see COSY in Supplementary Figure S114.

¹³C-NMR could not be obtained due to relaxation issues.

IR ν_{\max} (neat): 3447, 2251, 2125, 1656, 1054, 1026, 1007 cm⁻¹.

HRMS (ESI): C₂₅H₂₁N₆O₄ [M+H]⁺ calculated 469.1619, found 469.1620.

4.87: *N*-(1-(1-(7-hydroxy-2-oxo-2*H*-chromen-3-yl)-1*H*-1,2,3-triazol-4-yl)-1*H*-benzo[*d*]imidazol-6-yl)-5-(1-((2*S*,3*S*,5*R*)-2-(hydroxymethyl)-5-(5-methyl-2,4-dioxo-3,4-dihydropyrimidin-1(2*H*)-yl)tetrahydrofuran-3-yl)-1*H*-1,2,3-triazol-4-yl)pentanamide



Prepared using General Procedure A (0.1 mmol scale). Brown oil (55 mg, 75%). Purification on silica gel using 9/1 DCM/MeOH + 2% NEt₃.

¹H-NMR (DMSO-*d*₆, 500 MHz): δ 11.35 (br. s, 1H), 10.08 (br. s, 1H), 9.11–8.73 (m, 2H), 8.53–8.31 (m, 1H), 8.05–7.67 (m, 3H), 7.55–7.45 (m, 1H), 7.88–7.83 (m, 2H), 6.49–6.40 (m, 1H), 5.52–5.30 (m, 2H), 4.38–4.19 (m, 1H), 3.84–3.68 (m, 2H), 3.61–3.60 (m, 1H), 2.86–2.62 (m, 4H), 2.39–2.38 (m, 2H), 1.83–1.80 (m, 3H), 1.78–1.66 (m, 4H). Two protons under D₂O peak, see COSY in Supplementary Figure S114.

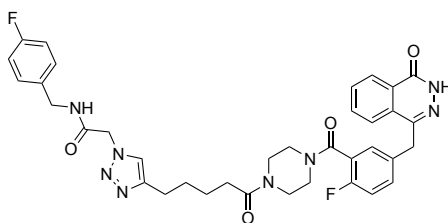
¹³C-NMR could not be obtained due to relaxation issues.

IR ν_{max} (neat): 3443, 2251, 2125, 1682, 1612, 1054, 1026, 1007 cm⁻¹.

HRMS (ESI): C₃₅H₃₄N₁₁O₈ [M+H]⁺ calculated 736.2586, found 736.2595.

4.7.4.3 Product from Scheme 4.21

4.94: 2-(4-(5-(4-(2-fluoro-5-((4-oxo-3,4-dihydrophthalazin-1-yl)methyl)benzoyl)piperazin-1-yl)-5-oxopentyl)-1*H*-1,2,3-triazol-1-yl)-*N*-(4-fluorobenzyl)acetamide



Prepared using General Procedure A (0.1 mmol scale at 3 mL/min). Yellow oil (59 mg, 86%). No purification needed.

¹H-NMR (CDCl₃, 400 MHz): δ 8.42–8.36 (m, 1H), 7.78–7.68 (m, 3H), 7.51 (d, *J* = 9.8 Hz, 1H), 7.31–7.30 (m, 2H), 7.25–7.23 (m, 1H), 7.17–7.13 (m, 2H), 7.06–6.99 (m, 2H), 6.95–6.87

(m, 2H), 5.06 (d, $J = 16.8$ Hz, 2H), 4.42 (d, $J = 6.1$ Hz, 1H), 4.36–4.34 (m, 2H), 4.28 (s, 2H), 4.03 (s, 1H), 3.72–3.67 (m, 2H), 3.52–3.49 (m, 1H), 3.46–3.43 (m, 1H), 3.33–3.23 (m, 2H), 2.75–2.69 (m, 2H), 2.36–2.32 (m, 2H), 1.73–1.64 (m, 4H);

$^{19}\text{F-NMR}$ (CDCl_3 , 376 MHz) δ -114.5, -114.7, -117.8, -118.0.

$^{13}\text{C-NMR}$ could not be obtained due to relaxation issues.²⁸⁶

IR ν_{max} (neat): 3296, 3071, 2926, 2865, 1638, 1511, 1437, 1225 cm^{-1} .

HRMS (ESI): $\text{C}_{36}\text{H}_{37}\text{F}_2\text{N}_8\text{O}_4$ $[\text{M}+\text{H}]^+$ calculated 683.2900, found 683.2891.

4.7.5 Characterisation of ODNs

Alkyne modified **ODN4.1-3** were prepared using General Procedure B, purified by preparative RP-HPLC and characterised by MALDI-TOF MS and analytical RP-HPLC.

ODN4.1: $\text{C}_{130}\text{H}_{166}\text{N}_{24}\text{O}_{85}\text{P}_{12}$ MW 3796.53 g/mol.

MALDI-TOF MS (+ve mode; matrix 3-hydroxypicolinic acid) m/z $[\text{M}+\text{H}]^+$ found 3797.66.

RP-HPLC $R_T = 20.5$ min.

ODN4.2: $\text{C}_{130}\text{H}_{165}\text{N}_{27}\text{O}_{84}\text{P}_{12}$ MW 3821.54 g/mol.

MALDI-TOF MS (+ve mode; matrix 3-hydroxypicolinic acid) m/z $[\text{M}+\text{H}]^+$ found 3821.57.

RP-HPLC $R_T = 19.1$ min.

ODN4.3: $\text{C}_{127}\text{H}_{158}\text{N}_{42}\text{O}_{75}\text{P}_{12}$ MW 3844.57 g/mol.

MALDI-TOF MS (+ve mode; matrix 3-hydroxypicolinic acid) m/z $[\text{M}+\text{H}]^+$ found 3844.72.

RP-HPLC $R_T = 16.3$ min.

Triazole **ODN4.4-6** were prepared using General Procedure C and characterised by MALDI-TOF MS and analytical RP-HPLC.

ODN4.4 (4.95a): $\text{C}_{145}\text{H}_{185}\text{N}_{29}\text{O}_{87}\text{P}_{12}\text{S}$ MW 4129.94 g/mol.

MALDI-TOF MS (+ve mode; matrix 3-hydroxypicolinic acid) m/z $[\text{M}+\text{H}]^+$ found 4130.83.

RP-HPLC $R_T = 25.7$ min.

ODN4.5 (4.95b): $\text{C}_{145}\text{H}_{184}\text{N}_{32}\text{O}_{86}\text{P}_{12}\text{S}$ MW 4154.95 g/mol.

MALDI-TOF MS (+ve mode; matrix 3-hydroxypicolinic acid) m/z $[\text{M}+\text{H}]^+$ found 4155.26.

RP-HPLC $R_T = 25.6$ min.

ODN4.6 (4.95c): C₁₄₂H₁₇₇N₄₇O₇₇P₁₂S MW 4177.96 g/mol.

MALDI-TOF MS (+ve mode; matrix 3-hydroxypicolinic acid) *m/z* [M+H]⁺ found 4178.88.

RP-HPLC R_T= 23.4 min.

4.7.6 Characterisation of Peptides

Alkyne modified peptides **4.96a-e** were prepared using General Procedure D, purified by preparative RP-HPLC and characterised by MALDI-TOF MS, ESI-HRMS and analytical RP-HPLC.

4.96a: C₆₇H₁₂₆N₂₆O₁₂ MW 1487.92 g/mol.

MALDI-TOF MS (+ve mode; matrix α-cyano-4-hydroxycinnamic acid) *m/z* [M+H]⁺ found 1487.96.

HRMS (ESI) (+ve mode) *m/z* [M/2+H]⁺ calculated 744.5097, found 744.5083.

RP-HPLC R_T= 19.7 min.

4.96b: C₇₀H₁₃₁N₂₇O₁₃S MW 1591.05 g/mol.

MALDI-TOF MS (+ve mode; matrix α-cyano-4-hydroxycinnamic acid) *m/z* [M+H]⁺ found 1590.97.

HRMS (ESI) (+ve mode) *m/z* [M/2+H]⁺ calculated 796.0143, found 796.0129.

RP-HPLC R_T= 21.0 min.

4.96c: C₇₂H₁₃₅N₂₇O₁₃S MW 1619.11 g/mol.

MALDI-TOF MS (+ve mode; matrix α-cyano-4-hydroxycinnamic acid) *m/z* [M+H]⁺ found 1619.01.

HRMS (ESI) (+ve mode) *m/z* [M/2+H]⁺ calculated 810.0299, found 810.0282.

RP-HPLC R_T= 22.5 min.

4.96d: C₇₃H₁₃₃N₂₉O₁₃ MW 1625.06 g/mol.

MALDI-TOF MS (+ve mode; matrix α-cyano-4-hydroxycinnamic acid) *m/z* [M+H]⁺ found 1625.04.

HRMS (ESI) (+ve mode) *m/z* [M/2+H]⁺ calculated 813.0392, found 813.0376.

RP-HPLC R_T= 18.1 min.

4.96e: C₇₆H₁₃₅N₂₇O₁₄ MW 1651.09 g/mol.

MALDI-TOF MS (+ve mode; matrix α -cyano-4-hydroxycinnamic acid) m/z [M+H]⁺ found 1651.02.

HRMS (ESI) (+ve mode) m/z [M/2+H]⁺ calculated 826.0414, found 826.0395.

RP-HPLC R_T= 21.7 min.

Triazole peptides **4.97a-e** were prepared using General Procedure C and characterised by MALDI-TOF MS, ESI-HRMS and analytical RP-HPLC.

4.97a: C₈₂H₁₄₅N₃₁O₁₄S MW 1821.33 g/mol.

MALDI-TOF MS (+ve mode; matrix α -cyano-4-hydroxycinnamic acid) m/z [M+H]⁺ found 1821.09.

HRMS (ESI) (+ve mode) m/z [M/2+H]⁺ calculated 911.0727, found 911.5724.

RP-HPLC R_T= 22.5 min.

4.97b: C₈₅H₁₅₀N₃₂O₁₅S₂ MW 1924.46 g/mol.

MALDI-TOF MS (+ve mode; matrix α -cyano-4-hydroxycinnamic acid) m/z [M+H]⁺ found 1924.19.

HRMS (ESI) (+ve mode) m/z [M/2+H]⁺ calculated 962.5772, found 962.5773.

RP-HPLC R_T= 23.6 min.

4.97c: C₈₇H₁₅₄N₃₂O₁₅S₂ MW 1952.52 g/mol.

MALDI-TOF MS (+ve mode; matrix α -cyano-4-hydroxycinnamic acid) m/z [M+H]⁺ found 1952.21.

HRMS (ESI) (+ve mode) m/z [M/2+H]⁺ calculated 976.5929, found 977.0945.

RP-HPLC R_T= 24.9 min.

4.97d: C₈₈H₁₅₂N₃₄O₁₅S MW 1958.47 g/mol.

MALDI-TOF MS (+ve mode; matrix α -cyano-4-hydroxycinnamic acid) m/z [M+H]⁺ found 1958.17.

HRMS (ESI) (+ve mode) m/z [M/2+H]⁺ calculated 979.6021, found 980.1034.

RP-HPLC R_T= 21.0 min.

4.97c: C₉₁H₁₅₄N₃₂O₁₆S MW 1984.50 g/mol.

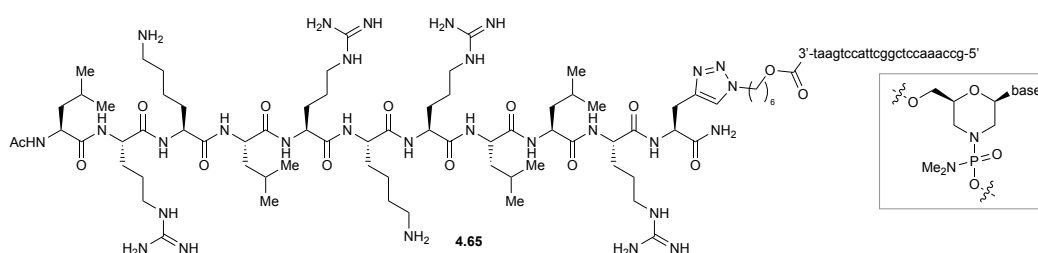
MALDI-TOF MS (+ve mode; matrix α -cyano-4-hydroxycinnamic acid) m/z [M+H]⁺ found 1984.17.

HRMS (ESI) (+ve mode) m/z [M/2+H]⁺ calculated 992.6043, found 993.1051.

RP-HPLC R_T= 24.1 min.

4.7.7 Peptide-PMO Conjugate Synthesis and Characterisation Data

ApoE-PMO (**4.65**)²⁸⁰



PMO azide **4.98** (10 μ L, 10 nmol, 1 equiv.), peptide **4.96a** (20 μ L, 100 nmol, 10 equiv.) and 3-methylbenzo[*d*]thiazol-3-ium **4.70** (1.0 mg, 1000 nmol, 100 equiv.) were dissolved in of 5/1 MeCN/H₂O (50 μ L). CuAAC reaction was carried out in a commercial chemical flow reactor equipped with a 2 mL copper reactor (easy-Scholar from Vapourtec) at a flow rate of 1 mL/min at 37 °C. The reaction mixture was collected after 15 cycles through the reactor and lyophilised. The residue was suspended in H₂O and subjected to a round of spin concentration using spin concentration Vivaspin 500 (Sartorius) for 30 min at 13.5 rpm, affording the expected conjugate **4.65** with 60% yield. The yield was calculated by measuring the absorbance of the product and the purity assessed by analytical HPLC (Phenomenex C18, 250 \times 4.6 mm) at a flow rate of 1 mL/min, gradient 5–20% MeCN/0.1% TFA over 35 min.

4.65: C₃₆₉H₆₀₀N₁₇₅O₁₁₃P₂₅ MW 10070.32 g/mol.

MALDI-TOF MS (+ve mode; matrix sinapinic acid) m/z [M+H]⁺ found 10070.49.

RP-HPLC R_T= 7.81 min.

Chapter 5

Future Directions Towards the Development of Aromatic Ynamines as Novel, Bio-orthogonal Reactive Groups for CuAAC Bioconjugation

Bio-orthogonal chemistry has become an indispensable tool in for the investigation of living systems. Although extensive efforts have been made to advance current strategies, all have been hindered by inherent limitations. Some of the current chemistries are not truly bio-orthogonal, competing with the reactivities of native nucleophiles (*e.g.*, cysteine, lysine, glutathione) and resulting in the formation of undesired side-products. Even those that can claim bio-orthogonality are hindered; limited by the structural features of cells and biomolecules. Scaffold size and chemical characteristics often impair cellular uptake and probe affinity, leading to lower effective concentrations. In order to combat these issues, research has focused on increasing the kinetics of different bioconjugation strategies; however, few display better kinetics than native thiol/maleimide conjugation ($734 \text{ M}^{-1} \text{ s}^{-1}$).¹⁰⁹ Finally, cross-reactivity between the different strategies prevents their use in sequential ligations.

CuAAC ligation remains the gold-standard for bioconjugation. It is one of the very few bio-orthogonal cycloadditions that combines the formation of a single product with rapid kinetics and minimal perturbation of living systems. Unfortunately, the toxicity associated with the use of copper remains a considerable limitation of this strategy. The initial hypothesis of this project was that modifying the reactivity of the alkyne surrogate, using an aromatic ynamine functional group, would (i) increase the reaction rate and therefore decrease biomolecule/catalyst interaction times, (ii) reduce copper loading and (iii) modulate chemoselectivity to allow sequential bioconjugation.

This thesis describes the preparation and application of aromatic ynamines as novel, bio-orthogonal reactive groups for CuAAC ligations of both small and large molecules. Aromatic ynamines were rapidly prepared *via* microwave-assisted synthesis (5 to 20 min). The enhanced reactivity of aromatic ynamines allowed for the development of a new, orthogonal, chemoselective CuAAC platform which functioned both inter- and intra-molecularly. A silyl protecting group was capable of temporally disguising reactivity of the aromatic ynamine, therefore improving the modularity of this system.

Aromatic ynamines are easily incorporated into oligodeoxyribonucleotides (ODNs) in both internal and terminal positions. CuAAC bioconjugation of ODNs using aromatic ynamines is fast (2 h versus 16 h for conventional alkynes) and high yielding with a wide range of azides. More importantly, the enhanced reactivity of aromatic ynamines permits the reduction of copper loading to a catalytic amount (10 mol %) as opposed to the supra-stoichiometric amount required with conventional alkynes.^{60,61} This represents an enormous advantage as it

allows CuAAC ligations to be performed under conditions favourable for biomolecules.⁸¹ This reactivity difference between aromatic ynamines and aromatic alkynes is conserved for biomolecule conjugation, providing a new platform for the chemoselective, sequential bioconjugation of ODNs. Importantly, the incorporation of aromatic ynamines into DNA does not alter DNA structure, rendering this functional group ideal for ODN bioconjugation.

This thesis culminates in the development of a rapid and mild continuous flow platform for CuAAC ligations using a copper reactor. Benefits of this platform include the use of mild conditions (room temperature, ambient pressure) and the omission of additives. Importantly, no additional catalyst was required, and ICP-MS analysis of final products measured extremely low copper concentrations (< 15 ppm), minimising toxicity. The efficiency of this platform was demonstrated for the ligation of small molecules (≤ 10 min) and the ligation of a PARP1 inhibitor to a PET probe mimic (3 min). Furthermore, this platform provided for the fast conjugation of biomolecules, such as oligonucleotides (≤ 1 min) and peptides (≤ 8 min), without degradation of even the most oxidation-sensitive substrates. Finally, the utility of this platform was demonstrated for the mild, fast and degradation-free bioconjugation of an azide-modified PMO with an alkyne-modified CPP (30 min).

This work develops a next generation platform for fast, mild and efficient bioconjugation. The use of aromatic ynamines and flow chemistry allows the formation of bioconjugates at extremely low copper loading, thus avoiding biomolecule degradation.

Further developments of this work include:

- (i) Extending the use of aromatic ynamines to the bioconjugation of peptides and proteins by incorporating an ynamine moiety into a peptide/protein via unnatural amino acids.
- (ii) Expanding the repertoire of DNA/RNA-labelling alkynes, such as EdU, to include the more reactive aromatic ynamines.
- (iii) Developing a FRET platform for metal qualification/quantification derived from its chelation by aromatic ynamines (Figure 5.1).

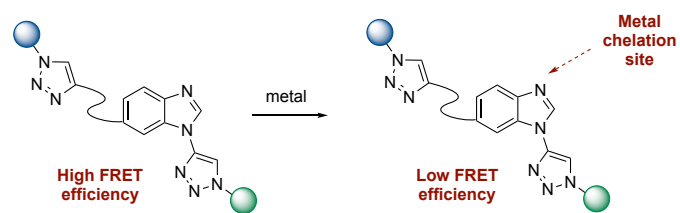


Figure 5.1. Establishment of a FRET platform for metal detection.

References

- (1) Fleischmann, R. D.; Adams, M. D.; White, O.; Clayton, R. A.; Ewen, F.; Kerlavage, A. R.; Bult, C. J.; Tomb, J.; Dougherty, B. A.; Merrick, J. M.; Mckenney, K.; Sutton, G.; Fitzhugh, W.; Fields, C.; Gocayne, J. D.; Scott, J.; Shirley, R.; Liu, L.; Glodek, A.; Jenny, M.; Weidman, J. F.; Phillips, C. A.; Spriggs, T.; Hedblom, E.; Matthew, D.; Utterback, T. R.; Hanna, M. C.; Nguyen, D. T.; Saudek, D. M.; Brandon, R. C.; Fine, L. D.; Fritchman, J. L.; Fuhrmann, J. L.; Gnehm, C. L.; McDonald, L. A.; Small, K. V.; Fraser, C. M.; Smith, H. O.; Venter, J. C. "Whole-Genome Random Sequencing and Assembly of Haemophilus Influenzae Rd." *Science* (80-.). **1995**, *269*, 496–512.
- (2) McPherson, A. "A Brief History of Protein Crystal Growth." *J. Cryst. Growth* **1991**, *110*, 1–10.
- (3) Tsien, R. Y. "The Green Fluorescent Protein." *Annu. Rev. Biochem.* **1998**, *67*, 509–544.
- (4) Peng, L.; Chen, X. "Antibody-Drug Conjugates." *Bioconjug. Chem.* **2015**, *26*, 2169.
- (5) Agarwal, P.; Bertozzi, C. R. "Site-Specific Antibody-Drug Conjugates: The Nexus of Bioorthogonal Chemistry, Protein Engineering, and Drug Development." *Bioconjug. Chem.* **2015**, *26*, 176–192.
- (6) Gunnoo, S. B.; Madder, A. "Bioconjugation – Using Selective Chemistry to Enhance the Properties of Proteins and Peptides as Therapeutics and Carriers." *Org. Biomol. Chem.* **2016**, *14*, 8002–8013.
- (7) Sen Gupta, A.; Von Recum, H. A. "*Organic Nanoparticles Based Bioconjugates*"; 2014.
- (8) Li, F.; Mahato, R. I. "Bioconjugate Therapeutics: Current Progress and Future Perspective." *Mol. Pharm.* **2017**, *14*, 1321–1324.
- (9) Cui, L.; Rao, J. "*Chemical Methodology for Labelling and Bioconjugation*"; 2015.
- (10) Sletten, E. M.; Bertozzi, C. R. "Bioorthogonal Chemistry: Fishing for Selectivity in a Sea of Functionality." *Angew. Chemie - Int. Ed.* **2009**, *48*, 6974–6998.
- (11) Güell, O. "*A Network-Based Approach to Cell Metabolism*"; 2017.
- (12) Schatz, G.; Dobberstein, B. "Common Principles of Protein Translocation across Membranes." *Science* (80-.). **1996**, *271*, 1519–1526.
- (13) DeGruyter, J. N.; Malins, L. R.; Baran, P. S. "Residue-Specific Peptide Modification: A Chemist's Guide." *Biochemistry* **2017**, *56*, 3863–3873.
- (14) Junutula, J. R.; Raab, H.; Clark, S.; Bhakta, S.; Leipold, D. D.; Weir, S.; Chen, Y.; Simpson, M.; Tsai, S. P.; Dennis, M. S.; Lu, Y.; Meng, Y. G.; Ng, C.; Yang, J.; Lee, C. C.; Duenas, E.; Gorrell, J.; Katta, V.; Kim, A.; McDorman, K.; Flagella, K.; Venook, R.; Ross, S.; Spencer, S. D.; Lee Wong, W.; Lowman, H. B.; Vandlen, R.; Sliwkowski,

- M. X.; Scheller, R. H.; Polakis, P.; Mallet, W. "Site-Specific Conjugation of a Cytotoxic Drug to an Antibody Improves the Therapeutic Index." *Nat. Biotechnol.* **2008**, *26*, 925–932.
- (15) Perols, A.; Honarvar, H.; Strand, J.; Selvaraju, R.; Orlova, A.; Eriksson Karlström, A.; Tolmachev, V. "Influence of DOTA Chelator Position on Biodistribution and Targeting Properties of ¹¹¹In-Labeled Synthetic Anti-HER2 Affibody Molecules." *Bioconjug. Chem.* **2012**, *23*, 1661–1670.
- (16) Means, G. E.; Feeney, R. E. "Chemical Modifications of Proteins: History and Applications." *Bioconjug. Chem.* **1990**, *1*, 2–12.
- (17) Algar, W. R. "A Brief Introduction to Traditional Bioconjugate Chemistry"; 2017.
- (18) Koniev, O.; Wagner, A. "Developments and Recent Advancements in the Field of Endogenous Amino Acid Selective Bond Forming Reactions for Bioconjugation." *Chem. Soc. Rev.* **2015**, *44*, 5495–5551.
- (19) Chalker, J. M.; Bernardes, G. J. L.; Lin, Y. A.; Davis, B. G. "Chemical Modification of Proteins at Cysteine: Opportunities in Chemistry and Biology." *Chem. - An Asian J.* **2009**, *4*, 630–640.
- (20) McKay, C. S.; Finn, M. G. "Click Chemistry in Complex Mixtures: Bioorthogonal Bioconjugation." *Chem. Biol.* **2014**, *21*, 1075–1101.
- (21) Baldwin, A. D.; Kiick, K. L. "Tunable Degradation of Maleimide - Thiol Adducts in Reducing Environments." *Bioconjug. Chem.* **2011**, *22*, 1946–1953.
- (22) Veredas, F. J.; Cantón, F. R.; Aledo, J. C. "Methionine Residues around Phosphorylation Sites Are Preferentially Oxidized in Vivo under Stress Conditions." *Sci. Rep.* **2017**, *7*, 1–14.
- (23) Kramer, J. R.; Deming, T. J. "Preparation of Multifunctional and Multireactive Polypeptides via Methionine Alkylation." *Biomacromolecules* **2012**, *13*, 1719–1723.
- (24) Gharakhanian, E. G.; Deming, T. J. "Versatile Synthesis of Stable, Functional Polypeptides via Reaction with Epoxides." *Biomacromolecules* **2015**, *16*, 1802–1806.
- (25) Lin, S.; Yang, X.; Jia, S.; Weeks, A. M.; Hornsby, M.; Lee, P. S.; Nichiporuk, R. V.; Iavarone, A. T.; Wells, J. A.; Toste, F. D.; Chang, C. J. "Redox-Based Reagents for Chemoselective Methionine Bioconjugation." *Science (80-.)*. **2017**, *355*, 597–602.
- (26) Seim, K. L.; Obermeyer, A. C.; Francis, M. B. "Oxidative Modification of Native Protein Residues Using Cerium(IV) Ammonium Nitrate." *J. Am. Chem. Soc.* **2011**, *133*, 16970–16976.
- (27) Higgins, H. G.; Harrington, K. J. "Reaction of Amino Acids and Proteins with Diazonium Compounds. II. Spectra of Protein Derivatives." *Arch. Biochem. Biophys.*

- 1959, 85, 409–425.
- (28) McFarland, J. M.; Joshi, N. S.; Francis, M. B. “Characterization of a Three-Component Coupling Reaction on Proteins by Isotopic Labeling and Nuclear Magnetic Resonance Spectroscopy.” *J. Am. Chem. Soc.* **2008**, 130, 7639–7644.
- (29) Dawson, P. E.; Muir, T. W.; Clark-Lewis, I.; Kent, S. B. H. “Synthesis of Proteins by Native Chemical Ligation.” *Science (80-.)*. **1994**, 266, 776–779.
- (30) Hermanson, G. T. “*Functional Targets for Bioconjugation*”; 2013.
- (31) Ruhaak, L. R.; Zauner, G.; Huhn, C.; Bruggink, C.; Deelder, A. M.; Wuhrer, M. “Glycan Labeling Strategies and Their Use in Identification and Quantification.” *Anal. Bioanal. Chem.* **2010**, 397, 3457–3481.
- (32) Bode, J.; Goetze, S.; Heng, H.; Krawetz, S. A.; Benham, C. “From DNA Structure to Gene Expression: Mediators of Nuclear Compartmentalization and Dynamics.” *Chromosom. Res.* **2003**, 11, 435–445.
- (33) Morris, K. V; Mattick, J. S. “The Rise of Regulatory RNA.” *Nat. Rev. Genet.* **2014**, 15, 423–437.
- (34) Chu, B. C. F.; Wahl, G. M.; Orgel, L. E. “Derivatization of Unprotected Polynucleotides.” *Nucleic Acids Res.* **1983**, 11 (6513–6529).
- (35) Zamecnik, P. C.; Stephenson, M. L.; Scott, J. F. “Partial Purification of Soluble RNA.” *Proc. Natl. Acad. Sci. U. S. A.* **1960**, 46, 811–822.
- (36) Reese, C. B. “Oligo- and Poly-Nucleotides: 50 Years of Chemical Synthesis.” *Org. Biomol. Chem.* **2005**, 3, 3851–3868.
- (37) Singh, Y.; Murat, P.; Defrancq, E. “Recent Developments in Oligonucleotide Conjugation.” *Chem. Soc. Rev.* **2010**, 39, 2054–2070.
- (38) Row, R. D.; Prescher, J. A. “Constructing New Bioorthogonal Reagents and Reactions.” *Acc. Chem. Res.* **2018**, acs.accounts.7b00606.
- (39) Lang, K.; Chin, J. W. “Bioorthogonal Reactions for Labeling Proteins.” *ACS Chem. Biol.* **2014**, 9, 16–20.
- (40) Rideour, D. “Self-Assembling Cytotoxins.” *Science (80-.)*. **1986**, 233, 561–563.
- (41) Jacobs, C. L.; Yarema, K. J.; Mahal, L. K.; Nauman, D. A.; Charters, N. W.; Bertozzi, C. R. “Metabolic Labeling of Glycoproteins with Chemical Tags through Unnatural Sialic Acid Biosynthesis.” *Methods Enzymol.* **2000**, 327, 260–275.
- (42) Datta, D.; Wang, P.; Carrico, I. S.; Mayo, S. L.; Tirrell, D. A. “A Designed Phenylalanyl-TRNA Synthetase Variant Allows Efficient in Vivo Incorporation of Aryl Ketone Functionality into Proteins.” *J. Am. Chem. Soc.* **2002**, 124, 5652–5653.
- (43) Nauman, D. A.; Bertozzi, C. R. “Kinetic Parameters for Small-Molecule Drug Delivery

- by Covalent Cell Surface Targeting.” *Biochim. Biophys. Acta - Gen. Subj.* **2001**, *1568*, 147–154.
- (44) Staudinger, H.; Meyer, J. “Ueber Neue Organische Phosphorverbindungen III. Phosphinmethylenetivate Und Phosphinimine.” *Helv. Chim. Acta* **1919**, *2*, 635–646.
- (45) Saxon, E.; Bertozzi, C. R. “Cell Surface Engineering by a Modified Staudinger Reaction.” *Science (80-.)*. **2000**, *287*, 2007–2010.
- (46) Saxon, E.; Armstrong, J. I.; Bertozzi, C. R. “A ‘Traceless’ Staudinger Ligation for the Chemoselective Synthesis of Amide Bonds.” *Org. Lett.* **2000**, *2*, 2141–2143.
- (47) Van Berkel, S. S.; Van Eldijk, M. B.; Van Hest, J. C. M. “Staudinger Ligation as a Method for Bioconjugation.” *Angew. Chemie - Int. Ed.* **2011**, *50*, 8806–8827.
- (48) Tera, M.; Glasauer, S. M. K.; Luedtke, N. W. “In Vivo Incorporation of Azide Groups into DNA by Using Membrane-Permeable Nucleotide Triesters”. *ChemBioChem* **2018**, *19*, 1939–1943.
- (49) Ren, X.; El-Sagheer, A. H.; Brown, T. “Azide and Trans-Cyclooctene DUTPs: Incorporation into DNA Probes and Fluorescent Click-Labeling.” *Analyst* **2015**, *140*, 2671–2678.
- (50) Nainar, S.; Beasley, S.; Fazio, M.; Kubota, M.; Dai, N.; Corrêa, I. R.; Spitale, R. C. “Metabolic Incorporation of Azide Functionality into Cellular RNA.” *ChemBioChem* **2016**, *17*, 2149–2152.
- (51) Beatty, K. E.; Fisk, J. D.; Smart, B. P.; Lu, Y. Y.; Szychowski, J.; Hangauer, M. J.; Baskin, J. M.; Bertozzi, C. R.; Tirrell, D. A. “Live-Cell Imaging of Cellular Proteins by a Strain-Promoted Azide-Alkyne Cycloaddition.” *ChemBioChem* **2010**, *11*, 2092–2095.
- (52) Zhang, X.; Zhang, Y. “Applications of Azide-Based Bioorthogonal Click Chemistry in Glycobiology.” *Molecules* **2013**, *18*, 7145–7159.
- (53) Weisbrod, S. H.; Marx, A. “A Nucleoside Triphosphate for Site-Specific Labelling of DNA by the Staudinger Ligation.” *Chem. Commun.* **2007**, *18*, 1828–1830.
- (54) Liu, C. C.; Schultz, P. G. Adding New Chemistries to the Genetic Code. *Annu. Rev. Biochem.* **2010**, *79*, 413–444.
- (55) Yanagisawa, T.; Ishii, R.; Fukunaga, R.; Kobayashi, T.; Sakamoto, K.; Yokoyama, S. “Multistep Engineering of Pyrrolysyl-TRNA Synthetase to Genetically Encode Nε-(o-Azidobenzoyloxycarbonyl) Lysine for Site-Specific Protein Modification.” *Chem. Biol.* **2008**, *15*, 1187–1197.
- (56) Tam, A.; Soellner, M. B.; Raines, R. T. “Electronic and Steric Effects on the Rate of the Traceless Staudinger Ligation.” *Org. Biomol. Chem.* **2008**, *6*, 1173–1175.

- (57) Shih, H. W.; Prescher, J. A. "A Bioorthogonal Ligation of Cyclopropenones Mediated by Triarylphosphines." *J. Am. Chem. Soc.* **2015**, *137*, 10036–10039.
- (58) Row, R. D.; Shih, H. W.; Alexander, A. T.; Mehl, R. A.; Prescher, J. A. "Cyclopropenones for Metabolic Targeting and Sequential Bioorthogonal Labeling." *J. Am. Chem. Soc.* **2017**, *139*, 7370–7375.
- (59) Row, R. D.; Prescher, J. A. "A Cyclopropenethione-Phosphine Ligation for Rapid Biomolecule Labeling." *Org. Lett.* **2018**, *20*, 5614–5617.
- (60) Walters, C. R.; Szantai-Kis, D. M.; Zhang, Y.; Reinert, Z. E.; Horne, W. S.; Chenoweth, D. M.; Petersson, E. J. "The Effects of Thioamide Backbone Substitution on Protein Stability: A Study in α -Helical, β -Sheet, and Polyproline II Helical Contexts." *Chem. Sci.* **2017**, *8*, 2868–2877.
- (61) Choudhary, A.; Raines, R. T. "An Evaluation of Peptide-Bond Isosteres." *ChemBioChem* **2011**, *12*, 1801–1807.
- (62) Curtius, T. "Ueber Die Einwirkung von Salpetriger Saure Auf Salzauren Glycocollather." *Ber. Dtsch. Chem. Ges.* **1883**, *16*, 2230–2231.
- (63) Buchner, E. "Einwirkung von Diazoessigather Auf Die Aether Ungesattigter Säuren." *J. Chem. Inf. Model.* **1888**, *487*, 2637–2647.
- (64) Gothelf, K. V.; Jorgensen, K. A. "Asymmetric Metal-Catalyzed 1,3-Dipolar Cycloaddition Reactions." *Chem. Rev.* **1998**, *98*, 863–909.
- (65) Huisgen, R. "1,3-Dipolar Cycloadditions." *Proc. Chem. Soc.* **1961**, 357–396.
- (66) Huisgen, R. "Kinetics and Mechanism of 1,3-Dipolar Cycloadditions." *Angew. Chemie - Int. Ed.* **1963**, *2*, 633–645.
- (67) Rostovtsev, V. V.; Green, L. G.; Fokin, V. V.; Sharpless, K. B. "A Stepwise Huisgen Cycloaddition Process: Copper(I)-Catalyzed Regioselective 'ligation' of Azides and Terminal Alkynes." *Angew. Chemie - Int. Ed.* **2002**, *114*, 2708–2711.
- (68) Tornøe, C. W.; Christensen, C.; Meldal, M. "Peptidotriazoles on Solid Phase: [1,2,3]-Triazoles by Regiospecific Copper(I)-Catalyzed 1,3-Dipolar Cycloadditions of Terminal Alkynes to Azides." *J. Org. Chem.* **2002**, *67*, 3057–3064.
- (69) Himo, F.; Lovell, T.; Hilgraf, R.; Rostovtsev, V. V.; Noodleman, L.; Sharpless, K. B.; Fokin, V. V. "Copper(I)-Catalyzed Synthesis of Azoles. DFT Study Predicts Unprecedented Reactivity and Intermediates." *J. Am. Chem. Soc.* **2005**, *127*, 210–216.
- (70) Meldal, M.; Tomoe, C. W. "Cu-Catalyzed Azide - Alkyne Cycloaddition." *Chem. Rev.* **2008**, *108*, 2952–3015.
- (71) Binder, W. H.; Sachsenhofer, R. "Click Chemistry in Polymer and Materials Science." *Macromol. Rapid Commun.* **2007**, *28*, 15–54.

- (72) Lutz, J. F. "1,3-Dipolar Cycloadditions of Azides and Alkynes: A Universal Ligation Tool in Polymer and Materials Science." *Angew. Chemie - Int. Ed.* **2007**, *46*, 1018–1025.
- (73) Shih, H.-W.; Chen, K.-T.; Chen, S.-K.; Huang, C.-Y.; Cheng, T.-J. R.; Ma, C.; Wong, C.-H.; Cheng, W.-C. "Combinatorial Approach toward Synthesis of Small Molecule Libraries as Bacterial Transglycosylase Inhibitors." *Org. Biomol. Chem.* **2010**, *8*, 2586–2593.
- (74) Lober, S.; Rodriguez-Loaiza, P.; Gmeiner, P. "Click Linker: Efficient and High-Yielding Synthesis of a New Family of SPOS Resins by 1,3-Dipolar Cycloaddition." *Org. Lett.* **2003**, *5*, 1753–1755.
- (75) Breinbauer, R.; Kohn, M. "Azide-Alkyne Coupling: A Powerful Reaction for Bioconjugate Chemistry." *ChemBioChem* **2003**, *4*, 1147–1149.
- (76) Allen, S. E.; Walvoord, R. R.; Padilla-Salinas, R.; Kozlowski, M. C. "Aerobic Copper-Catalyzed Organic Reactions." *Chem. Rev.* **2013**, *113*, 6234–6458.
- (77) Cantillo, D.; Ávalos, M.; Babiano, R.; Cintas, P.; Jiménez, J. L.; Palacios, J. C. "Assessing the Whole Range of CuAAC Mechanisms by DFT Calculations - on the Intermediacy of Copper Acetylides." *Org. Biomol. Chem.* **2011**, *9*, 2952–2958.
- (78) Appukkuttan, P.; Dehaen, W.; Fokin, V. V.; Van der Eycken, E. "A Microwave-Assisted Click Chemistry Synthesis of 1,4-Disubstituted 1,2,3-Triazoles via a Copper(I)-Catalyzed Three-Component Reaction." *Org. Lett.* **2004**, *6*, 4223–4225.
- (79) Pachon, L. D.; Van Maarseveen, J. H.; Rothenberg, G. "Click Chemistry: Copper Clusters Catalyse the Cycloaddition of Azides with Terminal Alkynes." *Adv. Synth. Catal.* **2005**, *347*, 811–815.
- (80) Abel, G. R.; Calabrese, Z. A.; Ayco, J. A.; Hein, J. E.; Ye, T. "Measuring and Suppressing the Oxidative Damage to DNA during Cu(I)-Catalyzed Azide-Alkyne Cycloaddition." *Bioconjug. Chem.* **2016**, *27*, 698–704.
- (81) Gierlich, J.; Burley, G. A.; Gramlich, P. M. E.; Hammond, D. M.; Carell, T. "Click Chemistry as a Reliable Method for the High-Density Functionalisation of Alkyne-Modified Oligodeoxyribonucleotides." *Org. Lett.* **2006**, *8*, 3639–3642.
- (82) Chan, T. R.; Hilgraf, R.; Sharpless, K. B.; Fokin, V. V. "Polytriazoles as Copper(I)-Stabilizing Ligands in Catalysis." *Org. Lett.* **2004**, *6*, 2853–2855.
- (83) Hong, V.; Presolski, S. I.; Ma, C.; Finn, M. G. "Analysis and Optimization of Copper-Catalyzed Azide-Alkyne Cycloaddition for Bioconjugation." *Angew. Chemie - Int. Ed.* **2009**, *48*, 9879–9883.
- (84) Wang, W.; Hong, S.; Tran, A.; Jiang, H.; Triano, R.; Liu, Y.; Chen, X.; Wu, P.

- “Sulfated Ligands for the Copper(I)-Catalyzed Azide-Alkyne Cycloaddition.” *Chem. - An Asian J.* **2011**, *6*, 2796–2802.
- (85) Uttamapinant, C.; Tangpeerachaikul, A.; Grecian, S.; Clarke, S.; Singh, U.; Slade, P.; Gee, K. R.; Ting, A. Y. “Fast, Cell-Compatible Click Chemistry with Copper-Chelating Azides for Biomolecular Labeling.” *Angew. Chemie - Int. Ed.* **2012**, *124*, 5954–5958.
- (86) Soriano Del Amo, D.; Wang, W.; Jiang, H.; Besanceney, C.; Yan, A. C.; Levy, M.; Liu, Y.; Marlow, F. L.; Wu, P. “Biocompatible Copper (I) Catalysts for in Vivo Imaging of Glycans.” *J. Am. Chem. Soc.* **2010**, *132*, 16893–16899.
- (87) Szafranski, P. W.; Kasza, P.; Cegła, M. T. “A New Water-Soluble Ligand for Efficient Copper-Catalyzed Huisgen Cycloaddition of Aliphatic Azides and Alkynes.” *Tetrahedron Lett.* **2015**, *56*, 6244–6247.
- (88) Kuang, G. C.; Guha, P. M.; Brotherton, W. S.; Simmons, J. T.; Stanke, L. A.; Nguyen, B. T.; Clark, R. J.; Zhu, L. “Experimental Investigation on the Mechanism of Chelation-Assisted, Copper(II) Acetate-Accelerated Azide-Alkyne Cycloaddition.” *J. Am. Chem. Soc.* **2011**, *133*, 13984–14001.
- (89) Brotherton, W. S.; Michaels, H. A.; Simmons, J. T.; Clark, R. J.; Dalal, N. S.; Zhu, L. “Apparent Copper(II)-Accelerated Azide-Alkyne Cycloaddition.” *Org. Lett.* **2009**, *11*, 4954–4957.
- (90) King, A. E.; Ryland, B. L.; Brunold, T. C.; Stahl, S. S. “Kinetic and Spectroscopic Studies of Aerobic Copper(II)-Catalyzed Methoxylation of Arylboronic Esters and Insights into Aryl Transmetalation to Copper(II).” *Organometallics* **2012**, *31*, 7948–7957.
- (91) Glaser, C. “Beitrage Zur Kenntniss Des Acetenylbenzols.” *Chem. Ber* **1869**, *153*, 422–424.
- (92) Rodionov, V. O.; Fokin, V. V.; Finn, M. G. “Mechanism of the Ligand-Free CuI-Catalyzed Azide-Alkyne Cycloaddition Reaction.” *Angew. Chemie - Int. Ed.* **2005**, *44*, 2210–2215.
- (93) Rodionov, V. O.; Presolski, S. I.; Díaz, D. D.; Fokin, V. V.; Finn, M. G. “Ligand-Accelerated Cu-Catalyzed Azide-Alkyne Cycloaddition: A Mechanistic Report.” *J. Am. Chem. Soc.* **2007**, *129*, 12705–12712.
- (94) Worrell, B. T.; Malik, J. A.; Fokin, V. V. “Direct Evidence of a Dinuclear Copper Intermediate in Cu(I)-Catalyzed Azide-Alkyne Cycloadditions.” *Science (80-.)*. **2013**, *340*, 457–460.
- (95) Jin, L.; Tolentino, D. R.; Melaimi, M.; Bertrand, G. “Isolation of Bis(Copper) Key

- Intermediates in Cu-Catalyzed Azide-Alkyne Click Reaction.” *Sci. Adv.* **2015**, *1*, 1–5.
- (96) Döhler, D.; Michael, P.; Binder, W. H. “CuAAC-Based Click Chemistry in Self-Healing Polymers.” *Acc. Chem. Res.* **2017**, *50*, 2610–2620.
- (97) Zabarska, N.; Stumper, A.; Rau, S. “CuAAC Click Reactions for the Design of Multifunctional Luminescent Ruthenium Complexes.” *Dalt. Trans.* **2016**, *45*, 2338–2351.
- (98) Zhai, W.; Chapin, B. M.; Yoshizawa, A.; Wang, H. C.; Hodge, S. A.; James, T. D.; Anslyn, E. V.; Fossey, J. S. “Click-Fluors”: Triazole-Linked Saccharide Sensors”. *Org. Chem. Front.* **2016**, *3*, 918–928.
- (99) Zhai, W.; Male, L.; Fossey, J. S. “Glucose Selective Bis-Boronic Acid Click-Fluor.” *Chem. Commun.* **2017**, *53*, 2218–2221.
- (100) Cernat, A.; Tertiş, M.; Cristea, C.; Săndulescu, R. “Applications of Click Chemistry in the Development of Electrochemical Sensors.” *Int. J. Electrochem. Sci.* **2015**, *10*, 6324–6337.
- (101) He, X. P.; Zeng, Y. L.; Zang, Y.; Li, J.; Field, R. A.; Chen, G. R. “Carbohydrate CuAAC Click Chemistry for Therapy and Diagnosis.” *Carbohydr. Res.* **2016**, *429*, 1–22.
- (102) Wang, Q.; Chan, T. R.; Hilgraf, R.; Fokin, V. V.; Sharpless, K. B.; Finn, M. G. “Bioconjugation by Copper(I)-Catalyzed Azide-Alkyne [3 + 2] Cycloaddition.” *J. Am. Chem. Soc.* **2003**, *125*, 3192–3193.
- (103) Wang, Q.; Kaltgrad, E.; Lin, T.; Johnson, J. E.; Finn, M. . “Natural Supramolecular Building Blocks: Wild-Type Cowpea Mosaic Virus.” *Chem. Biol.* **2002**, *9*, 805–811.
- (104) Wang, Q.; Lin, T.; Johnson, J. E.; Finn, M. G. “Natural Supramolecular Building Blocks: Cysteine-Added Mutants of Cowpea Mosaic Virus.” *Chem. Biol.* **2002**, *9*, 813–819.
- (105) Deiters, A.; Cropp, T. A.; Mukherji, M.; Chin, J. W.; Anderson, J. C.; Schultz, P. G. “Adding Amino Acids with Novel Reactivity to the Genetic Code of *Saccharomyces Cerevisiae*.” *J. Am. Chem. Soc.* **2003**, *125*, 11782–11783.
- (106) Evans, M. J.; Cravatt, B. F. Mechanism-Based Profiling of Enzyme Families. *Chem. Rev.* **2006**, *106* (8), 3279–3301.
- (107) Speers, A. E.; Adam, G. C.; Cravatt, B. F. “Activity-Based Protein Profiling in Vivo Using a Copper(I)-Catalyzed Azide-Alkyne [3 + 2] Cycloaddition.” *J. Am. Chem. Soc.* **2003**, *125*, 4686–4687.
- (108) Saito, F.; Noda, H.; Bode, J. W. “Critical Evaluation and Rate Constants of Chemoselective Ligation Reactions for Stoichiometric Conjugations in Water.” *ACS*

- Chem. Biol.* **2015**, *10*, 1026–1033.
- (109) Agard, N. J.; Prescher, J. A.; Bertozzi, C. R. “A Strain-Promoted [3 + 2] Azide-Alkyne Cycloaddition for Covalent Modification of Biomolecules in Living Systems.” *J. Am. Chem. Soc.* **2004**, *126*, 15046–15047.
- (110) Wittig, G.; Krebs, A. “Zur Existenz Niedergliedriger Cycloalkine.” *Chem. Ber.* **1961**, *94*, 3260–3275.
- (111) Meier, H.; Petersen, H.; Kolshorn, H. “Die Ringspannung von Cycloalkinen Und Ihre Spektroskopischen Auswirkungen.” *Chem. Ber.* **1980**, *113*, 2398–2409.
- (112) Thomas, J. D.; Cui, H.; North, P. J.; Hofer, T.; Rader, C.; Burke, T. R. “Application of Strain-Promoted Azide-Alkyne Cycloaddition and Tetrazine Ligation to Targeted Fc-Drug Conjugates.” *Bioconjug. Chem.* **2012**, *23*, 2007–2013.
- (113) Baskin, J. M.; Preschner, J. A.; Laughlin, S. T.; Agard, N. J.; Chang, P. V.; Miller, I. A.; Lo, A.; Codelli, J. A.; Bertozzi, C. R. “Copper-Free Click Chemistry for Dynamic in Vivo Imaging.” *Proc. Natl. Acad. Sci. U. S. A.* **2007**, *104*, 16793–16797.
- (114) Laughlin, S. T.; Baskin, J. M.; Amacher, S. L.; Bertozzi, C. R. “In Vivo Imaging of Membrane-Associated Glycans in Developing Zebrafish.” *Science (80-)*. **2008**, *320*, 664–667.
- (115) Agard, N. J.; Baskin, J. M.; Prescher, J. A.; Lo, A.; Bertozzi, C. R. “A Comparative Study of Bioorthogonal Reactions with Azides.” *ACS Chem. Biol.* **2006**, *1* (644–648).
- (116) Debets, M. F.; Van Berkel, S. S.; Schoffelen, S.; Rutjes, F. P. J. T.; Van Hest, J. C. M.; Van Delft, F. L. “Aza-Dibenzocyclooctynes for Fast and Efficient Enzyme PEGylation via Copper-Free (3+2) Cycloaddition.” *Chem. Commun.* **2010**, *46*, 97–99.
- (117) Jewett, J. C.; Sletten, E. M.; Bertozzi, C. R. “Rapid Cu-Free Click Chemistry with Readily Synthesized Biarylazacyclooctynones.” *J. Am. Chem. Soc.* **2010**, *132*, 3688–3690.
- (118) Ning, X.; Guo, J.; Wolfert, M. A.; Boons, G. J. “Visualizing Metabolically Labeled Glycoconjugates of Living Cells by Copper-Free and Fast Huisgen Cycloadditions.” *Angew. Chemie - Int. Ed.* **2008**, *120* (12), 2285–2287.
- (119) Dommerholt, J.; Schmidt, S.; Temming, R.; Hendriks, L. J. A.; Rutjes, F. P. J. T.; Van Hest, J. C. M.; Lefeber, D. J.; Friedl, P.; Van Delft, F. L. “Readily Accessible Bicyclononynes for Bioorthogonal Labeling and Three-Dimensional Imaging of Living Cells.” *Angew. Chemie - Int. Ed.* **2010**, *49*, 9422–9425.
- (120) Chigrinova, M.; McKay, C. S.; Beaulieu, L. P. B.; Udachin, K. A.; Beauchemin, A. M.; Pezacki, J. P. “Rearrangements and Addition Reactions of Biarylazacyclooctynones and the Implications to Copper-Free Click Chemistry.” *Org.*

- Biomol. Chem.* **2013**, *11*, 3436–3441.
- (121) Chang, P. V.; Prescher, J. A.; Sletten, E. M.; Baskin, J. M.; Miller, I. A.; Agard, N. J.; Lo, A.; Bertozzi, C. R. “Copper-Free Click Chemistry in Living Animals.” *Proc. Natl. Acad. Sci.* **2010**, *107*, 1821–1826.
- (122) Poole, T. H.; Reisz, J. A.; Zhao, W.; Poole, L. B.; Furdai, C. M.; King, S. B. “Strained Cycloalkynes as New Protein Sulfenic Acid Traps.” *J. Am. Chem. Soc.* **2014**, *136*, 6167–6170.
- (123) Plass, T.; Milles, S.; Koehler, C.; Schultz, C.; Lemke, E. A. “Genetically Encoded Copper-Free Click Chemistry.” *Angew. Chemie - Int. Ed.* **2011**, *50*, 3878–3881.
- (124) McKay, C. S.; Moran, J.; Pezacki, J. P. “Nitrones as Dipoles for Rapid Strain-Promoted 1,3-Dipolar Cycloadditions with Cyclooctynes.” *Chem. Commun.* **2010**, *46*, 931–933.
- (125) Ning, X.; Temming, R. P.; Dommerholt, J.; Guo, J.; Ania, D. B.; Debets, M. F.; Wolfert, M. A.; Boons, G. J.; Van Delft, F. L. “Protein Modification by Strain-Promoted Alkyne-Nitron Cycloaddition.” *Angew. Chemie - Int. Ed.* **2010**, *49*, 3065–3068.
- (126) Sanders, B. C.; Friscourt, F.; Ledin, P. A.; Mbuu, N. E.; Arumugam, S.; Guo, J.; Boltje, T. J.; Popik, V. V.; Boons, G. J. “Metal-Free Sequential [3 + 2]-Dipolar Cycloadditions Using Cyclooctynes and 1,3-Dipoles of Different Reactivity.” *J. Am. Chem. Soc.* **2011**, *133*, 949–957.
- (127) Singh, I.; Heaney, F. “Solid Phase Strain Promoted ‘Click’ Modification of DNA via [3+2]-Nitrile Oxide-Cyclooctyne Cycloadditions.” *Chem. Commun.* **2011**, *47*, 2706–2708.
- (128) Jawalekar, A. M.; Reubsæet, E.; Rutjes, F. P. J. T.; Van Delft, F. L. “Synthesis of Isoxazoles by Hypervalent Iodine-Induced Cycloaddition of Nitrile Oxides to Alkynes.” *Chem. Commun.* **2011**, *47*, 3198–3200.
- (129) Boger, D. L. “Diels-Alder Reactions of Heterocyclic Aza Dienes: Scope and Applications.” *Chem. Rev. (Washington, DC, United States)* **1986**, *86*, 781–794.
- (130) Carboni, R. A.; Lindsey, R. V. “Reactions of Tetrazines with Unsaturated Compounds. A New Synthesis of Pyridazines.” *J. Am. Chem. Soc.* **1959**, *81*, 4342–4346.
- (131) Thalhammer, F.; Wallfaher, U.; Sauer, J. “Reaktivität Einfacher Offenkettiger Und Cyclischer Dienophile Bei Diels-Alder-Reaktionen Mit Inversem Elektronenbedarf.” *Tetrahedron Lett.* **1990**, *31*, 6851–6854.
- (132) Blackman, M. L.; Royzen, M.; Fox, J. M. “Tetrazine Ligation : Fast Bioconjugation Based on Inverse-Electron-Eemand Diels - Alder Reactivity.” *J. Am. Chem. Soc.* **2008**, *130*, 13518–13519.

- (133) Taylor, M. T.; Blackman, M. L.; Dmitrenko, O.; Fox, J. M. "Design and Synthesis of Highly Reactive Dienophiles for the Tetrazine-Trans-Cyclooctene Ligation." *J. Am. Chem. Soc.* **2011**, *133*, 9646–9649.
- (134) Chen, W.; Wang, D.; Dai, C.; Hamelberg, D.; Wang, B. "Clicking 1,2,4,5-Tetrazine and Cyclooctynes with Tunable Reaction Rates." *Chem. Commun.* **2012**, *48*, 1736–1738.
- (135) Patterson, D. M.; Nazarova, L. A.; Xie, B.; Kamber, D. N.; Prescher, J. A. "Functionalized Cyclopropenes as Bioorthogonal Chemical Reporters." *J. Am. Chem. Soc.* **2012**, *134*, 18638–18643.
- (136) Devaraj, N. K.; Weissleder, R.; Hilderbrand, S. a. "Tetrazine-Based Cycloadditions : Application to Pretargeted Live Cell Imaging." *Bioconjug. Chem.* **2008**, *19*, 2297–2299.
- (137) Vrabel, M.; Kolle, P.; Brunner, K. M.; Gattner, M. J.; Lopez-Carrillo, V.; De Vivie-Riedle, R.; Carell, T. "Norbornenes in Inverse Electron-Demand Diels-Alder Reactions." *Chem. - A Eur. J.* **2013**, *19*, 13309–13312.
- (138) Han, H. S.; Devaraj, N. K.; Lee, J.; Hilderbrand, S. A.; Weissleder, R.; Bawendi, M. G. "Development of a Bioorthogonal and Highly Efficient Conjugation Method for Quantum Dots Using Tetrazine-Norbornene Cycloaddition." *J. Am. Chem. Soc.* **2010**, *132*, 7838–7839.
- (139) Pipkorn, R.; Waldeck, W.; Didinger, B.; Koch, M.; Mueller, G.; Wiessler, M.; Braun, K. "Inverse-Electron-Demand Diels-Alder Reaction as a Highly Efficient Chemoselective Ligation Procedure: Synthesis and Function of a BioShuttle for Temozolomide Transport into Prostate Cancer Cells." *J. Pept. Sci.* **2009**, *15*, 235–241.
- (140) Engelsma, S. B.; Willems, L. I.; Van Paaschen, C. E.; Van Kasteren, S. I.; Van Der Marel, G. A.; Overkleeft, H. S.; Filippov, D. V. "Acylazetine as a Dienophile in Bioorthogonal Inverse Electron-Demand Diels-Alder Ligation." *Org. Lett.* **2014**, *16*, 2744–2747.
- (141) Stairs, S.; Neves, A. A.; Stöckmann, H.; Wainman, Y. A.; Ireland-Zecchini, H.; Brindle, K. M.; Leeper, F. J. "Metabolic Glycan Imaging by Isonitrile-Tetrazine Click Chemistry." *ChemBioChem* **2013**, *14*, 1063–1067.
- (142) Karver, M. R.; Weissleder, R.; Hilderbrand, S. A. "Synthesis and Evaluation of a Series of 1,2,4,5-Tetrazines for Bioorthogonal Conjugation." *Bioconjug. Chem.* **2011**, *22*, 2263–2270.
- (143) Keliher, E. J.; Reiner, T.; Turetsky, A.; Hilderbrand, S. A.; Weissleder, R. "High-Yielding, Two-Step ¹⁸F Labeling Strategy for ¹⁸F-PARP1 Inhibitors."

- ChemMedChem* **2011**, *6*, 424–427.
- (144) Van Berkel, S. S.; Dirks, A. J.; Debets, M. F.; Van Delft, F. L.; Cornelissen, J. J. L. M.; Nolte, R. J. M.; Rutjes, F. P. J. T. “Metal-Free Triazole Formation as a Tool for Bioconjugation.” *ChemBioChem* **2007**, *8*, 1504–1508.
- (145) Evano, G.; Coste, A.; Jouvin, K. “Ynamides: Versatile Tools in Organic Synthesis.” *Angew. Chemie - Int. Ed.* **2010**, *49*, 2840–2859.
- (146) Besanceney-Webler, C.; Jiang, H.; Zheng, T.; Feng, L.; Soriano Del Amo, D.; Wang, W.; Klivansky, L. M.; Marlow, F. L.; Liu, Y.; Wu, P. “Increasing the Efficacy of Bioorthogonal Click Reactions for Bioconjugation: A Comparative Study.” *Angew. Chemie - Int. Ed.* **2011**, *50*, 8051–8056.
- (147) Best, M. D. “Click Chemistry and Bioorthogonal Reactions: Unprecedented Selectivity in the Labeling of Biological Molecules.” *Biochemistry* **2009**, *48*, 6571–6584.
- (148) Kislukhin, A. A.; Hong, V. P.; Breitenkamp, K. E.; Finn, M. G. “Relative Performance of Alkynes in Copper-Catalyzed Azide – Alkyne Cycloaddition.” *Bioconjug. Chem.* **2013**, *24*, 684–689.
- (149) Bohme, A.; Thaens, D.; Schramm, F.; Paschke, A.; Schüürmann, G. “Thiol Reactivity and Its Impact on the Ciliate Toxicity of α,β -Unsaturated Aldehydes, Ketones, and Esters.” *Chem. Res. Toxicol.* **2010**, *23*, 1905–1912.
- (150) Mather, B. D.; Viswanathan, K.; Miller, K. M.; Long, T. E. “Michael Addition Reactions in Macromolecular Design for Emerging Technologies.” *Prog. Polym. Sci.* **2006**, *31*, 487–531.
- (151) Kacprzak, K. “Efficient One-Pot Synthesis of 1,2,3-Triazoles from Benzyl and Alkyl Halides.” *Synlett* **2005**, *6*, 943–946.
- (152) Feldman, A. K.; Colasson, B.; Sharpless, K. B.; Fokin, V. V. “The Allylic Azide Rearrangement: Achieving Selectivity.” *J. Am. Chem. Soc.* **2005**, *127*, 13444–13445.
- (153) Aucagne, V.; Leigh, D. A. “Chemoselective Formation of Successive Triazole Linkages in One Pot: ‘Click-Click’ Chemistry.” *Org. Lett.* **2006**, *8* (20), 4505–4507.
- (154) Hein, J. E.; Tripp, J. C.; Krasnova, L. B.; Sharpless, K. B.; Fokin, V. V. “Copper(I)-Catalyzed Cycloaddition of Organic Azides and 1-Iodoalkynes.” *Angew. Chemie - Int. Ed.* **2009**, *48*, 8018–8021.
- (155) Yamamoto, K.; Bruun, T.; Kim, J. Y.; Zhang, L.; Lautens, M. “A New Multicomponent Multicatalyst Reaction (MC)²R: Chemoselective Cycloaddition and Latent Catalyst Activation for the Synthesis of Fully Substituted 1,2,3-Triazoles.” *Org. Lett.* **2016**, *18*, 2644–2647.
- (156) Wang, W.; Wei, F.; Ma, Y.; Tung, C. H.; Xu, Z. “Copper(I)-Catalyzed Three-

- Component Click/Alkynylation: One-Pot Synthesis of 5-Alkynyl-1,2,3-Triazoles.” *Org. Lett.* **2016**, *18*, 4158–4161.
- (157) Yuan, Z.; Kuang, G. C.; Clark, R. J.; Zhu, L. “Chemoselective Sequential ‘click’ Ligation Using Unsymmetrical Bisazides.” *Org. Lett.* **2012**, *14*, 2590–2593.
- (158) Shea, K. J.; Kim, J.-S. “Influence of Strain on Chemical Reactivity. Relative Reactivity of Torsionally Strained Double Bonds in 1,3-Dipolar Cycloadditions.” *J. Am. Chem. Soc.* **1992**, *114*, 4846–4855.
- (159) Yoshida, S.; Hatakeyama, Y.; Johmoto, K.; Uekusa, H.; Hosoya, T. “Transient Protection of Strained Alkynes from Click Reaction via Complexation with Copper.” *J. Am. Chem. Soc.* **2014**, *136*, 13590–13593.
- (160) Zaugg, H.; Swett, L.; Stone, G. “An Unusual Reaction of Propargyl Bromide.” *J. Org. Chem.* **1958**, *23*, 1389–1390.
- (161) Viehe, H. G. “Synthesis of Substituted Acetylenic Compounds.” *Angew. Chemie - Int. Ed.* **1963**, *2*, 477.
- (162) Ficini, J. “Ynamine: A Versatile Tool in Organic Synthesis.” *Tetrahedron* **1976**, *32*, 1449–1486.
- (163) Ficini, A.; Krief, J. “Stereochemical Control in the Hydrolysis of an Ynamine-Cyclopentenone Adduct: A Stereoselective Route to Diastereoisomeric 2-(1-Cyclopentyl-3-Oxo)-Propionic Acids.” *Tetrahedron Lett.* **1970**, *17*, 1397–1400.
- (164) IJsselstijn, M.; Cintrat, J. C. “Click Chemistry with Ynamides.” *Tetrahedron* **2006**, *62*, 3837–3842.
- (165) Burley, G. A.; Davies, D. L.; Griffith, G. A.; Lee, M.; Singh, K. “Cu-Catalyzed N-Alkynylation of Imidazoles, Benzimidazoles, Indazoles, and Pyrazoles Using PEG as Solvent Medium.” *J. Org. Chem.* **2010**, *75*, 980–983.
- (166) Altman, R. A.; Buchwald, S. L. “Cu-Catalyzed Goldberg and Ullmann Reactions of Aryl Halides Using Chelating N- and O-Based Ligands.” *Nat. Protoc.* **2007**, *2*, 2474–2479.
- (167) Burley, G. A.; Boutadla, Y.; Davies, D. L.; Singh, K. “Triazoles from N-Alkynylheterocycles and Their Coordination to Iridium.” *Organometallics* **2012**, *31* (3), 1112–1117.
- (168) Zhang, P.; Cook, A. M.; Liu, Y.; Wolf, C. “Copper(I)-Catalyzed Nucleophilic Addition of Ynamides to Acyl Chlorides and Activated N-heterocycles.” *J. Org. Chem.* **2014**, *79*, 4167–4173.
- (169) Hu, L.; Xu, S.; Zhao, Z.; Yang, Y.; Peng, Z.; Yang, M.; Wang, C.; Zhao, J. “Ynamides as Racemization-Free Coupling Reagents for Amide and Peptide Synthesis.” *J. Am.*

- Chem. Soc.* **2016**, *138*, 13135–13138.
- (170) Seath, C. P.; Burley, G. A.; Watson, A. J. B. “Determining the Origin of Rate-Independent Chemoselectivity in CuAAC Reactions: An Alkyne-Specific Shift in Rate-Determining Step.” *Angew. Chemie Int. Ed.* **2017**, *56*, 3314–3318.
- (171) Hatit, M. Z. C.; Sadler, J. C.; McLean, L. A.; Whitehurst, B. C.; Seath, C. P.; Humphreys, L. D.; Young, R. J.; Watson, A. J. B.; Burley, G. A. “Chemoselective Sequential Click Ligations Directed by Enhanced Reactivity of an Aromatic Ynamine.” *Org. Lett.* **2016**, *18*, 1694–1697.
- (172) Husken, N.; Gasser, G.; Koster, S. D.; Metzler-Nolte, N. “Four-Potential Ferrocene Labeling of PNA Oligomers via Click Chemistry.” *Bioconjug. Chem.* **2009**, *20*, 1578–1586.
- (173) Haldar, S.; Chattopadhyay, A. “Application of NBD-Labeled Lipids in Membrane and Cell Biology.” *Springer Ser. Fluoresc.* **2012**, 37–50.
- (174) Hatit, M. Z. C.; Seath, C. P.; Watson, A. J. B.; Burley, G. A. “A Strategy for Conditional Orthogonal Sequential CuAAC Reactions Using a Protected Aromatic Ynamine.” *J. Org. Chem.* **2017**, *82*, 5461–5468.
- (175) Dilauro, A. M.; Seo, W.; Phillips, S. T. “Use of Catalytic Fluoride under Neutral Conditions for Cleaving Silicon-Oxygen Bonds.” *J. Org. Chem.* **2011**, *76*, 7352–7358.
- (176) Sun, H.; DiMugno, S. G. “Anhydrous Tetrabutylammonium Fluoride.” *J. Am. Chem. Soc.* **2005**, *127*, 2050–2051.
- (177) Wang, X. N.; Yeom, H. S.; Fang, L. C.; He, S.; Ma, Z. X.; Kedrowski, B. L.; Hsung, R. P. “Ynamides in Ring Forming Transformations.” *Acc. Chem. Res.* **2014**, *47*, 560–578.
- (178) Zhang, X.; Hsung, R. P.; You, L. “Tandem Azidation– and Hydroazidation–Huisgen [3 + 2] Cycloadditions of Ynamides. Synthesis of Chiral Amide-Substituted Triazoles.” *Org. Biomol. Chem.* **2006**, *4*, 2679–2682.
- (179) Tale, R. H.; Gopula, V. B.; Toradmal, G. K. “‘Click’ Ligand for ‘click’ Chemistry: (1-(4-Methoxybenzyl)-1-H-1,2,3-Triazol-4-Yl)Methanol (MBHTM) Accelerated Copper-Catalyzed [3+2] Azide-Alkyne Cycloaddition (CuAAC) at Low Catalyst Loading.” *Tetrahedron Lett.* **2015**, *56*, 5864–5869.
- (180) Zheng, Z.; Shi, L. “An Efficient Regioselective Copper-Catalyzed Approach to the Synthesis of 1,2,3-Triazoles from N-Tosylhydrazones and Azides.” *Tetrahedron Lett.* **2016**, *57*, 5132–5134.
- (181) Taher, A.; Nandi, D.; Islam, R. U. I.; Choudhary, M.; Mallick, K. “Microwave Assisted Azide–Alkyne Cycloaddition Reaction Using Polymer Supported Cu(i) as a Catalytic

- Species: A Solventless Approach.” *RSC Adv.* **2015**, *5*, 47275–47283.
- (182) Bolje, A.; Urankar, D.; Kosmrlj, J. “Synthesis and NMR Analysis of 1,4-Disubstituted 1,2,3-Triazoles Tethered to Pyridine, Pyrimidine, and Pyrazine Rings.” *European J. Org. Chem.* **2014**, *36*, 8167–8181.
- (183) Krall, N.; Da Cruz, F. P.; Boutureira, O.; Bernardes, G. J. L. “Site-Selective Protein-Modification Chemistry for Basic Biology and Drug Development.” *Nat. Chem.* **2016**, *8*, 103–113.
- (184) Foley, T. L.; Burkart, M. D. “Site-Specific Protein Modification: Advances and Applications.” *Curr. Opin. Chem. Biol.* **2007**, *11*, 12–9.
- (185) Joo, C.; Balci, H.; Ishitsuka, Y.; Buranachai, C.; Ha, T. Advances in Single-Molecule Fluorescence Methods for Molecular Biology”. *Annu. Rev. Biochem.* **2008**, *77*, 51–76.
- (186) Stryer, L. “Fluorescence Energy Transfer as a Spectroscopic Ruler.” *Annu. Rev. Biochem.* **1978**, *47*, 819–846.
- (187) Junager, N. P. L.; Kongsted, J.; Astakhova, K. “Revealing Nucleic Acid Mutations Using Förster Resonance Energy Transfer-Based Probes.” *Sensors (Switzerland)* **2016**, *16*, 1173–1192.
- (188) Maruani, A.; Smith, M. E. B.; Miranda, E.; Chester, K. A.; Chudasama, V.; Caddick, S. “A Plug-and-Play Approach to Antibody-Based Therapeutics via a Chemoselective Dual Click Strategy.” *Nat. Commun.* **2015**, *6*, 6645–6654.
- (189) Pretze, M.; Pietzsch, D.; Mamat, C. “Recent Trends in Bioorthogonal Click-Radiolabeling Reactions Using Fluorine-18.” *Molecules* **2013**, *18*, 8618–8665.
- (190) Maruani, A.; Richards, D. A.; Chudasama, V. “Dual Modification of Biomolecules.” *Org. Biomol. Chem.* **2016**, *14*, 6165–6178.
- (191) Debets, M. F.; Van Hest, J. C. M.; Rutjes, F. P. J. T. “Bioorthogonal Labelling of Biomolecules: New Functional Handles and Ligation Methods.” *Org. Biomol. Chem.* **2013**, *11*, 6439–6455.
- (192) Schoch, J.; Staudt, M.; Samanta, A.; Wiessler, M.; Jaschke, A. “Site-Specific One-Pot Dual Labeling of DNA by Orthogonal Cycloaddition Chemistry.” *Bioconjug. Chem.* **2012**, *23*, 1382–1386.
- (193) Gramlich, P. M. E.; Warncke, S.; Gierlich, J.; Carell, T. “Click-Click-Click: Single to Triple Modification of DNA.” *Angew. Chemie - Int. Ed.* **2008**, *47*, 3442–3444.
- (194) Astakhova, I. K.; Wengel, J. “Interfacing Click Chemistry with Automated Oligonucleotide Synthesis for the Preparation of Fluorescent DNA Probes Containing Internal Xanthene and Cyanine Dyes.” *Chem. - A Eur. J.* **2013**, *19*, 1112–1122.
- (195) Pourceau, G.; Meyer, A.; Vasseur, J. J.; Morvan, F. “Synthesis of Mannose and

- Galactose Oligonucleotide Conjugates by Bi-Click Chemistry.” *J. Org. Chem.* **2009**, *74*, 1218–1222.
- (196) Jawalekar, A. M.; Meeuwenoord, N.; Cremers, J. G. O.; Overkleeft, H. S.; Van Der Marel, G. A.; Rutjes, F. P. J. T.; Van Delft, F. L. “Conjugation of Nucleosides and Oligonucleotides by [3+2] Cycloaddition.” *J. Org. Chem.* **2008**, *73*, 287–290.
- (197) Yim, C. Bin; Dijkgraaf, I.; Merkx, R.; Versluis, C.; Eek, A.; Mulder, G. E.; Rijkers, D. T. S.; Boerman, O. C.; Liskamp, R. M. J. “Synthesis of DOTA-Conjugated Multimeric [Tyr3]Ostreotide Peptides via a Combination of Cu(I)-Catalyzed Click Cycloaddition and Thio Acid/Sulfonyl Azide Sulfo-Click Amidation and Their in Vivo Evaluation.” *J. Med. Chem.* **2010**, *53*, 3944–3953.
- (198) Means, A. R.; Vanberkum, M. F. A.; Bagchi, I.; Lu, K. U. N. P.; Rasmussen, C. D. “Regulatory Functions of Calmodulin.” *Pharmac. Ther.* **1991**, *50*, 255–270.
- (199) Kim, J.; Seo, M. H.; Lee, S.; Cho, K.; Yang, A.; Woo, K.; Kim, H. S.; Park, H. S. “Simple and Efficient Strategy for Site-Specific Dual Labeling of Proteins for Single-Molecule Fluorescence Resonance Energy Transfer Analysis.” *Anal. Chem.* **2013**, *85* (3), 1468–1474.
- (200) Rashidian, M.; Kumarapperuma, S. C.; Gabrielse, K.; Fegan, A.; Wagner, C. R.; Distefano, M. D. “Simultaneous Dual Protein Labeling Using a Triorthogonal Reagent.” *J. Am. Chem. Soc.* **2013**, *135*, 16388–16396.
- (201) Mühlberg, M.; Hoesl, M. G.; Kuehne, C.; Dervede, J.; Budisa, N.; Hackenberger, C. P. R. “Orthogonal Dual-Modification of Proteins for the Engineering of Multivalent Protein Scaffolds.” *Beilstein J. Org. Chem.* **2015**, *11*, 784–791.
- (202) Kalia, J.; Raines, R. T. “Advances in Bioconjugation.” *Curr. Org. Chem.* **2010**, *14*, 138–147.
- (203) Kele, P.; Mezö, G.; Achatz, D.; Wolfbeis, O. S. “Dual Labeling of Biomolecules by Using Click Chemistry: A Sequential Approach.” *Angew. Chemie - Int. Ed.* **2009**, *48*, 344–347.
- (204) Ledin, P. A.; Friscourt, F.; Guo, J.; Boons, G. J. “Convergent Assembly and Surface Modification of Multifunctional Dendrimers by Three Consecutive Click Reactions.” *Chemistry (Easton)*. **2011**, *17*, 839–846.
- (205) Beal, D. M.; Albrow, V. E.; Burslem, G.; Hitchen, L.; Fernandes, C.; Laphorn, C.; Roberts, L. R.; Selby, M. D.; Jones, L. H. “Click-Enabled Heterotrifunctional Template for Sequential Bioconjugations.” *Org. Biomol. Chem.* **2012**, *10*, 548–554.
- (206) Sachdeva, A.; Wang, K.; Elliott, T.; Chin, J. W. “Concerted, Rapid, Quantitative, and Site-Specific Dual Labeling of Proteins.” *J. Am. Chem. Soc.* **2014**, *136*, 7785–7788.

- (207) Winz, M.-L.; Linder, E. C.; Becker, J.; Jaschke, A. "Site-Specific One-Pot Triple Click Labeling for DNA and RNA." *Chem. Commun.* **2018**, 11781–11784.
- (208) Sasmal, P. K.; Carregarl-Romero, S.; Han, A. A.; Streu, C. N.; Lin, Z.; Namikawa, K.; Elliot, S. L.; Koster, R. W.; Parak, W. J.; Meggers, E. "Catalytic Azide Reduction in Biological Environments." *ChemBioChem* **2012**, *13*, 1116–1120.
- (209) Taskova, M.; Madsen, C. S.; Jensen, K. J.; Hansen, L. H.; Vester, B.; Astakhova, K. "Antisense Oligonucleotides Internally Labeled with Peptides Show Improved Target Recognition and Stability to Enzymatic Degradation." *Bioconjug. Chem.* **2017**, *28*, 768–774.
- (210) Wang, K.; Sachdeva, A.; Cox, D. J.; Wilf, N. W.; Lang, K.; Wallace, S.; Mehl, R. A.; Chin, J. W. "Optimized Orthogonal Translation of Unnatural Amino Acids Enables Spontaneous Protein Double-Labeling and FRET." *Nat. Chem.* **2014**, *6*, 393–403.
- (211) Beaucage, S. L.; Caruthers, M. H. "Deoxynucleoside Phosphoramidites - A New Class of Key Intermediates for Deoxypolynucleotide Synthesis." *Tetrahedron Lett.* **1981**, *22*, 1859–1862.
- (212) Caruthers, M. H.; Barone, A. D.; Beaucage, S. L.; Dodds, D. R.; Fisher, E. F.; McBride, L. J.; Matteucci, M.; Stabinsky, Z.; Tang, J. Y. "Chemical Synthesis of Deoxyoligonucleotides by the Phosphoramidite Method." *Methods Enzymol.* **1987**, *154* (287–313).
- (213) Tataurov, A. V.; You, Y.; Owczarzy, R. "Predicting Ultraviolet Spectrum of Single Stranded and Double Stranded Deoxyribonucleic Acids." *Biophys. Chem.* **2008**, *133*, 66–70.
- (214) Kallansrud, G.; Ward, B. "A Comparison of Measured and Calculated Single- and Double-Stranded Oligodeoxynucleotide Extinction Coefficients." *Anal. Biochem.* **1996**, *236*, 134–138.
- (215) Hatit, M. Z. C.; Reichenbach, L. F.; Tobin, J. M.; Vilela, F.; Burley, G. A.; Watson, A. J. B. "A Flow Platform for Degradation-Free CuAAC Bioconjugation." *Nat. Commun.* **2018**, *9*, 4021–4029.
- (216) Flynn, G. E.; Withers, J. M.; Macias, G.; Sperling, J. R.; Henry, S. L.; Cooper, J. M.; Burley, G. A.; Clark, A. W. "Reversible DNA Micro-Patterning Using the Fluorous Effect." *Chem. Commun.* **2017**, *53*, 3094–3097.
- (217) Hein, C. D.; Liu, X. M.; Wang, D. "Click Chemistry, a Powerful Tool for Pharmaceutical Sciences." *Pharm. Res.* **2008**, *25*, 2216–2230.
- (218) Willibald, J.; Harder, J.; Sparrer, K.; Conzelmann, K. K.; Carell, T. Click-Modified Anandamide siRNA Enables Delivery and Gene Silencing in Neuronal and Immune

- Cells. *J. Am. Chem. Soc.* **2012**, *134* (30), 12330–12333.
- (219) Wang, W.; Chen, K.; Qu, D.; Chi, W.; Xiong, W.; Huang, Y.; Wen, J.; Feng, S.; Zhang, B. “One Pot Conjugation of Small Molecules to RNA Using Click Chemistry.” *Tetrahedron Lett.* **2012**, *53*, 6747–6750.
- (220) Deng, W. G.; Zhu, Y.; Montero, A.; Wu, K. K. “Quantitative Analysis of Binding of Transcription Factor Complex to Biotinylated DNA Probe by a Streptavidin-Agarose Pulldown Assay.” *Anal. Biochem.* **2003**, *323*, 12–18.
- (221) RICHARDSON, C. C.; KORNBERG, A. “A Deoxyribonucleic Acid Phosphatase-Exonuclease from Escherichia Coli.” *J. Biol. Chem.* **1963**, *239*, 242–250.
- (222) Watson, J. D.; Crick, F. H. C. “Molecular Structure of Nucleic Acids.” *Nature* **1953**, *171*, 737–738.
- (223) Stubbert, B. D.; Marks, T. J. Constrained Geometry Organoactinides as Versatile Catalysts for the Intramolecular Hydroamination/Cyclization of Primary and Secondary Amines Having Diverse Tethered C-C Unsaturation”. *J. Am. Chem. Soc.* **2007**, *129*, 4253–4271.
- (224) Barthes, N. P. F.; Gavvala, K.; Bonhomme, D.; Dabert-Gay, A. S.; Debayle, D.; Mély, Y.; Michel, B. Y.; Burger, A. "Design and Development of a Two-Color Emissive FRET Pair Based on a Photostable Fluorescent Deoxyuridine Donor Presenting a Mega-Stokes Shift. *J. Org. Chem.* **2016**, *81*, 10733–10741.
- (225) Zhao, Z.; Peng, G.; Michels, J.; Fox, K. R.; Brown, T. “Synthesis of Anthraquinone Oligonucleotides for Triplex Stabilization.” *Nucleosides, Nucleotides and Nucleic Acids* **2007**, *26*, 921–925.
- (226) Lee, T.; Kang, H. R.; Kim, S.; Kim, S. “Facile One-Pot Syntheses of Bromoacetylenes from Bulky Trialkylsilyl Acetylenes.” *Tetrahedron* **2006**, *62*, 4081–4085.
- (227) Elvira, K. S.; i Solvas, X. C.; Wootton, R. C. R.; DeMello, A. J. “The Past, Present and Potential for Microfluidic Reactor Technology in Chemical Synthesis.” *Nat. Chem.* **2013**, *5*, 905–915.
- (228) De La Hoz, A.; Díaz-Ortiz, Á.; Moreno, A. “Microwaves in Organic Synthesis. Thermal and Non-Thermal Microwave Effects.” *Chem. Soc. Rev.* **2005**, *34*, 164–178.
- (229) Yoshida, J. I. “Flash Chemistry: Flow Microreactor Synthesis Based on High-Resolution Reaction Time Control.” *Chem. Rec.* **2010**, *10*, 332–341.
- (230) Mingos, M. P.; Baghurst, D. R. “Applications of Microwave Dielectric Heating Effects to Synthetic Problems in Chemistry.” *Chem. Soc. Rev.* **1991**, *20*, 1–47.
- (231) Kappe, C. O. “Controlled Microwave Heating in Modern Organic Synthesis.” *Angew. Chemie Int. Ed.* **2004**, *43*, 6250–6284.

- (232) Glasnov, T. N.; Kappe, C. O. "The Microwave-to-Flow Paradigm: Translating High-Temperature Batch Microwave Chemistry to Scalable Continuous-Flow Processes." *Chem. - A Eur. J.* **2011**, *17*, 11956–11968.
- (233) Porta, R.; Benaglia, M.; Puglisi, A. "Flow Chemistry: Recent Developments in the Synthesis of Pharmaceutical Products." *Org. Process Res. Dev.* **2016**, *20*, 2–25.
- (234) Watts, P.; Haswell, S. J. "Continuous Flow Reactors for Drug Discovery." *Drug Discov. Today* **2003**, *8*, 586–593.
- (235) Colombo, M.; Peretto, I. "Chemistry Strategies in Early Drug Discovery: An Overview of Recent Trends." *Drug Discov. Today* **2008**, *13*, 677–684.
- (236) Razzaq, T.; Kappe, C. O. "Continuous Flow Organic Synthesis under High-Temperature/Pressure : Conditions." *Chem. - An Asian J.* **2010**, *5*, 1274–1289.
- (237) Snead, D. R.; Jamison, T. F. "End-to-End Continuous Flow Synthesis and Purification of Diphenhydramine Hydrochloride Featuring Atom Economy, in-Line Separation, and Flow of Molten Ammonium Salts." *Chem. Sci.* **2013**, *4*, 2822–2827.
- (238) Gutmann, B.; Cantillo, D.; Kappe, C. O. "Continuous-Flow Technology - A Tool for the Safe Manufacturing of Active Pharmaceutical Ingredients." *Angew. Chemie - Int. Ed.* **2015**, *54*, 6688–6728.
- (239) Bogdan, A. R.; Sach, N. W. "The Use of Copper Flow Reactor Technology for the Continuous Synthesis of 1,4-Disubstituted 1,2,3-Triazoles." *Adv. Synth. Catal.* **2009**, *351*, 849–854.
- (240) Murray, P. R. D.; Browne, D. L.; Pastre, J. C.; Butters, C.; Guthrie, D.; Ley, S. V. "Continuous Flow-Processing of Organometallic Reagents Using an Advanced Peristaltic Pumping System and the Telescoped Flow Synthesis of (E/Z)-Tamoxifen." *Org. Process Res. Dev.* **2013**, *17*, 1192–1208.
- (241) Battilocchio, C.; Deadman, B. J.; Nikbin, N.; Kitching, M. O.; Baxendale, I. R.; Ley, S. V. "A Machine-Assisted Flow Synthesis of SR48692: A Probe for the Investigation of Neurotensin Receptor-1." *Chem. - A Eur. J.* **2013**, *19*, 7917–7930.
- (242) Lange, H.; Carter, C. F.; Hopkin, M. D.; Burke, A.; Goode, J. G.; Baxendale, I. R.; Ley, S. V. "A Breakthrough Method for the Accurate Addition of Reagents in Multi-Step Segmented Flow Processing." *Chem. Sci.* **2011**, *2*, 765–769.
- (243) Guetzoyan, L.; Nikbin, N.; Baxendale, I. R.; Ley, S. V. "Flow Chemistry Synthesis of Zolpidem, Alpidem and Other GABAA Agonists and Their Biological Evaluation through the Use of in-Line Frontal Affinity Chromatography." *Chem. Sci.* **2013**, *4*, 764–769.
- (244) Snead, D. R.; Jamison, T. F. "A Three-Minute Synthesis and Purification of Ibuprofen:

- Pushing the Limits of Continuous-Flow Processing.” *Angew. Chemie - Int. Ed.* **2015**, *54*, 983–987.
- (245) Anciaux, A. J.; Demonceau, A.; Noels, A. F.; Hubert, A. J.; Warin, R.; Teyssié, P. “Transition-Metal-Catalyzed Reactions of Diazo Compounds. 2.1 Addition to Aromatic Molecules: Catalysis of Buchner’s Synthesis of Cycloheptatrienes.” *J. Org. Chem.* **1981**, *46*, 873–876.
- (246) O’Neill, S.; O’Keeffe, S.; Harrington, F.; Maguire, A. R. “Enhancement of Enantioselection in the Copper-Catalysed Intramolecular Büchner Reaction by Variation of the Counterion.” *Synlett* **2009**, *14*, 2312–2314.
- (247) Crowley, D. C.; Lynch, D.; Maguire, A. R. “Copper-Mediated, Heterogeneous, Enantioselective Intramolecular Buchner Reactions of α -Diazoketones Using Continuous Flow Processing.” *J. Org. Chem.* **2018**, *83*, 3794–3805.
- (248) Burguete, M. I.; Fraile, J. M.; García, J. I.; García-Verdugo, E.; Luis, S. V.; Mayoral, J. A. “Bis(Oxazoline)Copper Complexes Covalently Bonded to Insoluble Support as Catalysts in Cyclopropanation Reactions.” *J. Org. Chem.* **2000**, *2*, 3905–3908.
- (249) Sonogashira, K. “Development of Pd-Cu Catalyzed Cross-Coupling of Terminal Acetylenes with Sp²-Carbon Halides.” *J. Organomet. Chem.* **2002**, *653*, 46–49.
- (250) Zhang, Y.; Jamison, T. F.; Patel, S.; Mainolfi, N. “Continuous Flow Coupling and Decarboxylation Reactions Promoted by Copper Tubing.” *Org. Lett.* **2011**, *13*, 280–283.
- (251) Lam, P. Y. S.; Clark, C. G.; Saubern, S.; Adams, J.; Winters, M. P.; Chan, D. M. T.; Combs, A. “New Aryl/Heteroaryl C-N Bond Cross-Coupling Reactions via Arylboronic Acid/Cupric Acetate Arylation.” *Tetrahedron Lett.* **1998**, *39*, 2941–2944.
- (252) Chan, D. M. T.; Monaco, K. L.; Wang, R.-P.; Winters, M. P. “New N- and O-Arylations with Phenylboronic Acids and Cupric Acetate.” *Tetrahedron Lett.* **1998**, *39*, 2933–2936.
- (253) Evans, D. A.; Katz, J. L.; West, T. R. “Synthesis of Diaryl Ethers through the Copper-Promoted Arylation of Phenols with Arylboronic Acids. An Expedient Synthesis of Thyroxine.” *Tetrahedron Lett.* **1998**, *39*, 2937–2940.
- (254) Hili, R.; Yudin, A. K. “Making Carbon-Nitrogen Bonds in Biological and Chemical Synthesis.” *Nat. Chem. Biol.* **2006**, *2*, 284–287.
- (255) Mallia, C. J.; Burton, P. M.; Smith, A. M. R.; Walter, G. C.; Baxendale, I. R. “Catalytic Chan-Lam Coupling Using a “tube-in-Tube” Reactor to Deliver Molecular Oxygen as an Oxidant.” *Beilstein J. Org. Chem.* **2016**, *12*, 1598–1607.
- (256) Ullman, F.; Sponagel, P. “Ueber Die Phenyl- Irlung von Phenolen.” *Eur. J. Inorg.*

- Chem.* **1905**, 388, 2211–2212.
- (257) Meldal, M. “Polymer ‘Clicking’ by CuAAC Reactions.” *Macromol. Rapid Commun.* **2008**, 29, 1016–1051.
- (258) Sonawane, M. D.; Nimse, S. B. “Surface Modification Chemistries of Materials Used in Diagnostic Platforms with Biomolecules.” *J. Chem.* **2016**, 2016, 1–19.
- (259) Pasini, D. “The Click Reaction as an Efficient Tool for the Construction of Macrocyclic Structures.” *Molecules* **2013**, 18, 9512–9530.
- (260) Fuchs, M.; Goessler, W.; Pilger, C.; Kappe, C. O. “Mechanistic Insights into Copper(I)-Catalyzed Azide-Alkyne Cycloadditions Using Continuous Flow Conditions.” *Adv. Synth. Catal.* **2010**, 352, 323–328.
- (261) Iijima, J.; Lim, J. W.; Hong, S. H.; Suzuki, S.; Mimura, K.; Isshiki, M. “Native Oxidation of Ultra High Purity Cu Bulk and Thin Films.” *Appl. Surf. Sci.* **2006**, 253, 2825–2829.
- (262) EMEA European Medicines Agency. “Guideline on the Specification Limits for Residues of Metal Catalysts or Metal Reagents.” *Regul. Doc.* **2008**, Doc. Ref. CPMP/SWP/QWP/4446/00.
- (263) Baxendale, I. R.; Ley, S. V.; Mansfield, A. C.; Smith, C. D. “Multistep Synthesis Using Modular Flow Reactors: Bestmann–Ohira Reagent for the Formation of Alkynes and Triazoles.” *Angew. Chemie - Int. Ed.* **2009**, 48, 4017–4021.
- (264) Otvos, S. B.; Mandity, I. M.; Kiss, L.; Fulop, F. “Alkyne–Azide Cycloadditions with Copper Powder in a High-Pressure Continuous-Flow Reactor: High-Temperature Conditions versus the Role of Additives.” *Chem. - An Asian J.* **2013**, 8, 800–808.
- (265) Shao, C.; Wang, X.; Zhang, Q.; Luo, S.; Zhao, J.; Hu, Y. “Acid-Base Jointly Promoted Copper(I)-Catalyzed Azide-Alkyne Cycloaddition.” *J. Org. Chem.* **2011**, 76, 6832–6836.
- (266) Leibfarth, F. A.; Johnson, J. A.; Jamison, T. F. “Scalable Synthesis of Sequence-Defined, Unimolecular Macromolecules by Flow-IEG.” *Proc. Natl. Acad. Sci.* **2015**, 112, 10617–10622.
- (267) Mijalis, A. J.; Thomas, D. A.; Simon, M. D.; Adamo, A.; Beaumont, R.; Jensen, K. F.; Pentelute, B. L. “A Fully Automated Flow-Based Approach for Accelerated Peptide Synthesis.” *Nat. Chem. Biol.* **2017**, 13, 464–466.
- (268) Maeda, H.; Yamamoto, K.; Kohno, I.; Hafsi, L.; Itoh, N.; Nakagawa, S.; Kanagawa, N.; Suzuki, K.; Uno, T. “Design of a Practical Fluorescent Probe for Superoxide Based on Protection-Deprotection Chemistry of Fluoresceins with Benzenesulfonyl Protecting Groups.” *Chem. - A Eur. J.* **2007**, 13, 1946–1954.

- (269) Taiwo, F. A. “Mechanism of Tiron as Scavenger of Superoxide Ions and Free Electrons.” *Spectroscopy* **2008**, *22*, 491–498.
- (270) Itoh, T.; Nagata, K.; Okada, M.; Ohsawa, A. “The Reaction of 3-Methylthiazolium Derivatives with Superoxide.” *Tetrahedron* **1993**, *49*, 4859–4870.
- (271) Morales, J. C.; Li, L.; Fattah, F. J.; Dong, Y.; Bey, E. A.; Patel, M.; Gao, J.; Boothman, D. A. “Action and Rationale for Targeting in Cancer and Other Diseases.” *Crit Rev Eukaryot Gene Expr* **2014**, *24*, 15–28.
- (272) Jacobson, O.; Kiesewetter, D. O.; Chen, X. “Fluorine-18 Radiochemistry, Labeling Strategies and Synthetic Routes.” *Bioconjug. Chem.* **2015**, *26*, 1–18.
- (273) Zhang, Q.; Lv, H.; Wang, L.; Chen, M.; Li, F.; Liang, C.; Yu, Y.; Jiang, F.; Lu, A.; Zhang, G. “Recent Methods for Purification and Structure Determination of Oligonucleotides.” *Int. J. Mol. Sci.* **2016**, *17* (1–16).
- (274) Valverde, I. E.; Lecaille, F.; Lalmanach, G.; Aucagne, V.; Delmas, A. F. “Synthesis of a Biologically Active Triazole-Containing Analogue of Cystatin A through Successive Peptidomimetic Alkyne-Azide Ligations.” *Angew. Chemie - Int. Ed.* **2012**, *51*, 718–722.
- (275) Li, S.; Cai, H.; He, J.; Chen, H.; Lam, S.; Cai, T.; Zhu, Z.; Bark, S. J.; Cai, C. “Extent of the Oxidative Side Reactions to Peptides and Proteins during the CuAAC Reaction.” *Bioconjug. Chem.* **2016**, *27*, 2315–2322.
- (276) Re, F.; Cambianica, I.; Zona, C.; Sesana, S.; Gregori, M.; Rigolio, R.; La Ferla, B.; Nicotra, F.; Forloni, G.; Cagnotto, A.; Salmona, M.; Masserini, M.; Sancini, G. “Functionalization of Liposomes with ApoE-Derived Peptides at Different Density Affects Cellular Uptake and Drug Transport across a Blood-Brain Barrier Model.” *Nanomedicine Nanotechnology, Biol. Med.* **2011**, *7*, 551–559.
- (277) Taskova, M.; Mantsiou, A.; Astakhova, K. “Synthetic Nucleic Acid Analogues in Gene Therapy: An Update for Peptide–Oligonucleotide Conjugates.” *ChemBioChem* **2017**, *18*, 1671–1682.
- (278) Sharma, V. K.; Sharma, R. K.; Singh, S. K. “Antisense Oligonucleotides: Modifications and Clinical Trials.” *Medchemcomm* **2014**, *5*, 1454–1471.
- (279) Yin, H.; Saleh, A. F.; Betts, C.; Camelliti, P.; Seow, Y.; Ashraf, S.; Arzumanov, A.; Hammond, S.; Merritt, T.; Gait, M. J.; Wood, M. J. A. “Pip5 Transduction Peptides Direct High Efficiency Oligonucleotide-Mediated Dystrophin Exon Skipping in Heart and Phenotypic Correction in Mdx Mice.” *Mol. Ther.* **2011**, *19*, 1295–1303.
- (280) Betts, C.; Saleh, A. F.; Arzumanov, A. A.; Hammond, S. M.; Godfrey, C.; Coursindel, T.; Gait, M. J.; Wood, M. J. “Pip6-PMO, a New Generation of Peptide-Oligonucleotide

- Conjugates with Improved Cardiac Exon Skipping Activity for DMD Treatment.” *Mol. Ther. - Nucleic Acids* **2012**, *1*, 1–13.
- (281) Zhang, X.; Liu, P.; Zhu, L. “Structural Determinants of Alkyne Reactivity in Copper-Catalyzed Azide-Alkyne Cycloadditions.” *Molecules* **2016**, *21*, 1697–1714.
- (282) Coelho, A.; Diz, P.; Caamaño, O.; Sotelo, E. “Polymer-Supported 1,5,7-Triazabicyclo [4.4.0] Dec-5-Ene as Polyvalent Ligands in the Copper-Catalyzed Huisgen 1,3-Dipolar Cycloaddition.” *Adv. Synth. Catal.* **2010**, *352*, 1179–1192.
- (283) Santos, C. M.; Kumar, A.; Zhang, W.; Cai, C. “Functionalization of Fluorous Thin Films via “click” Chemistry”. *Chem. Commun.* **2009**, No. 20, 2854–2856.
- (284) Martin, M. M.; Lindqvist, L. “The PH Dependence of Fluorescein Fluorescence.” *J. Lumin.* **1975**, *10*, 381–390.
- (285) Sirivolu, V. R.; Vernekar, S. K. V.; Ilina, T.; Myshakina, N. S.; Parniak, M. a; Wang, Z. “Clicking 3'-Azidothymidine into Novel Potent Inhibitors of Human Immunodeficiency Virus.” *J. Med. Chem.* **2013**, *56*, 8765–8780.
- (286) Ovenall, D. W.; Chang, J. J. “Carbon-13 NMR of Fluorinated Compounds Using Wide-Band Fluorine Decoupling.” *J. Magn. Reson.* **1977**, *25*, 361–372.

Appendix

Supplementary data for Chapter 2 compounds can be found at the following links:

<https://pubs.acs.org/doi/suppl/10.1021/acs.orglett.6b00635>

<https://pubs.acs.org/doi/suppl/10.1021/acs.joc.7b00545>.

Supplementary data for Chapter 4 compounds can be found at the following link:

[https://static-content.springer.com/esm/art%3A10.1038%2Fs41467-018-06551-](https://static-content.springer.com/esm/art%3A10.1038%2Fs41467-018-06551-0/MediaObjects/41467_2018_6551_MOESM1_ESM.pdf)

[0/MediaObjects/41467_2018_6551_MOESM1_ESM.pdf](https://static-content.springer.com/esm/art%3A10.1038%2Fs41467-018-06551-0/MediaObjects/41467_2018_6551_MOESM1_ESM.pdf)

5.1 RP-HPLC and LC-MS Method Parameters

5.1.1 RP-HPLC

5.1.1.1 Analytical RP-HPLC generic method (small molecules/peptides)

Column specification: Aeris 3.6 μm WIDEPORÉ XB-C18, 250 x 4.6 mm.

Column temperature 25 °C

Mobile phase A: 0.1% v / v TFA in water

Mobile phase B: 0.1% v / v TFA in acetonitrile

Flow rate 1.0 mL/min

Gradient profile:

Time (mins)	%A	%B
0	95	5
5	95	5
40	40	60
43	40	60
44	10	90
47	10	90
48	95	5
50	95	5

The UV detection signal was recorded at 254 nm.

5.1.1.2 8-Minute generic method (small molecules)

Column specification: Phenomenex Luna C18(2), 50 x 2.0 mm, 3 m.

Column temperature: 40 °C

Mobile phase A: 0.05% v / v TFA in water

Mobile phase B: 0.05% v / v TFA in acetonitrile

Flow rate: 1 mL/min

Gradient profile:

Time (mins)	%A	%B
0	100	0
8	5	95
8.01	100	0

The UV detection signal was recorded at 254 nm.

5.1.1.3 Analytical RP-HPLC generic method (ODNs)

Column specification: Phenomenex Clarity 5 µM Oligo-RP, 250 x 4.6 mm.

Column temperature 25 °C

Mobile phase A: 0.1 M TEAA in water

Mobile phase B: 0.1 M TEAA in acetonitrile/water 8/2

Flow rate 1.0 mL/min

Gradient profile:

Time (mins)	%A	%B
0	90	10
5	90	10
35	50	50
40	10	90
55	10	90
57	90	10
67	90	10

The UV detection signal was recorded at 260 nm.

5.1.2 LC-MS

LC Conditions: The HPLC analysis was conducted on a Zorbax 45mm x 150mm C18 at 40 °C.

The solvents employed were:

A = 5 mM ammonium acetate in water.

B = 5 mM ammonium acetate in acetonitrile.

The gradient employed was:

Time (min)	Flow (ml/min)	Rate	% A	% B
0	1		95	5
1.48	1		95	5
8.5	1		0	100
13.5	1		0	100
16.5	1		95	5
18	1		95	5

The UV detection signal was recorded at 254 nm.

MS Conditions

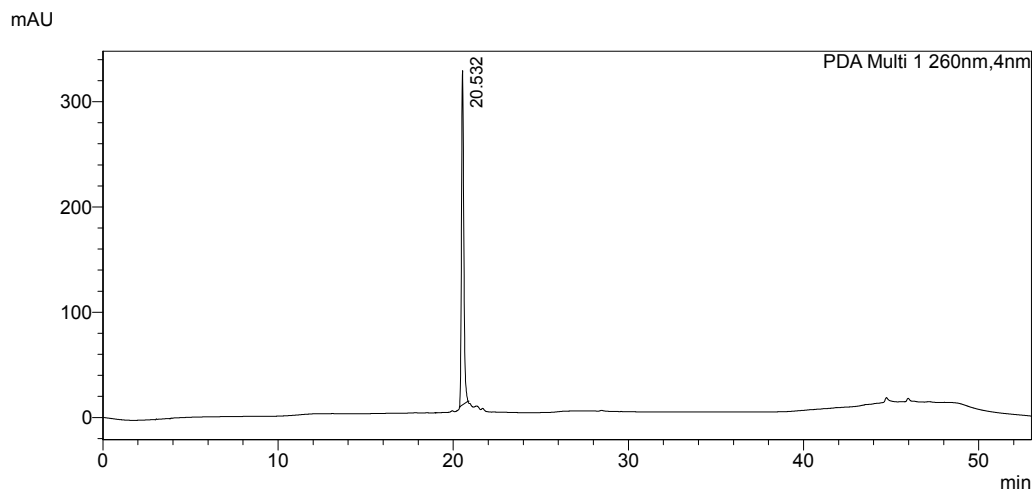
MS: Agilent Quadrupole

Ionisation mode: Positive and/or negative electrospray.

Scan Range: 100 to 1000 AMU positive, 120-1000 AMU negative.

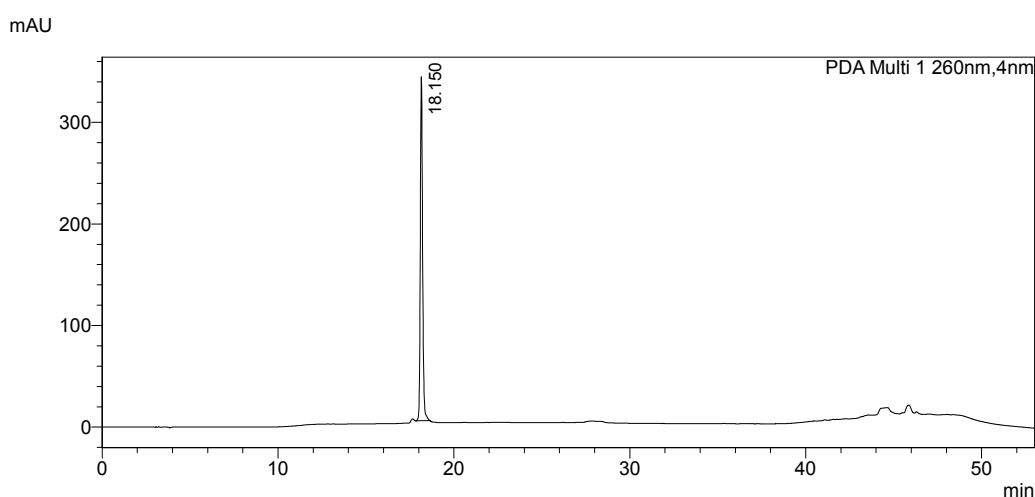
5.2 RP-HPLC Traces

5.2.1 RP-HPLC Traces from Scheme 3.18

**<Peak Table>**

PDA Ch1 260nm

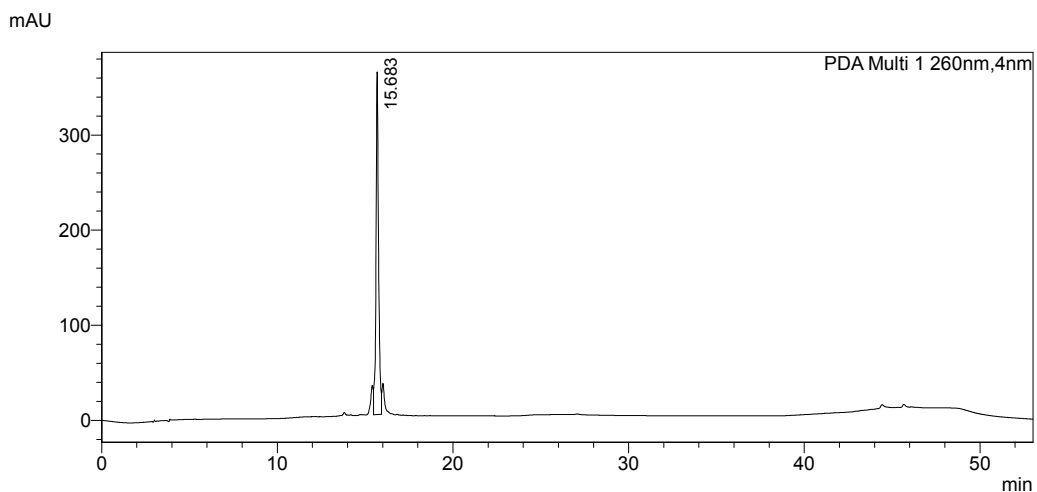
Peak#	Ret. Time	Area	Height	Conc.	Unit	Mark	Name
1	20.532	2880185	317429	0.000		M	
Total		2880185	317429				

Appendix 1: RP-HPLC trace of ODN3.18.**<Peak Table>**

PDA Ch1 260nm

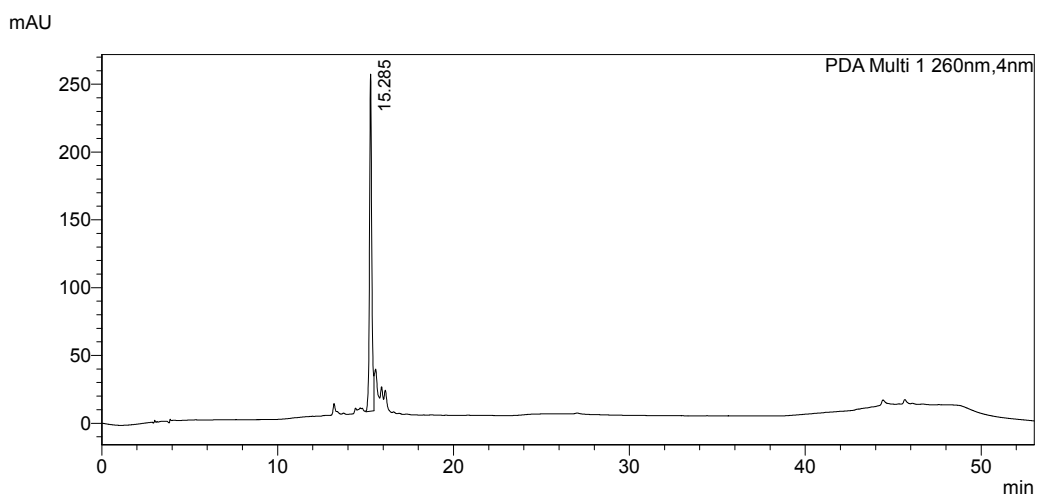
Peak#	Ret. Time	Area	Height	Conc.	Unit	Mark	Name
1	18.150	3070720	338674	0.000	nmol	M	dna ynamine
Total		3070720	338674				

Appendix 2: RP-HPLC trace of ODN3.19.

**<Peak Table>**

PDA Ch1 260nm

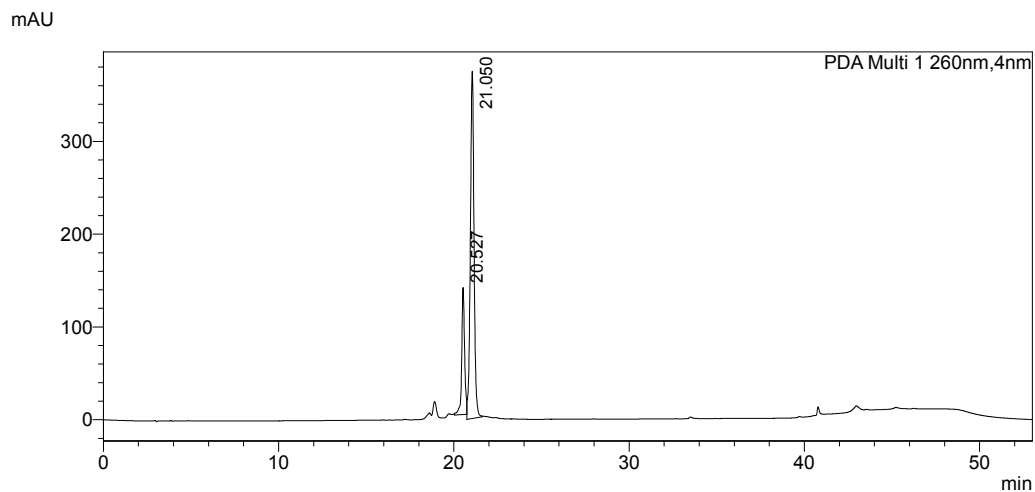
Peak#	Ret. Time	Area	Height	Conc.	Unit	Mark	Name
1	15.683	3629160	360099	0.000		M	
Total		3629160	360099				

Appendix 3: RP-HPLC trace of ODN3.20.**<Peak Table>**

PDA Ch1 260nm

Peak#	Ret. Time	Area	Height	Conc.	Unit	Mark	Name
1	15.285	2223490	248561	0.000		M	
Total		2223490	248561				

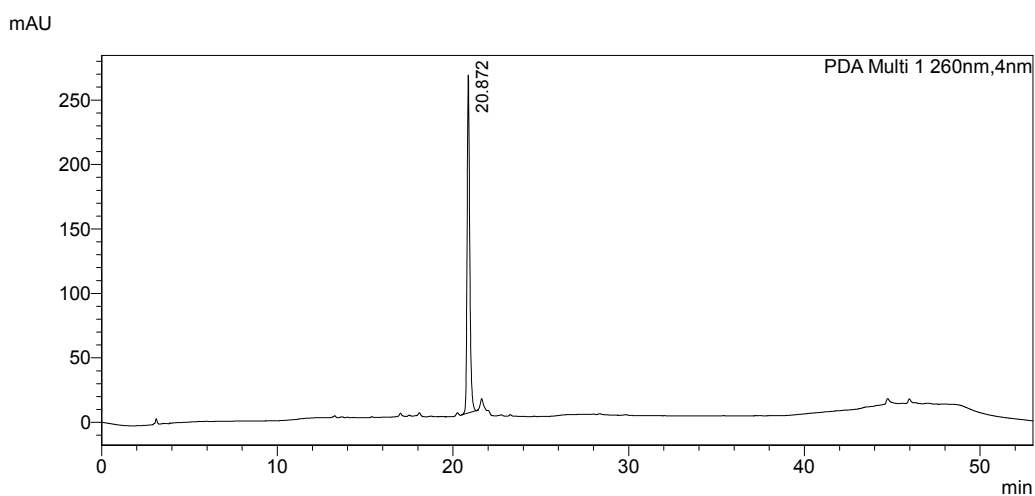
Appendix 4: RP-HPLC trace of ODN3.21.

**<Peak Table>**

PDA Ch1 260nm

Peak#	Ret. Time	Area	Height	Conc.	Unit	Mark	Name
1	20.527	1560013	136876	0.000		M	
2	21.050	5479996	373895	0.000		M	
Total		7040009	510772				

Appendix 5: RP-HPLC trace of ODN3.22.

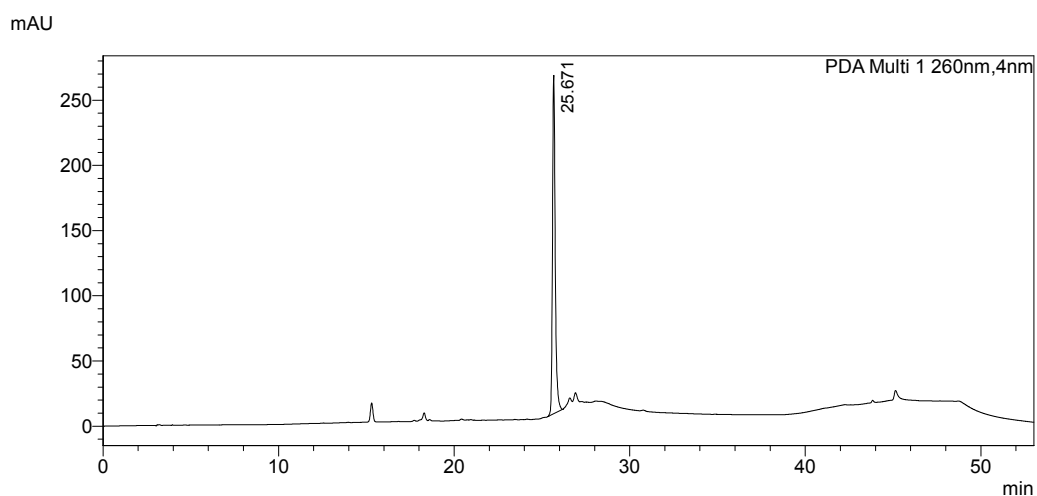
5.2.2 HPLC Chromatograms from Figure 3.14**<Peak Table>**

PDA Ch1 260nm

Peak#	Ret. Time	Area	Height	Conc.	Unit	Mark	Name
1	20.872	2716125	262058	0.000		M	
Total		2716125	262058				

Appendix 6: RP-HPLC trace of ODN3.24a.

5.2.3 RP-HPLC Chromatograms from Scheme 3.19

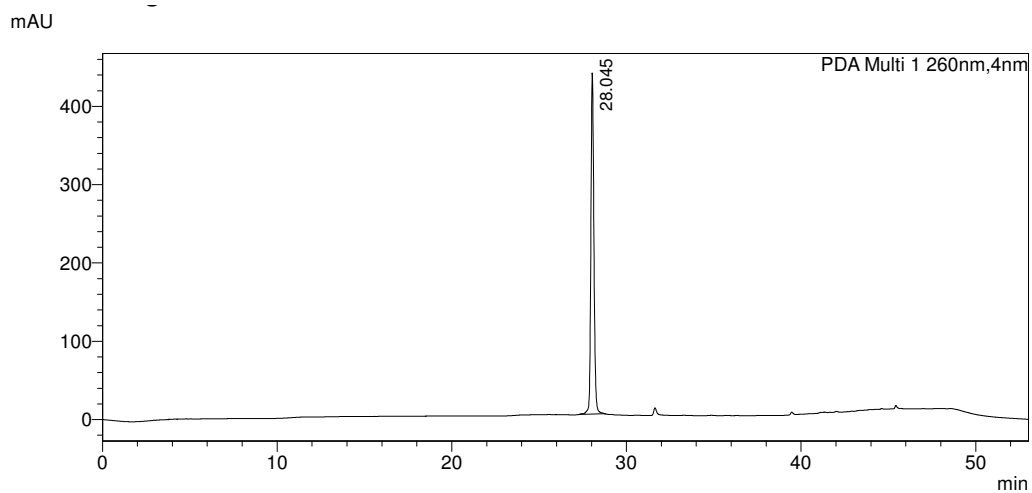


<Peak Table>

PDA Ch1 260nm

Peak#	Ret. Time	Area	Height	Conc.	Unit	Mark	Name
1	25.671	2816905	259386	0.000		M	
Total		2816905	259386				

Appendix 7: RP-HPLC trace of ODN3.23a.

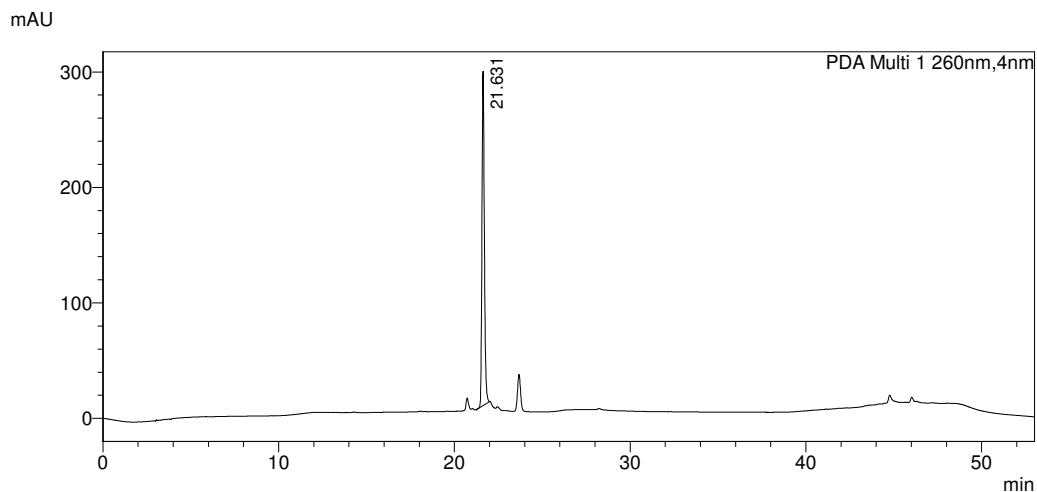


<Peak Table>

PDA Ch1 260nm

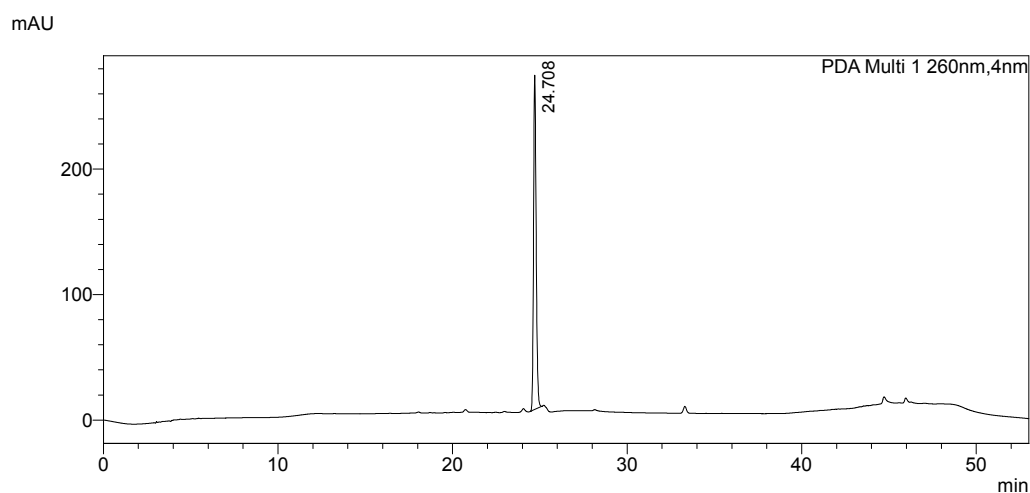
Peak#	Ret. Time	Area	Height	Conc.	Unit	Mark	Name
1	28.045	5261811	435574	0.000		M	
Total		5261811	435574				

Appendix 8: RP-HPLC trace of ODN3.23b.

**<Peak Table>**

PDA Ch1 260nm

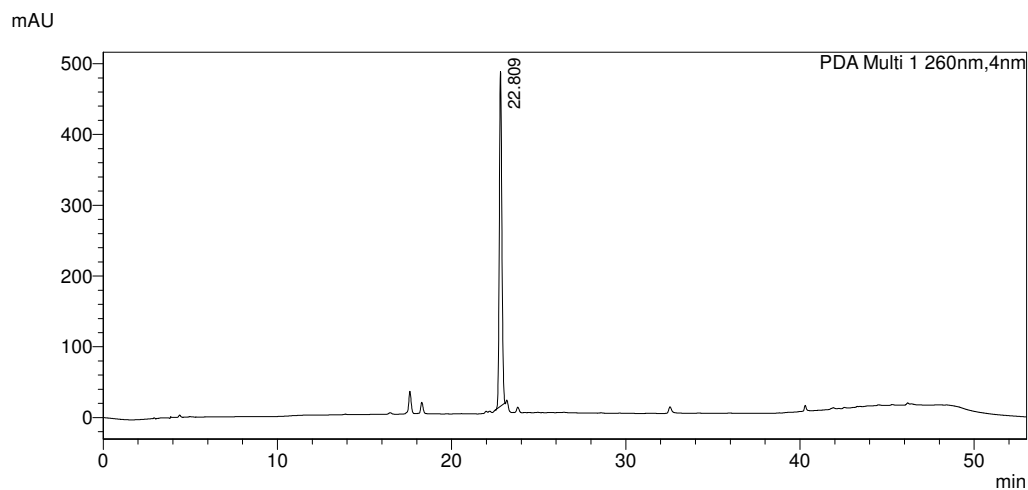
Peak#	Ret. Time	Area	Height	Conc.	Unit	Mark	Name
1	21.631	2754976	289375	0.000		M	
Total		2754976	289375				

Appendix 9: RP-HPLC trace of ODN3.23c.**<Peak Table>**

PDA Ch1 260nm

Peak#	Ret. Time	Area	Height	Conc.	Unit	Mark	Name
1	24.708	2752667	266278	0.000		M	
Total		2752667	266278				

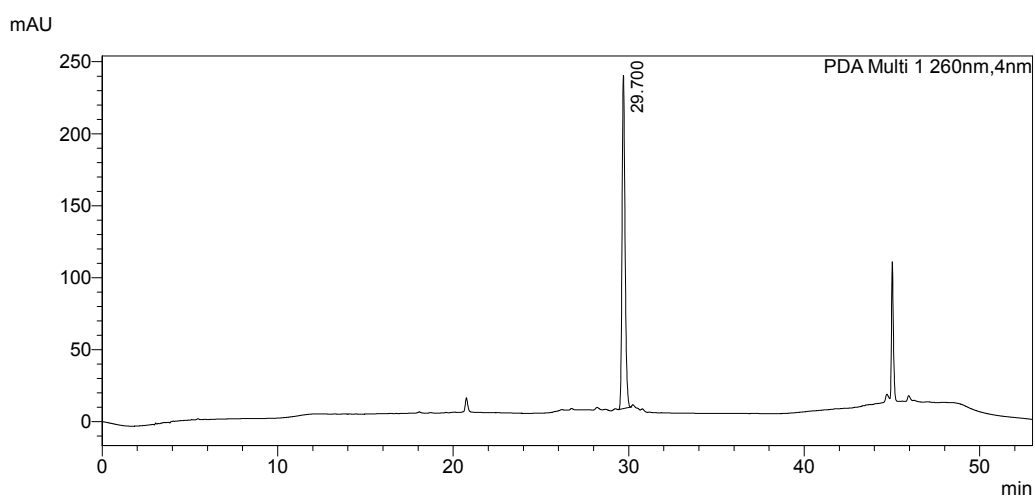
Appendix 10: RP-HPLC trace of ODN3.23d.

**<Peak Table>**

PDA Ch1 260nm

Peak#	Ret. Time	Area	Height	Conc.	Unit	Mark	Name
1	22.809	4828969	472804	0.000		M	
Total		4828969	472804				

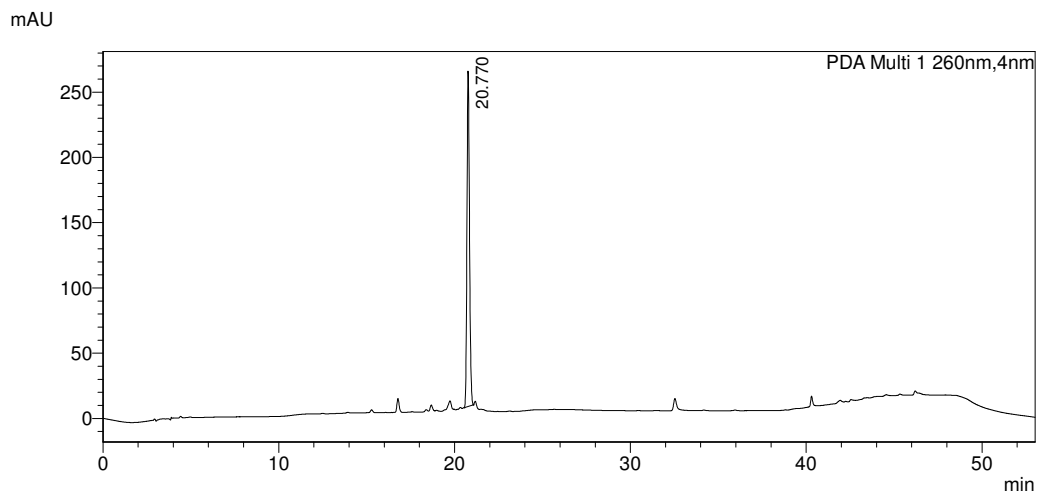
Appendix 11: RP-HPLC trace of ODN3.23e.

**<Peak Table>**

PDA Ch1 260nm

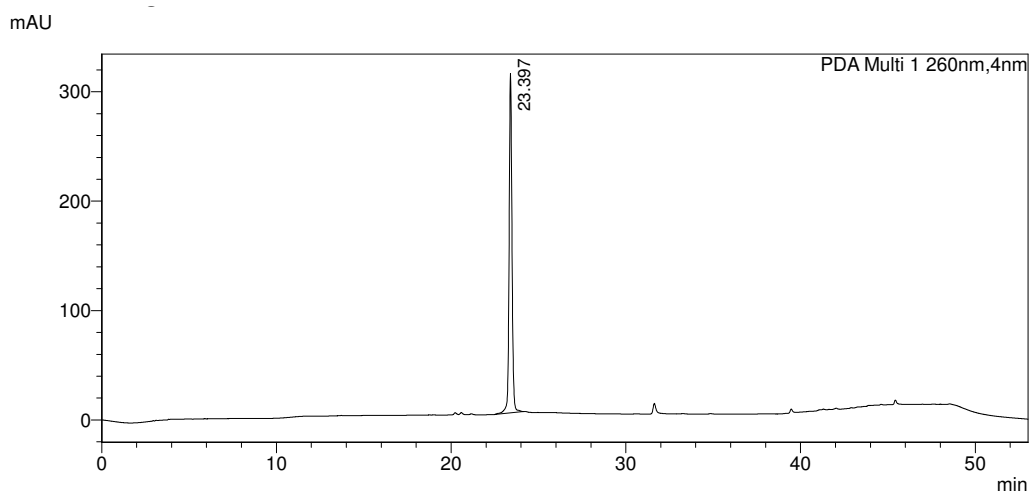
Peak#	Ret. Time	Area	Height	Conc.	Unit	Mark	Name
1	29.700	2738753	231323	0.000		M	
Total		2738753	231323				

Appendix 12: RP-HPLC trace of ODN3.23f.

**<Peak Table>**

PDA Ch1 260nm

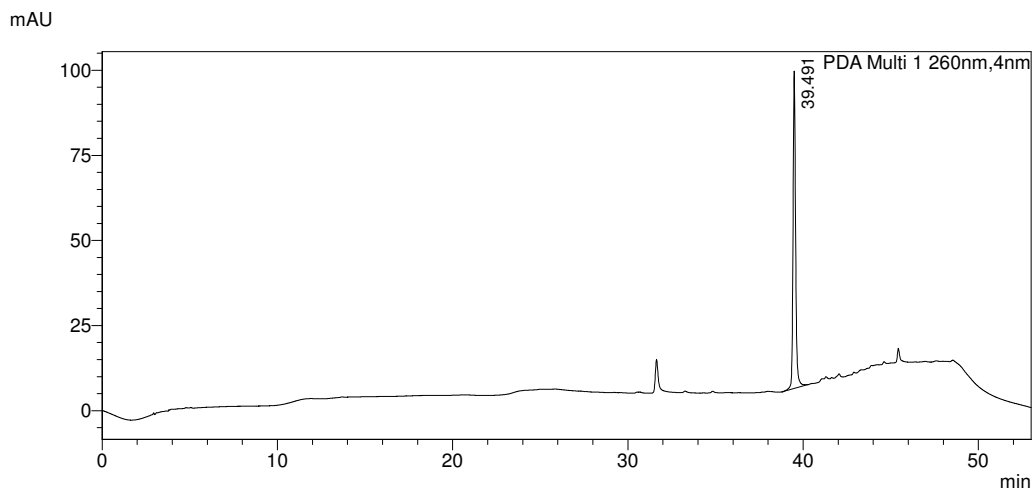
Peak#	Ret. Time	Area	Height	Conc.	Unit	Mark	Name
1	20.770	2585679	256899	0.000		M	
Total		2585679	256899				

Appendix 13: RP-HPLC trace of ODN3.23g.**<Peak Table>**

PDA Ch1 260nm

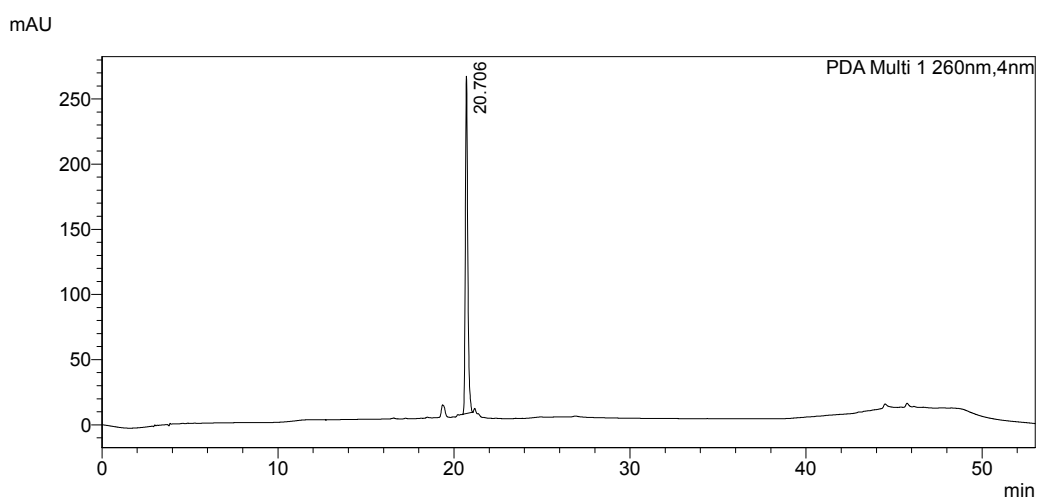
Peak#	Ret. Time	Area	Height	Conc.	Unit	Mark	Name
1	23.397	3544483	310063	0.000		M	
Total		3544483	310063				

Appendix 14: RP-HPLC trace of ODN3.23h.

**<Peak Table>**

PDA Ch1 260nm

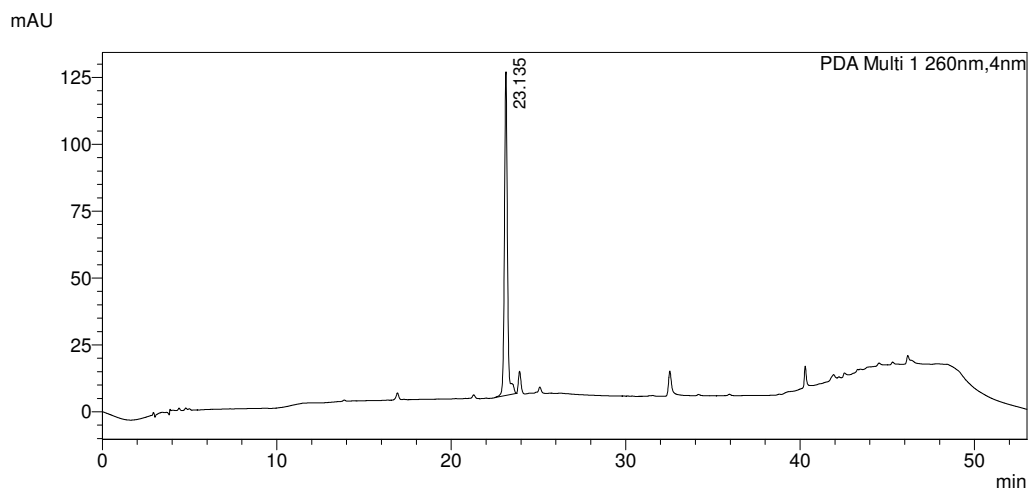
Peak#	Ret. Time	Area	Height	Conc.	Unit	Mark	Name
1	39.491	944233	93197	0.000		M	
Total		944233	93197				

Appendix 15: RP-HPLC trace of **ODN3.23i**.**<Peak Table>**

PDA Ch1 260nm

Peak#	Ret. Time	Area	Height	Conc.	Unit	Mark	Name
1	20.706	2448158	258748	0.000		M	
Total		2448158	258748				

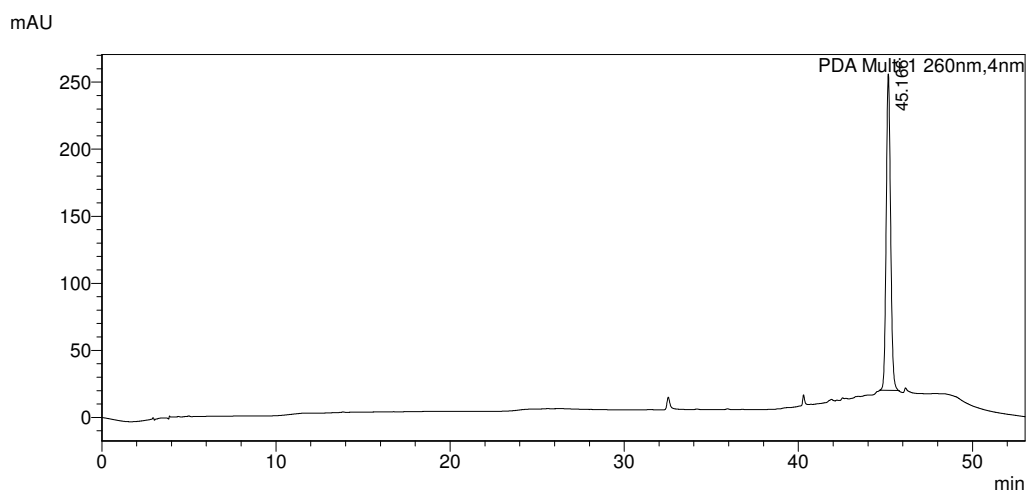
Appendix 16: RP-HPLC trace of **ODN3.23j**.

**<Peak Table>**

PDA Ch1 260nm

Peak#	Ret. Time	Area	Height	Conc.	Unit	Mark	Name
1	23.135	1442553	120940	0.000		M	
Total		1442553	120940				

Appendix 17: RP-HPLC trace of ODN3.23k.

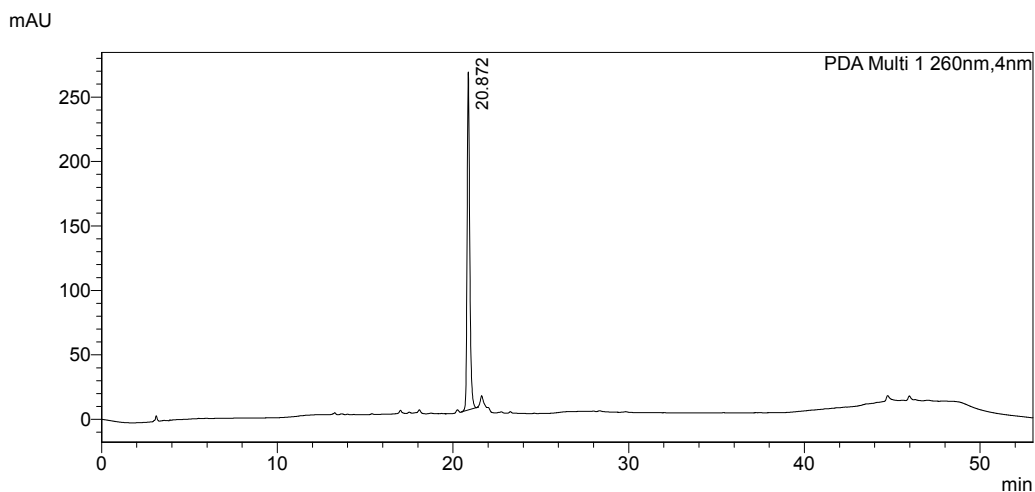
**<Peak Table>**

PDA Ch1 260nm

Peak#	Ret. Time	Area	Height	Conc.	Unit	Mark	Name
1	45.166	4122437	235879	0.000		M	
Total		4122437	235879				

Appendix 18: RP-HPLC trace of ODN3.23l.

5.2.4 RP-HPLC Chromatograms from Figure 3.15

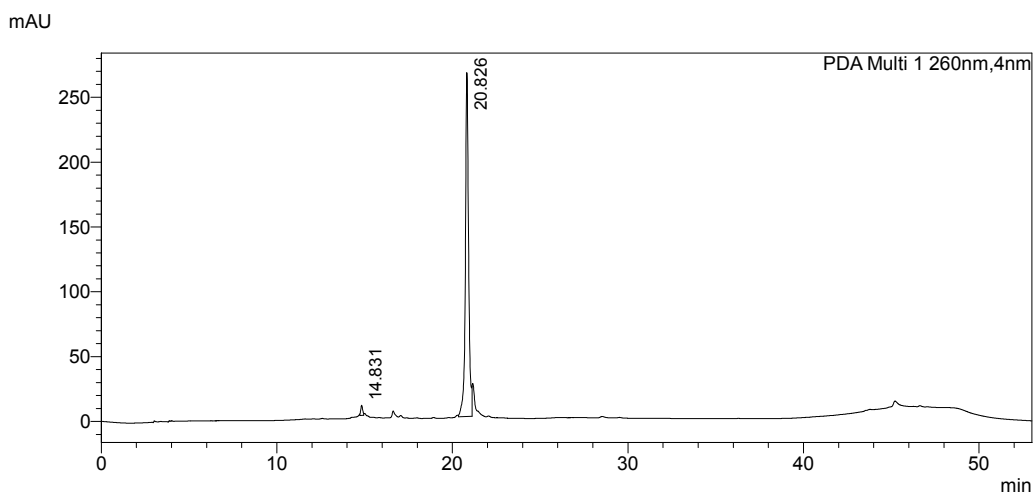


<Peak Table>

PDA Ch1 260nm							
Peak#	Ret. Time	Area	Height	Conc.	Unit	Mark	Name
1	20.872	2716125	262058	0.000		M	
Total		2716125	262058				

Appendix 19: RP-HPLC trace of ODN3.25a.

5.2.5 RP-HPLC Chromatograms from Figure 3.16

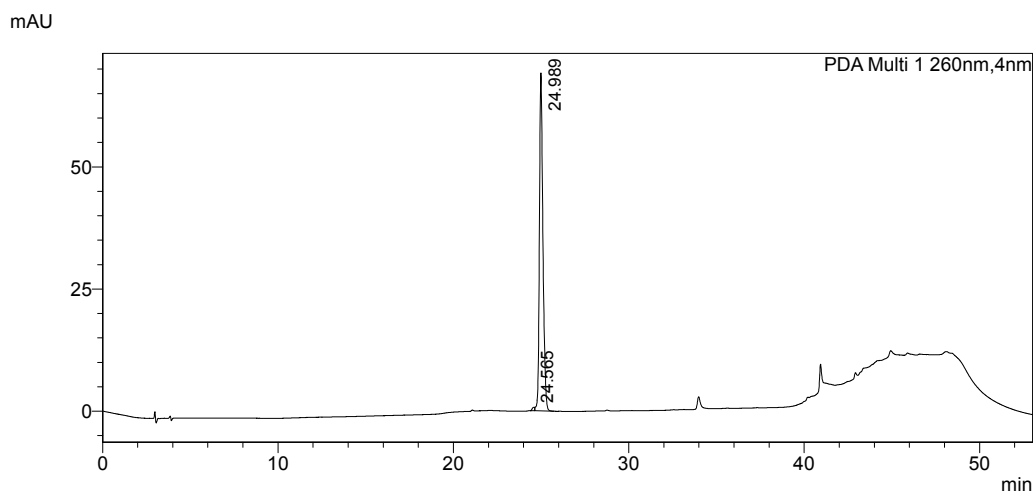


<Peak Table>

PDA Ch1 260nm							
Peak#	Ret. Time	Area	Height	Conc.	Unit	Mark	Name
1	14.831	59907	7900	0.000		M	
2	20.826	3395247	265147	0.000		M	
Total		3455154	273047				

Appendix 20: RP-HPLC trace of ODN3.26a.

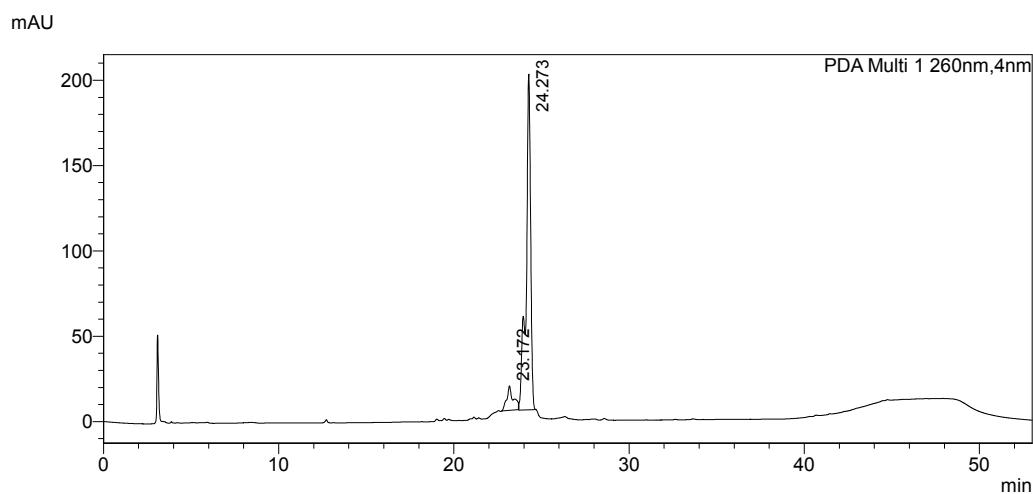
5.2.6 RP-HPLC Chromatograms from Scheme 3.20



<Peak Table>

PDA Ch1 260nm							
Peak#	Ret. Time	Area	Height	Conc.	Unit	Mark	Name
1	24.565	6906	710	0.000			
2	24.989	964281	69166	0.000		V	
Total		971187	69875				

Appendix 21: RP-HPLC trace of ODN3.27.

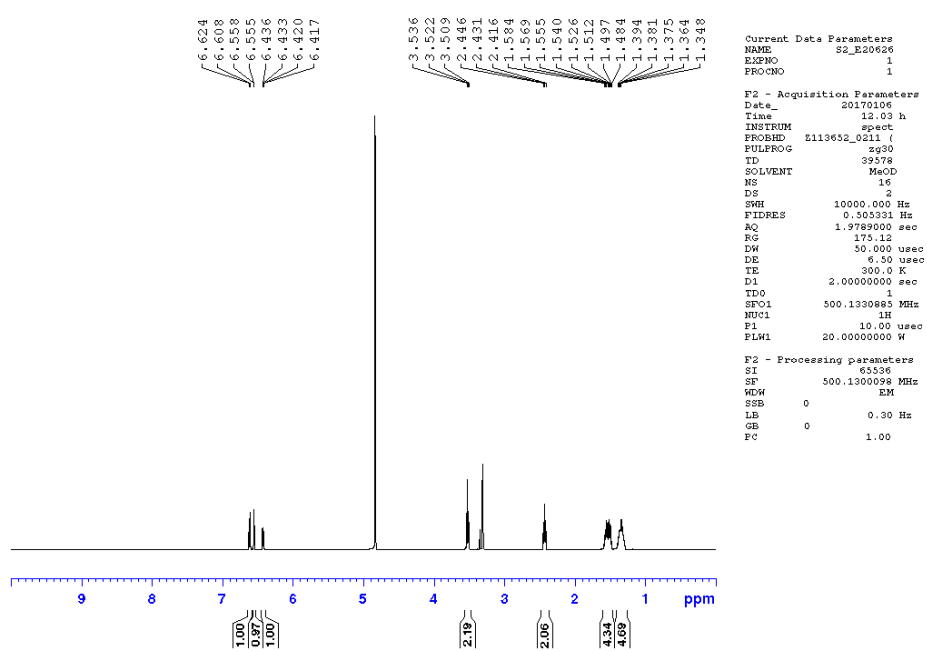
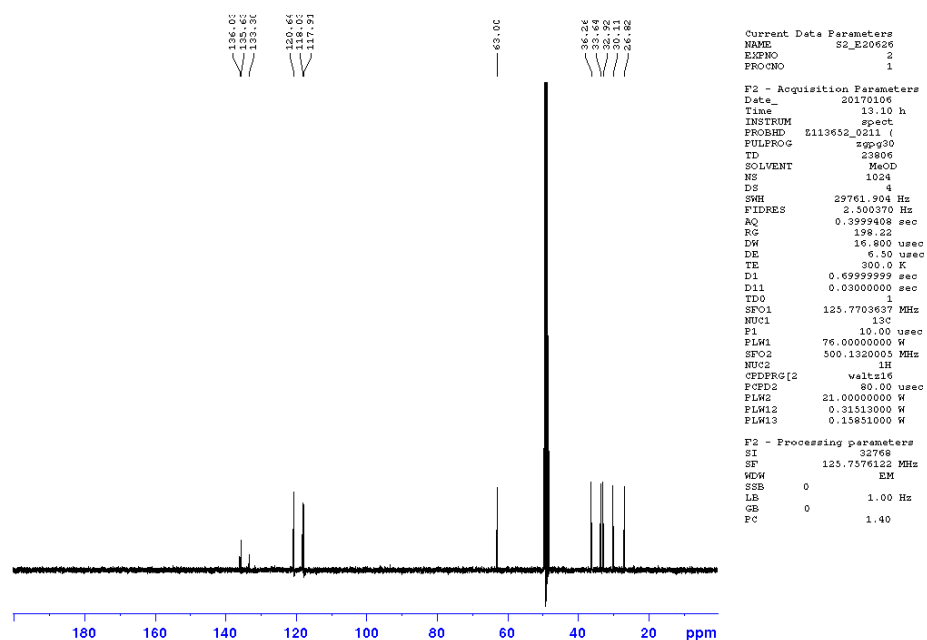


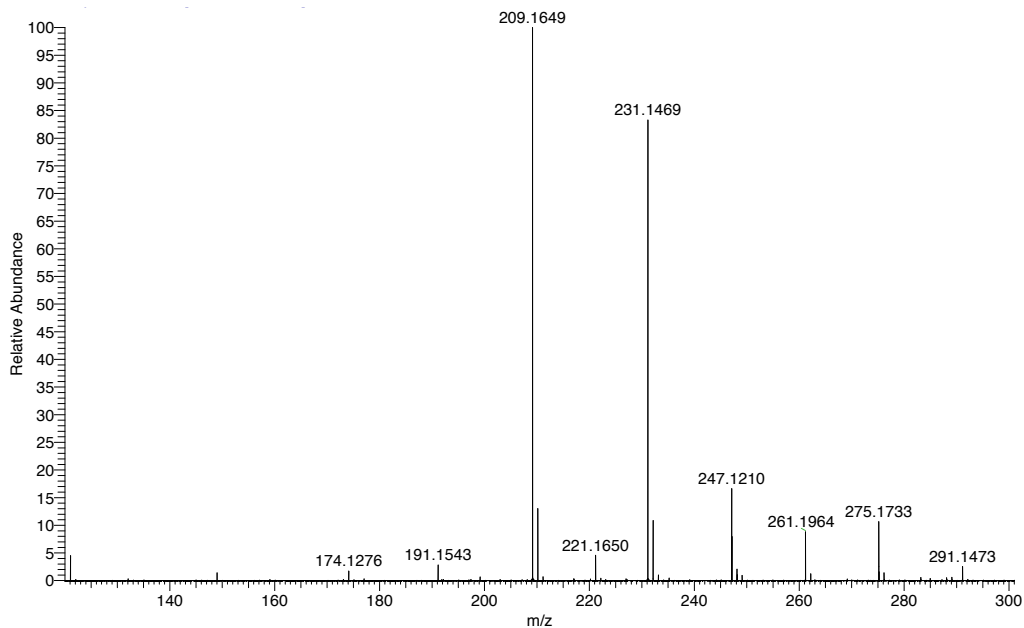
<Peak Table>

PDA Ch1 260nm							
Peak#	Ret. Time	Area	Height	Conc.	Unit	Mark	Name
1	23.172	372042	14350	0.000		M	
2	24.273	3541993	196704	0.000		M	
Total		3914035	211054				

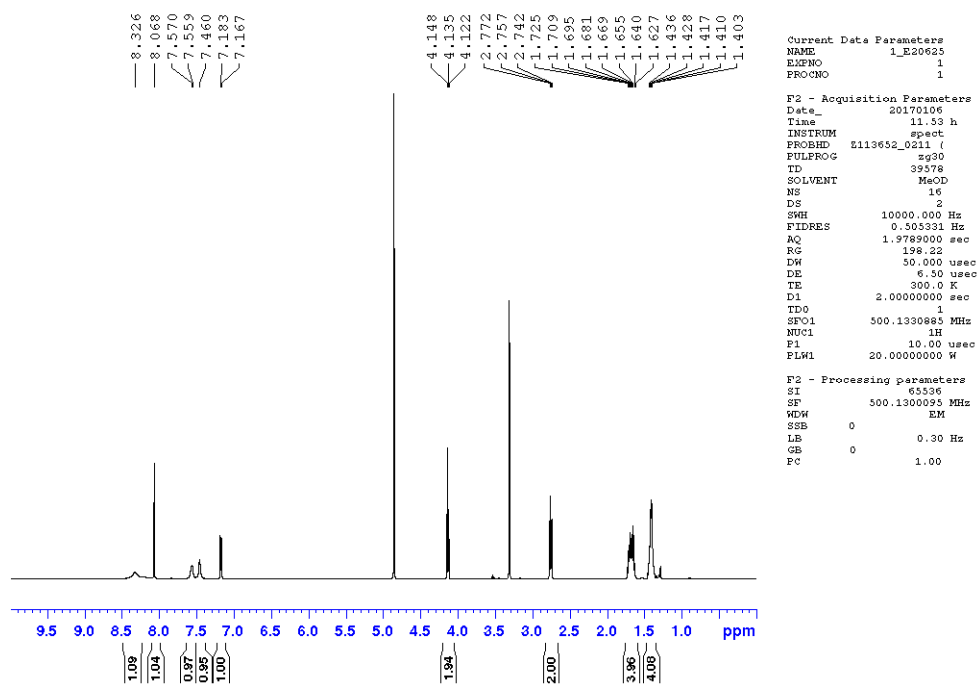
Appendix 22: RP-HPLC trace of ODN3.28.

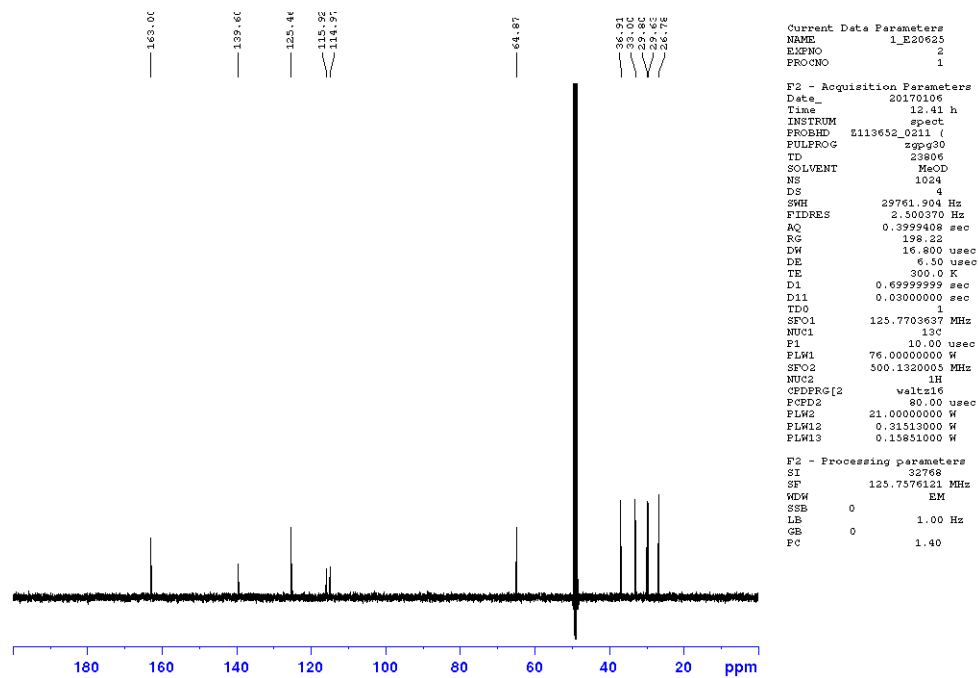
5.3 NMR and MS Spectrums

Appendix 23: ¹H NMR spectrum of 3.32.Appendix 24: ¹³C NMR spectrum of 3.32.

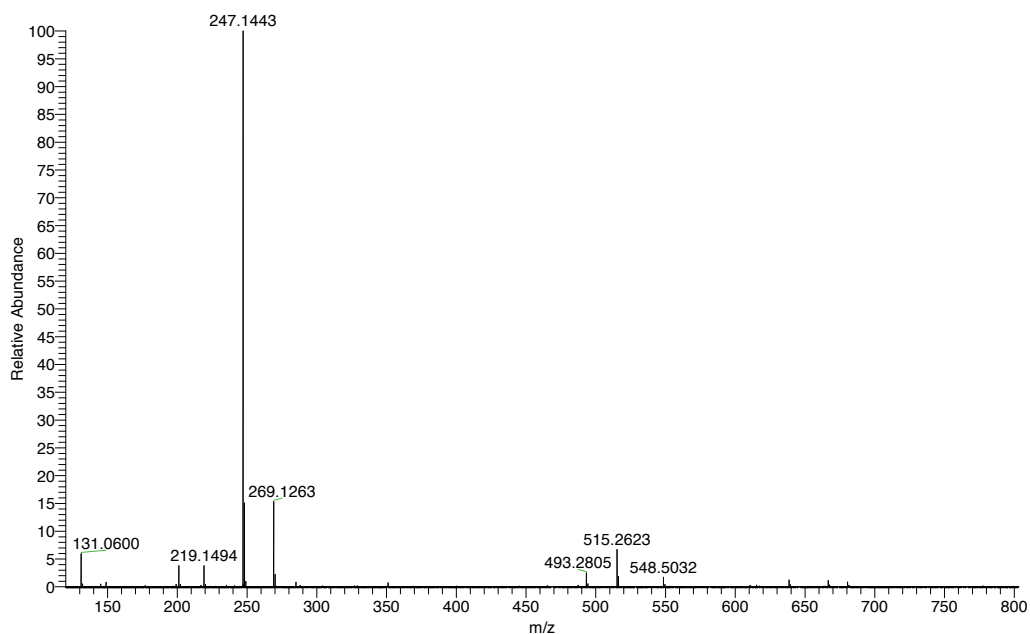


Appendix 25: HRMS spectrum of 3.32.

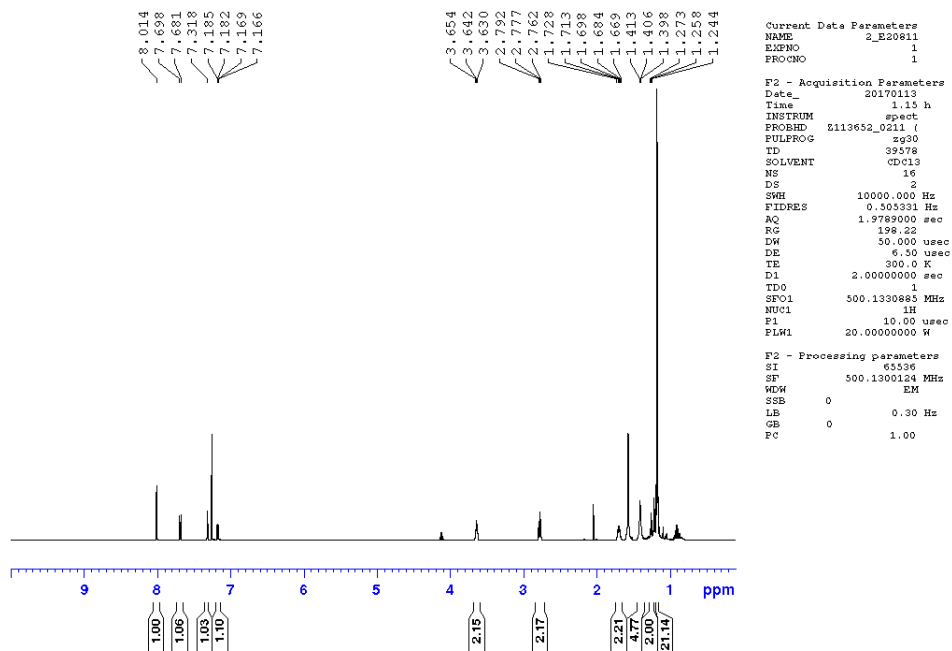
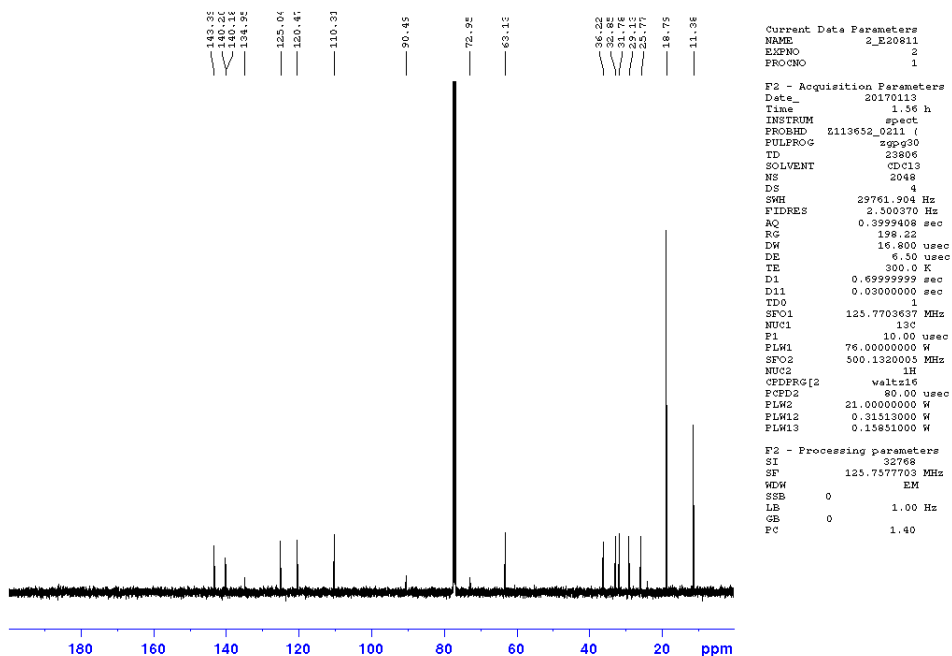
Appendix 26: ¹H NMR spectrum of 3.33.

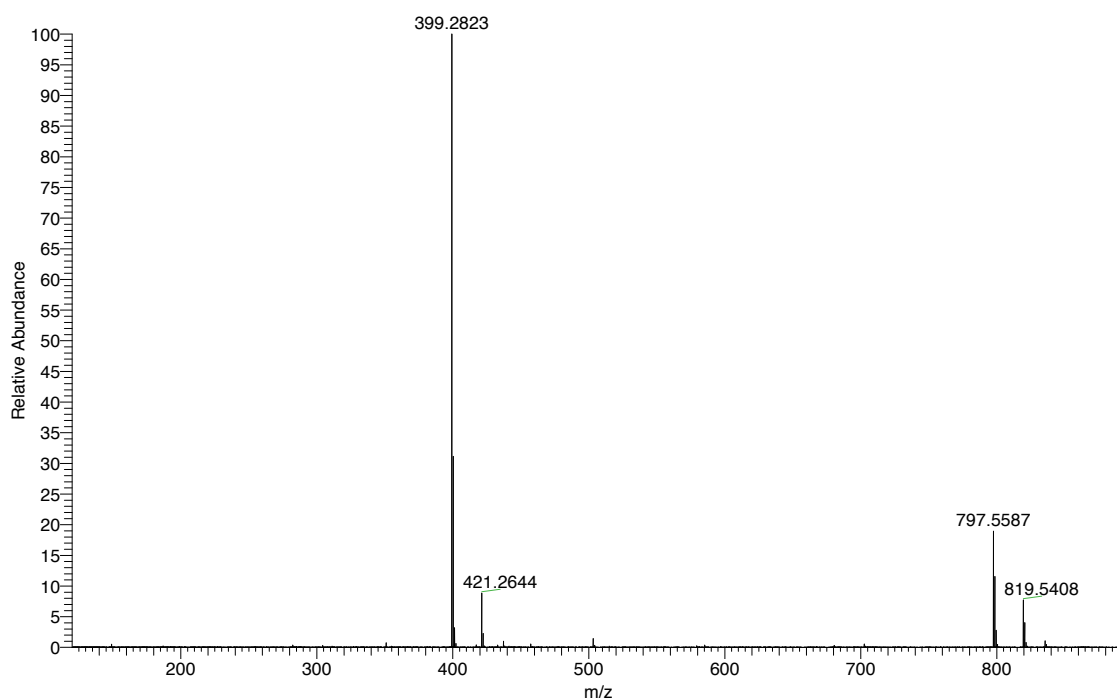


Appendix 267: ¹³C NMR spectrum of 3.33.

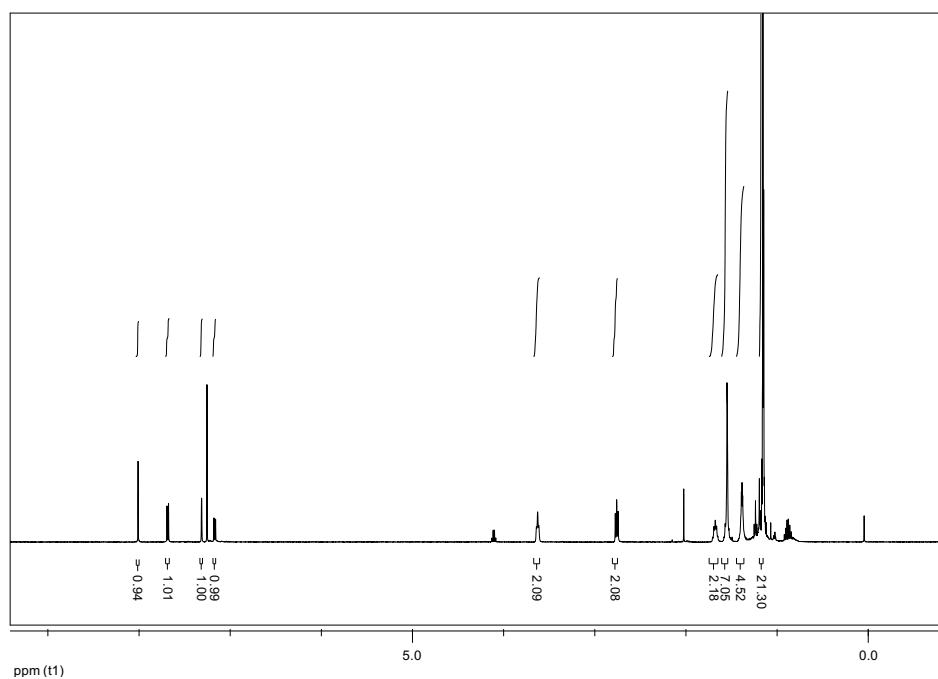


Appendix 28: HRMS spectrum of 3.33.

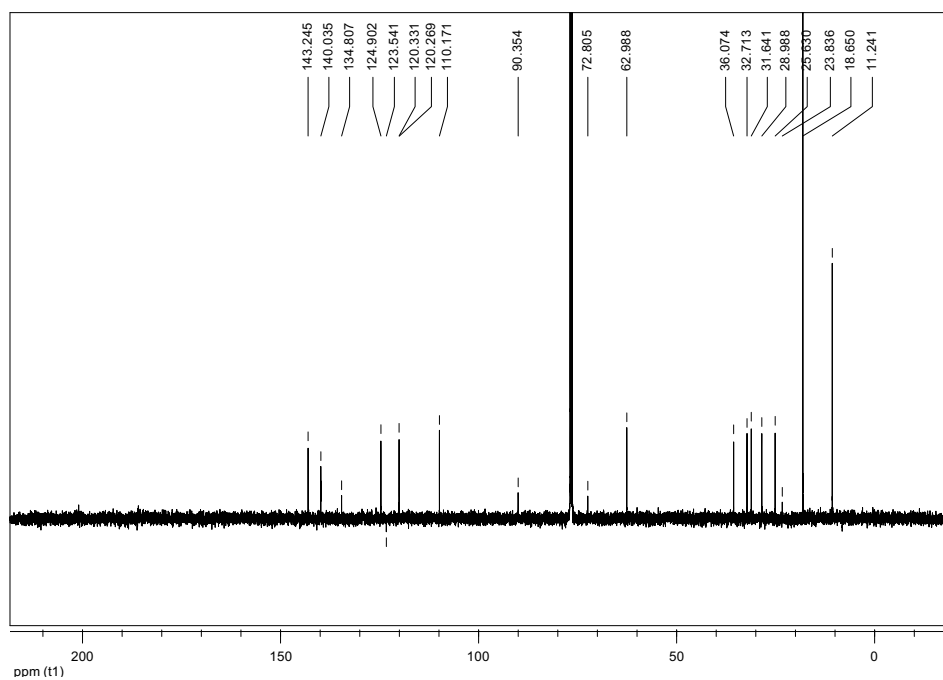
Appendix 29: ¹H NMR spectrum of 3.34a.Appendix 30: ¹³C NMR spectrum of 3.34a.



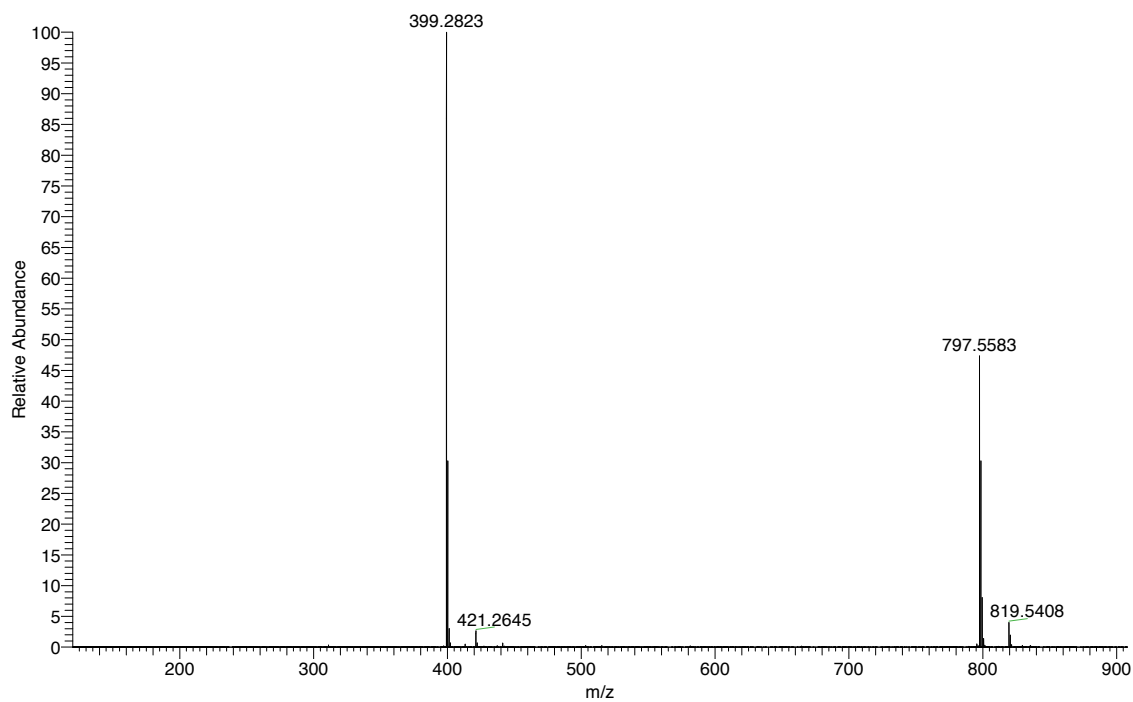
Appendix 31: HRMS spectrum of 3.34a.



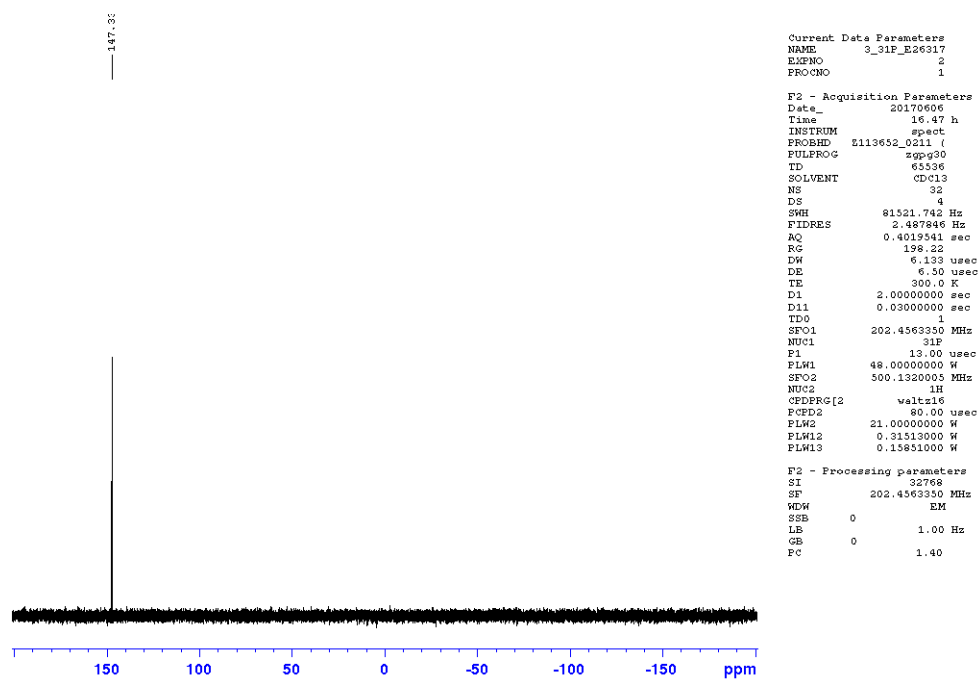
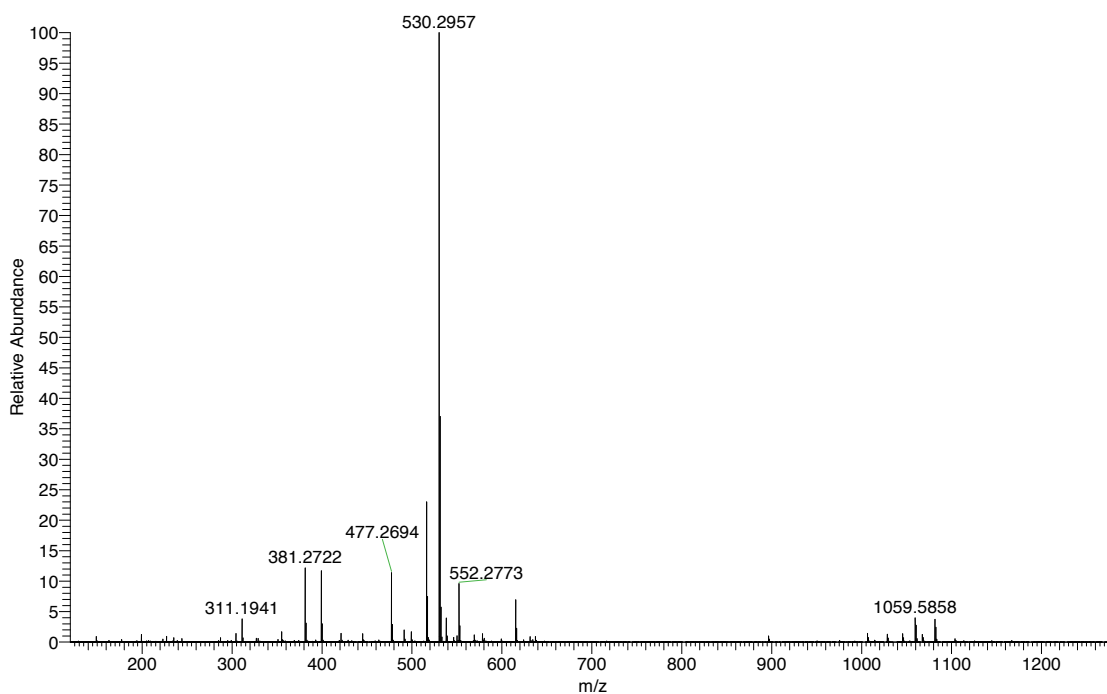
Appendix 32: ¹H spectrum of 3.34b.

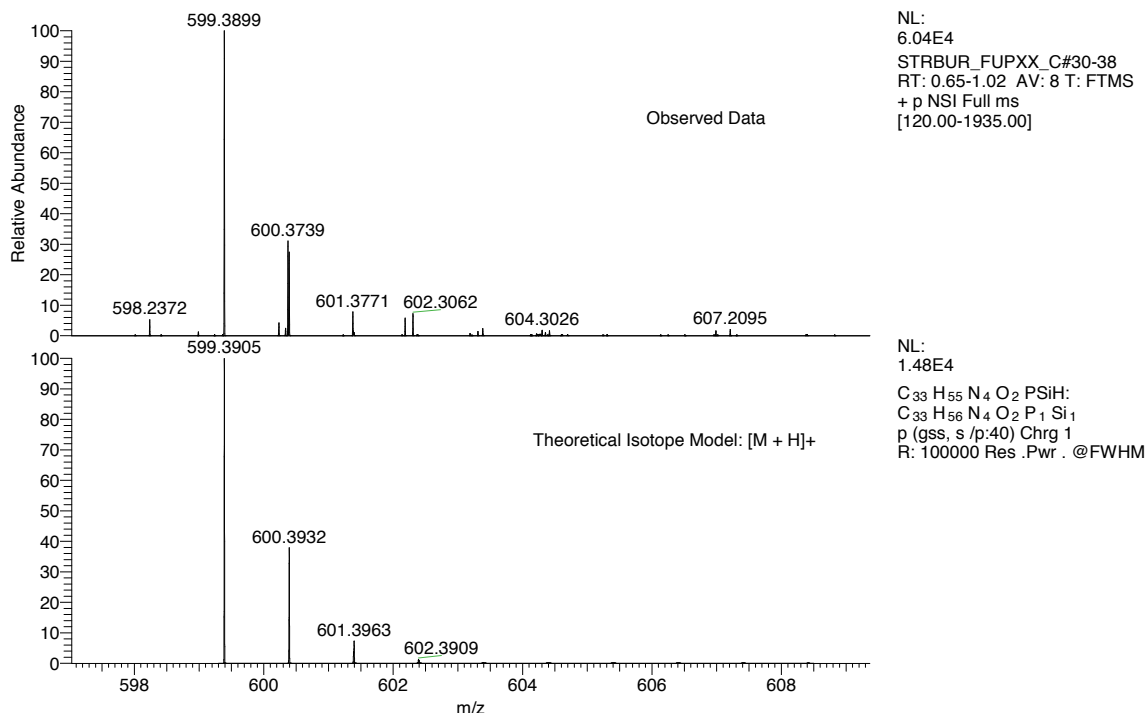


Appendix 34: ¹³C spectrum of 3.34b.

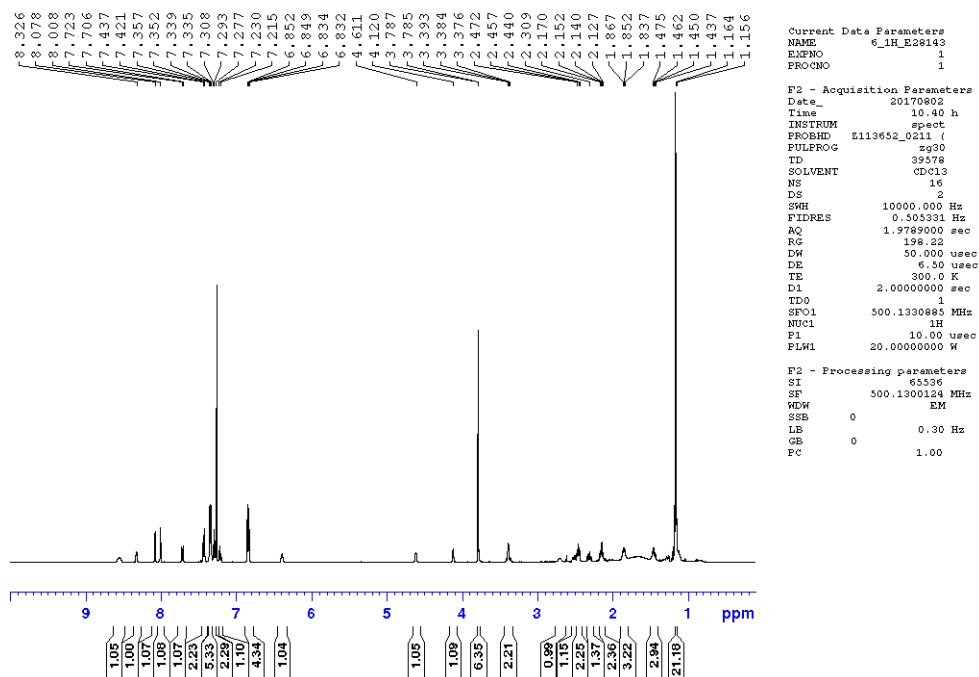


Appendix 35: HRMS spectrum of 3.34b.

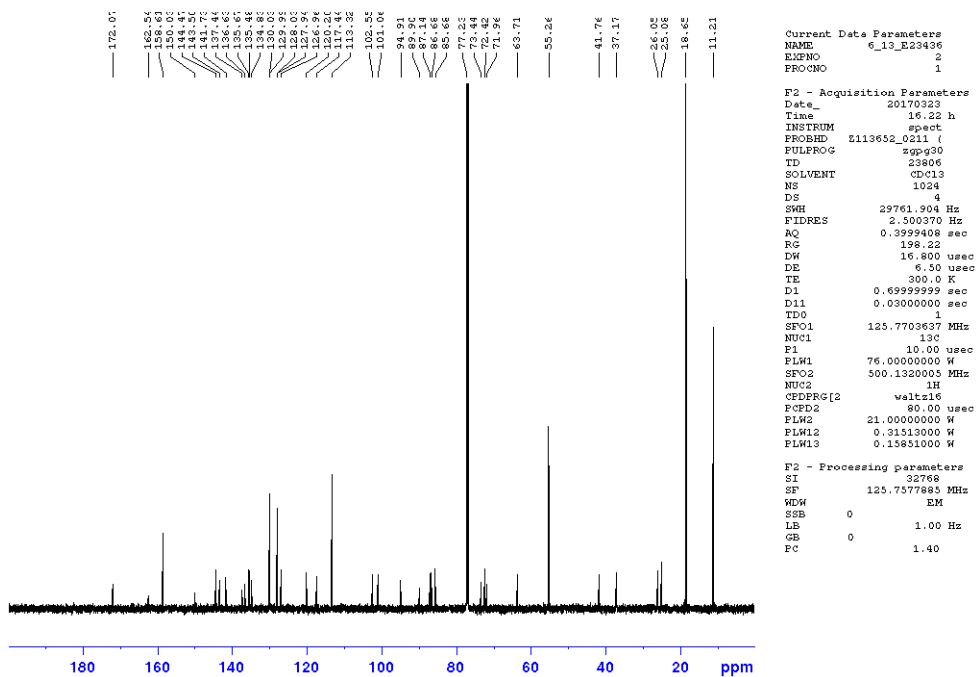
Appendix 38: ^{31}P NMR spectrum of **3.27**.Appendix 39: HRMS spectrum of **3.27**.



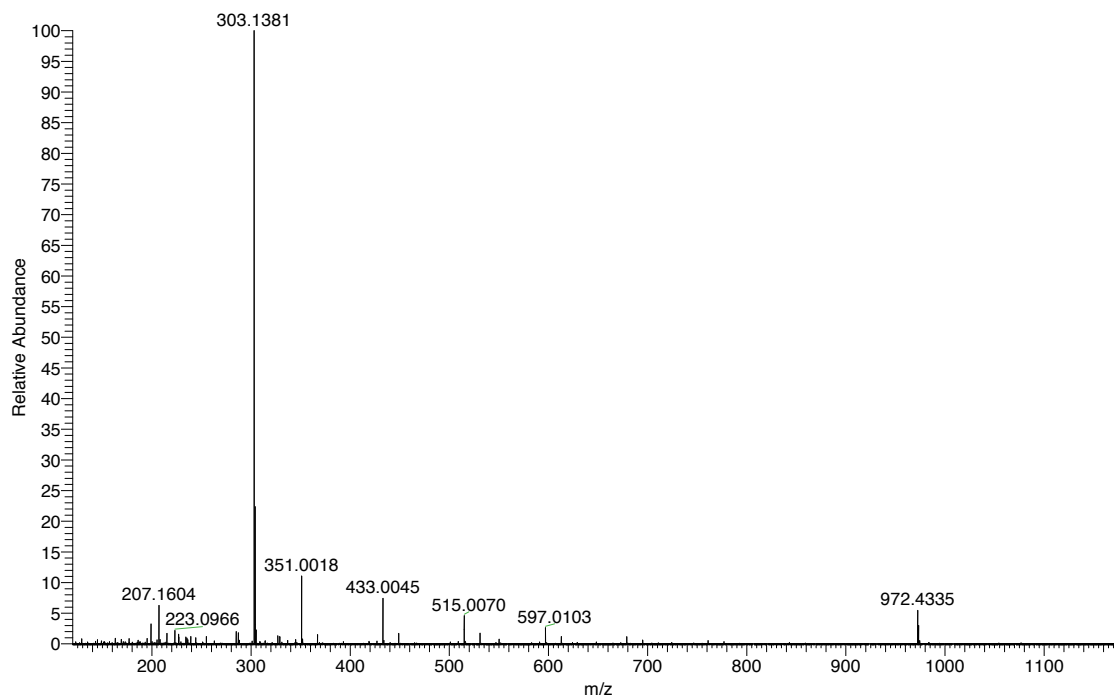
Appendix 40: Zoom HRMS spectrum of 3.27.



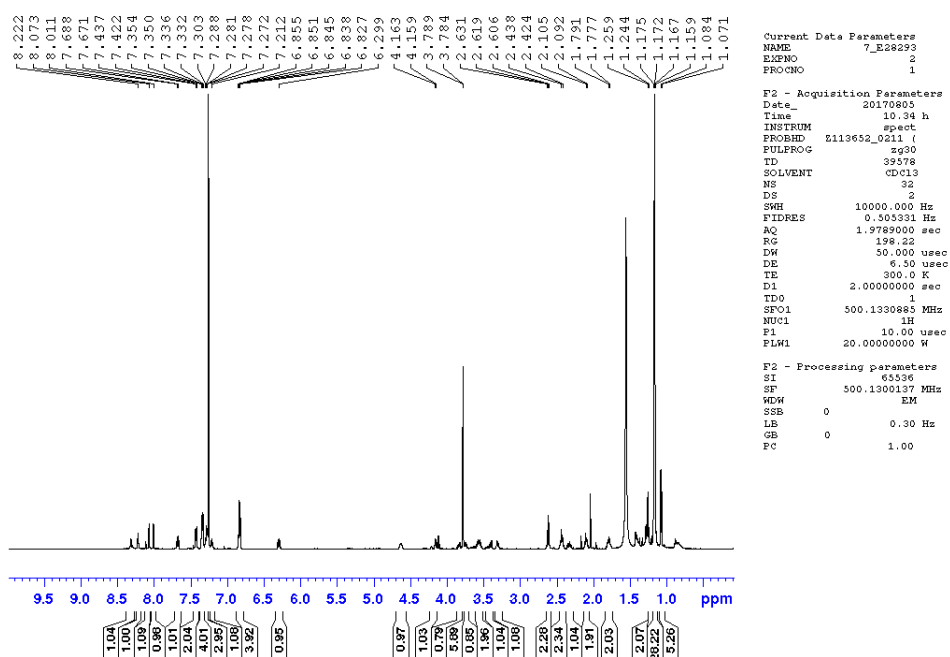
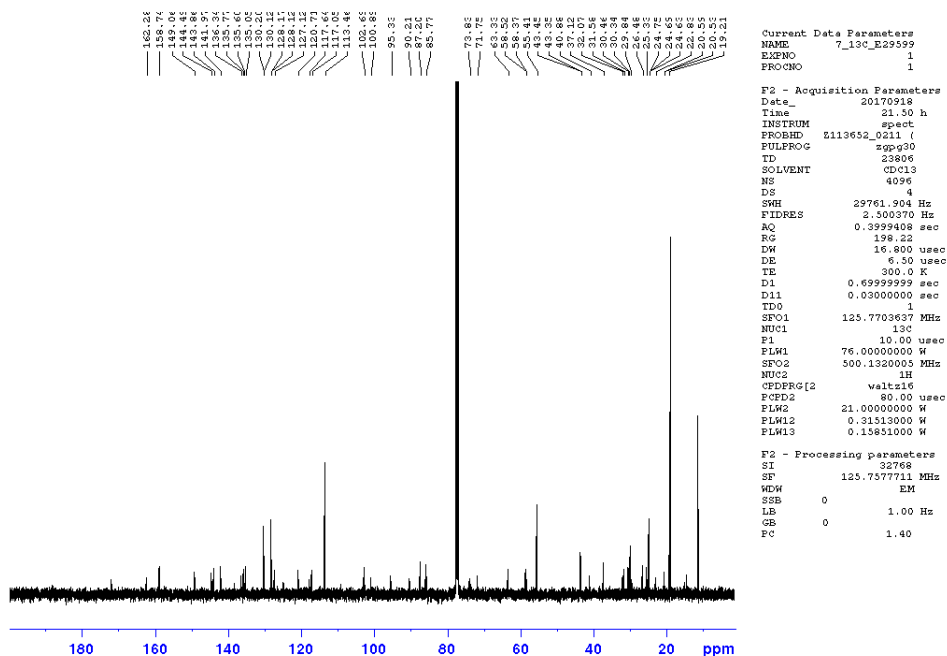
Appendix 41: ¹H NMR spectrum of 3.39.

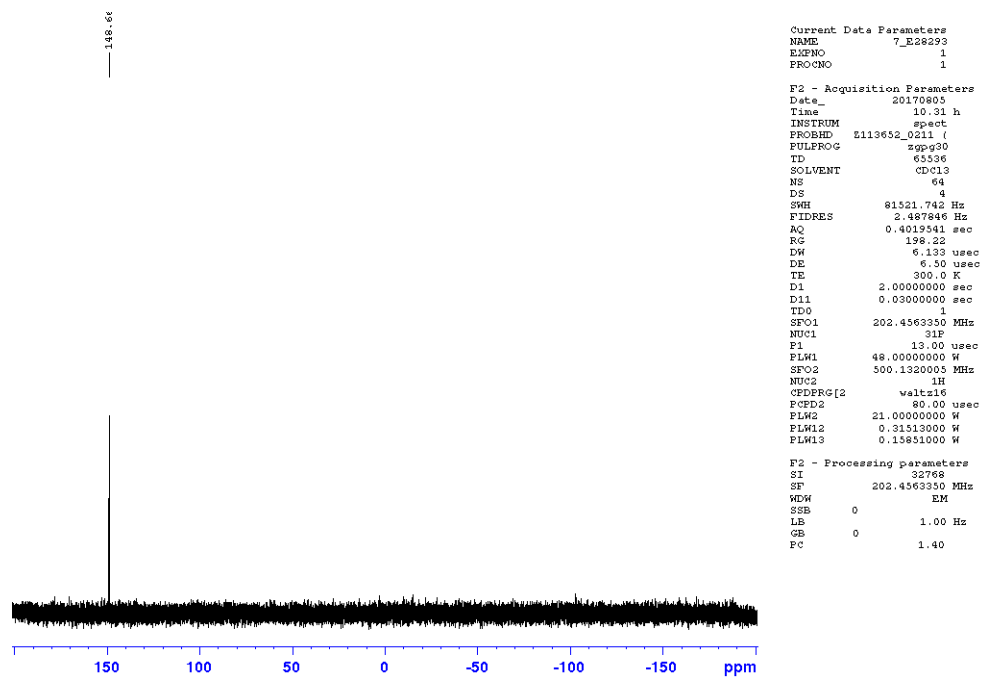
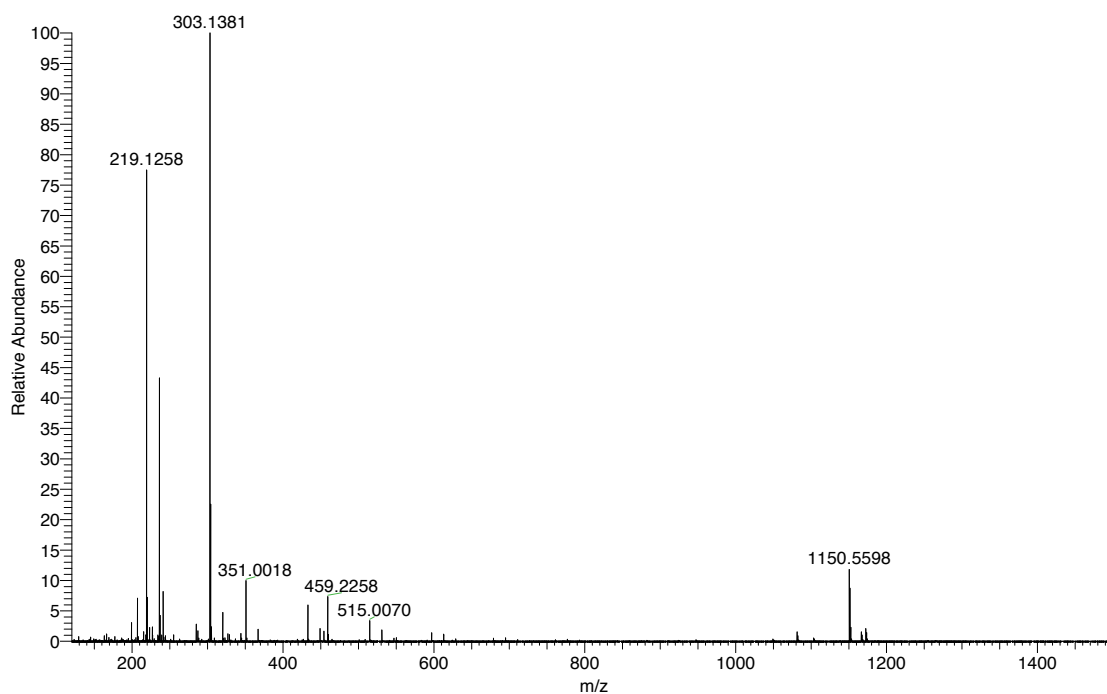


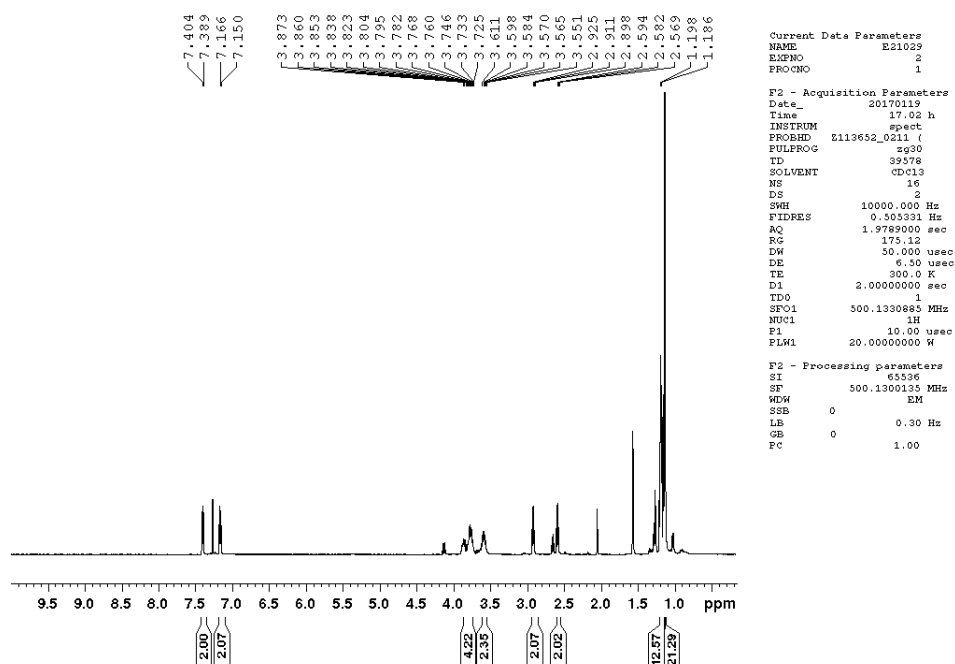
Appendix 42: ¹³C NMR spectrum of 3.39.



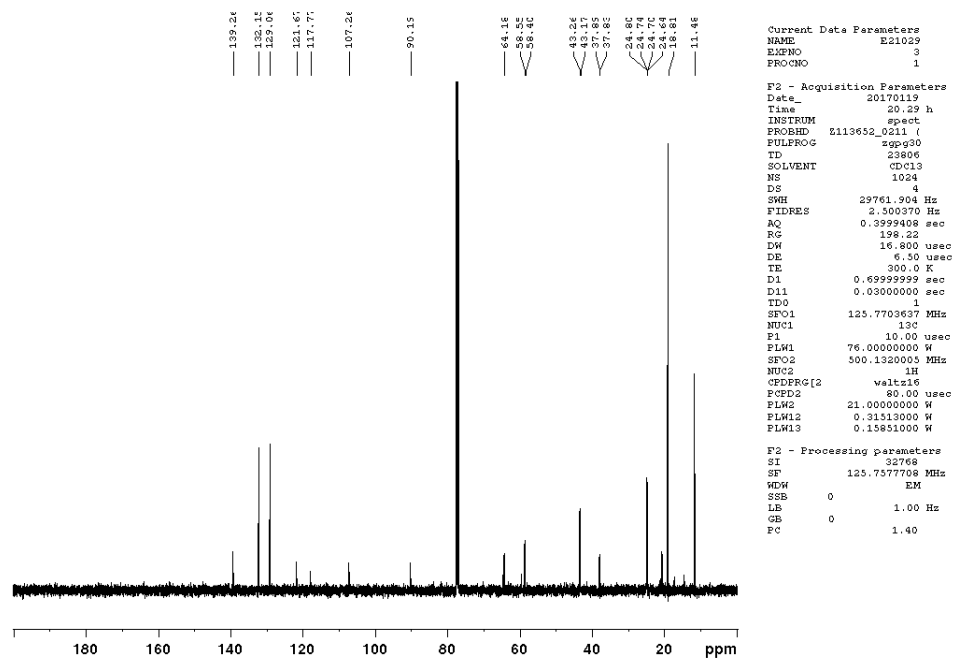
Appendix 43: HRMS spectrum of 3.39.

Appendix 44: ^1H NMR spectrum of 3.28.Appendix 45: ^{13}C NMR spectrum of 3.28.

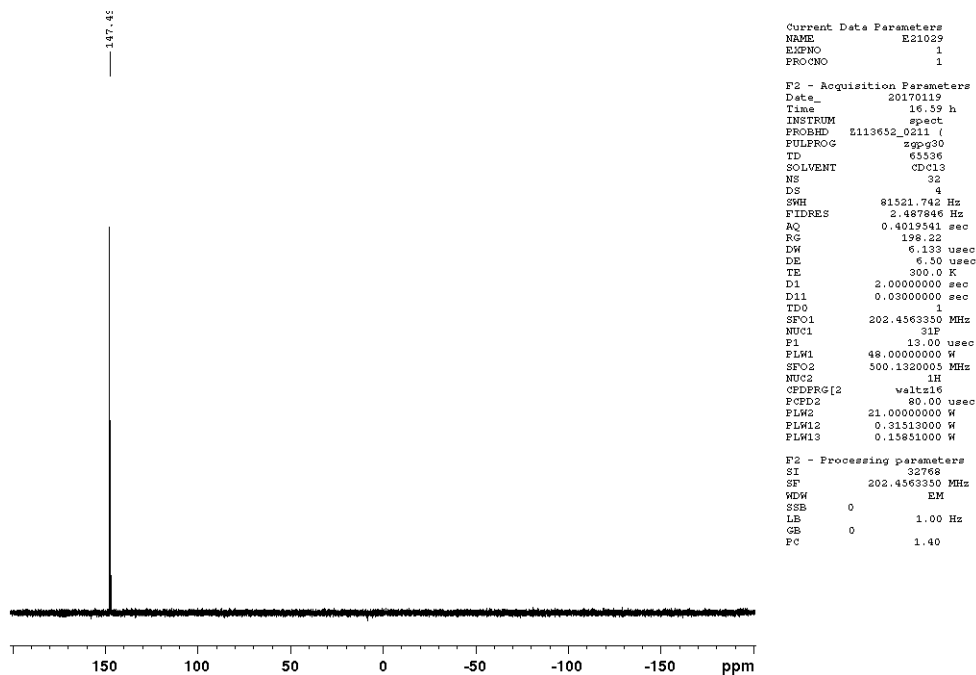
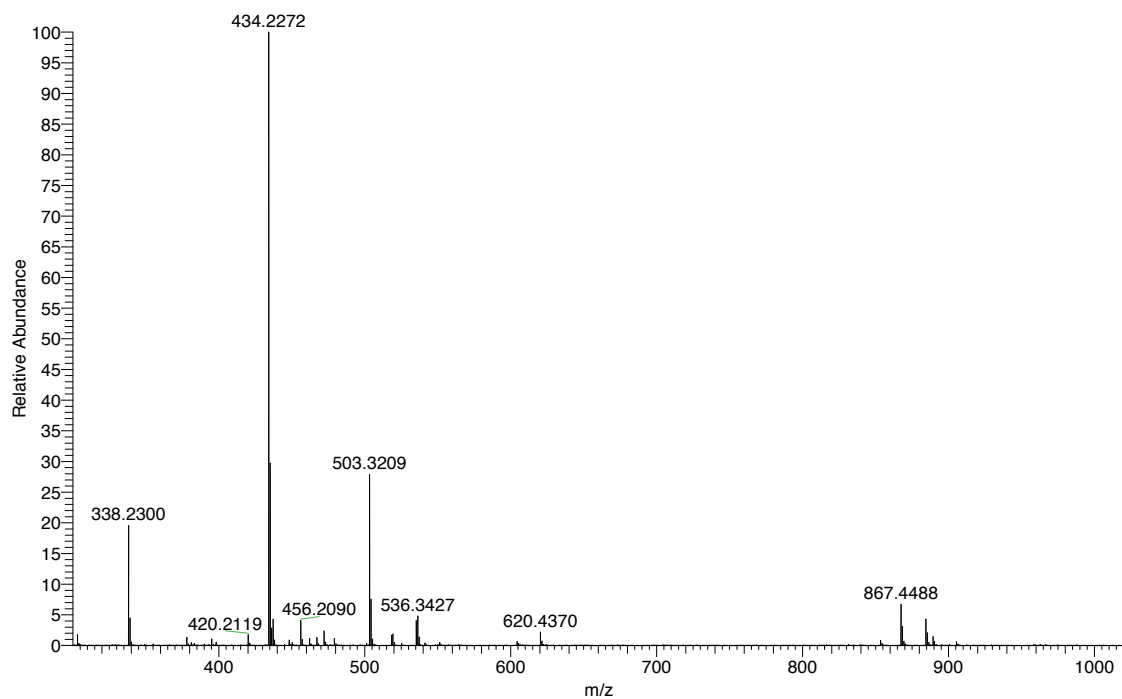
Appendix 46: ^{31}P NMR spectrum of **3.28**.Appendix 47: HRMS spectrum of **3.28**.



Appendix 48: ¹H NMR spectrum of 3.42.



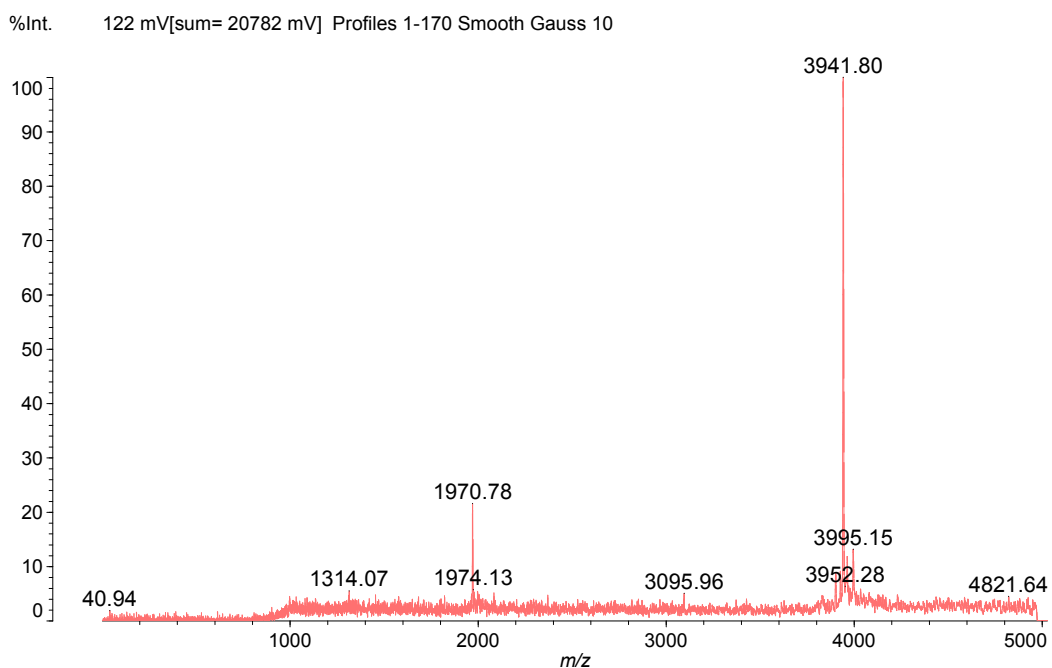
Appendix 49: ¹³C NMR spectrum of 3.42.

Appendix 50: ^{31}P NMR spectrum of 3.42.

Appendix 51: HRMS spectrum of 3.42.

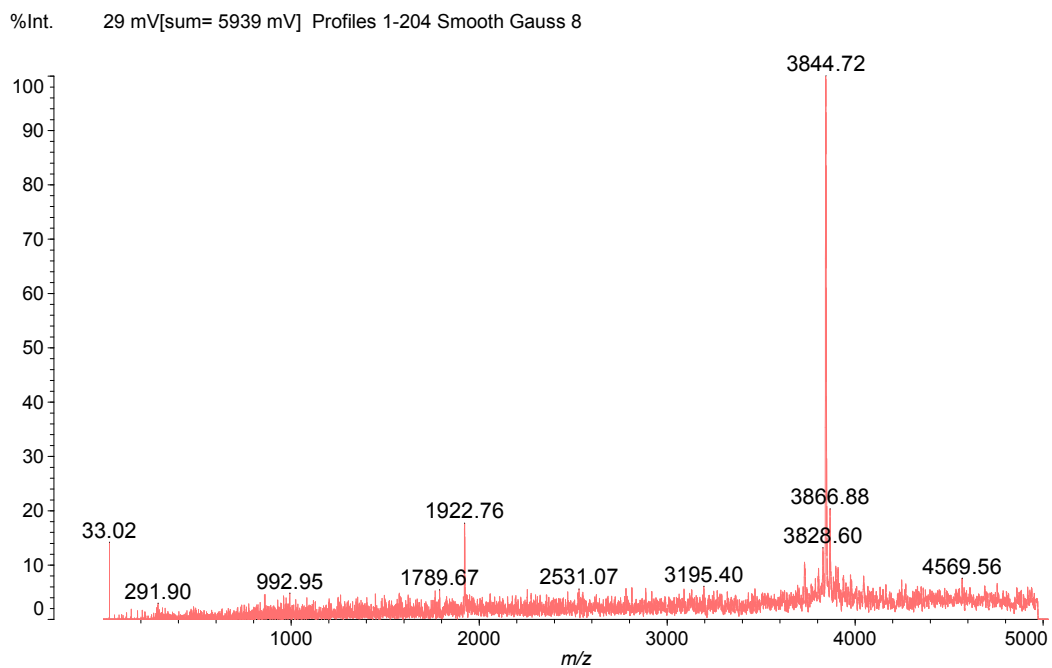
5.4 MALDI Spectra

Data: LR_416_15min0001.2H1[c] 14 Feb 2017 16:57 Cal: Small mols neg NUK 14 Feb 2017 16:27
Shimadzu Biotech Axima CFR 2.8.3.20080616: Mode reflectron_neg, Power: 137, Blanked, P.Ext. @ 4000 (bin 198)



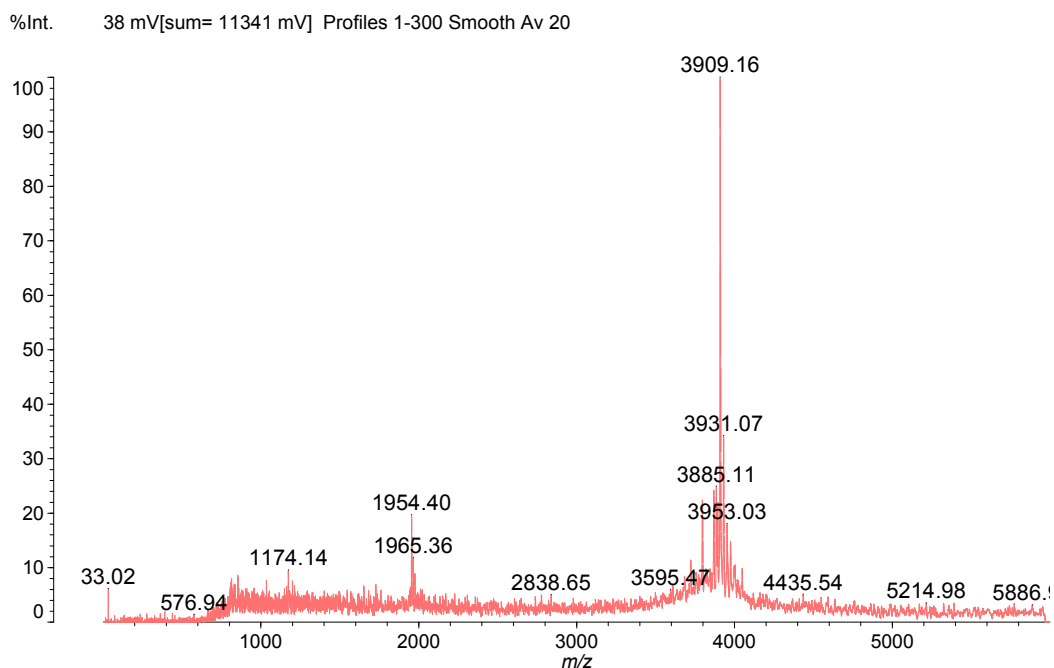
Appendix 52: MALDI spectrum of ODN3.18.

Data: LR_LR4140001.2D1[c] 31 Mar 2017 15:24 Cal: Small mols neg NUK 31 Mar 2017 15:23
Shimadzu Biotech Axima CFR 2.8.3.20080616: Mode reflectron_neg, Power: 132, Blanked, P.Ext. @ 4000 (bin 198)



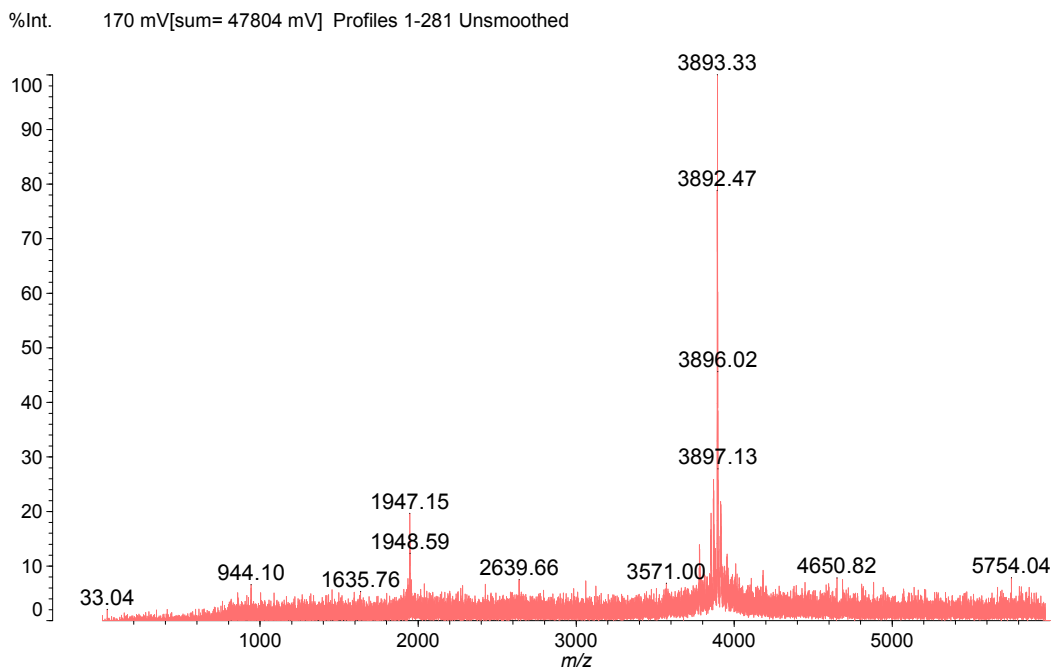
Appendix 53: MALDI spectrum of ODN3.19.

Data: LR474_desalted0001.3J1[c] 19 Apr 2017 15:55 Cal: Small mols pos 19 Apr 2017 15:49
Shimadzu Biotech Axima CFR 2.8.3.20080616: Mode reflectron_neg, Power: 145, Blanked, P.Ext. @ 4200 (bin 203)



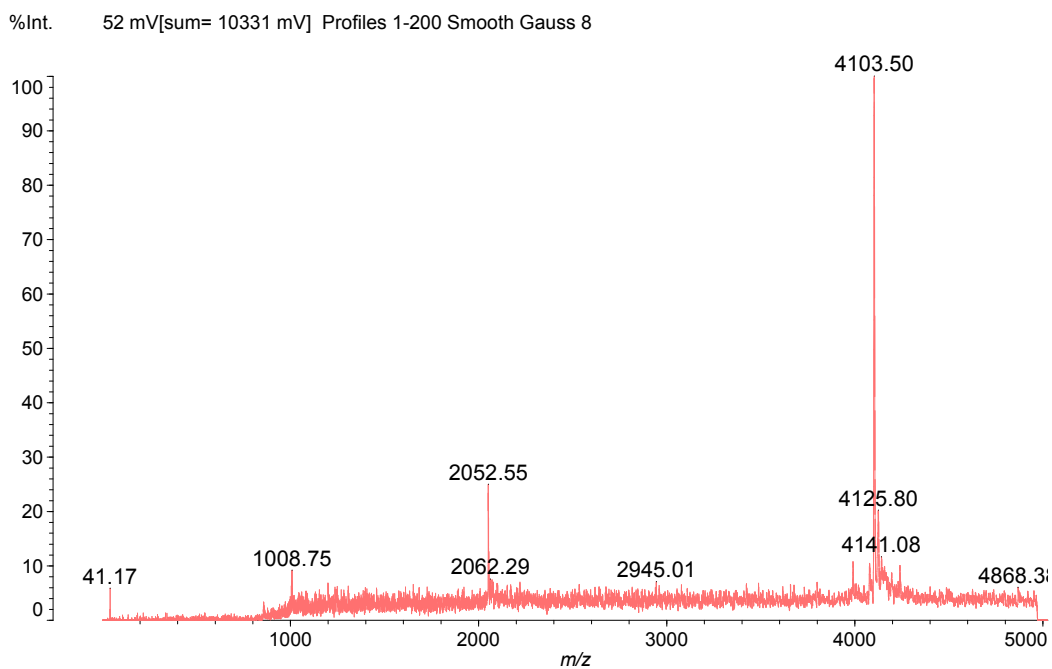
Appendix 54: MALDI spectrum of ODN3.20.

Data: LR473_desalted_really4730001.3K1[c] 19 Apr 2017 16:00 Cal: Small mols pos 19 Apr 2017 15:49
Shimadzu Biotech Axima CFR 2.8.3.20080616: Mode reflectron_neg, Power: 142, Blanked, P.Ext. @ 4200 (bin 203)



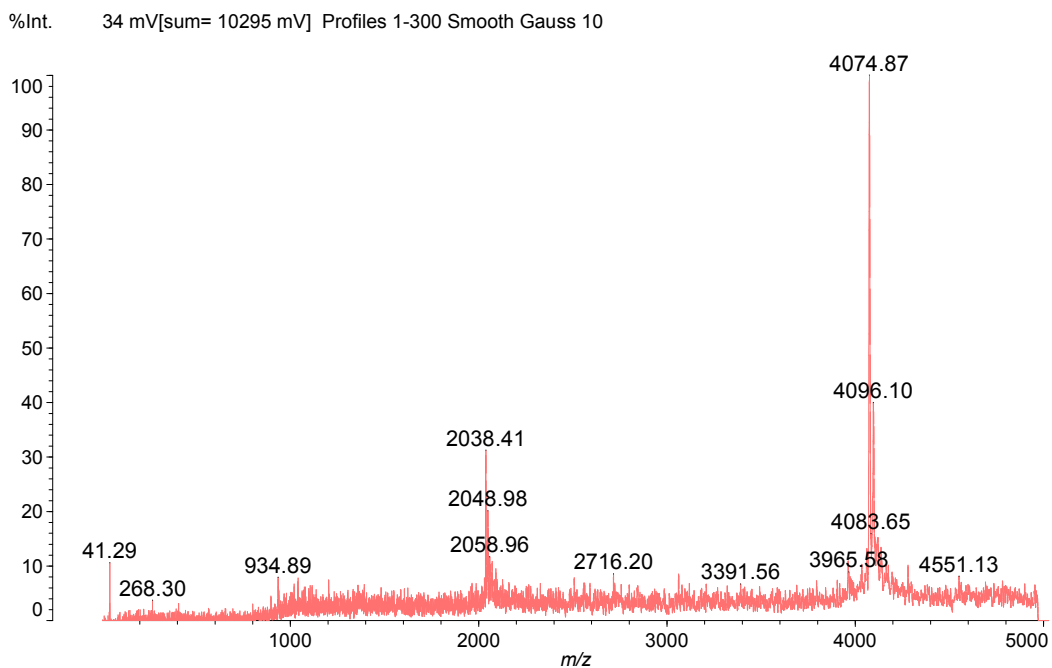
Appendix 55: MALDI spectrum of ODN3.21.

Data: LR534-10to120001.3K1[c] 25 Aug 2017 15:06 Cal: small mols neg LIN 25 Aug 2017 15:06
Shimadzu Biotech Axima CFR 2.8.3.20080616: Mode reflectron_neg, Power: 133, Blanked, P.Ext. @ 4100 (bin 200)



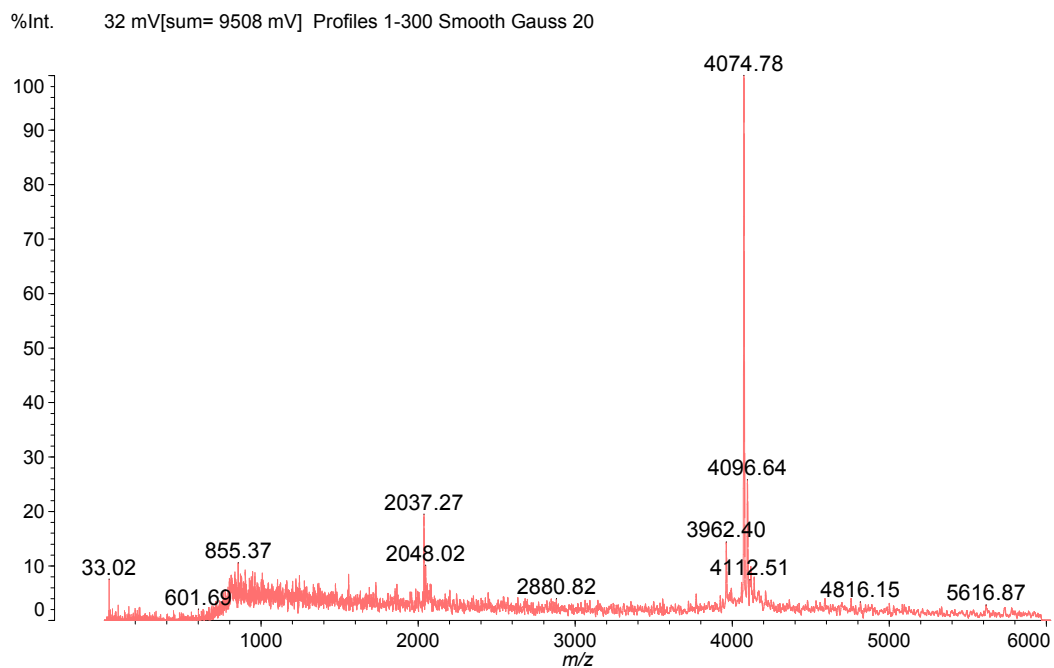
Appendix 56: MALDI spectrum of ODN3.22.

Data: LR447_20001.2K2[c] 17 Feb 2017 13:27 Cal: Small mols neg NUK 17 Feb 2017 13:22
Shimadzu Biotech Axima CFR 2.8.3.20080616: Mode reflectron_neg, Power: 139, Blanked, P.Ext. @ 4000 (bin 198)



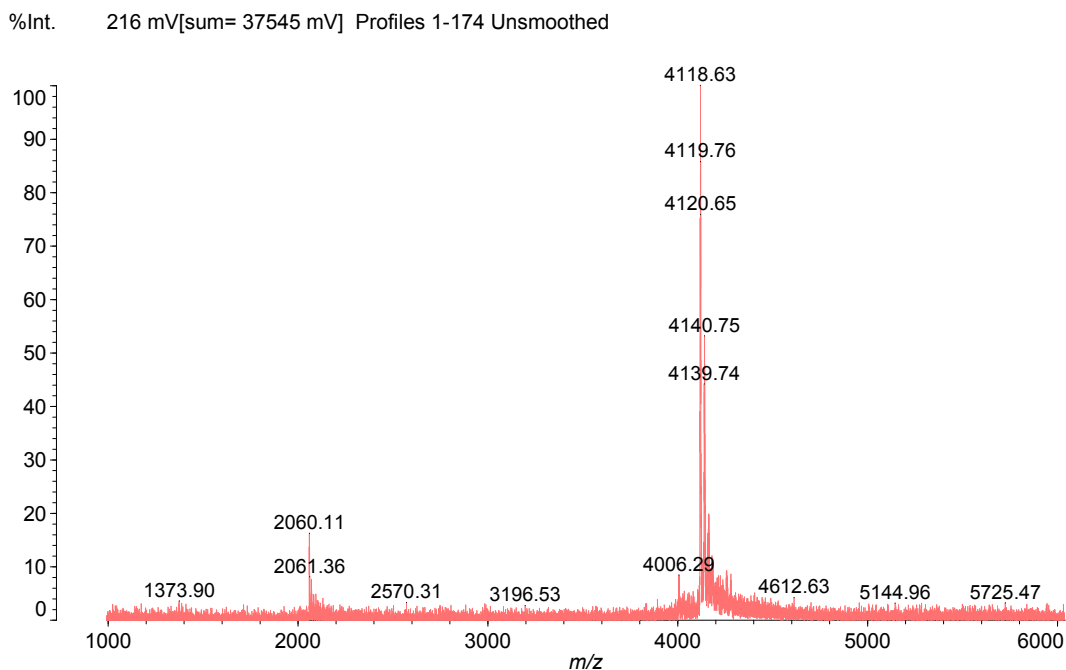
Appendix 57: MALDI spectrum of ODN3.23a.

Data: MH4220002.211[c] 21 Apr 2017 16:24 Cal: Small mols pos 21 Apr 2017 15:44
Shimadzu Biotech Axima CFR 2.8.3.20080616: Mode reflectron_neg, Power: 142, Blanked, P.Ext. @ 4000 (bin 198)



Appendix 58: MALDI spectrum of ODN3.23b.

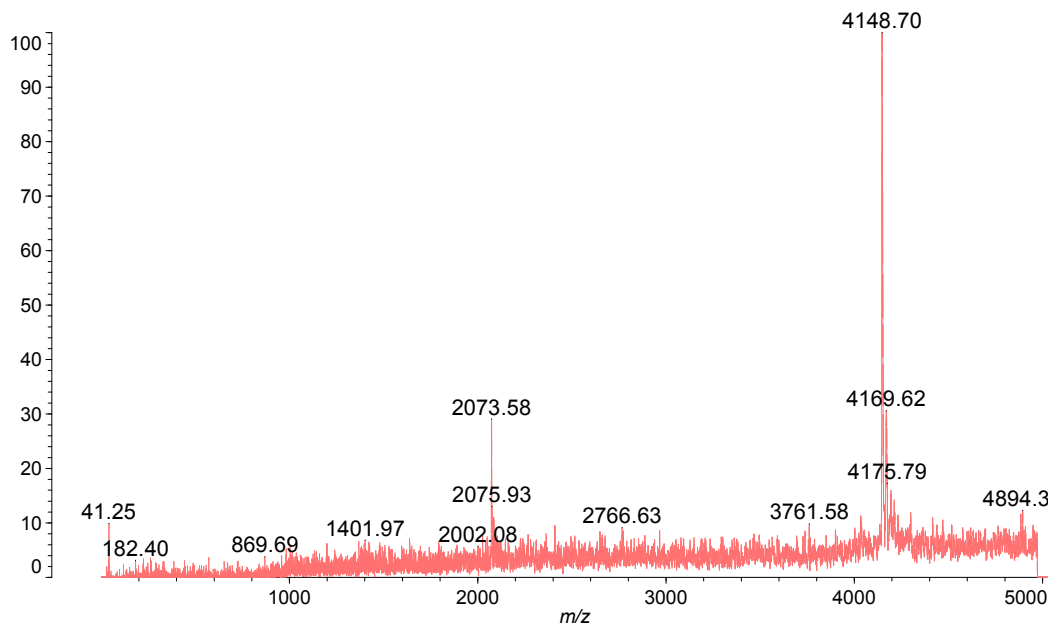
Data: MH_661_39pt9_ref_pos0001.3K1[c] 10 Aug 2018 16:07 Cal: 3 PEP MIX 10 Aug 2018 16:05
Shimadzu Biotech Axima CFR 2.8.3.20080616: Mode reflectron, Power: 140, P.Ext. @ 4100 (bin 200)



Appendix 59: MALDI spectrum of ODN3.23c.

Data: MH413_20001.2C2[c] 12 Apr 2017 16:07 Cal: Small mols neg NUK 12 Apr 2017 15:41
Shimadzu Biotech Axima CFR 2.8.3.20080616: Mode reflectron_neg, Power: 133, Blanked, P.Ext. @ 4000 (bin 198)

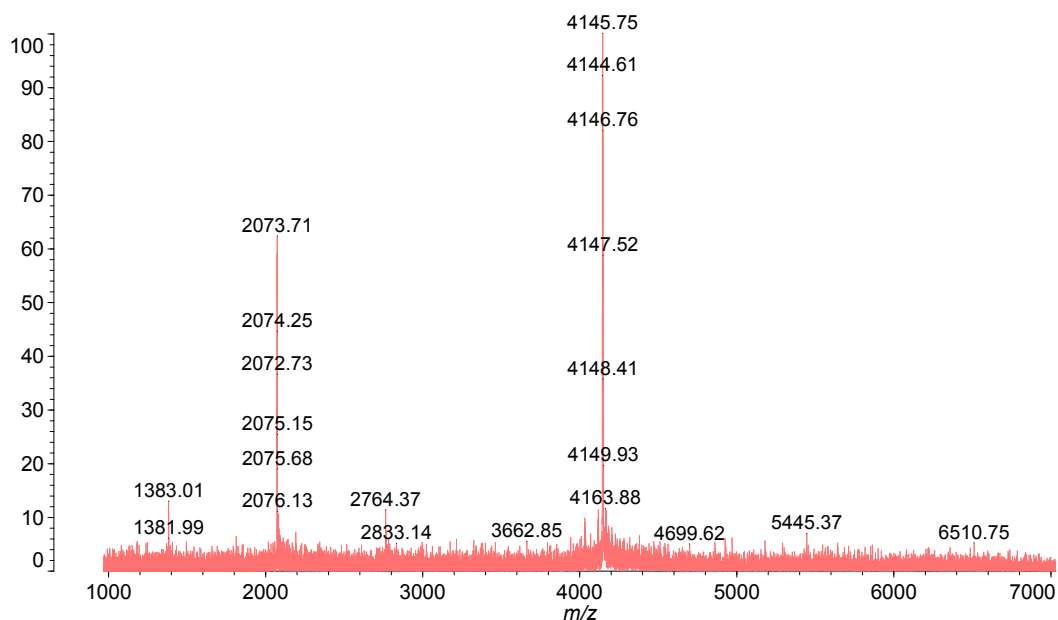
%Int. 43 mV[sum= 9248 mV] Profiles 1-217 Smooth Gauss 8



Appendix 60: MALDI spectrum of ODN3.23d.

Data: MH_662_32pt5_ref_pos0002.3L3[c] 3 Jul 2018 17:03 Cal: 3 PEP MIX 3 Jul 2018 16:48
Shimadzu Biotech Axima CFR 2.8.3.20080616: Mode reflectron, Power: 136, P.Ext. @ 4100 (bin 200)

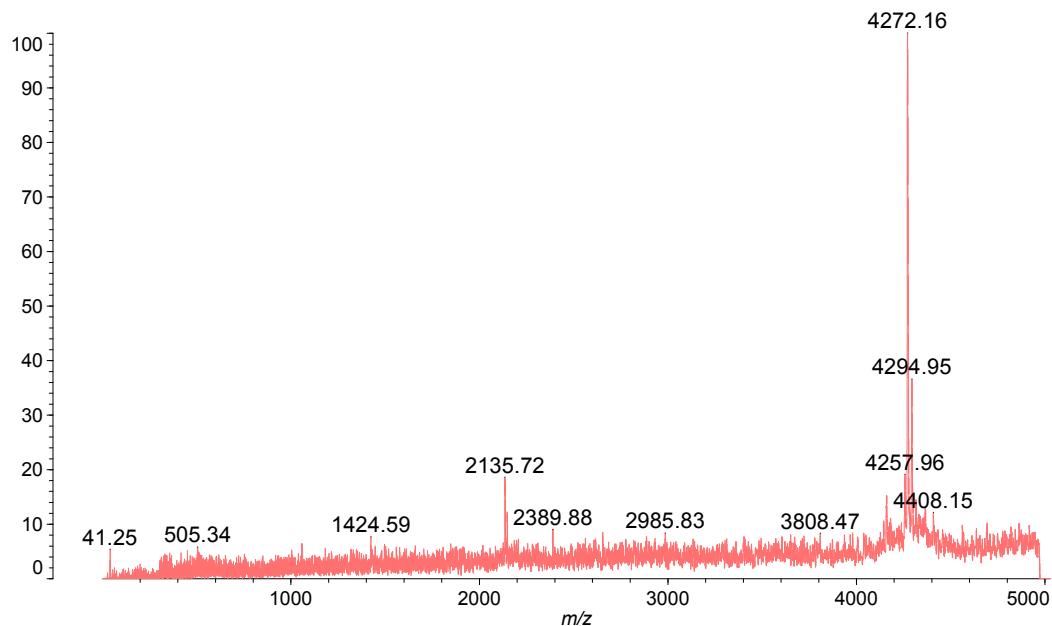
%Int. 148 mV[sum= 23459 mV] Profiles 1-159 Unsmoothed



Appendix 61: MALDI spectrum of ODN3.23e.

Data: MH410_20001.2D3[c] 12 Apr 2017 16:10 Cal: Small mols neg NUK 12 Apr 2017 15:41
Shimadzu Biotech Axima CFR 2.8.3.20080616: Mode reflectron_neg, Power: 133, Blanked, P.Ext. @ 4000 (bin 198)

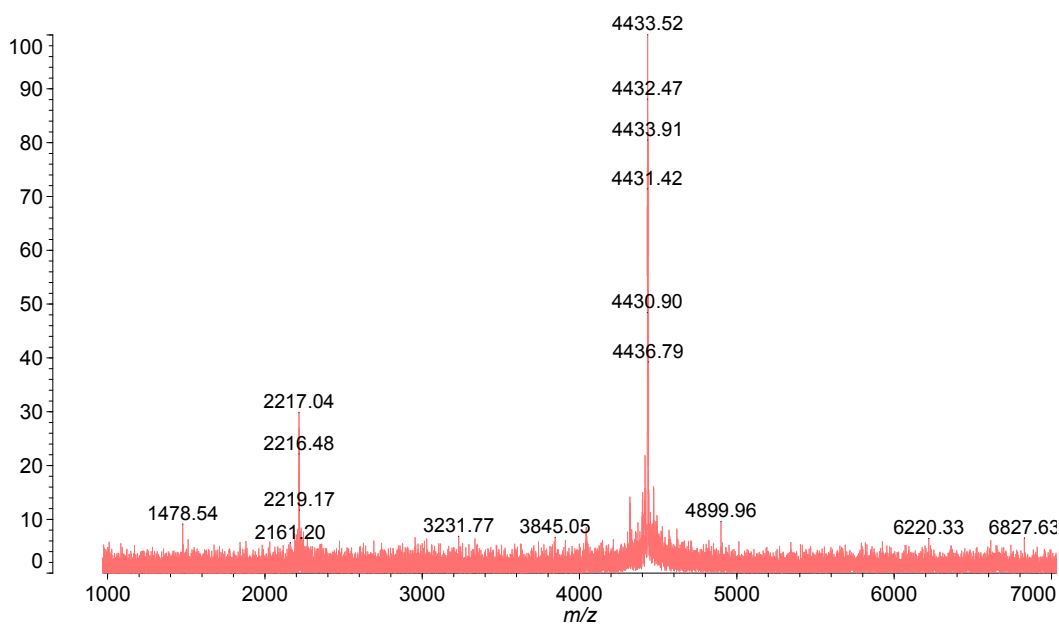
%Int. 65 mV[sum= 13403 mV] Profiles 1-205 Smooth Gauss 8



Appendix 62: MALDI spectrum of ODN3.23f.

Data: MH_663_29pt0_ref_pos0001.3l3[c] 3 Jul 2018 17:17 Cal: 3 PEP MIX 3 Jul 2018 16:48
Shimadzu Biotech Axima CFR 2.8.3.20080616: Mode reflectron, Power: 140, P.Ext. @ 4400 (bin 207)

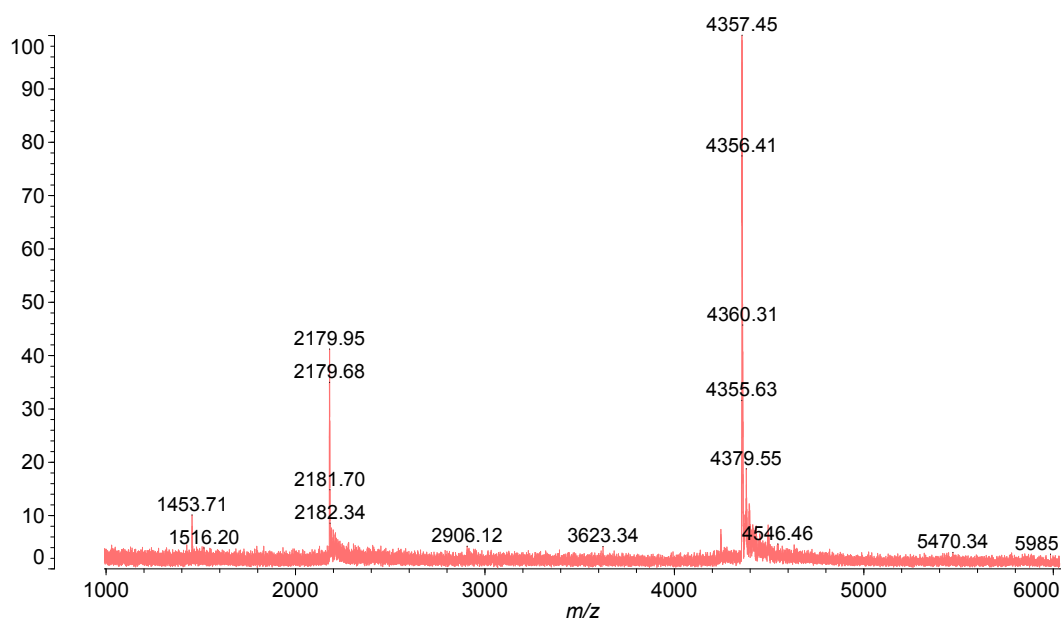
%Int. 217 mV[sum= 26894 mV] Profiles 1-124 Unsmoothed



Appendix 63: MALDI spectrum of ODN3.23g.

Data: MH_664_39pt7_ref_pos0001.3J2[c] 10 Aug 2018 16:11 Cal: 3 PEP MIX 10 Aug 2018 16:05
Shimadzu Biotech Axima CFR 2.8.3.20080616: Mode reflectron, Power: 146, P.Ext. @ 4100 (bin 200)

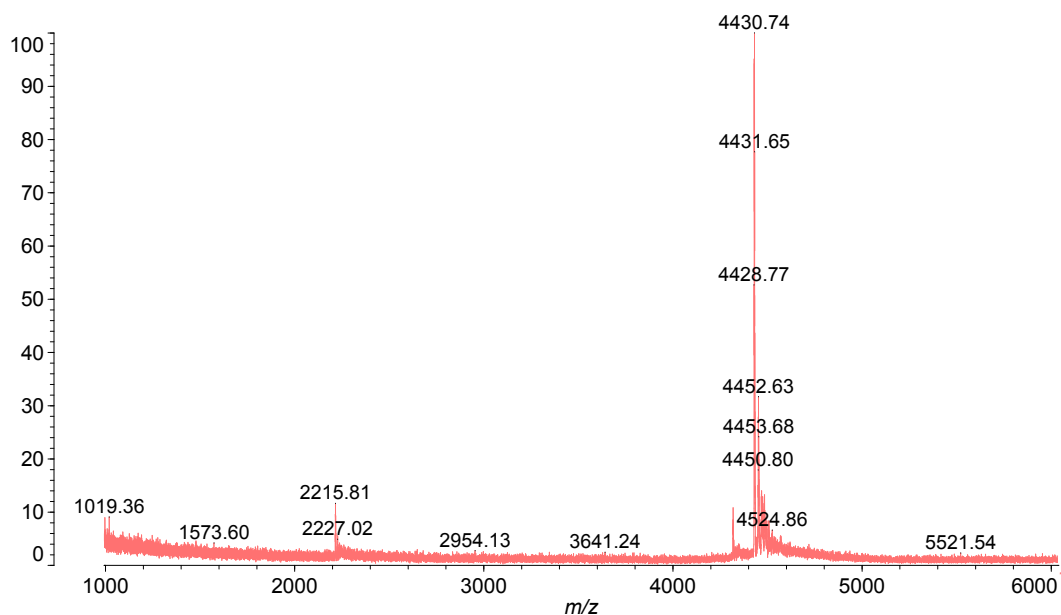
%Int. 599 mV[sum= 68259 mV] Profiles 1-114 Unsmoothed



Appendix 64: MALDI spectrum of ODN3.23h.

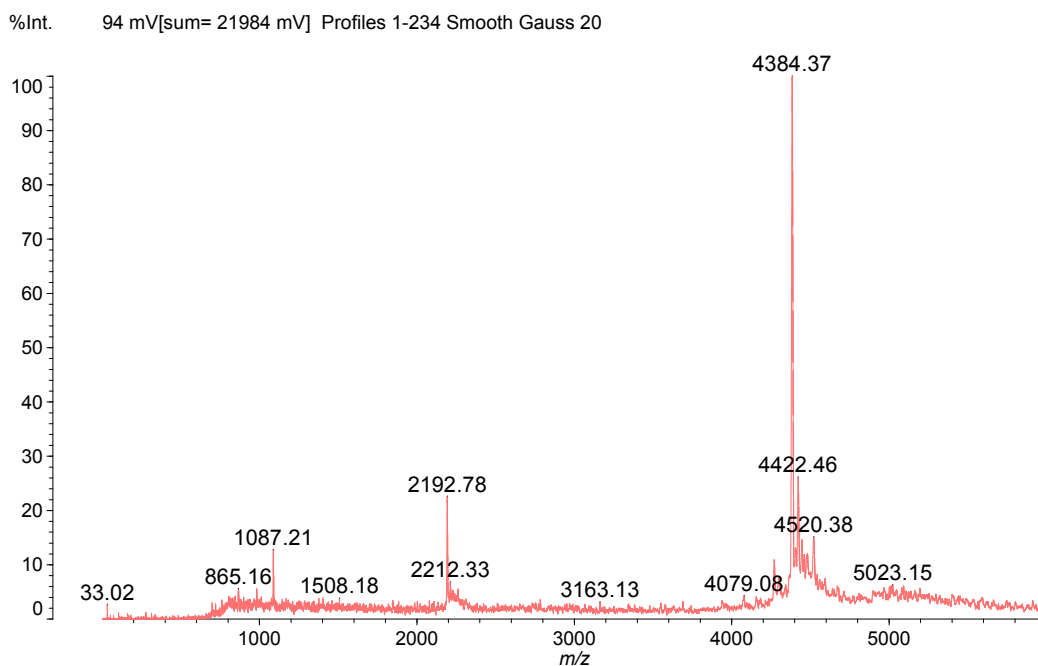
Data: MH_665_53pt2_ref_pos0002.3K3[c] 10 Aug 2018 16:17 Cal: 3 PEP MIX 10 Aug 2018 16:05
Shimadzu Biotech Axima CFR 2.8.3.20080616: Mode reflectron, Power: 150, P.Ext. @ 4400 (bin 207)

%Int. 384 mV[sum= 101380 mV] Profiles 1-264 Unsmoothed



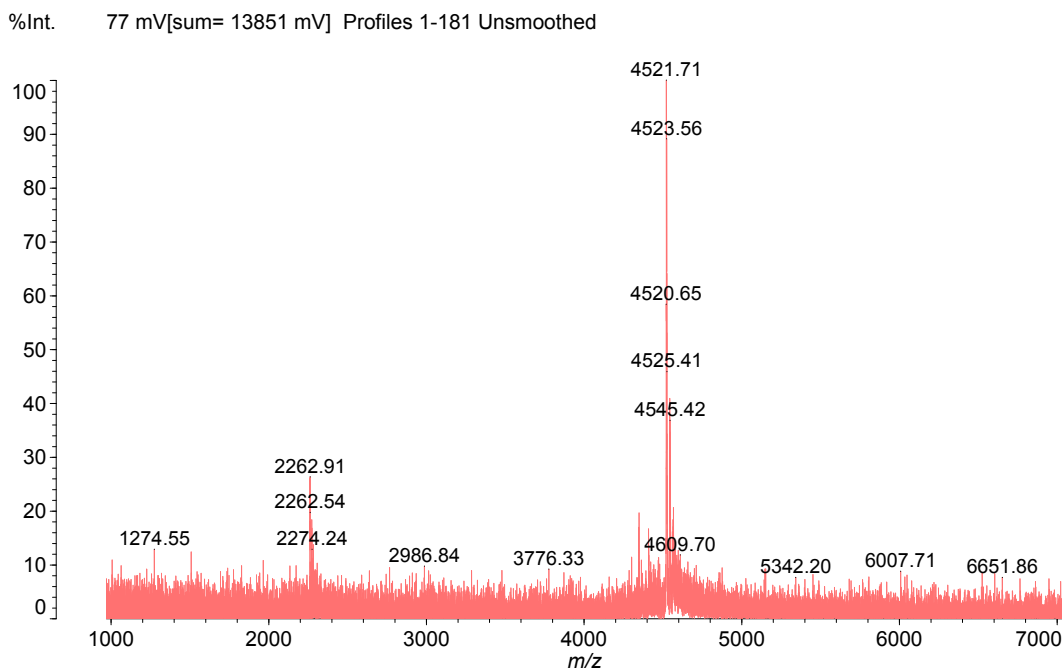
Appendix 65: MALDI spectrum of ODN3.23i.

Data: MH4150001.3E2[c] 19 Apr 2017 16:39 Cal: Small mols pos 19 Apr 2017 15:49
Shimadzu Biotech Axima CFR 2.8.3.20080616: Mode reflectron_neg, Power: 142, Blanked



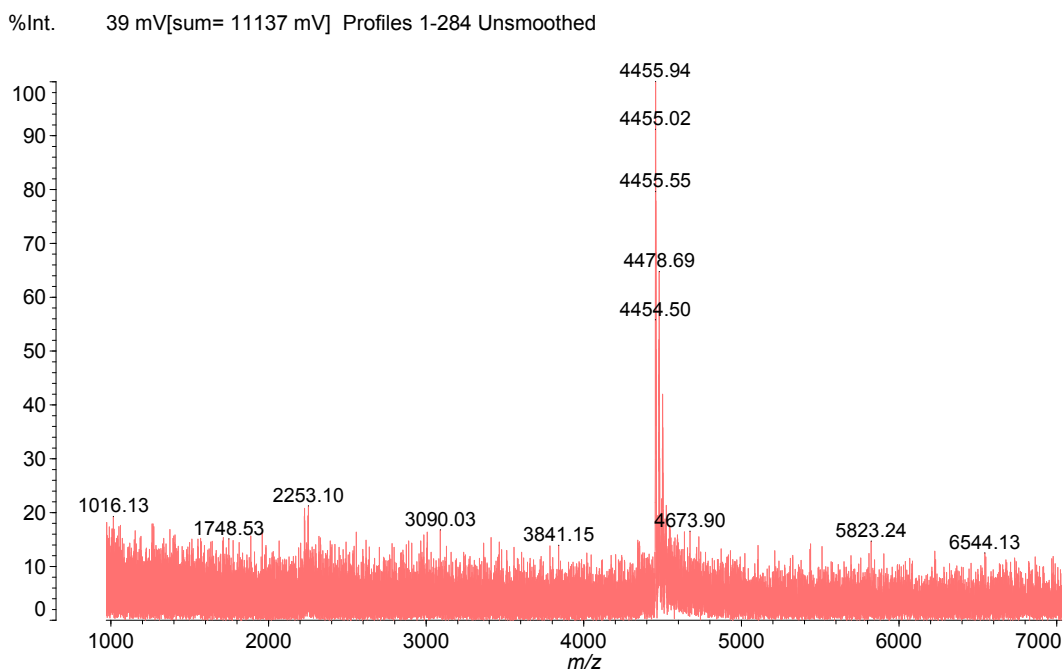
Appendix 66: MALDI spectrum of ODN3.23j.

Data: MH_666_29pt6_ref_pos0001.3F4[c] 3 Jul 2018 17:33 Cal: 3 PEP MIX 3 Jul 2018 16:48
Shimadzu Biotech Axima CFR 2.8.3.20080616: Mode reflectron, Power: 140, P.Ext. @ 4500 (bin 210)



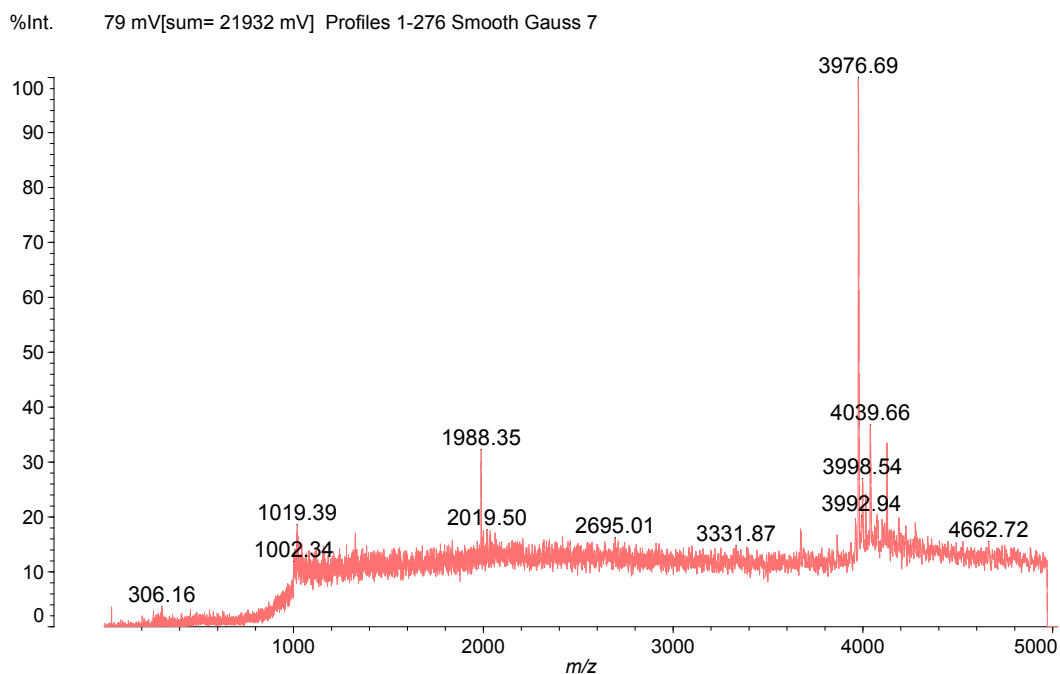
Appendix 67: MALDI spectrum of ODN3.23k.

Data: MH_667_54pt3_ref_pos0002.3C3[c] 3 Jul 2018 17:48 Cal: 3 PEP MIX 3 Jul 2018 16:48
Shimadzu Biotech Axima CFR 2.8.3.20080616: Mode reflectron, Power: 141, P.Ext. @ 4400 (bin 207)



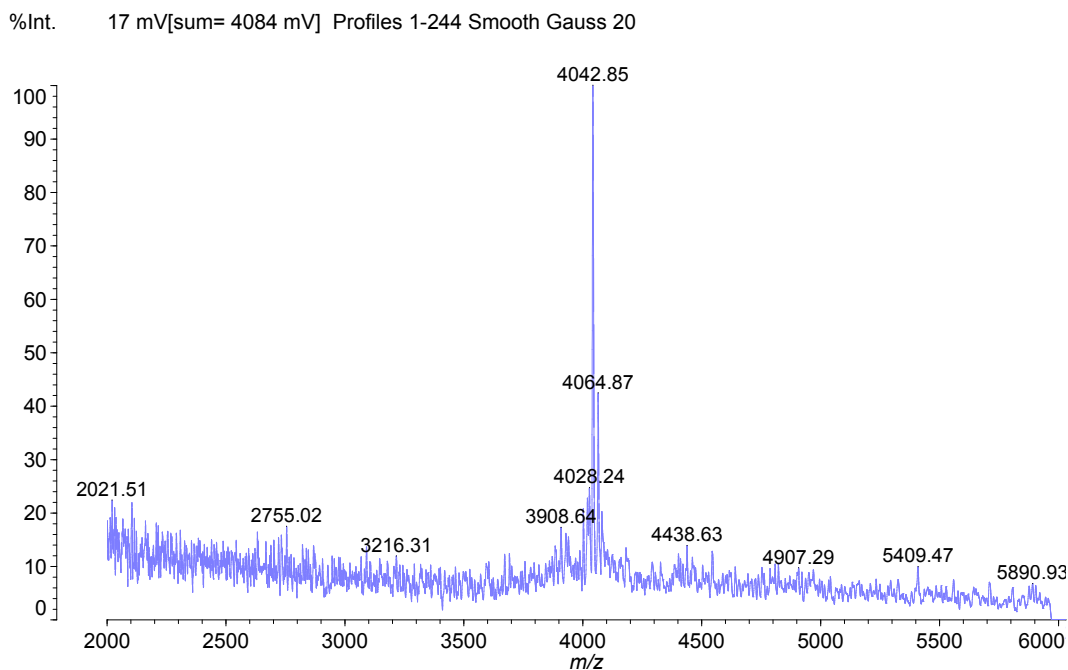
Appendix 68: MALDI spectrum of ODN3.23I.

Data: LR_MH376_alkyne_DNA_BnClick20001.2J4[c] 22 Mar 2017 15:41 Cal: Small mols neg NUK 22 Mar 2017 15:35
Shimadzu Biotech Axima CFR 2.8.3.20080616: Mode reflectron_neg, Power: 138, Blanked, P.Ext. @ 3850 (bin 194)



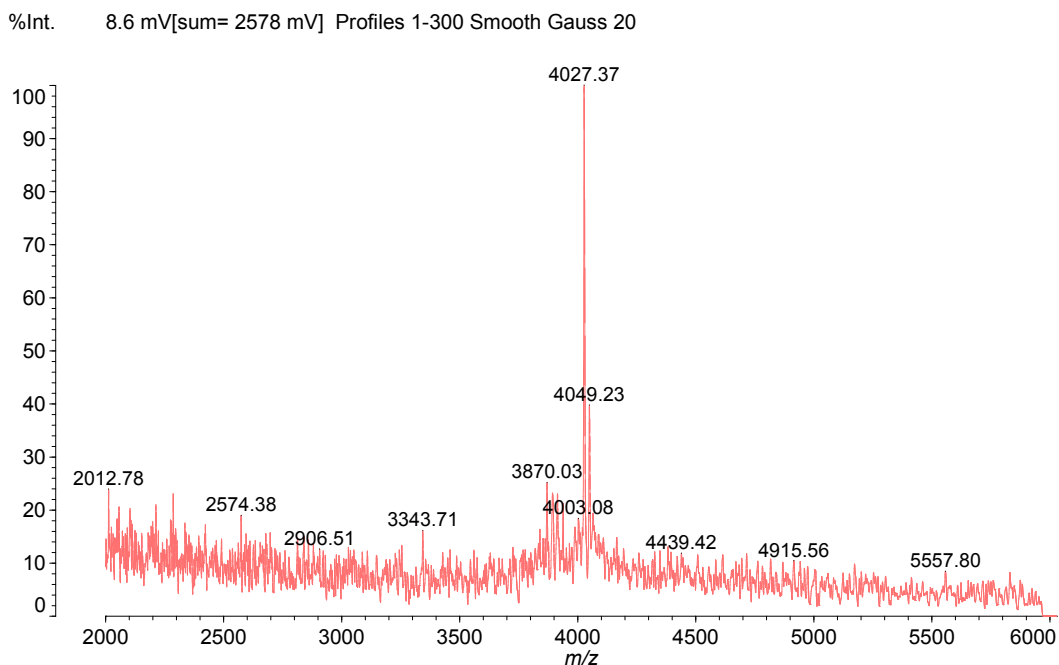
Appendix 69: MALDI spectrum of ODN3.24a.

Data: MH4500001.2G3[c] 21 Apr 2017 16:05 Cal: Small mols pos 21 Apr 2017 15:44
Shimadzu Biotech Axima CFR 2.8.3.20080616: Mode reflectron_neg, Power: 143, Blanked, P.Ext. @ 4000 (bin 198)



Appendix 70: MALDI spectrum of ODN3.25a.

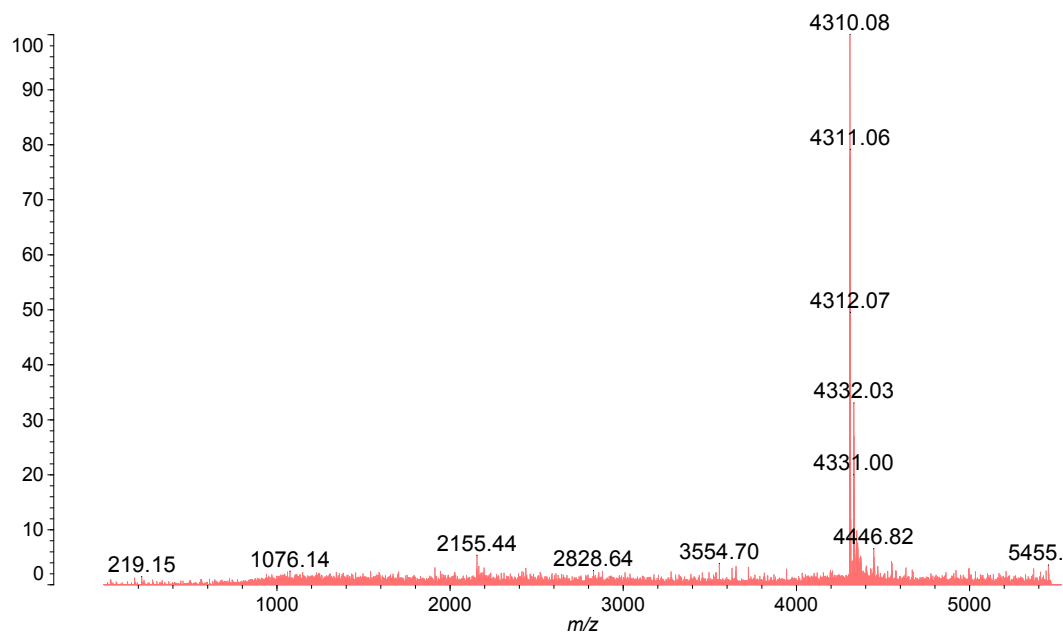
Data: MH448_20001.2E4[c] 21 Apr 2017 16:19 Cal: Small mols pos 21 Apr 2017 15:44
Shimadzu Biotech Axima CFR 2.8.3.20080616: Mode reflectron_neg, Power: 143, Blanked, P.Ext. @ 4000 (bin 198)



Appendix 71: MALDI spectrum of ODN3.26a.

Data: MH6150001.311[c] 29 Aug 2017 15:26 Cal: Small mols neg NUK 29 Aug 2017 15:13
Shimadzu Biotech Axima CFR 2.8.3.20080616: Mode reflectron_neg, Power: 146, Blanked, P.Ext. @ 4300 (bin 205)

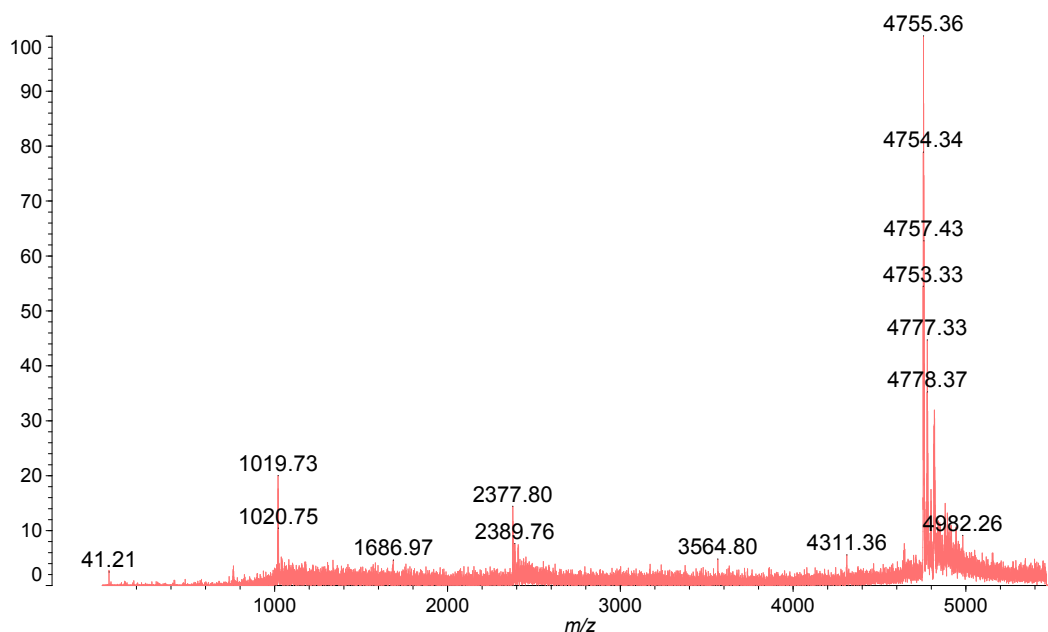
%Int. 346 mV[sum= 47066 mV] Profiles 1-136 Unsmoothed -Baseline 3



Appendix 72: MALDI spectrum of ODN3.27.

Data: LR_MH616_spot1_better0001.1K1[c] 30 Aug 2017 15:54 Cal: small mols neg LIN 30 Aug 2017 15:32
Shimadzu Biotech Axima CFR 2.8.3.20080616: Mode reflectron_neg, Power: 137, Blanked, P.Ext. @ 4700 (bin 214)

%Int. 214 mV[sum= 64267 mV] Profiles 1-300 Unsmoothed



Appendix 73: MALDI spectrum of ODN3.28.